Process Intensification: A Study of Micromixing and Residence Time Distribution Characteristics in the Spinning Disc Reactor

by

Salah Al-hengari B.Sc., M.Sc.

Thesis submitted for the degree of Doctor of Philosophy in the Faculty of Science Agriculture and Engineering of the Newcastle University

Process Intensification Group
School of Chemical Engineering And Advanced materials
Newcastle University
Newcastle upon Tyne
NE1 7RU
U. K.

October 2011

Abstract

Micromixing phenomena (i.e. mixing at molecular level) play a very important role in the chemical industry when the time scale of the chemical reaction involved have the same magnitude or smaller than the time scale of mixing process. The study of micromixing is very critical to the understanding of important processes such as polymerization, precipitation, crystallization and competing fast chemical reactions. It has long been recognised that the intense mixing characteristics of thin films in the spinning disc reactor (SDR), play an important role in improving the selectivity, yield, and quality of final products of a chemical reaction. However, to date, there has been no systematic study of micro and macro mixing in SDR thin films.

The first part of this study reports on the fundamental study undertaken to characterise micromixing in the thin films formed in 10 cm and 30 cm SDRs operating under a wide range of operating conditions. A well-established parallel-competitive reaction test scheme was adopted to quantify micromixing in terms of the segregation index (Xs) or micromixedness ratio (α), the power dissipation (ε) and micromixing time(t_m). The micromixing data obtained from 10cm and 30cm SDRs were benchmarked against both a 1.37 *l* conventional semi-batch reactor (SBR) and continuous tubular flow reactors in the form of narrow channels (NCRs) of 1.0 mm diameter and three different lengths namely 5 cm, 10 cm and 15 cm (Y and T shape junctions). The effects of various operating parameters such as disc rotation rates, disc size, disc surface configurations, feed flowrates, feed distribution systems, liquid feed concentrations and viscosities were investigated. It was observed that, at an acid concentration of 1 M, the lowest segregation index of 0.05 was achieved for a feed of 0.001Ns/m^2 viscosity at the highest flowrate of 5ml/s (corresponding to Re_{film}=72) and highest rotational speed of 2400 rpm in the 10cm diameter disc. Greatly improved micromixing was obtained on the larger disc of 30 cm diameter, especially at the lower Re_{film} of 15 and 42, in comparison to the smaller disc. Under optimised conditions, the micromixing time(t_m) in the water-like film on the 30cm diameter disc was estimated to be as low as 0.3ms with corresponding power dissipation (ε) of 1025 W/kg. In contrast, the SBR could only achieve, under optimised conditions, segregation indices of no lower than 0.13 corresponding to a micromixing time of above 1ms with power dissipation of no more than about 21 W/kg. On the other hand, the NCRs could only achieve, under optimised conditions, a

micromixing time of about 19 ms corresponding to power dissipation (ε) of about 208 W/kg. Therefore, when compared with other mixing devices such as conventional SBRs or NCRs, the SDR is shown to give significantly better micromixing performance which highlights its potential as an alternative device for processes where a high degree of mixing is critically important.

In the second part of this study, the residence time distribution (RTD) of the liquid flow in the 30 cm SDR was characterised for a range of operating conditions including disc rotational speeds, disc configuration (smooth vs. grooved), total flow rate of liquid and viscosity in order to determine the conditions for which plug flow profile became more prevalent in the SDR films. The dispersion number from the RTD results and Peclet number were also estimated for the purpose of further characterising the extent of axial dispersion in the thin film flow on the rotating disc. All the mentioned operating conditions were found to have a profound influence on the overall Mean Residence Time, ($t_{overall\,mean}$), variance,(σ^2), dispersion number and Peclet number, (Pe). More specifically, the lowest value for the $t_{overall\,mean}$ of 10.1 s was achieved for a feed of 0.001 Ns/m^2 viscosity at the highest flowrate of 15ml/s and highest rotational speed of 1200 rpm on the smooth disc with corresponding σ^2 of 2.16. The dispersion number and Pe were 0.010 and 100 respectively, showing that the degree of axial dispersion was very small. A considerable reduction in the dispersion number and Pe was observed when the smooth disc was replaced by grooved disc. Thus, under the above mentioned hydrodynamic conditions, whilst the $t_{overall\,mean}$ was almost unchanged at 10.10 s on grooved disc, the corresponding variance of 1.03 was significantly lower, indicating even more reduced axial dispersion in the film on the grooved disc. This is further substantiated by dispersion number and Pe of 0.005 and 200 respectively. In general the RTD curves become narrower and the values of $t_{overall\,mean}$ and σ^2 decreased as the disc rotational speed and flowrates increased and as the feed viscosity decreased. For the given operating conditions used in this research, it was confirmed that the 30 cm SDR approaches plug-flow regime which had a positive influence on the micromixing intensity on the SDR.

Key words: Spinning disc reactor; micromixing; segregation index; micromixedness ratio; micromixing time; power dissipation; residence time distribution.

Acknowledgements

This work could not have been carried out without the help and support of numerous people. I would like to take this opportunity to express my deepest appreciation and heartfelt thanks to all of the following people:

First of all, I owe my supervisor Dr. Kamelia Boodhoo many special thanks for accepting me as PhD student under her supervision, for her continued support and for giving me the freedom to develop and pursue my own ideas in the field of spinning disc reactor technology and micromixing. Our discussions were always stimulatingly helpful to me finding my way.

I would also like to acknowledge financial support I received from Libyan Petroleum Institute (LPI) for this project. Also I would like to manifest my appreciation to LPI's former Manager and my Supervisor there for their support and guidance during my PhD research programme. I would like to thank Dr. Bourima A. Belgasem (The former LPI General Manager), Dr. Mohammed El-Bousiffi .

My thanks also go to Mr. Brian E. Grover, Mr. Stuart Latimer, Mr. Ian Strong, Mr. Jimmy Banks and Mr. Simon Daley who offered me help and support (when it was needed most) during the rigs construction.

I would like to extend further thanks to our lab technicians: Mr. Rob Dixon, Mr. Paul Sterling, for their help during work with my project in the Millennium Lab.

Thanks to all my friends and colleagues in the school of Chemical Engineering and Advanced materials and Process Intensification Group who gave me their help and support during this work especially Miss Claire Thompson, Mr. Ankur Mukherjee, and Dr. Edward McCarthy. I would also like to thank Mr. Musa Bashir for support and encouragement I received from him during entire period of my PhD study.

Finally, I would like to thank my family who have been a tremendous source of encouragement to me.

Table of Contents

List of Figures

List of Tables

Nomenclature

Symbol	Description	Units
ω	Angular velocity of the disc	s^{-1}
ρ	liquid density	kg/m^3
μ	liquid viscosity	Ns/m^2
γ	Shear rate at given radial distance	s^{-1}
σ	Surface tension	kg/s^2
ν	Kinematic viscosity	m^2/s
ε	Power dissipation	W/kg
δ	Film thickness	m
U	Average radial velocity of the liquid solution on the disc	m/s
t_{res}	Residence time of the liquid solution on the disc ()	s
Re	Film Reynolds number	-
r	Radial distance from centre at the point of measurement	m
r	radial distance from the centre of the disc	m
Q_L	flow rate on the disc	m^3/sec
Q	volumetric flow rate	m^3/s
D	molecular diffusivity	m^2s^{-1}
γ_{max}	average maximum shear rate	s^{-1}
k_k	Kolmogorov wavenumber (-)	-
t_{res}	mean residence time	s
k_B	Batchelor wavenumber	-
W_e	Weber number	-
V_r	Radial velocity	m/s
Q_c	critical flow rate	Kg/s^2
ρ_L	liquid density	kg/m^3
μ_L	dynamic liquid Viscosity	Pa.s
ω	angular velocity of the disc	s^{-1}
C_{B0}	Initial concentration of B	M
L_c	Integral scale for concentration fluctuations	-
N_P	Power number	-
k_{OC}	Characteristic wave number of large eddies	-
t_D	Mesomixing time based on the turbulent diffusion/dispersion	s
t_{DS}	Micromixing time due to diffusion and shear	s
t_E	Micromixing time by engulfment	s
t_R	Reaction time	s
t_{cr}	Mean circulation time	s
t_m	Macromixing time	s
t_s	Mesomixing time constant by eddy disintegration	
$\bar{\varepsilon}$	Average power dissipation	W/kg
ε_{av}	Mean rate of energy dissipation	W/kg
d	Impeller diameter	m

D	Diffusion coefficient	m^2/s
D	Impeller diameter	m
G (k)	Spectral density of concentration fluctuation	-
k	Wave number	-
k	Reaction rate constant	$m^3/mol\ .s$
N	Stirring speed	s^{-1}
Ø	Relative power dissipation	-
P	Power consumption of the stirrer	W
Po	Power number	-
T	Tank diameter	m
t_r	Reaction time	s
V	Liquid volume	L
V	Liquid volume in the reactor,	l
Xs	Segregation index	-
ε	Local Power dissipation	W/kg
ν	Kinematic viscosity	m^2/s
Q	Impeller pumping rate,	m^3/s
Sc	Schmidt number, $Sc = (\nu/D)$	-
V	Liquid volume,	m^3
n	Global kinetic order of the reaction	-
α,	Micromixedness ratio	-
R	Total flowrate ratio	-
RTD	Residence time Distribution	-
σ_θ^2	Normalized variance of residence time distribution	-
σ^2	Variance of residence time distribution	-
t_m	Experimental mean residence time	s
D	Longitudinal or axial dispersion coefficient	m^2/s
L	Length of system	m
U	Average fluid velocity	m/s
$\left(\frac{D}{UL}\right)$	Dispersion number	-
NCR	Narrow channel reactors	-
Pe	Peclet number	-
SBR	Semi-batch reactor	-
SDR	Spinning disc reactor	-
λ	Wavelength	nm
D_λ	absorbance	-
ε_λ	Molar extinction coefficient	(m^2/mol)
l	Optical path length	m
δ_0	Striation thickness	m
$\dot{\gamma}$	Shear rate	s^{-1}
$[H^+]$	Acid ion concentration	M
t_{res}	Reactants residence time in the channel	s
L	length of the channel	m
U	Mean velocity of the flow	m/s
d_i	Internal diameter of narrow channel reactor	m
U	Mean velocity of the flow	m/s
η	Energetic efficiency of mixing	-
Pe	Peclet number = $\frac{UL}{di} = R_e Sc$	-

Re	Reynolds number (-)	
Sc	Schmidt number	-
ε	Power input (power dissipation)	W/kg
ν	Kinematic viscosity	m/s^2

1. Introduction

1.1 Process Intensification

The term process intensification (PI) has been used to describe the strategy of making dramatic reductions in the plant volume in order to meet a given production objective. The concept was developed by Professor Colin Ramshaw when he was leading a research programme concerning the Process intensification at Imperial Chemical Industries (ICI) during the early 1980's. The primary goal was to reduce the capital cost of a production system without affecting their production rate. While cost reduction was the original target for PI, it quickly became apparent that there were other important benefits, particularly in respect to improved energy efficiency and intrinsic safety, reduced environmental impact and energy consumption(Stankiewicz and Moulijn, 2000a) (Stankiewicz and Moulijn, 2000b; Ramshaw, 2003). Process intensification is one of the new concepts that have recently been added to the field of chemical engineering. As mentioned above, the first target for process intensification was capital cost reduction. This could be achieved by minimising pipe works; civil engineering structures and instrumentation by influencing the way plant is organised. To be fully effective, process intensification must be applied across the whole plant range. The decrease in process equipment size will correspondingly result in increase in the heat and mass transfer rates thereby minimizing the undesirable by-products (Stankiewicz and Moulijn, 2004). The second target for process intensification is the improvement of intrinsic safety. If the volume of the process equipments (inventory) is reduced the hazard is correspondingly reduced. Process intensification is one of the important tools to achieve the sustainability in the chemical industry and could be achieved by many routes as summarised in (Akay et al., 1997) including the use of centrifugal forces, flow field/fluid microstructure interactions, periodic flow, high/ultra-high pressure, electric field, and diffusion/conduction path reduction. The main features of process intensification can be summed as follows: smaller, safer and cheaper processes compared with the current processes. In literature review Chapter, the process intensification advantages, barriers, methods and equipments will be discussed in details.

1.2 Spinning Disc Reactor

The spinning disc reactor **(**SDR) technology offers the possibility of a step change in manufacturing operations, particularly with respect to the ability to cope with very fast chemical reactions such as combustion, polymerization, crystallization and competing fast chemical reactions. The SDR can be horizontally or vertically mounted on an axle. Liquid is fed near or at the centre and flows across the disc surface under the influence of the centrifugal force. The centrifugal force which stretches and contorts the film allows for high rates of heat/mass transfer properties. This type of reactor was successfully used at Newcastle University for industrial applications. Two distinguished examples of these applications are: polystyrene production (Boodhoo, 1999) and precipitation of barium sulphate from aqueous solutions (Cafiero et al., 2002). Results of these two applications showed promising results for the SDR when compared with the conventional batch reactor.

As stated previously, the relevant area to this research is the spinning disc reactor technology which is an example of an intensified reactor. This technology presents important opportunities due to the following attributes (Ramshaw, 2003) :

- High level of heat and mass transfer rates in solid/liquid, liquid/liquid and liquid/vapour systems and has ability to cope with very fast exothermic reactions (corresponding to heat fluxes of up to 100 kW/m^2).
- Ideal for micromixing processes (mixing in molecular level) in the liquid film.
- High selectivity in system which include parallel reactions and production of several products at the same time.
- Low inventory/intrinsic safety (liquid film thickness is 50 – 200 μm).
- Controllable and short time of reacting with fluid. Liquid residence times on the SDR disc are in the range of 1- 5 seconds compared with a few hours in a stirred tank reactor. Therefore, reactions with mixing times in the 0.1-1 s range most likely to be completed on the disc surface.
- Easy operating (start up and showdown), repairing and cleaning.
- Resistance to fouling or plugging technical problems during the ruining of the reactor.
- Close control (due to short residence times).

- Possibility to introduce different rotation surface (smooth, grooved, meshed).
- High shear rate crated between the disc surface and the liquid film flowing on the disc. Consequently, the micromixing for the reactants will be intensified than in the conventional reactors, i.e. stirred tank reactor even for high viscous liquids.

From the above mentioned attributes, it can be concluded that the SDR is a reactor that can be considered as being opposite to the traditional reactors in carrying out some defined reactions or processes.

1.3 Mixing and its effects on reactions

Mixing is used to reduce the degree of non-uniformity or gradient of a property in a system. The non-uniformity could be temperature, viscosity or concentration (Paul et al., 2004). Mixing can achieve a desired degree of homogeneity to the molecular scale, in addition to promoting both heat and mass transfer when a system is undergoing a chemical reaction. Poor mixing usually results from a combination of high viscosity and low diffusivity, typically found in polymerisations (Nauman and Buffham, 2003) . The quality of mixing of materials greatly determines the success and efficiency of many industrial processes, especially where product quality is concerned. Mixing plays an important role in many industries such as automotive finishes and paints, biotechnology, cosmetics and consumer products, drinking and waste water treatment, fine chemicals and pharmaceuticals, food, petrochemicals, polymer processing, (Paul et al., 2004) where chemical reactions such as combustion, biological growth, neutralization, precipitation and continuous polymerization take place. The quality of the output of these processes is highly depended on the mixing conditions.

It is well known that problems in controlling the formation of by-products often result from an ineffective mixing process. The subsequent important economic and environmental impacts of this issue cannot be underestimated.

Chemical reactions are not affected by the mixing process if the reagents are completely mixed down to the molecular scale (micromixing) before significant reaction takes place. This means that the time scale of the mixing process involved is less than the time constant of the reactions. On the other hand, if the time constants of the reactions are relatively close to or smaller than the time scale of the mixing process, the product

distribution and the quality of the fast multiple reactions can be affected (Bourne, 1993). The relative values of reaction time, t_r , and the mixing time, t_m, explain the competition between reaction and mixing, which direct to different product distributions and can be summarized as shown below (Paul et al., 2004; Baldyga and Bourne, 1999):

I. $t_m << t_r$: *slow regime*, homogenization is fast and precedes reaction. The reaction rate controls the process and the product distribution is chemically controlled.

II. $t_m \approx t_r$: *fast regime* , the reaction rate is influenced by both physical and chemical factors. In this regime, both the mixing and kinetics determine the product distribution.

III. $t_m >> t_r$: *instantaneous regime*, reaction is extremely fast, the reaction rate is limited by the rate of mixing by diffusion and the product distribution is controlled by the degree of mixing

1.4 Motivation and Background

It has long been recognised that the intense mixing characteristics and particularly the micromixing (i.e. mixing at the molecular scale) characteristics of the thin films in the SDR, play an important role in the improvements observed for the reactions carried out in the novel reactor. However, to date, there has been no systematic study undertaken to characterise the micromixing in the thin films. Also, there is no comprehensive study reported to date examining the flow behaviour of the SDR film i.e whether the film exhibits more plug flow or backmixed characteristics and, more specifically, assessing the hydrodynamic conditions which cause the flow to deviate from plug flow regime. Therefore, the purpose of this work is to fill this gap by studying (1) the fundamental science underlying the micromixing characteristics taking place within the thin films in the SDR and (2) the Residence Time Distribution of the film under a range of conditions.

1.5 Thesis Layout

This thesis consists of seven Chapters. The introduction, motivation and background of the research are discussed in this Chapter (Chapter 1). A critical literature review is presented in Chapter 2 where the general aspects of the Process Intensification are covered followed by a review of the spinning disc reactor (SDR) technology, mixing principles and its mechanisms, the time constants of single-phase mixing, the chemical methods for mixing quality characterization, the Iodide-Iodates technique and its aspects were summarized. In addition, Chapter 2 concludes with the Residence time Distribution and its relevant aspects related to this research. Chapter 3 describes the aims and objectives of the current research whilst Chapter 4 describes the experimental facilities and procedures that were followed in carrying out the research. Chapter 5 presents the results and discussion for the micromixing experiments that were conducted in four different reactors followed by the comparison of the reactors' performance based on their micromixing efficiency. Chapter 6 presents the Residence Time Distribution experimental results for the 30cm SDR and the discussion on the findings. Chapter 7 presents the conclusions that were drawn from the research for both the micromixing and Residence Time Distribution experiments. The Recommendations for future work is also presented in this Chapter.

2. Literature Review

2.1 Introduction

The aim of this Chapter is to, firstly, introduce the reader to Process Intensification and its benefits to the chemical industry. The principles of operation of the Spinning Disc Reactor (SDR) technology are then described in detail, followed by a review of previous work on heat/mass transfer and chemical reactions previously undertaken in the SDR.

Secondly, the basic principles of mixing, the mixing mechanisms, time constants of single-phase mixing are reviewed. The physical and chemical methods for characterisation of the quality of mixing as well as the test reactions that have been developed over the years for characterising the intensity of micromixing in particular are discussed in detail.

Finally, this Chapter concludes with a review of the Residence Time Distribution (RTD) concept, RTD measurement techniques and last but not least, the dispersion models available for quantitative estimation of dispersion in a given reactor type.

2.2 Process Intensification and its benefits

As stated earlier in Chapter one, the term process intensification (PI) has been used to describe the strategy of making dramatic reductions in the plant volume i.e. remarkable reductions in physical size of process equipment in the chemical plants in order to meet a given production objective which means no impacting on production capacity or quality of the products. Figure 2.1 shows the main benefits that process intensification could offer to the chemical industry (Stankiewicz and Moulijn, 2004; Ramshaw, 1999). These benefits may be categorized into four areas as discussed below:

- **Cost:** This is one of the main benefits that process intensification offers. It is highly critical because reduction in cost directly affects the number of elements on a plant. An example of this is the reduction in the cost of land where the intensified unit would be located. The benefit of this could be achieved from having much higher production capacity and/or number of products per unit of manufacturing area. Another benefit is the reduction in the investment costs which may also be reduced as a result of cheaper, more compact equipment with reduced piping etc., fewer raw materials being needed due to higher yields/selectivities. The cost of utilities (electricity, steam, cooling water etc.)

may also be reduced due to higher energy efficiency. Another important aspect of the cost reduction is that there would be less waste generation from intensified plants so that the cost of waste processing and disposal may be significantly cut.

- **Safety:** Since the size of process intensification unit is small, the plant volume is reduced. Hence, the toxic and flammable inventories of intensified plant are correspondingly reduced thereby making a major contribution to higher levels of intrinsic safety.

- **Time to market**: An expected outcome of process intensification is that reactor residence times may be reduced significantly, probably from hours to seconds which means it that the products can be produced rapidly. This implies that the production rate would be increased to meet the rapidly changing demands in the markets.

- **Company image**: Nowadays the chemical companies do recognise the importance of having good image because it plays a very significant role in the success of their business, especially where public perception is concerned. Process intensification provides safer and environmentally friendly processing. This is considered the key issue to the improved corporate integrity of the chemical plants.

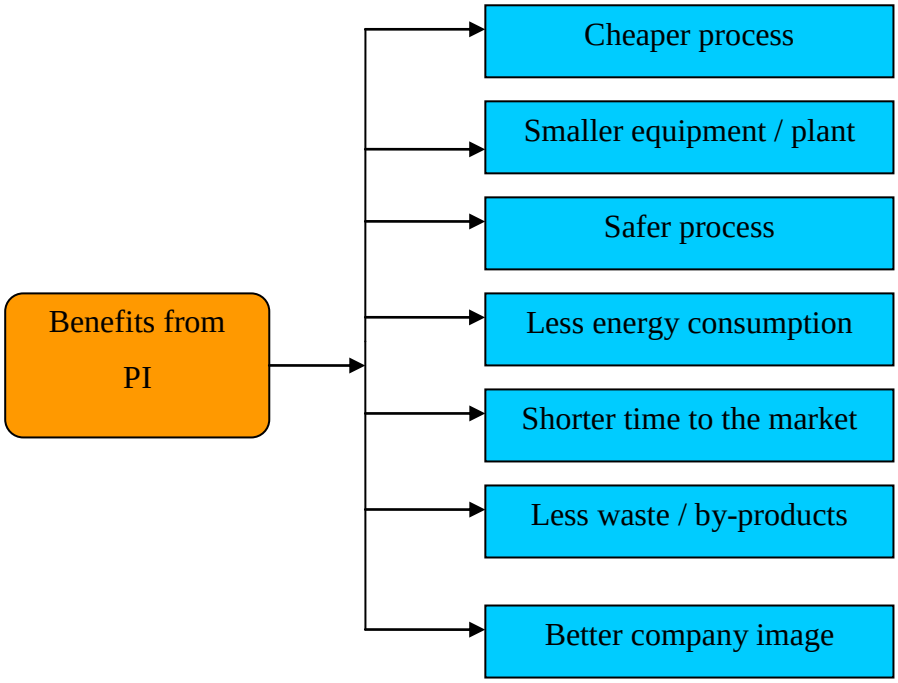

Figure 2.1: Main benefits of the process intensification (Stankiewicz and Moulijn, 2004)

2.2.1 Barriers of Process Intensification

Ramshaw (2003) summarises the barriers that may affect the implementation of the process intensification in the chemical industry in seven points as follows:

- Step changes in equipment design and operation is a required condition for implementing the PI in the chemical industry. This creates problems when there is already an established process investment, as it will be exceedingly difficult to justify a ‘’scrap and start again ‘’ policy.

- Very wide range of technology must be developed, covering all the main unit operations, for PI to be fully effective.

- Most plant managers ‘’rush to be second’’ and require full scale evidence of successful operation before they are prepared to take any risk.

- Design codes are needed for new equipment.

- There is need to distinguish between slow (> 5 sec) and fast (< 5 sec) reactions. Use different PI technology for each.

- Culture shock in batch – dominated industries.
- Fouling may be a problem.

2.2.2 Process Intensification Toolbox

Stankiewicz and Moulijn (2004) divided the PI toolbox into two groups, namely the process intensification equipment (*PI hardware*) and the process intensification method (*PI software*). Figure 2.2 shows the toolbox for the process intensification according to Stankiewicz's vision.

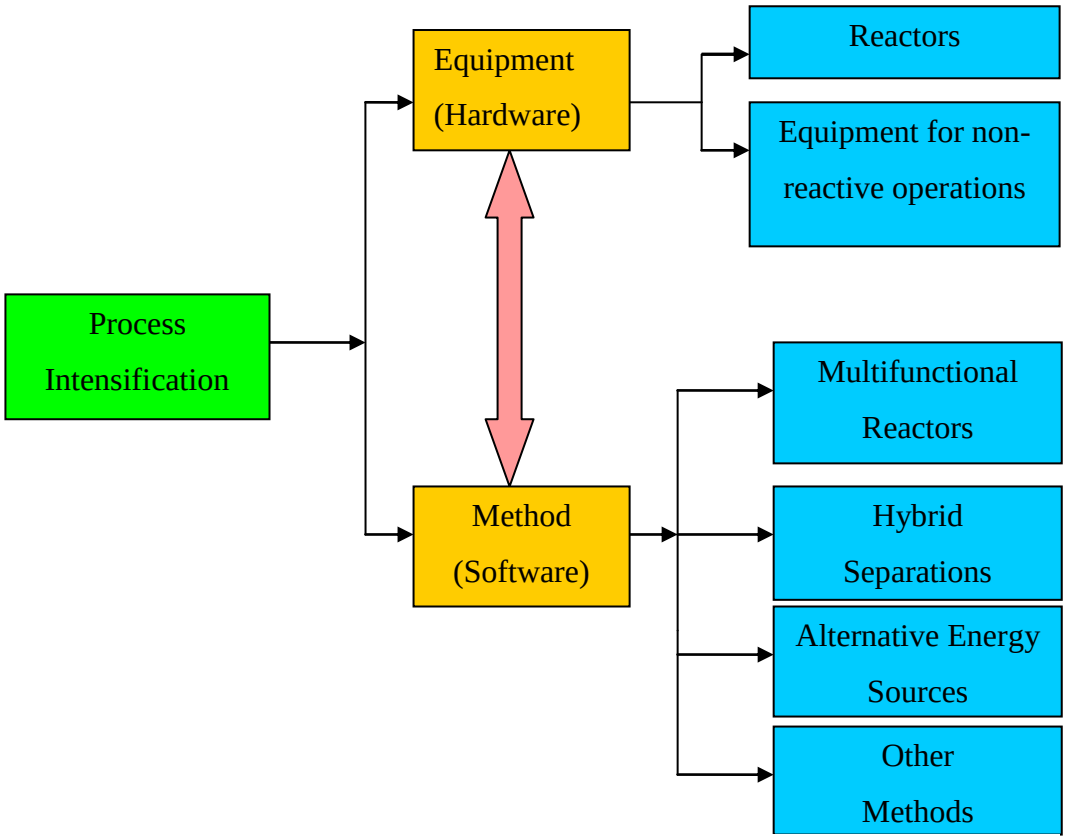

Figure 2.2: Process intensification toolbox (Stankiewicz and Moulijn, 2004)

2.2.3 Process intensifying methods

Process intensifying methods were classified by Stankiewicz and Moulijn (Stankiewicz and Moulijn, 2004; 2000a) as multifunctional reactors, hybrid separations, alternative energy sources and other methods. These four main groups are discussed below in details.

- **Multifunctional reactors**: This reactor combines at least two functions that conventionally would be performed in separate equipment in order to enhance chemical conversion and achieve a higher degree of integration. An example being the reverse – flow reactor which integrates reaction and heat transfer by periodic flow reversal.

- **Hybrid separations**: in hybrid separations, the integration of membranes with another separation technique is involved. An example is in membrane absorption where membrane plays a role of permeable barriers between the gas and liquid phase. Compact equipment and great mass transfer area can be achieved by using hollow-fiber membrane modules.

- **Alternative energy sources**: This type of source concerns the unconventional types of energy instead of the traditional sources. These sources include the use of centrifugal fields, ultrasound, solar energy, microwaves, electric fields, microwaves, and plasma technology.

- **Other methods**: This group puts together all the other methods not involved in the previous groups. Supercritical fluids, dynamic/periodic reactor operation are example of these methods.

2.2.4 Equipment for Process Intensification

Process intensification equipment has been classified by Stankiewicz and Moulijn (2004) according to their application. The first group consists of equipment used for carrying out chemical reactions and the other one has put together equipment for unit operations where chemical reactions are not involved. Some examples of intensification equipment are discussed in details below.

2.2.4.1 Equipment for carrying out chemical reactions

2.2.4.1.1 Spinning disc reactor

The spinning disk reactor (SDR) or more generally a rotating surface of revolution reactor (Stankiewicz and Moulijn, 2004) is designed to create highly sheared thin liquid films which have excellent heat/mass transfer properties. A schematic diagram of

spinning disk reactor is shown in Figure 2.3.

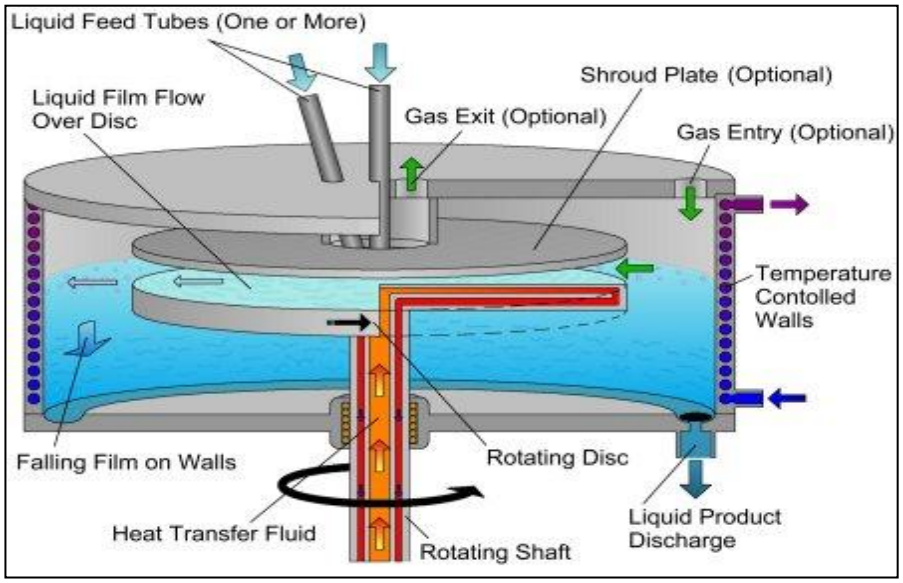

Figure 2.3: Schematic diagram of spinning disk reactor. adopted from (Ramshaw, 2003)

In SDR liquid is supplied to the disc at or near its centre and is flung outwards towards the disc periphery by the centrifugal acceleration. Depending upon the liquid viscosity and the disc speed, the film can be as thin as $25\ \mu m$ or even less (Boodhoo et al., 2004). This short diffusion and conduction path length is the basis for the very high mass and heat transfer rates respectively which are generated between the gas phase and the liquid, and the liquid and the disc. As can be seen from the accompanying photo (Figure 2.4) the liquid film is not smooth, except for a very limited set of conditions. It appears that any liquid film moving over a solid surface is intrinsically unsTable so that however uniform it may be initially, any tiny perturbations are ultimately amplified to visible waves. As the film proceeds, the initial spiral wave structure breaks down until the waves pattern becomes utterly chaotic (Stankiewicz and Moulijn, 2004). The liquid viscosity is responsible for exerting a damping influence and it can be shown that the advent of ripples is delayed as the viscosity increases. This means that the simple calculations of the film thickness and velocity, based upon Nusselt's approach, are more realistic for viscous liquids.

Figure 2.4: Thin film flows on smooth disc (adopted from (Vicevic, 2004))

Brauner and Maron (1982) studied the local instantaneous film thickness and mass transfer rate for a water film moving down a smooth inclined surface. They showed that there was a direct relationship between the intensity of the wavy films and the fluctuations in heat/mass transfer observed, as the larger waves could penetrate deeper into the liquid film. The passage of a ripple corresponded remarkably well with a marked instantaneous rise in the local heat and mass transfer coefficient.. Thus ripples are "a good thing" and are to be encouraged.

The use of rotating surface has contributed to the development of the concept of thin film, as has been reported recently. This surface generates high centrifugal force which provides the driving force for the flow ($F=rw^2$). The acceleration on the disc surface can be 100-1000 times the acceleration due to gravity. The use of the spinning disc for mass transfer operations can be traced to the NASA space research programme (Rahman and Faghri, 1993). In space conventional mass transfer, contacting devices are unsuiTable because the driving force of a liquid flowing under gravitational force cannot be performed in zero gravity conditions. NASA carried out a research to establish the use of such a device to generate centrifugal forces upon a liquid such that it generated a thin film for a mass transfer operation to occur. There is no doubt that the reason for the relatively poor performance of viscous systems is that ripples are effectively damped. This issue raises the prospect of modifying the disc surface in order to disturb the flow and enhance the disc performance. Intensive work on this subject has already been done with grooved disc (including some done by this author) and the results are encouraging (Boodhoo and Jachuck, 2000a). More attention will be paid later to further developments and application of the SDR technology in this Chapter.

A new configuration spinning disc reactor (Figure 2.5) , i.e. Multiple Rotor – stator disc reactor has been modified at the Eindhoven University of Technology in the Netherlands (Meeuwse, 2011). One stage in this modified SDR consists of a rotator disc in a cylindrical housing. The distance between the rotor and wall (the stator) is order of 1mm. The Liquid is the first stream which is fed to the reactor from the top inlet, near the rotating axis. The gas is the second stream where injected through an orifice in the bottom stator; a large velocity gradient, and therefore a large shear force, is created due to the high rotational disc speed. Due to the high rotational disc speed, a large velocity gradient, and consequently a large shear force is created. This large shear force breaks up gas bubbles, in case of a gas-liquid systems, or liquid drops, in case of liquid-liquid systems, this consequential in a large two phase interfacial area. The high energy input per unit volume results a high degree of turbulence. Consequently, the surface renewal rate is increases; this gives a high mass transfer coefficient. The combination of the large interfacial area and the high mass transfer coefficient leads to high volumetric mass transfer rates.

Meeuwse et al.,(2010b; 2010a) carried out an experimental work considering the gas-liquid mass transfer and Liquid – solid mass transfer in the rotor-stator spinning disc reactor. The results of these investigations prove that the rotor-stator spinning disc reactor shows high rates of mass transfer for both cases of gas-liquid / liquid- solid mass transfer in comparison to the conventional multiphase reactors. In the case of gas-liquid mass transfer, the volumetric gas– liquid mass transfer coefficient per unit volume of gas was much higher than for conventional reactors, 20.5 $m_L^3 m_G^{-3} s^{-1}$ instead of 0.5 $m_L^3 m_G^{-3} s^{-1}$ for bubble columns. In the case of liquid- solid mass transfer, the values of the volumetric liquid-solid mass transfer coefficient vary from 0.02 $m_L^3 m_R^{-3} s^{-1}$ at 1560 rpm to 0.22 $m_L^3 m_R^{-3} s^{-1}$ at 9420 rpm, which is higher than in conventional reactors such as a packed bed. The results show that the rotor stator spinning disc contactor is very appropriate for gas-liquid or liquid-solid processes.

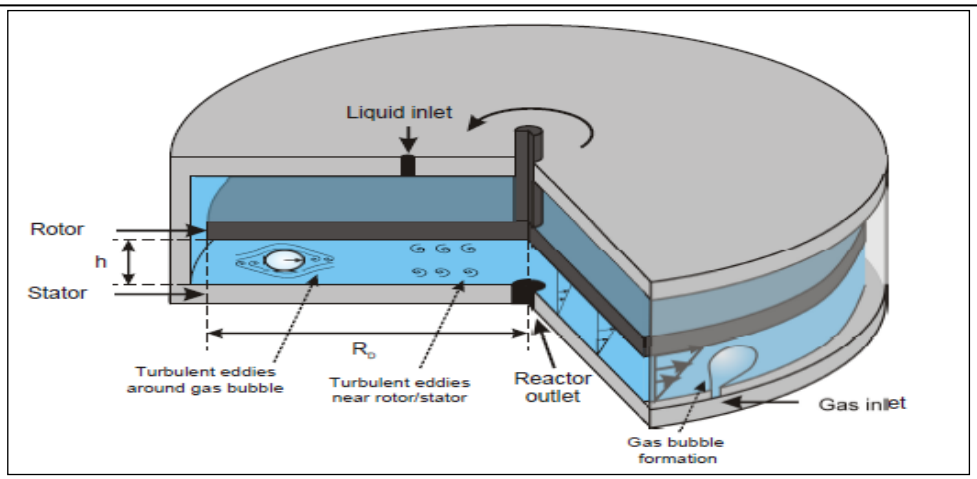

Figure 2.5: Schematic diagram of the rotor-stator spinning disc reactor with a gas inlet in the bottom stator (adopted from (Meeuwse, 2011))

2.2.4.1.2 Rotating packed bed reactors (RPBs)

This type of reactors (HIGEE) uses rotational speeds which are typically in the range of 500 rpm to 3000 rpm and high centrifugal accelerations that are in the range of 100 (g) to 500 (g). The Rotating packed bed reactors (RPBs) utilise this high centrifugal accelerations to intensify the mass transfer (Hassan-Beck, 1997; Bums, 1996; Ramshaw and Mallinson, 1981). Some key advantages of the RPBs are as follows:

1. It is less sensitive to external movement or vibration which makes it easier to operate offshore.
2. It has a reduced size of equipment due to small heat transfer unit (HTU) and high throughput leading to lower inventories and improved plant safety.
3. It has lower and more controllable residence times which allow RPB's to work as precision fast reactors.
4. It is capable of handling highly viscous liquids due to high driving acceleration (Burns et al., 2000).

The RPB's were used in many chemical industry's applications such as absorption, extraction and distillation as well as the counter-current gas/liquid mass transfer (Burns and Ramshaw, 1996). Figure 2.6 shows an RPB that was used in one of the studies carried at Newcastle University.

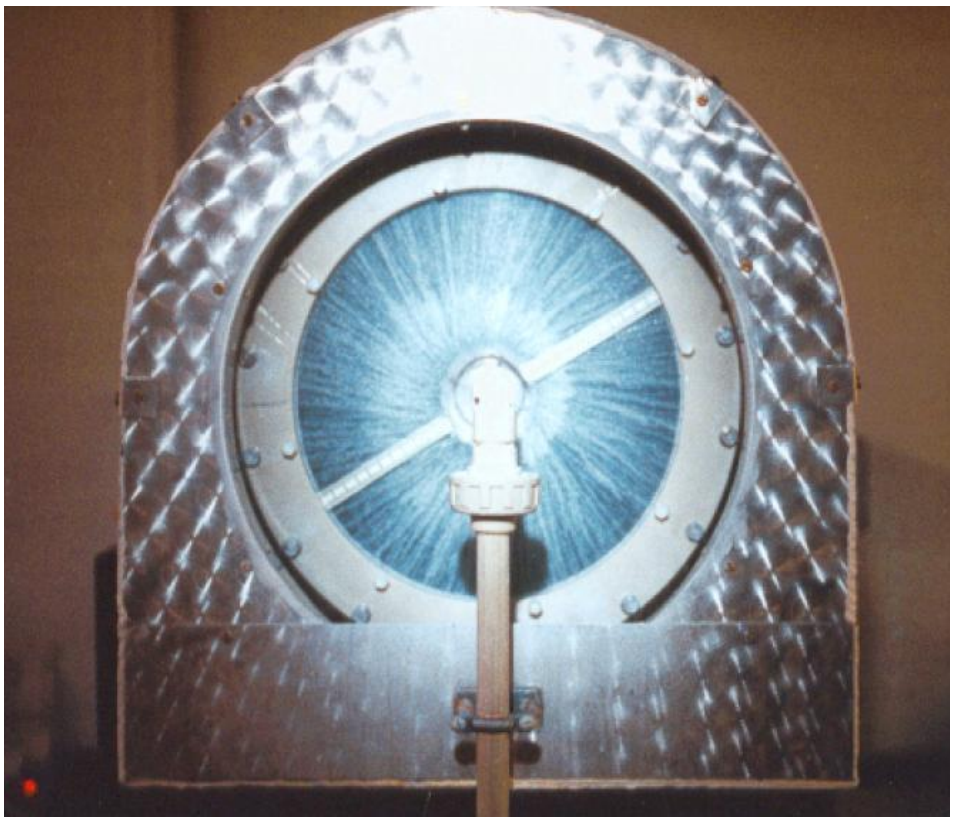

Figure 2.6: Rotating Packed Bed (adopted from (Burns, 1996))

2.2.4.1.3 Oscillatory baffled reactors (OBR's)

The Oscillatory baffled reactor is one of the new designs of intensified reactors. The OBR is made of baffled tube. The oscillatory flow mixing is achieved in the oscillatory baffled reactor at a typical frequency of 0.5 to 15 Hz at the amplitude of typically 1 to 100 mm (Harvey et al., 2001). The oscillating fluid motion combined with the baffles to form vortices. Consequently, the oscillating fluid motion provides excellent local and global mixing. This type of reactors has many advantages such as high heat/mass transfer, plug flow behaviour and it is easy to operate. The production of biodiesel was one of the OBR's successful applications. It has been shown that the SBR can be used for the production of biodiesel with accepTable conversions in times lower than in batch reactor (Harvey et al., 2003). Figure 2.7 illustrate the OSB arrangement.

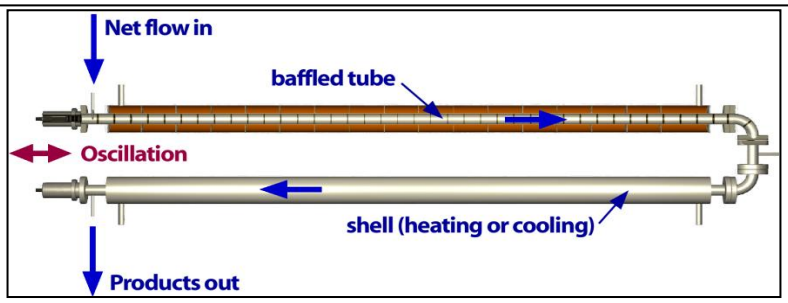

Figure 2.7: Oscillatory baffled reactor (http://pig.ncl.ac.uk/obrs.htm) accessed on 30/05/2011

2.2.4.1.4 Microreactors / Narrow Channel Reactors

The Microreactors (Figure 2.8) and Narrow Channel Reactors (Figure 2.9) are in the scale space of micrometers and millimetres respectively. The type of flow in these reactors is genially to be laminar with diffusion being the main controlling factor in heat and mass transfer. The advantage of using Microreactors/Narrow Channel Reactors in the high heat/mass transfer rates and effectual mixing due to the short diffusion path lengths is determined by the reactor diameter. Consequently, the molecular diffusion for the reactants could be improved. In addition, other advantages of using Microreactors/Narrow Channel Reactors is that their much higher surface area to volume ratio, when compared with stirred tank reactor geometries, provides a very high heat transfer per unit volume of the reactor. The flow rate in these channels is usually low. Scaling up of this kind of reactors requires the use of many channels in parallel and each channel can be considered as individual reactor which has identical conditions as all the other channels. The two sections below give more details on Microreactors / Narrow Channel Reactors technology.

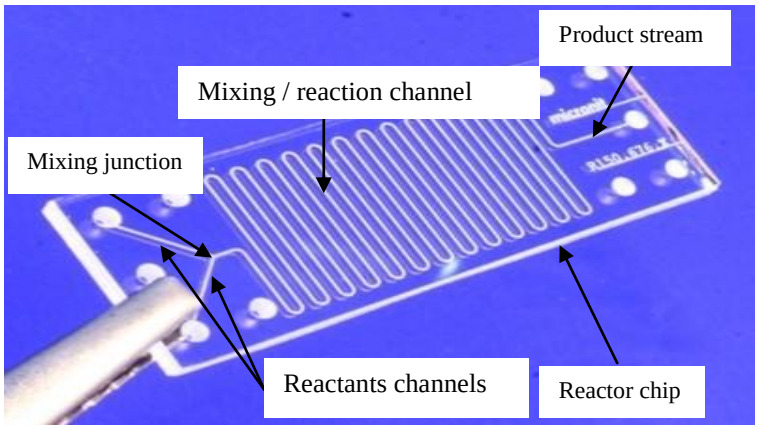

Figure 2.8: Glass Microreactor, the channels of the chip are 150 µm wide and 150 µm deep (http://en.wikipedia.org/wiki/Microreactor) accessed on 31/05/2011

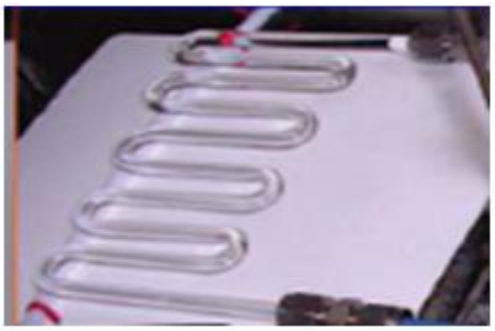

Figure 2.9: Glass narrow channel reactor made of made of borosilicate with internal diameter of 1.5 mm (Jachuck and Nekkanti, 2008)

2.2.4.1.5 Microreactors

Advances in micromachining have led to the development of microreactors that can be used for a wide range of continuous processing applications. The manufacturing methods stem from established microelectronics techniques(Hessel and Lowe, 2003a). Microreactors for analytical purposes and synthesis applications have been designed. The channels typically have diameters of less than a millimetre. They are machined in different materials including polymers, glass and metals.

Microreactor processing is used to create products using continuous operation, with microchannels of diameters less than 1mm. Microreactors have high surface to volume ratios, in the order of 10,000 – 50,000 m^2/m^3 compared with 100 m^2/m^3 in conventional reactors. High surface to volume ratios, inherent in smaller volumes, are associated with the potential for high heat and mass transfer rates, which reduce temperature and concentration gradients (McCarthy et al., 2007). Microchannels can also be machined onto both sides of a plate which partially overlap, to further increase the contact area for heat transfer(Horstwood, 2009). The high transfer rates give the potential for higher yields and better selectivity than in conventional reactors as more aggressive operating conditions can be achieved, due to the potential for homogeneity to be achieved within the reactor volume. Within the majority of microreactors, low values for Reynolds number are observed and the flow regime is laminar and turbulence is hard to induce (Kockmann et al., 2006).

The characteristics of fluid flow within narrow channels differ to the fluid flow in microchannels. Within a microchannel, the surface tension between the fluid and the pipe wall is more significant, as is the relative magnitude of the friction at the surface wall compared to the diameter of the channel (Hessel and Lowe, 2003a) .

Microreactors also allow for improved safety, this is associated with a reduction in the waste produced and the employment of distributed processing of hazardous and toxic chemicals. Due to the potential for small reaction channels, explosive mixtures such as hydrogen and oxygen can be mixed relatively safely (Hessel and Lowe, 2003a) . The selectivity and yield of the microreactor can be increased in comparison to conventional reactors due to the tight control of residence time(Yoshida et al., 2005). This increase in selectivity can lead to cost savings; costs savings can also be associated with a reduction in utilities, a reduction in size and the significantly smaller residence times required.

Micromixers can be generally categorised into two groups: active and passive. Active micromixers require an external disturbance and power input and are considered more complicated than passive micromixers (Hessel et al., 2005; Nguyen and Wu, 2005). Active micromixers can be both expensive and challenging to integrate into a micro-fluidic system in comparison to passive micromixers which are considered robust and sTable in operation.

Microreactors allow for simpler optimisation, rapid design implementation and easier scale up than conventional reactors, as scale up can be achieved by simply numbering up. Microreactors can reduce the time to the start up of the plant; as in many circumstances the laboratory scale reactor may be the same size as the plant scale. Due to the micro dimensions of the channels, diffusion path lengths are significantly shorter than in conventional reactor systems leading to decreased diffusion time and hence faster mixing of the reactants, as in laminar flow diffusion is the limiting mixing mechanism.

A transparent microreactor may be beneficial for photochemical reactions where yields are low; an increase in yield could be achieved when a reactor is in close proximity to the radiation source(Hessel and Lowe, 2003b).

Studies on mixing performance in microreactors have shown that the performance is affected by increasing the mean residence time (Adeosun and Lawal, 2005), which for a given channel diameter and fluid flowrate may be achieved by increasing the channel length (Schneider et al., 2004).

Two barriers have been identified to the use of microreactors in industry. The first barrier is the competition between a microreactor for existing production processes and a depreciated plant, which affects the overall economic attractiveness. Second barrier is the issue of fouling, for channels with small dimensions problems with fouling can occur.

Axiva, Frankfurt (Germany) have found that less fouling occurs for the polymerisation of acrylates when using micromixers. Merck Company, Darmstadt , (Germany) have also found industrial benefits to the use of micromixers: an organometallic reaction led to an increase in yield of 25% in comparison to batch processing (Hessel and Lowe, 2003a). Micro packed bed reactors have also been developed, in the case of hydrogenation of conjugated olefins; yields of 100% were achieved.

2.2.4.1.6 Narrow Channel Reactors

As mentioned earlier in this Chapter, narrow channel reactors have larger dimensions than microreactors (millimetre scale rather than micrometer scale); with those used as part of this research having channel diameters of 1mm. A narrow channel reactor can be considered to be made up of two sections. The first section usually consists of a T or Y junction, which serves as a point of contact (mixing junction) for the fluids where vortices are induced. The second section can consist of a straight channel or a meandering structure. This allows further inline mixing and mixing enhancement, it also provides the residence time required for reactions to take place (Kockmann et al., 2006). Due to the small diameters in narrow channel reactors, the flow regime is usually laminar and the main mixing mechanisms present are diffusion and chaotic advection. Although a laminar flow regime is usually observed in narrow channel reactors, there can be considered to be three different laminar flow regimes, which affect the degree of mixing achieved (Engler et al., 2004) :

I. *Stratified Laminar:* This regime is observed at low flowrates and Reynolds numbers. The mixing occurs by diffusion only. The streamlines are not bent and follow the channel walls.

II. *Vortex Flow:* The mixing mechanism observed is diffusion at the border faces of the streams as in stratified laminar flow, however there are vortices beginning to form. The swirling vortices begin to mix the fluid layers from the middle of the channel to the walls of the channel, whilst axial symmetry is retained, leading to an improvement of mixing.

III. *Engulfment Flow*: This laminar flow regime is observed with higher flowrates and Reynolds numbers. The streamlines interweave and reach the opposite channel wall, leading to the termination of symmetry, and resulting in significantly improved mixing.

2.2.4.1.7 Heat exchange (HEX) reactors (HEX-Reactors)

The heat exchange (HEX) reactor is another type of intensified narrow channel reactors. The main characteristic of the HEX reactors is that it has large heat transfer area per unit volume. This leads to reduction in space, weight and cost when compared with the conventional heat exchangers. There are many types of HEX reactors that derive from the existing compact heat exchanger such as the printed circuit (PRC) reactor (which has the benefits of using fine channels in view of their short conduction path lengths) polymer film heat exchanger and plate-fin heat exchanger (Anxionnaz et al., 2008). The HEX-reactors can be used in many industries including nitration, polymerisations, hydrogenations, halogenations and aminations (Reay et al., 2008) . Figure 2.9 shows an example of compact plate heat exchanger.

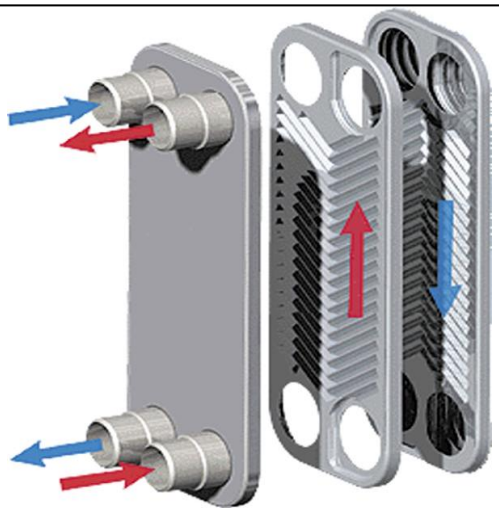

Figure 2.10: Schematic view of compact plate heat exchanger (Anxionnaz et al., 2008)

2.2.4.2 Equipment for operations not involving chemical reactions.

The Rotating devices applied in physical operations (i.e. those that do not involve chemical reactions apart from those mentioned before such as rotating packed beds) include centrifugal adsorber, which is a new continuous device that has good characteristics for either ion-exchange or adsorption processes or both of them. The device is an extremely compact and effective separation equipment in which centrifugal field establishes counter-current flow between liquid phase and very small particles of adsorbent. Examples of intensified equipment that do not involve chemical reaction are: Static mixers, Compact heat exchangers, Micro-channel exchangers, Rotor/stator mixers, Rotation packed beds, Centrifugal adsorbers and Disc bowl centrifuge.

The static mixers (the motional mixers) are equipments used for mixing two fluid materials. The static mixers used to mix the liquid and gas streams with liquids, i.e. Disperse gas into liquid or disperse immiscible liquids. The static mixers consist of mixer elements contained in a cylindrical (tube / pipe) or squared housing. These tubes / pipes are varying from about 6 mm to 6 meters diameter. Static mixer elements consist of a series of baffles made from metal or a variety of plastics it depends of application. The housing of mixer can be also made from metal or plastic. The static mixers are used for a wide range of different applications, for example, wastewater treatment, chemical processing, desalting of crude oil, the polymer production. The static mixers design incorporates a method for delivering two streams of fluids into the static mixer. As the streams move through the mixer, the non-moving elements (baffles) continuously mix

the fluids. A high degree of mixing is dependent on fluid properties, tube / pipe diameter, the number of baffles and their configuration.

The Rotor-stator mixers are single-shaft mixers with an impeller rotating in close proximity to a stationary housing. The Rotor-stator mixers are used to rapidly break separately solid particles in a liquid phase, or to blend a liquid into another. The impeller (rotor) provides high-shear forces to the elements. Rotor-stator mixers have been used effectively in a number of applications, including emulsification and viscous blending (Sparks, 1996). Rotor-stator mixers looks like centrifugal pumps and some designs have significant pumping capacities. The main difference between centrifugal pumps and rotor-stator-mixers is the narrow gap between the rotor and stator, known as the shear gap in the rotor-stator mixer where high shear forces disperse and homogenise any fluid passing through it. In contrast, the impeller in a centrifugal pump rotates with a large clearance from the stationary pump housing.

2.3 Spinning Disc Reactor (SDR) Technology

The Spinning Disc Reactor (SDR) has already been introduced earlier in section 2.4.2.1.1 of this Chapter. As the focus of the present research is on SDRs, it is appropriate to provide a detailed review of the hydrodynamics of thin film flow on a rotating disc, together with an analysis of the power dissipation on the spinning disc, and the previous work on heat/mass transfer and chemical reactions in the SDR.

2.3.1 The Hydrodynamics of a Thin Film Flow on a Rotating Disc

Over the past century there has been much interest in studying the flow of thin liquid films down a vertical or inclined surface under the effects of gravity (Andreev, 1964; Nusselt and Ver.Deut. Ingr. Z., 1916). These early investigations could be credited as being the lead investigations on this subject, which have resulted in present studies of thin films generated by rotating surfaces. These studies found that it was quite clear that these films were characterised by superior rates of heat and mass transfer which were linked to the strong mixing characteristics of the surface waves generated by the gravitational field (Fulford, 1964; Kirkbride, 1934).

2.3.1.1 Flow Models of the Thin Films Flows on the Disc Surface

In order to illustrate the flow of the thin liquid films on smooth horizontal rotating surface, the modified Navier-Stokes equation for conservation of momentum and the equation of continuity for the conservation of mass was used (Boodhoo, 1999) The simplified version of the Navier-Stoke equation can be used to derive the velocity distribution, film thickness and residence time on the surface of rotation. These versions of the equations are related to smooth, fully developed laminar flow which is only obtained for a certain range of operating conditions such as flowrates and disc rotational speeds.

2.3.1.1.1 The Centrifugal Model

This model is based on the assumptions that the liquid on the spinning surface flows radially and the motion is caused by the effect of centrifugal force on the liquid and it is balanced by the viscous drag. The flow on the disc in this type of model is steady and symmetrical around the axis of rotation which does not give any velocity variation in the angular direction. Another important consideration for the model is that the disc and the flow have similar velocity, i.e there is no slip. Other considerations are smaller thickness of the film when compared to the radius, surface tension and fraction with surrounding medium is negligible. Again, the simplified version of the Navier-Stoke equation which is a reduction and subsequent integration of the general Navier-Stoke equation, would give the equation for the radial velocity, film thickness, the shear rate at a given radial distance across the smooth disc surface and residence time on the surface disc for liquid flow between two radial points on the disc. These equations are summarised below (Boodhoo, 1999; Wood and Watts, 1973).

The radial velocity, (V_r), is given by expression:

$$V_r = \frac{\omega^2 r}{\nu}\left(\delta z - \frac{z^2}{2}\right) \tag{2.1}$$

The shear rate at a given radial distance across the smooth disc surface can be calculated as:

$$\gamma = \frac{dV_r}{dz} = \frac{\omega^2 r}{\nu}(\delta - z) \tag{2.2}$$

It can be seen that the shear rate is zero when the Z=δ and the maximum value of the shear rate will be obtained at the fluid/disc interface where Z=0. Then the maximum shear rate at a given radial distance across the smooth disc surface is given by:

$$\gamma_{max} = \frac{\omega^2 r}{v} (\delta) \tag{2.3}$$

The average maximum shear rate across the disc surface can be calculated as:

$$\gamma_{max} = \frac{1}{n} \sum_{i=1}^{n} \gamma_i \tag{2.4}$$

Where n is the number of shear rate measurements. For the 10 and 30 cm SDR, the average maximum shear rate on the disc surface was calculated on the basis of four shear rate values at four radial positions on the disc surface for each set of operating condition of the total flowrate and disc rotational speed.

The film thickness at the specific radial position on the disc surface is given by:

$$\delta = \left(\frac{3Qv}{2\pi\omega^2 r^2} \right)^{\frac{1}{3}} \tag{2.5}$$

Where the angular velocity, ω, is defined in terms of the disc rotational speed, *N*:

$$\omega = \frac{2.\pi.N}{60} \tag{2.6}$$

The average value of the film thickness across the disc surface can be estimated as:

$$\delta_{av} = \frac{1}{n} \sum_{i=1}^{n} \delta_i \tag{2.7}$$

Where n is the number of the film thickness across the disc surface measurements. For the 10 and 30 cm SDR, the average film thickness on the disc surface was calculated on

the basis of four film thickness values at four radial positions on the disc surface for each set of operating condition of the total flowrate and disc rotational speed.

The mean residence time of the fluid on the disc is another important parameter when considering reactions on the SDR. This can be expressed as:

$$t_{res} = \frac{3}{4}\left(\frac{12\pi^2\nu}{\omega^2 Q^2}\right)^{1/3}\left(r_0^{4/3} - r_i^{4/3}\right) \tag{2.8}$$

Where r_i and r_o are radii of the distributor and the disc respectively as illustrated in Figure (2.11) below:

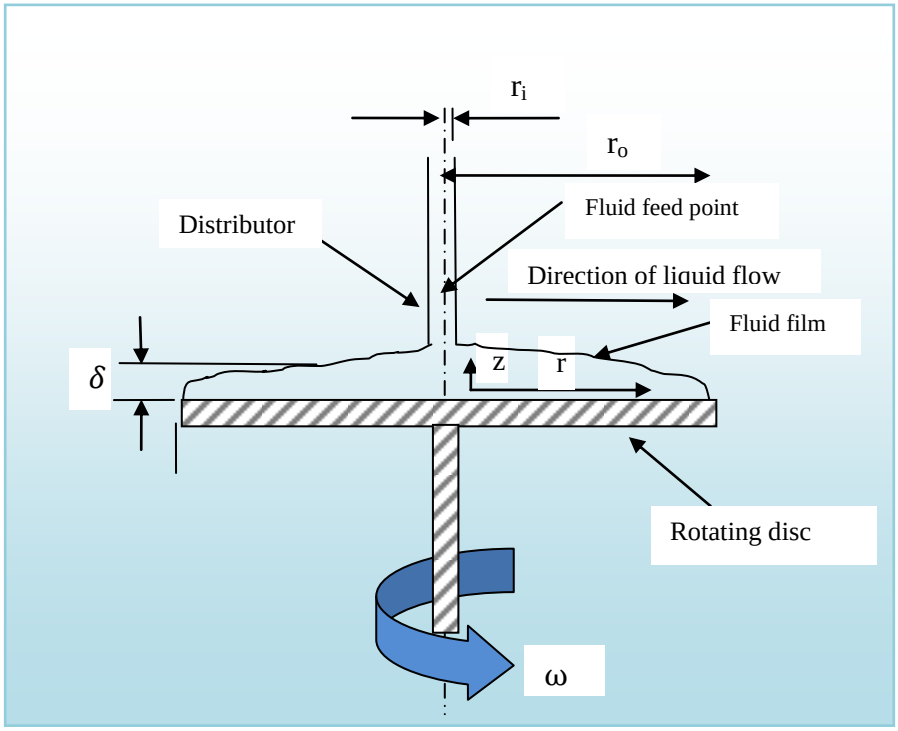

Figure 2.11: Thin film flow on spinning disc surface

2.3.1.1.2 The Coriolis Model

This model was based on the consideration of the Coriolis force that acts in a circumferential direction opposite to the direction of rotation of the disc. The effect of this force causes the liquid film to move with a lower speed than the disc. Emslie et al (1958) have stated that the Coriolis effect can be ignored if the centrifugal force is much greater than the Coriolis force, i.e. $\omega^2 r >> 2\omega V_r$.

2.3.1.1.3 The General Models

Most studies in the recent past have come up with various models that take into account the effect of inertial and Coriolis force on the disc. Venkataramen et al (1966) found that the effects of the inertial and Coriolis forces are only significant at a small distance from the distributor. Hence, if the disc is rather large (condition $\delta << r$ satisfied), the simple centrifugal model is sufficient to describe the flow.

2.3.1.2 Flow regimes and transitions

The type of flow on the surface of the rotating disc under given flow rate and disc rotational speed is one of the main characteristics which must be included in the study of the hydrodynamic of SDR because it directly affects the rate of mixing, mass and heat transfer rates in the fluid as it flows on the disc. The regimes can be predicted on the basis of the Reynolds number criteria that have been defined for thin film flows on the disc.

2.3.1.2.1 Reynolds Number Criteria

Reynolds number (Re) is the ratio of the inertial forces to the viscous forces of the fluid. As the velocity varies with the radial distance across disc surface (r), the Reynolds number becomes radius-dependent instead of rotational rate-dependent. The Reynolds number of the thin film flows on the smooth rotating disc can be evaluated as shown below (Vicevic, 2004):

$$R_e = \frac{2Q\rho}{\pi\mu r} \tag{2.9}$$

The criteria governing the type of flow regimes (smooth laminar, wavy laminar and turbulent) obtained on a plane vertical surface have been measured experimentally by various researchers (Fulford et al., 1964; Binnie, 1957; Friedman and Miller, 1941; Kirkbride, 1934). These criteria are:

Re < 16: smooth laminar flow (no surface waves)

16 ≤ R e < 40: Undulations across the film (small amplitude waves)

40≤ Re < 80: Sinusoidal waves gradually replaced by regular waves

80≤ Re < 1000 - 2000: Random surface waves (wavy laminar flow)

Re ≥ 1000 - 2000: Turbulent regime

One important issue that needs to be mentioned, even though the above criteria have been defined on the basis of film flow under gravity, is the fact that the above criteria are also applicable to films formed by the action of high centrifugal fields.

2.3.1.2.2 Flow Regimes

Over the recent past, some researchers have carried out investigation on different types of flow regimes associated with thin films formed on rotating discs. Charwat et al (1972) have described the different types of flow regimes associated with thin films formed on smooth rotating discs with low flow rates and disc rotational speeds. Hence, his study was limited to smooth discs only. However, from the study, a plot of flowrate against rotational speed was generated for the ranges of 0 to 7 cm^3/s and 6 to 75 radians/s respectively. Distinct boundaries between the flows regimes were observed depending on the operating conditions as follows: smooth film, spiral waves and concentric waves as shown in Figure 2.12. At low disc rotational speeds and flowrates the film surface was smooth. With increase in the flowrate at a fixed speed, concentric waves were formed. These waves move in radial direction outward and then decompose while the outer part of the film surface remained smooth. Another type of waves, which are spiral in structure, was developed at high disc rotational speed and low liquid flow rates. These waves were developed away from the centre of the disc, and decayed close to the disc edge but in most cases the waves first broke up into a very rough and non-uniform pattern of disconnected wedge-like wavelets. The highly unsTable film was produced by a combination of very high liquid flow rate and disc rotational speeds.

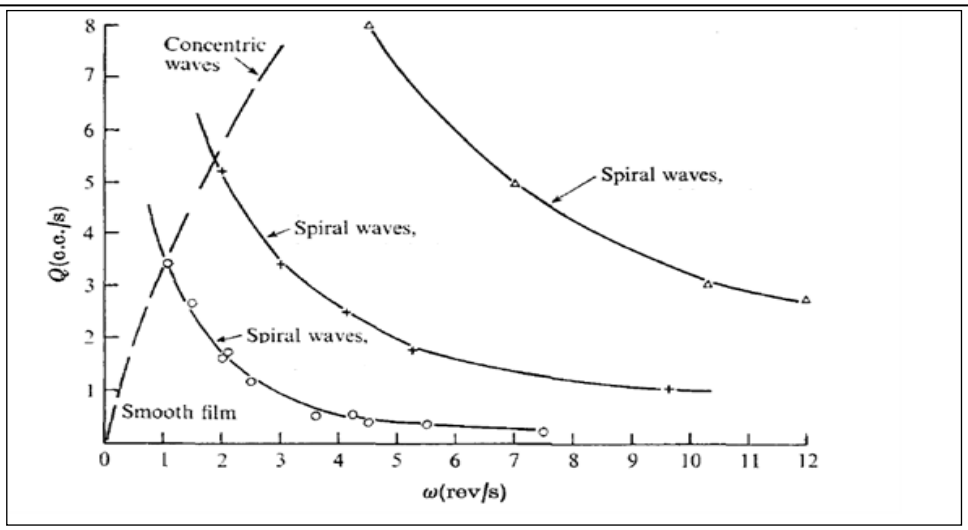

Figure 2.12: Flow regimes on the rotating disc surface. (Adopted from (Charwat and Kelly, 1972))

The behaviour of flow on the smooth disc experiments have been intensely investigated by Bell (1975) for the liquid flowrates up to 300 cm^3/s. Bell's diagram reproduced in Figure 2.13 indicates that there are three new zones which were not present in Charwat's flow diagram. At low flow rates, Bell observed that the film is broken and liquid flows in the form of rivulets.

However, the diagram does not clearly show how the film breakdown varies with radius but it was assumed that at least part of the disc is wetted at all flowrates for the graph of Charwat to make sense. Increasing the flow rates above 100 cm^3/s at disc rotational speeds below 20 radians/s caused jetting from the inlet nozzle. This was caused by the inlet nozzle being too small, which resulted in velocities in excess of the natural value at the exit of the nozzle.

At high speeds and high flowrates, the film surface appears to be very agitated. Bell interpreted this phenomenon as a result of centrifugal action causing the crests of ripples or jets to break off and impact upon flowing fluid. This was referred by Bell as a gray film.

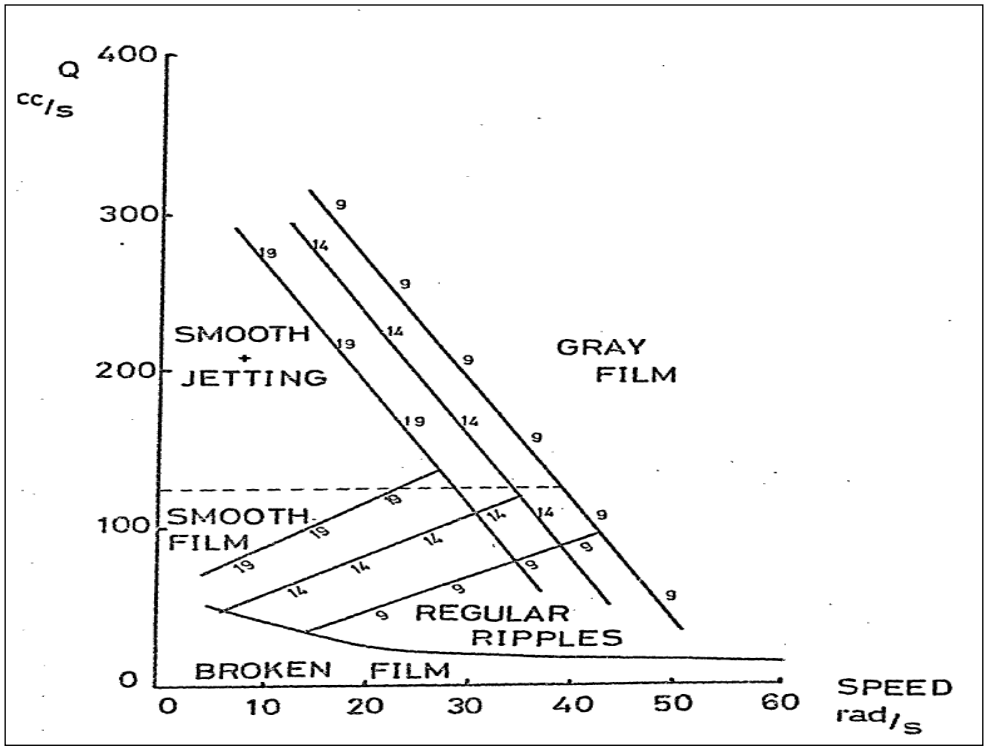

Figure 2.13: Flow regimes on the rotating disc surface. (adopted from (Ball, 1975)

2.3.1.3 Film breakdown

The occurrence of the breakdown of the thin film formed on a smooth rotating surface has been extensively studied over the past years. A critical review of these studies revealed that incomplete films with dry spots were observed at certain conditions especially at a combination of high rotational speeds and low liquid flow rates. Charwat et al (1972) described the mechanism of the film breakdown in great detail. The authors suggested that two distinct mechanisms that could be responsible for this phenomenon. In very thin films, even particles that stick to the surface of the disc can cause breakdown when the thickness drops to 20 μm Also, in the case of the thicker films, the breakdown occurred naturally even without physical disturbance as the function of flow parameters, particularly the Weber number can be estimated as shown below:

$$W_e = \frac{\sigma/\rho}{\delta_{film}\overline{V_r^2}} = 9\left(\frac{2\pi}{3}\right)^{5/3}\left(\frac{\sigma^3 \nu r^4}{\rho^3 Q^5 \omega^2}\right)^{1/3} \quad (2.10)$$

Where σ is the surface tension (kg/s^2)

One other noTable study in this area was carried out by Hartley and Murgatoyd (1964) in which the phenomenon of film breakdown investigated. They came up with a proposed model that was based on the assumption that film breakdown occurs when the sum of rates of surface and kinetic energy was at a minimum. Using the centrifugal velocity model profile and then differentiating it with respect to σ and summing it up to zero to obtain the minimum condition, the expression for the critical flow rate at which film breakdown would occur can be obtained using the equation given below:

$$Q_c = 5.5 \left(\frac{\nu r^4}{\omega^2}\right)^{\frac{1}{5}} \left(\frac{\sigma}{\rho}\right)^{\frac{3}{5}} \quad (2.11)$$

Where σ is the surface tension (Kg/s^2)

The results of the Bell's experiments (1975) have qualitatively proven these expectations. However, the results found that the experimental values for Q_c was about 30% lower than the predicted ones. This significantly affected the performance characteristics of the rotating disc by promoting the film breakdown which led to reduced available interfacial area across which mass or heat transfer occurs. Consequently, the film break down phenomenon negatively affected the intensity of mixing of the film on the disc due to the under utilisation of the complete disc surface in the process of mixing. Hence it is recommended that working below the critical flow rate should be avoided.

2.3.2 Power Dissipation on the Spinning Disc Reactor

It is very important to determine the amount of energy transferred into the fluid by the action of the disc rotation. The energy transferred to the fluid is an indication of the rate of mixing achieved in the SDR. This hydrodynamic characterisation is also important for comparison of the SDR mixing performance with other reactors. Furthermore, the power dissipation values are needed for calculating the micromixing time on the disc (section 2.4.4.1).

Khan (1986) proposed that the kinetic energy given to the liquid by the spinning disc was equal to the frictional power dissipated by the fluid; and it is expressed by:

$$P_{K.E} = \frac{1}{2} Q_f \{\rho_0 (r^2\omega^2 + U_m^2)_0 - \rho_i (r^2\omega^2 + U_m^2)_i\} \quad (2.12)$$

It should be noted that there is no change in the fluid density when the fluid flows from the centre to the edge of the disc. The fluid temperature remained constant on the disc surface as the experiments were carried out at 20°C. Therefore, equation 2.12 can be written as shown in the 2.13 below.

$$P_{K.E} = \frac{1}{2} Q_f \rho \{(r^2\omega^2 + U_m^2)_0 - (r^2\omega^2 + U_m^2)_i\} \quad (2.13)$$

Where:

Q_f = Volumetric flowrate (m^3/s)

ρ = film density (Kg/m^3)

r = radial distance from centre of disc (m)

ω^2 = angular velocity ($=2\pi N/60$) ($rads^{-1}$)

N = rotational speed (rpm)

U_m^2 = mean velocity of film on disc (m/s)

The subscripts 'i' and 'o' indicate conditions at the inner and outer radius of the disc respectively and *U* is the average radial velocity of the liquid solution on the disc (m/s) is given by:

$$U = \left(\frac{\rho_L \, Q_L^2 \, \omega^2}{12 \, \pi^2 \mu_L \, r} \right)^{\frac{1}{3}} \quad (2.14)$$

Where μ is dynamic viscosity (Ns/m^2), hence the total power dissipation, (ε), can be estimated as:

$$\varepsilon = \frac{P_{K.E}}{m} = \frac{1}{2} \frac{Q_f \rho}{m} \{(r^2\omega^2 + U_m^2)_0 - (r^2\omega^2 + U_m^2)_i\} \quad (2.15)$$

Where m is the mass of the fluid, (kg), and total power dissipation, (ε), equation could be written in as:

$$\varepsilon = \frac{P_{K.E}}{m} = \frac{1}{2}\ \frac{\dot{m}}{m}\ \{(r^2\omega^2 + U_m^2)_0 - (r^2\omega^2 + U_m^2)_i\} \quad (2.16)$$

Where ṁ is the mass flowrate (kg/s) and therefore,

$$\dot{m} = \frac{m}{t_{res}} \quad (2.17)$$

Therefore, the total power dissipation is directly proportional to the volumetric flowrate and the square of the disc speed. This finding has also corroborated the work of Cafiero et al., (2002) in which they described the total power dissipation given to the fluid by the action of disc rotation as:

$$\varepsilon = (0.5\ t_{res})\{(r^2\omega^2 + U^2)_o - (r^2\omega^2 + U^2)_i\} \quad (2.18)$$

Where , (ε), is in W/kg

2.3.3 Previous Work on Heat/Mass Transfer and Chemical Reactions in Spinning Disc Reactor

As stated previously in the preceding sections, there has been an increasing interest in the technology of process intensification and specifically the spinning disc reactor. Alongside the studies on the hydrodynamic characteristics of the SDR as presented in the previous section, many other investigations have been undertaken to characterise the SDR in terms of its heat and mass transfer rates and its performance in a broad range of chemical reactions. These will be reviewed here.

In the case of the heat/mass transfer, Wood and Watts (1973) investigated the heat transfer characteristics of water flowing over a 30cm diameter spinning disc. They reported that water flowing over a 30cm diameter spinning disc has a film velocities in the range of 3.3 to l0 m/s with a film thickness in the region of 25μm. This film

thickness is relatively very small and it has led to the formation of extraordinary heat transfer properties. The authors found that the overall heat transfer coefficients were in the range of 5.7 to 11.4 kW/m^{2}K. In this same study, Wood and Watts (1973) measured the absorption rates of of CO_2 in a film of water formed on a 30cm diameter rotating disc for disc rotational speeds in range of 320 to 1100 rpm and flowrates in the range of 31.6 to 252 m1/s. They found that the total absorbed CO_2 was in the range of 0.27 - 1.08 mol/s. These results were compared to the mass transfer model proposed by Vankataraman (1966) and it was found that over the range of the experiments, a good agreement between the model and the experimental results was obtained. On the other hand, the experimental results did not follow a mass transfer rate as proportional to a $Q^{1/3}$ relationship as Vankataraman's model predicted. Wood and Watts concluded that the water was not behaving according to the Nusselt flow model (from which Vankataraman's model is derived) and for this reason the Nusselt flow model was deemed not to completely describe the mass transfer characteristics of thin liquid film on the disc.

Rahman and Faghri (1993) introduced an analytical and numerical solutionfor mass transfer to a thin liquid film on the spinning disc. They recognised that all transport phenomena were controlled by inertial and viscous resistance at smaller radii as well as the rotation at larger radii. It was proved that the spinning disc can offer large enhancement of mass transfer coefficient over the entire disc radius by increasing the disc rotational speed. On the other hand, the enhancement of mass transfer coefficient with increase in flowrate was limited to the inertia-dominated region.

Woods (1995) carried out an experiment using a visual study of the waves produced by flow of a thin film over 0.3 m rotating glass spinning disc using an optical technique and obtained the detailed quantitative measurements by determining the reflection and absorption of light passing through the wavy film. The photographs of the flow showed details of the interfacial waves at various locations across the disc. It was recognized that an initially uniform film was broken down into well-defined spiral ripples, which later on broke down into more confused wavelets as the film progresses radially outward. This investigation has shown that the nature, frequency and location of the wave-fronts were controlled by rotational speed and flowrate. In this research,

measurements of the average film thickness were also attained at four radial points on the disc.

Jachuck and Ramshaw (1994a) used a spinning disc reactor with a 0.36 m diameter brass disc that had a grooved disc surface, which were used as an intensified heat transfer device, in order to increase the heat transfer rates. They studied the heat transfer of water flowing on the surface of a spinning disc which was operated in a rotational disc speed ranged 250 – 890 rpm. They reported average heat transfer coefficients of up to 16 kW/m^2K. One important finding from this work was that the heat transfer performance was significantly improved when mechanically machined grooves were employed on the disc surface compared to a smooth disc surface. This behaviour can be attributed to a large number ripples that were created within the thin film when the grooved disc was used and these large number of ripples had significant effect upon heat transfer performance when compared with the smooth surface disc

(Aoune and Ramshaw, 1999) investigated the heat and mass transfer performance on a 0.5cm diameter smooth spinning disc made of brass. They reported that very high heat transfer rates were attained on the disc for water system. In the case of mass transfer study of the absorption of oxygen in de-aerated water, they found that the mass transfer rates were governed by disc speed. On the other hand, the liquid flowrate and disc radius were not as influential parameters as the disc speed. In this study, the local mass transfer coefficients were reported in the range of 2 to 10 x 10^4 m/s at the liquid flowrate of 80 cm^3/s. They compared their experimental results with the Higbie penetration model of mass transfer and found that the experimental values were over 5 times higher than those predicted by the Higbie's model. The authors attributed this finding to a transit time of a surface element used in the Higbie model prediction of mass transfer coefficient which is determined by the derived residence time of the velocity of the film on the surface. However, the authors assumed in their experiments that the exposure time of a fluid element is that of the residence time of the fluid flowing on the surface predicted in the Nusselt model that describes the flow. This would be reliable when compared with the work carried out by Moore (1986) in which he suggested that the film instabilities and the propagation of the ripples and the instabilities of the film cause exposure times far less than the liquid surface residence time on the disc surface.

Polymerisation experiments were performed on a grooved SDR with 0.36m diameter disc by Boodhoo and Jachuck (2000a; 1999). As mentioned earlier, the grooves in the disc surface of the disc acted to create and introduce a large number of surface waves within the film. Accordingly, the heat and mass transfer for the film should be enhanced. The results of the polymerization of styrene obtained from the SDR were compared with the results from a stirred tank reactor. The results show that the use of a SDR gives rise to larger reaction rates and improved the product quality by producing a product with a tighter molecular weight distribution than those obtained using a standard stirred tank batch reactor. In addition, processing time for the completion of the process was reduced. Similar enhancements in reaction rates and product quality were obtained when the SDR was used for the continuous condensation polymerization to produce polyesters (Boodhoo and Jachuck (2000b)). It is also found that when the styrene polymerization experiments were performed on a grooved SDR, the rate of styrene polymerization is significantly increased (Boodhoo et al., 2002). Moreover, the molecular weight and the molecular weight distribution at a conversions of up to 80% in the SDR was found to be very close to those attained for the polymer at 60% conversions in the STR. The researchers attributed their findings as follows: the results indicated that the increase in polymerization rate is not the result of the Trommsdorff-Norrish effect, which would have resulted in an increase in the poly-dispersity. The shear rate experienced by the thin film provides intense mixing which is responsible for the above mentioned findings.

Also, Boodhoo *et al.* (2004; 2003) investigated the use of SDRs in the photo-polymerization reactions and they found that the SDRs can be applied successfully in this kind of processes due to high degree of mixing intensity achieved on the surface of the SDRs giving rise to fast rates of polymerization and tight molecular weight distributions at high molecular weights for the product.

In the case of cationic polymerization reaction, Boodhoo et al. (2006) studied the cationic polymerization of a styrene using SDR with silica-supported boron trifluoride (BF_3/SiO_2) catalyst in slurry form. Their study proves that the use of stirred batch reactor led to thermal runaway (uncontrollable) for monomer concentrations above 25% by weight and initial temperatures between 20-25 ^oC. In contrast, the use of SDR allowed controllable, essentially isothermal polymerization for monomer concentrations

as high as 75% by weight at 40 °C. In addition, the results of the study shows that a conversion increase of about 10% was achieved at 4100 s^{-1} average of shear rate, using a 200 mm diameter smooth disk with disc rotational speed of 400 rpm corresponding to mean residence times of approximately 1.0 s. These results proved that the use of SDR has the ability to enhance the heat and mass transfer rates associated with thin film which is driven by centrifugal forces on the surface of the spinning disc.

Cafiero *et al.* (2002) used the SDR with a 0.5 m diameter of smooth disc as intensifying reactor for investigating the precipitation process. The study was carried out to determine the precipitation of barium sulphate from aqueous solutions at 25 ^{o}C. The disc rotational speed was in the range of 900-1000 rpm. The article found that the SDR experimental results obtained were in good agreement with those found in the literature when a rapid T-mixer was used and the SDR was able to produce a very high specific number of crystals in the size range of 0.5-1 μm with a power dispersed of 115 W/kg. The study shows that the comparison of the induction and mixing time confirmed that at the adopted operating conditions homogeneous nucleation may occur. Accordingly, the spinning disc reactors appear to be an alternative to a reactor for carrying out a precipitation processes.

2.4 Mixing

2.4.1 General definition of Mixing

Mixing is defined as any process which can be used to reduce the inhomogeneity in order to achieve a desired process result. This inhomogeneity could be phase, concentration, temperature or pressure, etc. Mixing can reduce the scales of inhomogeneity down to molecular dimensions. The degree of mixing could affect mass transfer, reaction rate, and product properties, e.g. molecular weight and particle size distribution (Paul et al., 2004). Mixing operations are carried out in order to achieve the following objectives: accelerating and enhance the rate of heat and mass transfer for the system, distribution of immiscible materials and distributing one material in another to achieve uniform properties for the product. When the mixing process is occurring between two miscible liquids, two important factors for the mixer /reactors should be considered. These are:

I. No stagnant regions should exist within the mixer/reactor, i.e. the mixing must form an overall bulk or convective flow in the device.

II. High shear mixing must be offered by the mixing device. This will make the device capable of providing the reduction in system inhomogeneity or enhancing rate of heat / mass transfer that is required by the process duty.

During turbulent mixing in continuous or semi-continuous reactor, the kinetic energy input into the system is dissipated by viscous deformation during the following cascade of mechanisms (levels of mixing): macromixing, mesomixing and micromixing (Baldyga and Pohorecki, 1995b) which will be discussed in the following section The micromixing aspect of the mixing process is the key focus of this research.

2.4.2 Levels of mixing

The levels of mixing encountered in the mixing process for miscible fluids can be classified by three length scales, as depicted by (Johnson and Prud'homme, 2003) in Figure 2.14. These levels are: macromixing, mesomixing and micromixing.

I. *Macromixing:* is the mixing on a scale greater than the minimum eddy size. Macromixing is also the process of blending on the scale of the whole vessel (mixing at the macroscopic scale) which determines the environment concentrations for both mesomixing and micromixing. Macromixing is characterized by the blend time in a batch system or the residence time distribution in continuous systems. At this level of mixing, the fluid distribution throughout the vessel is by the bulk convection.

II. *Mesomixing*: is the mixing at intermediate level, which describes the mixing on an intermediate scale and, particularly, characterizes the inertial-convective mixing of a fresh feed stream. In other word, mesomixing is the formation of daughter vortices which grow by turbulent diffusion or inertial-convective mixing and engulf new fluid. In fact, the mesomixing level is referring to the dispersion of fresh feed stream shortly after it enters the reactor. At this level the mixing is at a scale roughly comparable with the size of the reactant feed pipe

and corresponding to mixing phenomena which occur on a scale smaller than macromixing and larger than micromixing (Baldyga and Bourne, 1992).

III. *Micromixing*: is the mixing on a scale smaller than the minimum eddy size (the last mixing stage). Micromixing is the mixing on the molecular scale, which is important for fast competitive chemical reactions. In micromixing scale, a further deformation of daughter vortices ultimately resulting in a lamellar structure (*momentum diffusion*) where molecular diffusion can eliminate regions of segregation in a local flow that is laminar (Johnson and Prud'homme, 2003; Baldyga and Bourne, 1984a).

The mixing phenomena at macromixing and mesomixing levels scales are better known and understood than micro-scale phenomena.

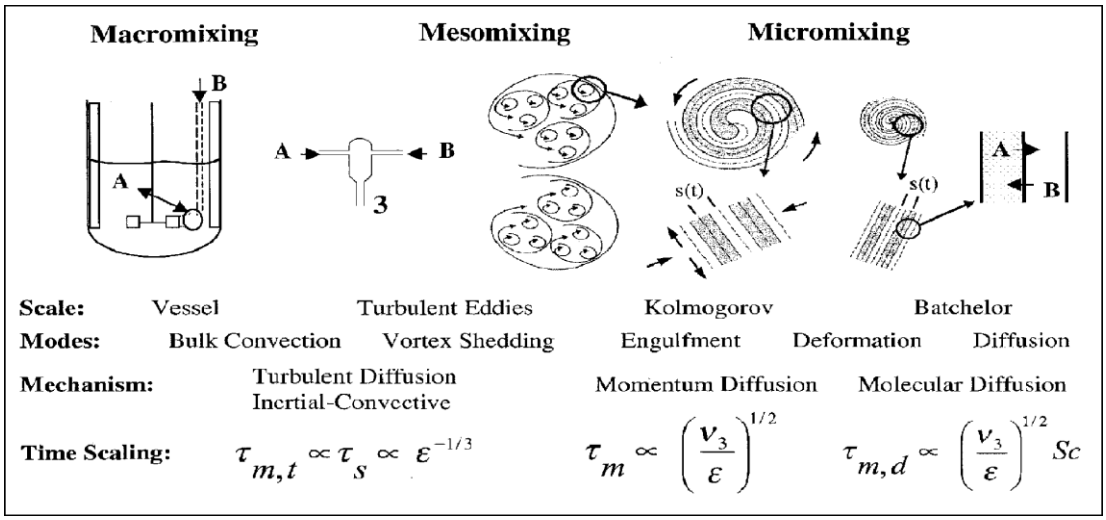

Figure 2.14: Turbulent mixing mechanisms through the three scales (adapted from Johnson and Prud'homme (2003))

2.4.3 Mixing Mechanisms

For miscible systems, mixing of two liquids can occur in three consecutive or sometimes parallel steps (Edward et al., 2004) and it can be summarised as follows:

a) At the beginning of the mixing process, one fluid is spreading in another (*Dispersion step*) so as to achieve a uniform average composition. On the microscale, however, the mixing consists of entirely segregated parts of the two

liquids and therefore the local concentration differences correspond to the difference of concentrations of non-mixed liquids.

b) The size of the segregated regions of the uniform composition increases and the contact area between the regions of different composition grows.

c) Mixing by molecular diffusion takes place to such an extent that segregated area disappears; the mixture reaches total homogeneity on the molecular level.

The first of these three stages represent the macromixing step while the other two stages are termed micromixing step. Thus micromixing is the process by which liquids contact and mixing process take place at the molecular scale.

Baldyga and Pohorecki (1995a) characterized mesomixing and micromixing processes by the spectral density function E(k) for turbulent kinetic energy and G(k) of the concentration fluctuations in the bulk liquid phase. The spectral densities are demonstrated in Figure 2.15 as a function of the wave number, (k), which is proportional to the reciprocal of the eddy size λ (λ ∝ 1/k). The k_{oc} is the wavenumber of large eddies, k_k is Kolmogorov wavenumber and k_B Batchelor wavenumber. Here the Kolmogorov micromixing (λ_k) can be defined as:

$$\lambda_k = \frac{1}{k_k} = \left(\frac{\nu^3}{\varepsilon}\right)^{\frac{1}{4}} \tag{2.19}$$

For the power dissipation of 1W/kg in water, the Kolmogorov microscale $(\lambda_k) \approx$ 30 μm.

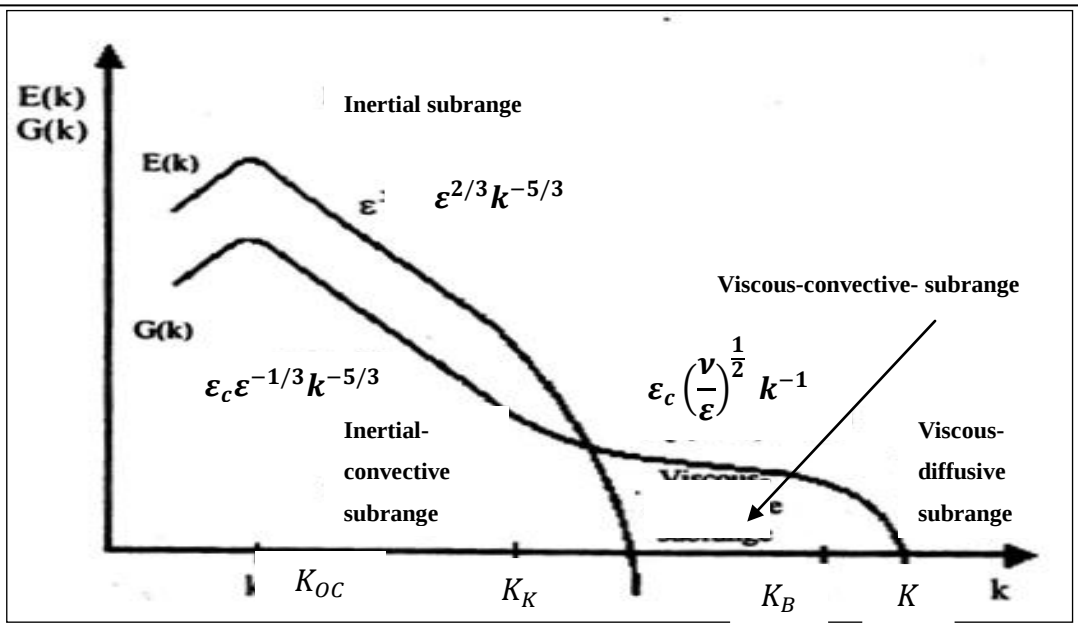

Figure 2.15: Kinetic energy spectrum E(k) and concentration spectrum G(k) for liquid mixture with Sc >> 1,log-log scale (adapted from (Baldyga and Pohorecki, 1995a)

The Batchelor micromixing length scale is defined as:

$$\lambda_B = \frac{1}{k_B} = \left(\frac{D^2\nu}{\varepsilon}\right)^{\frac{1}{4}} \quad , \quad Sc \gg 1 \tag{2.20}$$

For the power dissipation of 1 W/kg in water, the Batchelor microscale (λ_B) ≈ 1 μm. The integral scale for concentration fluctuations (L_c) is given as:

$$L_c = \frac{1}{k_{OC}} = \left(\frac{k^{3/2}}{\varepsilon}\right) \tag{2.21}$$

Where k_{OC} is the characteristic wave number of large eddies. For liquids, the spectral density of concentration fluctuation G (k) can be divided into three sub-ranges:

I. The inertial-convective sub-range;
II. The viscous-convective;
III. The viscous-diffusive sub-range.

The condition under which the inertial-convective sub-range occurs is given as: ($\lambda_k < l < L_c$ and $k_{oc} < k < k_k$), where l is the size of fluid elements. The deformation of the large blobs of fluid and their subsequent breaking up is cause by the fluid motion, which results in their scales being further reduced by viscous deformation, while their molecular diffusion becomes slowly active. This process can be identified within the process of the inertial-convective mesomixing.

The second sub-range of spectral density of concentration fluctuation occurs when the viscous-convective sub-range is the within the range of ($\lambda_B < l < \lambda_k$ and $k_K < k < k_B$), in which eddies are subjected to laminar strain that is depended on the viscosity. Consequently, the scales of eddies are further reduced by the effect of viscous deformation while molecular diffusion becomes slowly active.

The third sub-range of spectral density of concentration fluctuation is the viscous-diffusion sub-range which occurs within these conditions: ($\lambda_B > l$ and $k > k_B$). This begins when the laminar strain and molecular diffusion are of equal importance for even smaller eddies. The molecular diffusion of this smaller eddies rapidly dissipates the concentration variance. The spectral density of kinetic energy becomes negligible for eddies smaller than the Kolmogorov scale, hence the molecular diffusion becomes affected by the effect of viscous deformation only.

Baldyga and Bourne (1999) described visually the three sub-ranges discussed above. Figure 2.16 illustrates the development of small fluid element through the various mixing steps identified into the three sub-ranges and in particular the micromixing of solutions containing the reactants A and B.

Parts (a) and (b) (shown in Figure 2.16 below) represent the deformation of the large blobs of fluid B. This is because of the action of velocity fluctuations and their consequent reduction in size occurring in the inertial-convective sub-range. At this point, the micromixing will not occur but the structures formed will participate in the micromixing process. Part (c) describes the laminar deformation occurring at a finer scale recognized as the viscous-convective sub-range while part (d) concentrates on a small region and represents the action of vortices of the order of λ_k at the various times

t_i. This occurs in the inertial-convective sub-range. At this stage, mixing due to molecular diffusion occurs within the laminae formed because of the acting of vortex and their consequential stretching.

In conclusion, the micromixing process of solutions of A and B can be summarized as follows:

- ✓ First, an initial formation of fluid aggregates that are reduced to a scale on the order of the Kolmogorov scale , (λ_k), with no micromixing occurring.

- ✓ The above step is followed by the action of vortices that incorporated the fluids A and B of initial scale equal to λ_k which are then subjected to deformation and stretching. This allows the molecular diffusion within the laminae inside the vortex to be formed.

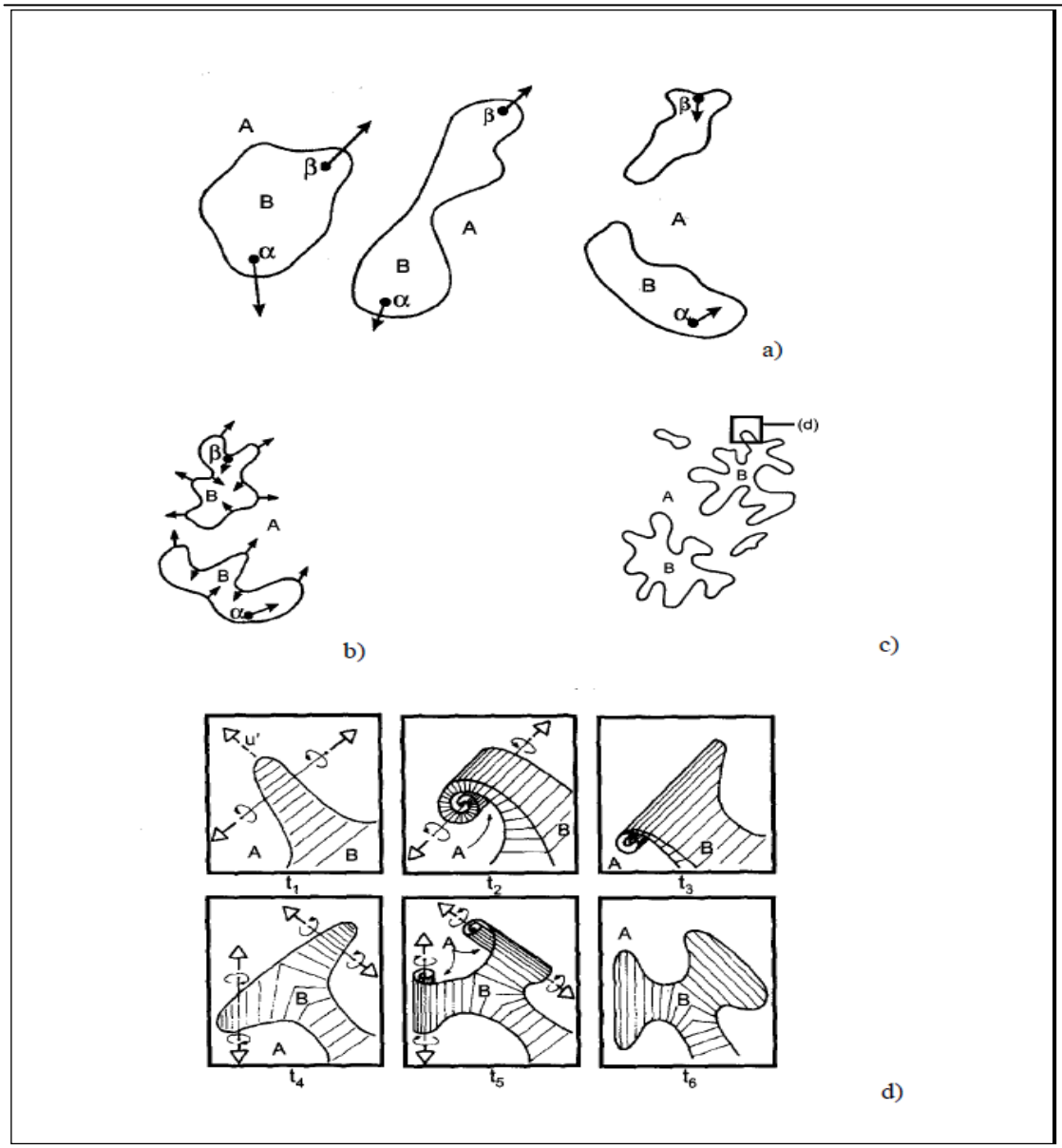

Figure 2.16: (a,b): Deformation of large blobs of fluid to a smaller scale in inertial-convective sub-range; (c): laminar deformation of the aggregates occurring in viscous-convective sub-range; (d): vortex action on small scale fluids elements forming laminae followed by molecular diffusion within the laminae. adopted from Baldyga and Bourne,(1999)

In summary, the initial macromixing step is very important because it defines the environment in which concentrations for mesomixing and micromixing occurs. The macromixing step also provides a medium through which the fluid elements in meso- and micromixing experience different turbulence properties. Mesomixing is a reflection of the coarse-scale turbulent dispersion between the fresh feed and its surroundings. A fast chemical reaction in mesomixing process is usually localized near the feed point and the plume of fresh feed. The plume is very large relative to micromixing scales but smaller than the scale of the system. Another aspect of meso-mixing is related to the

inertial-convective process of breaking down of large eddies. The effect of the breakdown of the large eddies on the mixing by the inertial-convective occurs without having any significant impact on molecular mixing. However, it is the erosive shrinking of the blobs of fresh feed; this means that it is the large eddies of the inertial-convective sub-range that determines the environment for micromixing. Micromixing is last step of turbulent mixing process which consists of the viscous-convective deformation of the fluid elements followed by molecular diffusion. The acceleration of the molecular diffusion by viscous-convective process is considered to be the most important characteristic of micromixing process.

2.4.4 Time constants of Single-phase mixing

2.4.4.1 Time constant for chemical reaction

The characteristic reaction time for second order reaction is given by:

$$t_R = \frac{1}{kC_{B0}^{n-1}} \qquad (2.22)$$

Fast reactions are defined as the ones whose characteristic time of reaction t_R is of the same order or smaller than the micromixing time t_m.

2.4.4.2 Time constant for macromixing

As previously explained in section (2.6.2), macromixing is the mixing process that occurs at the scale of the vessel. It is the process that determines the global environment in which other two scales i.e. meso- and micro-mixing may be involved and it consists of the fluid that consequently undergoes meso- and micromixing processes.

Harnby et al., (1992) reported that when a non-reactive material or tracer is entering the stirred tank, it joins the circulating flow and then it is dispersed by turbulence so that it

finally reaches all parts of the vessel. This bulk blending is followed experimentally by injecting a pulse of non reactive tracer at a particular position and its concentration (e.g., by electrical conductivity) is a function of time at one or several positions. The signal oscillates with a period of oscillation called the mean circulation time (t_{cr}). the mean circulation time can be defined as (Nienow, 1997):

$$t_{cr} = \frac{V}{Q} \tag{2.23}$$

Nienow (1997) found that for a number of mixers, the macromixing time is often a small multiple of t_{cr} ($i.e., t_m \approx 4\, t_{cr}$).

Tracer injection finally changes the concentration by Δc, and a possible definition of the macromixing (or bulk blending) time is the time following the injection when the concentration change at the measuring point becomes equal to $0.95\Delta c$. This is called the 95% mixing time. When the liquid depth in a baffled stirred tank is approximately equal to the tank diameter (T), good estimation of macromixing for a range of impeller types was estimated by Nienow (1997) as follows:

$$t_m = 5.9\left(\frac{T^3}{\varepsilon_{av} d}\right)^{\frac{1}{3}} \tag{2.24}$$

And

$$\varepsilon_{av} = \frac{P}{\rho V} = \frac{P_0 N^3 D^5}{V} \tag{2.25}$$

2.4.4.3 Time Constant for Mesomixing

2.4.4.3.1 Time Constant of Mesomixing by Eddy Disintegration

The first mechanism proposed by Baldyga and Bourne (1999) considers the disintegration of a fresh stream or a large spot entering a turbulent environment (e.g., in a stirred tank), from a scale as an initial scale (Λ_c) towards the Kolmogorov microscale (λ_k) where micromixing can occur. This break-up can be shown schematically in Figure 2.17. The mesomixing time constant by eddy disintegration, (t_s) is given by:

$$t_s \approx 2\left(\frac{\Lambda_c^2}{\varepsilon_T}\right)^{\frac{1}{3}} \tag{2.26}$$

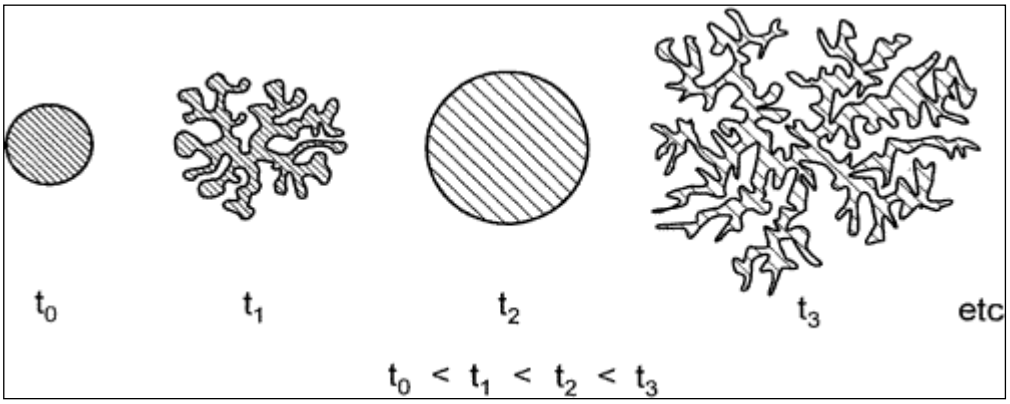

Figure 2.17: Disintegration of fluid element to scale where micromixing occurs (adopted from Baldyga and Bourne (1999))

For estimating the initial scale of "unmixdness",(Λ_c), Baldyga and Bourne (1999) have taken into account the different ways that the fluid has to enter the turbulent environment. One way was the fluid being fed to the environment through a small pipe into a large turbulent environment so that the momentum of the feed stream is not significant relative to that of the turbulent surrounding flow (velocity u). The Λ_c is given by:

$$\Lambda_c = \left(\frac{Q_B}{\pi u}\right)^{0.5} \tag{2.27}$$

Where Q_B is the feed flow rate

Conversely to the previous case, the feed enters with much higher velocity than the surrounding flow (higher than velocity) and a jet will be formed. In this case, Λ_c could be defined as equal to the radius of the feed pipe. Subsequently, the local power dissipation, ε_T, will be enhanced by the action of this jet (Bourne, 2003).

2.4.4.3.2 Time Constant of Mesomixing by turbulent diffusion/dispersion

The turbulent diffusion and turbulent dispersion are both used to indicate the spreading of the fresh feed into the surrounding fluid. The central point being that the mechanism is turbulent, not molecular (Bourne, 2003).

Figure 2.18 illustrates the initial spreading of a plume of fresh fluid injected into the system with flow rate of Q_B in the direction normal to its flow and the local volume fraction of feed material denoted as $X^0(r,x)$.

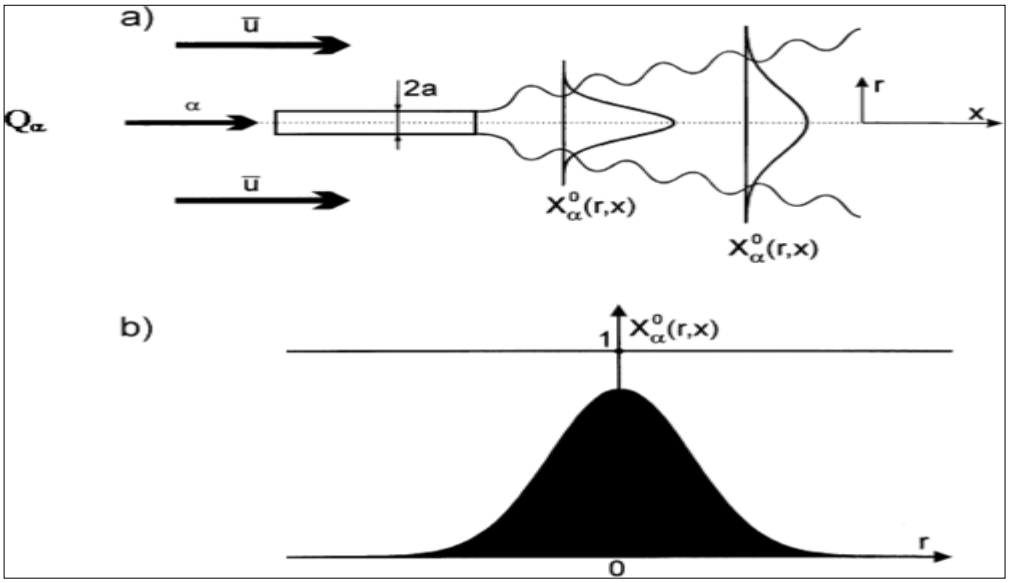

Figure 2.18: Turbulent dispersion of feed giving Gaussian concentration distribution normal to flow direction. adopted from Baldyga and Bourne (1999)

If the turbulent diffusivity (D_T) and local velocity (u) are constant during the feed dispersion, The Gaussian concentration distribution forms with a time constant (t_D),i.e., the characteristic time for mesomixing based on the turbulent diffusion/dispersion is given by:

$$t_D = \frac{Q_B}{uD_T} \tag{2.28}$$

the mesomixing time depends on the feed rate and the turbulence characteristics near the feed pip's outlet (Baldyga and Bourne, 1999).

2.4.4.4 Time Constant for Micromixing

2.4.4.4.1 Time Constant for Micromixing by Molecular Diffusion and Shear Force, (t_{DS})

Baldyga and Pohorecki (1995a) reported the micromixing time constant related to the processes of molecular diffusion (molecular diffusion within the laminae). As previously explained, during mixing process, the layers (laminae or thin film) of different composition come close to each other and the molecular diffusion occurs by homogenising the mixture at the molecular scale. In addition, during the diffusion step, the laminae or layers are deformed and the characteristic micromixing time for molecular diffusion and shear was defined by Baldyga and Pohorecki (1995a) as the time to decrease the thickness of the layer (laminae / thin film) from the Kolmogorov scale, λ_k , to the Batchelor scale, λ_B which is defined as follows:

$$t_{Ds} = 2\left(\frac{\nu}{\varepsilon}\right)^{0.5} arc\sinh\left(0.05\frac{\nu}{\mathrm{D}}\right) \tag{2.29}$$

As mentioned earlier in section 2.3.3 , the film flows on the disc of SDR can be as thin as *25 μm* or even less and also a high shear rate could be created between the thin film and the disc surface due to the centrifugal force. This physical property makes the Baldyga and Pohorecki model an important tool for calculating the micromixing time on the SDR due to the molecular diffusion and the shear force. Mixing down to molecular scale can often be achieved in the range of 0.1-1 s (Bourne, 2003).

2.4.4.4.2 Time Constant for Micromixing by Engulfment

Turbulent flow in micromixing is characterised by its vorticity and transitory vortex tubes. It can be deduced that small, energetic vortices acting near the Kolmogorov scale can be drawn (or engulfed) in the surrounding fluid to form a short-lived laminated structure within the vortex tube. Figure (2.19) illustrates the Vortex stretching causes by the engulfment of the fluid from the environment to form laminated structure.

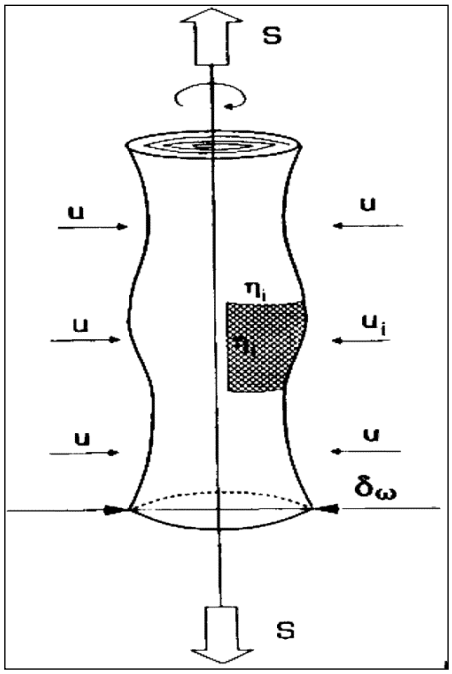

Figure 2.19: Vortex stretching which causes engulfment of fluid from the environment to form laminated structure (Adopted from (Baldyga and Bourne, 1999))

When a small amount of initially B-rich solution engulfs an A-rich surroundings, the rate of growth of the engulfed volume (*V*E) is given by:

$$\left(\frac{dV_E}{dt}\right) = EV_E \tag{2.30}$$

Where the engulfment rate coefficient (*E*) can be defined as:

$$E = 0.058\left(\frac{\varepsilon}{\nu}\right)^{\frac{1}{2}} \tag{2.31}$$

The time constant for micromixing by engulfment is the inverse of *E*, which is given as:

$$t_E = 17.5\sqrt{\frac{\nu}{\varepsilon}} \tag{2.32}$$

The power dissipation , (ε), has received considerable attention in both experiments and simulations. The total power input into a tank depends on the impeller diameter, impeller speed and the liquid volume to be stirred. The local power dissipation rate per unit mass of fluid can be specified as:

$$\varepsilon = \emptyset \ \frac{N_P N^3 \ D^5}{V} \tag{2.33}$$

The total power dissipation is not distributed homogeneously in the whole tank. The local power dissipation rate per unit volume of the fluid and local flow velocities in the tank depends strongly on the position in the tank. The greatest values are measured at the impeller discharge stream and specifically near the impeller tip where the engulfment rate has the highest value. The relative power dissipation (∅) is expressed by:

$$\emptyset = \frac{\varepsilon}{\bar{\varepsilon}} \tag{2.34}$$

Ø depends on the position and the geometry of the reactor. For example, assuming the values of the kinematic viscosity is ν = 10^{-6} m^2/s, diffusion coefficient, D =10^{-9} m^2/s and the local power dissipation, ε = 1 W/kg; using equations (2.29) and (2.32), the values of t_{DS} and t_E obtained are given as 9 ms and 17 ms respectively. Consequently, for low viscosity solutions, the engulfment mechanism is usually slower than the

diffusion one determining the micromixing rate. This can be concluded that the fast micromixing is due to low viscosity fluids and high values of local specific energy dissipation.

The time constants for micromixing are likely to fall in the range of 0.1-100 ms with existing sufficient intensive turbulence (Bourne, 2003).

2.4.5 Chemical Methods for Mixing Quality Characterization

These methods use test reactions called reactive tracers or more frequently test reactions, which are dependent on the reagent mixing state. This dependency is shown by their product distribution i.e. the segregation index, (Xs), since they are considered as molecular probes (Fournier et al., 1996a; Bourne et al., 1992). The technique consists in the injection of the feed of reagents into the mixing reactor, and after spontaneous reactions, the product distribution is determined by sampling the fluid at the outlet of reactor if the system is continuous, or from the mixture in the reactor if the reactor is semi-batch system.

2.4.5.1 Test Reactions for Micromixing Measurements

The chemical methods are test reactions which can be employed in experiments designed to evaluate the quantitative predictions of models claiming to describe the coupling between the mixing and reaction (quantifying the influence of the mixing process on reaction).

The following characteristics should be fulfilled by a set of test reactions and should be considered when the test reaction is chosen for testing the intensity of mixing (Baldyga and Bourne, 1999; Fournier et al., 1996a; Bourne et al., 1992; Bourne et al., 1977b);

- Reactions should be fast relative to mixing so that product distribution strongly depends on mixing and the time constants of these steps are of comparable magnitude. However, in those situations where a single reaction can be employed, it can also be instantaneously related to the mixing.

- Reactions should be irreversible so that the product distribution responds to the state of mixing in the reaction zone, but does not change during the rest of the residence time in the reactor and the period of chemical analysis.

- Unequivocal knowledge of all reactions and their kinetics is essential. The dependence of the reaction rates on all concentrations, ionic strength, pH, solvent, temperature and homogenous catalysts (e.g. acids and bases) should be clear. Substantial effort is necessary to attain this level of detail, especially for Fast reactions.

- All the reactants should be miscible because mass transfer between different phases could have a slower rate than mixing, which would make it difficult or impossible to characterize mixing.

- A simple, fast and accurate quantitative analysis method must be available to determine the product distribution.

- For general convenience and safety as well as ease of application at industrial scale, the reagents and products are inexpensive and non-toxic.

It is difficult for test reactions to satisfy all the above requirements strictly. in the literature (Baldyga and Bourne, 1999; Fournier et al., 1996a).These reactions can be grouped in three main stoichiometric types:

1) Single reaction: A+B→R;
2) Consecutive competing reactions: A+B→R, R+B→S;
3) Parallel competing reactions: A+B→R, C+B→S.

2.4.5.1.1 Single fast reactions

The single fast reactions generally involve the neutralization of a strong mineral acid with a base represented by the following scheme:

$$A + B \overset{k_1}{\rightarrow} R \qquad (2.35)$$

This type of reactions is instantaneous or very fast reactions with a characteristic reaction time *(t_r)* shorter than the mixing characteristic time *(t_m)*. They are suiTable for turbulent tubular reactors where reagent conversions as function of distance and hence also of time can be followed (Baldyga and Bourne, 1999). However, in a stirred tank reactor the local conversion in the moving fluid cannot usually be followed as a function of time.

The rate of mixing has a very important influence on the course of reaction. Insufficient mixing can limit the reaction rate. Thus the dependence of reaction rate on mixing can be used to evaluate the competition between turbulent mixing and reaction. Table 2.1 show some examples of single test reactions reported in the literature.

Table 2.1: Test reactions of type A + B → R (Single reaction)(Fournier et al., 1996a)

Reference	Reagent A	Reagent B	Rate of constant (25^oC) $[m^3.mol^{-1}.s^{-1}]$
(Worrell and Eagleton, 1964) (Keairns and Manning, 1969)	Sodium thiosulphate	Hydrogen peroxide	$k_1=2.83x10^{-4}$
(Keeler et al., 1965) (Torrest and Ranz, 1969) (Miyairi et al., 1971)	Ammonium hydroxide	Acetic acid	
(Mao and Toor, 1971)	Hydrochloric acid	Sodium hydroxide	$k_1=1.4x10^8$ at 25^oc
	Maleic acid	Sodium hydroxide	$k_1= 3x10^5$
	Nitrilotriacetic acid	Sodium hydroxide	$k_1=1.4x10^4$
	Carbon dioxide	Sodium hydroxide	$k_1= 8.32$
(Méthot and Roy, 1973)	Sodium thiosulphate	Sodium bromoacetate	$k_1= 10^{-4}$ At 20^oc
(Larosa and Manning, 1964) (Zoulalian and Villermaux, 1970) (Goto and Matsubara, 1975) (Lintz et al., 1975) (Makataka and Kobayashi, 1976)	Ethyl acetate	Sodium hydroxide	$k_1=1.34x10^4$ At 20^oc
(Aubry, 1972) (Klein et al., 1980)	Nitromethane	Sodium hydroxide	$k_1=2x10^{-2}$ At 20^oc

2.4.5.1.2 Multi-Step Fast Reactions

Fast reactions whose product distribution is dependent on the mixing quality require competitive steps. These may occur in a competitive-consecutive scheme or in a competitive- parallel scheme as explained below.

I. Competitive-consecutive scheme

Equations (2.36) and (2.37) shows the general *Competitive-consecutive scheme* where reagent A reacts with B, added as a limiting reagent, gives the primary product R in reaction (2.36) and then R further reacts with B to give the final product S in reaction (2.37). Reaction (2.36) is quasi-instantaneous and reaction (2.37) is fast and having a reaction time (t_m) of the same order as the micromixing time.

$$A + B \overset{k_1}{\rightarrow} R \qquad quasi - intantaneous: k_1\ very\ high \qquad (2.36)$$

$$R + B \overset{k_2}{\rightarrow} S \qquad \text{fast}, k_2 << \text{k}_1 \qquad (2.37)$$

Under good conditions of mixing ($t_m << t_R$ - *slow regime*) where kinetic process is the controlled regime and the mixing process has no any influence, it can be shown that the yield of the products R and S are only dependent on the stoichiometric ratio and on the rate constants ratio (k_1/ k_2). When ($t_m << t_R$). This means the reaction is slower when compared with the mixing process, so that mixing process will be completed before the reactions occur and there will be no mixing influence on the product distribution which depends on the initial stoichiometric reagents ratio and the ratio of the rate constants. By measuring the amount of products after total consumption of the reagent B, the segregation index, Xs, can be calculated as the fraction of the limiting reagent B present in the secondary unwanted product S, Xs where ;

$$X_S = \frac{2C_S}{2C_S + C_R} \qquad (2.38)$$

Contrary to the previous case where ($t_m >> t_R$ - *instantaneous regime*) and the mixing process is the controlled regime or intermediate regime, in this case the product R formed in reaction (2.36) will instantaneously react with reagent B in reaction (2.37)

which then gives the final product S. The amount of reagent R will be completely consumed and the segregation index, Xs, will be reached to the maximum value i.e. 1.0, where the total segregation state is present in the mixture.

The intermediate regime (the reaction is fast but not instantaneous i.e. ($t_m \approx t_R$ - *fast regime*) is the third case where the product distribution will be dependent on both the kinetics and rate of mixing.

In the early 80s, Baldyga and Bourne (Bourne et al., 1981) developed the first reaction schemes that showed the sensitivity to the maxing process. This set of reaction consists of the azo-coupling of 1-naphthol, A, with diazotized sulphanilic acid, B, having two products (R = monoazo and S= bisazo), which are dyes. This scheme was at the beginning simplified as a parallel-consecutive reaction system according to equations (2.36) and (2.37). In fact, the reaction produces two isomers of monoazo dye, the *para* and the *ortho* form. However, at the beginning(Bourne et al., 1981) the reactions involving the ortho product were not taken into account. Afterwards, the composition of *o-R* and *p -R* formed were determined and the new reaction scheme which now consists of four reactions (Bourne and Hilber, 1990b).

This type of test reaction has been successfully used on micromixing studies in several types of reactors e.g. (Bourne and Maire, 1991; Baldyga and Bourne, 1989b; Baldyga and Bourne, 1989a; Kusch et al., 1989). However, some disadvantages, regarding to this particular set of reaction is the degradation of the product (the temperature sensitivity of the products) not being straight forward in terms of preparation of the reactants and the difficulty to obtain the spectrum of product S (Wenger et al., 1992). The analytical errors and the risk of involving the product *S* (unwanted product) limit the application of this test system to reactors whose energy dissipation is less than 200 - 400 $W.kg^{-1}$ (Bourne et al., 1992).

Villermaux and his collaborators (Detrez et al., 1988; David et al., 1985; Barthole et al., 1982) developed another set of reaction which follows the *competitive-consecutive scheme,* equations (2.36) and (2.37). The test reaction is based on the precipitation of barium sulphate from the alkaline barium-EDTA complex under the influence of acid addition. Following this, it was found out that the reactions were not fast enough to

study performance of mixers/reactors. In addition, under certain circumstances, re-dissolution of the precipitate has been observed (Meyer et al., 1992). Table 2.3 show some examples of Competitive-consecutive scheme reactions reported in the literature.

II. Competitive-parallel scheme:

Equations (2.39) and (2.40) show the general *competitive-parallel scheme.* The common limiting reagent B reacts with A and C giving as products R and S. As for the prior case, reaction (2.39) is faster than the second reaction (2.40). When a small quantity of reagent B is added to an excess of reagent A and C, the quantity of product R and S will depend on the intensity of mixing and therefore the micromixing. Reaction (2.39) is quasi-instantaneous and the rate of reaction (2.40) is comparable to that of micromixing process.

$$A + B \overset{k_1}{\rightarrow} R \qquad quasi - intantaneous: k_1\ very\ high \qquad (2.39)$$

$$C + B \overset{k_2}{\rightarrow} S \qquad \text{fast}, k_2 << \mathrm{k}_1 \qquad (2.40)$$

As explained in *competitive-consecutive scheme*, in conditions where mixing does not have any influence, it can be shown that the yields of the products R and S are dependent only on the stoichiometric ratio and on the rate constants ratio (k_1/k_2). This can occur when the reaction is slow i.e. ($t_m << t_R$) and the product distribution i.e. segregation index, Xs, can be measured as the fraction of the limiting reagent B present in the secondary unwanted product S.

On the other hand, a mixing process controlled regime or an intermediate regime where ($t_m >> t_R$- *instantaneous or mixing controlled regime*) could alter the expected results of the kinetic controlled regime. In this case, the competition of reactant A and reactant C for reactant B will be controlled by the concentration of the reactants and not by the reaction rates.

The third case is the intermediate regime where the reaction is fast but not instantaneous i.e. ($t_m \approx t_R$ - *fast regime*). The product distribution will be dependent on both the kinetics and the rate of mixing.

For both competitive-consecutive and competitive-parallel schemes, there will be only the formation of product R and the segregation index, Xs, reaches 0 in the case of a perfectly micromixing system. Alternatively, the formation of product S will indicate a partial segregation of the mixture and the segregation index, Xs, will be in the range of 0 to 1.

These two kinds of reaction schemes have the advantage of keeping the memory of mixing efficiency through the distribution of products (Fournier et al., 1996a), i.e., the product distribution is limited by the consumption of the limiting reagent which is the reagent B. This makes two reactions well suited for studying the micromixing efficiency in different type of reactors. Therefore, a limited amount (lower than that given by stoichiometry) of *B* must be added to *A* ($N_{A0} > N_{B0}$ *or* $F_{A0} > F_{B0}$, where *N* is the number of moles in the case of semi-batch reactor systems and *F* is the volumetric flowrate in the case of continuous reactor systems) in the case of a competitive-consecutive reaction scheme or to the mixture of *A* and *C* ($N_{C0} > N_{B0}$ *or* $F_{A0}+F_{C0} > F_{B0}$*);* in the case of a competitive parallel reaction scheme, so that both reactions stop by total consumption of limiting reagent *B.*

Some examples of the consecutive and parallel reaction schemes are presented in the literature. Tables 2.2 and 2.3 show some of these examples for competitive-consecutive reaction scheme and competitive- parallel reaction scheme respectively as reported in the literature.

Table 2.2: Test reactions of type A + B → R, R + B→ S (Competitive- consecutive reaction) adapted from Fournier et al. (1996b)

Reference	Reagent A	Reagent B	Rate of constant (25^oC) [$m^3.mol^{-1}.s^{-1}$]
(Paul and Treybal, 1971) (Bourne and Rohani, 1983)	1-Tyrosine	Iodine	$k_1=3.5x10^{-2}$ $k_1/k_2=9.2$
(Zoulalian and Villermaux, 1974)	*p*-Cresol	Iodine	$k_1=3.25$ $k_2=1.28$ (pH=11)
(Zoulalian, 1973.) (Truong and Methot, 1976)	Glycol diacetate	Sodium hydroxide	$k_1=5.14x10^{8}$ $k_2= 2.27x10^{-4}$
(Bourne et al., 1977)	Resorcinol	Bromine	$K_2= 10^2$
(Nabholz and Rys, 1977)	Prehnitene Isodurene Durene	Nitronium salt	$k_2=3x10^{-1}$ $k_2=4x10^{-2}$ $k_2=10^{-1}$ $k_1/k_2>100$
(Bourne and Kozicki, 1977)	1,3,5-Trimetoxybenzene	Bromine	$k_1/k_2\approx27$
(Bourne et al., 1990)	1-Naphthol	Diazotized sulfanilic acid	$k_2=1.3x10^{4}$ $k_2=2.7$

Table 2.3: Test reactions of type A + B → R, C + B→ S (Parallel competing reaction), Adapted from Fournier et al.(1996b)

Reference	Reagent A	Reagent B	Reagent C	Rate of constant (25^oC) $[m^3.mol^{-1}.s^{-1}]$
(Treleaven and Tobgy, 1973)	1- Naphthol-6-sulphonic acid	4-sulphophenyl diazonium chloride	4-Toluene diazonium chloride	$k1 = 18.3x10^1$ $k2 = 2.46x\ 10^{-1}$
(Miyawaki et al., 1975)	Ammonia	Carbon dioxide	Sodium hydroxide	$k_1 = 4x10^1$ at 25^oc k_2=9.3
(Phelan and Stedman, 1981)	Hydrazine	Nitrous acid	Hydrogen azide	$k1 = 6.67$
(Paul et al., 1992)	Hydrochloric acid	Sodium hydroxide	Organic solvent	
(Bourne and Yu, 1994)	Hydrochloric acid	Sodium hydroxide	Ethyl chloroacetate	
(Bourne and Yu, 1994)	Hydrochloric acid	Sodium hydroxide	Methyl chloroacetate	$k1 = 1.3x10^8$ $k2 = 3.10x\ 10^{-2}$
(Guichardon and Falk, 2000; Fournier et al., 1996a)	Borate ion	Sulphuric acid	Iodide and iodate	$k1 = 10^8$ $k2 = f(I)$
(Baldyga et al., 1998)	Hydrochloric acid	Sodium hydroxide	2,2-dimethoxypropane	$k1 = 0.6$

Bourne et al., (Baldyga and Bourne, 1999; Bourne and Yu, 1994) investigated a set of reaction which follows the equations (2.39) and (2.40) for c*ompetitive- parallel scheme.* The set of reaction was a neutralization of hydrochloric acid and alkaline hydrolysis of monochloroacetate (methyl or ethyl) esters with sodium hydroxide as follows:

$$HCl + NaOH \xrightarrow{K_1} H_2O + NaCl \quad (2.41)$$

$$CH_2CLCOOC_2H_5 + NaOH \xrightarrow{k_2} C_2H_5OH + CH_2ClCOONa \quad (2.42)$$

The limitation in this set of reactions was the weaker flow fields (e.g. stirred tanks) where the energy dissipation should not be more than 1W/kg and 10 W/kg for ethyl ester and methyl ester system, respectively (Baldyga and Bourne, 1999). In addition, the authors found that this set of reaction requires a rapid gas chromatography analysis of the products because of the volatility of the components.

Another set of reaction that follows equation (2.39) and (2.40) is the iodide-iodate reaction which was first developed by Villermaux and his co-workers (Villermaux et al., 1993; Villermaux et al., 1992). This set of reaction was then further studied by (Guichardon and Falk, 2000; Fournier et al., 1996a; Falk et al., 1994) as an alternative system to assess the intensity of micromixing in the mixers/reactors. More details about this set of reaction are in the section below.

2.4.6 The Iodide- Iodate Technique

This set of reaction involves acid-base neutralization, (2.43), and an oxidation reaction, (2.44), called the Dushman reaction. The iodide-iodate reaction system (*coupling acid-base neutralization with Dushman reaction*) which belongs to the parallel competitive reaction scheme was implemented in this research as a model reaction to characterise the micromixing phenomena in intensified reactor systems, i.e. spinning disc reactors and microchannel reactors. The data were benchmarked against conventional semi-batch reactor using Rushton turbine impeller. The decision was taken after a very wide and careful screening of various reaction schemes that have been used as chemical probes to characterise the micromixing phenomena. The selection of the iodide-iodate reaction scheme has been made primarily on the basis of it being a well established and

well studied reaction system for micromixing characterisation. Also the chemicals involved in the system are not characterized by a high level of toxicity. Furthermore, the iodide-iodate reaction system fulfilled all the characteristics required when the test reaction was chosen for testing the intensity of mixing as discussed in section 2.7.1. In addition, the number of advantages associated with this reaction scheme as highlighted by Fournier et al. (1996a) are given as follows:

- Simple reaction schemes in order to avoid analysis of many products.
- Easy analysis of reaction products, i.e. spectrophotometeric technique.
- Known reaction kinetics, faster than mixing rate.
- Good sensitivity and reproducibility.
- Efficiency in stirred reactors, even in the case of fast mixing devices, i.e. rotating backed beds and spinning disc reactors.

These advantages encouraged the choice of the iodide-iodate reaction system as model reaction in this research to characterise the micromixing phenomena in intensified reactor systems. The iodide-iodate reaction system can be described in three steps as follows:

$$H_2BO_3^-{}_{(aq)} + H^+{}_{(aq)} \rightleftarrows H_3BO_{3(aq)} \quad \text{Acid-base neutralization, Quasi-instantaneous} \quad (2.43)$$

$$5I^-{}_{(aq)} + IO_3^-{}_{(aq)} + 6\,H^+{}_{(aq)} \rightleftarrows 3\,I_{2(aq)} + 3\,H_2O_{(aq)} \quad \text{Dushman reaction, Fast} \quad (2.44)$$

$$I_2 + I^- \rightleftarrows I_3^-{}_{(aq)} \quad \text{Equilibrium, Quasi-instantaneous} \quad (2.45)$$

The second reaction (2.44) which is a Redox reaction is fast being in the same time range as the micromixing process, but much slower than the acid-base neutralisation reaction (2.43). The iodine formed reacts further with iodide ions I^- to yield $I^-{}_3$ according to the quasi-instantaneous equilibrium (2.45). The degree of micromixing has a direct influence on reaction (2.44) and subsequently on reaction (2.45). The

measurement of I^-_3 by spectrophotometric absorption can therefore provide a good indication of the level of micromixing achieved in any given system. The lower the I^-_3 concentration, the lower is the segregation index, Xs, which means better micromixing. It should be noted that for perfect micromixing Xs = 0, the total segregation index is Xs = 1 and for partial segregation Xs varies between 0 and 1. This test system has been validated by different researchers including (Guichardon et al., 1997) for viscous media system, (Lin and Lee, 1997) for gas-liquid phase system,(Guichardon et al., 1995) for solid-liquid phase.

Recently, the iodide-iodate reaction system was the most used set of reaction for investigating the intensity of micromixing in different mixers/reactors by several research teams e.g. (Assirelli et al., 2008; Chu et al., 2007; Ferrouillat et al., 2006; Yang et al., 2006; Hai-Jian Yang, 2005).

2.4.6.1 Parameters to Characterise the Intensity of Micromixing

2.4.6.1.1 Segregation Index, Xs

The segregation index X_S, sometimes called product distribution, is defined as the value representing the actual yield of the undesired product (*Y*), compared with the maximum yield of undesired product (Y_{ST}), i.e. when the micromixing is infinitely slow and the total segregation occurs (Guichardon et al., 2000b; Guichardon and Falk, 2000; Fournier et al., 1996a). The segregation index is calculated by the following equation:

$$X_S = \frac{Y}{Y_{ST}} \qquad (2.46)$$

The segregation index, Xs, is a quantitative indicator of the degree of segregation in the reaction mixture. Its value is zero (0) in a homogeneous mixture and it increases as segregation appears. Its maximum value depends upon the initial composition of the reaction mixture, which is always less than 1. The value of X_S should be between $0 < X_S < 1$, $X_S = 0$ and $X_S = 1$, which indicates the maximum micromixing and segregation respectively:

Perfect micromixing: $X_S = 0$,

Total segregation: $X_S = 1$,

Partial segregation: $X_S = Y/Yst$.

The segregation index, X_S (product distribution), defined in that way shows the advantage to be easily measured experimentally. No measurement is necessary during the reaction. Only analysis of the initial and final reaction mixtures is required.

2.4.6.1.2 Micromixedness ratio, α

The micromixedness ratio, α, is another indicator that is used to measure the micromixing quality. The higher the value of micromixedness ratio, the lower the degree of segregation in the reaction mixture. The micromixedness ratio α can be defined as the fraction of a perfectly micro-mixed volume divided by the fraction of the volume remaining segregated and can be estimated as:

$$\alpha = \frac{1 - X_S}{X_S} \tag{2.47}$$

The significance of α is that it is closely related to the ratio of two characteristic times: that is, the reaction time and the micromixed time (Fournier et al., 1996a; Villermaux et al., 1992). Micromixedness ratio is derived from the segregation index, Xs, and is considered to describe the degree of segregation of the fluid. Guichardon and Falk (Guichardon et al., 2000b) described the micromixedness ratio, α, on the bases of the earlier ideas developed by Villermaux(Villermaux, 1986). They assumed that the real fluid is composed of two typical fluids, one which is perfectly micromixing of volume V_{PM} and the other fluid is totally segregated of volumeV_{ST}. This can be written as follows:

$$(V_{PM} + V_{ST})X_S = V_{PM}(X_S)_{perfectmicromixing} + V_{ST}(X_S)_{total\ segregation} \tag{2.48}$$

Where:

X_S = 0 for the perfect micromixing and X_S = 1 for the total segregation, then the micromixedness ratio α can be described by the following expression:

$$\alpha = \frac{V_{PM}}{V_{ST}} = \frac{1 - X_S}{X_S} \tag{2.49}$$

The complete procedure for the of segregation index (Xs) calculation (Guichardon et al., 2000b; Fournier et al., 1996a) is presented in Chapter 4, section 4.5 for both semi-batch and continues processes.

2.4.6.2 Considerations for Operating Conditions

2.4.6.2.1 Reactants Feed System Configuration in Semibatch Reactor

As reported in (section 2.6.4), the *coupling of acid-base neutralization with Dushman reaction* was chosen as a model reaction in this research in order to characterise the micromixing performance in four different types of reactors. In the first part of the research, the experiments were carried out in a Semibatch reactor (SBR) with two feed points where one of the reactants, i.e. sulphuric acid was added to a solution containing the others, i.e. H_3BO_3 , NaOH, KI and KIO_3. As Baldyga and Bourne (1999) suggested, there are three different possible feed strategies that can be implemented to carry out the iodide-iodate reaction. The reactants can be added using three different possible options:

I. Concentrated H_2SO_4 is added slowly to a pre-mixture of H_3BO_3, KI and KIO_3.

II. Concentrated H_3BO_3 and H_2SO_4 can be added slowly in separate streams to a more diluted solution of KI and KIO_3.

III. A concentrated pre-mixture of H_3BO_3 and KI and KIO_3 is slowly added to the diluted H_2SO_4.

For simplicity and practicality, all the SBR experiments were carried out based on the first option.

2.4.6.2.2 Influence of pH on the segregation index, Xs

As mentioned above in section (2.4.51.2), Villermaux et al. have developed and extensively studied the iodide-iodate system and have established the operating parameters that allow a correct application of this reaction scheme in relation to both the chemistry of the system and the type of measuring instruments. Originally, the iodide-iodate method was developed to characterize mixing efficiency in stirred tanks (Villermaux et al., 1992).

The application of the iodide-iodate reaction system requires that the hydrogen ions are in less than stoichiometric amount in respect to the borate ions. In addition to this, the spontaneous formation of iodine before the reactions take place must be prevented by controlling the pH (the initial pH) of the reactive mixture. To fulfil this condition, a sequence was followed for the preparation of the whole reactive mixture. First, the Sodium hydroxide is added to the solution containing borate ions to form a buffer solution. Then the iodide and iodate ions are added to this solution. The pH of buffer solution must be between 8.5 and 9.5 (Guichardon and Falk, 2000) . In the iodide-iodate reaction system, the borate ions play two roles. Firstly, they are reactants in the neutralisation reaction (2.39) and secondly, they had a role as buffer thus keeping the pH of the reactive mixture consonant.

Another consideration that was taken into account was the formation of iodine does not to occur spontaneously in order for the final concentration of iodine to reflect only the mixing conditions in the reaction environment. This means that the final pH (the pH of the product) does not have to be below the critical value of pH*, i.e. the value of pH from which iodine does not thermodynamically appear. pH* can be determined from the electric potential-pH diagram, depending on the total iodine concentration. When the final pH values become lower than the critical value (pH*), the formation of iodine from iodide and iodate ions becomes possible thermodynamically and therefore operating conditions with pH values lower than pH* must be adjusted .Conversely, if the final pH is too high, the iodine formed is unsTable and no tri-iodide ion can be detected by UV-vis spectrophotometer. It can be concluded that if the initial and the final values of pH are higher than pH*, the solution containing KI and KIO_3 is sTable and no iodine would thermodynamically appear. Hence, the measured tri-iodide can

only be formed due to the segregation of the fluid and wholly associated with the micromixing efficiency of the reactor.

As it is recommended by Guichardon and Falk (2000), the micromixing experiments must be carried out at pH values higher than pH*. The reactant concentrations in this micromixing experiments were chosen in order to fix the pH at 9.45 for the reactive mixture on an average and the pH for the buffer solution, i.e. H_3BO_3 and NaOH was in the range of 9.0 - 9.5. The pH value after finishing each experiment was measured and found to be always higher than the critical value (pH*) i.e., pH >7.

2.4.6.2.3 Influence of acid feed rate on the segregation index, Xs

Many researchers have invested a great deal of effort in studying the influence of the acid feed rate on the segregation index, Xs (Assirelli et al., 2002; Guichardon and Falk, 2000; Baldyga and Bourne, 1999; Fournier et al., 1996a; Bourne and Thoma, 1991). It has been observed that the segregation index can be strongly influenced by the acid feed rate if reaction is carried out in a semi-batch reactor (SBR). The feed time used in the experiments must exceed *a critical time (t_c)* in order to make sure that experiments are carried out in the micromixing-controlled regime.

In some more details, the *critical injection time* (t_c) is the time which the segregation index reaches a constant value at different injection time with constant hydrodynamic and concentration parameters, after which macromixing does not play any role during injection and segregation index reaches asymptotic values.

In addition, to only quantify the effect of micromixing in a semi-batch reactor, it is necessary to work in a medium where perfect macro-mixing conditions are fulfilled (Guichardon and Falk, 2000). When the reactor is perfectly macro-mixed and the state of segregation is uniform within the reactor volume, the extent of an instantaneous reaction with unmixed reactants is directly related to the strength of micro-mixing which controls the contact between reactants. Bourne and Thoma (1991) reported that for rapid acid injection conditions, i.e. changing in the feed time from low to high flow rates and keeping all the chemical and hydrodynamic conditions constant, the plume is not well dispersed in the tank and macroscopic concentration gradients may influence

the results by yielding high quantity of unwanted product, i.e., high value of the segregation index and for our particular case the segregation index,(Xs), becomes a function of the feeding rate.

In contrast, when acid injection rate is very low, macromixing effects are eliminated and the results which are given by chemical test reactions are only micromixing relevant.

In fact, critical injection time (t_c) should be determined for each new set of experimental conditions. This is however not practical. One solution to this problem is the determination of (t_c) under the worst experimental conditions, for instance, the lowest impeller rotational speed, the highest acid concentration and the nearest acid injection point to the fluid surface. Such t_c is then the longest t_c of all the experiments. If this t_c is used as the feed time, it is certain that all experiments are carried out in the micromixing-controlled regime. Figure (2.19) shows the influence of the feed rate on the Segregation Index (X_s) for a semi-batch stirred tank reactor (SBR).

In this research (section 5.2.1 in Chapter 5), the influence of acid feed rate in SBR system has been checked for the worst micromixing operating conditions for both water system and 75 wt% glycerol system.

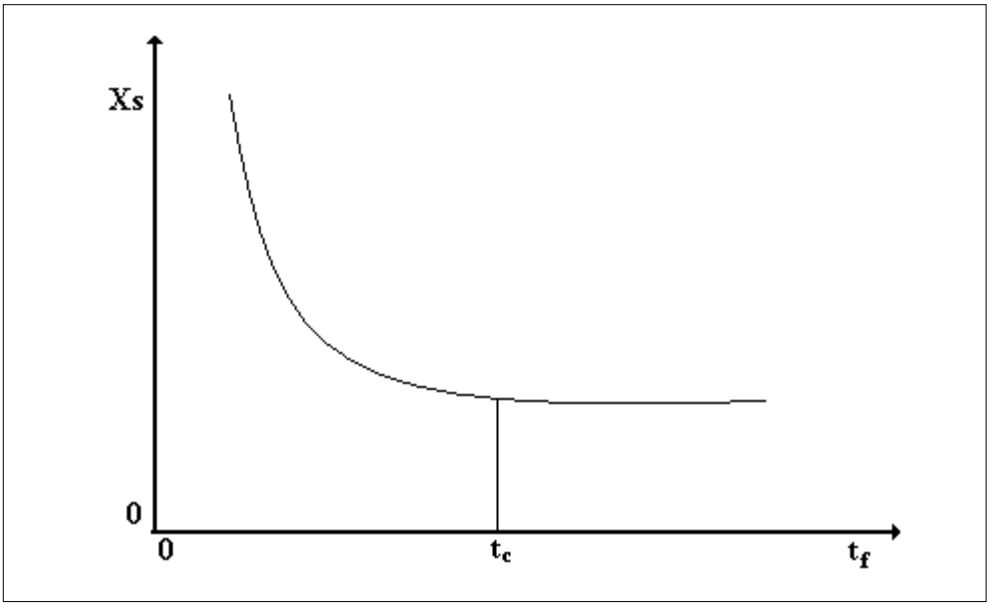

Figure 2.20: Segregation Index (X_s) as a function of feed time (t_f) for a semi-batch stirred tank reactor Adopted from (Baldyga and Bourne, 1992)

2.4.6.2.4 Feed pipe diameter effect on the segregation index,(Xs) in Semibatch reactor (SBR)

Fournier et. al. (1996a) studied the effect of feed pipe diameter on the segregation index. A pipe with diameters of 1 and 2 mm were used in the experiments for one litre SBR. The pipe diameter is an important parameter because it controls the size and the kinetic energy of initial acid eddies at the pipe outlet. The results confirmed at the impeller speed equals 7.5 s^{-1} the segregation index was found to increase with an increase in the pipe diameter. This confirmed that the larger the pipe diameter, the bigger eddy will be produced.

Guichardon and Falk (2000) characterised the micromixing efficiency by the iodide-iodate reaction system in a 1L stirred tank equipped with a Rushton turbine. The acid injection was done with a 2 mm diameter pipe. In the current work, acid was injected through a 1.78 mm diameter pipe made of stainless steel.

2.4.6.2.5 Influence of acid concentration and total flowrate ratio, ($\boldsymbol{R}$)

The sulphuric acid must be in stoichiometric default in the reactor with respect to all borate ions,($H_2BO_3^-$) (Monnier et al., 1999a) because there must remain iodide ions (I^-) to react with (I_2) form tri-iodide (I_3^-), the concentration of I_3^- characterizes the micromixing. If the concentration of the sulphuric acid is improperly selected, the amount of the tri-iodide (I_3^-) formed from reaction (2.45) is too high or too small and the optical density may not be in the range of the spectrophotometer scale.

To choose the proper flow rate ratios of the reactants, the following considerations need to be applied:

- The molar flow of acid ions (H^+) must be smaller than the molar flow of ($H_2BO_3^-$), (I^-) and (IO_3^-)because the acid must be in stoichiometric default.

- The residence time must be greater than the micromixing time.

- If $[I_3^-]$ is high then the spectrophotometer can be saturated. If the absorbance value (D) is too high. However it is necessary that locally $[H^+]$ is large.

In this research, we decide to start with flows rate ratio R (ratio of the volumetric iodide-iodate-borate flow rate, Q_I, and the acid flow rate, Q_H, where $R= Q_I/Q_H$)) equal to 7 as starting point (Yu-Shao CHEN, 2004; Monnier et al., 2000; Monnier et al., 1999a) .

2.5 Residence time Distribution (RTD)

2.5.1 Introduction

The residence time distribution (RTD) is a chemical engineering concept that was introduced by (Fogler, 2006; Cozewith and Squire, 2000; Levenspiel, 1972; Danckwerts, 1953), as a useful tool to investigate the mixing performance in the reactor at the level of macromixing, that is spatial distribution of materials on the macroscopic scale. The residence time distribution can also be described as the time history of a fluid inside a reactor. It is the probability distribution function that describes the amount of time a fluid element could spend inside the reactor. The residence time distribution has a direct influence on the yield and the selectivity of reactions, especially those that involve competitive reaction steps.

Ideal reactors are generally classified as having either plug-flow or perfectly-mixed characteristics depending on the RTD of material in the system. The RTD function can thus be used to compare the behaviour of real reactors to the ideal models.

2.5.2 The Residence Time Distribution Development History and Its Applications

It is a common knowledge that the mixing regime within a system does not instantly conform to the two theoretical mixing regimes of plug-flow or complete mixing which are universally, though incorrect, assumed in the design process (Danckwerts, 1953). This discrepancy can be investigated using the RTD, which describes the macromixing patterns within a mixing device.

Characterisation of the mixing regime using the RTD originated from the theoretical studies on laminar flow reactors (Bosworth, 1948) and the experimental measurements on fluidised beds (Gilliland and Mason, 1952). The generality of this method was due to the original work done by Danckwerts, (1953) and Zwietering (1959) in the 1950s. These researchers presented the general mathematical properties of residence time theory, with specific consideration to packed beds, blenders, reactors and tubular devices. Following this work, several publications have presented both detailed and summary of the developments in the RTD experimental and data analysis techniques that are currently available for use (Fogler, 1992; Nauman and Buf ham, 1983; Levenspiel, 1972).The concept RTD was first applied in the field of chemical engineering. Subsequently chemical reactors on which RTD studies have been conducted include the following:

I. tubular reactors (Danckwerts, 1953);
II. Fluidised beds (Levenspiel, 1972; Danckwerts et al., 1954);
III. Screw extruders (Wolf and White, 1976);
IV. Packed columns (Oliveros and Smith, 1982);
V. Bubble columns (Deckwer and Schumpe, 1993);
VI. Pulsed baffle bubble columns (Ni, 1994) both of varying operating i.e. co-current and counter-current

Due to the multiphase nature of some of these systems , investigation using the RTD is sometimes performed on the basis of the gas and solid phases. The RTD also has been utilized in a wide range of scientific fields including petroleum engineering (Hall and Hughes, 1993), medical (Lee et al., 1997) and geophysics (Robinson and Tester, 1984).

The RTD has been significantly gaining recognition in the most of chemical industries due to the emphasis being placed on design engineers to produce good and accounTable design for the process equipments. Knowledge of RTD would therefore be very helpful for the following reasons:

- ✓ Avoidance of any problems in the existing CSTR such as by-passing channelling and stagnates in packed-bed reactor (PBR).

- ✓ Prediction of the conversation or product distribution for new reaction in an existing reactor.
- ✓ Avoidance of stagnant regions and short-circuiting or bypass in plug-flow reactor (PFR).

2.5.3 Methods for RTD Measurement

The RTD can be obtained by stimulus-response technique**.** In this technique the inert chemical called a *tracer* is injected into the reactor (in the feed stream) at t=0 and then the tracer concentration(C) is measured in the effluent stream as a function of time. There two types of tracers i.e. coloured and radioactive materials. Besides being inert, the tracer needs to be soluble in the reactants and not be adsorbed on the walls of the reactor (where, for example, catalysed walls are employed). The most used injection methods are:

I. Pulse input
II. Step input

2.5.3.1 Pulse input injection method

In this method an amount of tracer is suddenly injected in one shot into the feed stream entering the reactor in as short time as possible. The effluent concentration is then measured as a function of time. The principal difficulties with the pulse technique lie in the problems connected with obtaining a reasonable pulse at reactor's entrance. The injection must take place over a period which is very short compared with residence the times in various segments of the reactor or reactor system, and there must be a negligible amount of dispersion between the point of injection and the entrance to the reactor system. If these conditions can be fulfilled, this technique represents a simple and direct way of obtaining the RTD (Fogler, 1992).

2.5.3.2 Step input injection method

In the step input method, a constant flow rate of tracer is added to the feed stream at time t=0. The concentration of tracer in the feed of the reactor is kept at this level until the concentration in the effluent is identical with the feed concentration.

The step input technique is usually easier to carry out experimentally than the pulse test. Its additional advantage over the pulse input technique is that the total amount of tracer in the feed over the period of the test does not have to be known as it does in the pulse test. One possible drawback of this technique is that it is sometimes difficult to maintain a constant tracer concentration in the feed. Obtaining the RTD from this test involves the differentiation of the data which presents an additional, and probably more serious, drawback to the technique. This is because the differentiation of data can guide to large errors. A third problem lies with the large amount of tracer needed for this test. If the tracer is very expensive, a pulse test is advised to use for minimizing the cost. Figure (2.21) shows the concentration curves that can be produced from pulse and step tracer injection method.

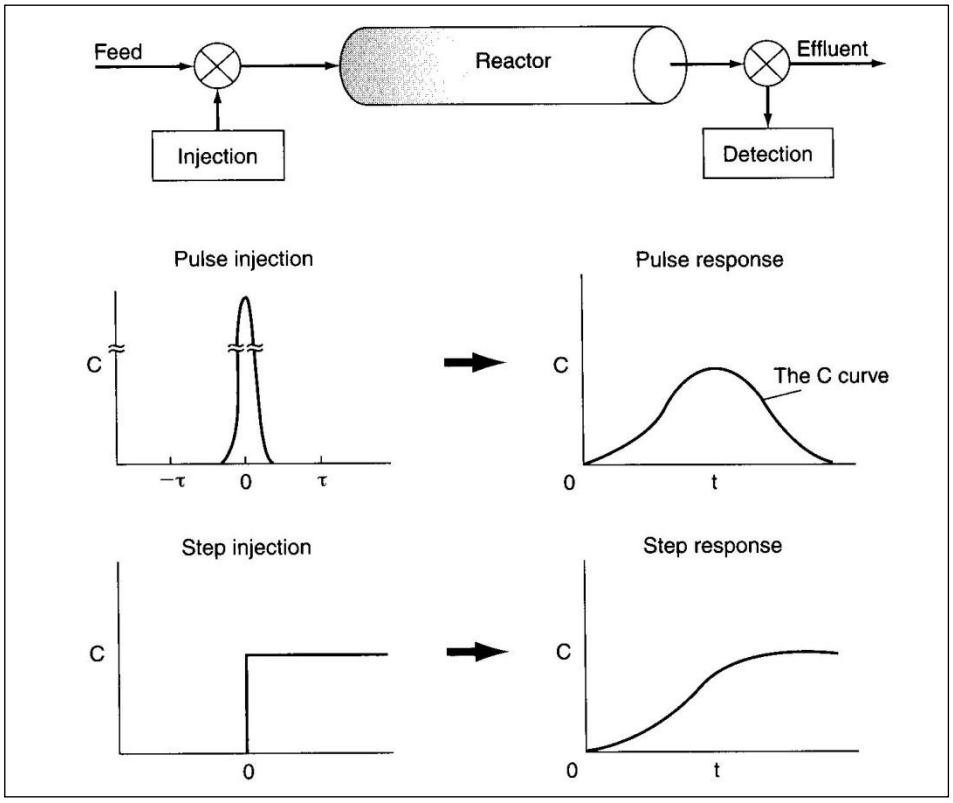

Figure 2.21: The C curve from Pulse and Step methods (adopted from Fogler (2006))

2.5.4 RTD Characterisation

To obtain the RTD, tracer concentration data collected from the reactor need to be analysed and manipulated so that functions E(t) and F(t) can be generated.

2.5.4.1 RTD Function E(t)

The function E(t) is called the residence time distribution function. It is a function that shows, in a quantitative manner, how much time different fluid elements have spent in the reactor. It is expressed as:

$$E(t) = \frac{C(t)}{\int_0^\infty C(t)dt} \tag{2.50}$$

Where:

C (t) is the concentration of the tracer in the outlet stream at time t after injection

$$\int_0^\infty C(t)dt = \text{area under the curve for C(t) vs. t} \tag{2.51}$$

E(t) represents the fraction of the tracer with a residence time between t and t+dt which can tell us how long different molecules have been in the reactor. The RTD function E(t) can be determined directly from a pulse input technique. Figure (2.22) shows the shape of E (t) function. Figure 2.23 shows the shapes of RTD for the different types of reactors that usually observed.

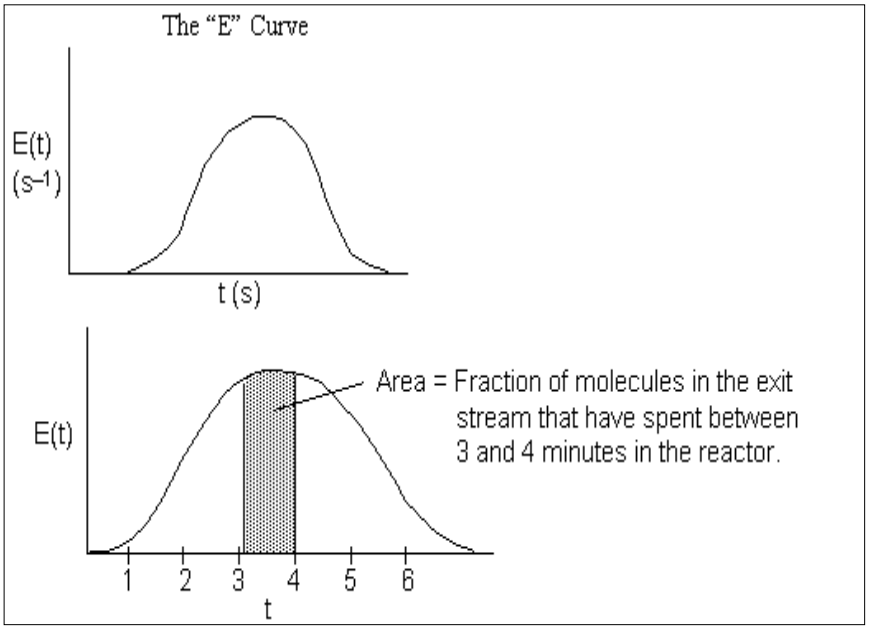

Figure 2.22: The residence time distribution function curve, E(t). adopted from Fogler (2006))

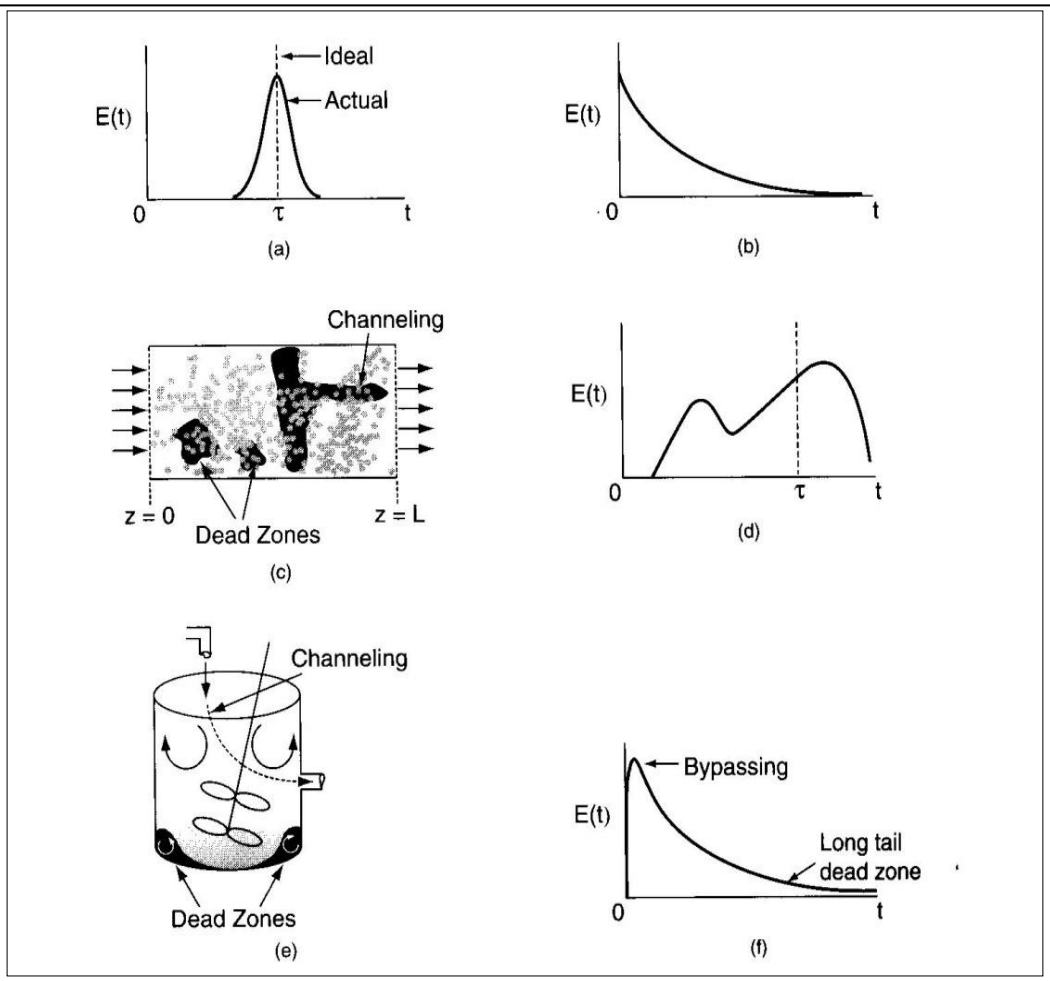

Figure 2.23: Typical E(t) curves for the different types of reactors that are commonly observed (a) near plug-flow reactor; (b)near perfectly mixed CSTR (c) packed-bed reactor with dead zones and channelling; (d)E(t) curve for packed-bed reactor in (c); (e) tank reactor with short-circuiting flow (by-bass); (f) E(t) for tank reactor with channelling (by-passing or short circuiting) and a dead zone in which the tracer slowly diffused in and out (adopted from Fogler (2006))

2.5.4.2 Cumulative RTD function F(t)

The Cumulative RTD Function F(t) can be determined directly from a step input technique. It is defined as the fraction of molecules exiting the reactor that have spent a time t or less in the reactor. The Cumulative RTD function F (t) can be derived as:

$$C_{out} = C_0 \int_0^t E(t)dt \qquad (2.52)$$

Dividing by C_0 yields

$$\left[\frac{C_{out}}{C_0}\right]_{step} = \int_0^t E(t)dt \tag{2.53}$$

$$F(t) = \left[\frac{C_{out}}{C_0}\right]_{step} \tag{2.54}$$

Differentiating the above expression to obtain the RTD function E (t), the RTD function E (t) can be defined as:

$$E(t) = \frac{d}{dt}\left[\frac{C(t)}{C_0}\right]_{step} = \frac{dF}{dt} = \frac{F(t)_2 - F(t)_1}{t_2 - t_1} \tag{2.55}$$

Numerically, the Cumulative RTD function *F (t)* can be determined from the area under the curve of the *F* (t) vs t. Figure 2.24 shows the shape of the F-curve produced from the step input technique.

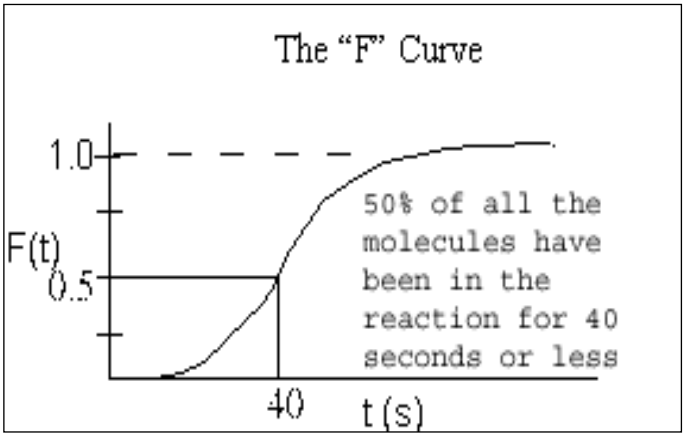

Figure 2.24: Cumulative distribution curve, F(t).adopted from Fogler(2006)

2.5.4.3 The Moments of the RTD (Mean residence Time and Variance)

It is common to characterize a distribution by some numerical values. For this purpose the most import measure is the location of the distribution (Fogler, 2006; Levenspiel, 1999; Levenspiel, 1972). This is called the mean value or the centroid of the distribution i.e. the mean residence time which is the measure of the average time spent by the molecules in the reactor. Thus mean residence time is given by:

$$t_{mean} = \int_0^{\infty} tE(t)dt \tag{2.56}$$

The value of the mean residence time (t_m) can be determined from the area under the curve of the t E(t) vs. t, as illustrated in Figure 2.25.

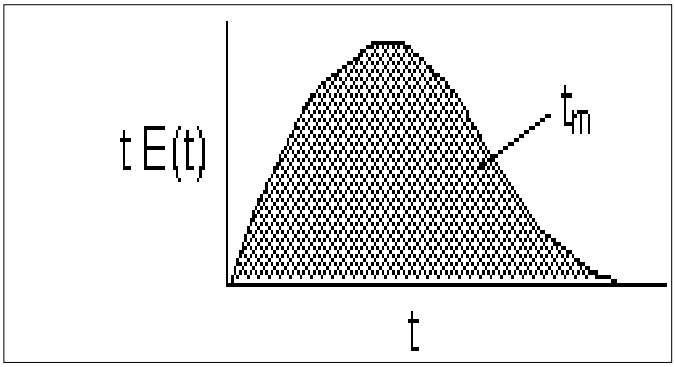

Figure 2.25: Calculating the mean residence time

The second important descriptive quantity is the variance which is defined as the square of standard deviation and which represents the the spread of the distribution. It has units of $(time)^2$; the greater the value of this factor, the greater the distribution spread will be. This can be calculated by the equation 2.57 given below.

$$\sigma^2 = \int_0^{\infty} (t - t_m)^2 E(t)dt \tag{2.57}$$

The value of the mean residence time (t_m) can be determined from the area under the curve of the $(t - t_m)^2$ E(t) vs. t, as shown in Figure 2.26.

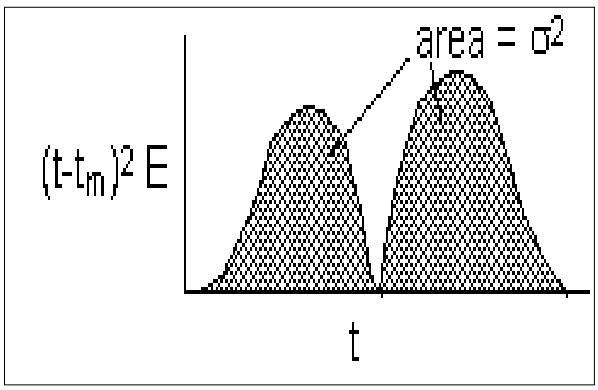

Figure 2.26: Calculating the variance. (Adopted from Fogler (2006))

2.5.5 Flow Models in the Reactors

The determination of the flow pattern is important for the prediction of the performance or diagnosis of the weakness of the reactor. The most two common flow models encountered in practice are dispersed plug flow model and back mixed model(Levenspiel and Bischoff, 1959).

2.5.5.1 Dispersed plug flow model

In dispersed plug flow (piston flow) model the flow rate and velocity profile are uniform over any cross section normal to the direction to fluid motion. Also there is negligible axial mixing due to either diffusion or convection. When carrying out competitive chemical reaction, plug flow is normally desirable so that products are removed quickly from any fresh reaction(Sparks, 1996; Ekpo, 1972).

2.5.5.2 Back-mixed flow model

This is usually applied for the stirrer tanks reactors where the concentration profile is similar at any point of the reactor. In this flow model, the products of the reaction will re-circulate back into the reaction zone to combine with the fresh reagents consequently the more undesirable products will be produced. This type of pattern is not preferred if the reaction is a competitive chemical reaction(Sparks, 1996).

2.5.6 The dispersion models

The dispersion model is a helpful tool used for demonstrating the flow in the real reactors for the purpose of analysing poor flow (poor mixing) and reactor scale up. There are different types of dispersion models which depends on the type of flow, whether the flow is close to plug, mixed, or somewhere in between the two. In the case of small deviation from plug flow, there are two types of models for this, namely, the tanks-in series model and axial dispersion model. These types of models may be applied to the following types of flow conditions: turbulent flow in pipes, laminar flow in very long tubes, flow in packed beds, shaft kilns, long channels, screw conveyers, etc(Levenspiel, 1999).

2.5.6.1 Tanks-in-Series Model

The tanks-in series model is simple and can be used with any kinetics. It can be extended without too much difficulty to any arrangement of compartments, with or without recycle. It demonstrates the effect of backmixing when setting up a series of N ideal stirred tanks along the reactor such that the outlet concentration of the *(i-1th)* tank is the inlet concentration for the *ith* tank. The flow pattern is quantified by estimating an appropriate N to represent the RTD data. Plug flow is approached when N= ∞, and it is mixed flow when N=1. This model can always be used along with the dispersion model for a not very large deviation from the plug flow(Levenspiel, 1999; Ekpo, 1972).

Both models give identical results for all practical purposes. The type of model used depends on the choice of the researcher.

The number of tanks in series is given as:

$$N = \frac{1}{\sigma_\theta^2} \tag{2.58}$$

Where σ_θ^2 is the normalized variance of residence time distribution (-) which can be estimated as:

$$\sigma_\theta^2 = \frac{\sigma^2}{t_m^2} \tag{2.59}$$

The number of tanks in series expression represents the number of tanks necessary to model the real reactor as N ideal tanks in series. As the number of tanks increases, the variance decreases.

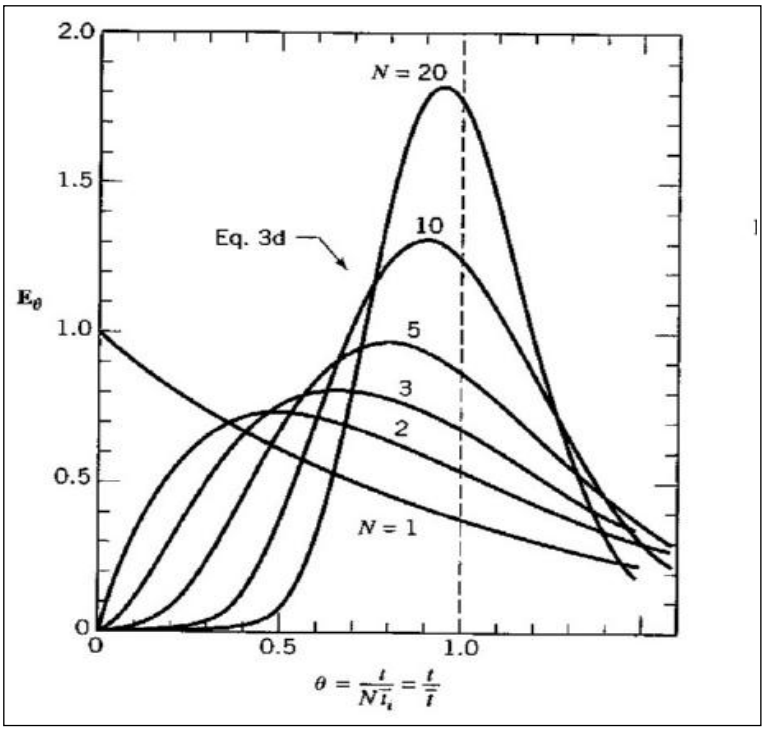

Figure 2.27: The RTD curves for the tanks-in-series model, (adopted from (Levenspiel, 1999))

2.5.6.2 Axial dispersion model

The main advantage of axial dispersion model is that all correlations for flow in real reactors are always based on this model. When a plug flow of a fluid is considered with some degree of back-mixing placed on top of it, its magnitude is independent of its position within the vessel. This condition implies that there exist no stagnant pockets and no gross bypassing or short-circuiting of fluid in the vessel. Thus, this flow model is called the axial dispersed plug flow model. Figure 2.28 illustrates the visualized conditions for the plug and dispersed flows. The velocity profile in the ideal plug flow is flat while it fluctuates in dispersed plug flow due to different flow velocities and due to molecular and turbulent diffusion (Levenspiel, 1999).

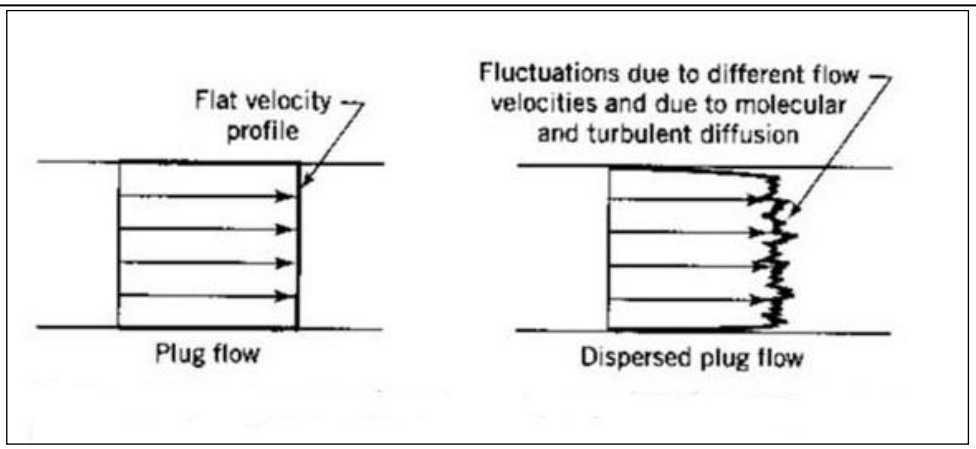

Figure 2.28: Illustration of the dispersion i.e. dispersed plug flow model (adopted from Levenspiel (1999))

In order to estimate the extent of deviation from ideal-plug flow conditions, a dispersion number is needed to be calculated. The dispersion number is a measure of the ratio of the rate of transport by diffusion and the ratio of transport by convection and it describes the non-ideal reactors, where the axial dispersion is applied to the plug flow of a fluid. The dispersion number can be defined as:

$$Dispersion\ number = \frac{D}{UL} \tag{2.60}$$

The axial dispersion coefficient (D) uniquely characterizes the degree of back mixing during flow. If the dispersion number approaches zero, dispersion is considered to be negligible and the behaviour of the reactor is approaching that of a PFR. If the dispersion number approaches infinity, there is a large degree of dispersion, and the behaviour of the reactor approaches mixed flow as in a STR. Thus,

D / UL → 0 the dispersion is negligible, hence plug flow
D / UL → ∞ means large dispersion, hence mixed flow.

Figure 2.29 illustrates the shape of Residence Time Distribution curves i.e. E (t) curve for dispersed plug flow and mixed flow.

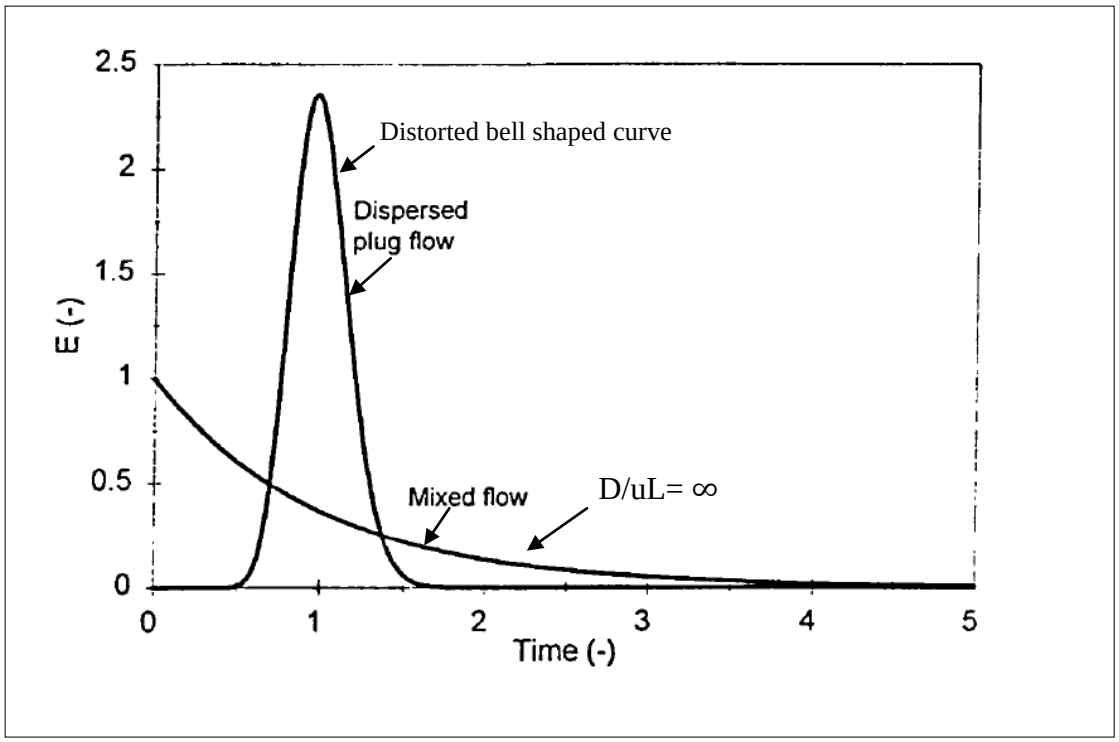

Figure 2.29: Residence Time Distribution curves for dispersed plug flow and mixed flow (adopted from Levenspiel (1972))

2.5.6.2.1 The Dispersion Model for Small Extents of Dispersion, $\frac{D}{UL} < 0.01$

As mentioned earlier, the dimensionless group D/*UL* is called the axial dispersion number. If the idealised pulse has been introduced to the flow, the flowing fluid then dispersion modifies this pulse as illustrated in Figure 2.30.

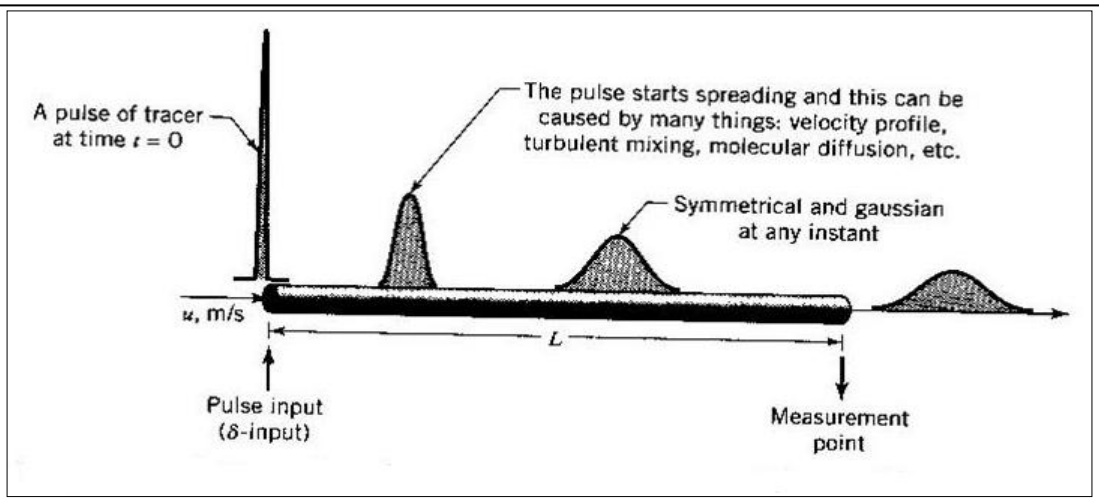

Figure 2.30: The spreading of tracer according to the dispersion model (adopted from Levenspiel (1999))

When D/*UL*, is small $\left(\frac{D}{UL} < 0.01\right)$, the extent of axial dispersion is very small, thus the spreading tracer curve does not considerably change in shape as it passes the measuring point (during the time it is being measured) and the E curve is a symmetrical Gaussian curve. There are a number of methods to calculate the axial dispersion number D/*UL* from the experimental curve which are given by the following:

I. by calculating its variance
II. by measuring its maximum height
III. by measuring its width at the point of inflection
IV. by finding the width which includes 68% of the area

The first method was considered in this research, Aris (1958) has shown, for small extents of dispersion i.e. $D/Ul < 0.01$, as

$$\sigma_\theta^2 = 2\left(\frac{D}{UL}\right) \tag{2.61}$$

and

$$\sigma_\theta^2 = \frac{\sigma^2}{t_m^2} \tag{2.62}$$

Where:

σ_θ^2 = normalized variance of residence time distribution (-)

$\sigma^2 =$ The variance of residence time distribution (-)

$t_m =$ The experimental mean residence time (sec)

$\left(\frac{\mathrm{D}}{\mathrm{UL}}\right)$ = dispersion number (-)

2.5.6.2.2 The Dispersion Model for Large Extents of Dispersion, $\frac{D}{UL} > 0.01$ (Levenspiel, 1999)

For large deviation from plug flow i.e. $\left(\frac{D}{UL} > 0.01\right)$, the pulse of response is broad and it passes the measurement point slowly enough that it changes shape, which gives a non-symmetrical E curve. In this case, $\frac{D}{UL}$ is usually evaluated according to the corresponding boundary conditions. Two types of boundary conditions are considered. These are: (i) the flow is undisturbed as it passes the entrance and exit boundaries (this is called the open B.C.), (ii) plug flow outside the vessel up to the boundaries (this is called the closed B.C.). This leads to four combinations of boundary conditions namely, (1) closed-closed, (2) open-open, (3) open-closed, (4) closed-open. These four boundaries are discussed in detail below:

I. The *closed vessel* can be defined as one in which fluid movement is by bulk flow only, and there is plug flow entering and leaving the streams. Diffusion and dispersion are absent at the entrance and exit and there is no movement of material upstream and out of the vessel by eddies.

II. The *open vessel* is one where neither the entering nor leaving fluid streams satisfies the plug flow requirements of the closed vessel.

When only the input or the output fluid stream satisfies the closed vessel requirements, the system can be considered as a *closed-open* or *open-closed* vessel. Figure 2.30

illustrates the various boundary conditions used with the dispersion model for open and close vessels.

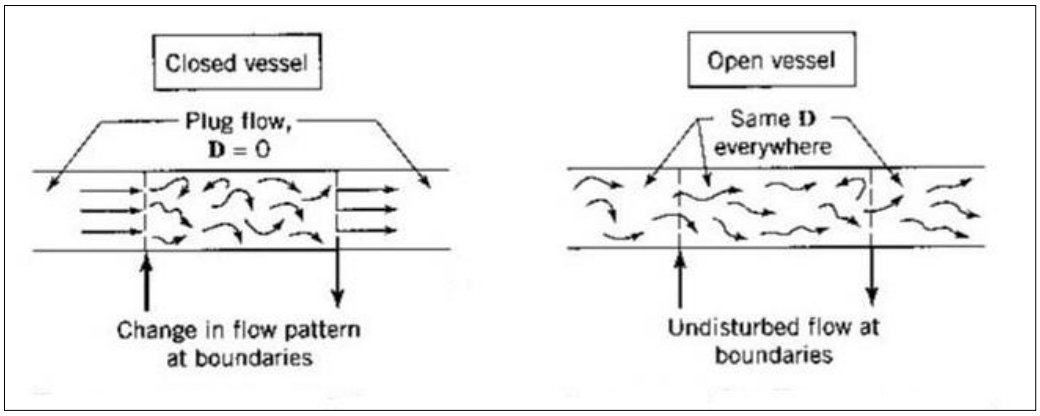

Figure 2.31: Various boundary conditions used with the dispersion model (adopted from Levenspiel (1999))

Levenspiel (1999) gives the mathematical expression for the axial dispersion number (D/UL) for the case when the Deviation from plug flow is large as follow:

I. For large Deviation from plug flow and open-open reactor boundary condition, D/UL > 0.01 (Levenspiel, 1999)

$$\sigma_{\theta,OO}^2 = 2\left(\frac{D}{UL}\right) + 8\left(\frac{D}{UL}\right)^2 \quad (2.63)$$

II. For large Deviation from plug flow and close-close reactor boundary condition, D/UL > 0.01 (Levenspiel, 1999)

$$\sigma_{\theta,cc}^2 = 2\left(\frac{D}{UL}\right) - 2\left(\frac{D}{UL}\right)^2 \left[1 - e^{-UL/D}\right] \quad (2.64)$$

2.5.6.3 The Peclet Number,(Pe)

The degree of dispersion in the axial direction can be also presented in terms of Peclet number (Pe). The Peclet number (Pe) is the inverse of the dispersion number (Pe = UL /D). The Peclet number (Pe) can be defined as:

$$\mathrm{Pe} = \frac{Rate\ of\ transport\ by\ convection}{Rate\ of\ transport\ by\ diffusion\ or\ dispersion} = \mathrm{UL}/\mathrm{D} \qquad (2.65)$$

The following Peclet number (Pe) values are used to categorize the degree of dispersion (Higgins, 2000; Levenspiel, 1972)

- Pe = <10 → large amount of dispersion;
- Pe = 10 -100 → Intermediate amount of dispersion;
- Pe = >100 → small amount of dispersion.

3. Aims and Objectives of the Present Investigation

The main aim of this research is to study the fundamental science underlying the micromixing characteristics taking place within the thin films flowing on the surface of rotating disc reactors. The research involves the use of a parallel competing reaction scheme namely the acid-base neutralization coupled with the Dushman reaction. This reaction scheme was chosen because most of the available literature on the experimental procedure and techniques for quantitative micromixing measurements in conventional semi-batch reactors (SBRs) is based on this particular reaction.

The research intends to quantify the micromixing in terms of the segregation index, (Xs), micromixedness ratio, (α), power dissipation (ε), micromixing time(t_m). It is also intended that the effects of various parameters as listed below will be investigated.

I. Disc rotation rates
II. Feed flow rates
III. Disc diameter
IV. Disc surface configurations (smooth, grooved, etc.)
V. liquids of varying concentration, and viscosities
VI. Various feed systems (i.e. single-point feed system/multi-point distributor) and locations.

The data obtained from 10 and 30cm SDRs micromixing experiments in terms of the segregation index,(Xs), micromixedness ratio, (α), power dissipation (ε), micromixing time (t_m) will be benchmarked against a 1.37 l conventional semi-batch reactor (SBR) using a conventional Rushton turbine impeller. . It is also intended as part of this study to compare the degree of micromixing in SDRs with that in continuous tubular flow reactors in the form of narrow channels (NCR) of 1.0mm diameter and three different lengths namely 5, 10 and 15 cm (Y and T shapes).

The characteristic segregation index, (Xs), will be obtained under a range of operating conditions of angular velocity of the disc, (ω), total flow rate and liquid, (Q_t) and viscosity, (μ), enabling the best micromixing conditions to be selected for a given reaction system in the SDR. To this end, a micromixing model linking these parameters

will be developed by regression analysis using Minitab software (Version 15.0) for the 10 and 30cm SDR on the basis of the data collected.

Another objective of this investigation is to experimentally determine the Residence Time Distribution (RTD) of the liquid flow in the 30cm SDR for a range of operating conditions including disc rotational speeds, (N), total flow rate of liquid, (Q_t) and viscosity, (μ), in order to predict the macromixing behaviour of the thin film flows on SDR i.e. either a plug flow or a back-mixed profile. The RTD study will be based on mixing an inert dye (methylene blue) into the liquid film and using offline UV-Vis spectroscopy to assess the level of dye in samples collected at various time intervals after the dye injection. It is also intended to estimate the Dispersion number from the RTD results for the purpose of characterising the extent of dispersion in the thin film flow on the rotating disc.

4. Experimental Facilities and Procedures

4.1 Introduction

This Chapter describes the experimental and analytical facilities and procedures used in the micromixing studies and the Residence Time Distribution (RTD) experiments.

Four different reactors rigs were used in the micromixing aspect of the study. The first rig is the semi-batch rig (SBR) which is used to characterise the micromixing performance for benchmarking purposes. The second and third rigs were the 10cm and 30cm SDRs. The fourth rig consisted of the Y and T- junction narrow channel reactors rig (NCRs) having varying lengths.

In order to compare the performance of the 10 and 30 cm SDRs in terms of the intensity of micromixing with the results obtained from the SBR as well as the Y and T- junction NCRs, a large number of micromixing experiments were performed. In addition, macromixing experiments were performed to predict the Residence Time Distribution (RTD) for the 30cm spinning disc reactor for the purpose of predicting the type of flow pattern on the rotating disc and to determine whether the spinning disc reactor behaves as plug-flow or a backmixed reactor.

4.2 Micromixing Reactor Facilities

4.2.1 Semi-Batch Reactor (SBR) Experimental Rig

Figure 4.1 shows the general view of the experimental rig setup used in performing the SBR experiments.

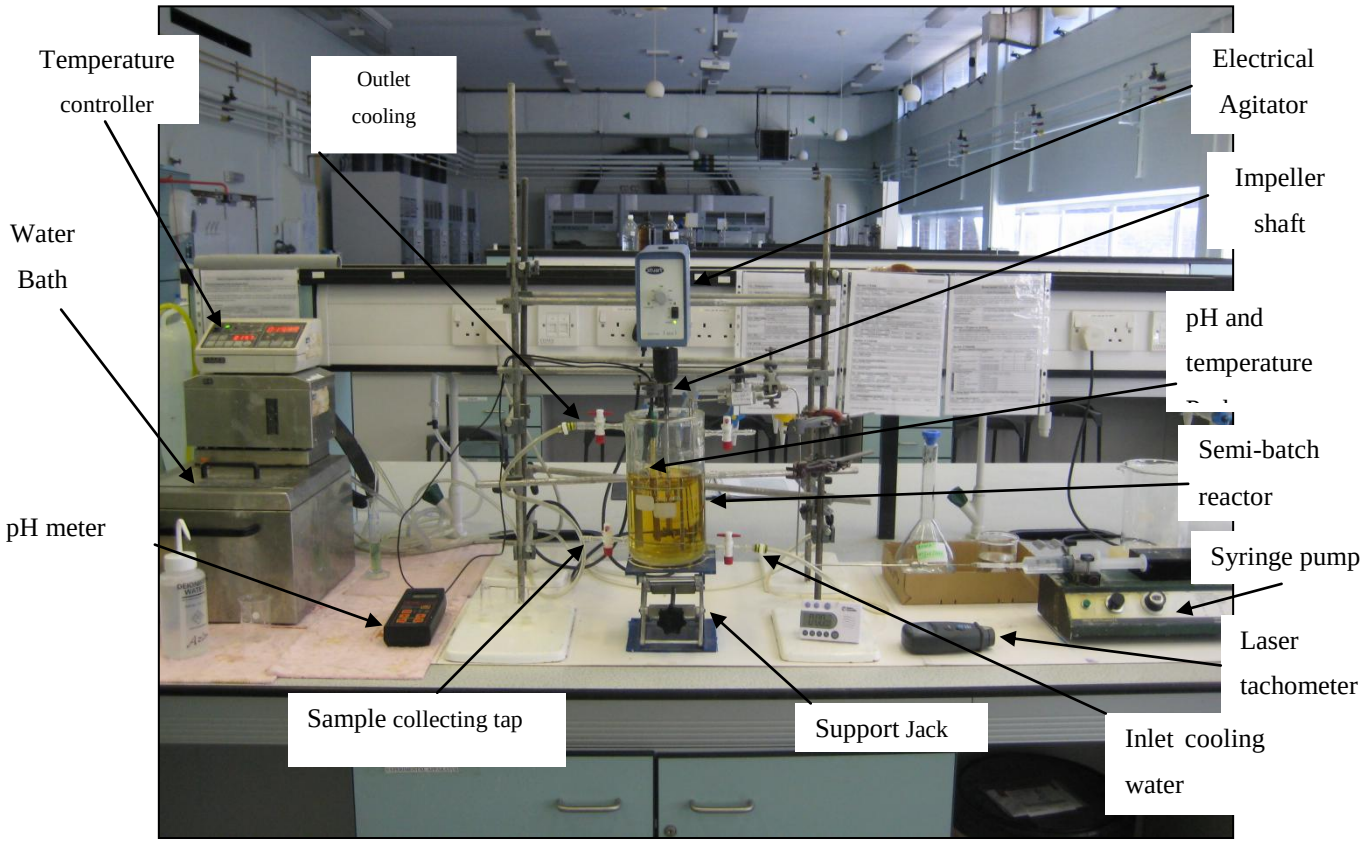

Figure 4.1: The set up for SBR Experimental Rig

4.2.1.1 The Semi-Batch Reactor (SBR)

At this stage of the research, a Semi-batch reactor (SBR) made of borosilicate was used. Figure 4.2 shows the SBR connected with the instruments and ancillary equipment that were employed to carry out the experiments.

The SBR had provision for a water jacket connected to a water bath in order to keep the temperature of the reacting liquid inside the vessel constant at 20 ^{O}C. The vessel shown in Figure 4.2 and Figure 4.3 was equipped with four fixed baffles (width B=12.3 mm), made of stainless steel. The dimensions of the vessel are given in Table 4.2 together with the clearance off the bottom of the reactor, C (mm), at which the Rushton turbine was placed. The four stainless steel baffles used in SBR are shown in Figure 4.4.

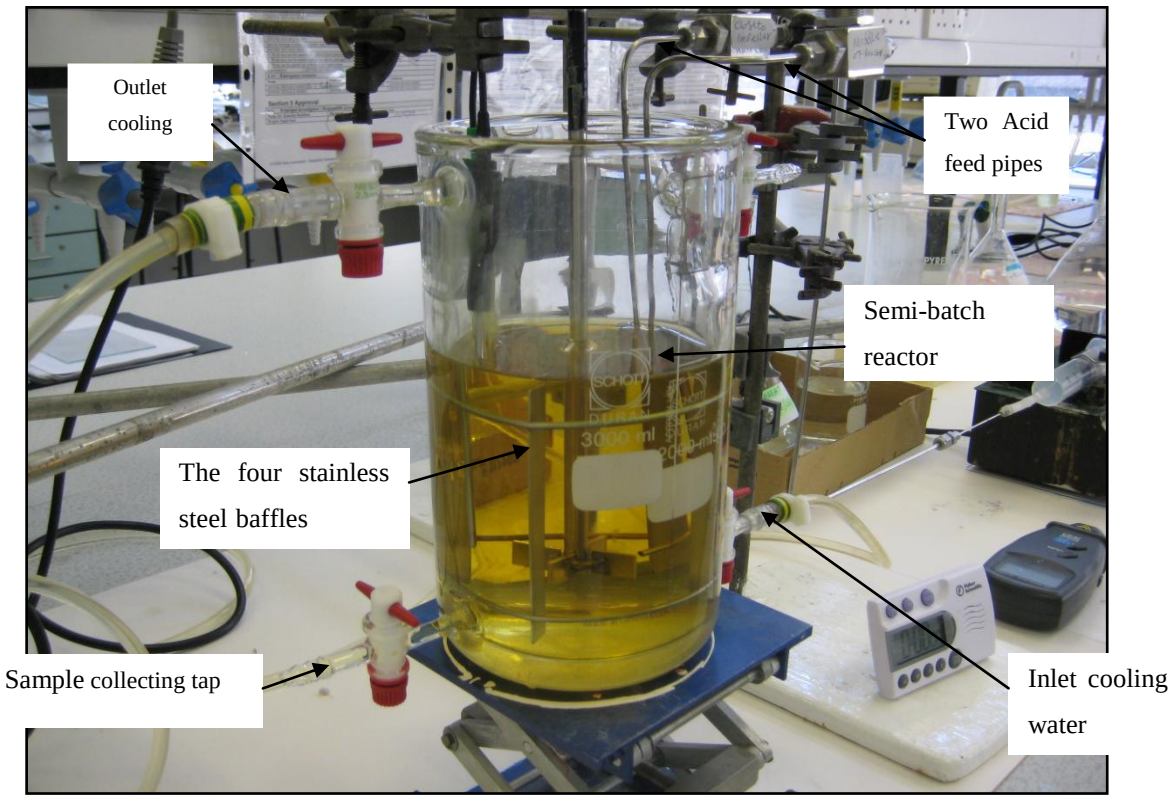

Figure 4.2: Semi-batch reactor (SBR) used in this work

Table 4.1: Reactor sizing - the geometric parameters for the SBR

Parameter	Size,(mm)
Liquid height, H	110.2 mm
Tank diameter, T	110.2 mm
Impeller diameter, D	44.0 mm
Impeller clearance, C	36.7 mm
Impeller Blade width, a	17.4 mm
Impeller Blade height, b	12.3 mm
Wall baffled width, B	15.9 mm

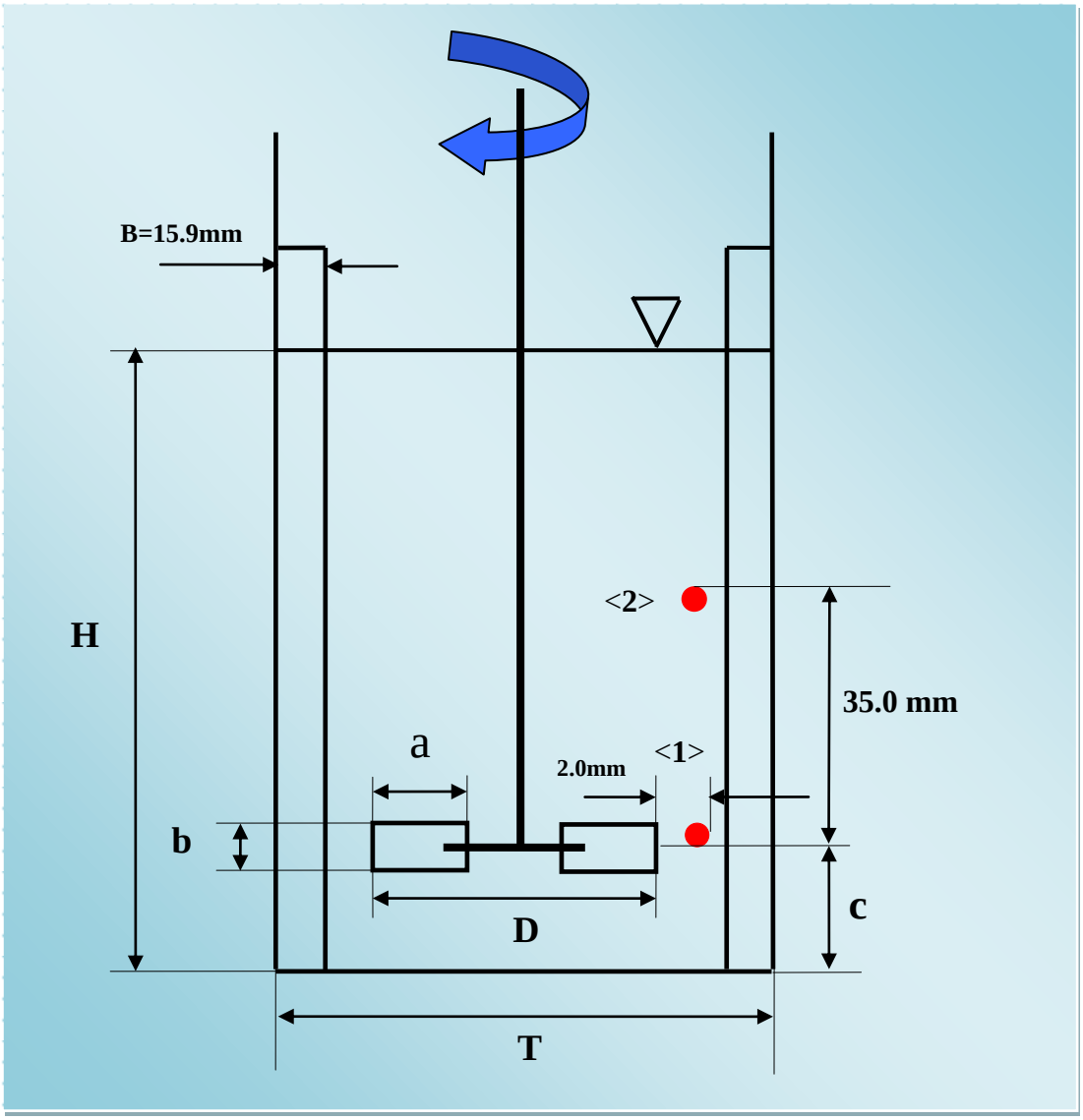

Figure 4.3: Geometry of SBR Showing Feed Locations, Agitator, Baffles and Rushton

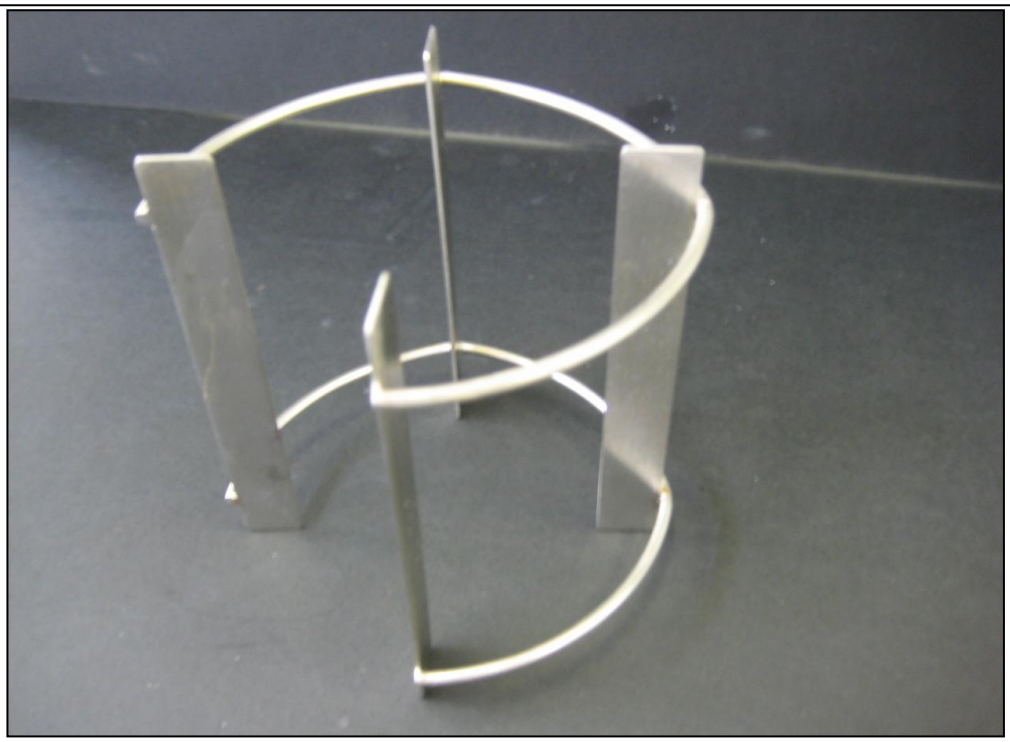

Figure 4.4: The four stainless steel baffles used in SBR

The design and the geometry of the reactor and its dimension ratios were adopted from (Tatterson, 1994) as a rule of thumb. The volume of the solution which comprises iodide, iodate, and borate solution, i.e. H_3BO_3, NaOH, KI and KIO_3 was 1.37 L for each experimental run.. The experiments were carried out with an aspect ratio H/T equal to 1.0. The clearance ratio, C/T=0.33. The impeller diameter Dwas set at 0.40T. The impeller speeds were 300, 600, 900 and 1200 rpm; the acid concentrations were 0.25, 0.5 and 1.0 M; the acid feed rate was 3.6 ml/min. Two acid feeding point positions were investigated. The first point < 1 >, was located at a distance of 2 mm (Assirelli et al., 2002) from the edge of the impeller blade in the same horizontal plane whilst the second point < 2 > was located directly above the first injection point, at a vertical distance of 35 mm. The two feed points were located at the vertical axis of symmetry of the reactor. In order to control the feed to these two points, two ball valves were used. These two feed points lie on a vertical line at 0.1 T from the wall of the reactor, where T is the diameter of the reactor. The reactor is equipped with an acid feed stainless steel tube of 1.78 mm internal diameter, which is connected to a syringe pump.

4.2.1.2 Ancillary Equipment Set-up

4.2.1.2.1 The syringe pump

Figure 4.5 shows the syringe pump (model 353, Sage Instruments) that was used to deliver the sulphuric acid to the SBR. The pumping rate at which the pump operates is measured in terms of percentage of flow (% flow). It was necessary to calibrate this pump in order that values for flowrate in terms of ml/min could be obtained. This calibration was made by using de-ionised water as the properties (the density and viscosity) are not far from highest concentration of sulphuric acid used in this work i.e. 1.0M. The ρ_{water} and $\rho_{\text{sulphuric acid}}$ at 25 ^{0}C are 999 kg/m^3 and 1070 kg/m^3 (Green and Perry, 2008)respectively. The μ_{water} and. $\mu_{\text{sulphuric acid}}$ at 25 ^{0}C are 1.003x 10^{-3} $Pa.s$ and 1.05x 10^{-3} $Pa.s$ (Rhodes and Barbour, 1923) respectively. Comparing the ρ_{water} vs. $\rho_{\text{sulphuric acid}}$ at 25^{0}C differ not more than 7% and the μ_{water} vs. $\mu_{\text{sulphuric acid}}$ at 25^{0}C differ not more than 5% . The pump was therefore allowed to run at various percentage of flow and the volume of de-ionised water collected in 1 minute was measured. In order to allow for the greatest degree of accuracy, the pump was operated as it would be when running a test, with the correct lengths of tubing and the feed and outlet maintained at the appropriate height. Figures A1 and A2 in appendix A show the calibration curves for the syringe pump equipped with one and two syringes respectively.

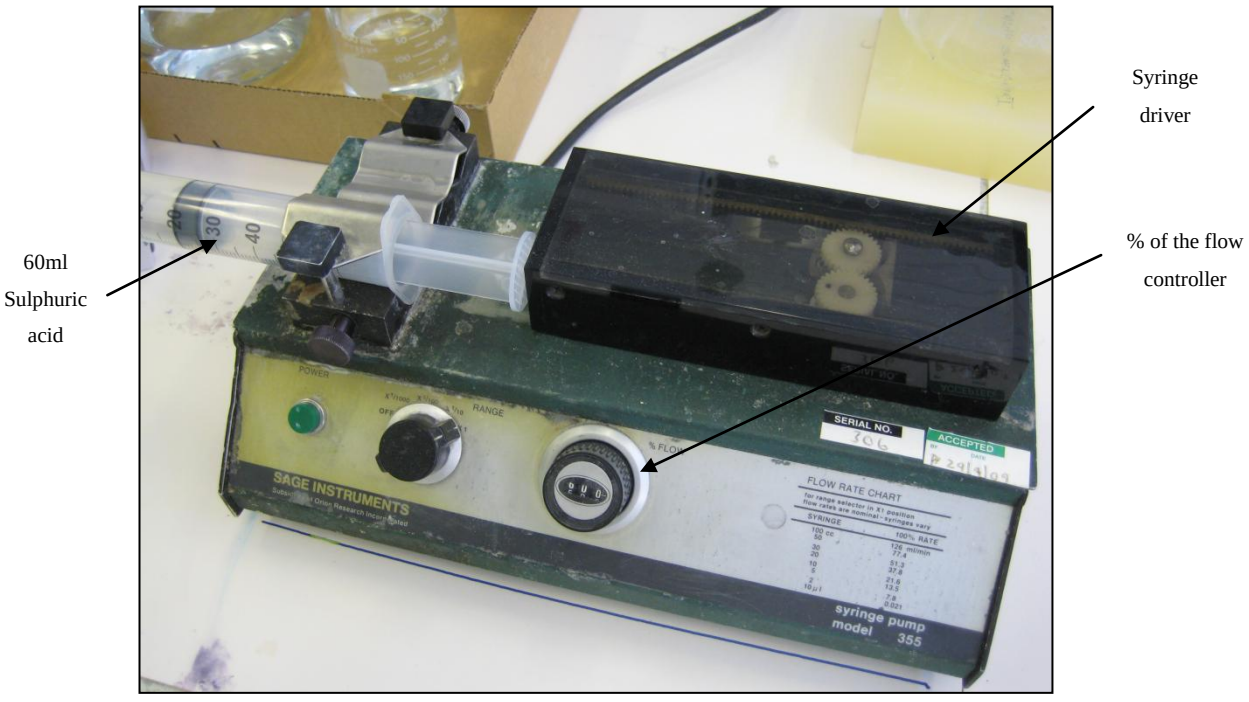

Figure 4.5: Syringe pump (model 353, Sage instruments)

4.2.1.2.2 Impeller System

In this part of the research, a Rushton Turbine which was manufactured at the school's workshop was used as the agitator. It was chosen because most of the relevant fluid dynamic and micromixing studies carried out in the stirred tank reactors were obtained with this type of impeller (Assirelli et al., 2002; Guichardon and Falk, 2000; Fournier et al., 1996a), thus making comparison of the data from the present study with the previous studies possible. Figure 4.6 shows the Rushton Turbine used in the SBR micromixing experiments

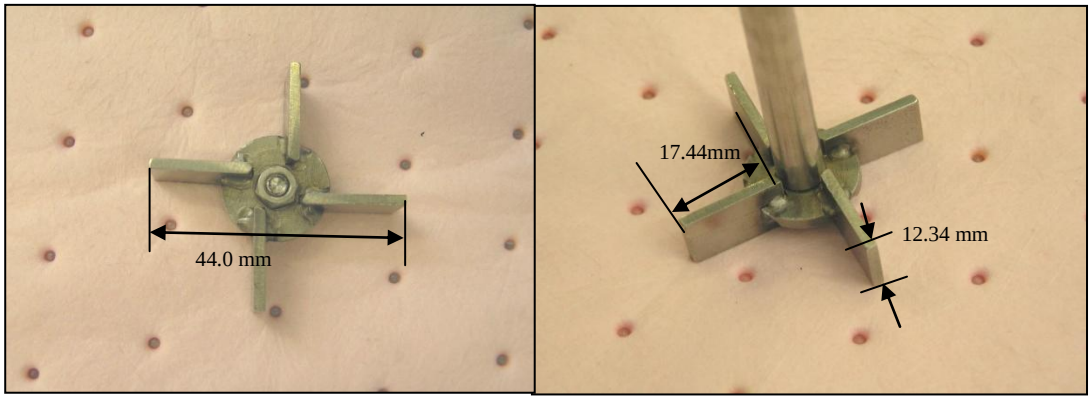

Figure 4.6: The Rushton Turbine used as agitator in the SBR

4.2.1.2.3 pH meter

The pH values for the chemical solutions used in the experiments as well as the reactants when the reaction was progressed were monitored by pH meter type of HANNA INSTRUMENTS HI 8424 microcomputer pH meter. The meter used was a digital type. The pH meter/probe was calibrated on daily basis before beginning the experimental work using standard buffer solution of pH 7 and then 4. The tip of the probe was washed with de-ionised water to remove any build up of impurities on the glass before immersing it into the buffer.

4.2.1.2.4 SBR Micromixing Experimental Procedure

All the experiments were performed with reaction volume of 1.37 litres of the solution which consists of Iodide, Iodate and Borate solution. The volumes of the sulphuric acid for injection into the SBR were calculated as shown in appendix B and its dependence on the acid concentration was used in the run.

As mentioned earlier in Chapter 2 section 8, the iodide-iodate reaction system belongs to the parallel competitive reaction scheme were implemented in this research as a model reaction to characterise the micromixing phenomena in intensified reactor systems, i.e. SDRs and NCRs. The data were benchmarked against conventional Semibatch reactor using Rushton turbine impeller. This set of reaction involves acid-base neutralization, (4.1), and an oxidation reaction, (4.2), called the Dushman reaction according to the following steps:

$$H_2BO_3^-{}_{(aq)} + H^+{}_{(aq)} \rightleftarrows H_3BO_{3(aq)} \qquad \text{Acid-base neutralization} \qquad (4.1)$$

Quasi-instantaneous

$$5I^-{}_{(aq)} + IO_3^-{}_{(aq)} + 6\,H^+{}_{(aq)} \rightleftarrows 3\,I_{2(aq)} + 3\,H_2O_{(aq)} \qquad \text{Dushman reaction} \qquad (4.2)$$

Fast

$$I_2 + I^- \rightleftarrows I_3^-{}_{(aq)} \qquad \text{Equilibrium} \qquad (4.3)$$

Quasi-instantaneous

The second reaction (4.2) which is Dushman reaction is fast being in the same time range as the micromixing process, but much slower than the acid-base neutralisation reaction (4.1). The iodine formed reacts further with iodide ions I^- to yield $I^-{}_3$ according to the quasi-instantaneous equilibrium (4.3). The degree of micromixing has a direct influence on reaction (4.2) and subsequently on reaction (4.3). The measurement of $I^-{}_3$ by spectrophotometric absorption can therefore provide a good indication of the degree of micromixing achieved in any given reactor.

The micromixing experiments were carried out using the reactant concentrations listed in Table 4.2 which was adopted from the work of Guichardon and Falk (2000). The work is regarded as the leading *"state of the art"* approach for using the iodide- iodate technique for characterisation of the micromixing reactor performance. This choice of concentrations allowed for a comparison of this research's results with those reported in the literature.

Table 4.2: the initial concentration of the reactants used in this work

Reactants	Concentration used (M)
$[H_3BO_3]$	0.1818 for water system and 0.0909 for 50 and 75wt% glycerol systems
[NaOH]	0.0909
[KI]	0.01167
$[KIO_3]$	0.00233
$[H^+]$	0.1,0.25,0.5,1.0M

The concentration of potassium iodide and potassium iodate were chosen to give a potential concentration of iodine as follows:

$$[I_2]_{potential} = 3[IO_3^-]_0 = \frac{3}{5}(I^-)_0 = 7.10^{-10}\ M \qquad (4.4)$$

Where $[I_2]_{potential}$ is the potential concentration of iodine which can be defined as the maximum total concentration of iodine that can be obtained at a complete conversion of the reaction (4.2). It is also the concentrations of the iodide and iodate ions which follow the stoichiometry of Dushman reaction.

Therefore, after mixing sodium hydroxide and boric acid, the initial concentration of the sodium borate is $[H_2BO_3^-] = [H_3BO_3] = 0.0909\ mol/l$, forming a buffer solution at $pH = pKa_1 = 9.14$ that corresponds to the first acidity equilibrium constant of the boric acid (Fournier et al., 1996a).

One of the restrictions that needed to be taken into account when carrying out a comparison between the performance of the various types of reactors studied is the ratio of the molar quantities of acid and the borate ions contacting each other. This parameter has to be maintained at a constant ratio in the continuous reactors i.e. NCRs and SDRs, as well as in the SBR for a valid comparison (Guichardon and Falk, 2000). The injected number of moles of hydrogen ions in the SBR was 0.020 moles for all experiments.

To utilise the above conditions for continuous reactor systems and to make a possible comparison between the micromixing performance of various reactor types (semi-batch reactor systems vs. continuous reactor systems), the ratio of the molar quantities of acid and the borate ions that are in contact with each other has to be considered. This ratio

has to be maintained constant in the continuous reactors as well as in the semi-batch for a valid comparison (Guichardon and Falk, 2000):

$$\left(\frac{n_{I_2\ potential}}{n_{H,0^+}}\right)_{Batch} = \left(\frac{q_{I_2\,potential}\quad [I_2]_{potential}}{q_{H,0^+}\ [H^+]_0}\right)_{Continuous} \tag{4.5}$$

and

$$\left(\frac{n_{H_2BO_3^-}}{n_{H,o^+}}\right)_{Batch} = \left(\frac{q_{H_2BO_3^-}\ [H_2BO_3^-]_0}{q_{H,O^+}\ [H^+]_0}\right)_{Continuous} \tag{4.6}$$

where $q_{H_2BO_3^-}$ and q_{H,o^+} are the Borate-Iodide and Iodate solution and the acid volumetric flow rate respectively.

Complete calculations of the sulphuric acid volumes which were injected into the SBR and also the ratios (R) of the solution of Iodide-Iodide-Borate ions and the acid volumetric flow rates were adopted in the SDR and NCR reactors which are shown in appendix B. The reactants concentrations shown in Table 4.2 in this section were used in the micromixing experiments performed in this research. Table 4.3 shows the initial concentrations for I and H solutions and the molar numbers ratio used in SBR. Table 4.4 shows the initial concentrations for I, i.e., the iodide-iodate-borate solution and H, i.e., the hydrogen ions solution and the molar numbers ratio used in SDRs and NCRs.

Table 4.3: The initial concentrations for I and H solutions and its molar numbers ratio of Reactants the used in SBR

Solution I			Solution H	
$C_{IO3^-,0}$	$C_{I^-,0}$	$C_{H2BO3^-,0}$	$C_{H^+,0}$(mol/l)	$\left(\frac{n_{H_2BO_3^-}}{n_{H,0^+}}\right)_{SBR}$
$2.3X10^{-3}$	$1.16X10^{-2}$	0.09	0.25	6.363
$2.3X10^{-3}$	$1.16X10^{-2}$	0.09	0.5	6.363
$2.3X10^{-3}$	$1.16X10^{-2}$	0.09	1.0	6.363

Table 4.4: The initial concentrations for I and H solutions and its flow rate ratios used in SDRs and NCRs

Solution I			Solution H	R=Q_I/Q_H	$\left(\frac{q_{H_2BO_3^-}[H_2BO_3]_0}{q_{H_0^+}[H^+]_0}\right)_{SDRs\&NCRs}$
$C_{IO_3^-,0}$	$C_{I^+,0}$	$C_{H2BO3^-,0}$	$C_{H^+,0}$(mol/l)		
$2.3X10^{-3}$*	$1.16X10^{-2}$ *	0.09 *	0.1 *	7 *	6.363
$2.3X10^{-3}$	$1.16X10^{-2}$	0.09	0.25	17.5	6.363
$2.3X10^{-3}$	$1.16X10^{-2}$	0.09	0.5	35	6.363
$2.3X10^{-3}$	$1.16X10^{-2}$	0.09	1.0	70	6.363

*Same as monnier et al. (2000)

10 *l* of Borate-Iodide-Iodate solution (solution H) was prepared every day to keep it fresh by dissolving the following amounts of solid reagents in de-ionised water in the case of water system experiments:

I. Water system

- 112.407 g of H_3BO_3 dissolved in $3000x10^{-3}$ l de-ionised water;
- 36.364 g of NaOH dissolved in $1000x10^{-3}$ l de-ionised water;
- 4.993 g of KIO_3 dissolve in $1000x10^{-3}$ l de-ionised water; and
- 19.367 g of KI dissolve in 100 $x10^{-3}$ l de-ionised water.

It is well known that addition of glycerol has influence on the redox potential of the Iodine/water couple (Guichardon et al., 1997) (Guichardon et al., 1997)(Guichardon et al., 1997)(Guichardon et al., 1997)(Guichardon et al., 1997)(Guichardon et al., 1997)(Guichardon et al., 1997)(Guichardon et al., 1997)(Guichardon et al., 1997)(Guichardon et al., 1997)(Guichardon et al., 1997)(Guichardon et al., 1997)(Guichardon et al., 1997)which will reduce the value of the pH to less than 7. To prove this, an Iodide/Iodate solution containing 50 wt% of glycerol in water was tested. The pH and the absorbance values were measured before adding any sulphuric acid and the results were 5.17 and 0.095 respectively at 20.7 ^oC which was evidence of the presence of I_3^- in the solution. To sort this matter out requires increasing the pH value for the water/glycerol system. The concentration of H_3BO_3 was reduced to 50% of the

that used in the water system. The number of H_3BO_3 moles was adjusted to 0.0909 for the 50 and 75 wt% glycerol system. The pH and the absorbance values were measured after this adjustment before adding any sulphuric acid and were measured as 11.0 and 0.000 at 20.1 ^oC respectively. This confirmed that the initial formation of iodine has diminished and becomes inexistent at pH = 11.0. The amounts of solid reagents used in the case of 50 and 75 wt% water / glycerol system are shown below:

II. 50 and 75 wt% water /glycerol system

- 56.205 g of H_3BO_3 dissolved in $3000x10^{-3}$ l de-ionised water;
- 36.364 g of NaOH dissolved in $1000x10^{-3}$ l de-ionised water;
- 4.993 g of KIO_3 dissolve in $1000x10^{-3}$ l de-ionised water; and
- 19.367 g of KI dissolve in 100 $x10^{-3}$ l de-ionised water.

The first step in the preparation of the solutions for these experiments was the weighing of the chemicals. This was followed by their dissolution in de-ionised water in the beakers. In order to obtain the volumes of the solutions, the volumetric flasks were used and the solutions were homogenised in a 10 *l* aspirator before each experiment. The solution of up to 10 *l* was made by addition of de-ionised water in the case of water system experiments or de-ionised water and glycerol in the case of 50 and 75wt% glycerol experiments.

The sequence that was followed for the preparation of the whole reactive mixture is very critical to the results of the experiments. First, the boric acid and the sodium hydroxide were added into the aspirator to obtain the buffer solution followed by KI and KIO_3. This procedure was important in order to avoid contact between KI and KIO_3 in the acid solution and the subsequent thermodynamic formation of I_2 (Guichardon and Falk, 2000).

For every batch of solution, the pH values for the buffer solution and final solution were checked to ensure that they meet the following rules:

- Buffer solution : 8.5< pH < 9.5;

- pH* must be close to 7.

where pH* is the average working pH from which iodine does not thermodynamically appear. All the solutions prepared in this study satisfied the above criteria.

The sulphuric acid was delivered to the SBR by the syringe pump (Model 353, Sage Instruments) using stainless steel tube of 1.78 mm internal diameter. The 60ml syringe was loaded with the desired concentration of sulphuric acid and inserted in its slot on the syringe driver. The sulphuric acid flowrate was 3.6 ml/min for all the experiments (water system; 50 wt% and 75 wt% water/ glycerol system) and set by selecting the % of the flow set point from the flow controller corresponding to the this flowrate according to the calibration curves as shown in AA-1 and AA-2 in appendix. The feed point needs to be selected by opening its ball valve and closing the other feed point's valve. After that, the pump was switched on to fill the feeding system up to the delivery point at the end of the tube. This was to ensure that the correct amount of sulphuric acid was injected in the SBR over a given time period as well as to ensure that the tube was free of air bubbles. Once the sulphuric acid appeared from the discharge of the feeding system, the pump was switched off and the tip of the tube was cleaned by wiper. The syringe was loaded again with the required volume of sulphuric acid that was needed for the given experiment and was inserted in its slot on the syringe driver. By this time, the SBR was located in its position having taken into consideration the impeller clearance, (C = 36.73 mm), as well as the location of the impeller shaft. This was done by manipulating the height of support jack. The SBR was located in a place on the support jack to ensure that the impeller is in the centre of the SBR and meet the dimensions shown in Figure 4.3 and Table 4.1. The SBR was filled with 1.37 *l* of Iodide, Iodate and Borate solution. In order to keep the temperature of the reacting liquid inside the vessel constant at 20 ^{o}C, the water bath temperature was set on 20^{o}C then switched on to deliver the cooling water to SBR water jacket. The pH and temperature values for the reaction were monitored by a microcomputer pH and temperature meter (HANNA INSTRUMENTS HI 8424) by means of a pH probe and thermocouple clamped to their supports and immersed in the solution. . Once the temperature reactants in SBR reached 20 ^{o}C, the impeller speed was measured using digital LED laser tachometer (CEM DT-6234B). At this stage the system was ready for the experiment to be performed by injecting the sulphuric acid in the SBR. The syringe

pump was switched on to deliver the required volume of sulphuric acid to the SBR. The syringe pump was switched off after finishing the injection of the acid into the SBR. Two minutes later, three samples were collected in three sample bottles from the sample collecting tap located at the bottom of the SBR for the absorbance analysis. The agitator was switched off and the waste was disposed. The SBR was flushed with de-ionised water and then dried by a paper towel. The system was readied for the next experiment.

4.2.1.2.5 Analysis of Experimental Product

The analysis of tri-Iodide (I_3^-) has been carried out as recommended by (Guichardon and Falk, 2000; Fournier et al., 1996a). In order to ensure a high level of accuracy in the measurements and to avoid disproportionation and iodine losses, the samples were analysed within five minutes of collection from the SBR (Yu-Shao CHEN, 2004; Guichardon and Falk, 2000). The collected product was analyzed in an off-line UNICAM 8700 UV-vis spectrophotometer. The wavelength used was λ = 353 nm (Guichardon and Falk, 2000).The samples were placed within a 10mm pathlenght cuvettes made of semi-optical polystyrene with a volume of 2.5 ml supplied by Fisher Scientific, UK except in a particular situation where the recorded absorbance was greater than 2.00, when the samples were transferred to Quartz 1mm pathlenght cuvettes with volume of 1.0 ml supplied by UNISPEC. Prior to the measurement of each absorbance of the sample, the spectrophotometer was set to zero using a cuvette containing the iodide, iodate and borate solution to act as calibrating solution for the measured absorbance of the sample. Thorough cleaning of the cuvette was done using de-ionised water and air for drying to ensure that no traces of previous samples were left in them or that marks affected the measured absorbance. Following the analysis of the absorbance of the experimental products, the pH and the temperature of the sample collected were recorded. These values were taken in order to ensure that the pH was above 7 as recommended by (Guichardon and Falk, 2000), which means that thermodynamically Iodine cannot be formed and the observed formation of tri-iodide can only occur due to segregation of the fluid and the temperature was valid for the rate constant used.

4.2.2 10cm spinning disc reactor (SDR) Experimental Rig

The second rig employed for the micromixing experiments was the 10cm SDR (the small SDR). Figure 4.7 shows the general layout for the 10cm SDR and the auxiliary equipments used in the micromixing experiments. The disc was driven by 125 W electric motor supplied by Parvalux Electric Motors. The rotational speed was controlled by a digital speed controller in the speed range of 300-4000 rpm. Cooling water was supplied through the sealed rotary union and the shaft allowed for cooling of the bearings and the internal machinery parts as well as the disc surface. A cooling circuit was also available for the reactor shell. The reactor shell and the rotary union were connected to a water bath (HAAKE circulators N4-B) in order to keep the temperature of the reacting liquid on the disc surface constant at 20 ^{o}C. In addition, a thermocouple was connected to the bottom side of the disc; digital thermometer was used to measure the temperature of the disc. The disc and the shell were constructed from stainless steel. The disc surface was a stainless steel plate attached by eight slotted stainless steel screws.

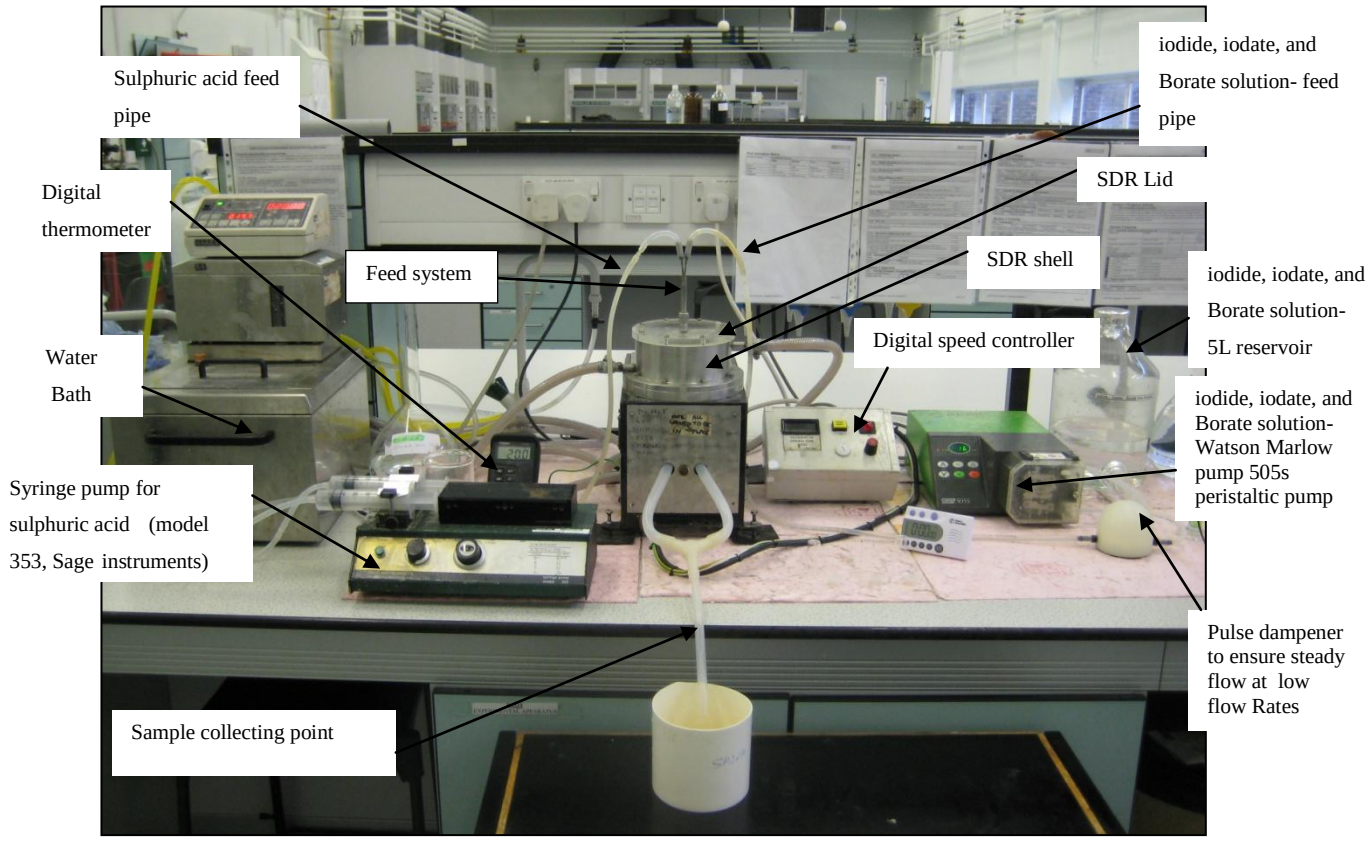

Figure 4.7: 10cm SDR Rig experimental set-up

4.2.2.1 The Mechanical Design of Spinning Disc Reactor

The spinning disc reactor consist of a disc surface (1), which is supported by a channel plate (2), through which disc service fluid is pumped up through the rotary union (8) then to the shaft for the control of the temperature reaction on the disc surface. It also consist of the reactor housing with water jacket for the purpose fluid circulation (7); the base plate (6) on the supporting frame; drive shaft with attached motor pulley (5) and bearing housing (4). The spinning disc reactor also has two product outlets (9) located at the bottom of the reactor base. The 10cm SDR rig was made of stainless steel and the rubber ring-seals were used as gaskets between the reactor plate and the reactor shell and also between the SDR polycarbonate lid and the external reactor jacket. The main parts of the spinning disc reactor of the 10cm SDR are shown in Figure 4.8. Figure 4.9 and 4.10 show the side aerial views of the 10cm SDR respectively. Figure 4.11 shows side view for 10cm SDR without side plate cover showing drive motor, rotary union, bearing, and connecting pulley.

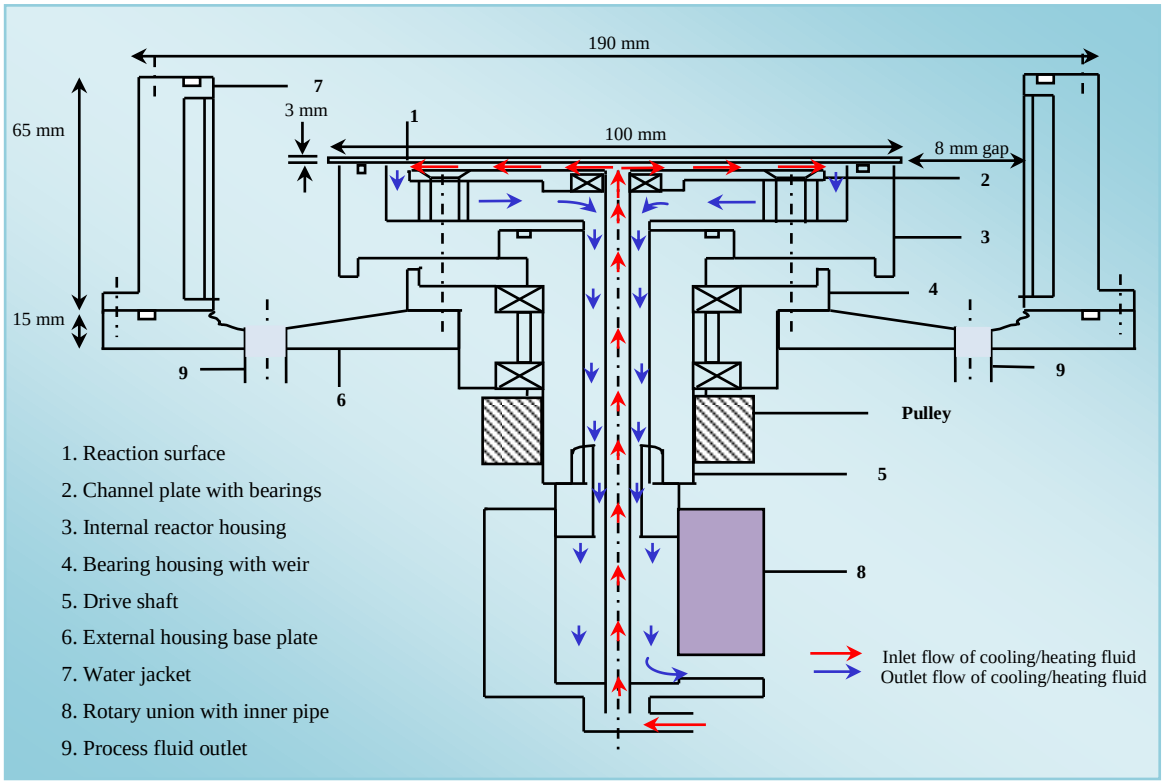

Figure 4.8: The mechanical Design of spinning disc reactor (adopted from McCarthy (2006)

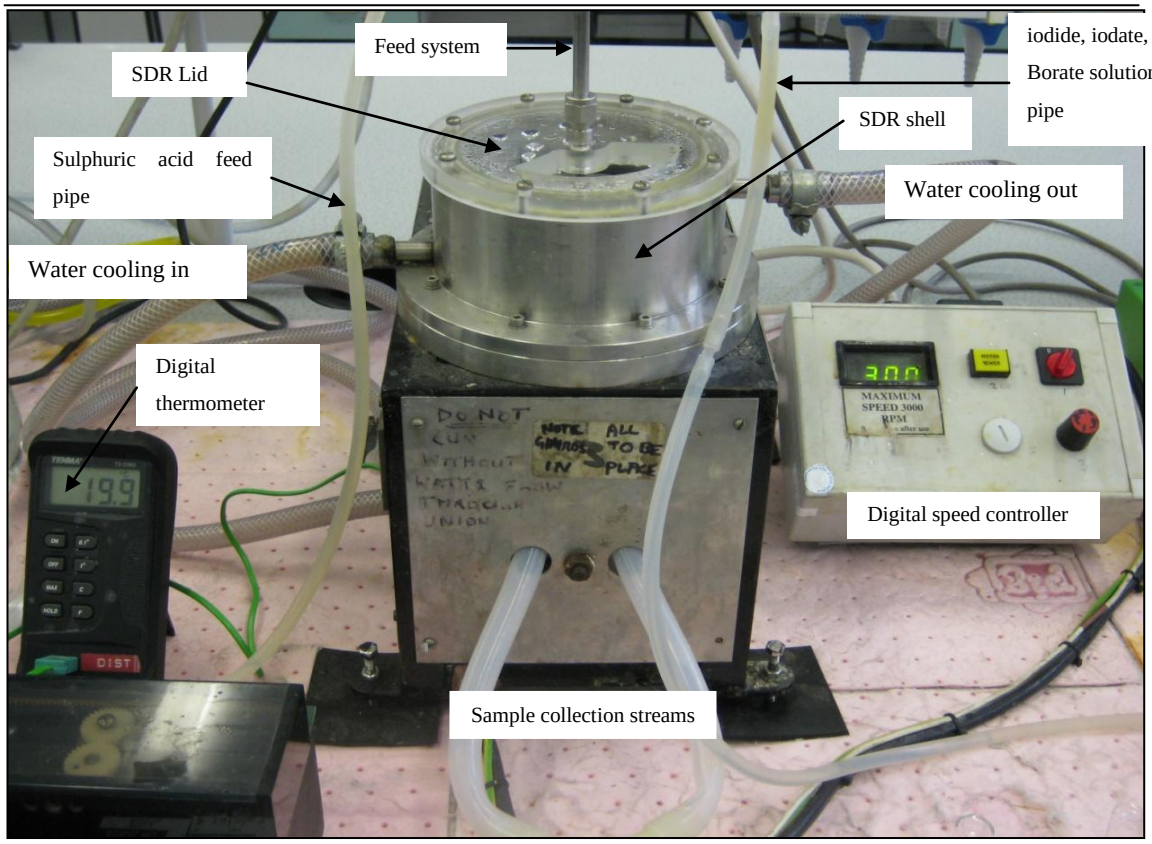

Figure 4.9: Side view of 10cm SDR

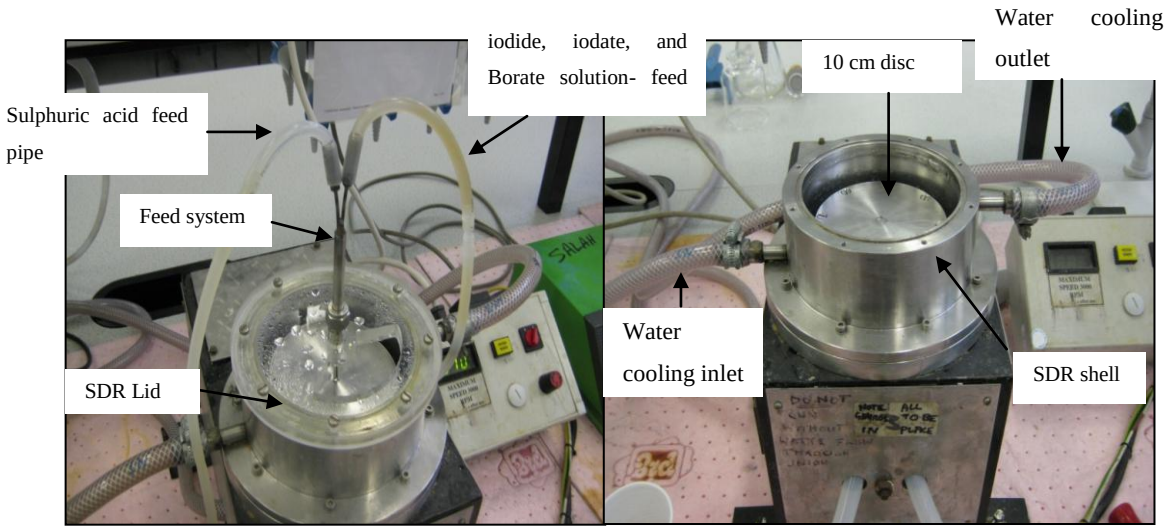

Figure 4.10: Two Aerial views of 10cm SDR, with (left) and without (right) lid

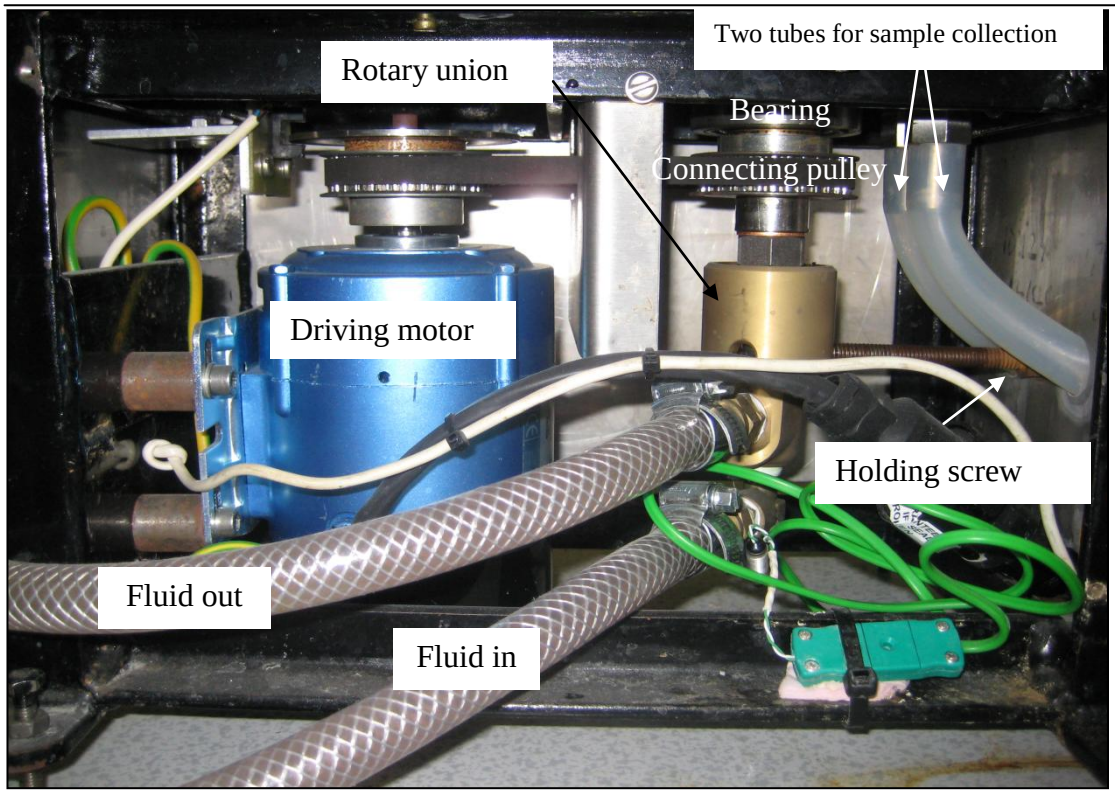

Figure 4.11: Side view for 10cm SDR without side plate cover

4.2.2.2 Liquid Feed Distributor (Single-Point Distributor)

The reactants were fed onto the spinning disc reactor surface through a feed distributor. The distributor consists of two pipes made of stainless steel: one for delivering the iodide, iodate and borate solution and the other for delivering the sulphuric acid as shown in Figure 4.12. Two feed distributors have been used with this rig, its usage depends on the total flow rate needs to be delivered to the disc. For example, at the total flowrate of 1 ml/s, a 0.65 mm pipe diameter was used for delivering the sulphuric acid while 1.65 mm pipe was used for delivering the iodide, iodate and borate solution. For the remaining total flowrates (3 and 5 ml/s), the two tubes have a 1.65 mm diameter. The choice of the feed tube diameters were carefully selected in order to achieved consistency in the introduction of the flow of reactants on the disc. The feed distributor was fixed on the lid so that it was located at the centre of the disc surface and was placed at 2.00 mm above the surface. This height could easily be adjusted by using a shim. The lid and feed systems for the 10cm SDR were in Figure 4.12 below.

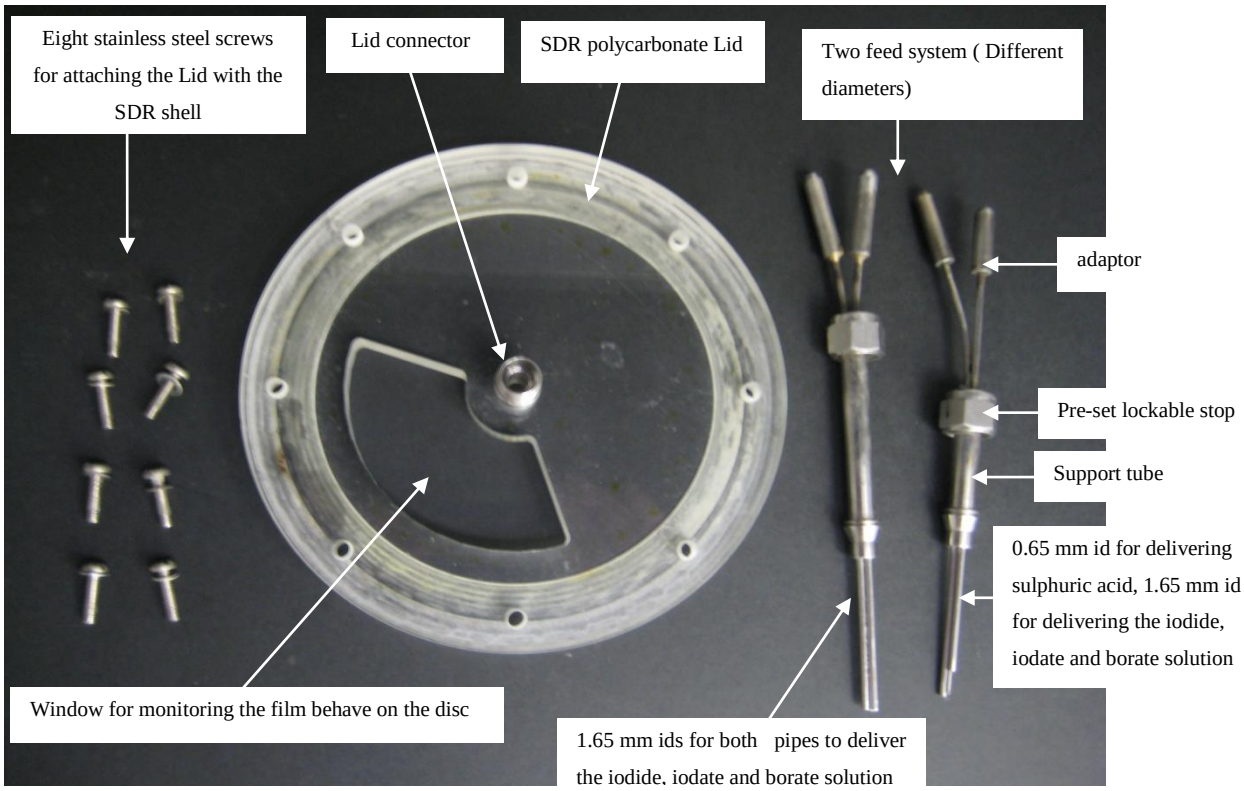

Figure 4.12: The lid and feed systems for the 10cm SDR

4.2.2.3 The Product Collector

The product was thrown off the edge of the disc which then hit the inner wall of the reactor housing and flowed down on the housing base. For the purpose of collecting the samples, there were two holes on the base of the reactor through which product continued to flow down through two pipes. These two pipes were combined to one pipe by a piece Y adaptor made of plastic to obtain a single outlet. From this pipe, the samples were collected for the purpose of analysis as shown in Figure 4.13.

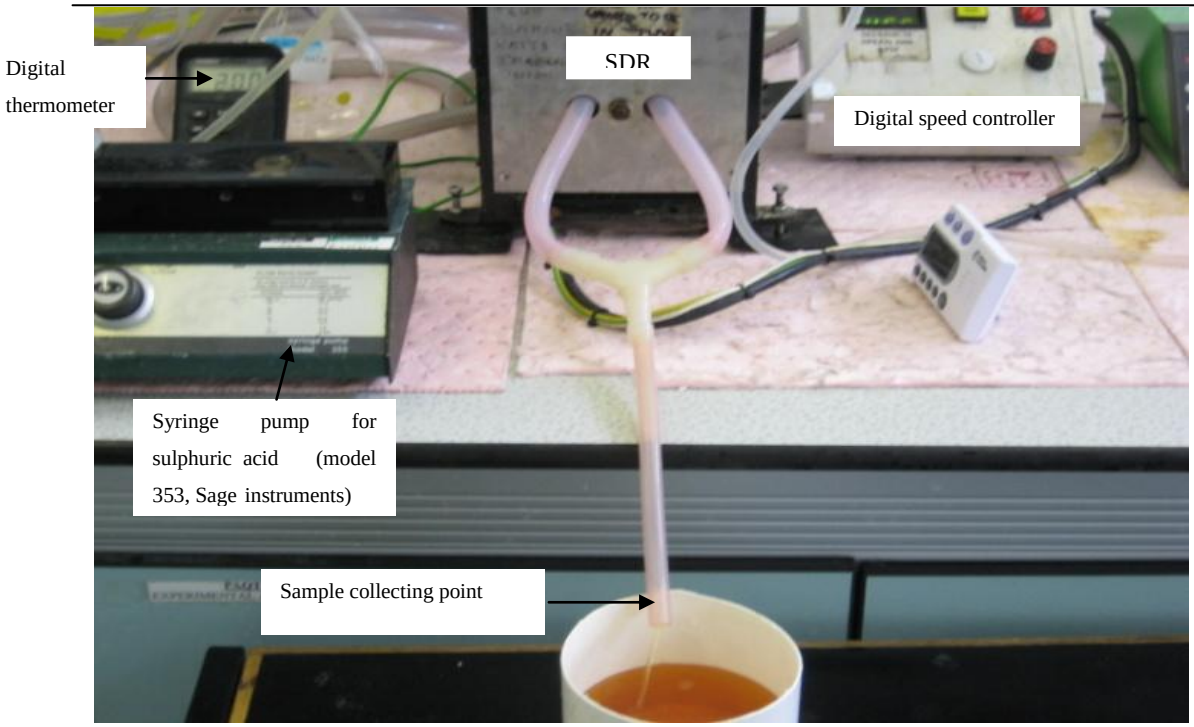

Figure 4.13: 10cm SDR product collector

4.2.2.4 Reactants pumping system for 10cm SDR

Two pumps were connected to the 10cm SDR to pump the reactants to the centre of the disc. The iodide, iodate and borate solution was delivered from Borosilicate 5 L reservoir by means of a peristaltic pump (Watson Marlow pump 505S) using 4.8 mm internal diameter Masterflex platinum cured silicone tubing as shown in Figure 4.14.

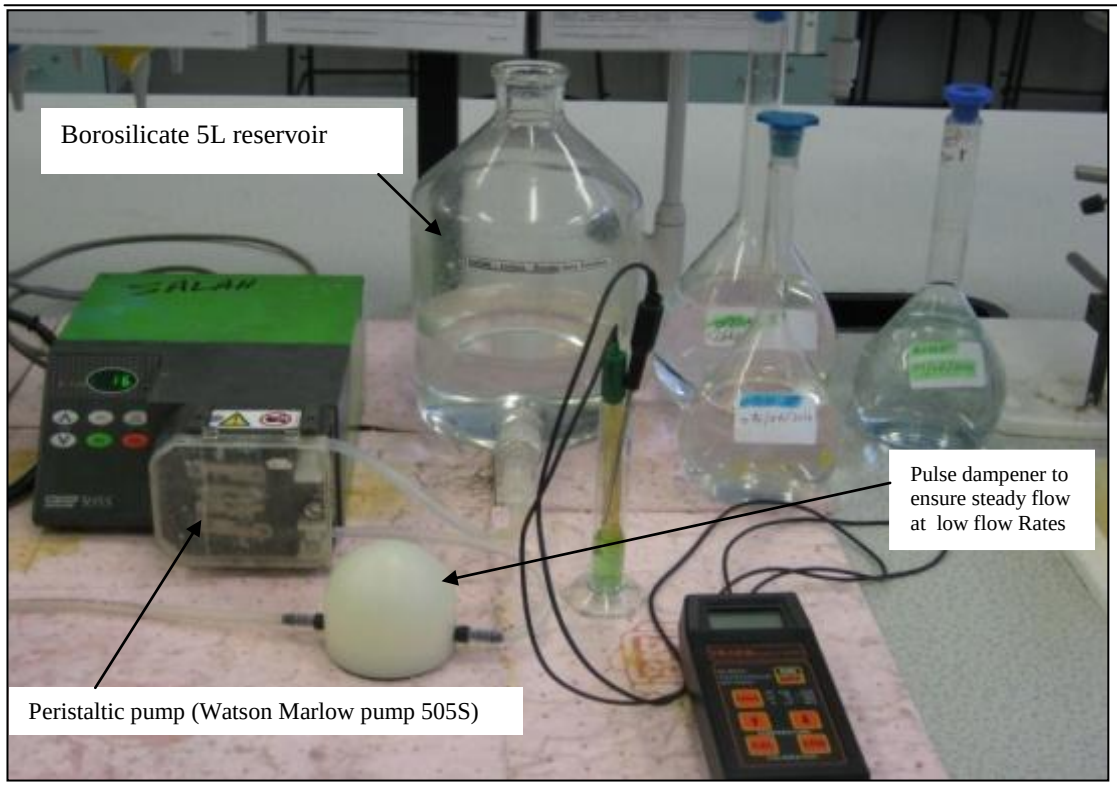

Figure 4.14: Peristaltic pump used for delivering of iodide, iodate, and Borate solution to 10cm SDR

Before the commencement of the experiments, the pump was calibrated so that the values for flowrate in terms of ml/min could be obtained. The pump was therefore allowed to run at various revolutions per minute (rpm) and the volume of de-ionised water collected in 1 minute was measured. The pump was operated as it would be when running a test, with the correct lengths of tubing for the feed and outlet maintained at the appropriate height. The pump calibration was performed with water system, 50 and 75 wt% glycerol systems. Figure C1 in appendix C show the calibration curve for the Watson Marlow pump505S with 4.8 mm internal diameter tubing feed pipe.

The sulphuric acid was delivered from two 60 ml syringes to the centre of the SDR disc by the syringe pump that was used in the SBR micromixing experiments which was shown previously in Figure 4.5. The calibration curves for the syringe pump (Model 353 Sage Instruments), are shown in Figure C2 to Figure C6 in appendix C.

4.2.2.5 10cm Micromixing Experimental Procedure

The flowrate of the borate/iodide/iodate solution was set by selecting the pump speed point (rpm) from the pump speed controller corresponding to the desired flowrate. The sulphuric acid flowrate was set by selecting the % of the flow set point from the flow controller that corresponds to the desired flowrate. The water bath temperature was set at 20 ^{o}C from the water bath temperature controller then switched on to deliver the cooling water to SDR through the sealed rotary union for the cooling of the bearing and the internal machinery parts as well as the disc surface and the reactor shell in order to keep the temperature of the reacting liquid on the disc surface constant at 20 ^{o}C (Guichardon and Falk, 2000). The samples bottles were cleaned using de-ionised water and then dried by the air and placed on the Table which is located close to the sample tube collector. When the reactor disc surface temperature reached to 20 ^{o}C (steady state condition), the syringe pump and the peristaltic pump were switched on to deliver the reactants to the centre of disc surface through the single single-point distributor. In the mean time the desired disc rotational speed was set from the digital disc speed controller and the disc started to rotate. To ensure the system is maintained in a total steady state condition, i.e. tubing and feeding system were air bubbles-free and reactants temperature on the disc surface reached the 20 ^{o}C, the disc was run for 5 minutes before taking any sample from the sample collector. After that, three samples were collected in the sample glass bottles at a time interval of 2 minutes from samples collector as shown in Figure 4.14. The disc and the both pumps were then stopped. The pH of the sample was measured and recorded to ensure that it was not lower than 7. This means thermodynamically iodine cannot form and the observed formation of tri-iodide can only be due to the segregation of the fluid. The samples were analysed for their absorbance values (D) within five minutes of the collection from the SDR sample collector using UNICAM 8700 UV-vis spectrophotometer. The samples were analysed using the same manner of the analytical procedure followed in the SBR experiments with the wavelength of λ = 353 nm (section 4.2.1.5). Upon completion of the experimental run, the disc lid was removed and the reactor was flushed with de-ionised water repeatedly then dried by using a paper towel. The lid was fixed back to its position by tightening the lid bolts. At this stage the SDR Rig became ready for performing the next experiment.

4.2.3 30cm Spinning Disc Reactor (SDR) Experimental Rig

The third rig employed in the micromixing experiments was 30cm SDR. Figures 4.15 and 4.16 show the aerial views of 30 cm SDR with and without the lid. In general, the mechanical design and construction for the 30 cm SDR are very much similar to the 10 cm SDR except for the difference in disc size. The disc was driven by a 0.37 kW motor type (ABB motors) attached with a toothed drive belt to prevent slippage of the belt. The designed maximum motor speed was 2870 rpm. From safety point of view, the maximum speed at which the reactor could be safely operated was 1200 rpm. The rotational disc speed was controlled by digital speed controller type (Varispeed 606 PC3) supplied by (YASKAWA). The disc speed was obtained from the speed controller as a unit of frequency (Hz). To determine the disc speed in terms of revolution per minute (rpm), a laser tachometer was used to measure the disc rotational speed in rpm and then speed calibration curve (Hz vs. rpm) for the 30 cm SDR was performed. Figure D-1 in appendix D shows the calibration curve for the 30 cm SDR speed.

The rig was made of stainless steel material. The disc (smooth/grooved) plate was also made from a stainless steel material which is attached to the circular rotating frame by eight slotted stainless steel screws. The SDR was covered by polycarbonate lid which was attached by twelve hex cap screws. Disc surfaces (smooth and grooved discs) were interchangeably used using counter sink screws through the surface disc into the main rotor sealed with a Viton 'O' ring. The rotor, shaft and reactor shell were supported on an angle iron framework with bearing supports using a self aligning bearing.

In order to keep the temperature of the reacting liquid on the disc surface constant at 20^{O}C as well as to avoid any mechanical damage that could occur to the bearing and other mechanical parts of the reactor due to the running of the reactor without a cooling system, cooling water was fed into the reactor through a central pipe co-axial with the main drive shaft connected to the 40 L feed tank via a rotary union supplied by Deublin UK. This cooling water makes contact with the bottom of the disc surface which centrally flows out to the periphery over a channel plate which then returns toward the centre until it makes contact with the annular pipe (formed by the feed drive shaft arrangement) where it flows down to the drain holed that is then discharged into the return fluid skirt and then to the tank again. The cooling water flow circulation was achieved partly by disc centrifugal force and water feed pump pressure. Figure 4.17

shows the cooling system for the 30cm SDR. Figure 4.18 shows the upper part of cooling system and driving system for 30 cm SDR.

To maintain the desired temperature for the SDR, two heaters were immersed in the tank. One end of a thermocouple was immersed in the tank and the other was connected to the digital temperature controller.

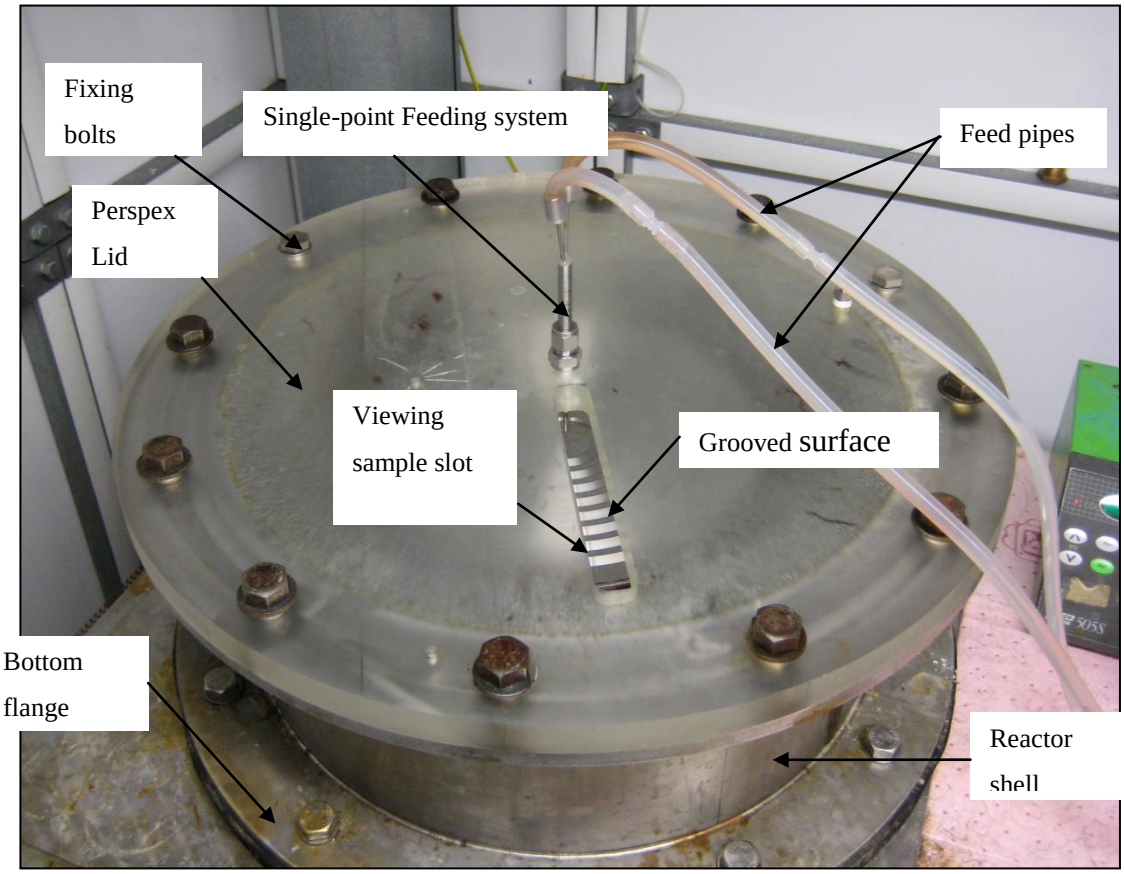

Figure 4.15: The Aerial view of 30cm SDR with the lid

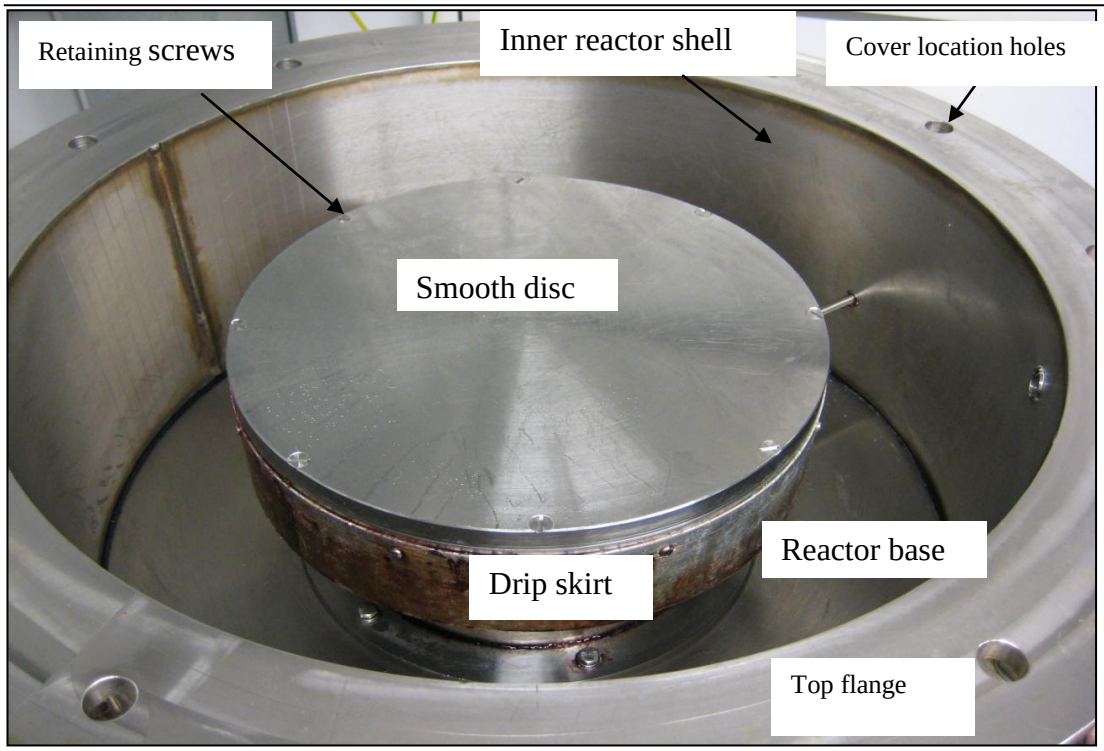

Figure 4.16: The Aerial view of 30cm SDR without the lid

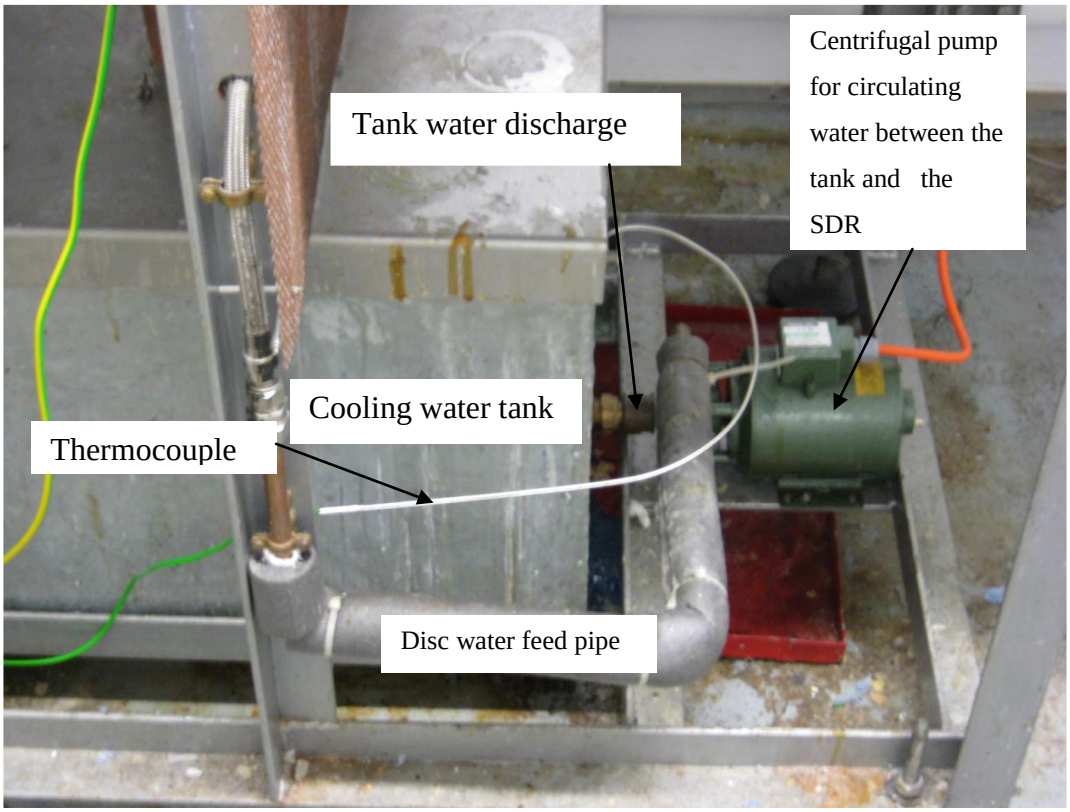

Figure 4.17: Cooling system for 30cm SDR

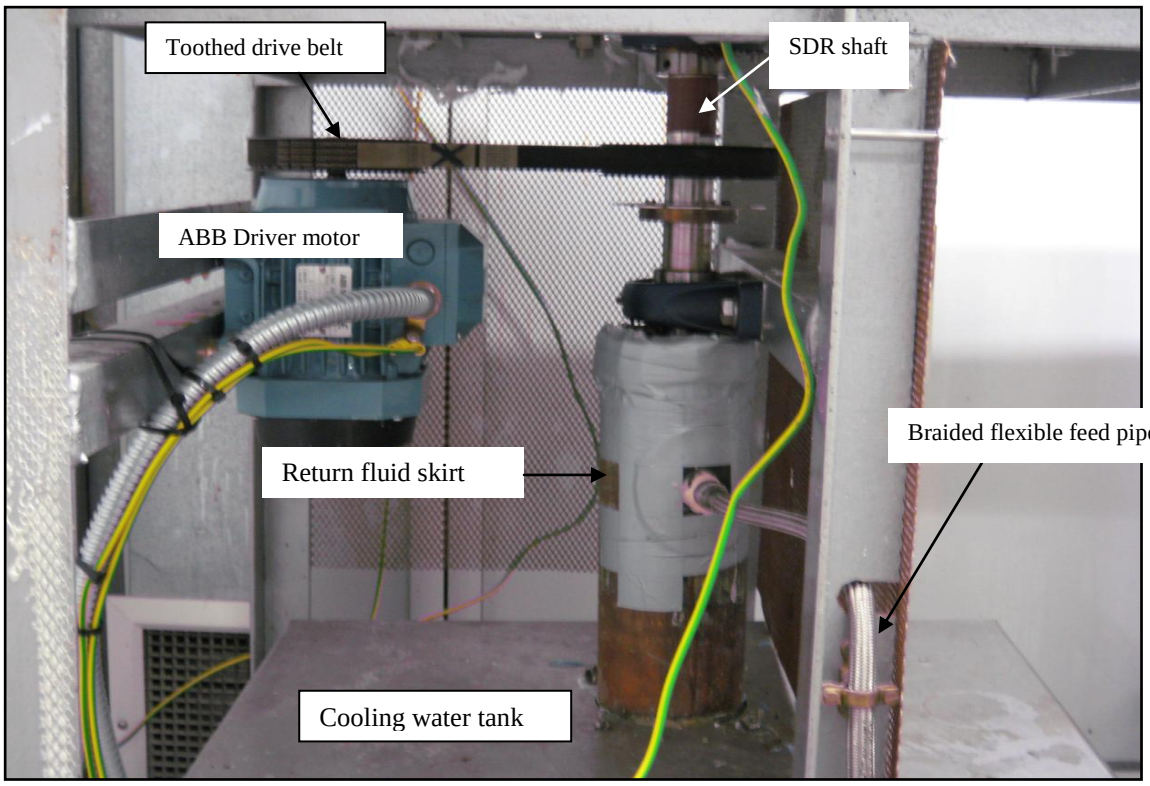

Figure 4.18: The upper part of cooling system and driving system for 30 cm SDR

4.2.3.1 Reactants Pumping System and Liquid Feed Distributor (Single-Point Distributor for 30 cm SDR

Two pumps were connected to the 30cm SDR to pump the reactants to the centre of the disc. The Iodide, Iodate and Borate solution was delivered from 10 L aspirator by means of the peristaltic pump that was used with 10cm SDR. The sulphuric acid was injected into the centre of the disc using the Syringe Pump type (NE-1000, New Era Syringe). The reactants were pumped into the disc through a Single-Point Distributor with a diameter of 3.0 mm for iodide, iodate and Borate solution stream and 1.65 mm for the sulphuric acid stream. The two pumps were calibrated with similar procedure that has been used for the pumps with the 10cm SDR. Figure 4.19 shows the pumping and feed system used with the 30 cm SDR. The feed system (the Single-Point Distributor) used with the 30 cm SDR was similar constriction to one was used with the 10 cm SDR. The distributor consists of two pipes made of stainless steel: one pipe of a 3.0 mm diameter for delivering the iodide, iodate and borate solution and the other pipe of a 1.7 mm diameter was used for delivering the sulphuric acid. The diameters of these feed tubes were carefully selected in order to achieve consistency in the introduction of

the flow of reactants on the disc. Similar to one used with 10 cm SDR, The feed distributor was fixed on the lid so that it was located at the centre of the disc surface and was placed at 2.00 mm above the surface. This height could easily be adjusted by using a shim. Figure AE-1 and Figure AE-2 in appendix E show the calibration curve for the Watson Marlow pump505S which was made by using de-ionised water. The calibration curve for the syringe pump, model NE-1000, New Era Syringe is also shown in Figure AE-3 in appendix E.

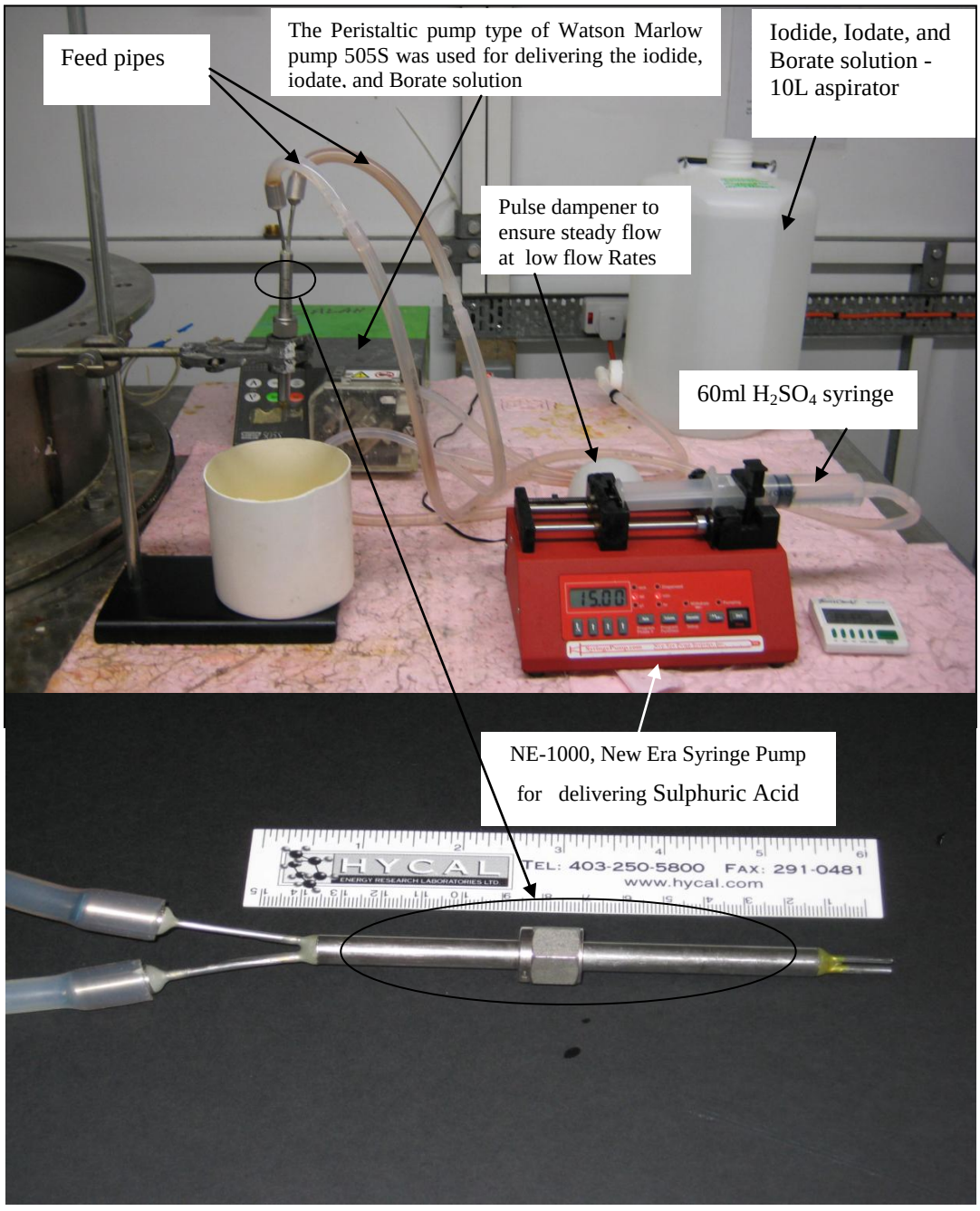

Figure 4.19: The pumping and feed systems for 30 cm SDR

4.2.3.2 Sulphuric Acid Multi-Point Distributor for 30 cm SDR Rig

The multi-point distributor was designed and constructed to give a high level distribution of the sulphuric acid with the Iodate-Iodate-Borate ions solution on the disc surface. This would enhance the quality of micromixing on the disc surface as shown in the results of the 30 cm SDR micromixing experiments (See Chapter 5 for the results). The multi-point distributor was manufactured by the in-house workshop except for the 0.2 mm holes (jets) that were drilled by Drill Service (Horley) Ltd.

The multi point distributor is a way of delivering two discrete streams of reactants on to a rotating surface at a known radius of contact without any prior mixing. This is done by using a central feed tube with the ability to change the feed tube diameter and height from the disc surface. This supports a 70.0 mm circular distributor block which has an annular groove machined in it. A feed tube was attached to this to provide the reactant. This annulus was then covered and sealed in place. The cover was made with a 1.5 mm stainless steel and it has four 0.2 mm feed holes (jets) machined in it. The diameters of the holes were very carefully chosen by carrying out pressure drop calculations due to frictional loses in the acid feed tube and the distributor holes.

The multi point distributor was used as a means of introducing reactant (1) one (the Iodide, Iodate and Borate solution stream) to the centre of the disc through a pipe of 3.5 mm diameter in order to couple it with the disc which allows it to form a rotating thin film. When the sulphuric acid was fed into the annulus, it first has to fill this and then build sufficient pressure to exit via the jets. The lower part of the distributor (the base plate) has four 0.2 mm diameter holes that was used to deliver reactant (2) two (The Sulphuric acid) onto the film surface as evenly as possible at a known discrete radius without significantly disrupting the film whilst still allowing good mixing to occur. Figures 4.20 and 4.21 show the multi-point distributor before and after assemble. Figure 4.22 shows the multi-point distributor's operational set-up in the 30 cm SDR.

Before commissioning the experiment, a flow test on the multi-point distributor was carried out using the lowest flowrate (3 ml/s). It was confirmed that there was flow through all the four holes.

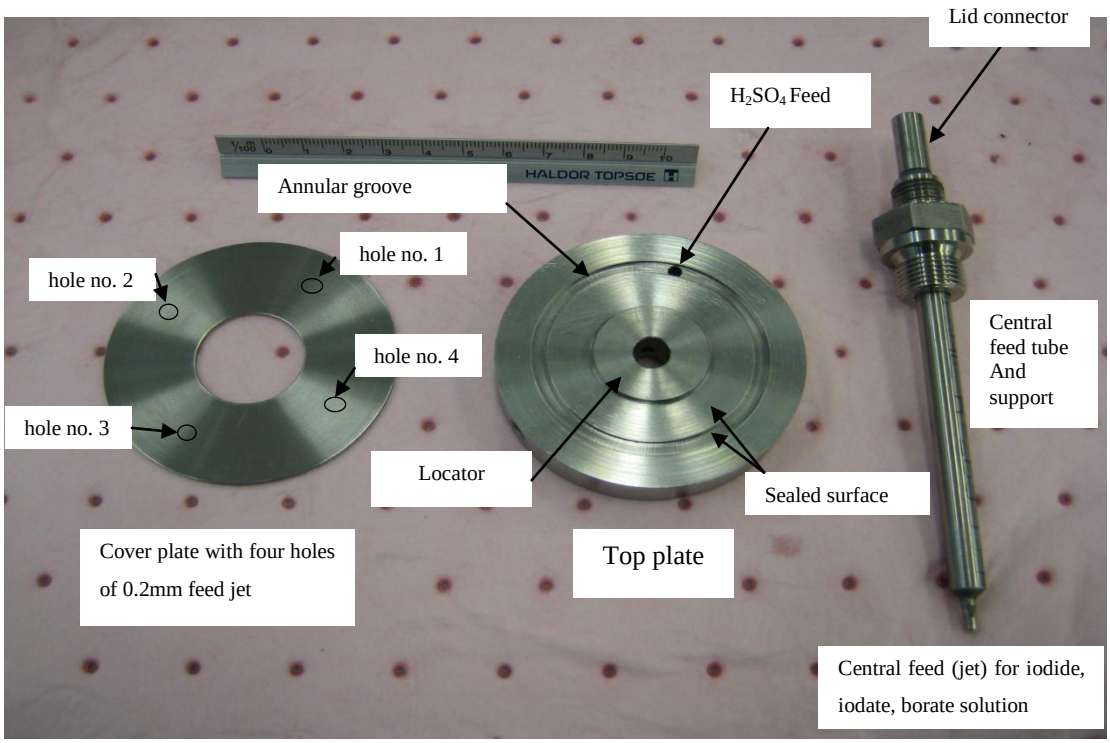

Figure 4.20: Multi point-distributor components before assembly

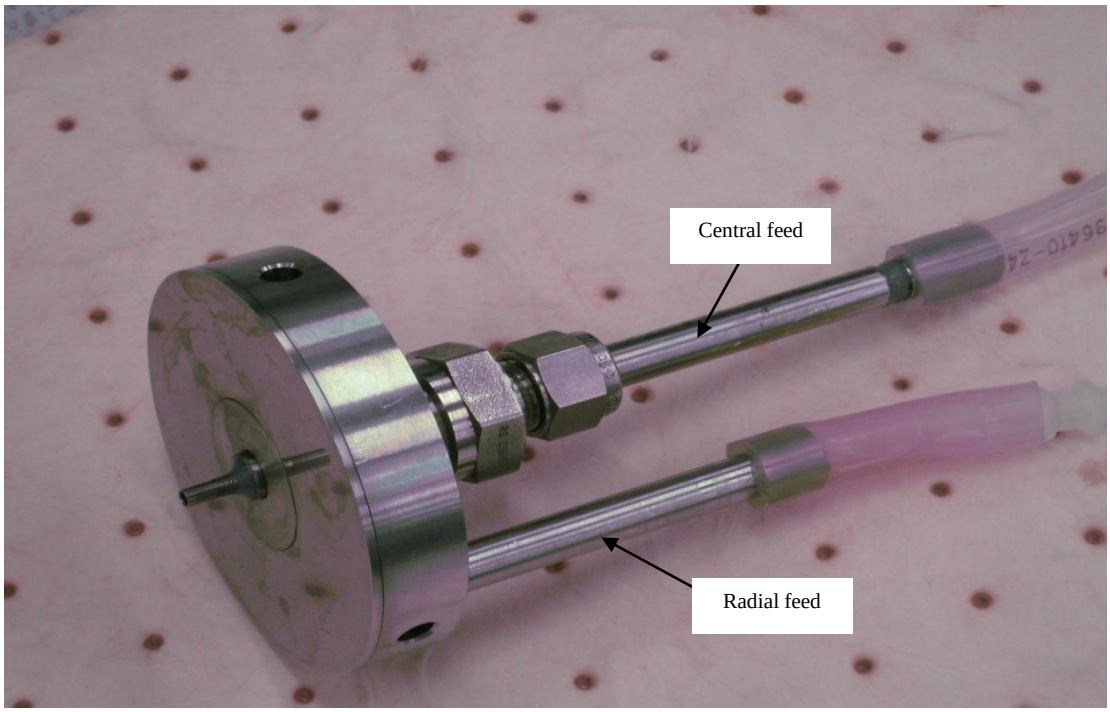

Figure 4.21: Multi point-distributor components after assembly

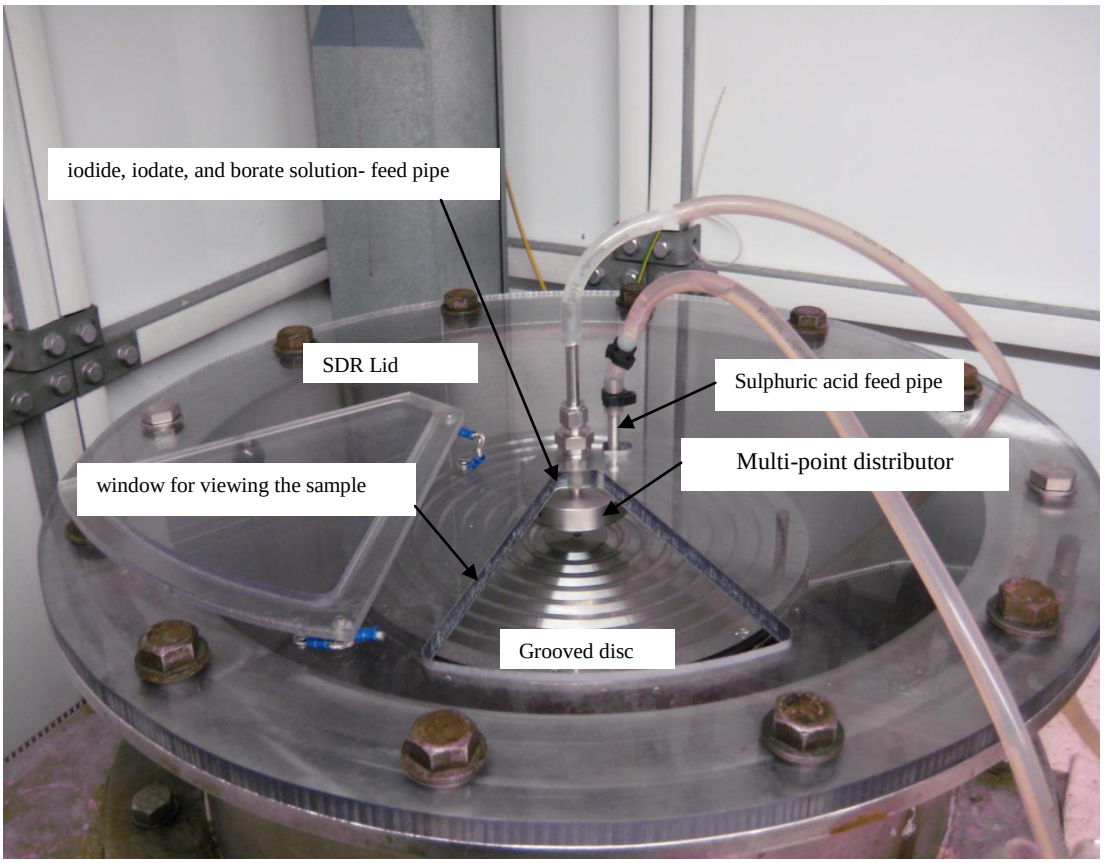

Figure 4.22: Multi-point distributor operational set-up

4.2.3.3 30 cm SDR Micromixing Experimental Procedure

The procedure for the 30 cm SDR micromixing experiments was very much similar to the one followed in the 10 cm SDR. A syringe pump type of (NE-1000, New Era Syringe Pump) was used for the delivering of the sulphuric acid into the centre of the disc surface using 4.8mm Masterflex platinum cured silicone tubing connected to a single or multi point-distributor which depends on the experimental mode. The iodide, iodate and borate solution was delivered by the peristaltic pump type of Watson Marlow pump 505S from a 10 L aspirator to the centre of the disc surface along with a 4.8 mm Masterflex platinum cured silicone tubing connected to a single point distributor or to the central pipe in the case of multi point distributor.

The 60 ml syringe was filled with sulphuric acid and was inserted in its slot on a syringe driver. The 10 L aspirator was filled with the Iodide, Iodate and Borate solution and was

connected to the peristaltic pump using 4.8mm silicone tubing. The water bath temperature was set at 20 ^{o}C from the water bath temperature controller.

The two electric immersion heaters were switched on followed by the centrifugal pump being switched on to deliver the cooling water from the water bath through the rotary union connected to the shaft. Before the commencement of the experiments, it was ensured that the reactor system temperature becomes constant and equals to the set point of 20 ^{o}C.

The iodide, iodate and borate solution and the sulphuric acid pumps were set at the desired flowrates and were turned on to fill the tubing system and the single-point / multi-point distributor. This was to ensure that tubing and feeding systems were completely full and air bubbles-free. Once the fluids appeared on the centre of the disc, the pumps were turned off and the disc was cleaned by a wiper; and at this time the system became ready for performing the experiments.

When the reactor disc surface temperature reached 20 ^{o}C (steady state condition), the desired disc rotational speed was set from the digital disc speed controller and the disc started to rotate. In the meantime, the samples bottles were cleaned by de-ionised water and were dried by the air and placed on the Table which was located close to where the sample tube collector were located at the bottom of the reactor. At this time, the iodide, iodate and borate solution and sulphuric acid pumps were turned on in order to introduce the two fluids to the centre of the disc through the single / multi -point distributor. To ensure that the system is maintained at a total steady state condition i.e. tubing and feeding system were air bubbles-free and reactants temperature on the disc surface reached the 20 ^{o}C, the disc was run for 5min before taking any sample from the sample collector. After that, three samples were collected in the sample glass bottles at a time interval of 2 minutes for the purpose of absorbance (D) analysis using (UNICAM 8700 UV/Vis) spectrophotometer. The disc and both of the pumps were then stopped. Before analysing the samples, the pH for the samples were measured and recorded to ensure that it was not lower than 7. The samples were analysed within five minutes of the collection from the SDR sample collector. The samples were analysed using the same manner of the analytical procedure followed in the SBR and 10cm SDR experiments with a wavelength of λ = 353 nm. After the experimental run, the disc lid

was removed and the reactor was flushed with de-ionised water and then dried by wiper and the lid was fixed back to its original position by tightening the lid bolts. At this stage the system was ready to perform the next experiment.

4.2.4 Narrow Channel Reactor (NCR) Experimental Rig

The fourth rig employed for the micromixing experiments was the Narrow Channel Reactors Rig (NCRs). Figure 4.23 shows the general layout of the NCRs rig and its auxiliary equipment. The narrow channel reactors used for the experimental runs were made of borosilicate glass and were fabricated at the Glass Blower Workshop in the Department of Chemistry – Newcastle University.

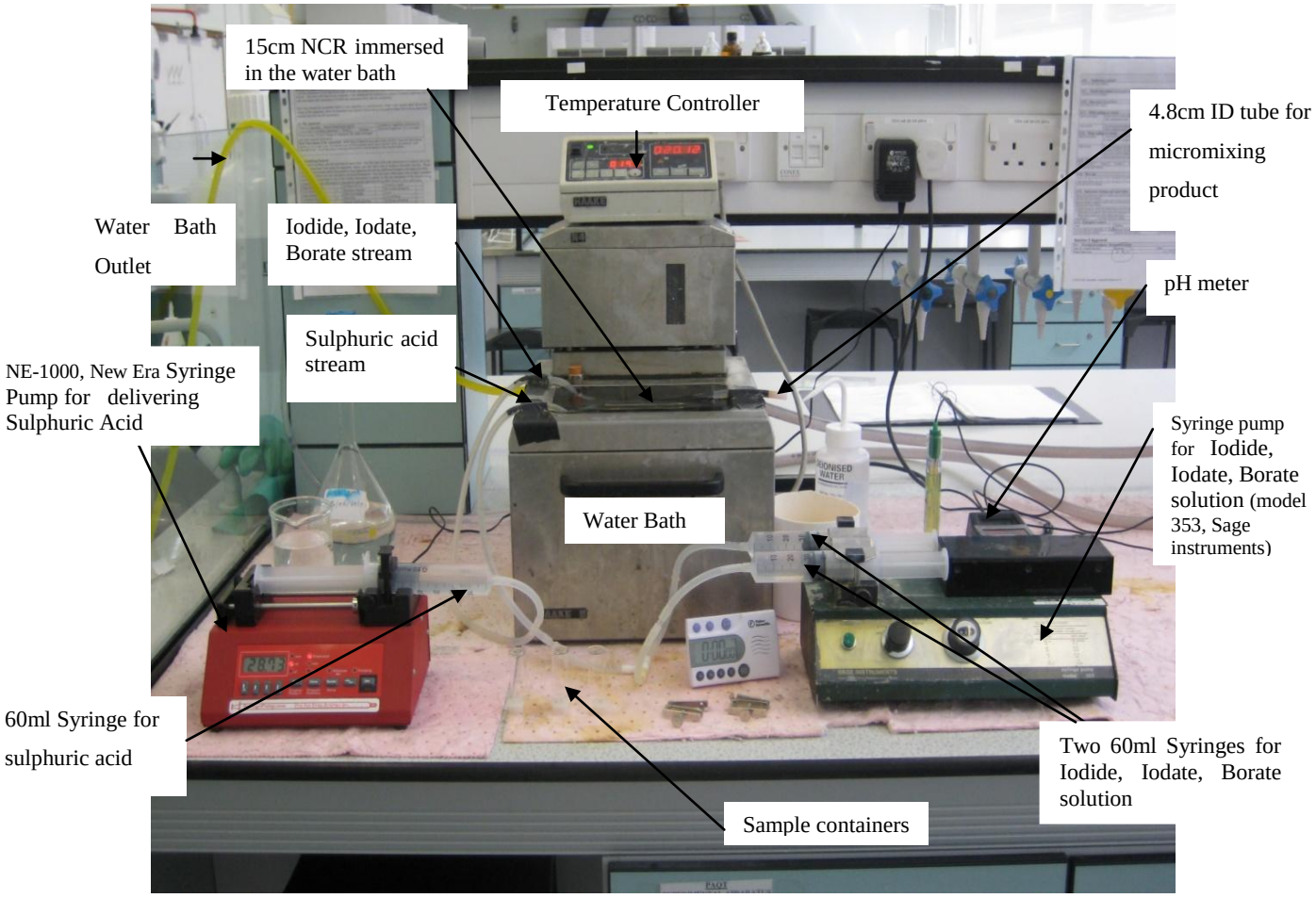

Figure 4.23: Set up of the NCR Rig

Figure 4.24, below shows the flow diagram for the process carried out with the Y and T- junction NCR. Two junction types were considered for the experiments, namely the T and Y, in order to investigate whether the junction type has any effect on the

micromixing. Three channel lengths were considered for each of the junction type, 5 cm, 10 cm and 15 cm, in order to determine whether the micromixing continues along the length of the channel. Figures 4.25 and 4.26 show the Y and T- junction Narrow Channel Reactors used in this part of the research.

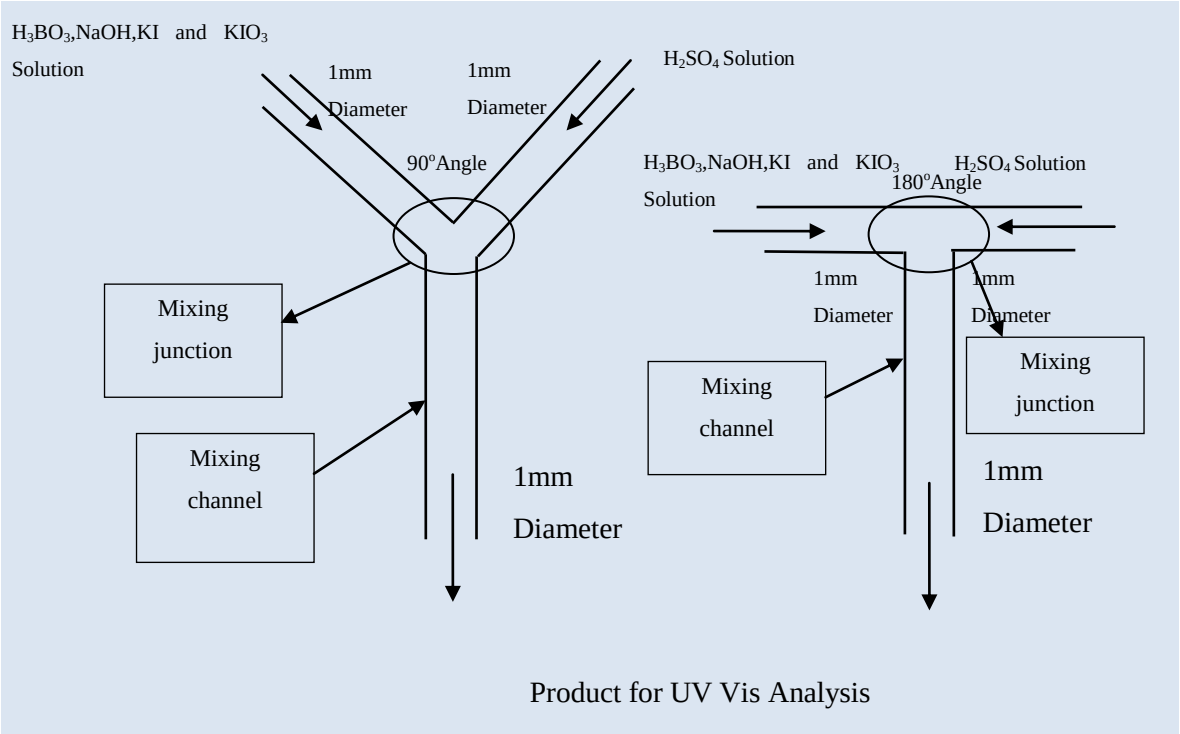

Figure 4.24: Schematic flow diagram for the mixing process carried out Y and T Junction NCR's

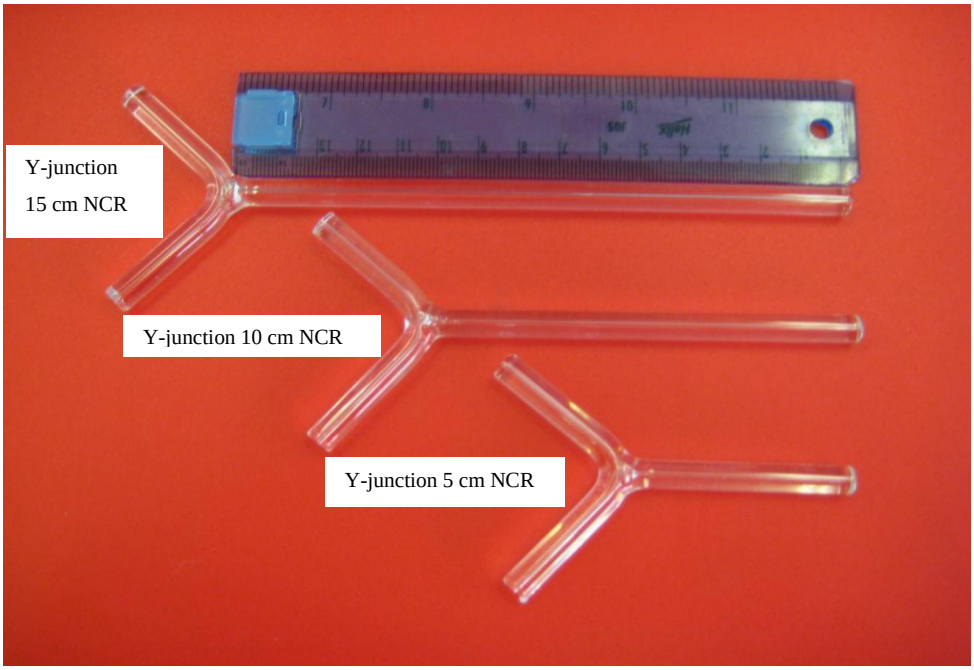

Figure 4.25: Y-junction Narrow Channel Reactors

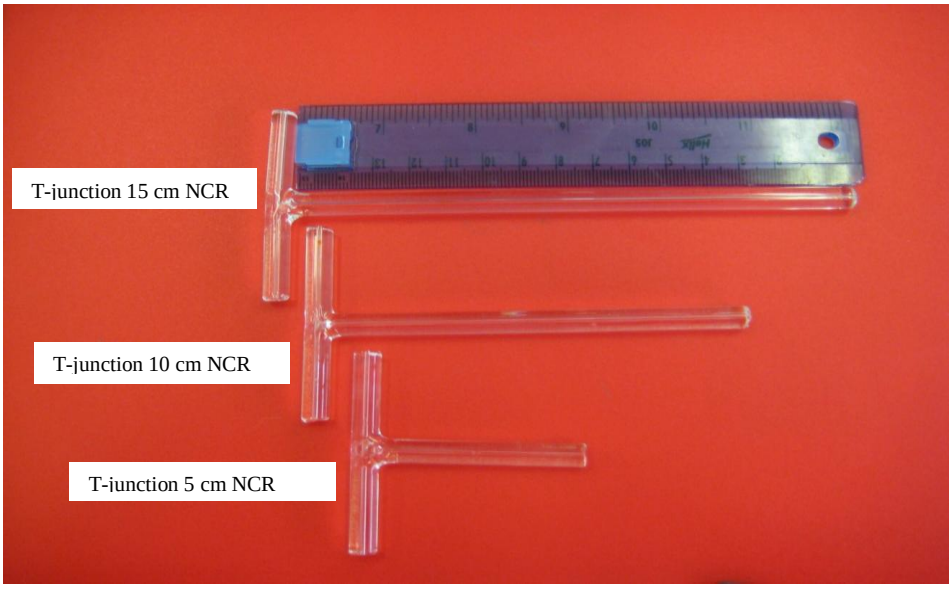

Figure 4.26: T-junction Narrow Channel Reactors

The narrow channel reactors were immersed in a water bath (HAAKE circulators N4-B) in order to keep the temperature of the reacting liquid in the narrow channel reactors constant at 20 ^{O}C. as mentioned earlier, this temperature is required in order to satisfy the validity of the rate constant used in the calculation of the iodine concentration, as determined by Guichardon *et al.* (2000) where it was found that the constant experiences no change between 20 ^{O}C and 35 ^{O}C . In addition, the narrow channel reactors were kept flat in the water bath to ensure that no back flow was allowed into the feed channels. Figure 4.27 shows an aerial view of 5cm Y- junction Narrow Channel Reactor in the water bath.

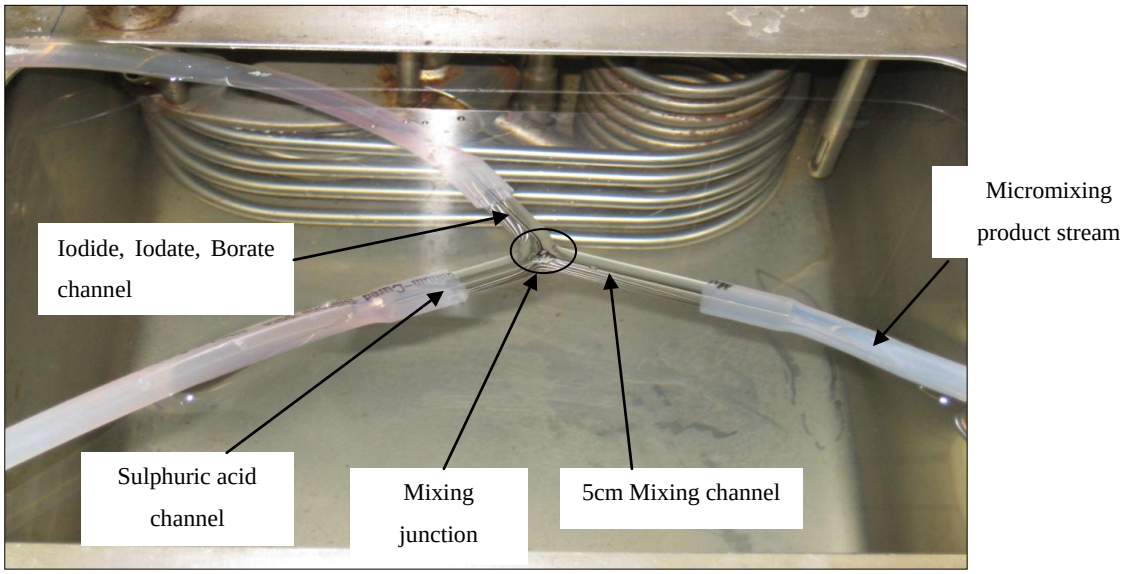

Figure 4.27: Aerial View of Y-junction 5cm NCR in water bath

The Y-junction narrow channel reactors used had a 90° angle between the two feed streams with 1mm diameter each. Both the feed channels (3 cm in length each) were followed by the mixing channel which has a diameter of 1mm. Y-Junction reactors were used with a mixing channel length following the mixing junction of 15 cm, 10 cm and 5 cm. Additionally, T-junction narrow channel reactors were used to aid the comparison of junction types with an angle of 180° between the two feed streams (1mm diameter each). The T-junction narrow channel reactors used as part of this research had a feed channels length of 3 cm each and followed by a mixing channel with a diameter of 1 mm and lengths of 5 cm, 10 cm and 15 cm, to allow for the direct comparison with the Y-junction reactors.

The tubing following the narrow channel reactor had an internal diameter (ID=4.8 mm) which is four times higher than that of the narrow channel reactor to prevent further micromixing following the narrow channel reactor (SCHNEIDER, 2004).

4.2.4.1 Reactants Pumping System for the NCR Experimental Rig

The syringe pump used for feeding the Iodide, Iodate solution (Model 353, Sage Instruments, shown in Figure 2) consist of two syringes with 60 ml capacity. The pump flowrates were varied by a percentage flow controller located within the pump. Calibration of the pump was achieved by altering the percentage flow and measuring the volume collected over a time period of one minute, thus allowing the determination of a flowrate in terms of ml/min. To ensure the accuracy of the calibration, the pump was operated with the piping and the narrow channel reactor in the positions to be used for the experimental runs. The pump was recalibrated for each narrow channel reactor and with both the water and viscous solutions. The calibration charts obtained can be seen in Appendix F.

A NE-1000, New Era programmable syringe pump was used to pump the sulphuric acid contained within the 60ml syringe. The flowrates can be specified on the pump in terms of ml/min. Calibration of the pumping speeds was completed to verify the pump flowrates by measurement of the volume of fluid collected over a period of a minute. As with the calibrations procedure of previous pump, the calibration for this pump was

completed with the piping and reactor in the same position as for the experimental runs. The calibration chart obtained can be found in Appendix F.

4.2.4.2 Micromixing Experimental Procedure for the NCR Rig

The continuous mixing of the Iodide, Iodate and Borate solution and the Sulphuric acid was carried out in a narrow channel reactor. The two feeds met at a junction with the mixing continuing along the length of the narrow channel reactor. The feed streams were pumped to the narrow channel reactor using syringe pumps The syringe pump type of (NE-1000, New Era Syringe Pump) equipped with one 60 ml syringe was used for the delivery of the sulphuric acid to the feed channel of the acid using 4.8 mm Masterflex platinum cured silicone tubing. The 60 ml syringes were loaded with sulphuric acid for a desired concentration and inserted in its slot on the syringe driver. The desired flowrate was set from the pump flowrate controller. The Syringe pump type (Model 353, Sage instruments) was used for delivering the Iodide, Iodate and Borate solution to the feed channel along with 4.8 mm Masterflex platinum cured silicone tubing; two 60 ml syringes were loaded with the Iodide, Iodate and Borate solution and were inserted in their slots on the syringe driver. The Iodide, Iodate and Borate solution flowrate was set by selecting the % of the flow set point from the flow controller that corresponds to the desired flowrate. The characterised narrow channel reactor was connected to the two feed tubing then immersed in the water bath. As mentioned earlier, the narrow channel reactor was kept flat in the water bath to ensure that no backflow was allowed into the feed channels. The water bath temperature was set at 20 ^{o}C from the water bath temperature controller. The samples bottles were cleaned using de-ionised water and then dried by the air and placed close to the rig. When the rig temperature reached 20 ^{o}C (steady state condition), the syringe pump and the peristaltic pump were switched on to deliver the reactants to the NCR. To ensure that the system is maintained in a total steady state condition i.e. tubing and feeding system were air bubbles-free and reactants temperature in NCR reached 20 ^{o}C, the reactants pumps were run for 5 min before taking any sample from the NCR outlet through sampling tubing. After that, three samples were collected in the sample glass bottles at a time interval of 2 min. Both of the pumps were then stopped. The pH for the sample was measured and recorded to ensure that it was not lower than 7. The absorbance (D) values of the samples were analysed within five minutes of the collection from the NCR outlet through sampling tubing using (UNICAM 8700 UV-vis) spectrophotometer. The

samples were analysed using the same manner of the analytical procedure followed in the SBR, 10 cm SDR and 30 cm SDR micromixing experiments with the wavelength of λ = 353 nm. Upon completion of the experimental run, the NCR was disconnected from the feed tubing and was flushed with de-ionised water repeatedly then dried by using a wiper. The NCR was fixed back to its position in the water bath and connected to the feed tubing. At this stage the NCR became ready for performing the next experiment.

4.3 Calculation Procedure for Tri-Iodide Concentration

The quantitative analysis of I_3^- was carried out as suggested by Fournier et al. (1996a). The product was analysed by UV/Vis Spectrophotometer at a wavelength of λ = 353 nm. The concentration of Tri-Iodide was therefore carried out on the basis that the Lambert-Beer law is valid which means that the absorbance, D_λ, is less than 2.0 at the particular wavelength and also it is directly proportional to the concentration of Tri-Iodide as follow:

$$D_\lambda = [I_3^-] \,.\, \varepsilon_\lambda \,.\, l \tag{4.7}$$

From the absorbance, D_λ, calculation of the concentration of Tri-Iodide became possible knowing that the molar extinction coefficient, ε_λ, and the optical path length, l as :

$$[I_3^-] = \frac{D_\lambda}{\varepsilon_\lambda \,.\, l} \tag{4.8}$$

Table 4.5 shows the values of molar extinction coefficient which are given in the literature.

Table 4.5: List of extinction molar coefficient determined in literature and respective wavelengths

References	Wavelengths, λ (nm)	Extinction molar coefficient, ε_λ (m^2/mol)
(Custer, 1949)	352	2590
(Awtrey and Connick, 1951)	353	2640
(Palmer et al., 1984)	350	2575
(Guichardon and Falk, 2000)(SB*)	353	2395.9
(Guichardon and Falk, 2000)(DB**)	353	2606
(Assirelli et al., 2002) (DB)	353	2541.2

(SB)= single beam*

*(DB**)= Double beam*

For this research, the spectrometer used was a single beam system *(SB)* and the value of extinction molar coefficient was 2395.9 m^2/mol.

4.4 Calculation Procedure for Xs using a single Injection method

The procedure of determining the quantity of the micromixing efficiency which is expressed by the segregation index, Xs, requires the determination of the concentration of Tri-Iodide (I_3^-) using Spectrophotometric analysis. The concentration of I_3^- was achieved by measuring the optical density of I_3^- and the subsequent application of the Beer-Lambert law (equation 4.7).

The segregation index, Xs, relating the actual yield of the undesired product, Y, to the maximum yield, Y_{ST}, as defined by Fournier et al.(1996a) and given as follows:

$$X_S = \frac{Y}{Y_{ST}} \tag{4.9}$$

Where

I. For the Semibatch process

$$Y = \frac{2\left(n_{I_2} + n_{I_3^-}\right)}{n_{H_0^+}} = \frac{2V_{tank}[(I_2) + (I_3^-)]}{V_{injection}(H^+)_0} \quad (4.10)$$

II- For the continuous process

$$Y = \frac{2\left(n_{I_2} + n_{I_3^-}\right)}{\left(n_{H^+,0}\right)} = \frac{2\left(C_{I_2} + C_{I_3^-}\right)Q_t}{\left(C_{H^+,0}\, Q_H\right)} \quad (4.11)$$

And

$$Y_{ST} = \frac{6(I_3^-)_0}{6(IO_3^-)_0 + (H_2BO_3^-)_0} \quad (4.12)$$

Where $Q_t = (Q_I + Q_H)$ represents the total liquid flowrate of the two solutions i.e. the iodide, iodate, and Borate solution and the sulphuric acid solution respectively introduced into the system, and the subscript 0 denotes the inlet conditions.

Y is considered to be the ratio of moles of acid consumed by Dushman reaction to produce I_2, which then produced I_3^-, over the total moles of acid injected to the system based on the measured values of I_3^-. Y_{ST} is the product of the reaction due to the total segregation conditions in which the quantity of iodine formed is mainly due to the stoichiometric ratio of the reactants. Consequently, the calculated segregation index, X_S, ranged between 0 and 1 in which X_S= 0, gives a perfect micromixing and X_S=1, gives total segregation. In general, 0 < X_S < 1, i.e., there is partial segregation.

In conclusion, for any given pair of competing parallel reaction, the lower the value of X_S, gives better micromixing. In order to determine the amount of I_2 produced, the mass balance on the iodine can be considered based on the given equation as follows:

$$(I^-) = (I^-)_0 - \frac{5}{3}\left[(I_2) + (I_3^-)\right] - (I_3^-) \quad (4.13)$$

$$K_B = \frac{(I_3^-)}{(I_2)(I^-)} \quad (4.14)$$

K_B = the equilibrium constant of reaction (4.3), which is defined by the equation below:

$$log_{10}K_B = \frac{555}{T} + 7.355 - 2.575log_{10} \quad (4.15)$$

At 20°C, K_B for the water system equal 788.89. Guichardon et al. (1997) studied the effect the glycerol mass fraction on the K_B and it was found that the K_B equals 2250 for the 50 wt% water/glycerol system and 6250 for the 75 wt% water/glycerol system.

The combination of Equations (4.13) and (4.14) gives a second order algebraic equation which can be solved to give the iodine concentration as follows:

$$-\frac{5}{3}(I_2)^2 + \left[(I^-)_0 - \frac{8}{3}(I_3^-)\right](I_2) - \frac{(I_3^-)}{K_B} = 0 \quad (4.16)$$

In determining the values of Xs using single injection method, for a given operating conditions, for four different reactants, a Microsoft Excel spreadsheet was developed.

4.5 Residence time Distribution (RTD) Experimental Facilities and Procedure

RTD experiments were performed on the 30cm SDR Rig that was employed in the micromixing experiments and which has been described in detail in section 4.3.3. To make this rig applicable for the RTD experiments, some technical modifications have been carried concerning the sampling system.

4.5.1 Technical modifications for the RTD Rig

4.5.1.1 Sampling probe (scooper)

The sampling probe (scooper) was designed and constructed for the purpose of collecting the samples from the edge of the disc. This will help to get the overall experimental mean resident time (t_m) on the disc itself. Figure 4.28 shows the set up of the sampling probe (scooper). The sampling probe was designed with some considerations for the vertical movement of probe, the angle of the pickup probe and the rotational disc speed in order to orientate the probe in the direction of the film on the disc so that bending to the probe can be avoided and also to minimise the disturbance of the film on the disc.

The scooper was a flexible device brought into contact with a rotating surface in an attempt to sample the film at a given radius. This was a Tygon tube with ID=1.6mm and it was flexible so as not to damage disc surface or disrupt the film unduly. The end tube was cut at an angle of 30^0 so as to build a pool within the tube which could then be drawn up via a syringe for later analysis. The scooper device was set to the position allocated for sampling but not in contact with the disc surface. The disc speed was set and disc stared.

The respective flow rate was set from the pumps before switching them on. When the steady conditions were observed for the liquid film on the disc, then the fine vertical adjustment was wound down to bring the flexible scooper tube in to contact with the liquid film on the rotating disc surface. The sampling syringe was then extended to attempt to draw up fluid from the surface. Unfortunately, due to the thinner film of the disc, it was not possible to collect the samples by the scooper. To address this technical problem, the scooper was replaced by shoe collector which is described in next section.

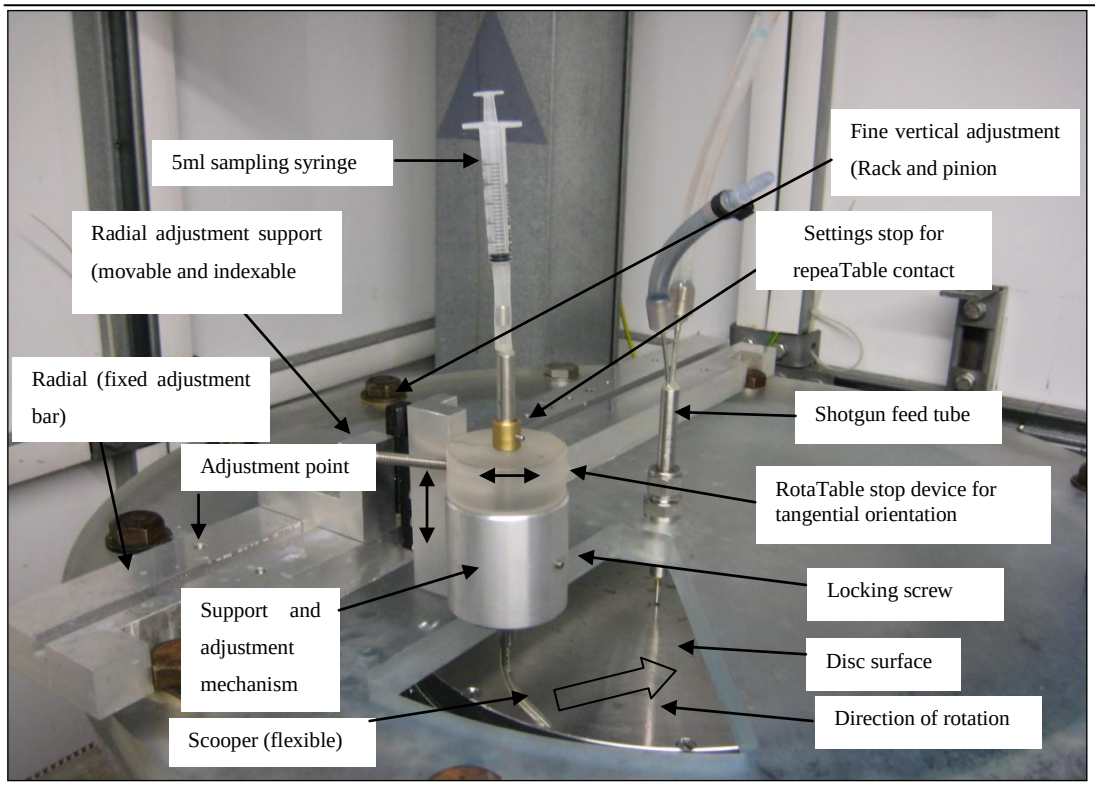

Figure 4.28: The set up of the sampling probe (scooper)

4.5.1.2 Sampling shoe

The shoe collector is a small box with the dimensions of 6.0 cm length x 2.0 cm width x 2.0 cm height arranged by welding together stainless steel plates. One side of the sampling shoe was left half enclosed on the side closer to the SDR (2.0 mm away from the edge of the disc) to provide an entrance for reactants to be collected and retained, if necessary, in a small reservoir. The shoe collector outlet size was engineered to provide minimal residence time in the shoe. The shoe is supported in the main collector by a heavy base annulus with a sturdy rod and an adjusTable setting mechanism to stop device to ensure accurate, repeaTable placement after removal. The shoe was tilted slightly to create a fall towards the outlet pipe thus reducing hold up further. This is then connected to small flexible pipe for sampling purposes. This sample pipe exits the reactor coaxially via the main drain pipe until and then through a small hole in the wall of the pipe enabling sample collection as close to the SDR surface as possible. Figures 4.29 and 4.30 showed the sample shoe set up before the assembly. Figures 4.31 and 4.32 show the sample shoe set up after the assembly and the Shoe operational set-up within the 30 cm SDR .

The methylene blue was delivered by syringe pump and the de-ionised water was delivered by the peristaltic pump. Both fluids were fed to the central disc surface via single feed-distributor (shotgun) that was used with the micromixing experiments using 30 cm SDR Rig. Before starting the RTD experiments, some considerations were taken into account. This was to ensure that the shoe meet its objectives. To confirm this, some trials were carried out with the shoe modified. The trials showed that the modified shoe performed very well in collecting the low flowrate sample but at the higher flowrates the shoe overflowed which caused problems in collecting fresh samples with short time intervals of 10 s. This problem occurred because of the small diameter of outlet pipe of 1.25 mm. This was addressed by increasing the outlet pipe diameter to 2.9 mm , which allowed the product to flow out of the tube more rapidly.

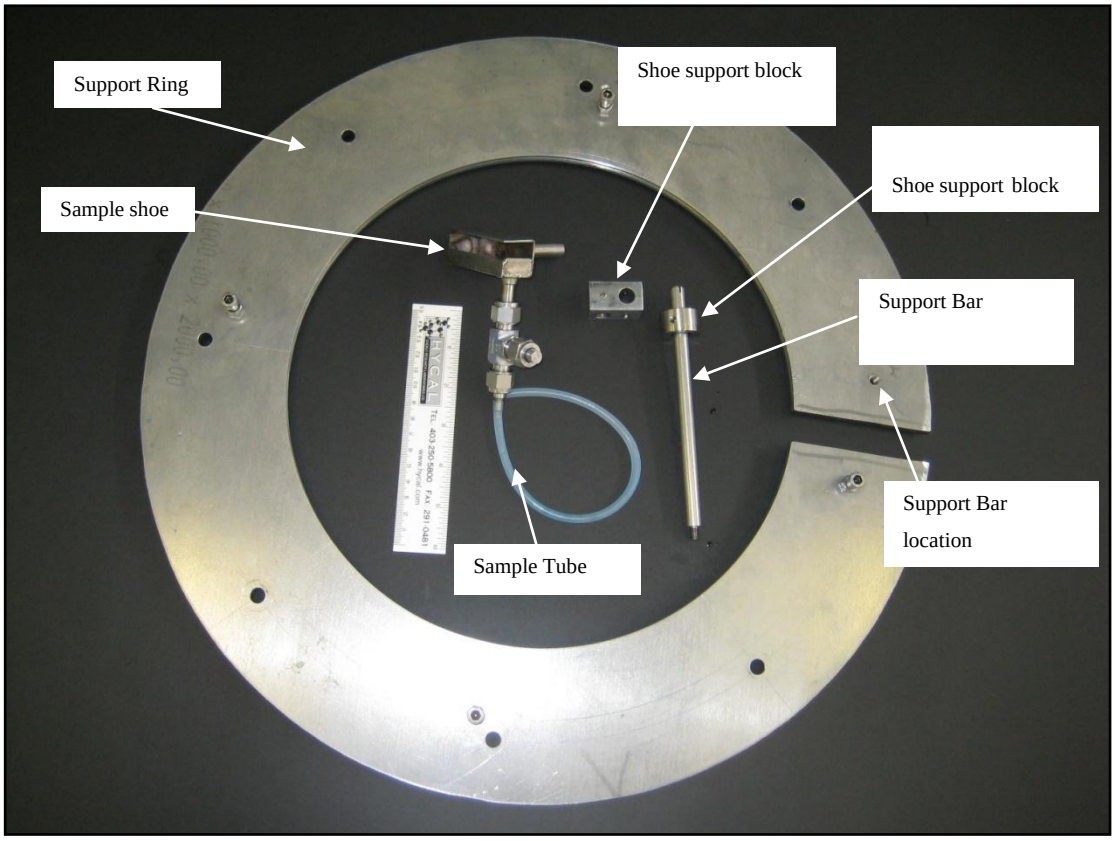

Figure 4.29: Sample shoe set up (before assembly)

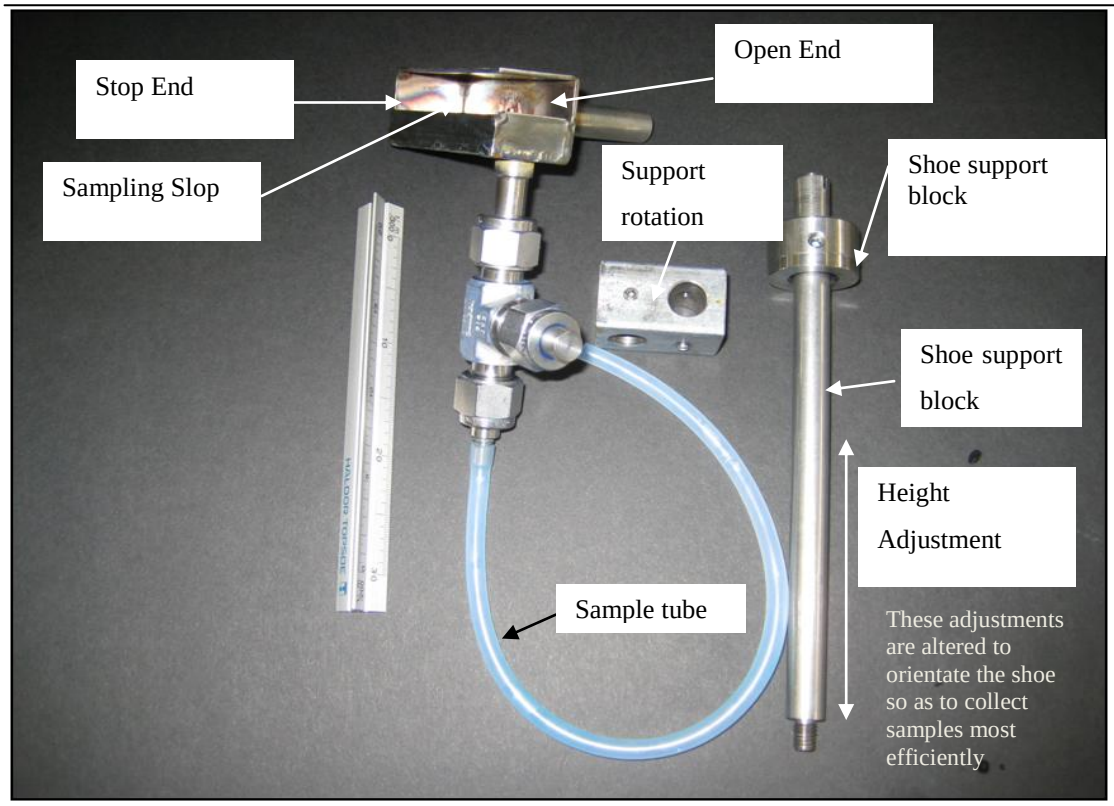

Figure 4.30: Sample shoe set up (before assembly)

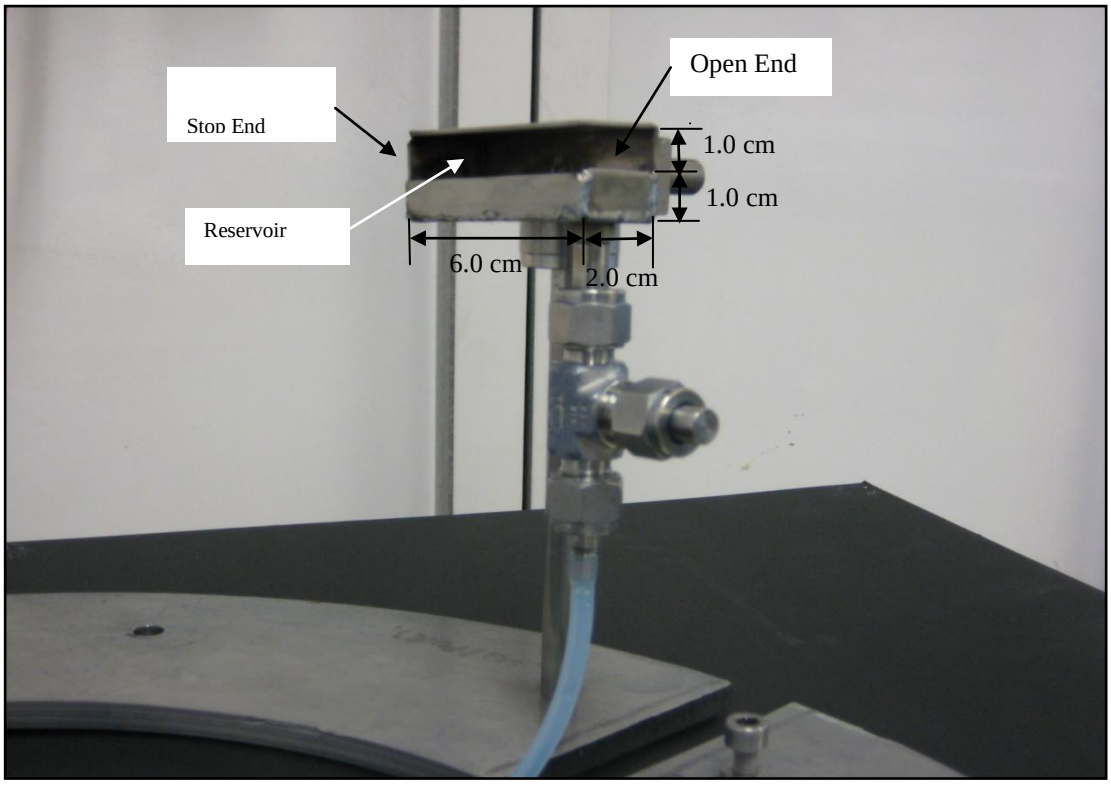

Figure 4.31: Sample shoe set up (after assembly)

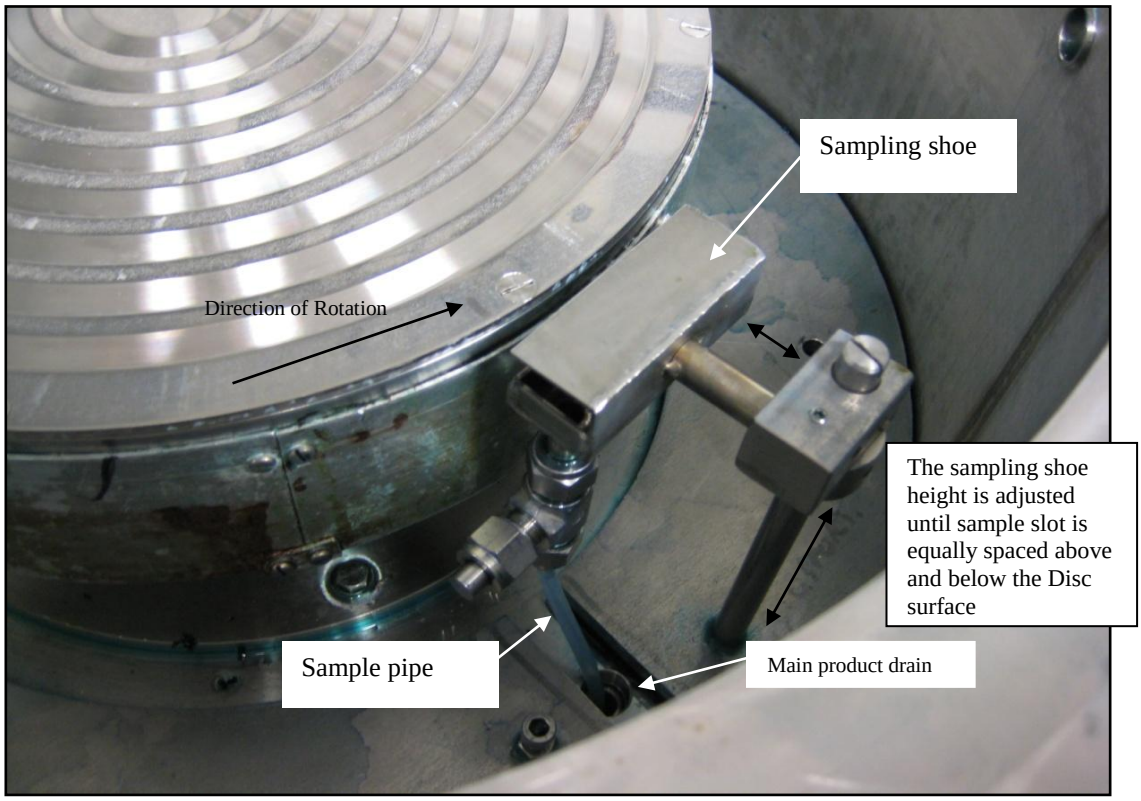

Figure 4.32: Shoe operational set-up

4.5.2 Residence time distribution: Experimental procedure

Methylene blue was used as a step-input tracer in the residence time distribution experiments. In order to ensure that accurate flow rates with no pulsation was achieved, a syringe pump type of (NE-1000, New Era Syringe Pump) was used for the delivering of the methylene blue into the centre of the disc surface using 4.8 mm Masterflex platinum cured silicone tubing connected to a single point distributor. The syringe pump was equipped with one 60 ml syringe. The working fluid (de-ionised water for water system or 50 wt% glycerol/water system) was fed from a 10 L aspirator to the centre of the disc surface using peristaltic pump type of Watson Marlow pump 505S supplied by Cole-Pamer-UK along with a 4.8 mm Masterflex platinum cured silicone tubing connected to a single point distributor. The desired flowrate was set from the pump speed controller that corresponds to the desired flowrate. The 10 L aspirator was filled with the de-ionised water and connected to the peristaltic pump using 4.8mm silicone tubing.

The 60 ml syringe was filled with methylene blue of 0.5 g/l concentration and was inserted in its slot on a syringe driver. The volumetric flowrate of methylene blue tracer was set from the pump flowrate controller and kept 5 ml/min for the entire course of experiments.

The water bath temperature was set at 25 ^{o}C (ambient temperature) from the water bath temperature controller. The two electric heaters were switched on and then the centrifugal pump was switched on to deliver the cooling water from the water bath through the rotary union connected to the shaft to allow for the cooling of the bearing and internal machinery parts as well as the disc surface. Before the commencement of the experiments, it was ensured that the reactor system temperature becomes constant and equals to the set point i.e. 25 ^{o}C to avoid any mechanical damage that could occur to the bearing and other mechanical parts of the reactor due to the running of the reactor without a cooling system. After that, the working fluid and methylene blue pumps were set at the desired flowrates and were turned on to fill the tubing system and the single-point distributor. This was to ensure that tubing and feeding systems were completely full and air bubbles-free. Once the fluids appeared on the centre of the disc, the pumps were turned off and the disc was wiped clean using a paper towel, at this stage the system was ready for performing the experiments. The desired disc rotational speed was set from the digital disc speed controller and the disc started to rotate. In the meantime, the samples bottles were cleaned by de-ionised water and were dried by the air and placed on the Table which was located close to the sample tube collector. The working fluid and methylene blue pumps were turned on in order to introduce the two fluids to the centre of the disc while the stop watch was turned on. The product, after being thrown off the edge of the disc, entered the sampling shoe and then flowed down through the 2.9 mm sample tubing. Twelve samples were collected with the time interval (Δt) of 10 s for the purpose of absorbance (D) analysis using UNICAM 8700 UV/Vis spectrophotometer. The samples were analysed using the same manner of the analytical procedure followed in micromixing experiments with the wavelength ($\lambda_{\max}$) ranged 662.7- 664.8 nm for both systems water and 50 wt% glycerol. After finishing the experimental run, the disc lid was removed and the reactor was flushed with de-ionised water, wiped clean and the lid was fixed back to its position by tightening the lid bolts. At this stage the system was ready to perform the next experiment.

5. Experimental Results and Discussion: Micromixing Studies

5.1 Semi-batch reactor (SBR)

The main objective of this set of experiments is to characterise the micromixing process in Semibatch reactor (SBR) and to compare its micromixing performance in terms of the segregation index (Xs), power dissipation (ε) and micromixing time(t_m) with results obtained from micromixing experiments using two different spinning discs of 10 and 30 cm in diameter and six different Narrow Channel Reactors (Y and T shape junctions, each of three different length; 5, 10 and 15 cm and 1 cm in diameter). This set of experiments has been carried out in a 1.37 L flat semi-batch reactor,(SBR), made of borosilicate glass, equipped with four baffles and an impeller of Rushton turbine-type with four flat blades, as described previously in Chapter 4.

As mentioned in Chapter 2, section 2.8, the iodide-iodate reaction system was implemented in this research as a model reaction to characterise the micromixing phenomena in intensified reactor systems. The iodide-iodate reaction system can be described in three steps as follows:

$$H_2BO_3^-{}_{(aq)} + H^+{}_{(aq)} \rightleftarrows H_3BO_{3(aq)} \quad \text{Acid-base neutralization, Quasi-instantaneous} \quad (5.1)$$

$$5I^-{}_{(aq)} + IO_3^-{}_{(aq)} + 6\,H^+{}_{(aq)} \rightleftarrows 3\,I_{2(aq)} + 3\,H_2O_{(aq)} \quad \text{Dushman reaction, Fast} \quad (5.2)$$

$$I_2 + I^- \rightleftarrows I_3^-{}_{(aq)} \quad \text{Equilibrium} \quad (5.3)$$

5.1.1 SBR Experimental design

MINITAB 15 software programme was utilized in order to generate an appropriate general full factorial experimental design for both water and 50 and 75w% glycerol systems (Table G1 in Appendix G). The variables incorporated into experimental design were:

- Impeller Agitation speed: 300,600,900 and 1200 rpm
- Acid concentration: 0.25,0.50,1.0 M

- Acid feed injection location: Middle of Reactor and Close to the Impeller
- Viscosity: water system(μ=1.005 mPa.s at 20 °C), 50wt% glycerol system (μ = 6.0 mPa.s at 20 °C) and 75 wt% glycerol system(μ=35.5 mPa.s at 20 °C)

72 experiments for three systems, i.e. water system, 50 wt% Glycerol system and 75 wt% glycerol system were carried out. Each experiment was repeated three times. The mean value of segregation index, Xs (mean), the standard deviation (σ), standard error (S) and relative error were estimated. The maximum relative error of experiments was only (7.2 %) and the results were satisfactorily reproducible. Calculation Procedure for the error analysis is shown in appendix H.

The acid ion concentrations and its injected volumes in the 2.0l SBR, containing 1.37 L of iodate and iodide ions in basic medium are shown in Table 5.1 below. The calculation of the sulphuric acid volumes which needs to be injected in the SBR is shown in appendix B. The acid injection rate was 3.6 ml/min (see section 5.1.2 for details).

Table 5.1: The acid ion concentrations and its injected volumes in the 2.0l SBR, containing 1.37 L of iodate and iodide ions in basic medium

Acid concentration,[H^+] mol	Volume of acid ion , V_{H^+} (ml)	Injection time,(min)
0.25	80	22.22
0.5	40	11.11
1.0	20	5.60

5.1.2 Influence of acid feed rate on the segregation index, Xs

As discussed previously in the literature review (Section 2.4.6.2.3 in Chapter 2), the segregation index can be strongly influenced by the acid feed rate if reaction is carried out in a semi-batch reactor. The feed time used in the experiments must exceed a critical time (t_c) in order to make sure that experiments are carried out in the micromixing-controlled regime.

The critical injection time was determined for the worst operating conditions used in the semi-batch experiments (i.e N=300 rpm, [H+] =1.0 M and acid injection point at the middle of the reactor) as shown in Figures 5.1 and 5.2 for water and

25%water/75%glycerol mixture respectively. The acid flowrates corresponding to each data point in Figures 5.1 and 5.2 are presented in Tables (G2) and (G3) in Appendix (G). The critical feed time was found to be 34 sec and 54 sec, for water system and 75wt%glycerol system respectively. A value of 335 sec, corresponding to an acid injection rate of 3.6 ml/min, was subsequently used for all experiments which was well above the critical injection time. Therefore, at such low acid injection rate used in semi-batch experiments, it is ensured that macromixing effects are eliminated and the results given by chemical test reactions are only micromixing relevant.

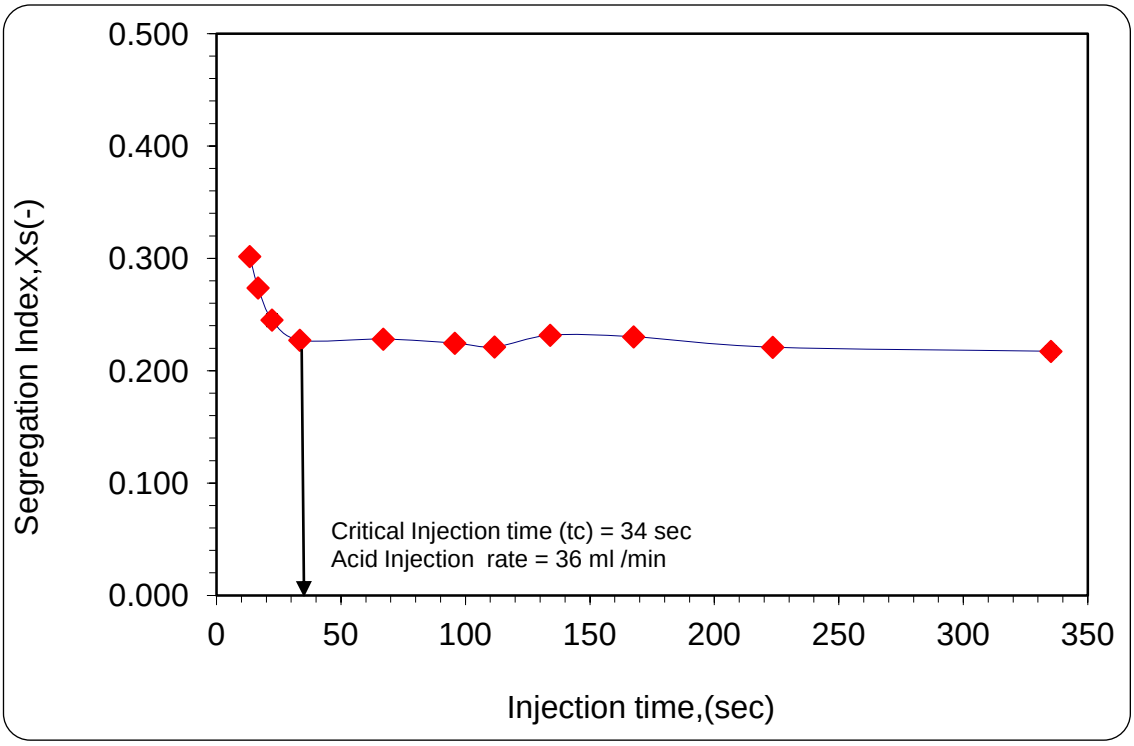

Figure 5.1: Influence of acid injection time on segregation index (Xs) using [H+]=1.0 M injected in water in the batch reactor with stirrer speed N of 300 rpm and feed point located in the middle of the reactor

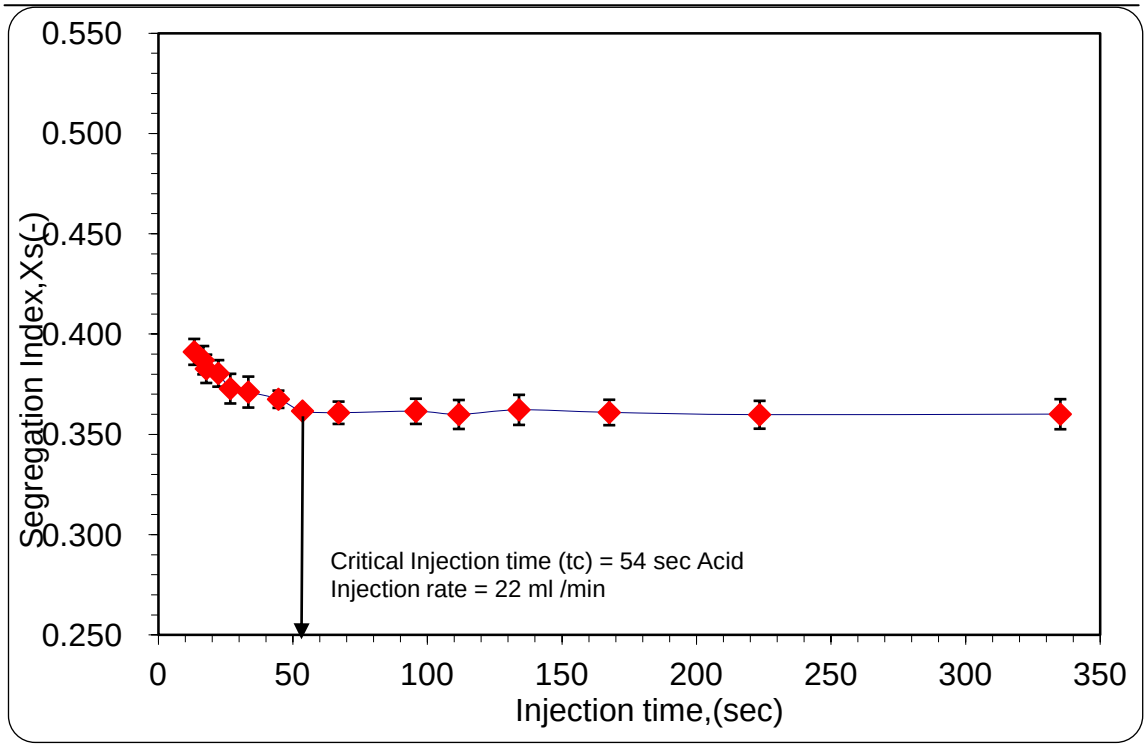

Figure 5.2: Influence of the acid feed rate on segregation index, (Xs) using [H+]=1.0 M injected in 25% water/75wt% glycerol mixture the batch reactor with stirrer speed N of 300 rpm and feed point located in the middle of the reactor

5.1.3 Influence of acid concentration and impeller rotational speed on segregation index, (X_s)

Figure 5.3 shows the effect of acid concentration on the segregation index (Xs) using three different acid concentrations in the range 0.25 to 1.0 M injected at position 2 (corresponding to the middle of the reactor, as shown in schematic diagram of the SBR, Figure 4.3 with four different stirrer speeds (300, 600, 900 and 1200 rpm). It is seen that the higher the concentration of acid, the higher the value of X_S at any rotational speed of the impeller. Similar trends have previously been reported for iodide-iodate reaction scheme as shown in Figure 5.4 (Fournier et al., 1996a). This behaviour is explained by considering the kinetics of the neutralization and of the Dushman reactions involved in this process. With a decrease of the acid concentration, the rates of the neutralization reaction and of the Dushman reaction are slowed down but the rate of the Dushman reaction is more sensitive because its order with respect to acid is higher and the difference between the two reaction rates is increased. Therefore, less iodine is produced and X_S decreases.

The effect of impeller rotational speed on the segregation index is also shown in Figure 5.3. It is observed that the segregation index Xs consistently decreases with increasing impeller rotational speed for all acid concentrations used in this study. In fact, an increase of the rotational speed corresponds to increasing the mean specific energy dissipation rate and consequently the local specific energy dissipation rate and engulfment rate also increases. Thus, as expected the intensity of micromixing is enhanced and X_s decreases. This is in agreement with the findings in other studies as shown in Figure 5.4.

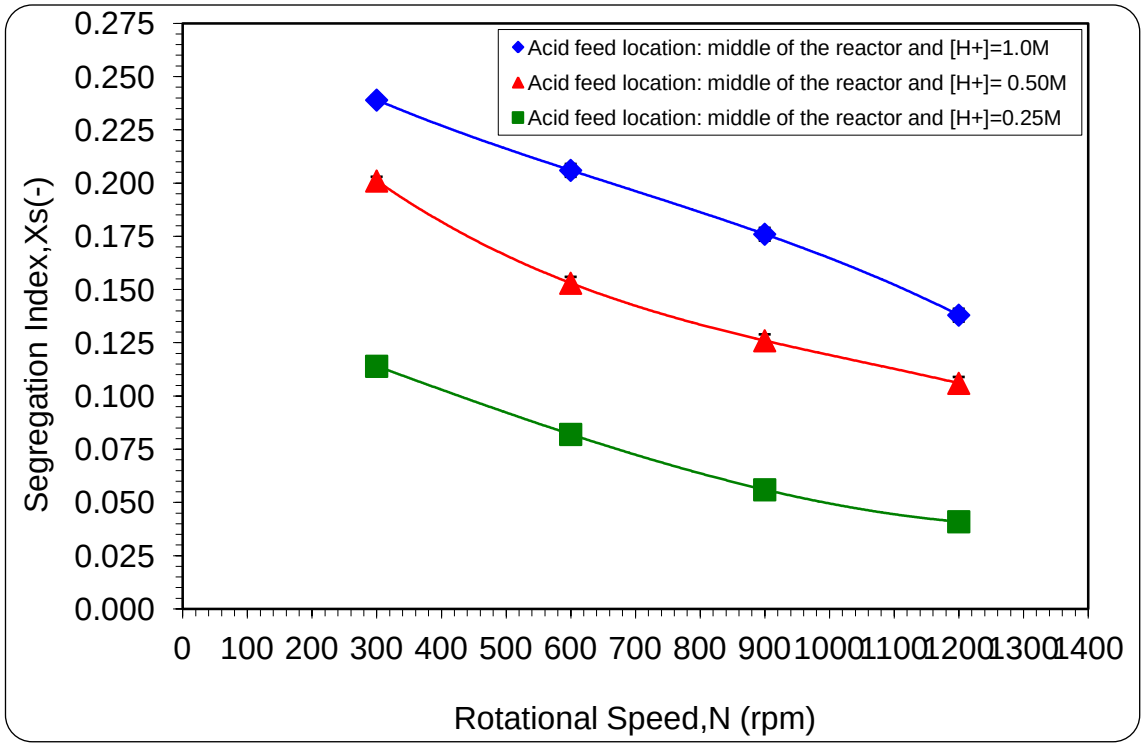

Figure 5.3: Influence of the acid concentration and stirrer speed on segregation Index (Xs) with feed point located at the middle of the reactor – water system

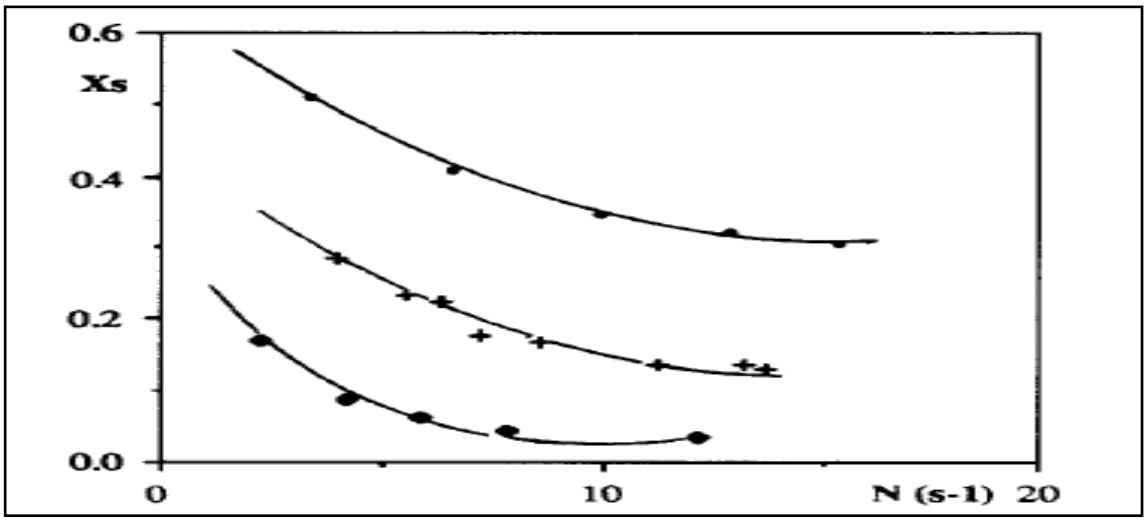

Figure 5.4: Segregation index, Xs, as a function of different acid concentration,(●) ([H+] =8 •10^{-2}, (+) ([H+] =8 x10-2, (♦) ([H+] =8 x10^{-2} (Fournier et al., 1996a)

5.1.4 Influence of viscosity on segregation index,(Xs)

Glycerol-water mixtures of two different concentrations (50 and 75wt % of Glycerol) were used in this task to obtain viscosities of 6 and 35.5 mPa.s at 20 ^{O}C . From Figure 5.5 and 5.6, the influence of viscosity on the segregation index can be seen for acid concentrations of 0.25 M and 1.0 M respectively. As viscosity increases from μ= 1.005 mPa.s to μ= 6 mPa.s and 35.3 mPa.s, Xs increases for all agitator speeds tested. This is most evident at the highest viscosity system used.

Clearly, the increase of viscosity slows down the micromixing rate and consequently, increases the micromixing time (t_m). Furthermore, it alters the intrinsic kinetics of the reaction. In fact, it could slow down the overall reaction rate, and this will result to shift of Xs to a higher value at high liquid viscosities (Guichardon et al., 1997).

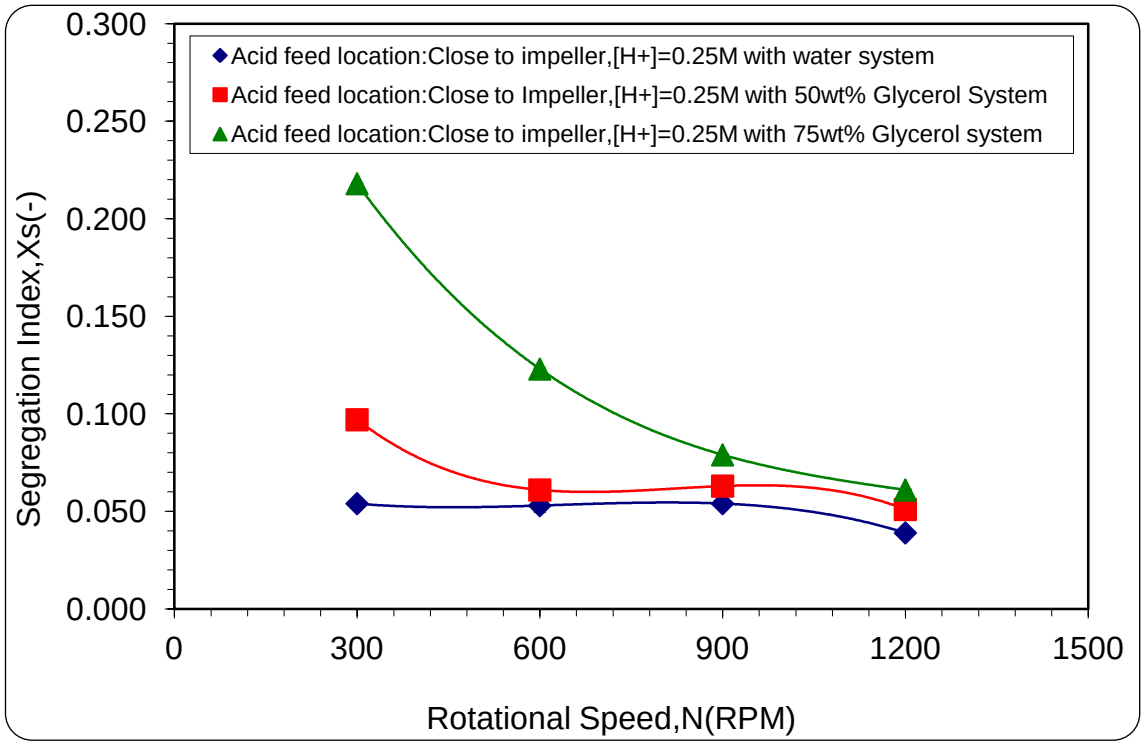

Figure 5.5: Dependence of the segregation Index, (Xs) on the liquid viscosity with [H+] =0.25 M and acid feed location close to impeller

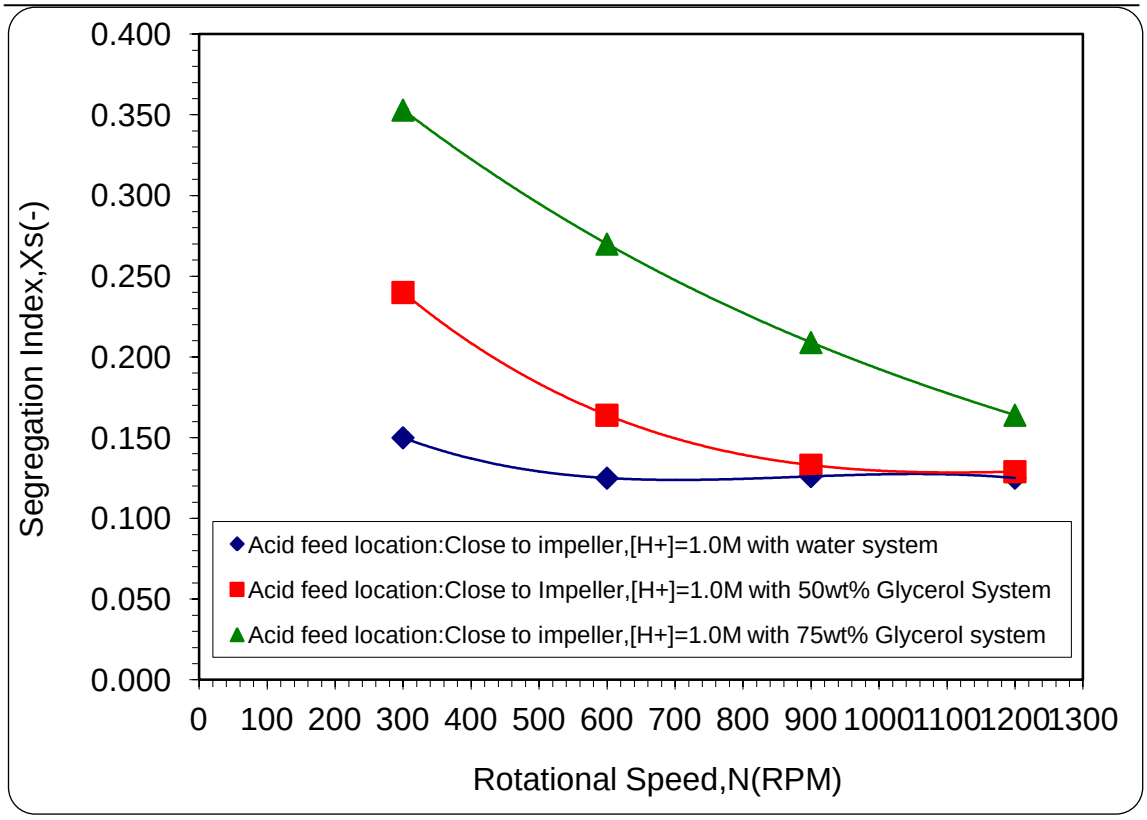

Figure 5.6: Dependence of the segregation Index, (Xs) on the liquid viscosity with [H+] =1.0 M and acid feed location close to impeller

5.1.5 Influence of feed location on segregation index,(Xs)

From the results displayed in Figure 5.7, it can be clearly seen that acid injection position has a remarkable effect on the values of segregation index, Xs. Thus for each impeller rotational speed, Xs decreases in going from injection position < 2 > to the injection position <1> (impeller discharge stream). This effect is attributed to the local power dissipation in the SBR i.e. from position of low to high local power dissipation, which is also reported by Geisler et al. (1994). The highest value of local power dissipation (ε) has been reached at the impeller discharge stream was 21.2 W/kg. Nevertheless, only 8.5 W/kg has been reached at the injection position < 2 >, i.e. the middle of the reactor and this confirmed the findings of LDV studies (Geisler et al., 1994). The effect of power dissipation on Xs is discussed in more detail in the following section.

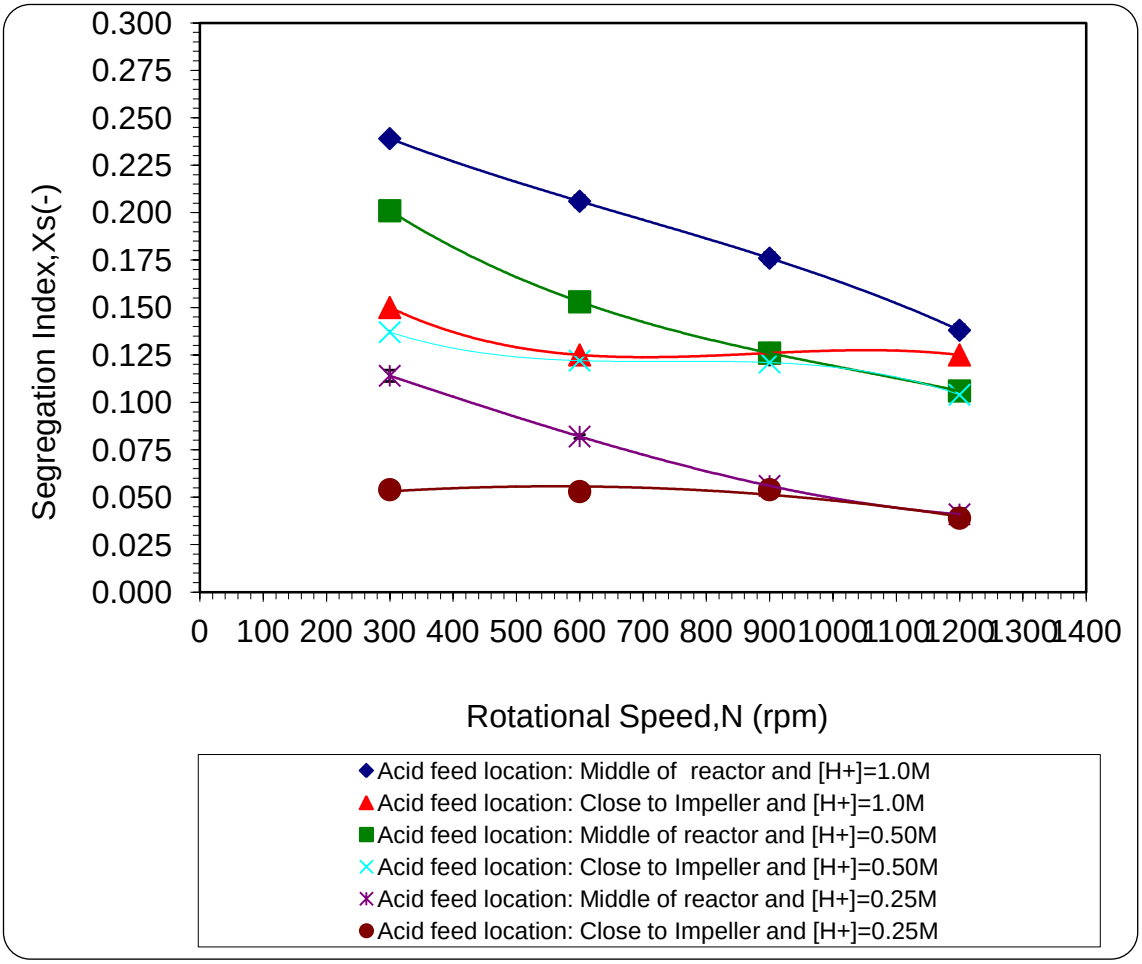

Figure 5.7: Influence of Acid feed location on segregation Index, (Xs) - water system

5.1.6 Estimation of Power dissipation,(ε), and its effect on Xs

As stated earlier in section 2.4.4.4.2, the total power dissipation is not distributed homogeneously in the whole tank. The local power dissipation per unit volume of the fluid and local flow velocities in the tank depends strongly on the position in the tank. The greatest values are measured at the impeller discharge stream and specifically near the impeller tip where the engulfment rate has the highest value. The relative power dissipation (Ø) is expressed by:

$$\emptyset = \frac{\varepsilon}{\bar{\varepsilon}} \qquad (5.4)$$

Ø is depends on the position and the geometry of the reactor. Ø at the region of radial flow in discharge equal 4 where the injection point <1> were located (Guichardon et al.,

2000b). Ø at the region of axial flow along the wall <2> has been calculated from the following empirical correlation (Baldyga and Bourne, 1999) :

$$\emptyset = 1.7exp(-2.5Z^*) \quad (5.5)$$

Where Z^* is the height of the injection point from the centre of the impeller which is 0.0252m. Then the value of Ø is 1.6. The power number is in the range of 3.5 – 5 and is dependent on the Reynolds number (Holland and Bragg, 1995).

The local power dissipation, (ε), in SBR was estimated by equation (2.33) given in Chapter 2 and reproduced here:

$$\varepsilon = \emptyset \frac{N_P N^3 D^5}{V} \quad (5.6)$$

Figure 5.8 shows the effect of the impeller rotational speed on the power dissipation, the higher the impeller rotational speed, the higher the power dissipation introduced to the fluid by the impeller. It can see from equation (5.6) the power dissipation is proportional, to N^3.

Figure 5.9 and Figure 5.10 show the segregation index, (Xs) as function of local power dissipation (ε) for three different acid concentrations and two different acid injection points. It is clear that from Figure 5.9 and Figure 5.10 the higher value of power dissipation leads to lower value of segregation index, (Xs). This is because a high impeller rotational speed corresponds to high energy input and therefore, to large engulfment rate, which enhances the micromixing process.

In Figure 5.9, the acid was injected close to the impeller, the local power dissipation (ε) values varied from 0.331 to 21.2 W/kg depending on the impeller rotational speed used. Alternatively in Figure 6.10, the acid was injected at middle of reactor, the local power dissipation (ε) values varied from 0.132 to 8.5 W/kg. At an impeller rotational speed of 1200 rpm and acid concentration of 1.0M injected in the middle of the reactor (Figure 5.10), the local power dissipation (ε) and Segregation index; (Xs) equalled 8.475W/kg

and 0.138 respectively. Under the same operating conditions with implementation of acid injection point close to the impeller, (Figure 5.9), the local power dissipation (ε) and segregation index, (Xs) equalled 21W/kg and 0.125 respectively. From Figure 5.9 and Figure 5.10, two facts can be confirmed. Firstly, the highest value of local power dissipation (ε) can be achieved at the impeller discharge stream and the lowest value will be at the acid injection point close to the liquid surface. Secondly, the segregation index (Xs) is inversely proportional to the local power dissipation (ε) and it is evident that the mixing intensity depends upon the mixing power input to the system, with higher power input increasing the intensity of mixing. Fournier et al. (1996a) use micromixedness ratio ($\alpha = \frac{1-X_S}{X_S}$) instead of segregation index, (Xs) in characterising micromixing efficiency. They found that micromixedness ratio is directly proportional to the local power dissipation (ε).

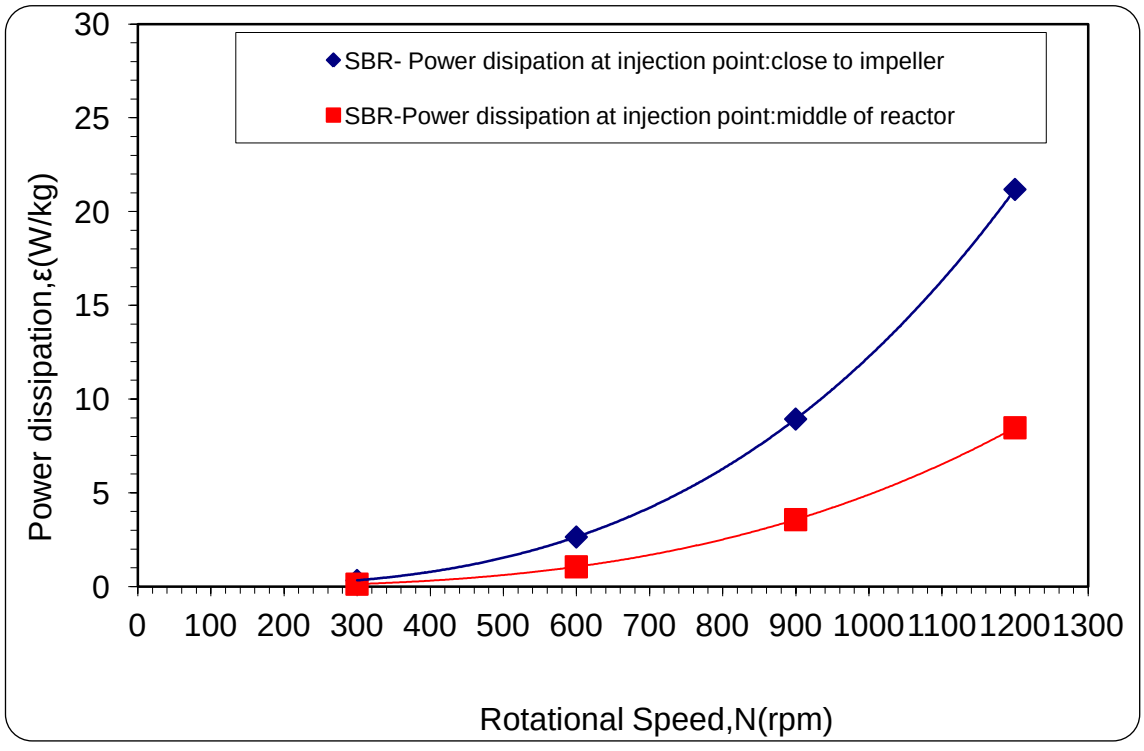

Figure 5.8: Dependence of the Power dissipation, (ε) on the impeller rotational speed,(N)- Water system

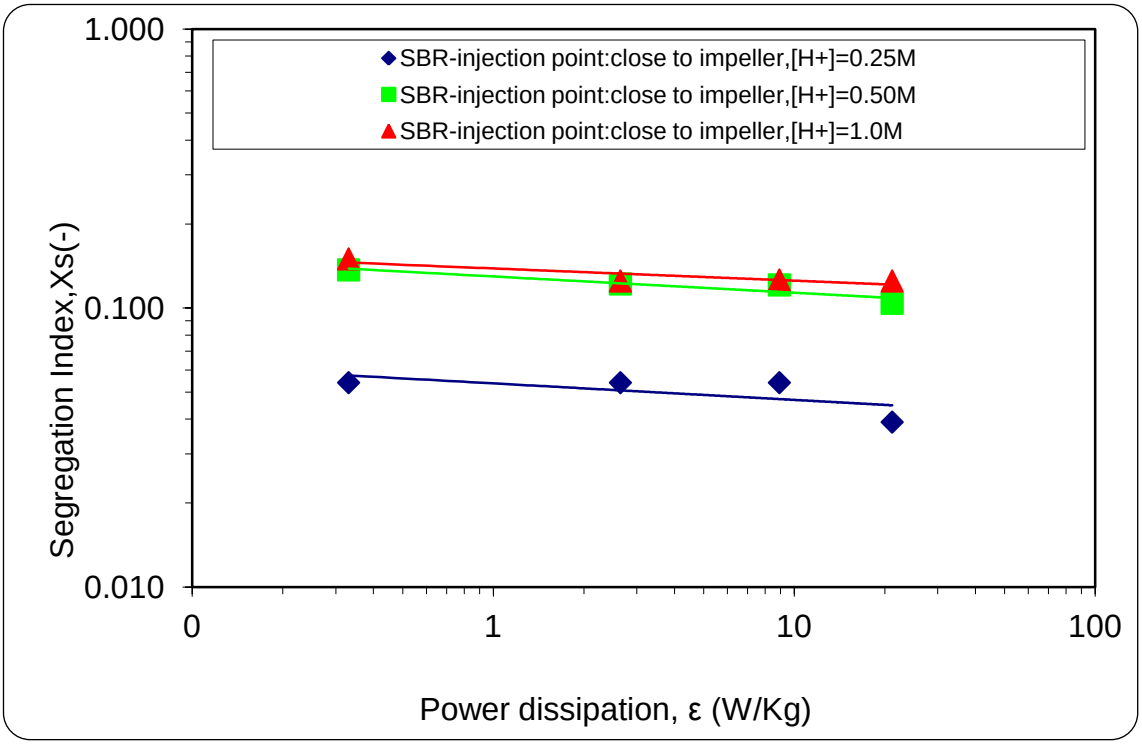

Figure 5.9:Dependence of the segregation Index, (Xs) on the Power dissipation: Water system - acid feed location is closed to impeller

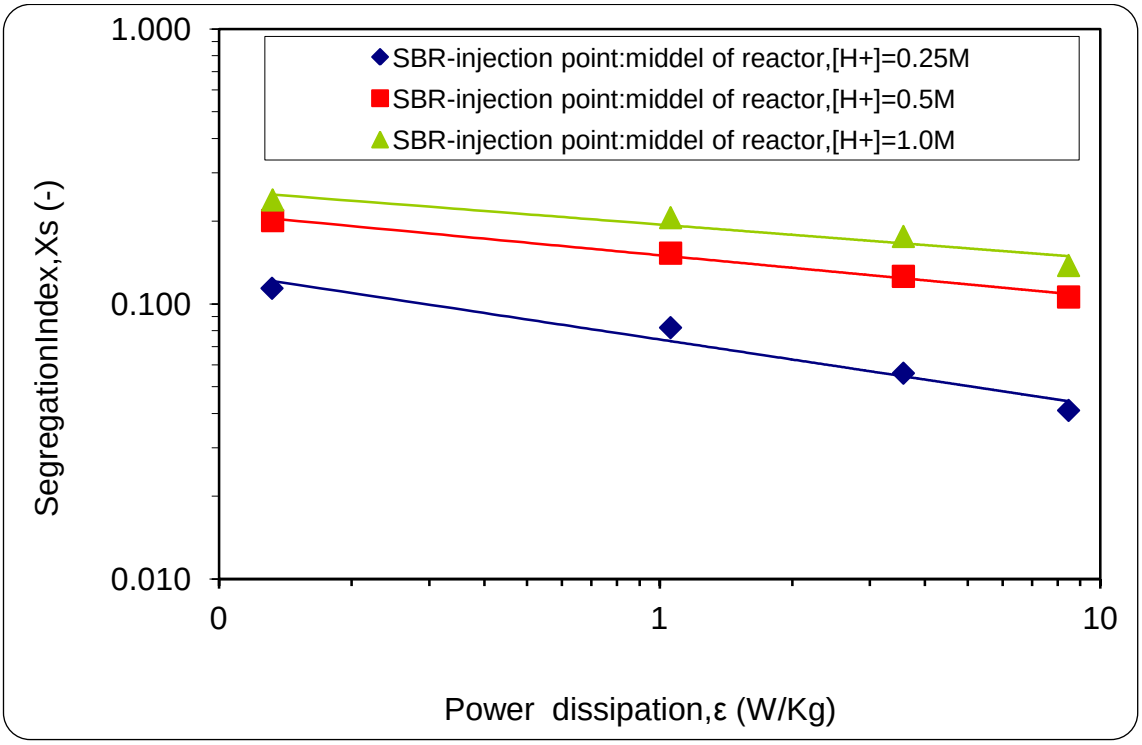

Figure 5.10: Dependence of the segregation Index, (Xs) on the Power dissipation: Water system - acid feed location at the middle of reactor

So far, the maps of Ø are well known for non-viscous media (Wu and Patterson, 1989; Costes and Couderc, 1988; Laufhuette and Mersmann, 1987; Okamoto et al., 1981). Up to date the published experimental data are available for the SBRs with capacity of 5 l. Guichardon (1995) confirmed that the maps of Ø are still valid in smaller SBRs, i.e. 1 l, as used in this study. Therefore, in this study $\emptyset = 4$ for the injection point <1> (corresponding to a location close to the impeller) and 1.6 for injection point <2> (corresponding to a location away from the impeller).

Guichardon el al.(1997) studied the effect of viscosity, up to 89 wt% Glycerol on the micromixing process. They assumed for moderately viscous solutions, that the power dissipation at a given location in the SBR and a given impeller rotational speed is the same as in water system. This is on the basis of Ø is proportional to $1/N_P$ and independent of viscosity.

On the basis of the above-mentioned assumptions, the values of power rate dissipation for 50 and 75 wt% Glycerol systems for this study at given a location in the SBR and a given impeller rotational speed are assumed to be as the values obtained for the water system.

5.1.7 Estimation of Micromixing time, (t_E) for SBR

The micromixing time is the time required to achieve complete mixing on molecular scale; in other words, the time required for the reagents to diffuse to one another. The degree of mixing can control the selectivity, quality or distribution of the final product only if micromixing time (t_E) is larger than the reaction time, (tr).

To choose the proper model for estimating the micromixing time in the SBR, the flow regime in the system needs to be characterised by calculating the impeller Reynolds number at the given operating conditions. The impeller Reynolds number can be specified as:

$$R_e = \frac{N D^2}{\nu} \qquad (5.7)$$

The flow is normally laminar if Re < 10, and turbulent for Re > 10000 the transition region between laminar and turbulent flow occurs over the range 10 < Re > 10000 (Cheremisinoff, 2000). The impeller Reynolds number is dependent on impeller rotational speed and its value was estimated for all three liquid systems studied, as follows:

Water system: 9680 ≤ Re ≤ 38720.

50wt% glycerol system: 7710 ≤ Re ≤ 1928 .

75wt% glycerol: 326 ≤ Re ≤ 1308 .

It is noted from these results that not all the experimental runs were carried out under turbulent conditions, i.e. Re ≥10000. This is because of the increased viscosity at higher glycerol concentrations: at 50 wt% and 75 wt% glycerol, operation was in the transition region.

Micromixing times for the SBR system were estimated for water system based on turbulence theory and the model proposed by Baldyga and Bourne (1999),i.e. equation (2.32). On the other hand, for non-turbulent flows, i.e. when the 50 and 75wt% glycerol system were used, the micromixing time or diffusion and deformation time model were applied (Baldyga and Bourne, 1984b), which is given as:

$$t_{DS} = \frac{1}{\dot{\gamma}2}\text{arcsinh}\left(\frac{0.76\dot{\gamma}\delta_0^2}{D}\right) \tag{5.8}$$

The above form of the micromixing time model is recommended by Baldyga and Bourne (1984b) for calculating the micromixing time (t_E) when the micromixing process occurring by engulfment of the fluid from the environment to form laminated structure within the vortex tube in the SBR and the flow regime in the system is non-turbulent flow.

Striation thickness (δ_0) is not equal to feeding pipe radius in the SBR (can be for fast feeding). Instead it depends on the feeding rate, (Q) and local fluid velocity close to the pipe and also is proportional to impeller speed (N) and impeller diameter (di). Hence,

from the material balance, $Q = \pi\, \delta_0^2\, u_{local}$. In this work the 50 and 75wt% glycerol system were injected close to the impeller (injection point < 2 >). In our work, the local velocity u_{local}, is the fluid velocity at the impeller suction, (U_s). Bhattacharya and Kresta (2002) carried on a CFD simulations to estimated the fluid velocity at the impeller suction as :

$$U_S = 0.25\pi Ndi \tag{5.9}$$

The shear rate at the impeller suction is the maximum shear rate in the SBR. Sanchez Perez et al.(2006) estimated the maximum shear rate in the stirred tank reactors as:

$$\gamma_{max} = 3.3\, N^{1.5} d_i \left(\frac{\rho}{\mu}\right)^{0.5} \tag{5.10}$$

Where d_i is the diameter of the impeller (m).

As mentioned above, the micromixing time for the water system was estimated from the turbulence theory model, equation (2.32). Figure 5.11 shows in logarithmic plot the estimation of micromixing time as function of local power dissipation for water system with two different acid injection locations and stirrer speed ranging 300 -1200 rpm. From Figure 5.11, it is clearly observed that the micromixing time is inversely proportional to the local power dissipation. As the power input increases, the micromixing time decreases.

The points lie on a straight line, in agreement with the findings of Fournier et al. (1996a) and Guichardon et al. (2000a). The micromixing time varies from 0.006 to 0.05 s at the injection point in the middle of reactor. At the injection point close to impeller it lies between 0.004 to 0.030 s. At the acid injection point close to impeller, the smallest value of micromixing time is achieved at 0.004 sec with the local power rate dissipation of 21.2 W/kg. On the other hand, at the injection point in middle of reactor, a micromixing time of 0.006 sec is achieved under similar operating conditions with a corresponding power rate dissipation of 8.5 W/kg.

Figures 5.12 and 5.13 demonstrate the relationship between the calculated micromixing time and the experimentally determined segregation index, (Xs), for the water system using $[H^+]$ =0.25, 0.5 and 1.0 M injected from both injection points (close to the impeller and the middle of reactor). From these two Figures, it is obvious that the shorter the micromixing time, the lower the value of segregation index achieved. This trend applies to any acid concentration used in this study.

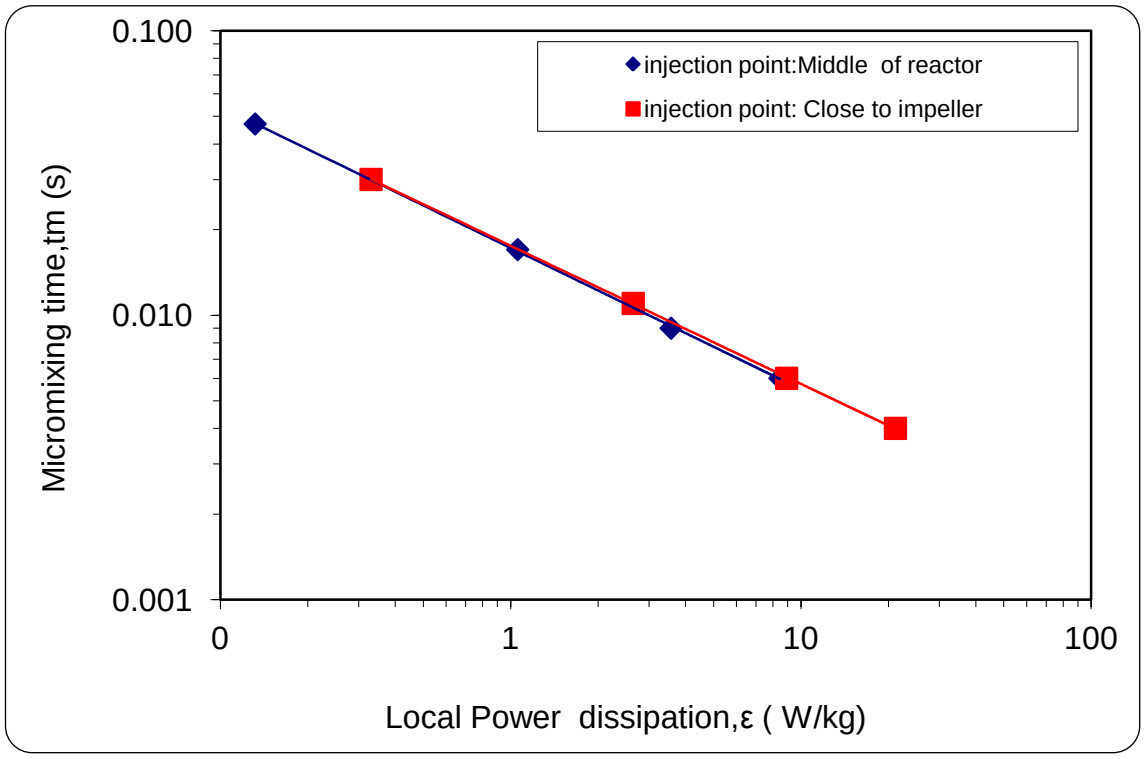

Figure 5.11: Micromixing time against Local Power Dissipation for two injection points- water system

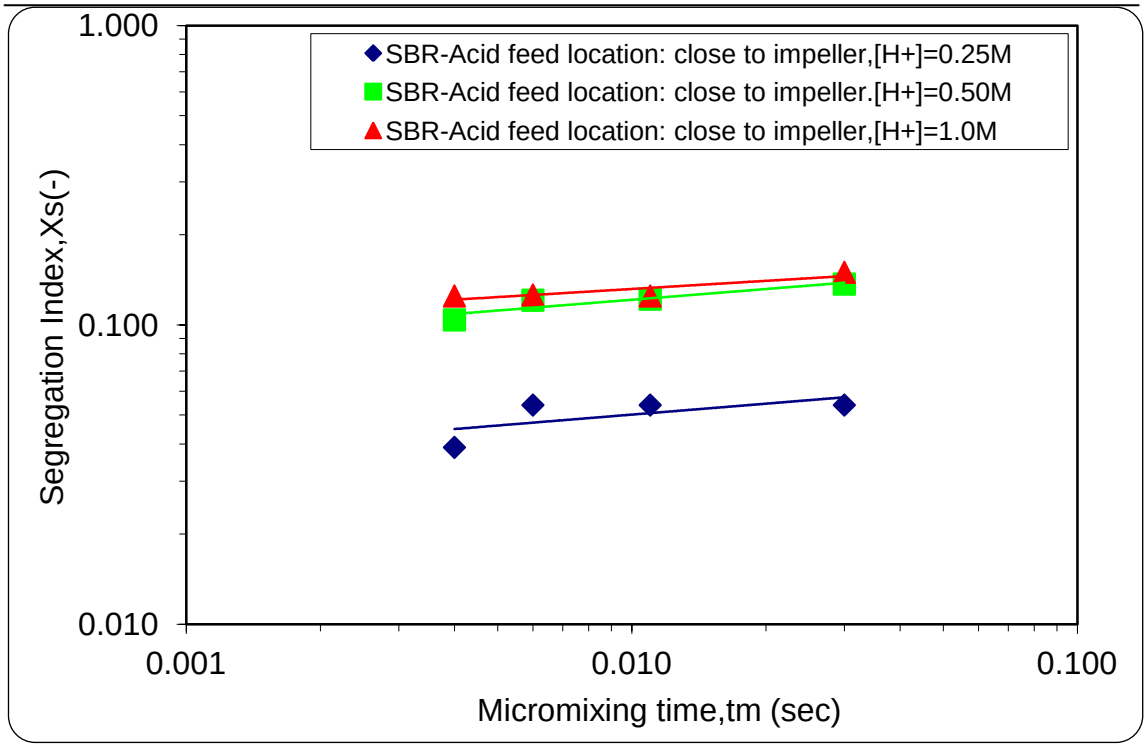

Figure 5.12: Dependence of the segregation Index, (Xs) on the Micromixing time for water system, the acid feed location is closed to impeller

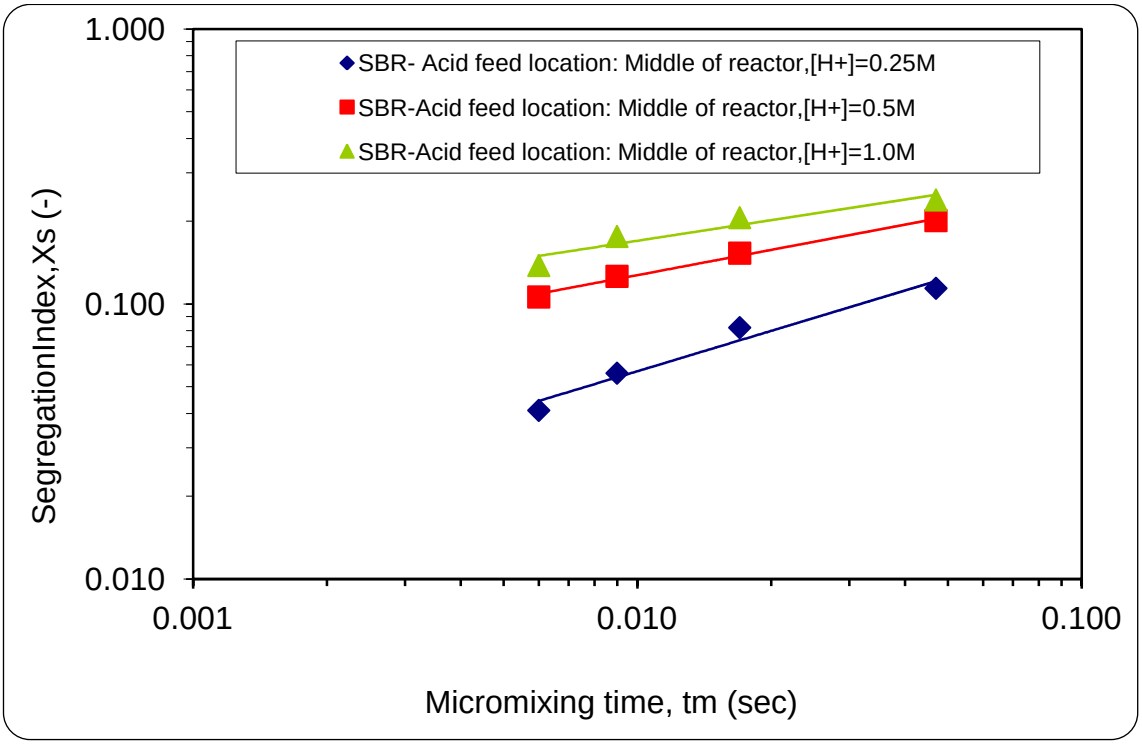

Figure 5.13: Dependence of the segregation Index, (Xs) on the Micromixing time for Water system, the acid feed location at the middle of reactor

Figures 5.14 and 5.15 demonstrate the relationship between the calculated micromixing time and the experimentally determined segregation index, (Xs), at the three different total flowrates for the water system, 50 wt% glycerol system and 75 wt% using $[H^+]$=0.5 and 1.0 M which injected from the injection point close to the impeller. From both Figures, it is obvious that the shorter the micromixing time, the lower the value of segregation index achieved.

From the findings above, it can be concluded that the impeller rotational speed play an important role in increasing the intensity of mixing in the SBR whereby the higher the impeller rotational speed, the higher the power dissipation. This in turn leads to shorter micro-mixing time between reacting molecules. Furthermore, at given impeller rotational speed, higher values of micromixing time were attained in the SBR by increasing the reactant viscosity. This is attributed to the fact that increasing the dynamic liquid viscosity (μ) results in a reduction in the maximum shear rate of the liquid solution in the SBR. Accordingly, the power dissipation to the fluid by the action of impeller rotation is reduced in higher viscosity media. In addition, the diffusivity, (D), is naturally slower when the feed viscosity increases and given that the micromixing time is inversely proportional to the diffusivity coefficient value (equation (5.8), micromixing time is higher.

Other factor resulting in the increase of segregation index, (X_S), is the change of reaction rate for the Dushman reaction (5.2) due to the present of glycerol in the reactant solution. Guichardon et al. (1997) found out that there is an inverse relationship between the glycerol mass fraction added to the reactant solution and rate constant of Dushman reaction . Consequently, the rate of reaction will be reduced and as result of that, the reaction is slowed down. Therefore, higher iodine is produced and Xs increases.

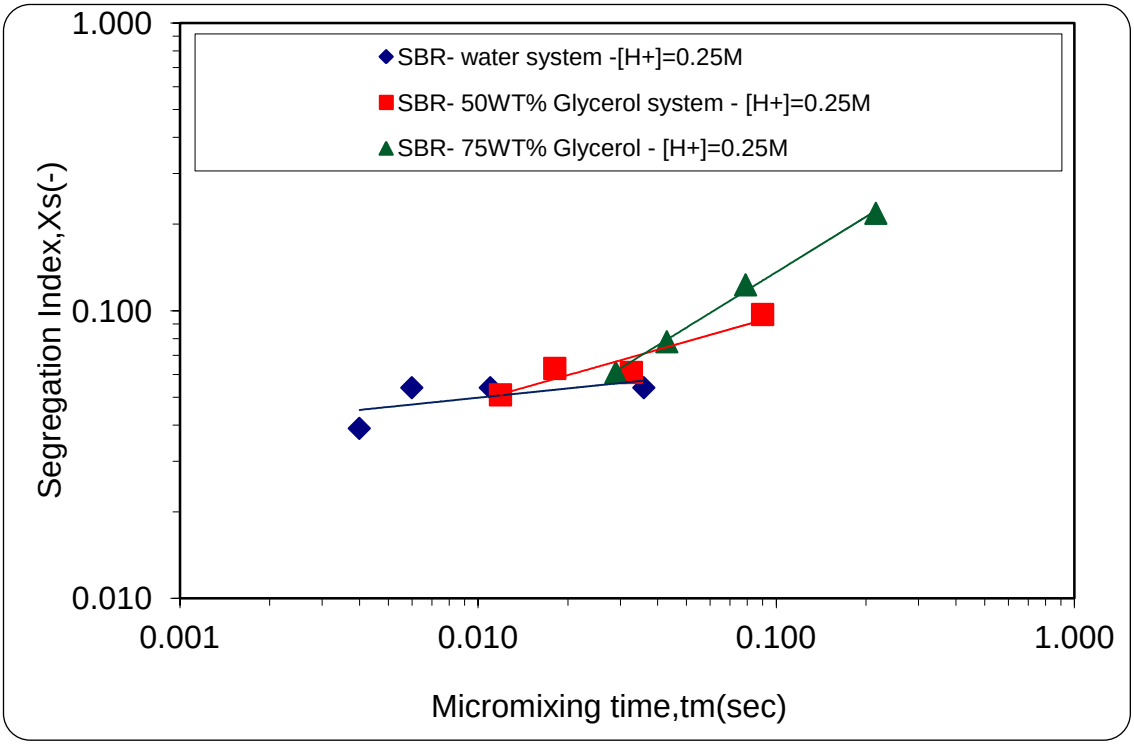

Figure 5.14: Dependence of the segregation Index, (Xs) on the Micromixing time for water, 50 and 75wt% Glycerol system with acid concentration of 0.25M injected closed to the impeller

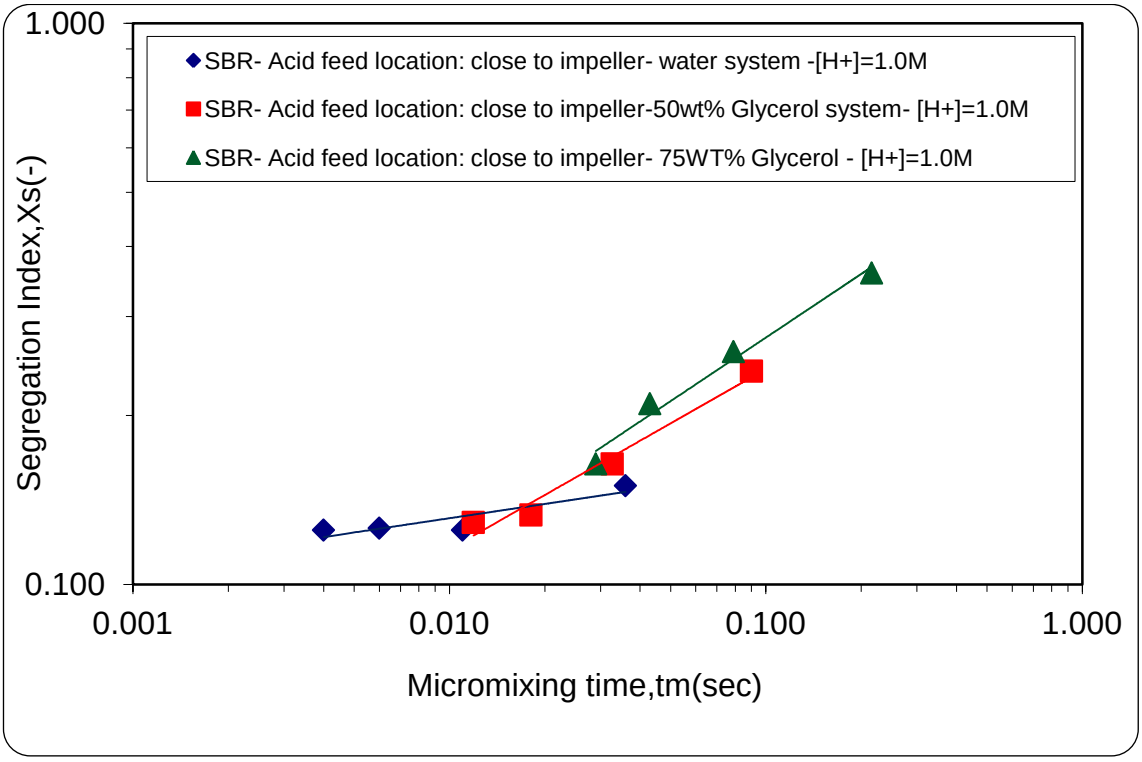

Figure 5.15: Dependence of the segregation Index, (Xs) on the Micromixing time for water, 50 and 75wt% Glycerol system with acid concentration of 1.0M injected close to the impeller

5.2 Micromixing Experimental Results: 10cm Spinning Disc Reactor

Micromixing intensity on the spinning disc is affected by many variables such as acid concentration, total feed flow rate (Qt), disc rotational speed, feed ratio R (ratio of the volumetric iodide-iodate-borate flow rate and the acid flow rate) and viscosity. In this part of the research all of the above mentioned variables were implemented to characterise the micromixing process within a thin film flowing in a 10cm diameter spinning disc reactor (SDR). These variables are presented in the next following section.

5.2.1 10cm SDR Experimental design

Randomized general full factorial experimental designs DOE for water, 50 wt% and 75wt% glycerol systems were performed using Minitab 15 (Table AI1 appendix I). For the 30 cm SDR experiments, the variables incorporated into the experimental design were:

- Disc rotational speed: 300 rpm, 800 rpm, and 1200 rpm,1600 rpm,2000 rpm and 2400 prm (2400 rpm was the maximum speed at which the reactor could be safely operated)
- Acid ion concentration: 0.1,0.25,0.5 and 1.0 M
- Total flowrate: 1, 3 and 5 ml/s
- Viscosity: water system(μ=1.005 mPa.s at 20 ^{0}C), 50 wt% glycerol system (μ = 6.0 mPa.s at 20 ^{0}C) and 75wt% glycerol system(μ=35.5 mPa.s at 20 ^{0}C)

The individual flowrates of the iodide-iodate-borate ions stream, (Q_I), and the acid ions stream, (Q_H), corresponding to each total flowrate indicated above are given in Tables 5.2 to 5.5 for acid concentrations of 0.1, 0.25, 0.5 and 1.0 M corresponding to the volumetric flowrate ratio,(R), of 7, 17.5, 35 and 70 respectively. The procedure of calculating the volumetric flowrate ratio (R), Q_I and Q_H are shown in appendix B.

Table 5.2: the individual flowrates of (QI) and (QH) corresponding to each total flowrate for acid concentrations 0.1M and volumetric flowrate ratio of 7, (R= QI / QH)

Qt,(ml/s)	Q_I,(ml/s)	Q_H,(ml/s)
1.0	0.875	0.125
3.0	2.625	0.375
5.0	4.375	0.625

Table 5.3: the individual flowrates of (QI) and (QH) corresponding to each total flowrate for acid concentrations 0.25M and volumetric flowrate ratio of 17.5, (R= QI / QH)

Qt,(ml/s)	Q_I,(ml/s)	Q_H,(ml/s)
1.0	0.946	0.054
3.0	2.838	0.162
5.0	4.730	0.270

Table 5.4: the individual flowrates of (QI) and (QH) corresponding to each total flowrate for acid concentrations 0.5M and volumetric flowrate ratio of 35, (R= QI / QH)

Qt,(ml/s)	Q_I,(ml/s)	Q_H,(ml/s)
1.0	0.972	0.027
3.0	2.916	0.083
5.0	4.86	0.138

Table 5.5: the individual flowrates of (QI) and (QH) corresponding to each total flowrate for acid concentrations 1.0 M and volumetric flowrate ratio of 70, (R= QI / QH)

Qt,(ml/s)	Q_I,(ml/s)	Q_H,(ml/s)
1.0	0.986	0.014
3.0	2.958	0.042
5.0	4.929	0.070

5.2.2 10cm Spinning Disc Reactor (SDR) water System Results

Seventy two water system experiments were carried out using the 10 cm SDR i.e. eighteen experiments for each sulphuric acid concentration. Each experiment was repeated three times (three replicates). The mean value of absorbance D_λ (mean), the standard deviation (σ) and standard error (S) and relative error were estimated. The maximum relative error of experiments was only (4.23 %) and the results were satisfactorily reproducible. Calculation Procedure for the error analysis is shown in appendix H.

5.2.3 Effects of disc rotational speed and flowrate on Xs.

The effect of the disc rotational speed and total feed flowrate on the segregation index is shown in Figure 5.16 and Figure 5.17. The flow rate, Qt, is the total flow rate of the two liquid streams, i.e. the volumetric iodide – iodate – borate flow rate Q_I and the acid flow rate Q_H. Two different flow rate ratios R (where $R=Q_I/Q_H$) were implemented (i.e. R= 7

and 70 corresponding to the acid ion concentration of $[H^+]$ = 0.1M and 1.0M and Concentration of H_2SO_4 of 0.05 and 0.5M respectively). With the total flow rate Qt = 1 ml/s, it is evident that the segregation index (Xs) decreases consistently with increasing rotational speed. At [H+]=0.1 M and Qt= 1ml/s (Figure 5.16), Xs was reduced from 0.073 at 300 rpm to its lowest value of 0.017 at 2100 rpm, representing a 77% drop in Xs.

On the other hand, at Qt at 3 and 5 ml/sec for two acid concentrations tested, the rotational disc speed seems to have no strong influence on the segregation index. This is more clearly observed in Figure 5.17 This would seem to suggest that the higher flowrates of 3 ml/s and 5 ml/s are sufficient to ensure a high degree of mixing intensity is achieved even when the disc speed was relatively low.

High degree of micro-mixing in terms of (Xs) can be achieved at high disc speeds and high feed flow rates. Under such conditions, higher shear forces are created between liquid film and the disc surface and thinner liquid film are formed. The higher shear rates and thinner films will cause the rate of mass transfer to be enhanced. Consequently the rate of reaction for the reaction (2.43) will be enhanced and most of sulphuric acid will be reacted and reaction (2.44) will not be involved.

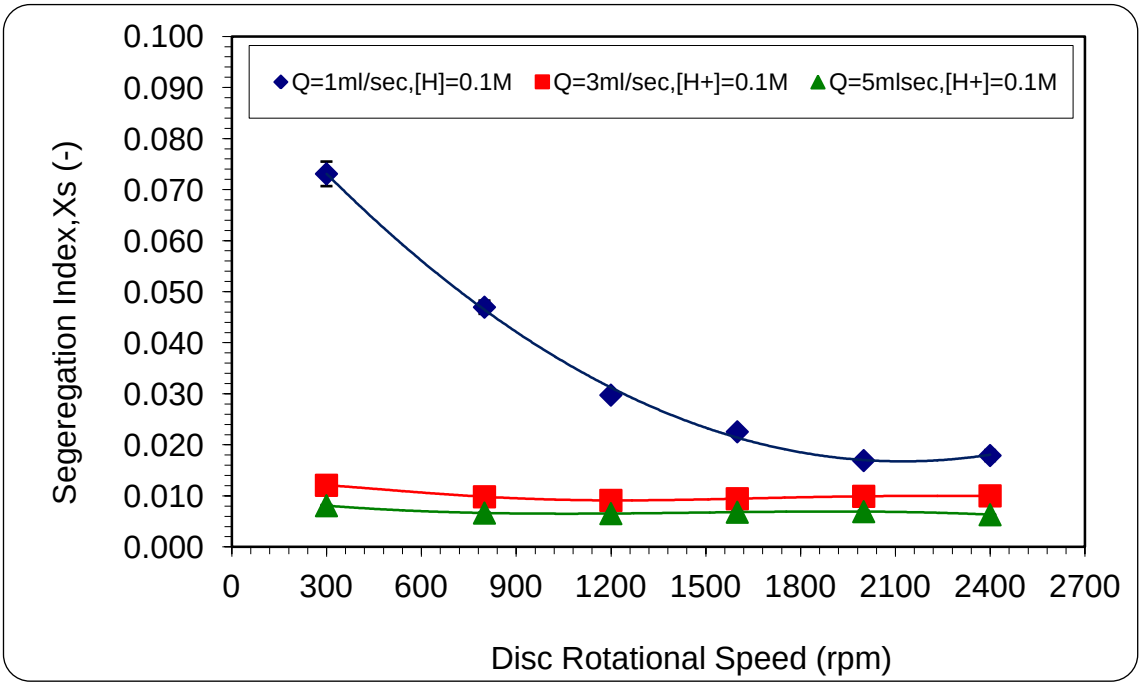

Figure 5.16: Effect of rotational speed and total flowrate on the segregation index at [H+] = 0.1 M and R=7

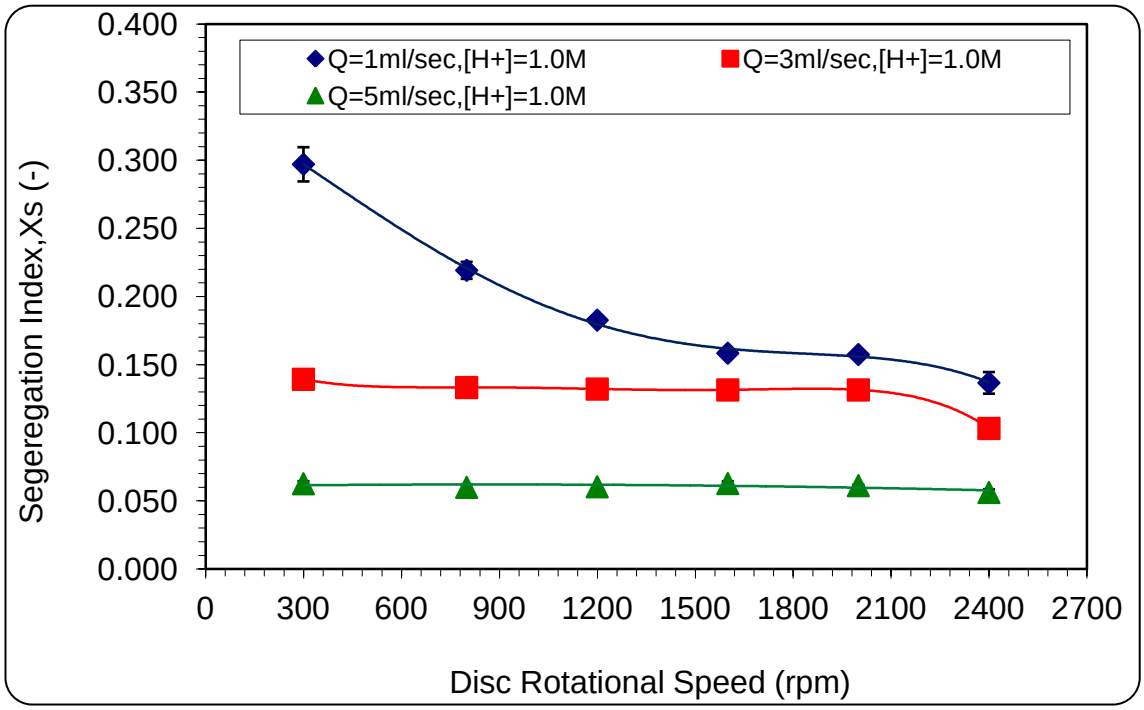

Figure 5.17: Effect of rotational speed and total flowrate on the segregation index at [H+] =1.0 M and R=70

Increasing the disc rotational speed affect both the maximum film shear rate, (γ_{max}) , and mean disc residence time, (t_{res}), as seen from eq. (2.3) and (2.8) which are reproduced here:

$$\gamma_{max} = \frac{\omega^2 r}{\nu}(\delta) \qquad 5.11$$

$$t_{res} = \frac{3}{4}\left(\frac{12\pi^2\nu}{\omega^2 Q^2}\right)^{1/3}\left(r_0^{4/3} - r_i^{4/3}\right) \qquad 5.12$$

It can be observed from Eq. (2.3) and (2.8) the residence time, t_{res} is proportional to $\omega^{-2/3}$ while the maximum shear rate (γ_{max}), which characterizes the intensity of mixing with the thin film, is proportional to the flow rate ω^2.

Similar observations with regards to the effect of the disc rotational speed and total feed flowrate on the segregation index, (Xs), in Figures 5.16 and 5.17 were obtained in Figures AI1 and AI2 in appendix I at all total flowrates for $[H^+]$=0.25 M and 0.5 M.

What can be concluded from the above findings is that micromixing depends strongly on the liquid flow rate in reactors utilising the centrifugal forces for enhancing heat and mass transfer of the reactants (Yang et al., 2006; Hai-Jian Yang, 2005; Yu-Shao CHEN, 2004; Lin et al., 2003; Chia-Chang and Hwai-Shen, 2000; Liu et al., 1996). In addition, the shear rate generated at the disc/liquid interface by liquid flowrate and disc rotational speed has an effect on the segregation index (Xs), the higher sheer rate the lower segregation index (Xs). The effect of the average maximum film shear rate (γ_{max}) and the mean disc residence time, (t_{res}), of the reactants on the intensity of the mixing on the disc will discussed in details in below.

As mentioned in section 2.3.1.1.1, the average maximum shear rate across the disc surface for the smooth disc was calculated on the basis of four shear rate values at four radial positions on the disc surface for each set of operating condition of total flowrate and disc rotational speed. The average maximum shear rate across the disc surface was estimated from equations (2.3) and (2.4). Figures 5.18 to 5.21 show the effect of average maximum shear rate across the disc surface on the segregation index, (Xs), for water system at three total flowrates and acid concentrations of $[H^+]$=0.1 M, 0.25 M, 0.50 M and 1.0 M. It is clear from the Figures that at the lower total flowrate Qt=1 ml/s, the intensity of mixing on the 10 cm SDR in terms of segregation index, (Xs), is strongly affected by the shear rate generated at the disc/liquid interface. The higher shear rate the lower segregation index, (Xs).On the other hand, at the highest flowrates Qt=3 and 5 ml/s, the intensity of mixing on the 10 cm SDR is not affected by the shear rate generated at the disc/liquid interface. This could be attributed to the limitation of mass transfer and the kinetics for the system at these operating parameters. In addition, the results in figure 5.16 and 5.17 show that the higher flowrates of 3 ml/s and 5 ml/s are sufficient to ensure a high degree of mixing intensity is achieved even when the shear rate was relatively low.

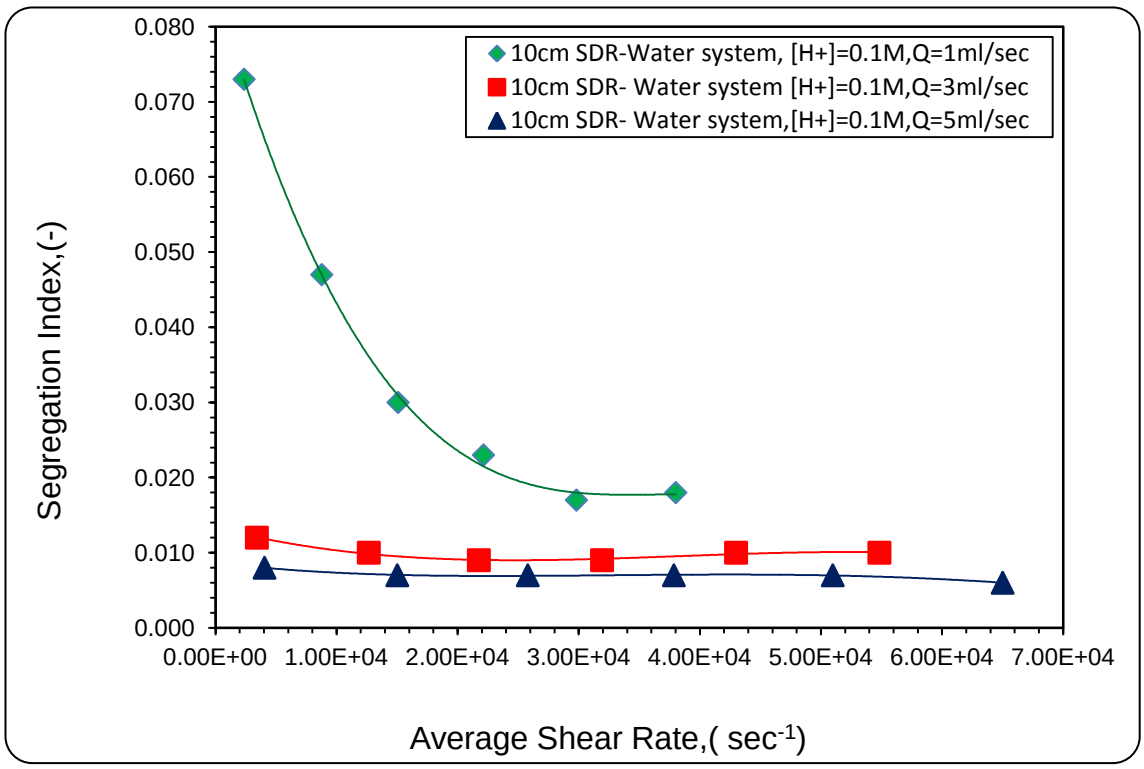

Figure 5.18: Effect of Average Shear Rate on segregation Index (Xs) in SDR at Various Total flowrate and [H+] =0.1 M and R=7

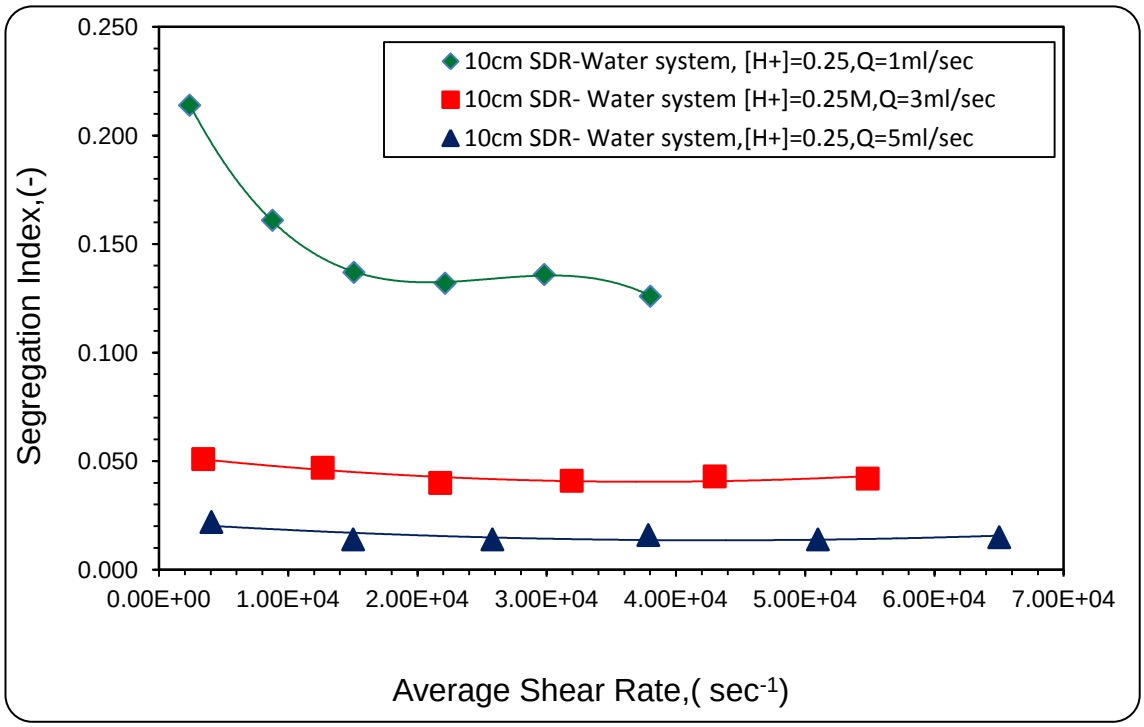

Figure 5.19: Effect of Average Shear Rate on segregation Index (Xs) in SDR at various total flowrate and [H+] =0.25 M

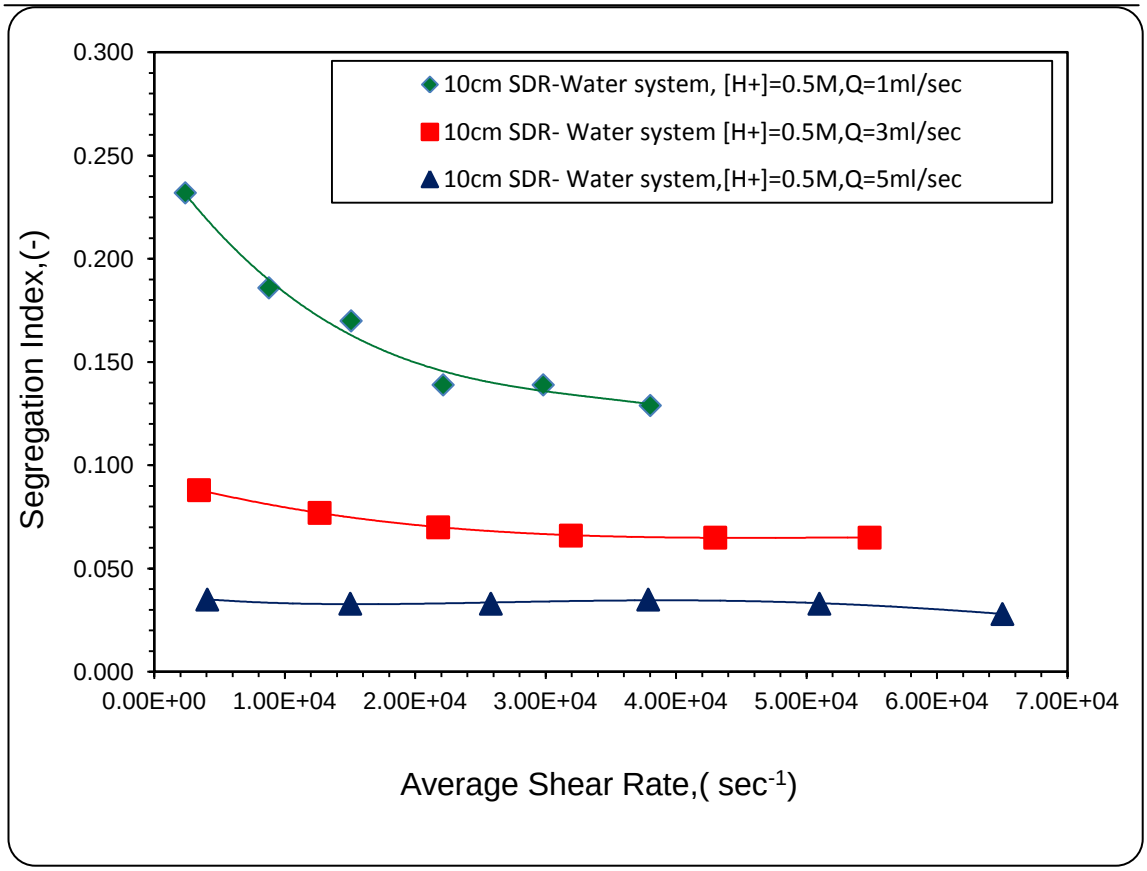

Figure 5.20: Effect of Average Shear Rate on segregation Index (Xs) in SDR at various total flowrate and [H+] =0.50 M and R=35

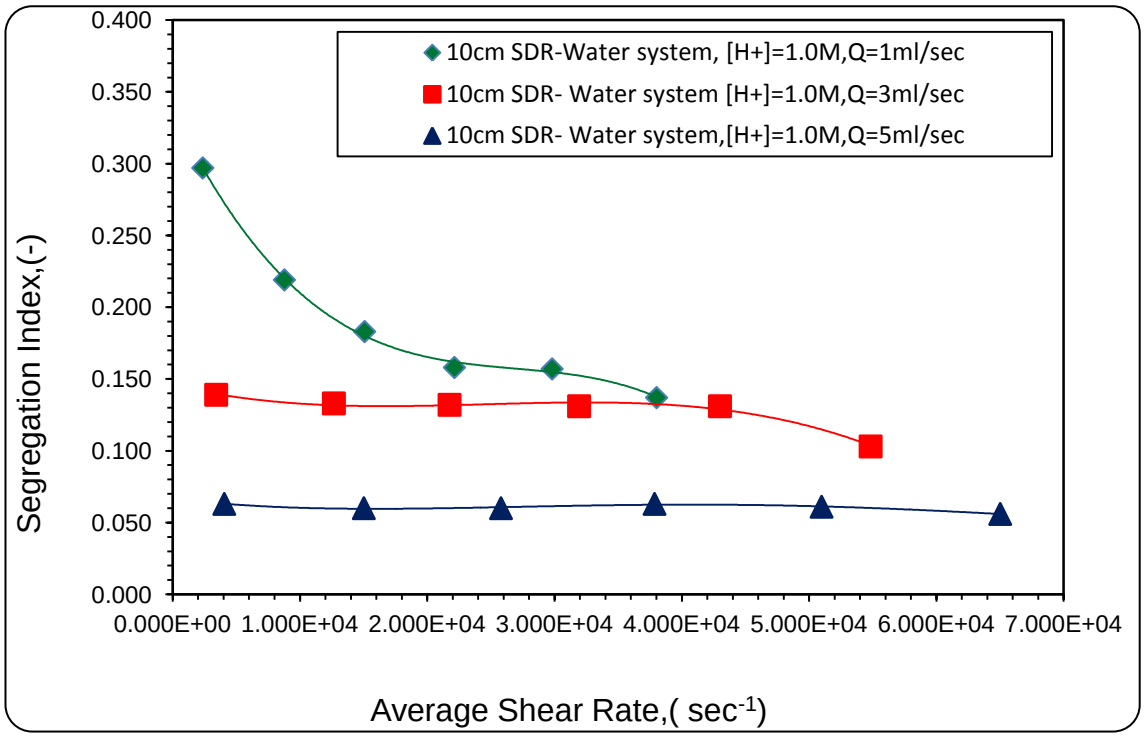

Figure 5.21: Effect of Average Shear Rate on segregation Index (Xs) in SDR at Various Total flowrate and [H+] =1.0 M and R=70

Another important parameter which needs to be considered when micromixing is taking place on the surface disc of the SDR is the residence time of the fluid on the disc. The liquid residence time on the disc needs to be greater than the required micro-mixing time; therefore it is possible for the micromixing taken place on the disc. Tables 5.6 to 5.8 show the predicted values of the residence (obtained from equation 2.8) and the micromixing times (estimated from equation 2.29) for the 10 cm SDR experiments at the given disc rotational speed and water, 50 wt% Glycerol and 75 wt% systems. It is clear that the residence times are much higher than the mixing times.

Table 5.6: Residence time and mixing time on 10cmSDR for water System

Disc rotational speed,(rpm)	Liquid total flowrate Qt, (ml/sec)	Residence time $t_{res,}$ (sec)	Micromixing time $t_{mix,}$ (sec)
300	1	0.6500	0.0067
800		0.3380	0.0018
1200		0.2580	0.0011
1600		0.2129	0.0007
2000		0.1835	0.0005
2400		0.1625	0.0004
300	3	0.3125	0.0047
800		0.1625	0.0013
1200		0.1240	0.0007
1600		0.1024	0.0005
2000		0.0882	0.0004
2400		0.0781	0.0003
300	5	0.2223	0.0040
800		0.1156	0.0011
1200		0.0882	0.0006
1600		0.0728	0.0004
2000		0.0628	0.0003
2400		0.0556	0.0002

Table 5.7: Residence time and mixing time on 10cmSDR for 50 wt% Glycerol System

Disc rotational speed,(rpm)	Liquid total flowrate Qt, (ml/sec)	Residence time $t_{res,}$ (sec)	Micromixing time $t_{mix,}$ (sec)
300	1	0.1184	0.0309
800		0.2276	0.0084
1200		0.2983	0.0049
1600		0.3613	0.0033
2000		0.4193	0.0025
300		0.4735	0.0019
800	3	0.2462	0.0215
1200		0.4735	0.0058
1600		0.6204	0.0034
2000		0.7516	0.0023
2400		0.8721	0.0017
300		0.9848	0.0013
300	5	0.3461	0.0182
800		0.6656	0.0049
1200		0.8721	0.0028
1600		1.0565	0.0019
2000		1.2260	0.0014
2400		1.3844	0.0011

Table 5.8: Residence time and mixing time on 10cmSDR for 75 wt% Glycerol System

Disc rotational speed,(rpm)	Liquid total flowrate Qt, (ml/sec)	Residence time $t_{res,}$ (sec)	Micromixing time $t_{mix,}$ (sec)
300	1	2.012	0.1407
800		1.046	0.0381
1200		0.798	0.0222
1600		0.659	0.0151
2000		0.568	0.0112
2400		0.503	0.0088
300	3	0.967	0.0977
800		0.503	0.0264
1200		0.384	0.0154
1600		0.317	0.0105
2000		0.273	0.0078
2400		0.242	0.0061
300	5	0.688	0.0825
800		0.358	0.0223
1200		0.273	0.0130
1600		0.225	0.0088
2000		0.194	0.0066
2400		0.172	0.0051

Figure 5.22 and Figure 5.23 show the effect of residence time on the segregation index, (Xs), at the three different total flowrates and disc rotational speed ranged 300-2400 rpm. From these two plots it is clear that the increase in residence time results in an increase in the segregation index, (Xs), for example from Figure 5.22 and Table 5.6, the residence time, (t_{res}) in longest (0.65 sec) for the lowest flowrate (1 ml/sec) and disc rotational speed of 300 rpm. As mentioned in the earliest of this section, when the liquid flow rate and disc rotational speed decrease, the average velocity of the reactants on the disc is also decreased, resulting in higher residence time and smaller power dissipation

generated at the disc/liquid interface. This causes poor micromixing which is reflected in higher segregation index. The residence time itself has no direct repercussion on the micromixing process but the power dissipation has a major influence on the intensity of the micromixing intensity. Nevertheless, for the other the flowrates of 3 ml/s and 5 ml/s, the residence time has no influence of segregation index. This could be attributed to that the higher flowrates of 3 ml/s and 5 ml/s are sufficient to ensure a high degree of mixing intensity is achieved even when the disc speed was relatively low.

From the above findings, it can be conclude that the segregation index (Xs) can be decreased when the liquid flow rate increased. as the liquid flow rate increased, the average radial velocity (U) of the reactants flow on the disc are increased results in decreasing residence time, (t_{res}) and increasing power dissipation, (ε). Although, the first phenomenon (i.e. the residence time) does not give any direct advantage to the micromixing, the second phenomenon (i.e. the power dissipation), however, is of considerable benefit to micromixing process. Consequently, the segregation index, (Xs) decreased.

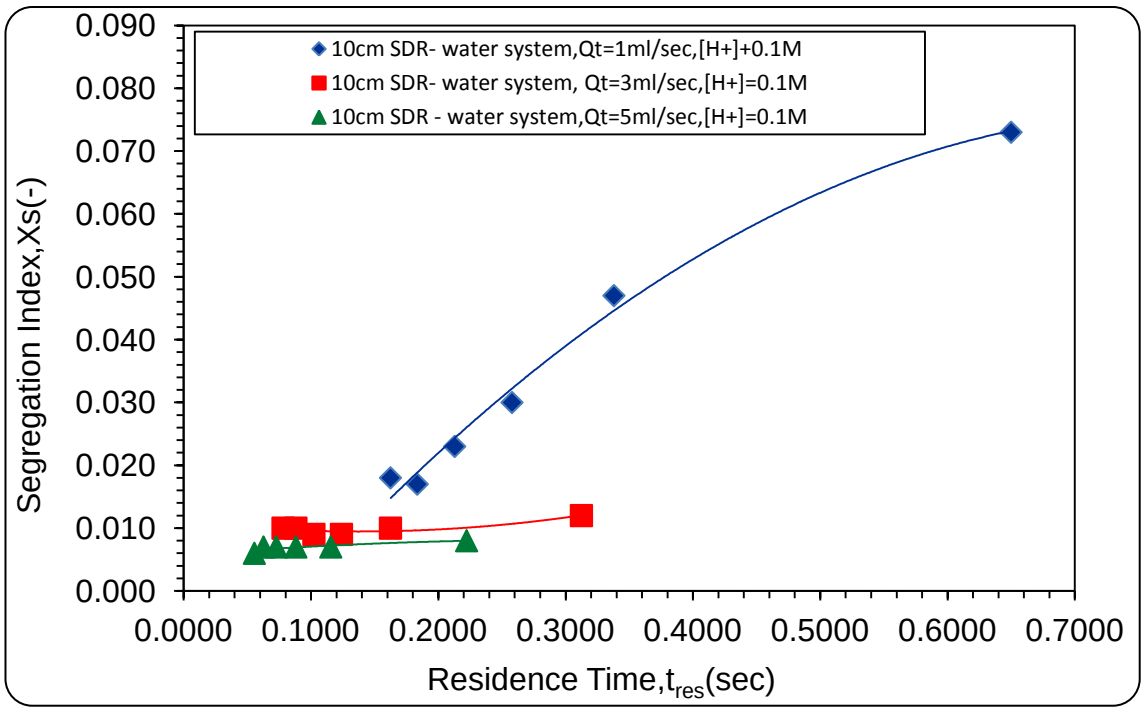

Figure 5.22: Effect of Residence time on segregation Index (Xs) in SDR at Various Total Flowrate and [H+] =0.1 M and R=7

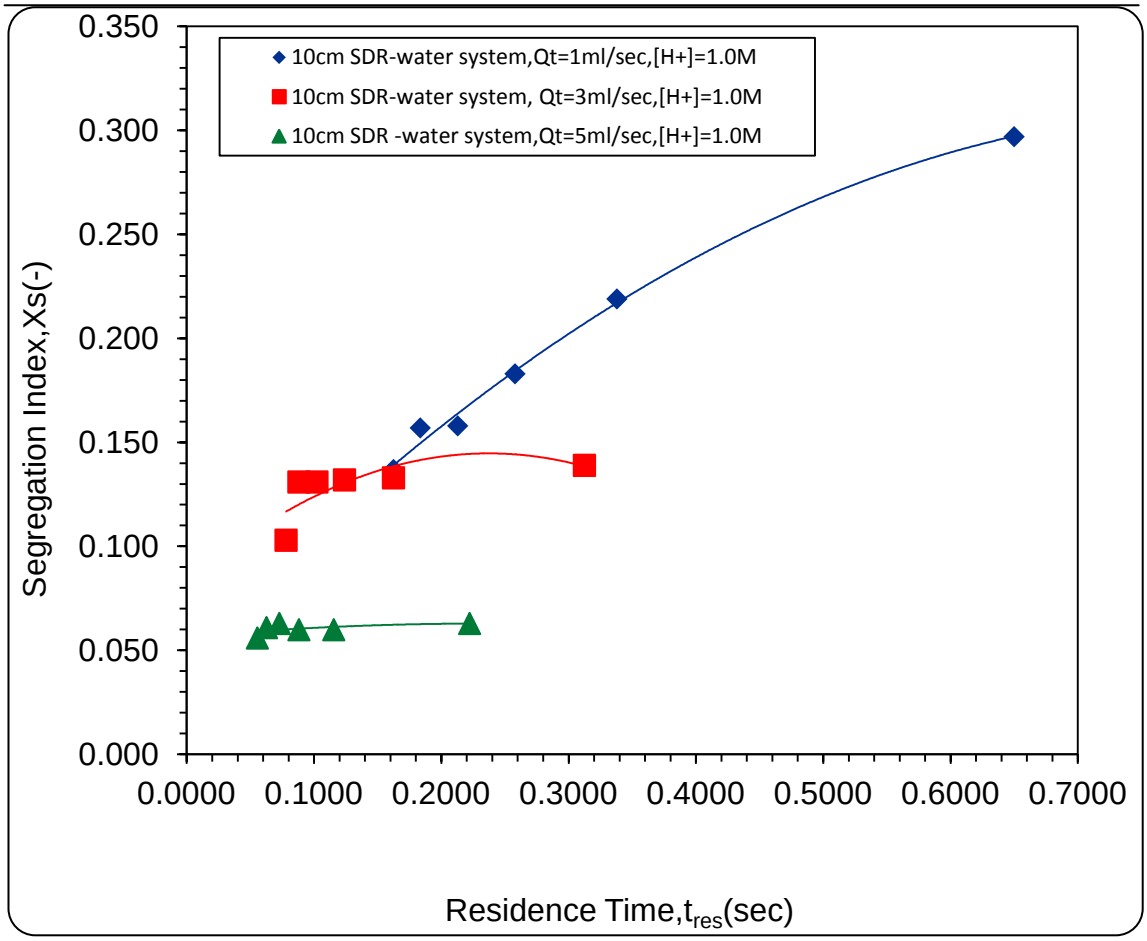

Figure 5.23: Effect of Residence time on segregation Index (Xs) in SDR at Various Total Flowrate and [H+] =1.0 M and R=70

It should be kept in mind that only micromixing rate depends on reactants total flowrate. Whereas intrinsic reaction rate is fixed once reagents concentration and temperature are fixed. When total flowrate increased further, the micromixing rate of SDR increased significantly because of higher shear rate between liquid film and the disc surface. Furthermore, the power dissipation provided by the disc to the reactants is increased. When the micromixing rate is much larger than reaction rate, the reactants can be homogeneously mixed before the reaction taken place. In this case the reaction will occur in a perfect uniform environment and controlled by reaction kinetics.

5.2.4 Effect of acid concentration on Xs

Figures 5.24 to 5.26 show the effect of acid concentration on the segregation index (Xs), with the operating conditions of three different acid concentrations (0.1 M, 0.25 M, and 0.5 M). The disc speed ranged from 300 to 2400 rpm and the flow rate was set at 1, 3 or

5 ml/s. From the experimental results it can observed that X_S is sensitive to the acid concentration.

At various flowrates, a decrease in X_S was observed as the acid concentration was decreased and this was obtained in all the experiments except with the flow rate 5ml/sec and the acid concentrations 0.1 and 0.25 M. Under the latter conditions, it is observed that there is no effect on the mixing intensity and the segregation index remains almost constant at all the rotational speeds in the range 800 rpm to 2400 rpm.

The increase of segregation index with increasing acid concentration could be interpreted by studying the iodide-iodate reaction scheme involved in this process. Since the rate of Dushman reaction, i.e. reaction (2.44) is more sensitive to acid concentration than that of reaction (2.43) because its reaction order with respect to acid is higher, reaction (2.44) increases at a faster rate than reaction (2.43) when the acid concentration is increased. Consequently more iodine and therefore more tri-iodide is formed. This causes segregation index (X_S) to be increased.

Similar effects of higher acid concentration on segregation index,(Xs), have been observed in previous micromixing studies carried on the intensifying reactors (Yang et al., 2009a; Chu et al., 2007; Yang et al., 2006; Hai-Jian Yang, 2005).

One important issue needs to be mentioned, it has been tried to investigate the effect of the effect of $[H^+]$ =1.0 M. The samples from these runs had pH values less that 7 and the absorbance values were higher than 2.0. For these reason, the results of this set of experiments has been rejected.

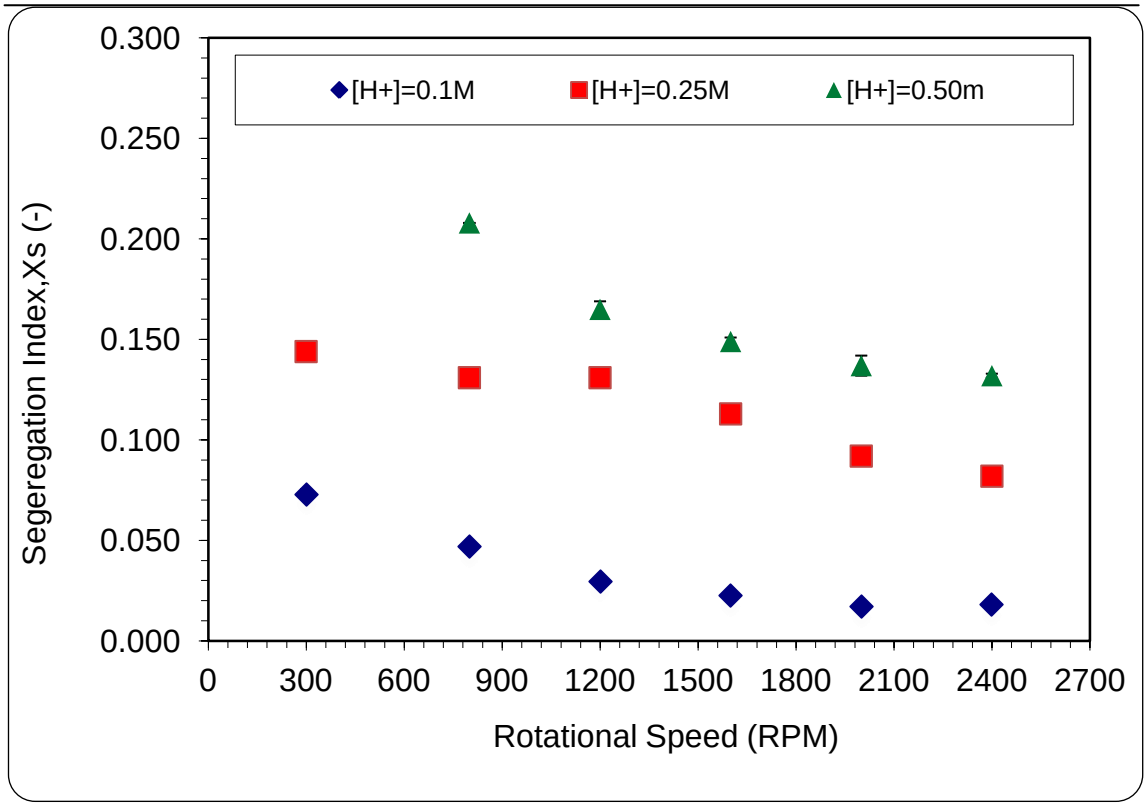

Figure 5.24: Acid Concentration Effect on Segregation Index, (Xs) at flow rate Q=1 ml/s, R=7 - Water System

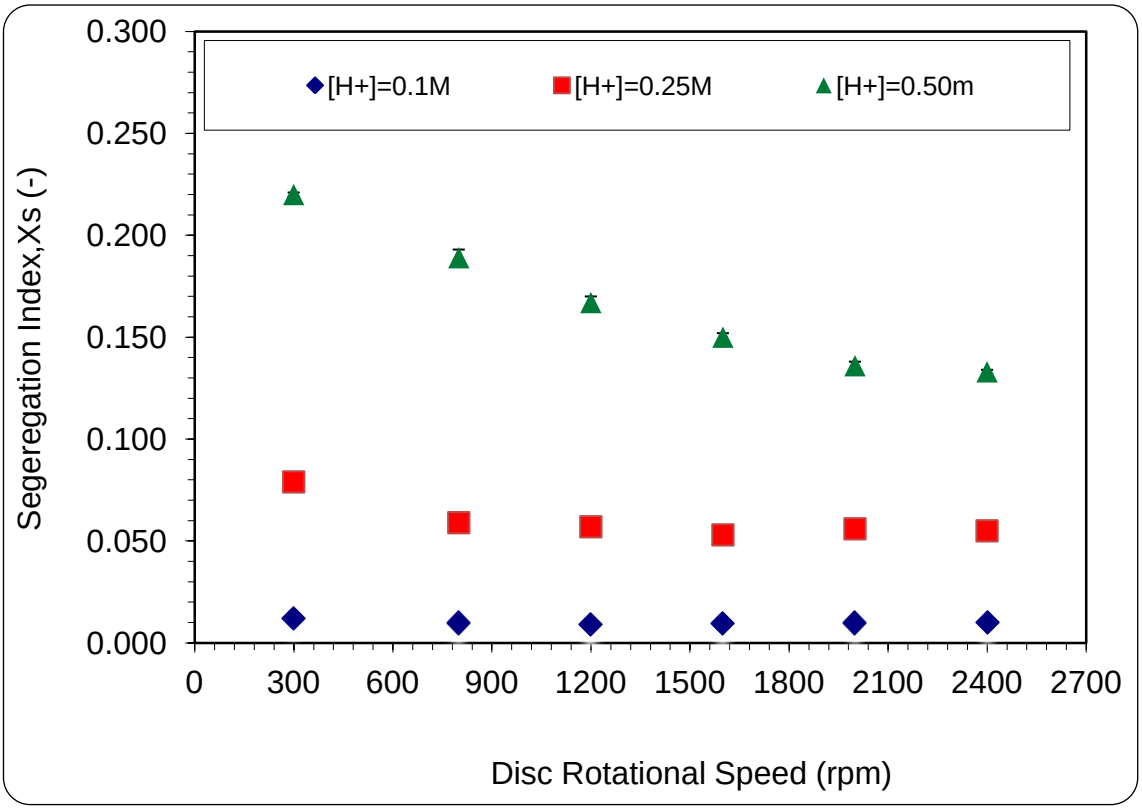

Figure 5.25: Acid Concentration Effect on Segregation Index, (Xs) at total flow rate Qt=3ml/sec, R=7 - Water System

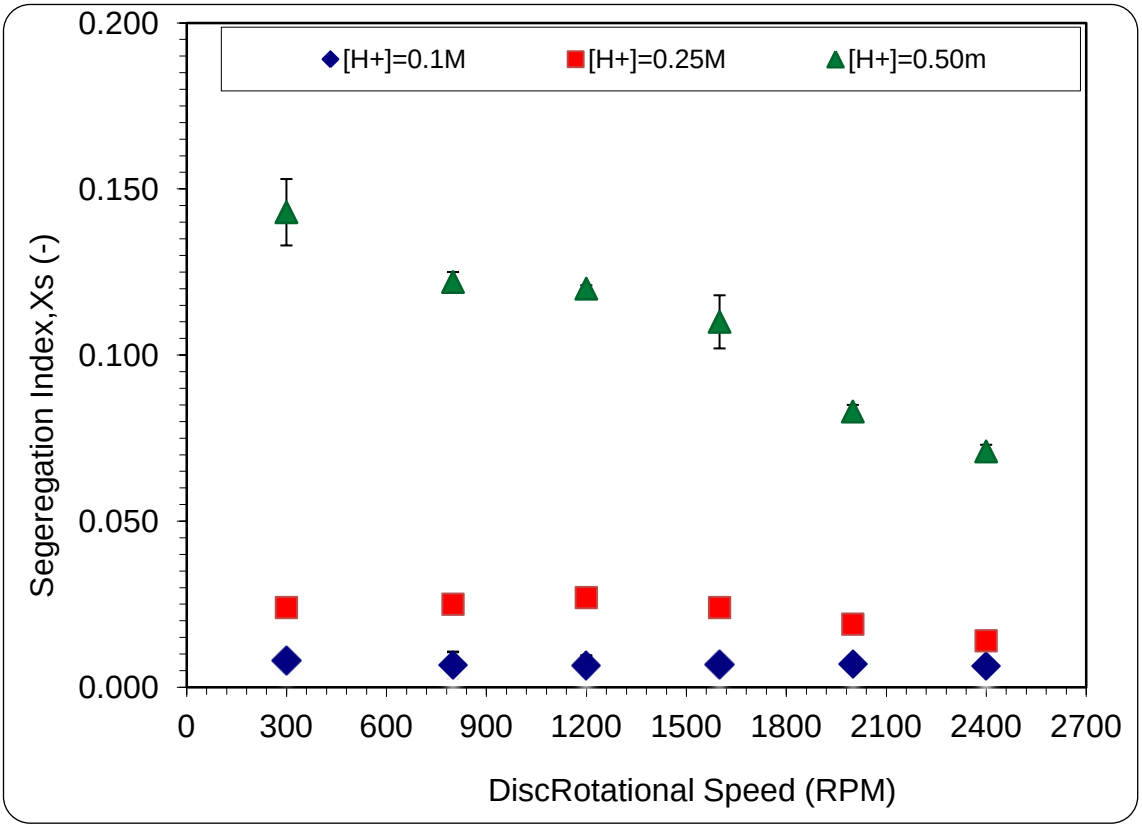

Figure 5.26: Acid Concentration Effect on Segregation Index, (Xs) at flow rate Q=5/sec, R=7 - Water System

5.2.5 Effect of Total Flowrate ratios (R) on XS

The effect of the flow rate ratio R (ratio of the volumetric iodide-iodate-borate flow rate, Q_I, and the acid flow rate, Q_H, where $R= Q_I/Q_H$) on the Xs was also investigated. The effect of total flowrate ratios, (R), on the segregation index, (X_S), is illustrated in Figures 5.27 to 5.29 below. Two different total flowrate ratios (R) namely 3 and 7 are implemented with constant acid concentration of $[H^+]$ = 0.1 M. The rotational disc speeds set at ranging of 300, 800, 1200, 1600 and 2400 rpm respectively. The total flow rates were 1, 3 and 5 ml/sec. From the Figures it can be observed that the segregation index, (X_S), is sensitive to the total flowrate ratio. When the value of total flowrate ratios (R) is decreased, the molar flow rate of acid ions (H^+) is increased. If the flowrate of iodate-borate ions stream is kept constant, the average concentration of (H^+) in the bulk of the solution will be increased. Although the acid reacts in reactions (2.43) and (2.44) simultaneously, the rate of the Dushman reaction (Reaction 2.44) is more sensitive to acid concentration than that of reaction acid-base neutralization (Reaction 2.43) because its reaction order with respect to acid is higher. This will make Dushman

reaction (reaction 2.44) faster remarkably and more iodine is formed, meaning an increasing of segregation index, (X_S).

Thus, as seen in Figures 5.27 to 5.29 below with condition of Qt =1, 3 and 5 ml/s with constant acid concentration of $[H^+]$ = 0.1 M, a lower value of R=3 results in a higher molar flow of (H^+) ions being introduced to the rotating disc. The relatively poor mixing at low rotational speeds combined with the larger amount of (H^+) ions in solution gives higher values of segregation index (Xs) at R=3 compared with R=7. The sulphuric acid must be in stoichiometric default in the reactor with respect to the borate ions because there must remain ions I^- to react with I_2: the concentration of I_2 characterizes the micromixing. If the acid is not in stoichiometric default, the $[I_2]$ would be always the same one for all characteristic time of micromixing. If the concentration of the sulphuric acid is improperly selected, the amount of the iodine formed from the Dushman reaction (reaction 2.44) is too high or too small and the optical density may not be in the range of the spectrophotometer scale.

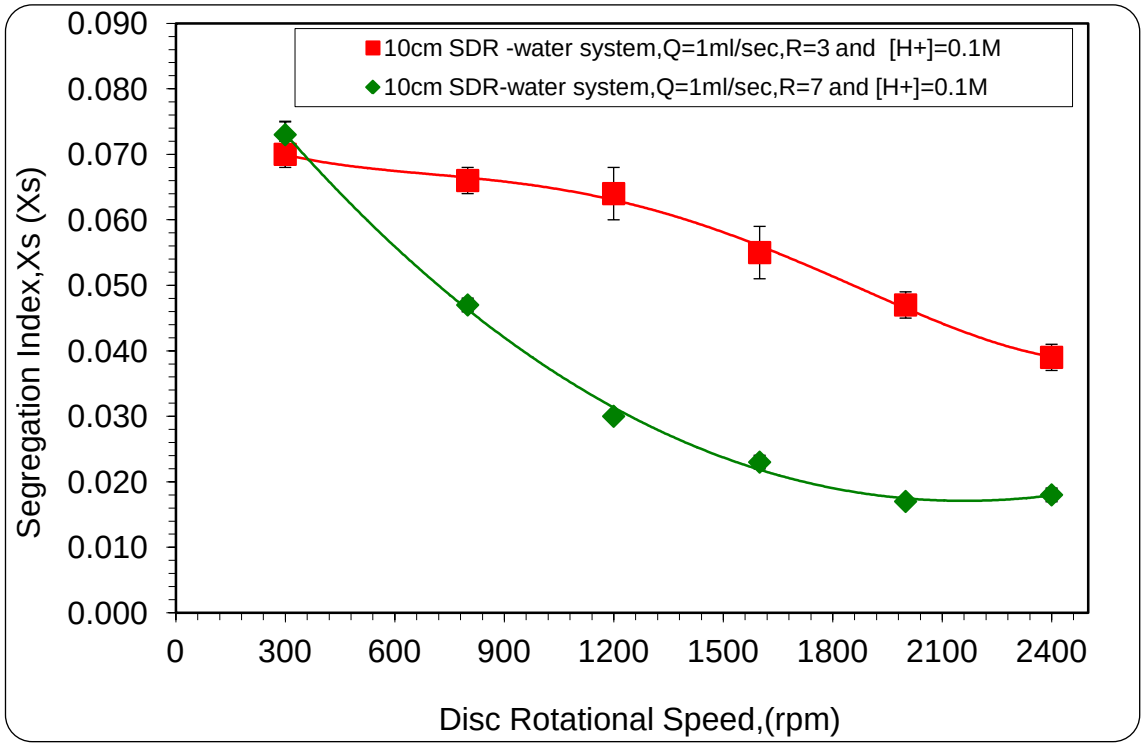

Figure 5.27: Effect of liquid feed ratios (R) on segregation Index (Xs) at a total flow rate Qt=1 ml/sec And various disc rotational disc speed

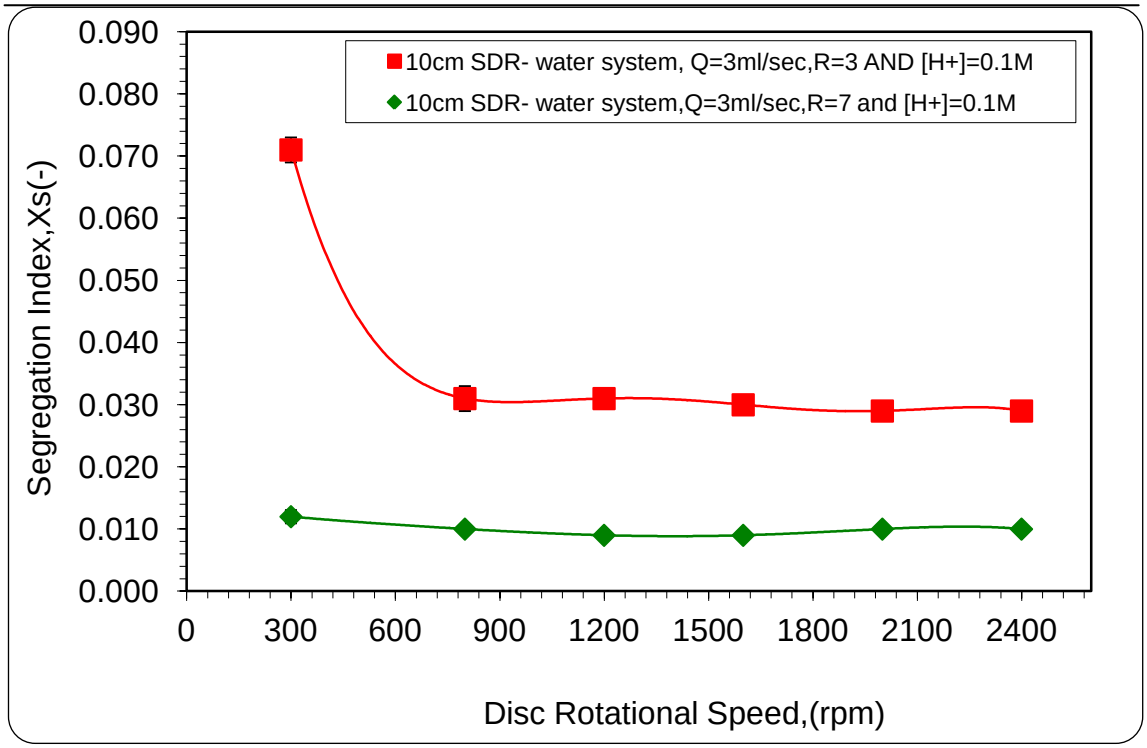

Figure 5.28: Effect of liquid feed ratios (R) on segregation Index (Xs at a total Flowrate Qt =3 ml/sec And various disc rotational disc speed

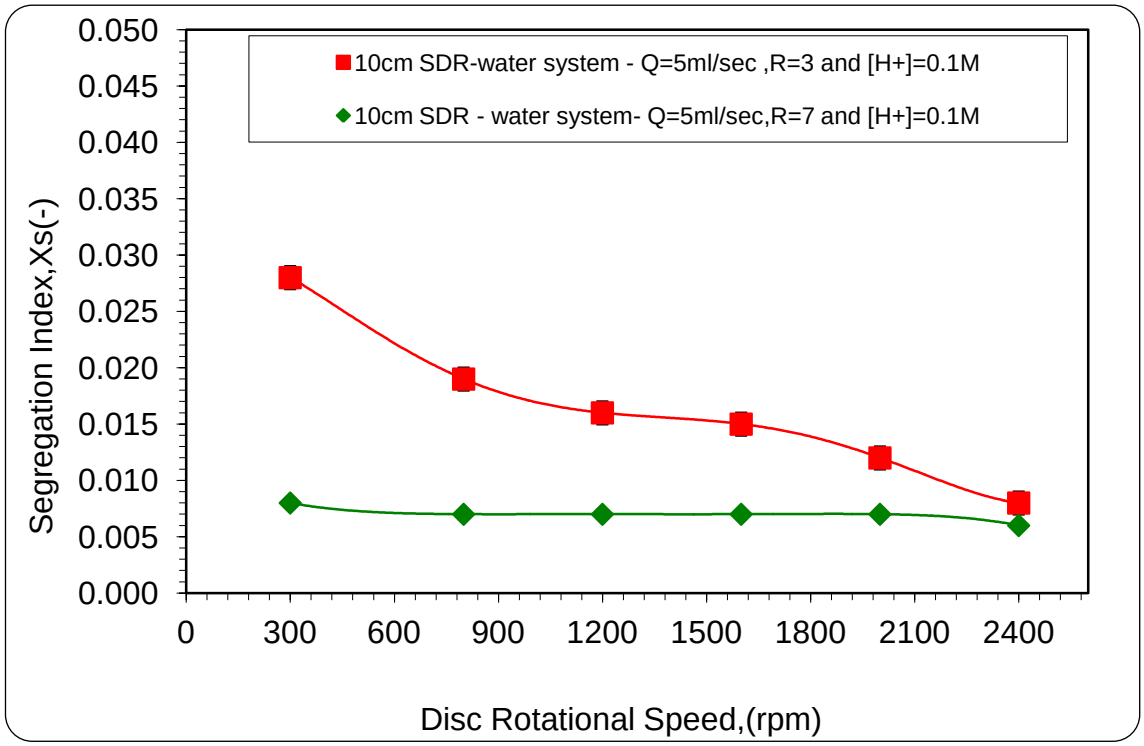

Figure 5.29: Effect of liquid feed ratios (R) on segregation Index (Xs) at a total Flowrate Qt=5 ml/sec and various disc rotational disc speed

5.2.6 Effect of feed Viscosity on Xs

In order to investigate the influence of viscosity on the micromixing intensity in terms of segregation index (Xs), glycerol was used to increase the viscosity of the aqueous reaction solution. Two different concentrations were used (50 and 75 wt% Glycerol-water mixture) corresponding to viscosity values of 6 and 35.5 mPa.s at 20 ^{O}C respectively. The iodide – iodate - borate solution was maintained close to pH value of 11.0 for all viscous media experiments to prevent the initial formation of iodine in the solution before any addition of the sulphuric acid (Guichardon et al., 1997). This was achieved by reducing the concentration of $H_2BO^-_3$ to 50% of the concentration of the aqueous reaction solution (water system), i.e. 0.0909M. The maximum relative error of experiments was only (9.14 %) and the results were satisfactorily reproducible.

The effect of feed viscosity on segregation index (Xs) in 10 cm SDR at different total flowrates and different acid concentrations are shown in Figure 5.30 and Figure 5.31. Figures 5.30 and 5.31 show the effect of viscosity on segregation index (Xs) at total flowrates of 1 and 3 ml/s respectively with acid concentration of [H+] =0.1 M.

From Figure 5.30, it is clearly that the segregation index is affected by the increasing the viscosity of the feed. At 1ml/sec and 300 rpm of disc rotational speed, the segregation index, (Xs) increased from 0.073 for the least viscous system (aqueous reaction solution) to 0.145 for most viscous solution (75 wt% glycerol-water solution of 35.5 mPa.s viscosity). This effect may be explained in terms of increased viscous shear forces acting against centrifugal forces on the surfaces of the disc, causing the flow to be retarded. Furthermore, as explained previously in section 5.1.4, the viscous media will slow down the micromixing rate and alter the intrinsic kinetics of the reaction (Yu-Shao CHEN, 2004; Guichardon et al., 1997). Interestingly, beyond a disc rotational speed of 1200 rpm, there is almost no viscosity effect (water system vs. 50 wt% glycerol system) on the segregation index as seen by the curves converging to similar values of Xs beyond 1200 rpm on Figure 5.31 when the total flowrate,(Qt) was 3ml/s. This is attributed to shear rate being greatly increased at the higher disc rotational speeds, resulting in more intimate contact between the layers in the liquid film. Under these high shear rate conditions, the viscosity effects can be overcome to a large extent

and the micromixing intensity is significantly improved even in the highly viscous solution.

It is to be noted that even at the higher viscosities, the centrifugal force created by the SDR still has positive influence on micromixing. For example, at the total flowrate of 1ml/s, an 81% reduction of Xs was obtained at 6 mPa.s as the rotational speed increased from 300 to 2400 rpm and a 75% reduction in Xs was obtained at 35.5 mPa.s.

Similar trends with regards to the effects of viscosity on the segregation index, (Xs), as highlighted in Figure 5.30 and Figure 5.31 were obtained in Figures AI3 to AI12 in the Appendix I for all the total flow rates and the acid concentration was 0.1 M, 0.25 M, 0.5 M and 1.0 M.

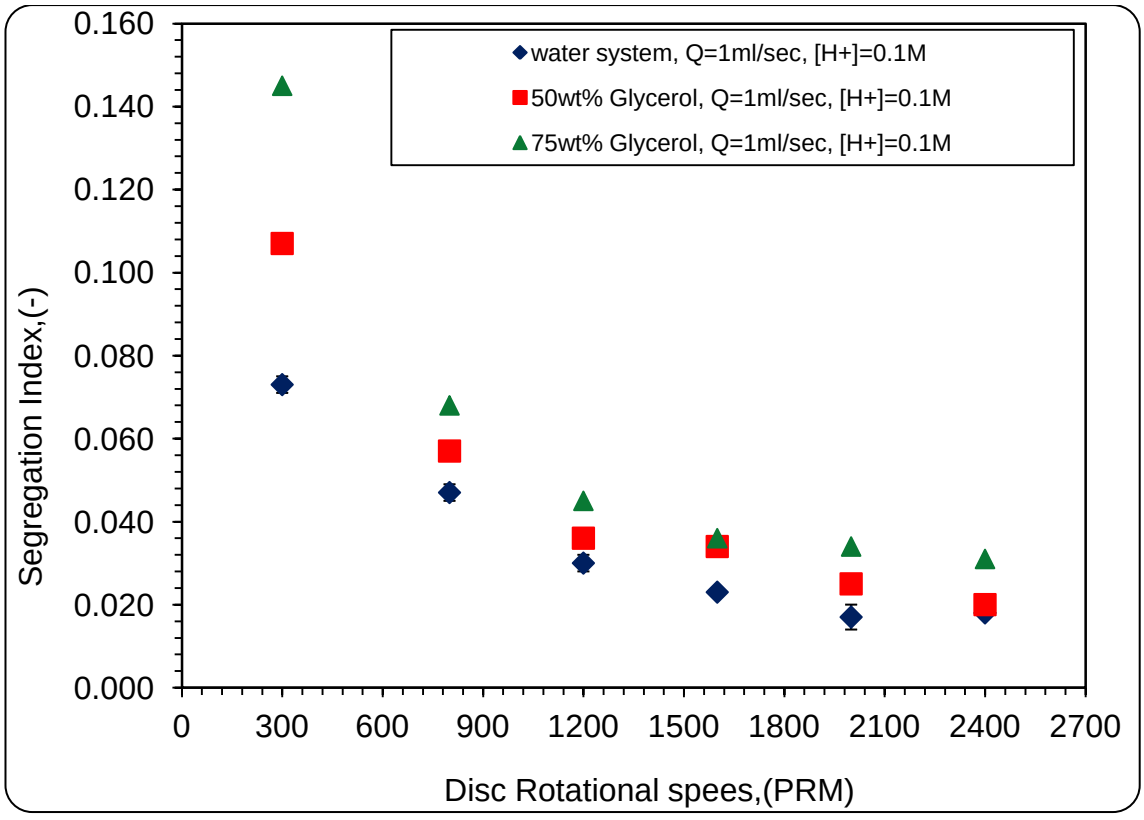

Figure 5.30: Effect of feed viscosity on segregation Index (Xs) in SDR at Q=1ml/sec Total flowrate and [H+] =0.1 M and R=7

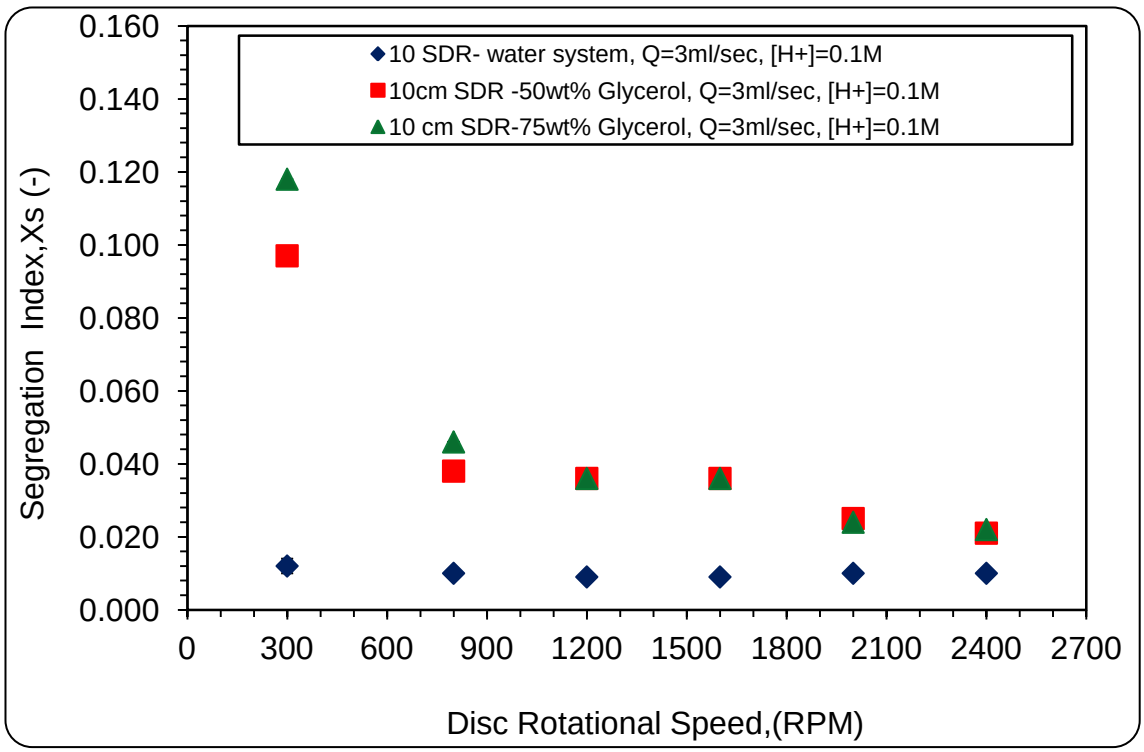

Figure 5.31: Effect of feed viscosity on segregation Index (Xs) in SDR at Q=3ml/sec total flow rates and [H+] =0.1 M and R=7

5.2.7 Effect of Power dissipation, (ε) on segregation index, Xs (-)

The Power dissipation, (ε) transferred into the fluid by action of disc rotation is another indication of the rate of the mixing achieved in the SDR. In addition, the Power dissipation, (ε) is also important character for the comparison the SDR micromixing performance with the other type of reactors. The power dissipation , (ε) was calculated by equation (2.18).

Figure 5.32 demonstrate the effect of disc rotational speed on power dissipation, at three total flowrates (1, 3 and 5 ml/sec) and disc rotational speeds in the range 300 to 2400 rpm, corresponding to power dissipation ranging 0.6-1392 W/kg. Three systems were used (water, 50 and 75 wt% glycerol systems). From Figure 5.37 certain facts were confirmed, notably the higher power dissipation could be achieved on the 10 cm SDR by the higher reactant total flowrate, higher disc rotational speeds and lower reactants viscosity. In addition, the higher the power dissipation given to the fluid by the action of disc rotation and higher total flowrates, the higher intensity of micromixing achieved on the disc. This can be seen clearly later in Figures 5.33 and 5.34.

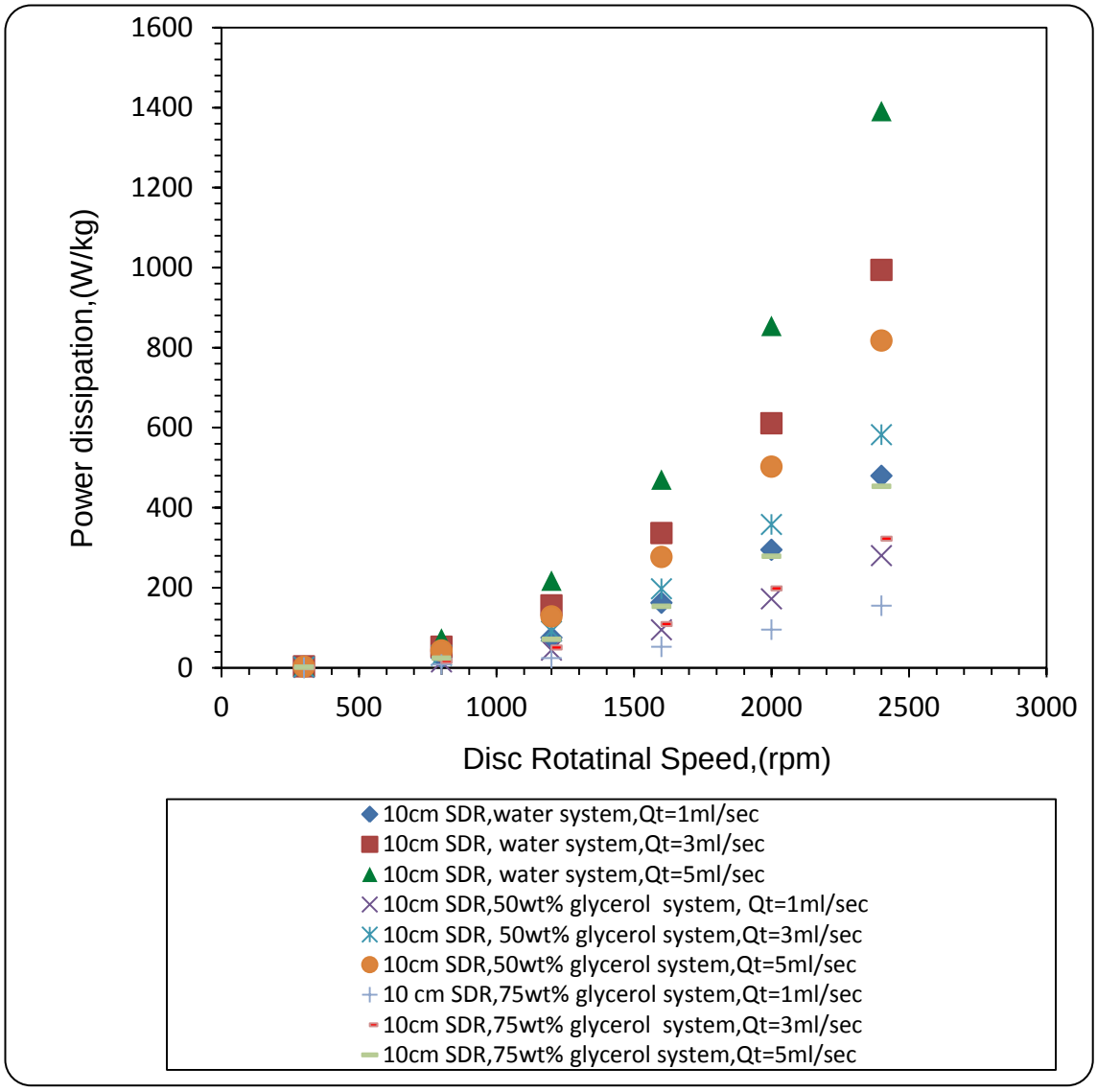

Figure 5.32: Effect of Disc Rotational speed on the power dissipation at different liquid total flowrates in 10cm SDR-water, 50 and 75wt% glycerol systems

Figure 5.33 and Figure 5.34 demonstrates the effect the Power dissipation on the segregation index, (Xs), at two flowrates of 1 and 5ml/s and six disc rotational speeds. The performance of 10cm SDR has been investigated using water, 50 and 57 wt% glycerol system, corresponding to viscosity values of 1,6 and 35.5mPa.s at 20 ^{o}C . The acid ion concentrations were 0.1 and 1.0 M.

The power dissipation was the range of 0.61-1392 W/kg. These values depend on the total flow rate, system viscosity and the disc rotational speed. These two Figures clearly indicated that the increase in power dissipation results in a decrease of the segregation index, (Xs) at a given disc rotational speed and total flowrate (Monnier et al., 2000;

Monnier et al., 1999b). The higher power rate dissipation provided to the fluid, the higher rate of mixing can be achieved.

From Figure 5.33, it is evident that the segregation index decreases consistently with increase in power dissipation. At the total flowrate of 1ml/s and water system using [H+] =0.1 M, the power dissipation increased from 1.9 W/kg at 300rpm to its highest value of 480 W/kg at 2400 rpm. This represents an increase of 99% in the power dissipation, corresponding to a reduction in Xs from 0.073 at 300 rpm to its lowest value of 0.018 at 2400 rpm thereby representing a 75% drop in Xs. Alternatively, at the same operating condition but with a replacement of the water system by 50 wt% glycerol system, the power dissipation increased from 1.1 W/kg at 300rpm to its highest value of 281W/kg at 2400 rpm which is an increase of 100% over this range of disc speed. As a result of that, the segregation index reduced from 0.107 at 300 rpm to its lowest value of 0.020 at 2400 rpm representing a 81% drop in Xs. Similar trends were observed at flowrate of 5 ml/s. In Figure 5.34 where [H+] =1.0 M, similar trends with regards to the effects of power dissipation on Xs as described above were obtained at all flowrates and for water system (μ=1 mPa.s); 50wt% glycerol system (μ=6 mPa.s) and 75wt% glycerol system (μ=35.5 mPa.s).

From Figures 5.33 to Figure 5.34, two observations can be made. Firstly, the higher value of power dissipation rate (ε) could be achieved on the 10cm SDR by the higher reactant total flowrate and higher disc rotational speeds. Secondary, at given disc rotational speed and reactant total flowrate the lower values of power dissipation could be attained on the disc by increasing in reactant viscosity. This could be attributed to the fact that, increasing in dynamic liquid viscosity (μ_L) results in decreasing in the average velocity of the liquid solution on the disc. Thus, the power dissipation given to the fluid by the action of disc rotation decreased and the kinetic energy given to the liquid will be reduced as well. Consequently, poor micromixing will occur, giving rise to higher segregation index.

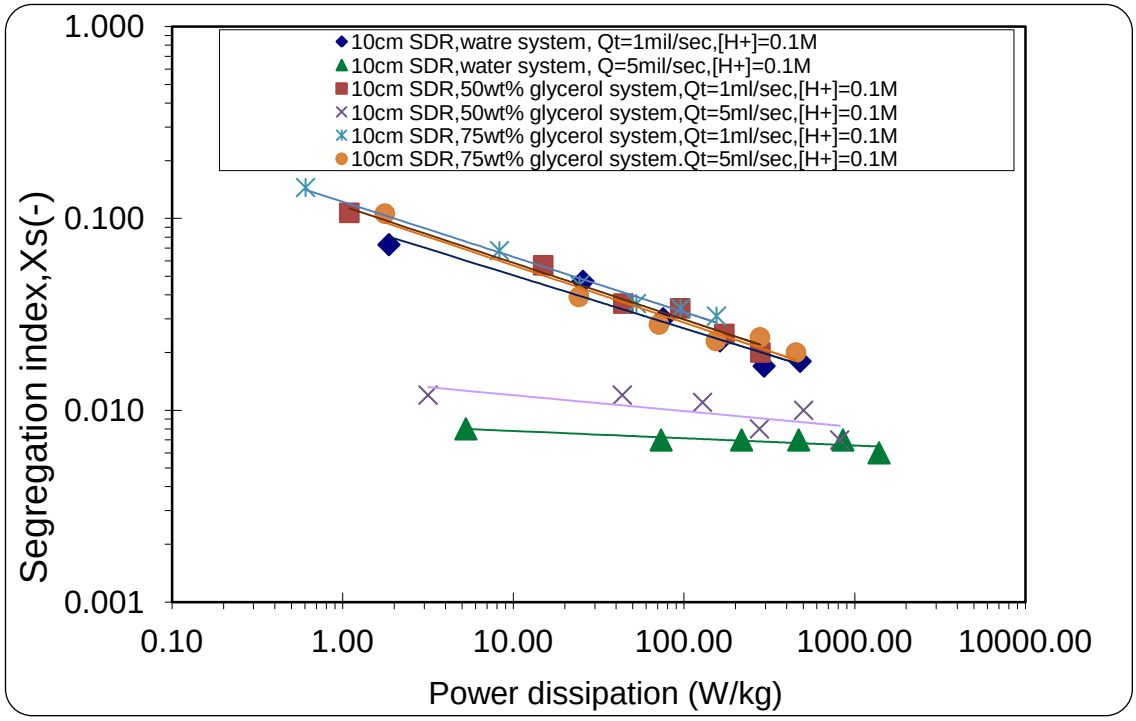

Figure 5.33: Effect of Power dissipation on Segregation Index, (-) at different liquid total flowrates – 10cm SDR –water, 50 and 75wt% glycerol systems,[H+]=0.1 M and R=7

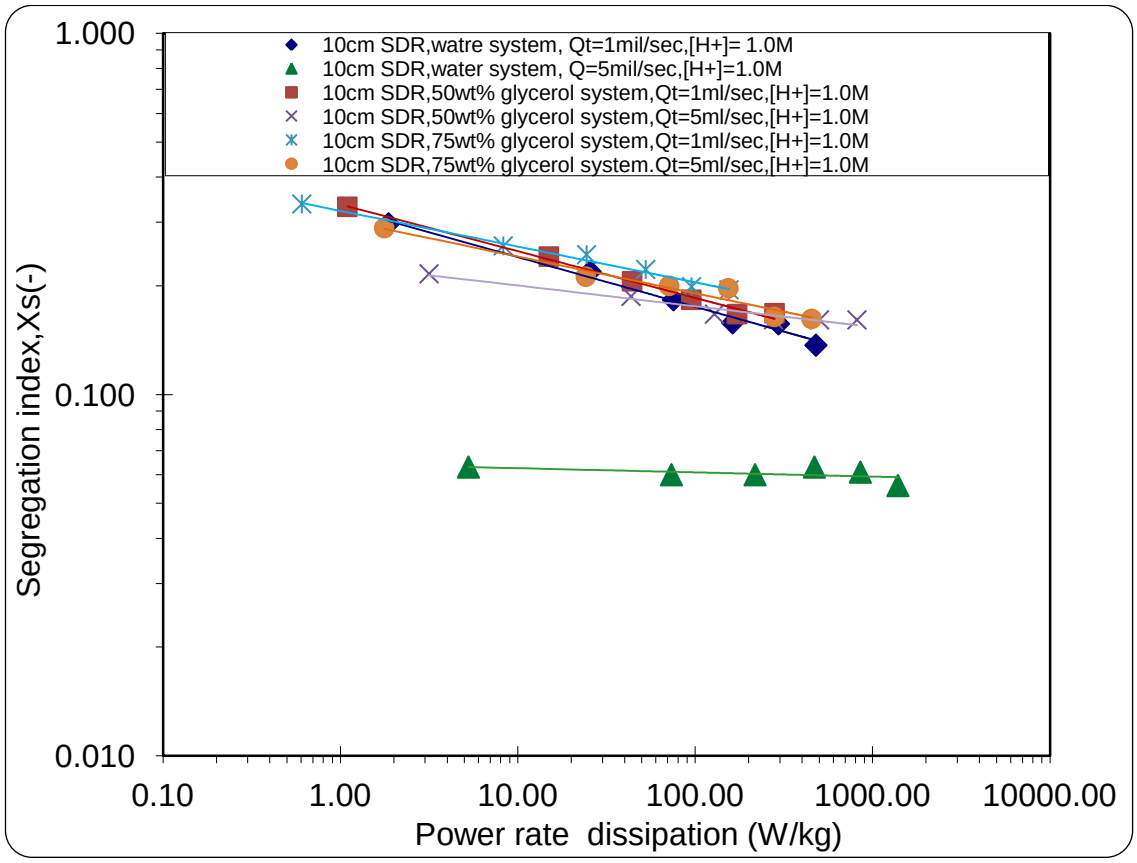

Figure 5.34: Effect of Power dissipation on Segregation Index, (-) at different liquid total flowrates – 10 cm SDR –water, 50 and 75wt% glycerol systems,[H+]=1.0 M and R=70

5.2.8 10cm SDR Micromixing time,(t_{DS}), and its Relationship with Segregation Index, (Xs), for water, 50 and 75 wt% Glycerol systems

As mentioned earlier in section 5.1.7, the micromixing time is the time required to achieve complete mixing on molecular scale; in other words, the time required for the reagents to diffuse to one another. The micromixing time of the reactant solution flowing on the rotating disc was calculated on the basis on the hydrodynamic properties of the fluid and the power dissipation, ε referring to the whole disc surface. The degree of mixing can control the selectivity, quality or distribution of the final product only if micromixing time is longer than the reaction time t_r ($t_m >> t_r$) which is equivalent to the residence time of the reactants on the disc. The micromixing on the disc are controlled by deformation and molecular diffusion (molecular diffusion and shear force). The micro-mixing times on the disc were given by equation (2.29).

Figure 5.35 below shows the effect of disc rotational speed and total feed flowrate on the estimated micromixing time in the 10 cm SDR. It is seen that higher disc speeds and higher flowrates result in shorter micromixing time. The lowest value of micromixing achieved on the 10 cm SDR was 0.0002 s at the disc rotational speed of 2400 rpm with a total flowrate of 5 ml/s when the water system was used. Moreover, at given disc rotational speed and reactant total flowrate, higher values of micromixing time were attained on the disc by increasing the reactant viscosity. This is attributed to the fact that increasing the dynamic liquid viscosity (μ_L) results in a reduction in the average radial velocity of the liquid solution on the disc. Accordingly, the power dissipation to the fluid by the action of disc rotation is reduced in higher viscosity media. In addition, as mentioned earlier, the diffusivity, (D), is naturally slower when the feed viscosity increases and given that the micromixing time is inversely proportional to the diffusivity coefficient value (equation 2.29), micromixing time is higher.

The combined effects of disc rotation speed and feed flowrate on micromixing time can be more clearly understood by analysing the effect of power dissipation on micromixing time. Figure 5.36 represent a logarithmic plot of the estimation of micromixing time for water ,50 wt% and 75 wt% glycerol systems as a function of power dissipation, calculated using equation (2.18) for three different total flow rates (1, 3 and 5 ml/s) and disc rotational speeds ranging between 300-2400 rpm.

The graph clearly shows that the micromixing time is inversely proportional to the power dissipation. As the power input increases, the time, required for the molecules to diffuse to one another and make contact (i.e. the micro-mixing time, t_{DS}) decreases. Accordingly, the micromixing intensity is improved. This also supports the explanation on the increases in the mixing efficiency with increased flowrates and rotational speed, which resulted in the power input increase. It is interesting to note that the data points for the higher viscosity systems are shifted upwards on Figure 5.36.

In conclusion, the lower value of micromixing time, t_{DS}, was achieved on the 10cm SDR by using higher values of power dissipation generated by a combination of higher reactant total flowrate, higher disc rotational speeds and lower reactants viscosity as shown in Figure 5.36 .

Figures 5.37 and 5.38 show the relationship between the calculated micromixing time and the experimentally determined segregation index, (Xs), at the three different total flowrates for water ,50 wt% and 75 wt% glycerol systems using $[H^+]$=0.1 and 1.0 M. From both Figures, it is evident that the shorter the micromixing time, the lower the value of segregation index achieved. For example at the total flowrate 1ml/s using water system and [H+] =0.1 M, the micromixing time lies between 0.0067- 0.0004 s corresponding to a segregation index of 0.073 and 0.018 respectively, depending on the disc rotational speed. The reduction of segregation index value of 75% was reached at the micromixing time of 0.0004s relative to the initial value of 0.0067 s. Similar trends were observed at flowrates of 3 ml/s and 5 ml/s. Similar trends with regards to the relationship between the micromixing time and segregation index as highlighted in Figure 5.37 were obtained for the higher acid ion concentration of 1.0 M (shown in Figure 5.38) at all flow rates for water system,50 wt% and 75 wt% glycerol systems .

According to the findings above, it can be concluded that flowrate plays an important role in increasing the intensity of mixing on the rotating disc surface whereby the higher flow rate, the higher power rate dissipation. This is in turn leads to shorter micro-mixing time between reacting molecules.

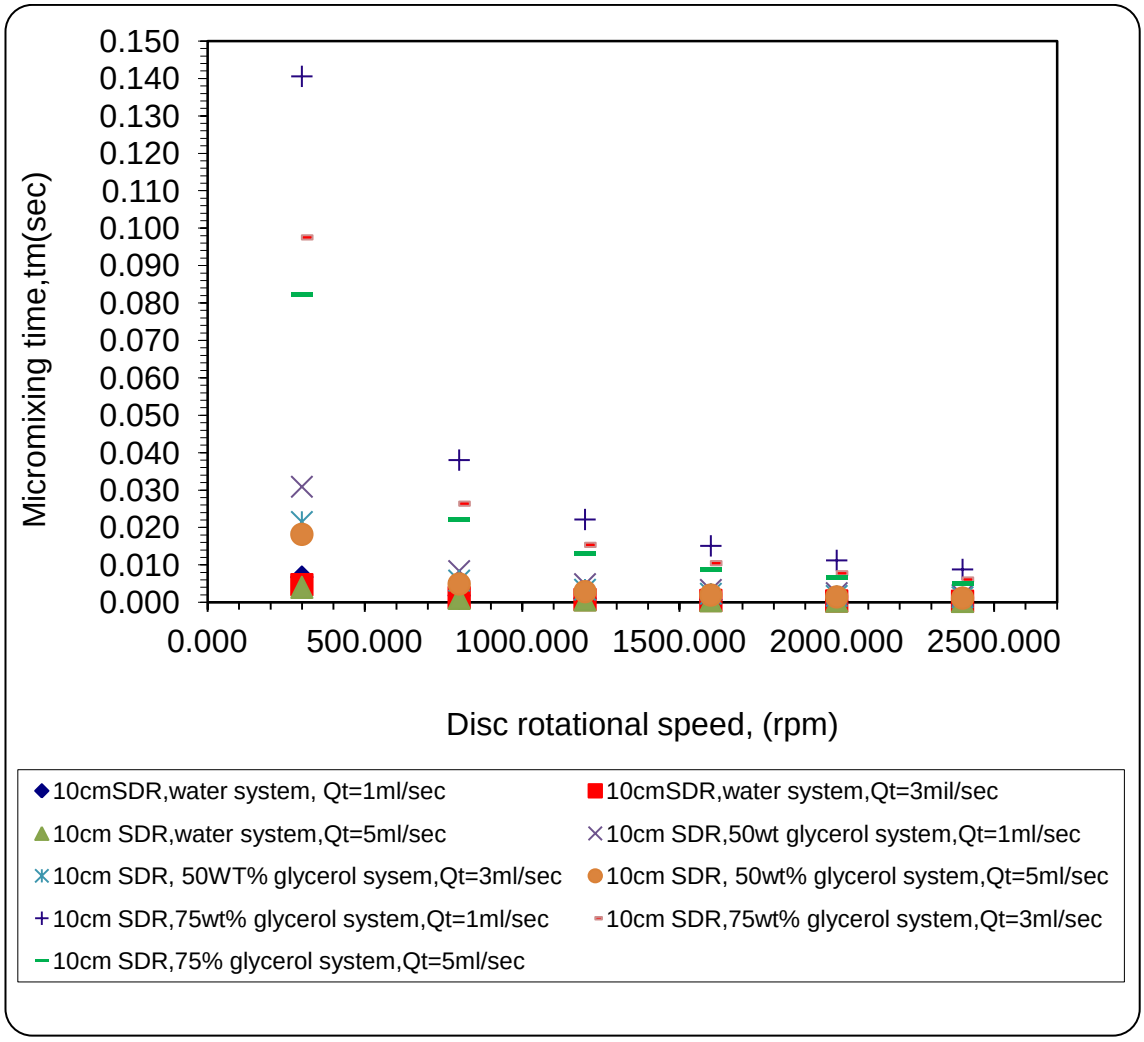

Figure 5.35: Micromixing time against disc rotational speed for 10 cm SDR at different Total flowrate and different viscosities (water, 50 and 75 wt% glycerol systems)

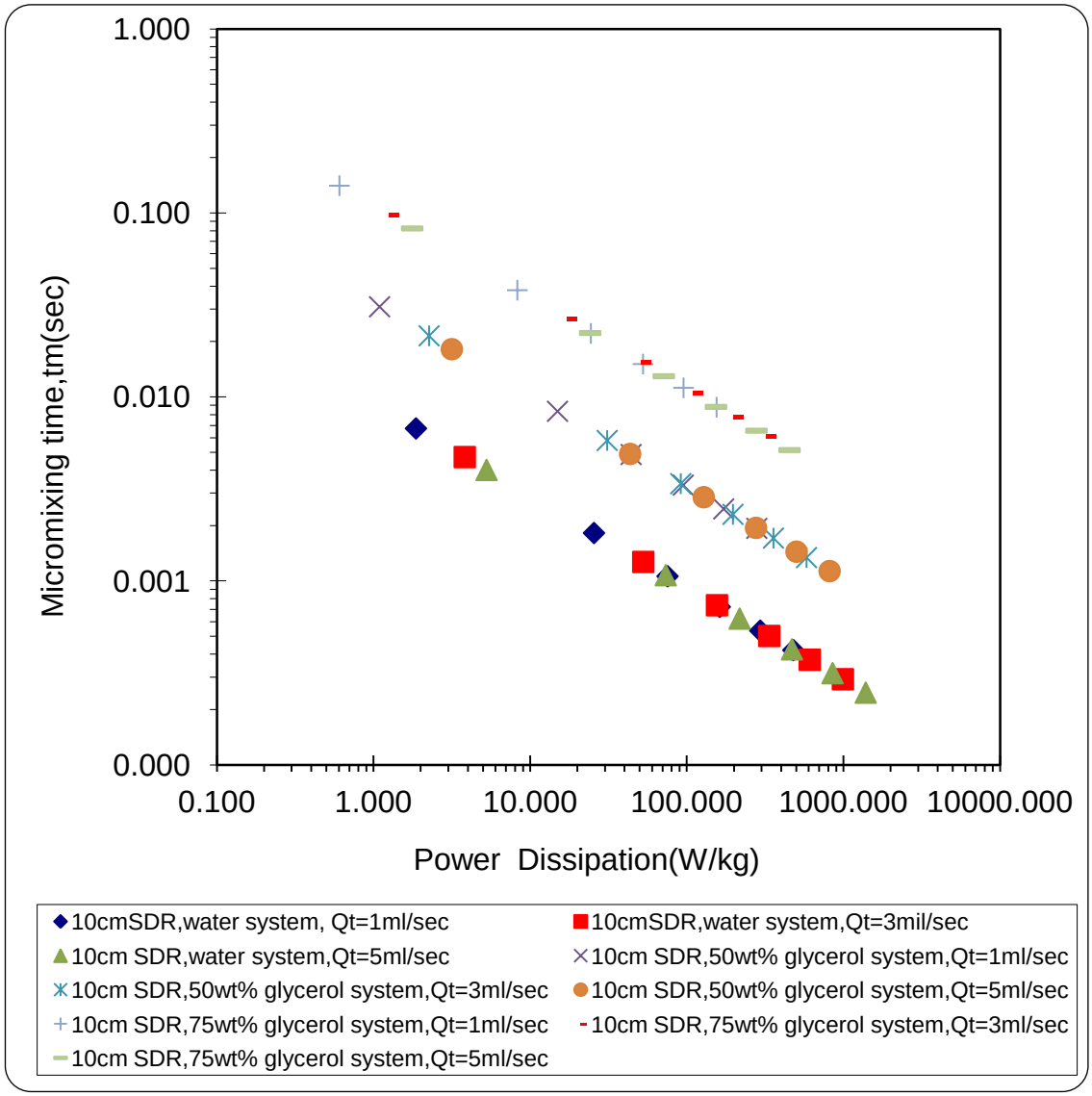

Figure 5.36: Micromixing time against power rate dissipation for 10 cm SDR at different Total flowrate and different viscosities (water, 50 and 75 wt% glycerol systems)

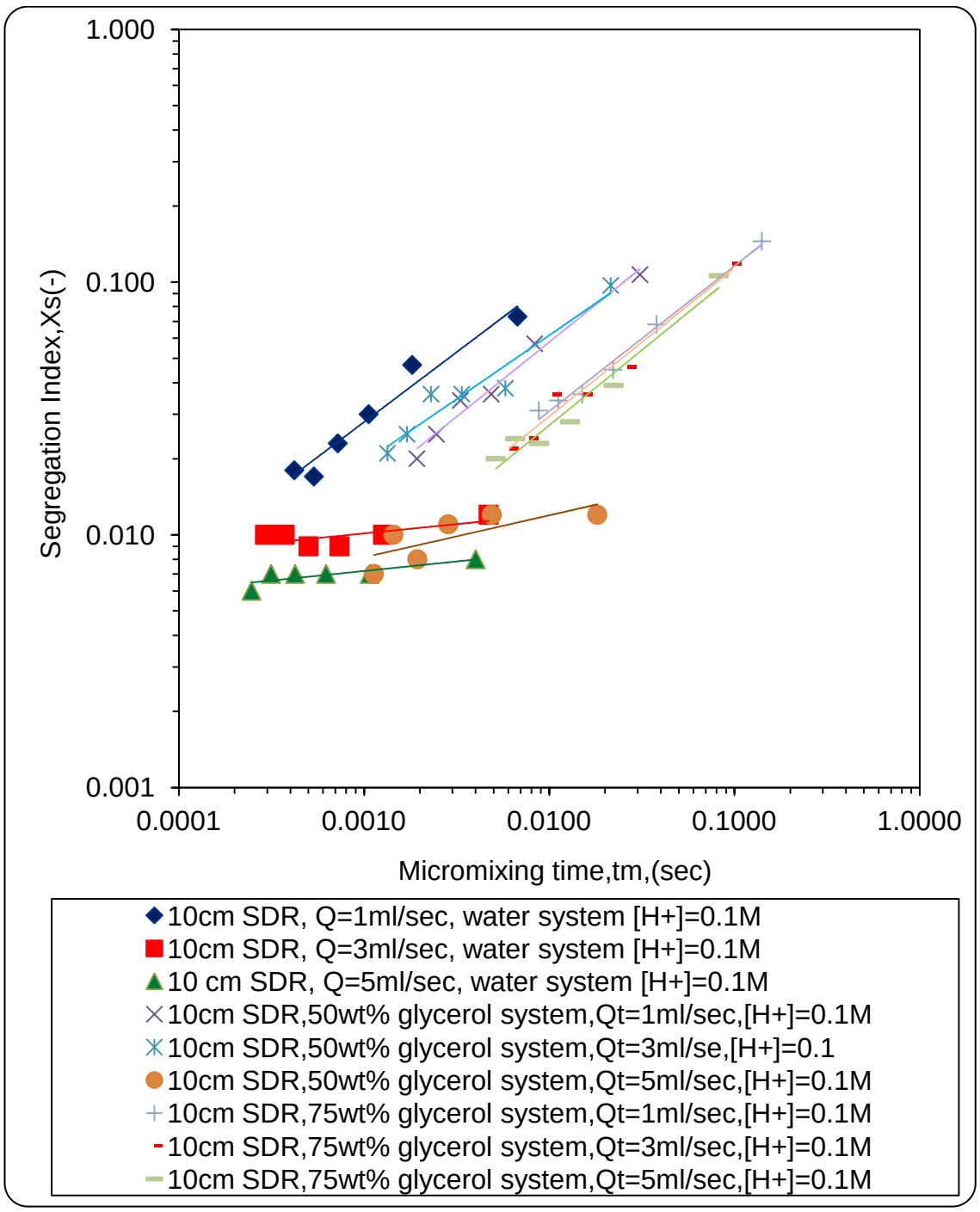

Figure 5.37: Relationship between Micromixing time and segregation at different total Flowrates and different viscosities (water, 50 wt% glycerol and 75 wt% glycerol systems) - [H+] =0.1 M and R=70

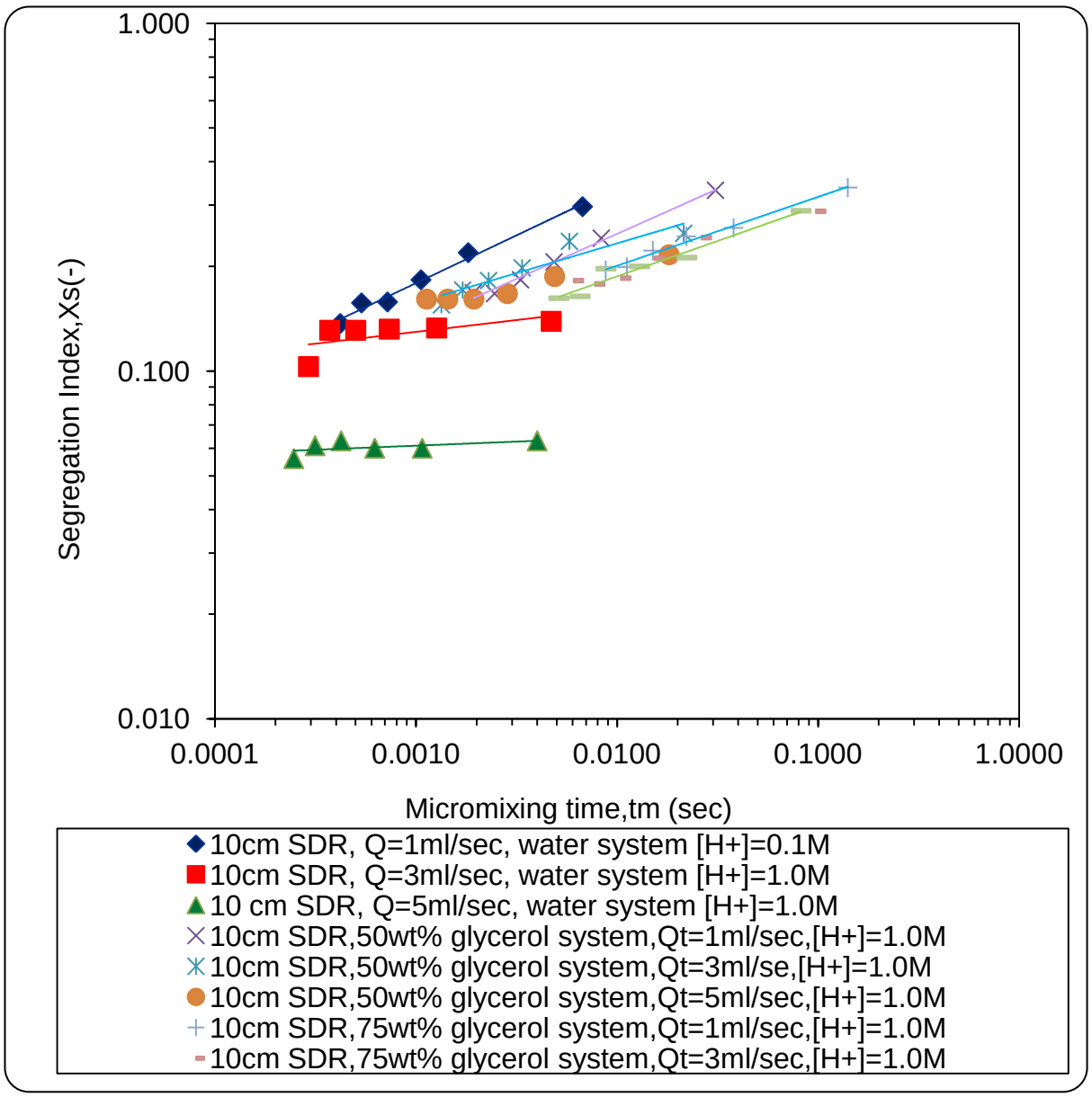

Figure 5.38: Relationship between Micromixing time and segregation at different total Flowrates and different viscosities (water, 50 wt% glycerol and 75 wt% glycerol systems) - [H+] =1.0 M and R=70

5.2.9 Regression Analysis on Segregation index for 10cm SDR

Regression analyses were performed for all the 10 cm SDR data (i.e. aqueous solution, 50 wt% Glycerol and 75 wt% Glycerol) using the regression tool in the Minitab 15 software. Four empirical models between Segregation index, (Xs) and the three variables (angular velocity of the disc, (ω), total flowrate, (Qt) and dynamic liquid viscosity, (μ) were obtained, one for each acid concentration tested.

For the regression analyses it was assumed that the segregation index, (Xs), could be represented by:

$$X_S = A.\omega^B.{Q_t}^C.\mu^D \quad (5.13)$$

Where A, B, C, D are regression parameters in the equation. Equation (5.13) can be written in a more appropriate form:

$$\log(X_S) = \log A + B\ log(\omega) + C\ log(Q_t) + D\ log\ (\mu) \quad (5.14)$$

Table (5.9) represent the calculated values of the parameters and R^2 for the segregation index models

Table 5.9: Segregation index Regression analysis results for 10 cm SDR

[H+],M	A	B	C	D	R^2(Adj)
0.1	+0.235	-0.453	-0.752	+0.293	0.749
0.25	+0.352	-0.287	-0.704	+0.343	0.769
0.50	+0.419	-0.266	-0.463	+0.266	0.770
1.0	+0.451	-0.222	-0.284	+0.183	0.681

Therefore following model equations which describe the segregation index in a 10 cm SDR can be written as:

$$\text{For } [\text{H}+] = 0.10 \text{ M:} \quad X_S = 0.235\ (\omega)^{-0.453}(Q_t)^{-0.752}(\mu)^{0.293} \tag{5.15}$$

$$\text{For } [\text{H}+] = 0.25 \text{ M:} \quad X_S = 0.352\ (\omega)^{-0.287}(Q_t)^{-0.704}(\mu)^{0.343} \tag{5.16}$$

$$\text{For } [\text{H}+] = 0.50 \text{ M:} \quad X_S = 0.419\ (\omega)^{-0.266}(Q_t)^{-0.463}(\mu)^{0.266} \tag{5.17}$$

$$\text{For } [\text{H}+] = 1.00 \text{ M:} \quad X_S = 0.451\ (\omega)^{-0.222}(Q_t)^{-0.284}(\mu)^{0.183} \tag{5.18}$$

From the 10cm SDR model equations that have been produced, it can be seen clearly that increases in angular velocity of the disc and liquid total flowrate cause significant decreases in segregation index, (Xs). While increases in the dynamic liquid viscosity cause an increase in segregation index, Xs. Moreover, increases in, ω and Q_t as the acid concentration cause increases in the segregation index. This corresponds well with what was observed in the experimentally observed data.

As seen in Table 5.1 R^2 values for the three correlations between 0.68 and 0.77 suggest a reasonably good fit of the regression to the data. P-values were obtained corresponding to the significance of each parameter with the regression. With assuming a significance level of 0.05 (i.e. 95% confidence interval) the p-values was zero to three decimal places (0.000) indication each parameter to be of significance within the regression.

In order to check the validity of the model equations, segregation index values were calculated using the regression models (equations 5.15 to 5.18) and compared to real (experimental) values by plotting the experimental values against predicted data.

If the experimental values and predicted data were in good agreement, the best linear fit would be y = x. It will be more realistic to expect that y = M x, where constant is close to 1. Figures 5.39 to 5.42 illustrate a good degree of correlation between the predicted and experimental results. One noTable issue about Figures 5.39 to 5.42, there is some scatter occurring at the higher Xs values.

For the regressions, the model equations are applicable within the following range of operation parameters:

$$31.4\ s^{-1} \leq \omega \leq 251.2\ s^{-1}$$

$$5\ ml/s \leq Q_t \leq 1\ ml/s$$

$$1.005\ mPa.s \leq \mu \leq 35.5\ mPa.s$$

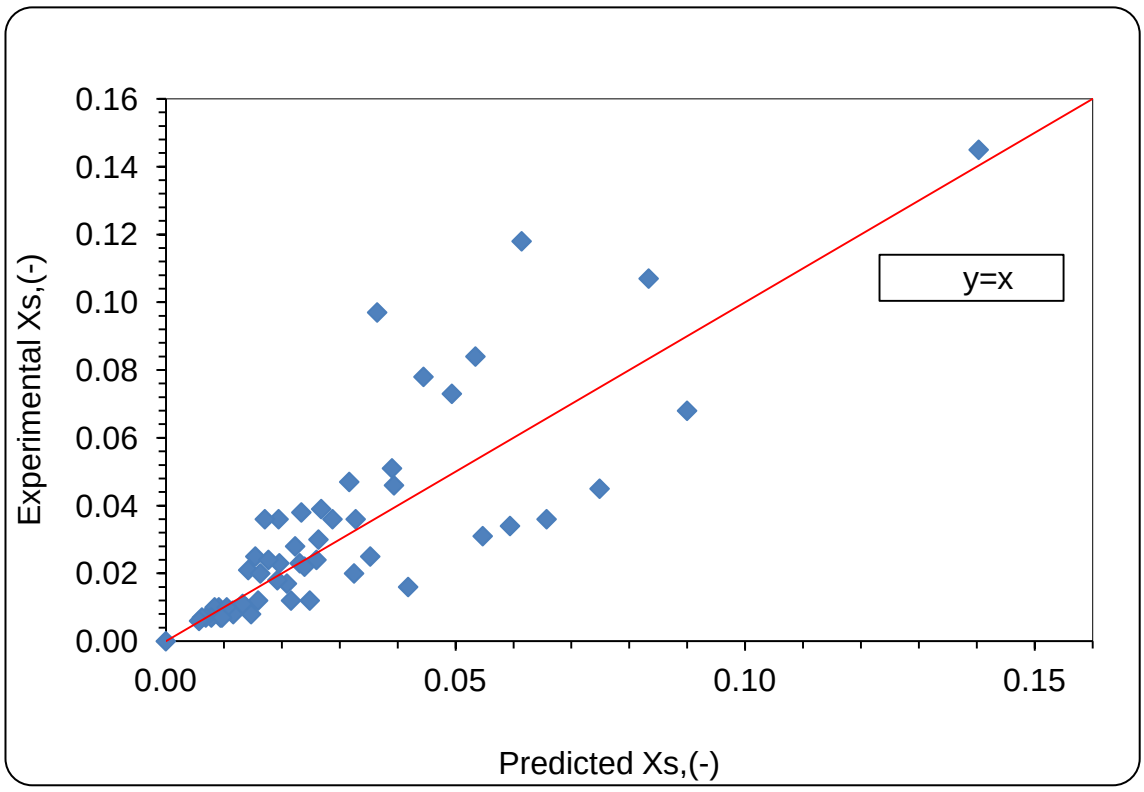

Figure 5.39: Experimental segregation index data against segregation index as predicted by Empirical model for [H+] = 0.1 M

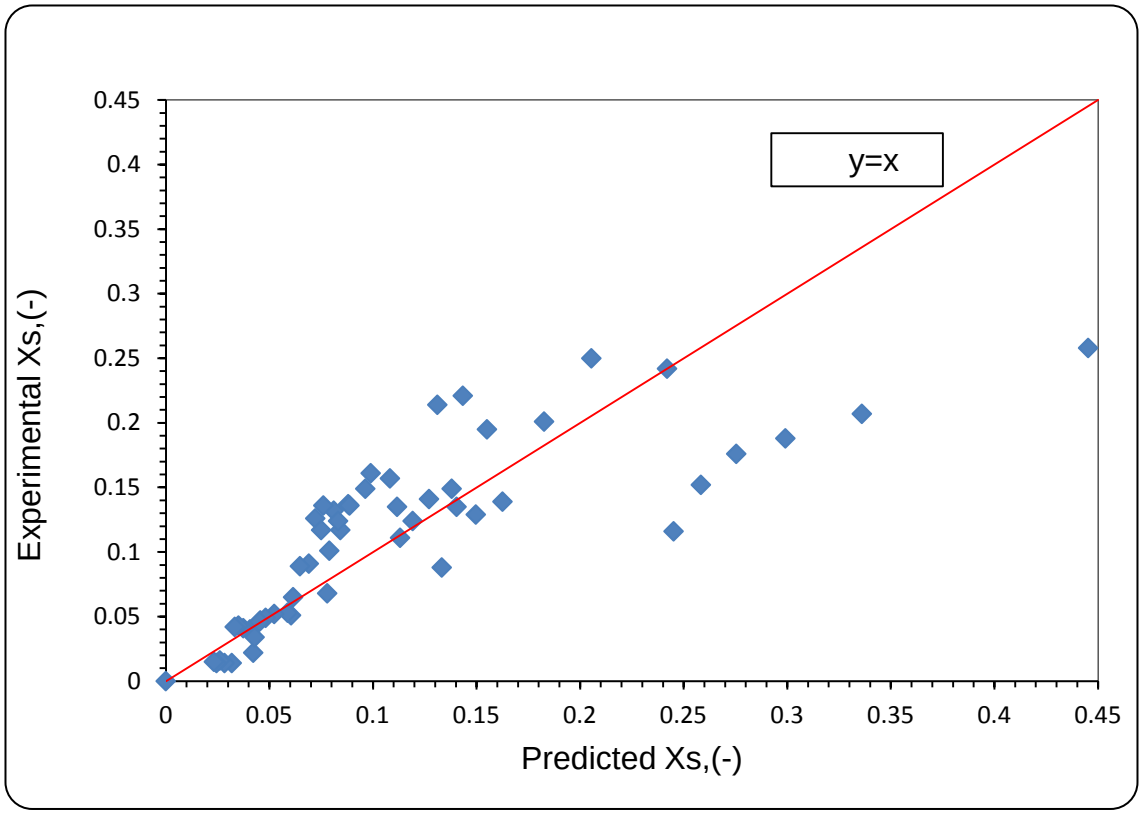

Figure 5.40: Experimental segregation index data against segregation index as predicted by Empirical model for [H+] = 0.25 M

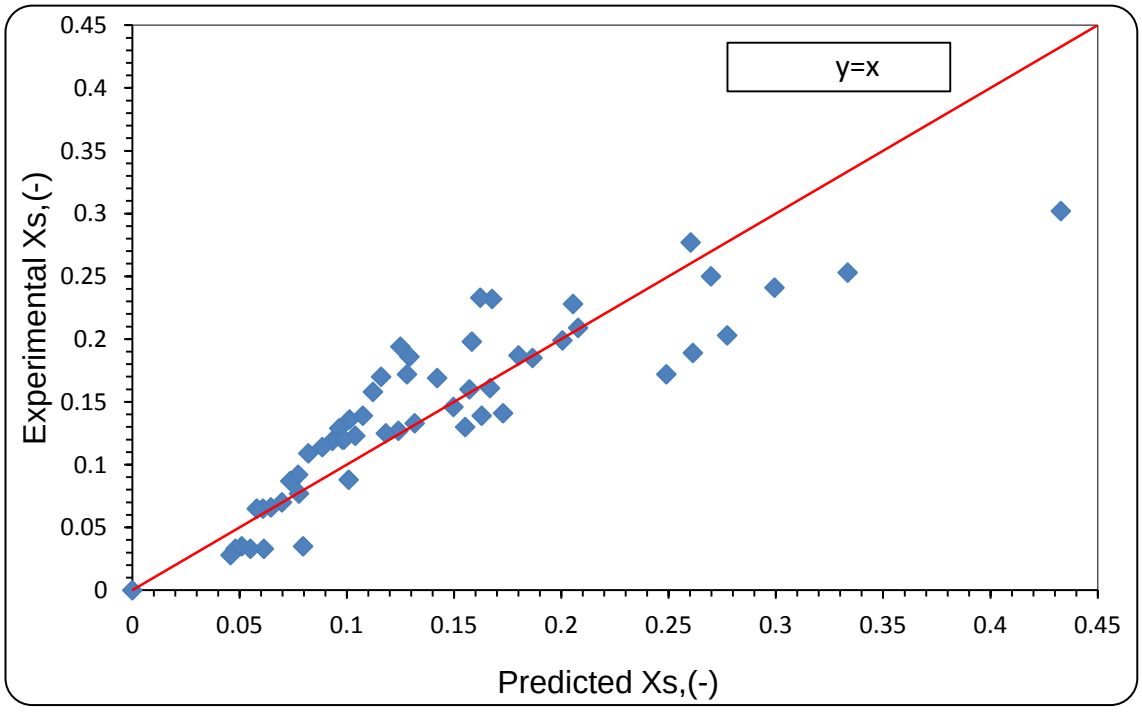

Figure 5.41: Experimental segregation index data against segregation index as predicted by Empirical model for [H+] = 0.50 M

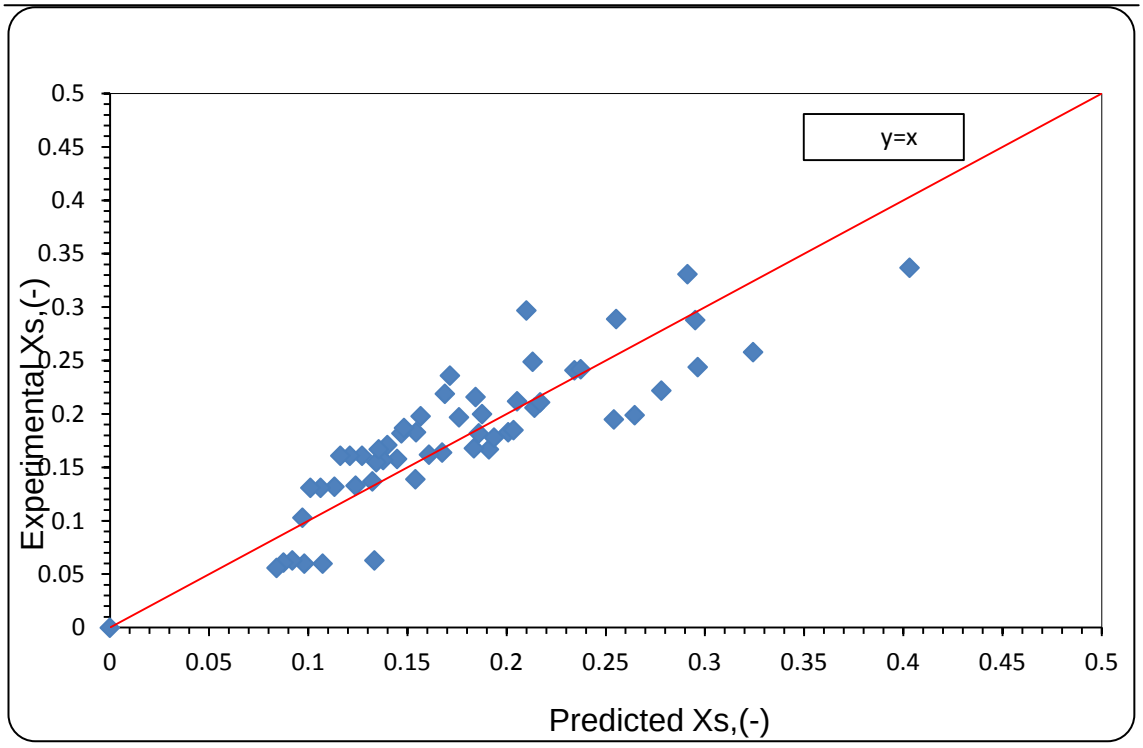

Figure 5.42: Experimental segregation index data against segregation index as predicted by Empirical model for [H+] = 1.0 M

5.3 Micromixing Experimental Results: 30cm Spinning Disc Reactor

The characterisation of micromixing on the 30 cm SDR adopted much the same procedure as used for the 10 cm SDR experiments. The 10 cm and 30 cm SDRs are identical in all aspects except for their rotating disc size. For a direct comparison of their micromixing performance under different operating conditions, the Reynolds number has been selected as a constant parameter in both reactors. The total flowrates used in the large SDR (30 cm) have therefore been calculated based on the Reynolds numbers employed in the 10 cm SDR (Table 5.10).

Table 5.10: the total flowrates used in 30 cm SDR based on the Reynolds numbers employed in the 10 cm SDR

Total flowrates in 10 cm SDR (ml/sec)	Total flowrates in 30 cm SDR (ml/sec)	Reynolds number, Re (-)
1	3	14.3
3	9	42.3
5	15	71.5

5.3.1 30cm SDR Experimental design

Randomized general full factorial experimental designs DOE for both water and 50 wt% water/50wt% glycerol systems were performed using Minitab 15 (AJ1). In this part of the research, ninety six experiments were carried out i.e. forty eight experiments for each liquid medium used (water and 50 wt% water/50wt % glycerol) using two different types of discs (stainless steel smooth disc and grooved disc). Three replicates of each experiment were carried out for data accuracy. The mean value of absorbance D_λ (-), the average segregation index Xs (-), the standard deviation (σ) and standard error (S) as well as the relative error were estimated. The maximum relative error of experiments was only (4.60%) and the results were satisfactorily reproducible.

For the 30 cm SDR experiments, the variables incorporated into the experimental design were:

- Disc rotational speed: 300 rpm, 500 rpm, 800 rpm and 1200 rpm (1200 rpm was the maximum speed at which the reactor could be safely be operated)
- Acid ion concentration: 0.5 and 1.0M
- Total flowrate: 3, 9 and 15 ml/s
- Viscosity: water system (μ=1.005 mP.s at 20 ^{o}C), 50wt% glycerol system (μ = 6.0 mPa.s at 20 ^{o}C) .
- Disc surface configuration: smooth and grooved disc.

5.3.2 30cm Smooth stainless steel disc results

5.3.2.1 Effects of rotational disc speed and total flowrate on Xs

The influence of the smooth 30cm disc rotational speed and reactants total flowrates on the segregation index is shown in Figures 5.43 to 5.46. Figure 5.43 and Figure 5.44 shows the influence of disc rotational speed on the segregation index (Xs) at three different total flowrates in the range 3 to 15 ml/s, with two different acid concentrations of 1.0 and 0.5 M respectively and the disc rotational speed ranged 300-1200 rpm.

The individual flowrates of the iodide-iodate-borate ions stream, (Q_I), and the acid ions stream, (Q_H), corresponding to each total flowrate indicated above are given in Tables

(5.11) and (5.12) for acid concentrations 1.0 M and 0.5 M respectively. Sample calculation of the volumetric flowrate ratio (R), Q_I and Q_H is shown in appendix (B).

Table 5.11: The individual flowrates of (QI) and (QH) corresponding to each total flowrate for acid concentrations 1.0 M and volumetric flowrate ratio of 70 , (R= QI / QH)

Qt,(ml/s)	Q_I,(ml/s)	Q_H,(ml/s)
3	2.957	0.042
9	8.873	0.1267
15	14.788	0.211

Table 5.12: The individual flowrates of (QI) and (QH) corresponding to each total flowrate for acid concentrations 0.5 M and volumetric flowrate ratio of 35 (R= QI / QH)

Qt (ml/s)	Q_I,(ml/s)	Q_H,(ml/s)
3	2.92	0.0833
9	8.75	0.250
15	14.58	0.416

It is observed that for each of the total flowrates employed, the segregation index,(Xs), decreases with increasing the disc rotational speed. As mentioned earlier in section 5.2.3, an increase of the disc rotational speed corresponds to an increase in shear rate generated at the disc/liquid interface. Consequently, the intensity of micromixing increases. At $[H^+]$ =1.0 M and total flowrate of 3ml/sec (Figure 4.43), the segregation index varied from 0.163 to 0.0062 depending on the disc rotational speed. The reduction in segregation index of 96% was attained at the disc rotational speed of 1200 rpm relative to starting disc rotational speed of 300 rpm. Similar observations with regards to the effect of disc rotational speed on the segregation index, (Xs), were obtained at the total flowrates of 9 ml/s and 15 ml/s over the entire range of disc rotational speeds tested.

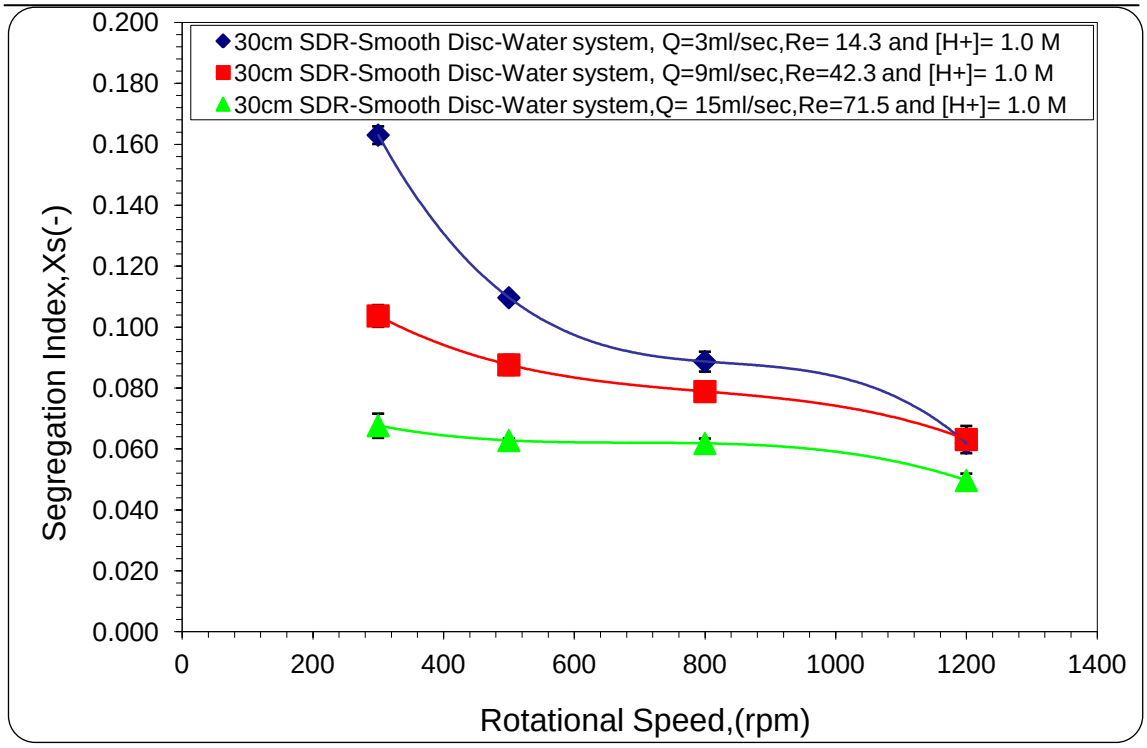

Figure 5.43: Effect of Disc Rotational Disc on segregation Index, Xs at Various total Flow rates - water system with [H+] =1.0 M

Analogous to Figure 5.43, the results in Figure 5.44 shows again the influence of disc rotational speed on the segregation index at three total flowrates using [H+]= 0.5 M. It is very clear that at the three total flowrates, the segregation index decreases with increase in the disc rotational speed. As explained earlier, an increase of the disc rotational speed corresponds to the increase in shear rate generated at the disc/liquid interface which therefore results in the increase of the micromixing intensity.

Figure 5.43 shows clearly that the worst case of the intensity of micromixing was achieved at the highest flowrate (i.e. 15 ml/s and Re= 71.5) over the entire range of disc rotational speeds tested. This was quite opposite to what was earlier established in 10 cm SDR experiments findings (section 5.2.3), where the highest total flowrate gave the lowest values of segregation index at a given disc rotational speed. This phenomenon is further studied and discussed in detail below.

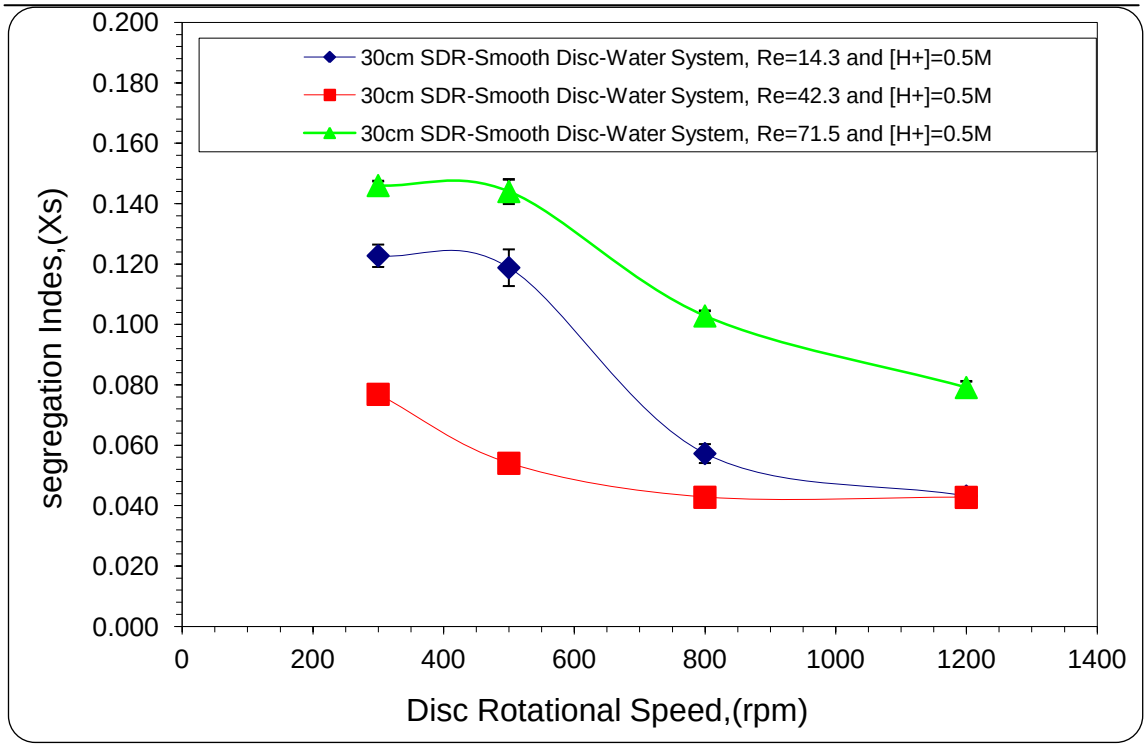

Figure 5.44: Effect of Disc Rotational Disc on Segregation Index, Xs at Various Total Flow Rates - Water System with [H+] =0.50 M

It can be concluded from the above Figures (5.43 and 5.44) is that micromixing in the 30 cm SDR depends strongly on the liquid flow rate in reactors utilising the centrifugal forces for enhancing heat and mass transfer of the reactants. This with agreement to what was earlier established in 10 cm SDR experiments findings. In addition, the shear rate generated at the disc/liquid interface by liquid flowrate and disc rotational speed has an effect on the segregation index (Xs), the higher sheer rate the lower segregation index (Xs).

The average maximum shear rate across the disc surface was estimated from equations (2.3 and 2.4). Figures 5.45 to 5.46 show the effect of average maximum shear rate across the disc surface on the segregation index, (Xs), for water system at three total flowrates and acid concentrations of $[H^+]$=1.0 M and 0.5 M. It is clearly from the Figures that the intensity of mixing on the 30 cm SDR in terms of segregation index, (Xs), is strongly affected by the shear rate generated at the disc/liquid interface. The higher shear rate the lower segregation index, (Xs).

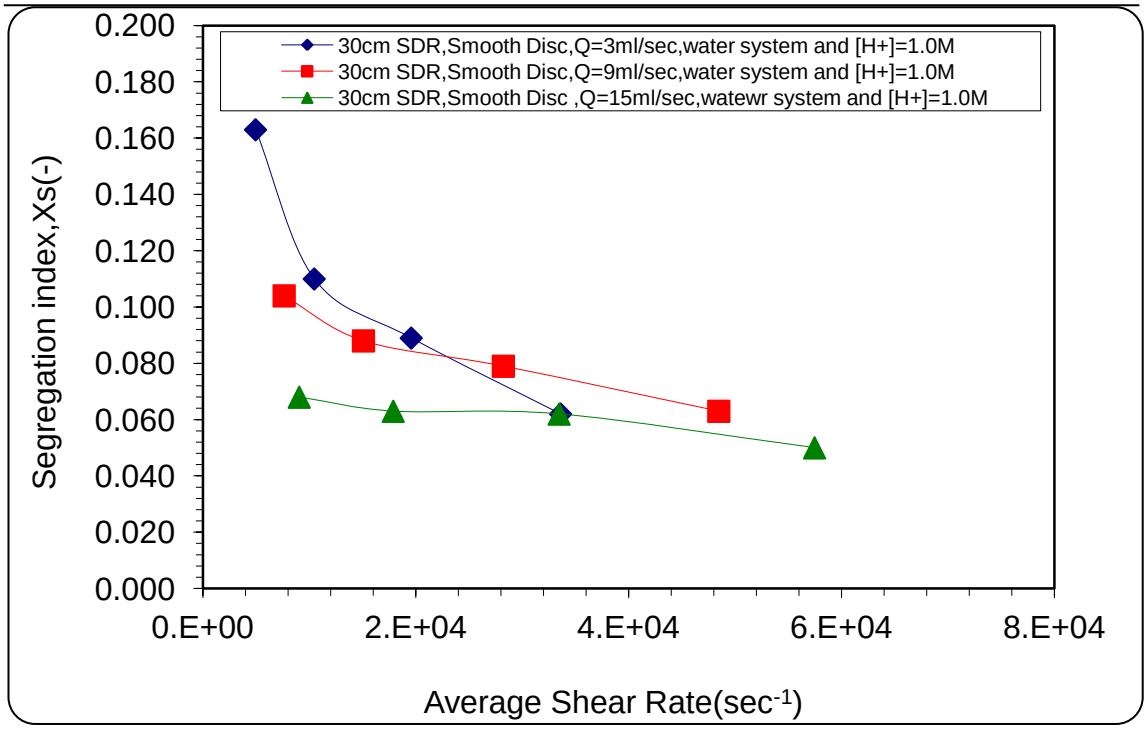

Figure 5.45: Effect of Average Shear Rate on segregation Index (Xs) in 30cmSDR at Various Total flowrate- smooth disc –water system, [H+] =1.0 M

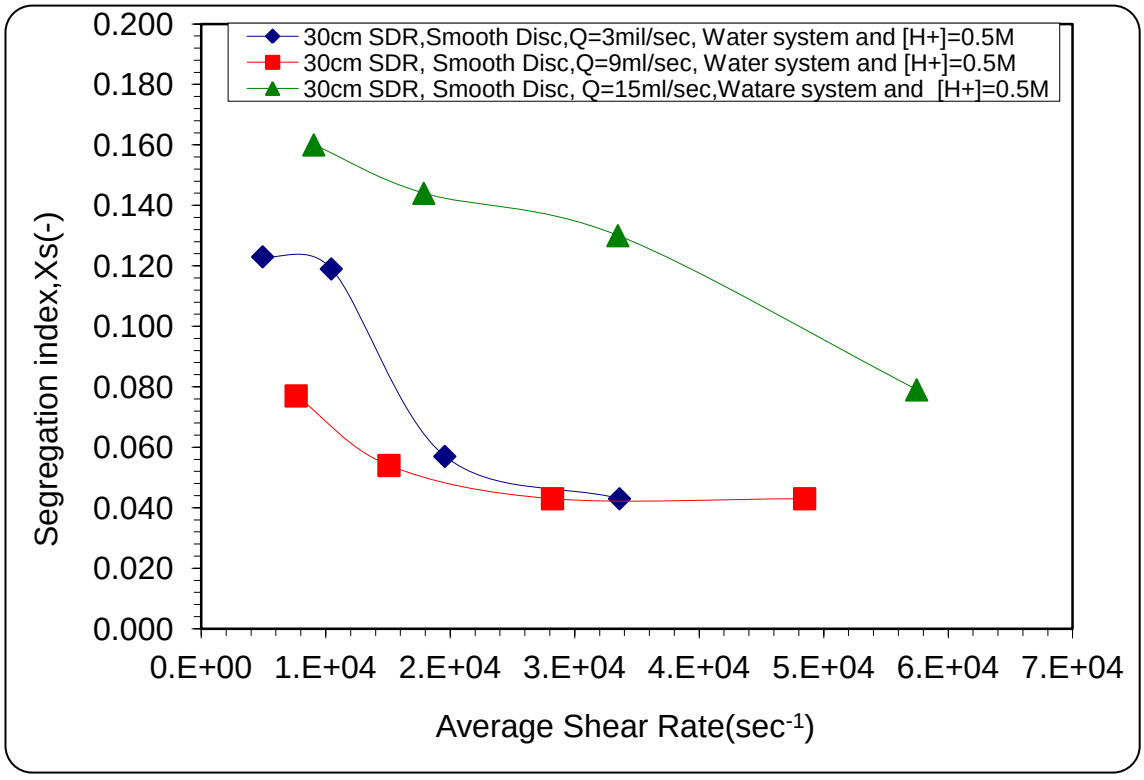

Figure 5.46: Effect of Average Shear Rate on segregation Index (Xs) in 30cmSDR at Various Total flowrate- smooth disc -water system, [H+] =0.5 M

It can be noted from Figure 5.43 that at the total flowrate of 15 ml/sec with $[H^+]$ =1.0 M, the SDR performance has improved compared to its performance when the acid ion

concentration was 0.5M in Figure 5.44. The influence of total flowrate on the segregation index can be more clearly demonstrated in Figures 5.47 and 5.48 for the two different acid concentrations used in this study.

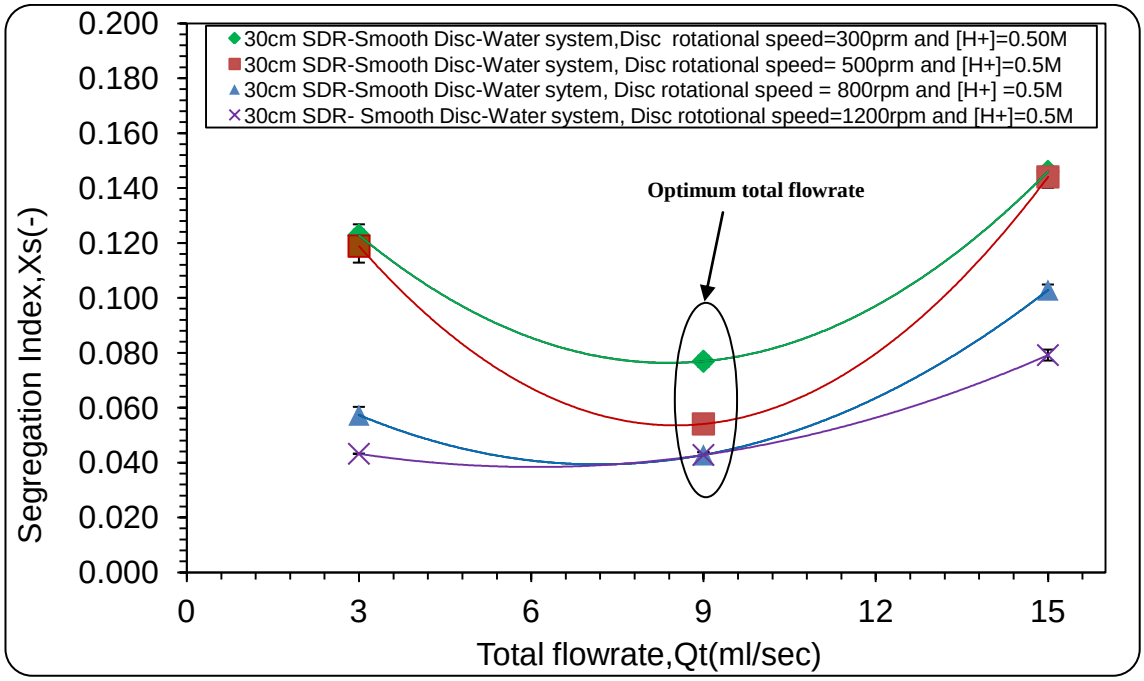

Figure 5.47: Effect total flowrate on the segregation index at Various Disc rotational Speed and [H+] =0.5 M

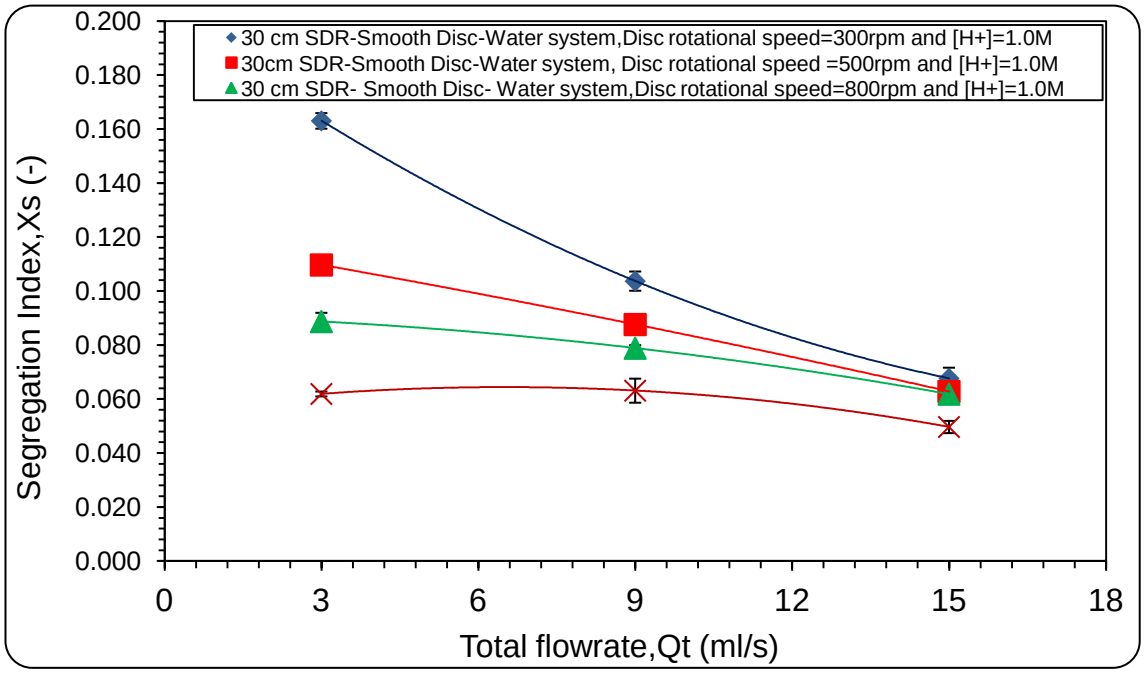

Figure 5.48: Effect total flowrate on the segregation index at Various Disc rotational speed and [H+] =1.0 M

Figure 5.47 shows the influence of total flowrate on the segregation index, (Xs) at four disc rotational speeds with an acid ion concentration of 0.5 M. It is noticeable that

between the total flowrates of 3ml/s and 9 ml/sec, the segregation index decreases with increase in the total flowrate in the entire range of disc rotation speed studied. Beyond 9 ml/s total flowrate, the segregation index appears to increase up until the maximum flowrate of 15 ml/s, indicating that an optimum flowrate for best micromixing performance exists in the range between 3 ml/s to 9 ml/s using an acid ion concentration of 0.5 M. In contrast, no optimum flowrate in the range tested in this study was apparent for 1.0 M acid ion concentration as seen in Figure 5.48 where a consistent decrease in segregation index was observed as total flowrate increased from 3 ml/s to 15 ml/s. From these findings it is clear that the intensity of micromixing on the 30cm SDR depends strongly on the liquid flow rate. Besides, the shear rate generated at the disc/liquid interface will increase as the total flowrate increases. The higher the shear rate the lower segregation index (Xs). From Figure 5.47**,** at total flow rate of 3ml/s and disc rotational speed of 300 rpm, the average shear rate on the disc has reached the highest value of 4943.5 sec^{-1}.On the other hand, with the total flowrate of 15 ml/s, the average shear rate was 9052 sec^{-1} at the similar disc rotational speed.

To interpret the observation of an optimum flowrate at acid ion concentration of 0.5 M, a simple SDR flow visualisation study was carried on. The canon camera model of (DIGITAL IXUS 70) was used for this purpose. Four photographs have been captured through the window of the SDR lid and presented in Figures 5.49 to 5.52 The observation of the four photographs allow the visualization of the different flow patterns that possibly occurred on the disc during experiments at a total flowrate of 15 ml/sec and different disc rotational speeds together with the effect of these parameters on the mixing intensity.

Figure 5.49, Photo 1 shows the flow pattern on the disc at the disc rotational speed of 300 rpm. The total flowrate of 15 ml/s combined with low disc rotational speed of 300 rpm results in a spiral flow path of the liquid stream close to the centre of the disc indicating that, on contact with the disc, the liquid does not instantly couple with the disc surface. This results in the liquid having an angular velocity lower than the disc itself. The spiral profile gradually disappears as the film thins at the periphery of the disc. The spiral flow behaviour is typical under conditions where the film thickness is high (i.e. closer to the disc centre, low disc speed, high flowrate) whereby the retarding Coriolis force becomes significant. Under such conditions, mixing between the two

liquid streams injected onto the disc is expected to be quite poor. Consequently, a substantial amount of tri-iodide would be expected in this inner region as evidenced by the yellow coloured area seen on the disc surface which appears to cover approximately 25% of the total disc area. Also, when examining the individual flowrate conditions for each of the borate ions and the H+ ions at 0.5 M and 1.0 M under identical total flowrates (see Table 5.11 and 5.12), it is clear that the flowrate of the sulphuric acid stream at 0.5 M is twice as high as that at 1.0 M. It is therefore reasonable to expect that it would be more challenging to completely integrate a higher flowrate of the acid into the borate ion stream to achieve good micromixing under identical disc rotation speeds. Instead, some of the sulphuric acid may flows on the surface of iodide-iodate-borate ions solution.

In Figure 5.50 - Photo 2, the disc rotational speed was 500 rpm, the phenomenon of poor integration of the sulphuric acid stream still occurred. Based on visual observation, the poor micromixing state was similar to the one at disc rotational speed of 300 rpm.

In Figure 5.51 (Photo 3) and Figure 5.52 (Photo 4), the disc rotational speed was 800 rpm and 1200 rpm respectively. It appears that the poor mixing of the sulphuric acid within the borate ion stream is limited to a region very close to the centre of the disc. The picture shows no obvious evidence of extensive spiral profile which means that the whole film coupled with the disc surface more effectively and closer to the centre. The film thickness would be much thinner at such high rotational speeds and would be expected to give better micromixing. This was reflected in the lower segregation index values at 800 and 1200 rpm of 0.103 and 0.079 respectively, as seen in Figure 5.44. However, the micromixing intensity was still not encouraging when compared with the intensity of micromixing at the total flowrate of 3ml/s and 9 ml/s (Figure 5.44).

Overall, two conclusions can be drawn from Figures 5.44**,** 5.47 and 5.48 and Figures 5.49 to 5.52. Firstly, the optimum total flowrate that gave the lowest values of segregation index with [H+] of 0.5 M is 9 ml/sc. Secondly, bad distribution of sulphuric acid with the iodide-iodate-borate ions solution occurred at the higher total flow rate of 15 ml/sc. Accordingly, the 30cm SDR failed to show superior performance at this higher total flowrate.

To eliminate the bad distribution of sulphuric acid with the iodide-iodate-borate ions solution, a *multi -point distributor* was introduced to the 30 cm SDR and was used in the course of micromixing experiments. The results for the micromixing experiments using the *multi -point distributor* are presented in section (5.3.4).

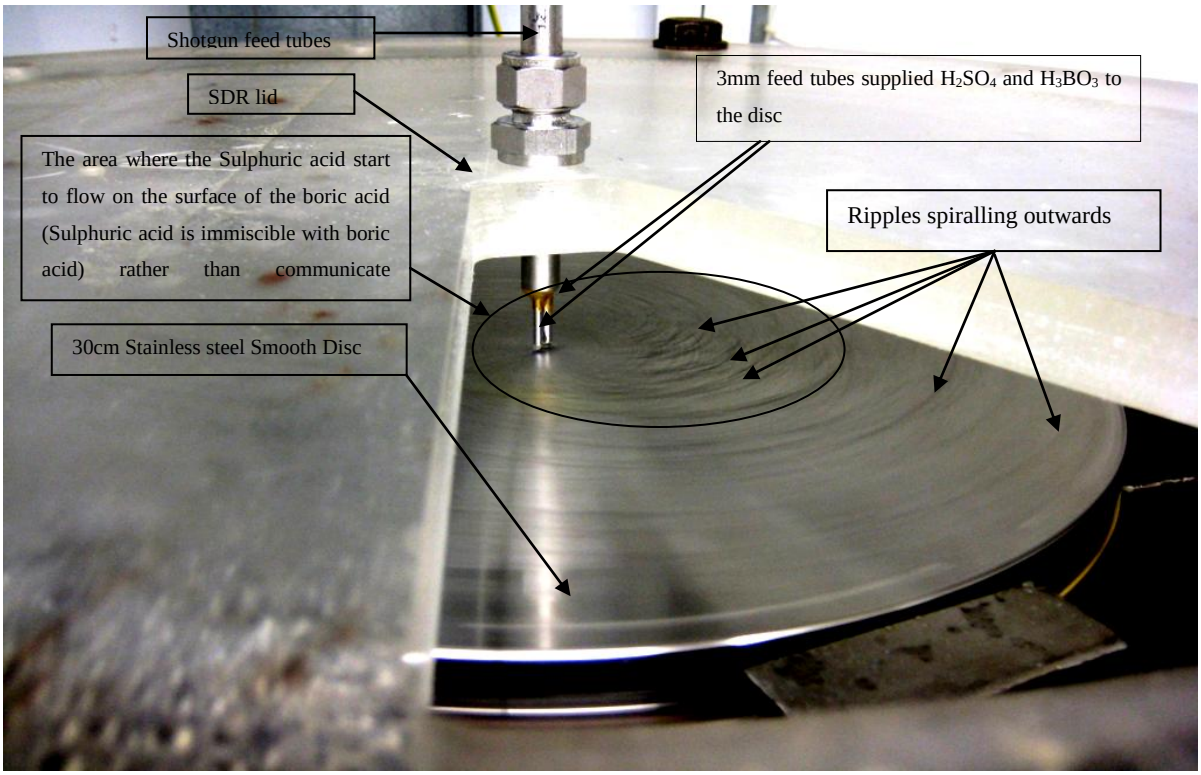

Figure 5.49: Water system- Smooth disc Single - Point distributor at N=300 rpm- Qt=15 ml/sec ,Q_I=875 ml/min, Q_H=25 ml/min, [H+]=0.5 M

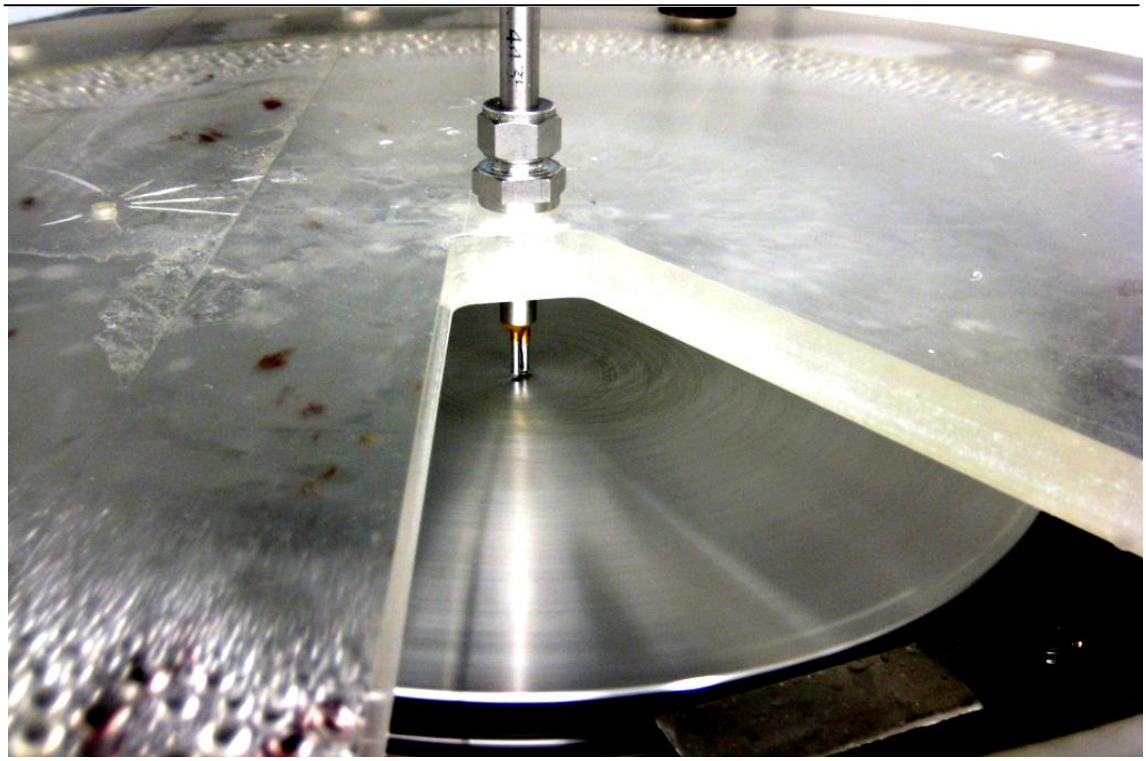

Figure 5.50: Water system- Smooth disc Single - Point distributor at N= 500 rpm- Qt=15 ml/sec, QI=875 ml//min,QH=25 ml/min, [H+]=0.5 M

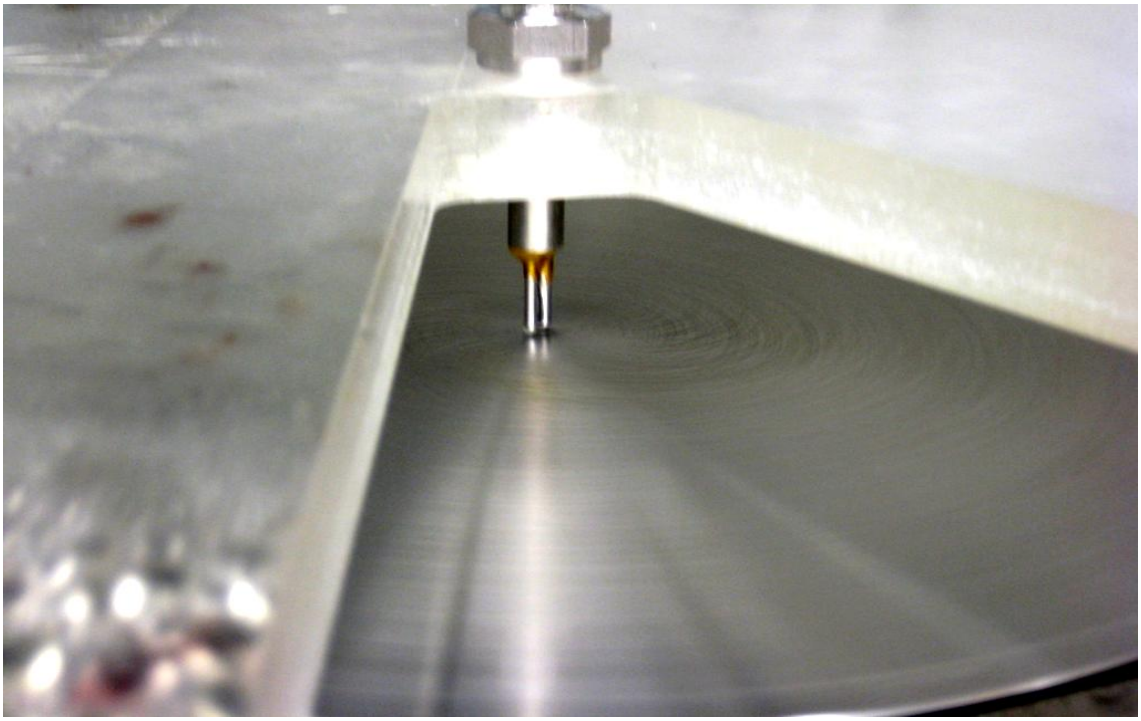

Figure 5.51: Water system- Smooth disc Single - Point distributor at N=800 rpm- Qt=15 ml/sec, QI=875 ml//min,QH=25 ml/min, [H+]=0.5 M

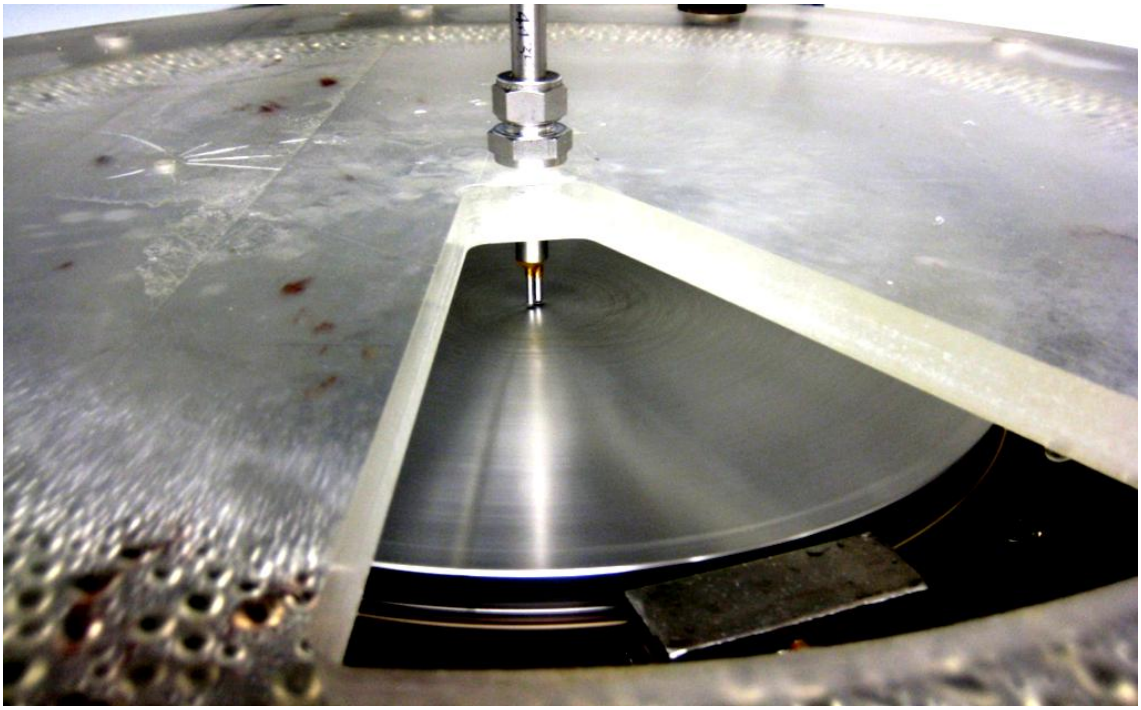

Figure 5.52: Water system- Smooth disc Single - Point distributor at N=1200 rpm - Qt=15 ml/sec, QI=875 ml//min,QH=25 ml/min, [H+]=0.5 M

5.3.2.2 Effect of feed viscosity on segregation Index (Xs)

The effect of feed viscosity on the segregation index in the 30 cm SDR was investigated by performing a set of micromixing experiments using a higher viscosity liquid medium consisting of a mixture of water and glycerol (50wt% of each component). The standard errors of the segregation index for all the experimental runs were calculated and plotted as standard error bars on the graphical plots. The relative experimental errors, based on three experiments for each set of conditions studied, were also estimated showing a maximum relative error of (5%), indicating that good reproducibility was achieved. The effect of feed viscosity on segregation index (Xs) in 30 cm SDR at three different total flowrates and different acid concentrations are shown in Figures 5.53 and 5.54 below.

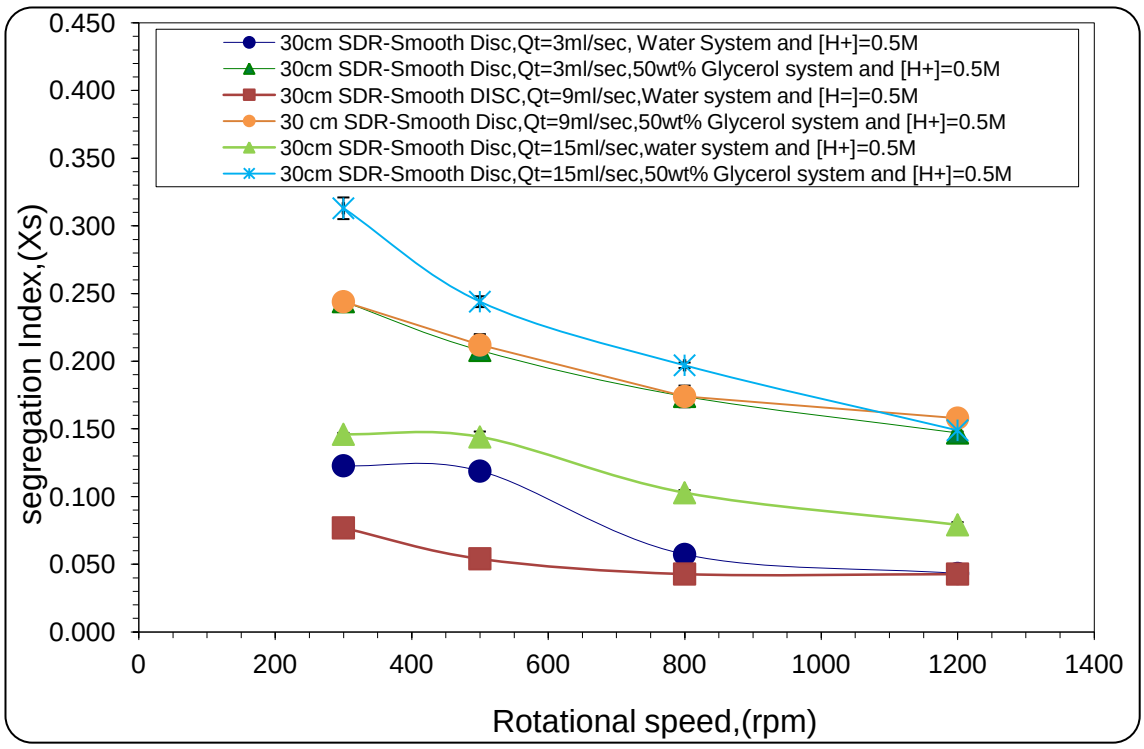

Figure 5.53: Effect of feed viscosity on segregation Index (Xs) in 30 cm SDR with Smooth disc at Qt =3, 9 and 15 ml/sec and [H+] =0.5 M

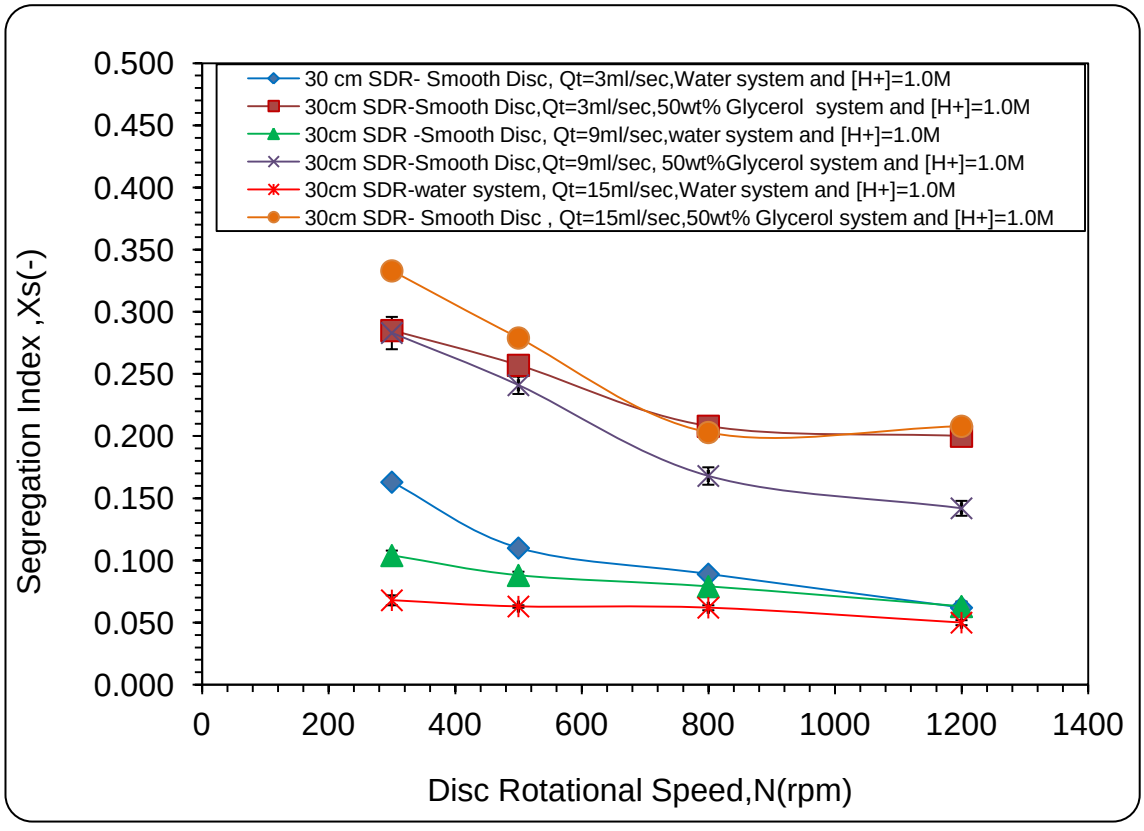

Figure 5.54: Effect of feed viscosity on segregation Index (Xs) in 30 cm SDR with Smooth disc at Qt =3, 9 and 15 ml/sec and [H+] =1.0 M

It is clear from Figure 5.54 which shows data for $[H^+]$ = 0.5 M that the segregation index increases as feed viscosity increases at any given disc rotational speed and total flowrate. For instance, at the 3 ml/s and disc rotational speed of 300rpm, the segregation index was increased by 50% for the 50wt% Glycerol solution (6 mPa.s) when compared with the segregation index of aqueous reaction solution (water system, 1 mPa.s). On the other hand, when the disc rotational speed was increased to 1200 rpm, the segregation index was increased by 71%. Similar trends were also observed at flowrates of 9 ml/s and 15 ml/s.

As demonstrated earlier in section 5.2.6 in 10 cm SDR experiments, this effect may be explained in terms of increased viscous shear forces acting against centrifugal forces on the surface of the disc, causing the flow to be retarded. Under such conditions, the shear rate, which is a measure of the mixing intensity within the film, is decreased. Therefore, as explained previously in section 5.2.6, the more viscous media has the effect of slowing down the micromixing rate and altering the intrinsic kinetics of the competitive reaction steps. Similar effects of viscosity on micromixing have been reported by several researchers in different reactor configurations (Yu-Shao CHEN, 2004; Guichardon et al., 1997) .

In addition, the diffusivity would naturally be slower in case of increase in the feed viscosity; this will result in reduction in the rate of mass transfer. Consequently, the rate of reaction in *neutralization reaction* will be reduced causing local accumulation of [H+] ions in solution. Under such conditions, the *Dushman reaction* is enhanced, producing a higher concentration of iodine and consequently tri-iodide whereby segregation index has a tendency to increase.

Besides, at a given total flowrate and disc rotational speed, increasing the feed viscosity will increase the average film thickness flowing on the disc. For example, at the total flowrate equal 3 ml/s and disc rotational speed of 300 rpm, the average film thickness across the whole disc surface for the water and 50 wt% Glycerol system equalled 36.611 and 108.933 μm respectively, representing a 3-fold increase in the average film thickness. Such an increase in film thickness will lead to an increase in the diffusion/conduction path length. Consequently, the mass and momentum transfer will be reduced and the rate of mixing will decrease.

The findings in Figure 5.54 where the acid ions concentration was 1.0 M were similar to the ones in Figure 5.53, in that the segregation index increases as feed viscosity increases at a given total flowrate. These findings were in agreement with the results that have been achieved in 10cm SDR experiments (section 5.2.6) and also with the works of previous researchers (Yu-Shao CHEN, 2004; Monnier et al., 1999a; Guichardon et al., 1997).

From Figure 5.53 and 5.54, one can note that even at the higher viscosities, the centrifugal force created by the 30cm SDR still has superior influence on micromixing, even at the higher viscosity. For example, at [H+] =0.5 M and Qt=15 ml/sec a 52% reduction of Xs was obtained at 6 mPa.s as the rotational speed increased from 300 to 1200 rpm. Similarly, a 38% reduction of Xs was obtained at [H+] =1.0 M as the rotational speed increased from 300 to 1200 rpm.

5.3.2.3 Effects of acid concentration on Xs

The effect of acid concentration at different disc rotational speeds and total flow rate of 3 ml/s on segregation index is shown in Figure 5.55 below. The acid ion concentrations were 0.5 and 1.0 M, the total volumetric flow rate ration,(R),was kept constant for the two concentrations (i.e. R = 35) for the purpose of demonstrating the acid concentration effect.

From the experimental results, it can be observed that the segregation index is sensitive to the acid concentration. In the disc rotational speed range between 300 and 1200 rpm, an increase of segregation index was observed as the acid concentration was increased. Over the entire range of disc rotational speed, the segregation index increased from 27.0 to 47.0% when the concentration acid ion was increased from 0.5 M to 1.0 M, depending on the disc rotational speed. These findings support the results that have been achieved in 10 cm SDR experiments (section 5.2.4). The reason behind the increase in segregation index with the increase in acid concentration can be explained by the studying the rate equations of the reactions taking place in this particular system.

The kinetics of second reaction (5.2) has been experimentally determined by (Guichardon et al., (2000b) as:

$$r = k[H^+][I^-]^2[IO_3^-] \quad (5.19)$$

Where the Kinetic constant (k) depends on the ionic strength, $(\boldsymbol{\mu})$, and given as:

$$\text{For } \boldsymbol{\mu} < 0.166\text{M}: \ log_{10}[k] = 9.28105 - 3.664\sqrt{\mu} \quad (5.20)$$

$$\text{For } \boldsymbol{\mu} > 0.166\text{M}: \ log_{10}[k] = 8.383 - 1.5112\sqrt{\mu} + 0.23689\mu \quad (5.21)$$

As shown in equations 5.1 and 5.2 above, the acid reacts in *neutralization reaction* and *Dushman reaction*. The rate of *Dushman reaction* is more sensitive to acid concentration than the *neutralization reaction* because the reaction order with respect to acid is higher. When the acid concentration is increased, the *Dushman reaction* becomes faster and consequently more iodine is produced. As a result, segregation index (X_S) increases. Similar effects of higher acid concentration on segregation index have been observed in previous micromixing studies (Yang et al., 2009a; Chu et al., 2007; Yang et al., 2006; Hai-Jian Yang, 2005).

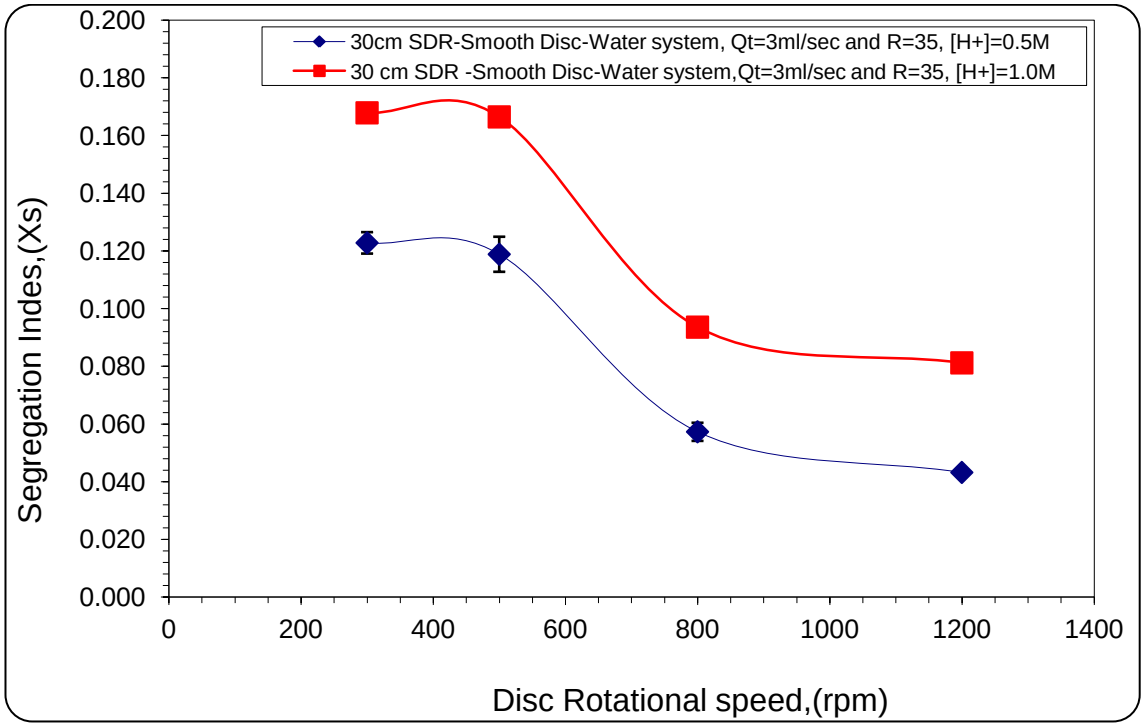

Figure 5.55: Effect of acid concentration on the segregation index at Various Disc Rotational Speed and Qt=3 ml/sec -water system flows on Smooth Disc, The total volumetric flow rate ratio, (R=35), [H+] = 0.5 and 1.0 M

5.3.2.4 Effect of power dissipation, (ε) on segregation index, (-)

Figures 5.56 show the effect of power dissipation on the segregation index for both water and 50 wt% glycerol system with an acid ion concentration of 0.5 M. The total flowrates were 3 ml/s, 9 ml/s and 15 ml/s and the disc rotational speed range was between 300 and 1200 rpm.

The power dissipation was the range of 5.1-1025 W/kg. These values depend on the total flow rate, water system or 50 wt% glycerol system and the disc rotational speed. This clearly indicates that the increase in power dissipation results in decrease in the segregation index at a given disc rotational speed and total flowrate (Monnier et al., 2000; Monnier et al., 1999b). The higher the power rate dissipation provided to the fluid, the higher rate of mixing that can be achieved.

From Figure 5.56, it is evident that the segregation index decreases consistently with increase in power dissipation. At the total flowrate of 3ml/s and water system using [H+] =0.5 M, the power dissipation increased from 9.0 W/kg at 300rpm to its highest value of 351 W/kg at 1200 rpm. This represents an increase of 98% in the power dissipation, corresponding to a reduction in Xs from 0.123 at 300 rpm to its lowest value of 0.043 at 1200 rpm thereby representing a 65% drop in Xs. Alternatively, at the same operating condition but with a replacement of the water system by 50 wt% glycerol system, the power dissipation increased from 5.1 W/kg at 300rpm to its highest value of 205 W/kg at 1200 rpm which is an increase of 98% over this range of disc speed. As a result of that, the segregation index reduced from 0.244 at 300 rpm to its lowest value of 0.147 at 1200 rpm representing a 40% drop in Xs. Similar trends were observed at flowrate of 9 ml/s and 15 ml/s. In Figure 5.57 where $[H^+]$ =1.0 M, similar trends with regards to the effects of power dissipation on Xs as described above were obtained at all flowrates and for both water system and 50 wt% glycerol system.

From Figure 5.58 and Figure 5.59 certain facts were confirmed. Firstly, the higher value of power dissipation could be achieved on the 30 cm SDR by the higher reactant total flowrate and higher disc rotational speeds as shown in Figure 5.58. Secondly, at a given disc rotational speed and reactant total flowrate, the lower values of power dissipation could be attained on the disc by increasing the reactant viscosity. This could be attributed to the fact that increasing the dynamic liquid Viscosity (μ_L) results in decrease

in the average velocity of the liquid solution on the disc. Therefore, the average shear rate generated at the disc/liquid interface at a given disc rotational speed decreases with increasing viscosity as shown in Figure 5.59. Accordingly, the power dissipation given to the fluid by the action of disc rotation decreased and the kinetic energy given to the liquid was reduced as well. For that reason, the intensity of micromixing also decreased.

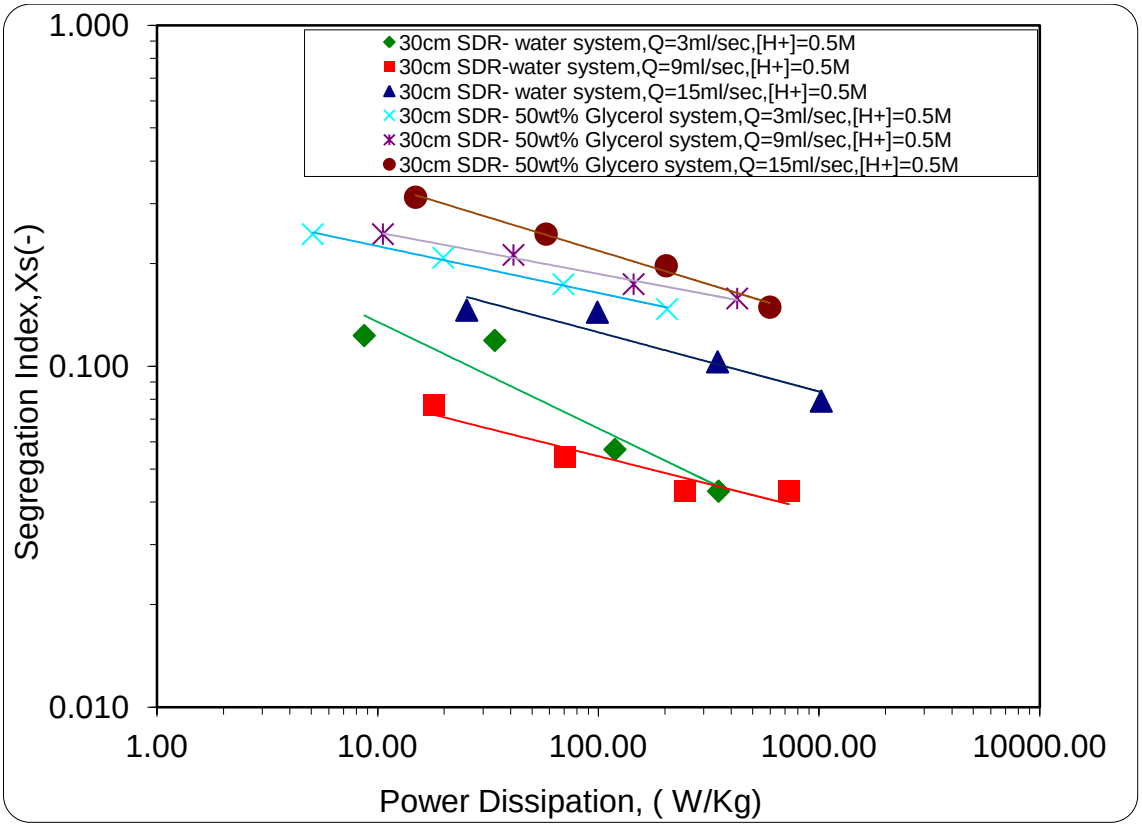

Figure 5.56: Effect of Power dissipation on Segregation Index, (-) at different liquid total Flowrates-30cm SDR smooth disc -water system and 50 wt% Glycerol system, [H+] =0.5 M

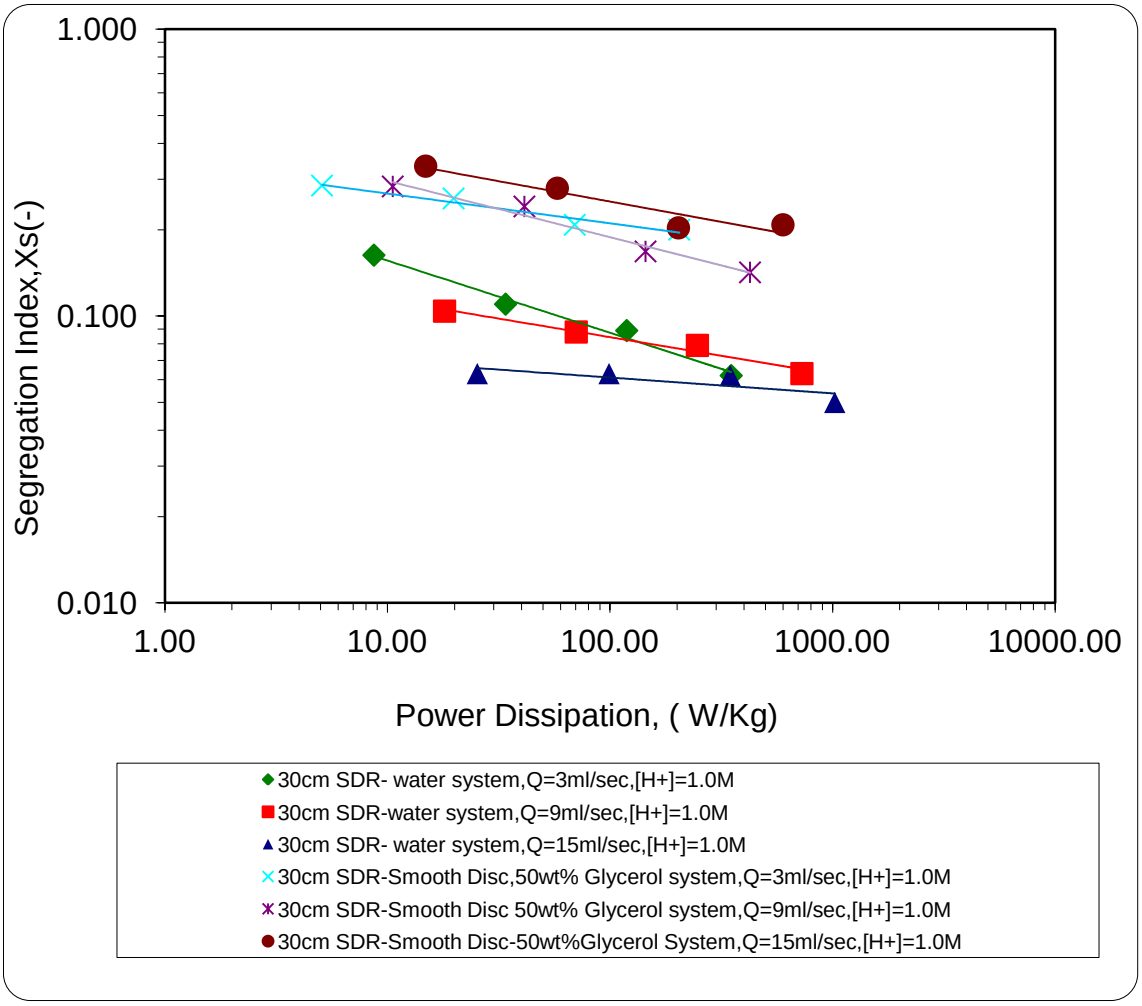

Figure 5.57: Effect of Power dissipation on Segregation Index, (-) at different liquid Total Flowrates- 30 cm SDR smooth disc -water system and 50 wt% Glycerol, [H+] =1.0 M

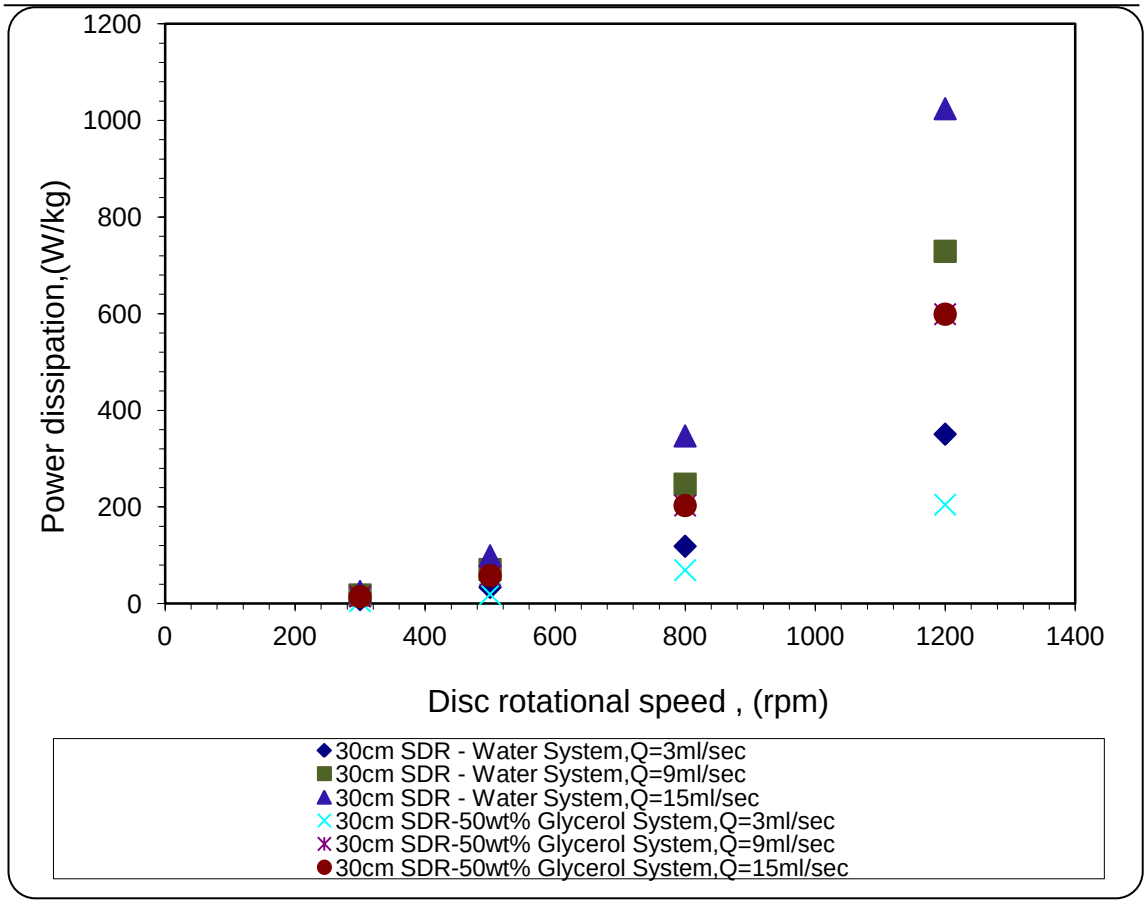

Figure 5.58: The effect of disc rotational speed on the power dissipation at Different total flowrates- 30 cm SDR smooth disc -water system and 50 wt glycerol system

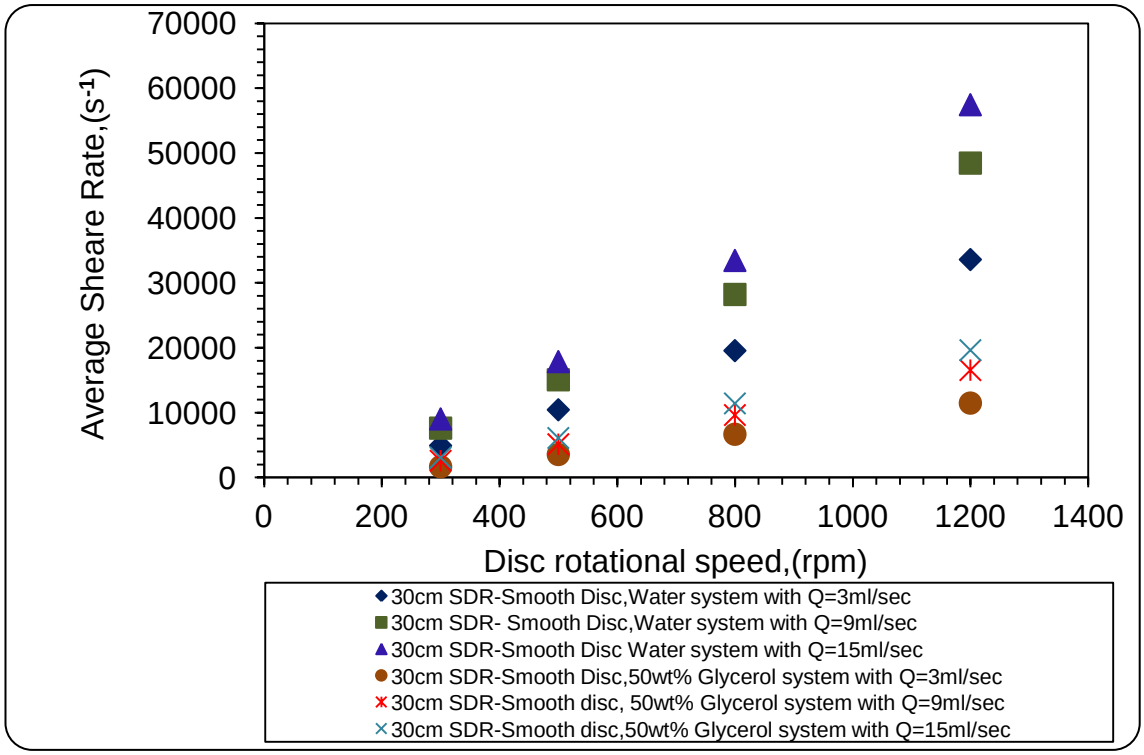

Figure 5.59: The effect of disc rotational speed on the average shear rate at different Liquid Total Flowrates- 30 cm SDR smooth disc -water system and 50 wt% glycerol system

5.3.2.5 30cm SDR Micromixing Time, (t_{DS}), and its Relationship with Segregation Index for Water and 50wt% Glycerol Systems

As mentioned earlier in section 5.2.8, the micromixing time on the disc is controlled by deformation and molecular diffusion. It has been calculated using equation (2.29) on the basis of the hydrodynamic properties of the fluid and the specific power dissipation across the whole disc surface. It is important to bear in mind that the micromixing time is a key parameter in determining the selectivity, quality or distribution of the final product if t_m value is less or close to reaction time, (t_r), which is equivalent to the residence time of the reactants on the disc.

As mentioned earlier in section 5.2.3, one important parameter needs to be considered when the micromixing taking place on the surface disc of the SDR is the residence time of the fluid on the disc. The liquid residence time on the disc needs to be greater than the required micro-mixing time; therefore it is possible for the micromixing taken place on the disc. Table AJ2 and Table AJ3 in appendix J show the predicted values of the residence (obtained from equation 2.8) and the micromixing times (estimated from equation 2.29) for the 30cm SDR experiments at the given disc rotational speed and water, 50 wt% Glycerol. It is clear that the residence times are much higher than the mixing times.

Figure 5.60 below shows the effect of disc rotational speed and total feed flowrate on the estimated micromixing time in the 30 cm SDR. It is seen that higher disc speeds and higher flowrates result in shorter micromixing time. The lowest value of micromixing achieved on the 30 cm SDR was 0.0003 s at the disc rotational speed of 1200 rpm with a total flowrate of 15 ml/s when the water system was used. Furthermore, at given disc rotational speed and reactant total flowrate, higher values of micromixing time were attained on the disc by increasing the reactant viscosity. This is attributed to the fact that increasing the dynamic liquid viscosity (μ_L) results in a reduction in the average velocity of the liquid solution on the disc. The average shear rate generated at the disc/liquid interface at a given disc rotational speed is consequently decreased as was shown in the above Figure (Figure 5.59). Accordingly, the power dissipation to the fluid by the action of disc rotation is reduced in higher viscosity media, as shown in Figure 5.61. In addition, as mentioned earlier, the diffusivity D is naturally slower when the feed

viscosity increases and given that the micromixing time is inversely proportional to the diffusivity coefficient value (equation (5.29), micromixing time is higher.

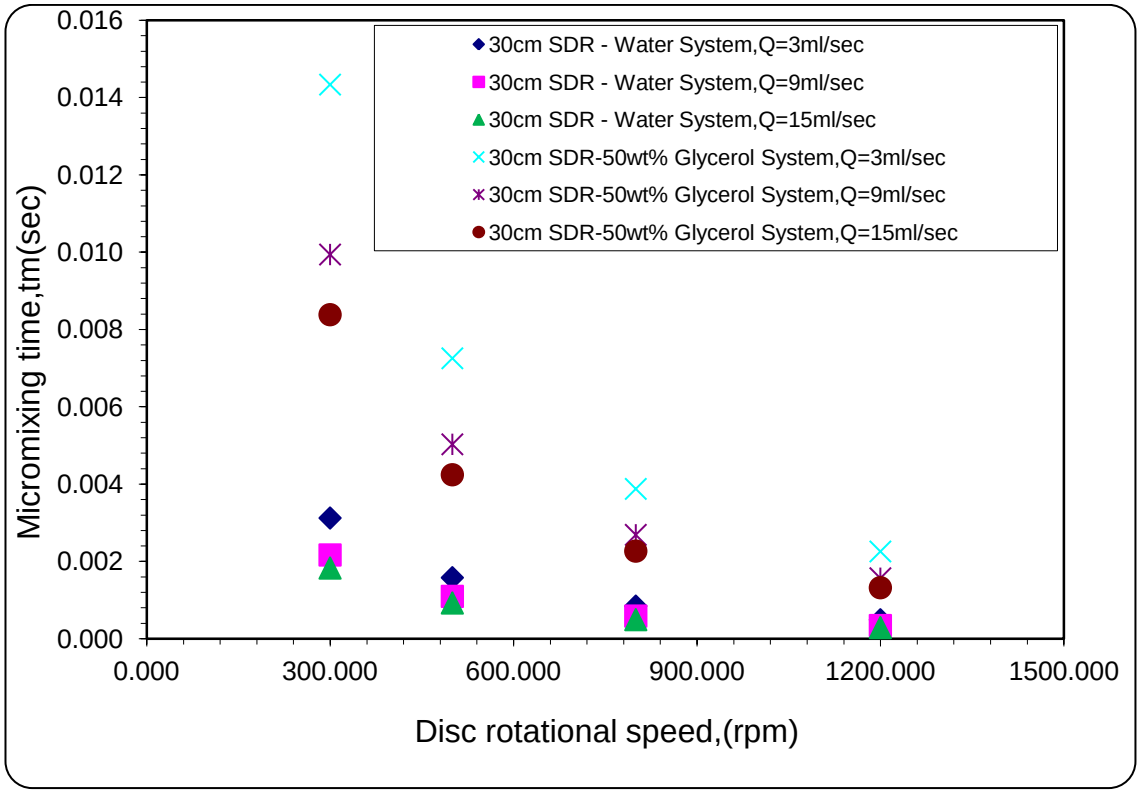

Figure 5.60: Micromixing time against disc rotational speed for 30 cm SDR-smooth disc

The combined effects of disc rotation speed and feed flowrate on micromixing time can be more clearly understood by analysing the effect of power dissipation on micromixing time. Figure 5.61 depicts a logarithmic plot of the estimation of micromixing time for both the water system and 50 wt% glycerol system as a function of power dissipation, calculated using equation (2.18) for three different total flow rates (3, 9 and 15 ml/s) and disc rotational speeds ranging between 300-1200 rpm.

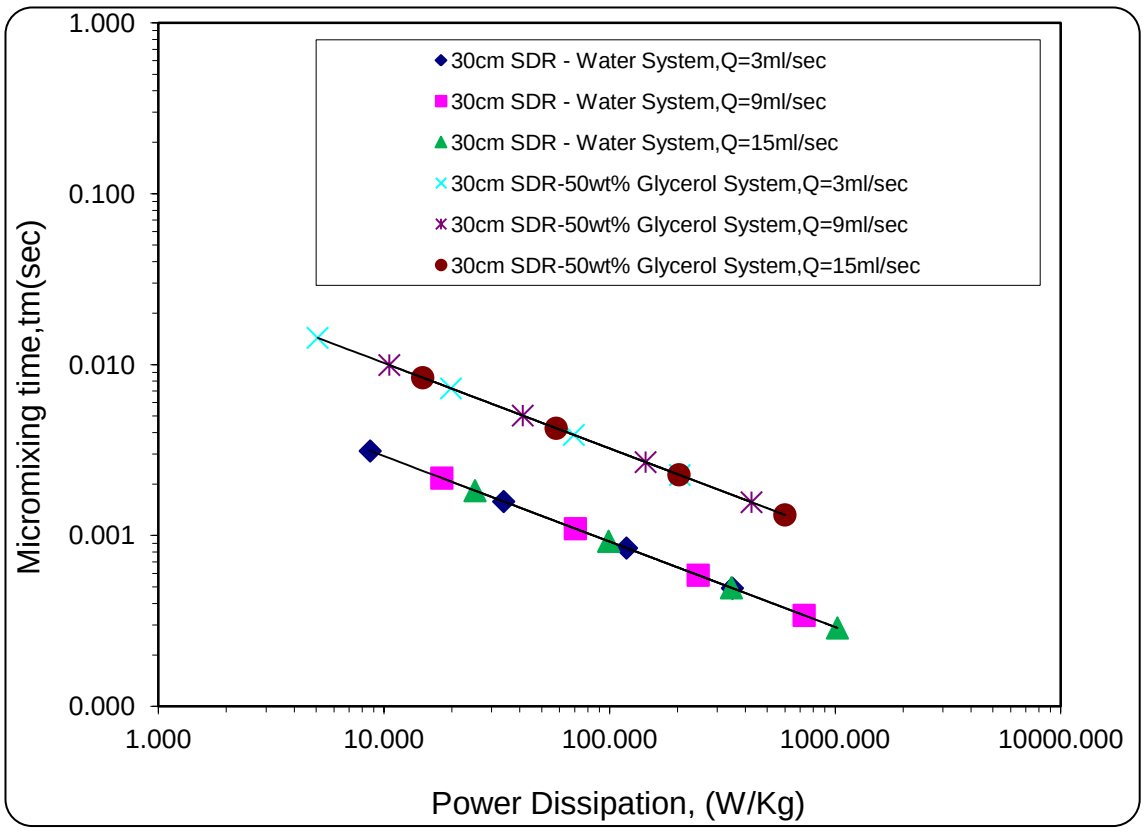

Figure 5.61: Micromixing time against power dissipation for 30 cm SDR-smooth disc at different total flowrate-water and 50 wt%Glycerol system

The graph clearly shows that the micromixing time is inversely proportional to the power dissipation. As the power input increases, the time, required for the molecules to diffuse to one another and make contact (i.e the micro-mixing time, tm) decreases. Accordingly, the micromixing intensity is improved. This also supports the explanation on the increases in the mixing efficiency with increased flowrates and rotational speed, which resulted in the power input increase.

In conclusion, the lower value of micromixing time, t_m, was achieved on the 30 cm SDR by using higher values of power dissipation generated by a combination of higher reactant total flowrate and higher disc rotational speeds as shown in Figure 5.61.

Figures 5.62 and 5.63 demonstrate the relationship between the calculated micromixing time and the experimentally determined segregation index, (Xs), at the three different total flowrates for both water system and 50 wt% glycerol system using $[H^+]$=0.5 and 1.0 M. From both Figures, it is obvious that the shorter the micromixing time, the lower

the value of segregation index achieved. For example at the total flowrate 3 ml/s using water system and $[H^+]$ =0.5 M, the micromixing time lies between 0.0031 – 0.0005 s corresponding to a segregation index of 0.123 and 0.043 respectively, depending on the disc rotational speed. The reduction of segregation index value of 65% was reached at the micromixing time of 0.0005 s relative to the initial value of 0.0031s. Similar trends were observed at flowrates of 9 ml/s and 15 ml/s. Similar trends with regards to the relationship between the micromixing time and segregation index as highlighted in Figure 5.62 were obtained for the higher acid ion concentration of 1.0 M (shown in Figure 5.63) at all flow rates for both water system and 50wt% glycerol .

From the findings above, it can be concluded that the total flowrate and disc rotational speed play an important role in increasing the intensity of mixing on the rotating disc surface whereby the higher the flow rate and the disc speed, the higher the power dissipation. This in turn leads to shorter micro-mixing time between reacting molecules. These findings were in agreement with the findings made from 10cm SDR experiments (see section 5.2.8).

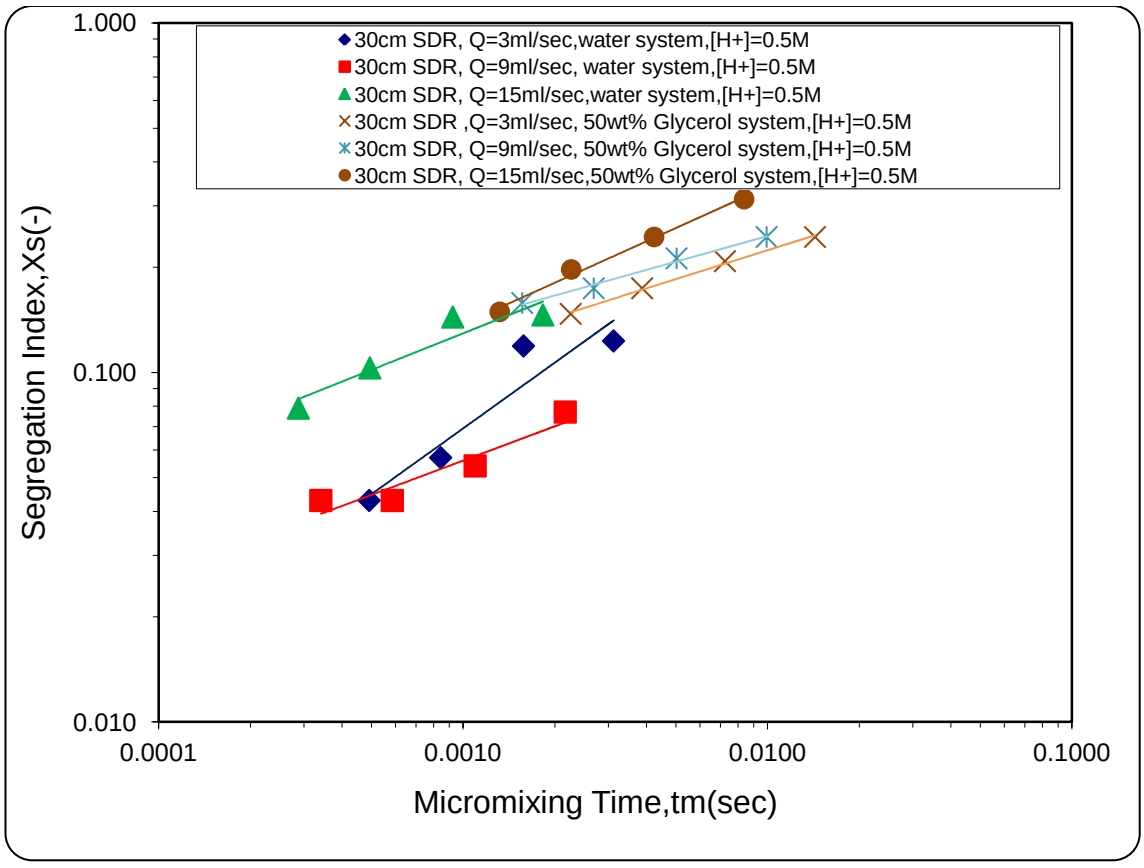

Figure 5.62: Relationship between Micromixing time and segregation index, (Xs) – 30 cm SDR-smooth disc at different Total Flowrate and [H+] =0.5 M for water and 50 wt% Glycerol system

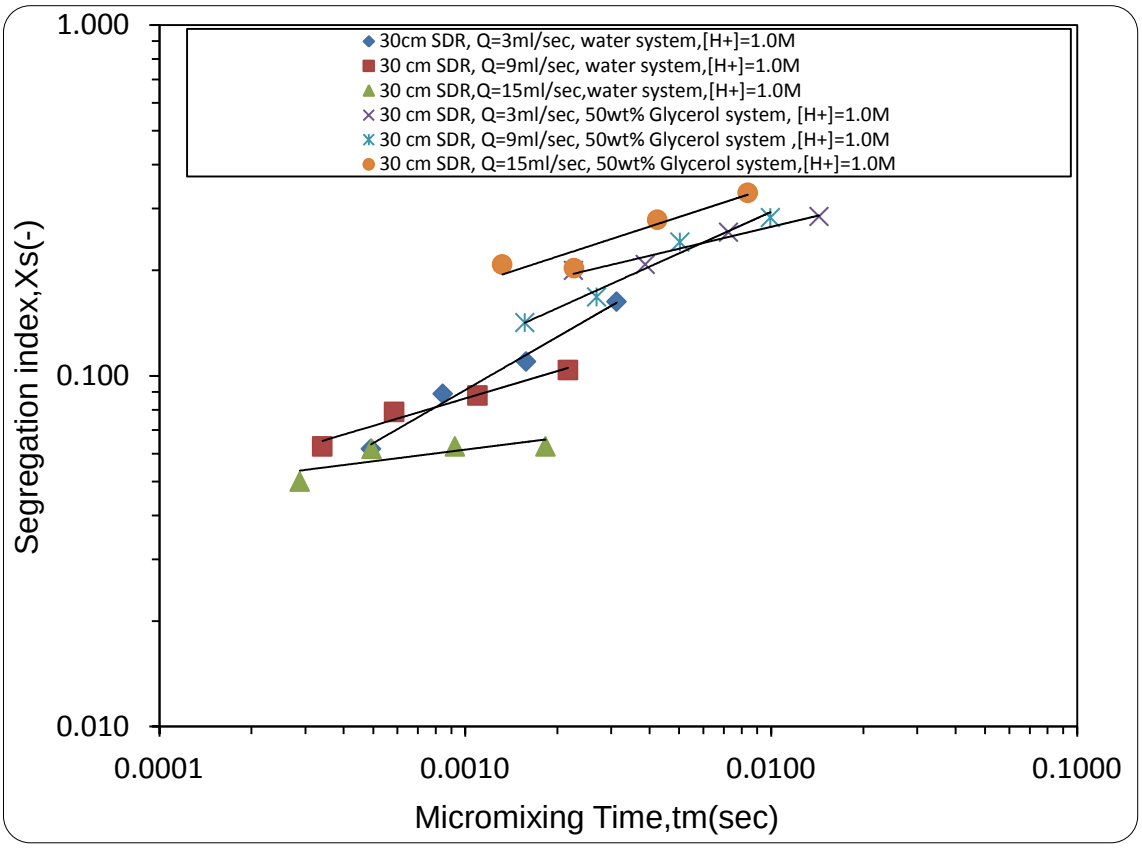

Figure 5.63: Relationship between Micromixing time and segregation index, (Xs) – 30 cm SDR-smooth at different Total Flowrate and [H+] =1.0 M for water and 50 wt% Glycerol system

5.3.3 30cm Grooved Stainless Steel Disc Results and its Comparison with Smooth Disc Results using 3.0mm Single-Point Distributor

As pointed out earlier in section (2.3.3), it has been recognised that the presence of grooves on the disc surface helps to enhance the heat and mass transfer performance by creating more waves of small amplitude and short wavelength at the film surface than the smooth disc (Jachuck and Ramshaw, 1994b). These waves have been shown to create increased instabilities in the film and also to increase the surface area available for heat and mass transfer. These features could lead to the improvement of the intensity of micromixing.

In view of this, micromixing experiments using 30 cm grooved stainless steel disc were performed to find out if the presence of grooves on the disc surface helps to enhance micromixing performance when compared with the smooth disc.

5.3.3.1 Effect of Disc Rotational Speed and Total Flowrate on Segregation Index (Grooved vs. Smooth Disc using 3.0 mm Single-Point Distributor)

Figures 5.64 and 5.65 show the performance of the 30cm SDR in terms of segregation index for both the grooved and smooth disc surfaces for the purpose of comparison. Three different total flow rates have been used in this set of experiments (3 ml/s, 9 ml/s and 15 ml/s). The disc rotational speed range was 300-1200rpm. The total flowrate ratios were, R= 35 and 70 with two different concentrations of H_2SO_4 of 0.25M and 0.5M corresponding to acid ion concentration of ([H+] =0.5 and 1.0 M) respectively.

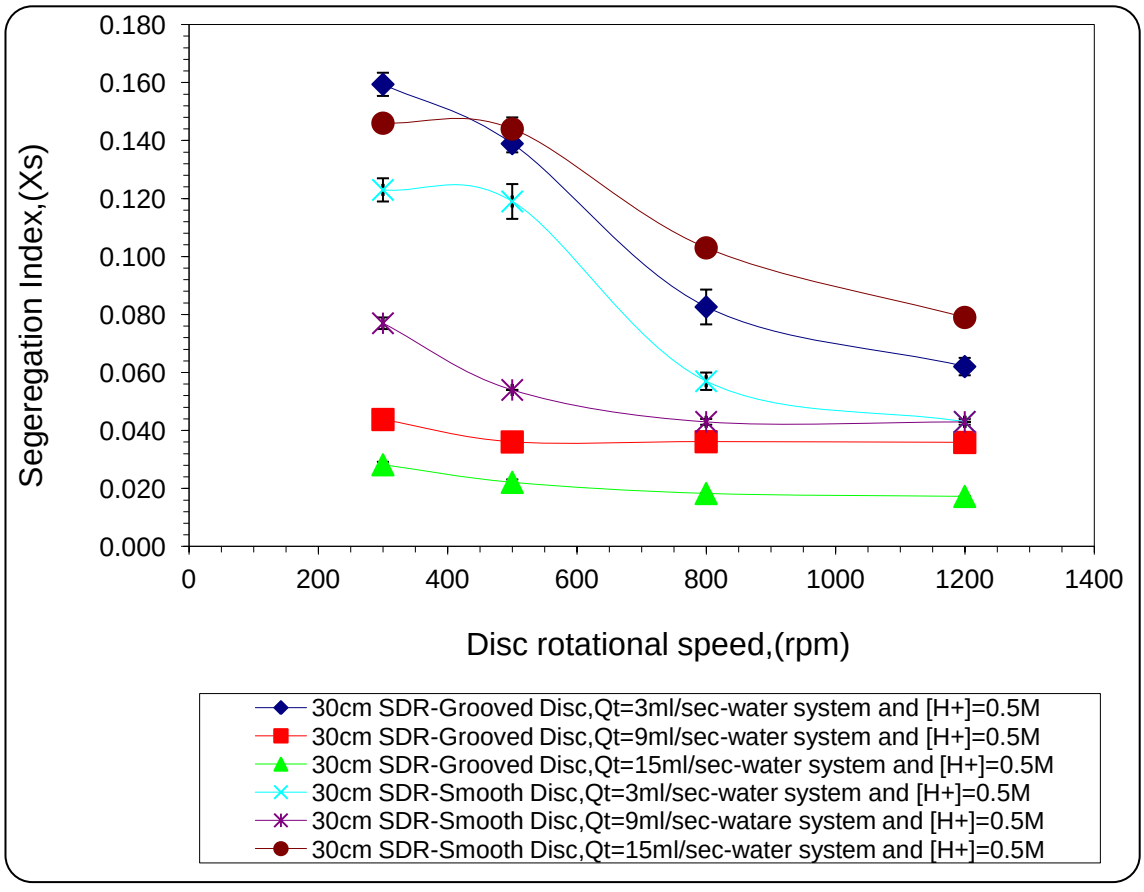

Figure 5.64: Effect of Disc Rotational Disc on segregation Index, Xs at Various total Flow Rates - water system with [H+] =0.5 M (Smooth disc Vs. Grooved Disc)

From Figure 5.64, it is apparent at Qt= 3 ml/s and the [H+] =0.5 M with rotational speed of 300 rpm Xs was 0.123 and 0.159 for smooth and grooved disc respectively. The segregation index was increased by 23% when the smooth disc was replaced by the grooved disc. On the other hand, when the disc rotational speed reached 1200 rpm, the

Xs was 0.043 and 0.062 for smooth and grooved disc respectively. The segregation index was increased by 31% when smooth disc was replaced by grooved disc. At this relatively low total flowrate, the grooved disc failed to perform better than the smooth disc. This could be attributed to the fact that when using grooved disc at low flowrates all grooves may not give good micromixing results if there is not sufficient reactants to wet the surface fully. In the presence of grooves, the valley or the lower section of the groove has to fill before passing on to the next groove with a tendency to create rivulets at low flowrates with increase in the radius of the groove. On visual inspection using a stroboscope, these rivulets formation was observed from about 3^{th} groove onwards for entire range of the disc rotational speed (300-1200 rpm). If a thin turbulent film does not form then good mixing will not occur. If the disc surface is not completely wetted, the formation of a uniform, sTable thin film is very unlikely. Low rotational speed with high flowrates tends to promote these conditions. Also high speed and very low flowrates can also produce similar effects.

In contrast to the low flowrate of 3 ml/s, at Qt= 9 ml/s and rotational speed of 300 rpm, Xs was observed to be 0.077 and 0.044 for smooth and grooved disc respectively. The segregation index was reduced by 43 % when smooth disc was replaced by grooved disc. A consistent decrease in Xs on the grooved disc was apparent when flowrates of 9 ml/s and 15 ml/s were employed at all disc speeds tested in this study.

After carrying out a visual inspection using a stroboscope at the Qt=9 ml/s and 15 ml/sec and the entire range of disc rotational speed, the rivulets totally disappeared and it became evident that there were sufficient reactants to wet the surface fully. This explains the improved micromixing achieved on the grooved disc compared to the smooth disc at the higher flowrates.

Another very important observation from Figure 5.64 is that when smooth disc was replaced by a grooved one and with conditions of Qt=15 ml/sec and $[H^+]$ =0.5 M, the phenomenon of bad distribution of sulphuric acid which was experienced with using smooth disc with the same operating conditions (see section 5.3.2.1) completely disappeared as shown in Figure 5.65. This is a strong indication that the grooved disc gives a superior degree of mixing than the smooth disc.

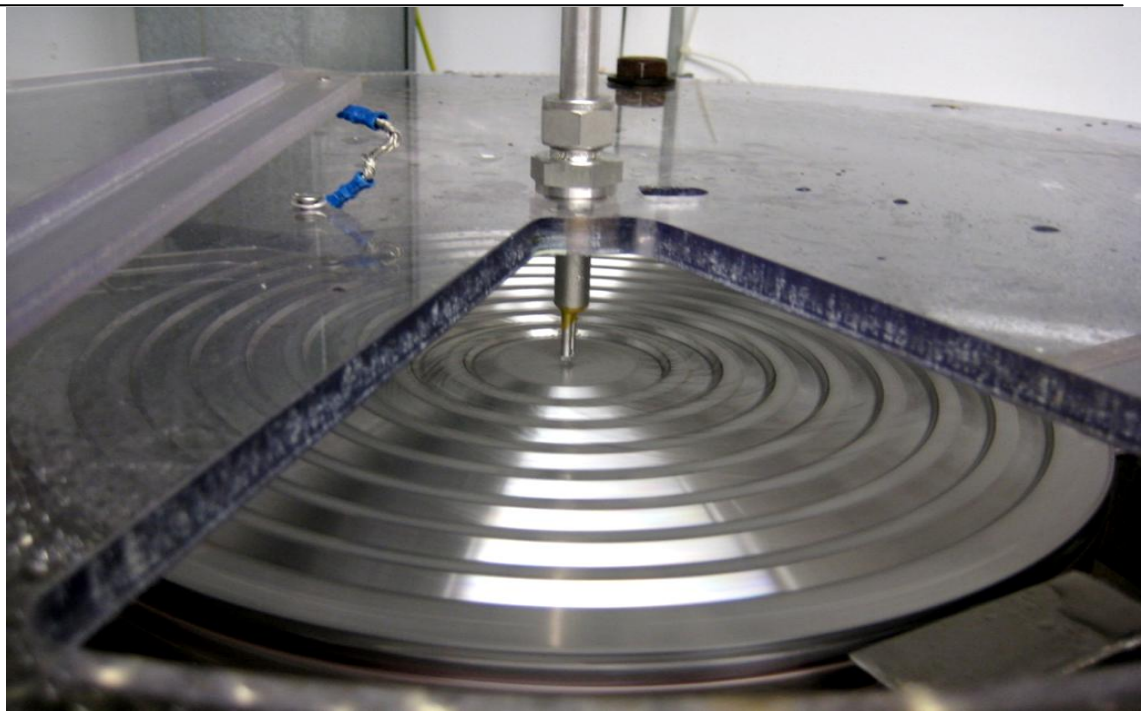

Figure 5.65: Photo of 30 cm SDR using Single- point Distributor with Grooved disc - Water System, Qt=15 ml/sec, QI=875 ml//min, QH=25 ml/min, [H+] =0.5 M- N=300 rpm

Similar trends with regards to the performance of grooved disc were compared with smooth disc as highlighted in Figure 5.64 were obtained in Figure 5.66 at all flow rates for $[H^+]$ =1.0 M.

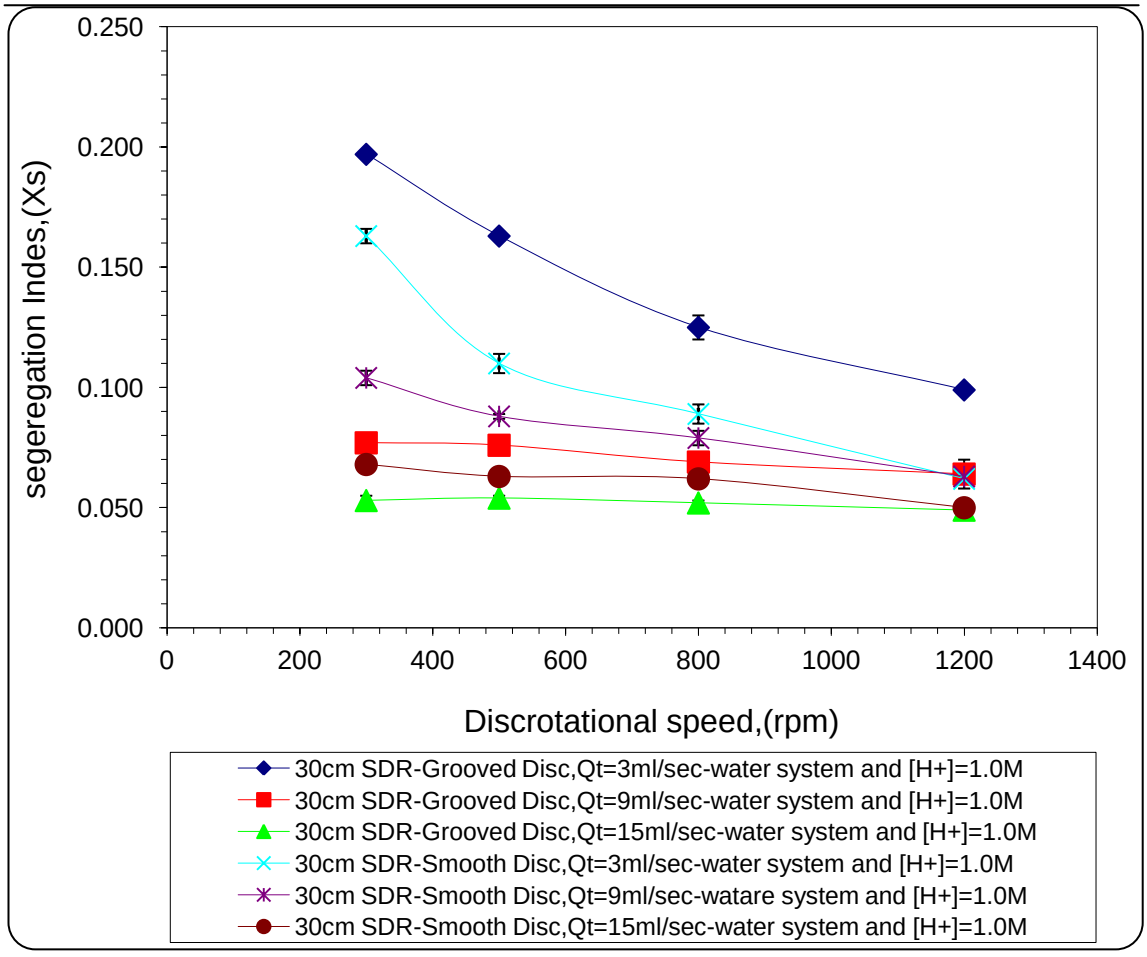

Figure 5.66: Effect of Disc Rotational Disc on segregation Index, Xs at Various total Flow Rates - water system with [H+] =1.0 M (Smooth disc Vs. Grooved Disc)

5.3.3.2 Effect of Feed Viscosity on Segregation Index (Grooved Vs. Smooth Disc) Using 3.0 mm Single-Point Distributor

In order to investigate the performance of 30 cm SDR using the grooved disc with the presence of viscous media, a 50 wt % glycerol system was employed to compare with the water medium. Similar conditions of flowrate, disc speed and acid concentration as described in section 5.3.2.2 were employed. Figures 5.67 to 5.69 **s**how the 30 cm SDR micromixing performance in terms of segregation index using 50 wt% glycerol with grooved disc in comparison to the micromixing performance with a smooth disc.

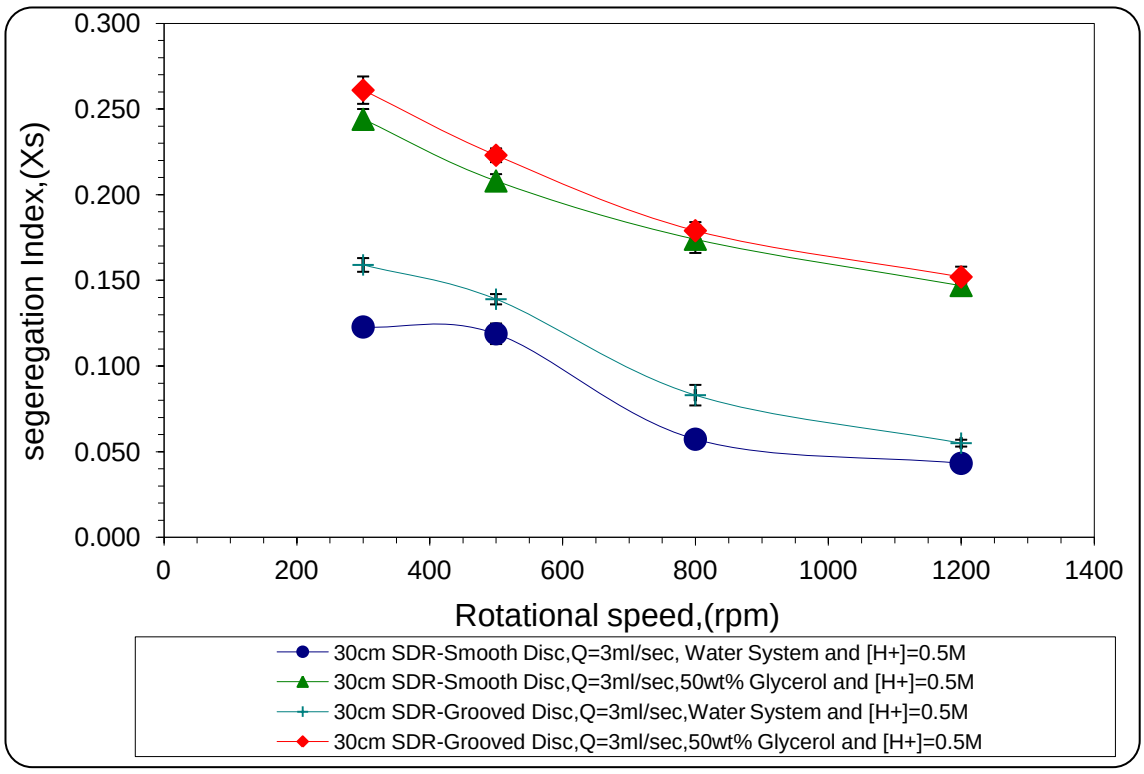

Figure 5.67: Effect of feed viscosity on segregation Index (Xs) in 30 cm SDR at Qt =3 ml/s and [H+] =0.5 M (Smooth disc Vs. Grooved Disc)

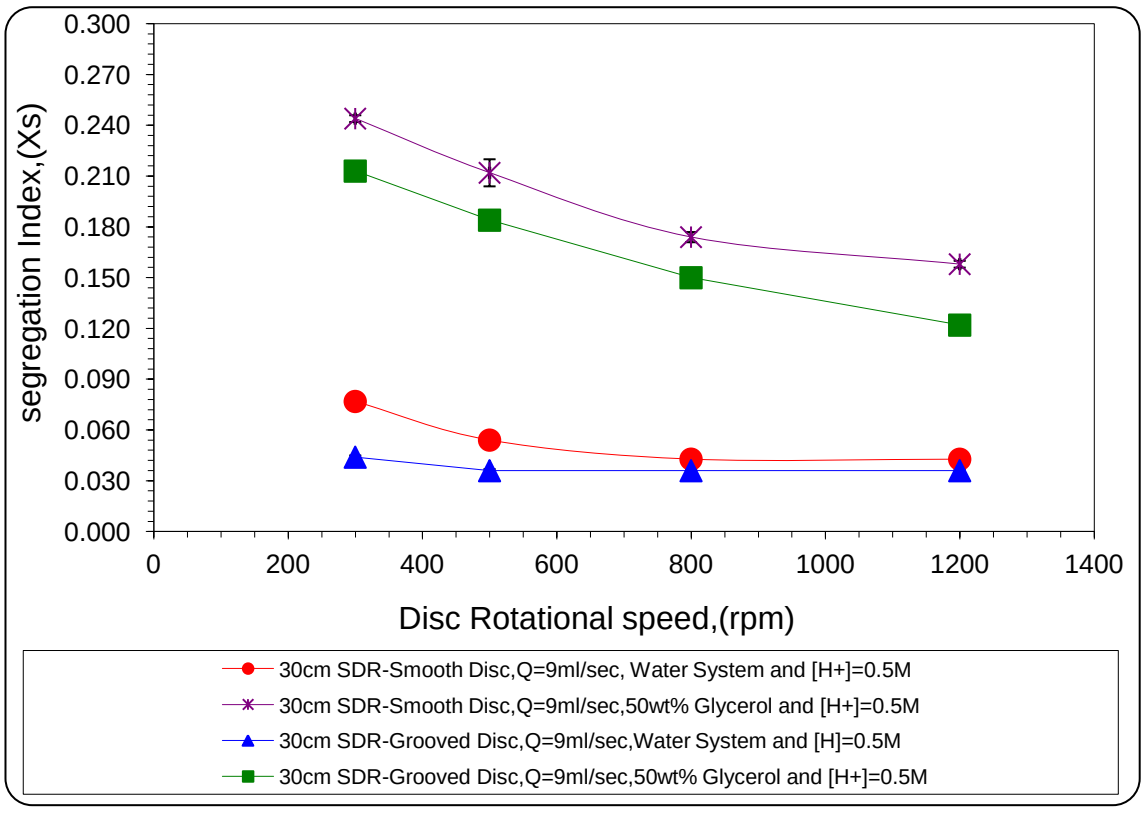

Figure 5.68: Effect of feed viscosity on segregation Index (Xs) in 30 cm SDR at Qt =9 ml/sec and [H+] =0.5 M (Smooth disc Vs. Grooved Disc)

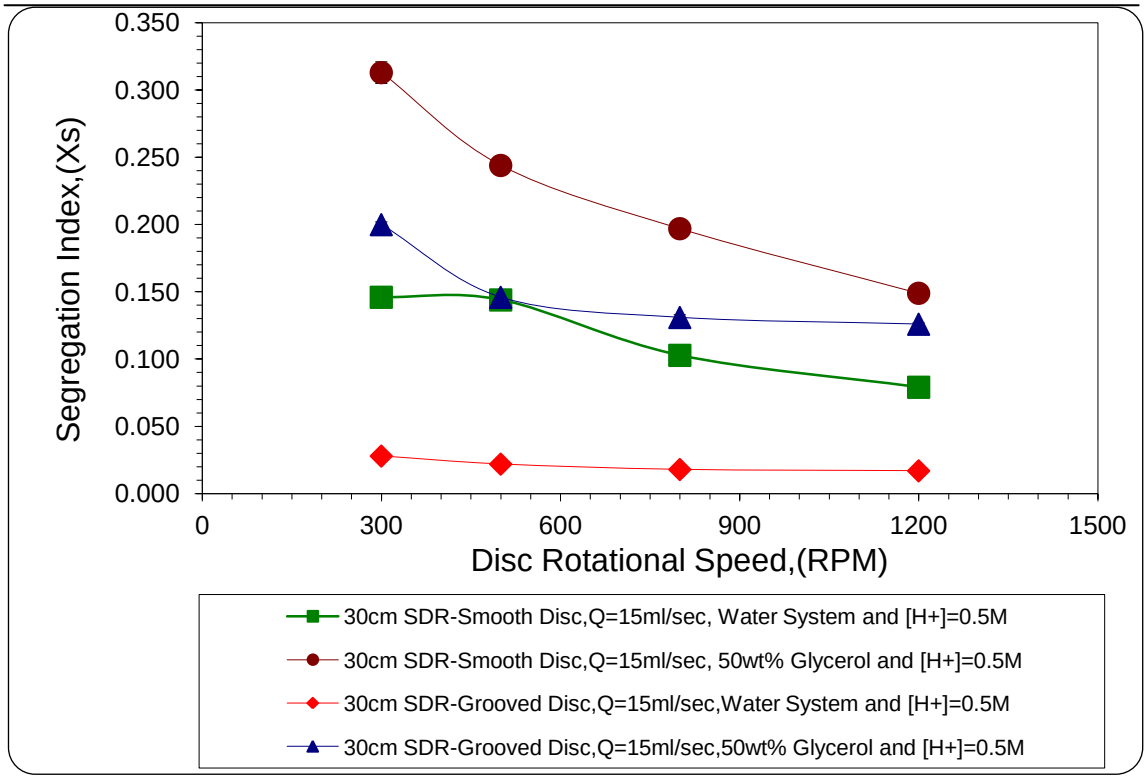

Figure 5.69: Effect of feed viscosity on segregation Index (Xs) in 30 cm SDR at Qt =15 ml/sec and [H+] =0.5 M (Smooth disc Vs. Grooved Disc)

It is clear from Figures 5.67 to 5.69 that the segregation index increases as feed viscosity increases for all the total flowrates at given disc rotational speed for both smooth disc and grooved disc. The effect of viscosity on the segregation index for the grooved disc can be said to be similar to what was explained earlier in section 5.3.2.2.

It is worth highlighting that at the lowest flowrate of 3ml/s (Figure 5.67), the smooth disc showed better performance than the grooved disc even with the higher viscosity medium, the reasons for which have already been discussed in terms of poor wetting at the such low flowrates in section 5.3.3.1 in relation to the water system In the presence of a more viscous fluids, the formation of a thin, sTable film would be even harder to achieve, which in turn prevents good micromixing. A stroboscope was used for the purpose of visual inspection of the film at the total flowrate of 3 ml/s which revealed the formation of the rivulets as observed from about 4th groove onwards for the entire range of the disc rotational speed (300-1200 rpm). In contrast, at the Qt=9 ml/s and 15ml/sec for the 50 wt% glycerol system within the disc rotational speed range of 300-1200 rpm, the rivulets were minimised and there were sufficient reactants to wet the surface fully. Consequently, all the grooves contributed to give good micromixing.

Similar observations with regards to the performance of grooved disc compared with smooth disc as highlighted in Figures 5.67 to 5.69 were obtained in Figures AJ1 to AJ3 in appendix J at all flow rates and [H+]=1.0 M .

5.3.4 30cm SDR Results using a Multi-Point Distributor

During the course of the micromixing experiments on the 30cm SDR, one of the research targets was to improve the intensity of micromixing by introducing different modifications to the reactor. One of options of meeting this target was the introduction of a grooved disc to the 30 cm SDR which was mentioned in section 5.3.3. When the smooth disc was replaced by the grooved disc**,** the micromixing was enhanced and the results were promising. Another modification that was introduced to the 30 cm SDR was a *70 mm diameter multi-point distributor* for the sulphuric acid feed stream which consisted of four feed holes, each having a diameter of 0.2 mm. The main reason behind the use of this multi-point distributor was to eliminate the problems related to the bad distribution of sulphuric acid within the boric acid stream that was experienced when using the smooth disc at an operating conditions of Qt=15 ml/s and [H+]=0.5 M for water system with single point distributor (see section 5.3.2.1). Another reason was that a good distribution of sulphuric acid on both the smooth and the grooved discs may be achieved with the use of a wider range of operating conditions (in terms of flowrate mainly) for both water system and 50 wt% glycerol system, giving the potential of further enhancing the micromixing intensity.

Three different total flow rates of water system have been used in these sets of experiments (3 ml/s, 9 ml/s and 15 ml/sec). The disc rotational speed range of 300-1200 rpm for these three total flowrates was equally used. The total flowrate ratios was R= 35 with the concentrations of H_2SO_4 (The acid concentration was of 0.25 M) corresponding to acid ion concentration of [H+] =0.5 M. The mean value of absorbance D_λ (-), the average segregation index Xs (-), the standard deviation (σ) and standard error (S) as well as the relative error were estimated. The maximum relative error of experiments was only (3.0%) which therefore indicates that a good reproducibility of the experiment was achieved.

5.3.4.1 Effects of Rotational Disc Speed and feed flowrate on Xs using 70mm Multi-Point Distributor

Figure 5.70 demonstrates the 30 cm SDR micromixing performance in terms of segregation index using the 70 mm diameter multi-point distributor and smooth disc.

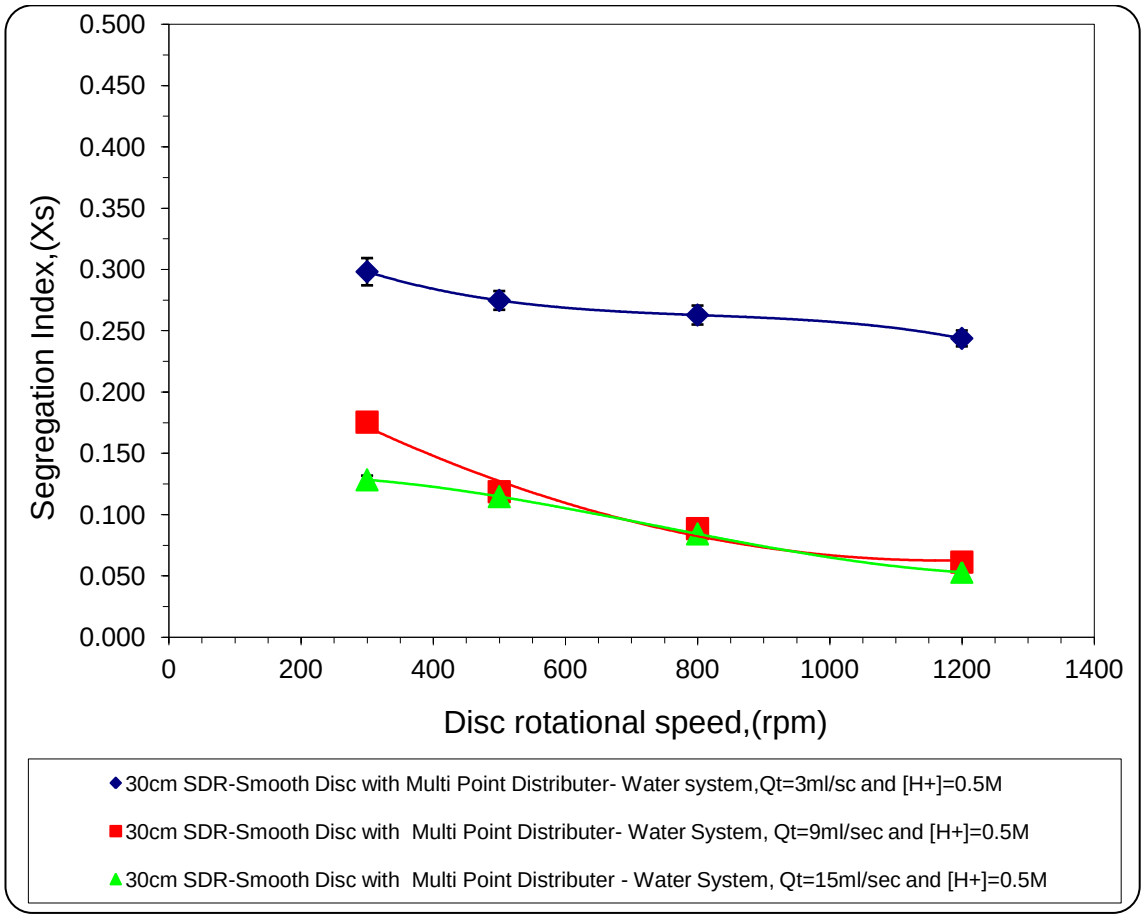

Figure 5.70: Effect of Disc Rotational Disc on Segregation Index, Xs at Various Total Flow Rates using 70 mm Multi-Point Distributor - Water System with [H+] = 0.5 M- (Smooth Disc)

It was noticeable from Figure 5.70 that for all the three total flowrates along with their disc rotation speed range, the segregation index decreases consistently with the increase in the total flowrate. This result confirmed the strong influence that flowrate has on the intensity of micromixing in the SDR, whereby the higher shear rate generated at the disc/liquid interface at higher flowrates causes intimate mixing between the two reactant streams. It is worth noting here that these trends are in sharp contrast to what was observed when using the single point distributor as will be examined in more detail below.

5.3.4.2 30cm SDR Performance (70mm Multi Point Distributor VS. 3.0mm Single Point Distributor with using Smooth and Grooved Discs)

Figures 5.71 to 5.75 demonstrate the performance of 30 cm SDR under a range of operating conditions in terms of segregation index using the 70 mm Multi Point Distributor and 3 mm Single Point Distributor for the purpose of disc performance comparison. From Figure 5.71 below it can be concluded that at the total flowrate of 15ml/sec, the micromixing has been improved by using the 70 mm Multi Point Distributor instead of the 3 mm Single Point Distributor as discussed in detailed in section 5.3.2.1. This is evident that a good distribution of sulphuric acid on the disc was achieved. Consequently, the contact between the sulphuric acid and other reactants was enhanced thereby yielding good micromixing.

Figure 5.72 shows a photo of flow pattern on the smooth disc using the 70 mm Multi - Point Distributor at rotational speed of 300 rpm using water system with total flowrate 15 ml/sec and $[H^+]$=0.5 M. It can be seen that the phenomenon of poor distribution of sulphuric acid on the disc has disappeared. This led to the improvement of the intensity of micromixing which evidently show that the 70 mm Multi-Point Distributor has improved the micromixing on 30 cm smooth disc.

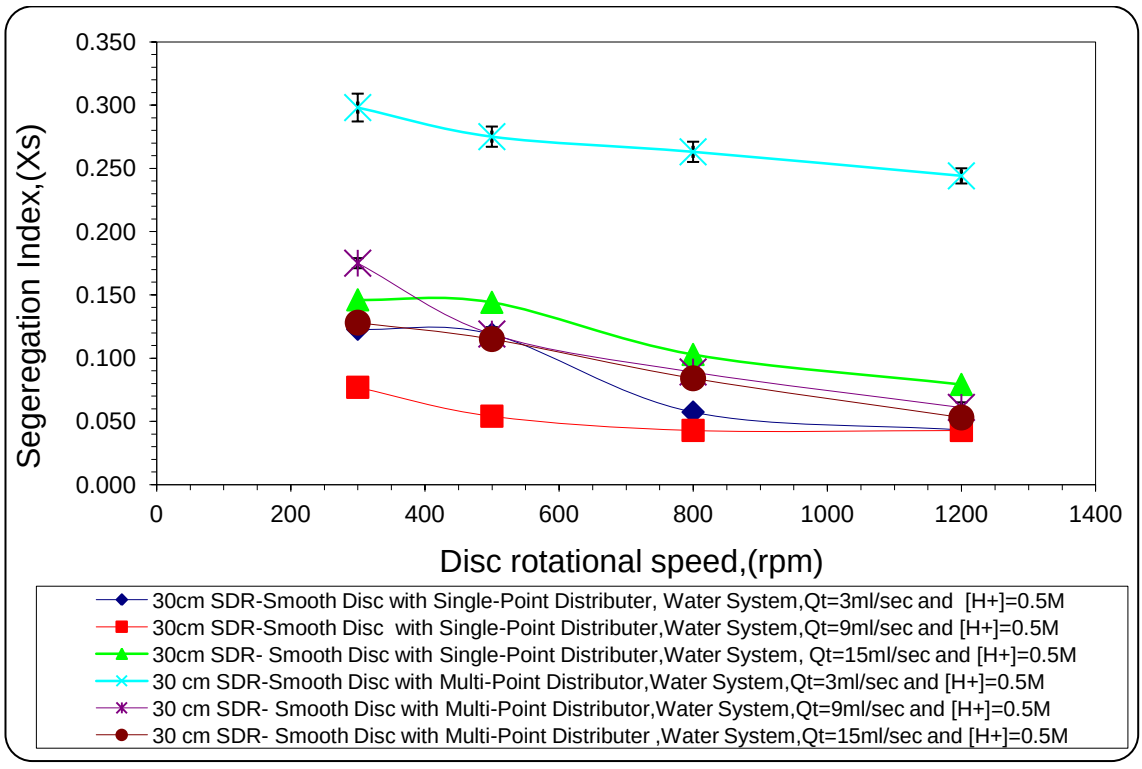

Figure 5.71: Effect of Disc Rotational Disc on segregation Index, Xs at Qt=3,9 and 15 ml/sec, Single-point distributor VS. Multi-point distributor - water system with [H+] =0.5 M- (Smooth Disc)

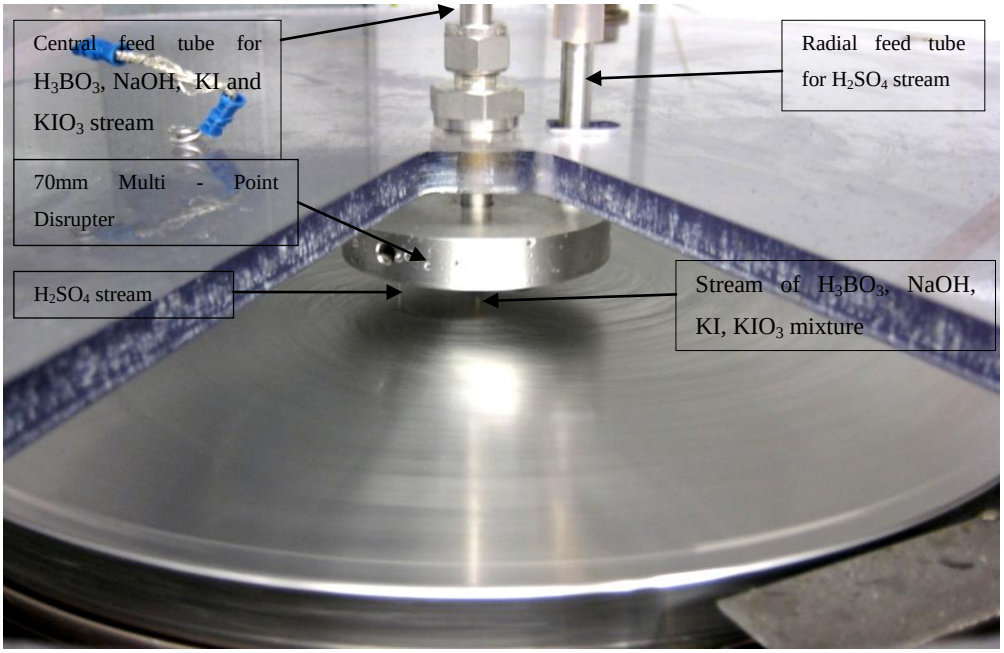

Figure 5.72: Water system- smooth disc Multi - Point Distributor at N=300 rpm- Qt=15ml/sec, QI=875ml//min, QH=25ml/min, [H+]=0.5 M

From Figure 5.71, the influence of the distributor system employed using the water system with [H+]=0.5 M flowing on a smooth disc can be summarised as follows:

- At Qt= 3 ml/sec which corresponded to a flowrate of 0.042 ml/s for the sulphuric acid stream, the 70 mm Multi-Point Distributor gave the worst mixing conditions, as evidenced by the highest segregation indices under these conditions. It is envisaged that this was as a result of unsteady flow and/or bad distribution of the sulphuric acid on the disc surface. It was noted in the course of performing the experiments that only two feed holes of the multi-point distributor were able to deliver sulphuric acid on the disc. Also, the very low flow rate of acid stream did not give continuous flow through each hole; instead droplets of sulphuric acid of unknown volume were formed intermittently (see Figure 5.73), which caused the rate of contact between the acid stream and the other reactants to be variable over the course of the run. The introduction of the sulphuric acid stream at such low flowrates can be more easily controlled in the 3mm diameter single point distributor, whereby careful selection of the delivery tube lengths can give sufficient holdup in the tube to assist in producing a more even flow and uniform delivery of the acid stream onto the disc.

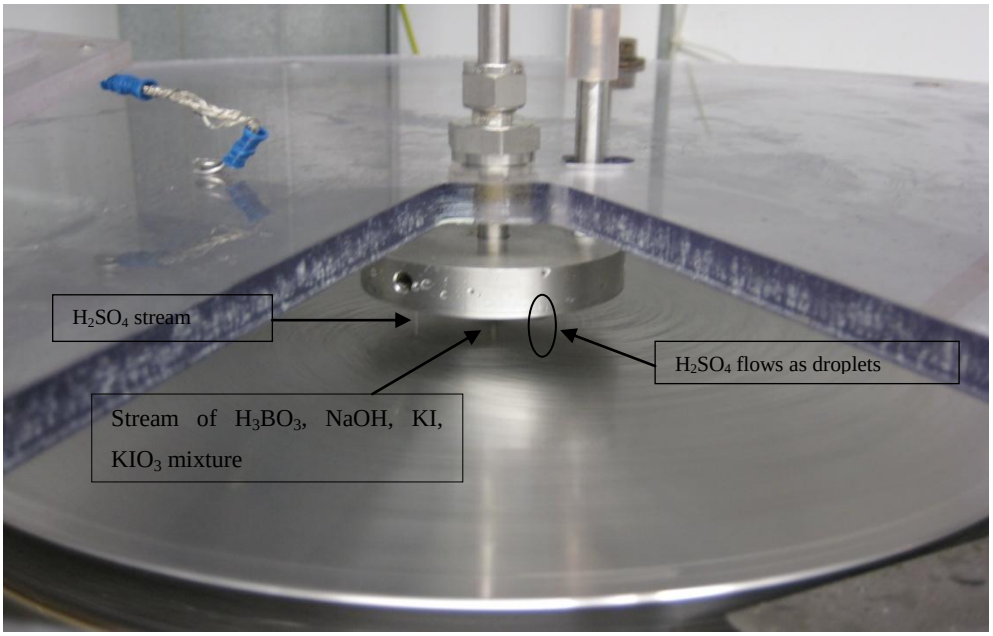

Figure 5.73: Water system smooth discs Multi - Point Distributor At N=300 rpm- Qt=3 ml/sec, QI=177.42 ml//min, QH=2.52 ml/min, [H+]=0.5 M

- At Qt= 9 ml/sec, the single point distributor again performed better than the multi-point Distributor, although the differences in segregation index were no more than 56% and 30% at the disc rotational speeds of 300rpm and 1200 rpm respectively which were significantly lower than the differences in Xs between the two distributors at 3 ml/s. In effect, the micromixing intensity at 9 ml/s with the multi-point distributor was almost similar to that at Qt= 15 ml/sec and for the disc rotational speed ranged 500-1200 rpm using the same type of distributor.

- At Qt=15 ml/sec with the multi-point distributor, the micromixing was marginally better than that at the same flowrate using the single-point distributor at all disc speeds. For instance, at a disc speed of 300 rpm, the Xs was 0.128 and 0.146 for multi-point distributor and single-point distributor respectively whilst when the disc rotational speed was 1200 rpm, the Xs achieved was 0.053 and 0.079 for multi-point distributor and the single-point distributor respectively..

- It is interesting to note that at Qt=15 ml/sec, the 30 cm SDR equipped with the multi-point distributor gave a lower micromixing performance when compared with Qt=9 ml/sec for the Single-Point Distributor.

different trends with regards to the effect of using 70mm Multi-Point Distributor with the smooth disc at total flowrate 15 ml/sec and [H+]=0.5 M which was described above in Figure 5.71 were obtained with $[H^+]$=1.0 as highlighted in Figure 5.74. It is clear from Figure 5.74 that at Qt=15 ml/sec and $[H^+]$ =1.0 M, the smooth disc with Multi-point distributor gives a lower micromixing performance when compared with the performance of smooth disc with single-point distributor at similar operation conditions of total flowrate and acid ion concentration. This was as resolute of the very low flow rate of acid stream, i.e. Q_H= 0.211 ml/s when $[H^+]$ = 0.1 M was used, instead the flow rate of acid stream was almost double when the $[H^+]$ =0.5 M). The very low rate of acid stream did not give continuous flow through each hole; instead droplets of sulphuric acid of unknown volume were formed intermittently, which caused the rate of contact between the acid stream and the other reactants to be variable over the course of the run. Again needs to be mentioned that the delivery of the sulphuric acid stream at low flowrates can be more easily controlled in the 3mm diameter single point distributor than the Multi-point distributor.

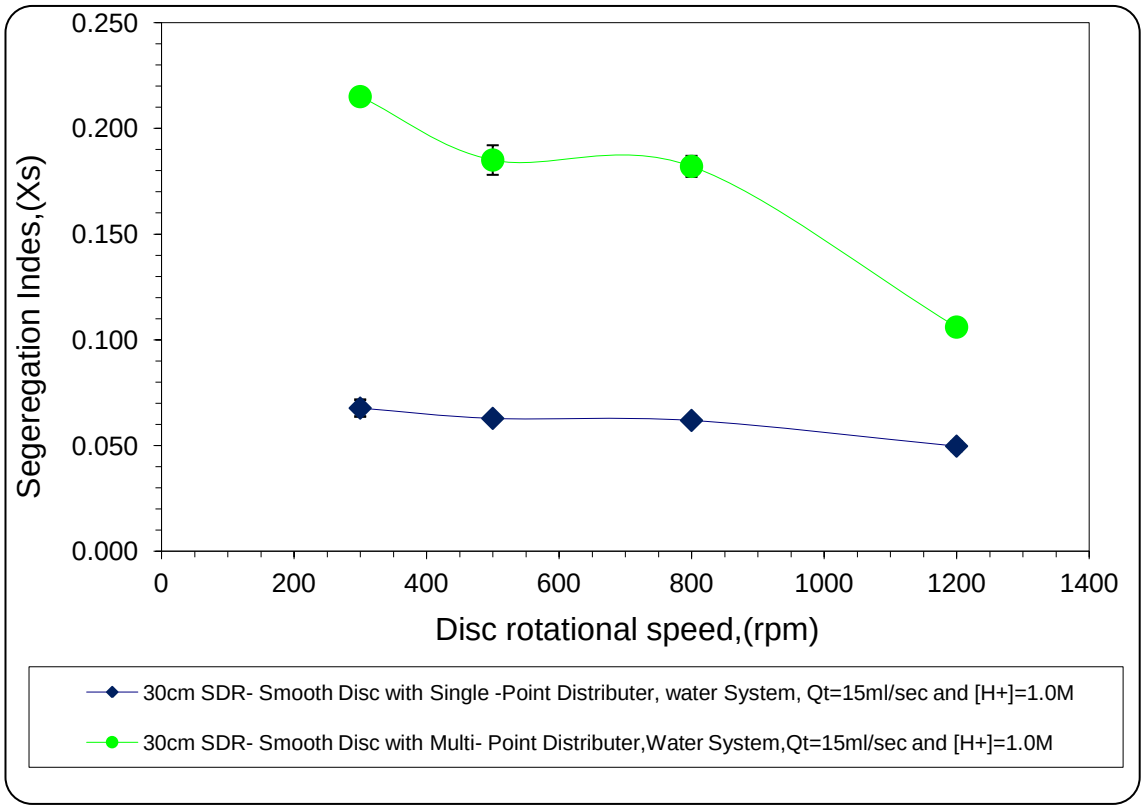

Figure 5.74: Effect of Disc Rotational Disc on segregation Index, Xs at Qt=15 ml/sec, Single- point distributor VS. Multi-point distributor - water system with 1.0 M- (Smooth Disc)

Figure 5.75 demonstrates the influence of total flowrate on the segregation index at four disc rotational speeds in the presence of 50 wt% glycerol flows on smooth disc. The acid ion concentration was 0.5 M. It was obvious that for the total flowrate of 15ml/sec using the using 70 mm Multi-Point Distributor, the micromixing was remarkably improved compared with the Qt= 15 ml/sec with Single-Point Distributor. For example at disc speed of 300 rpm the reduction in Xs was 31.0 %. On the other hand, at the disc speed of 1200 prm, the reduction in Xs was 28 %. From these results, it is evident that the 30 cm SDR perform better when the Single Point Distributor was replaced by 70 mm Multi-Point Distributor. This may be explained in terms of the improved distribution of sulphuric acid on the disc which has been achieved. Therefore, as good contact between the sulphuric acid and other reactants was achieved, high degree of micromixing was also achieved.

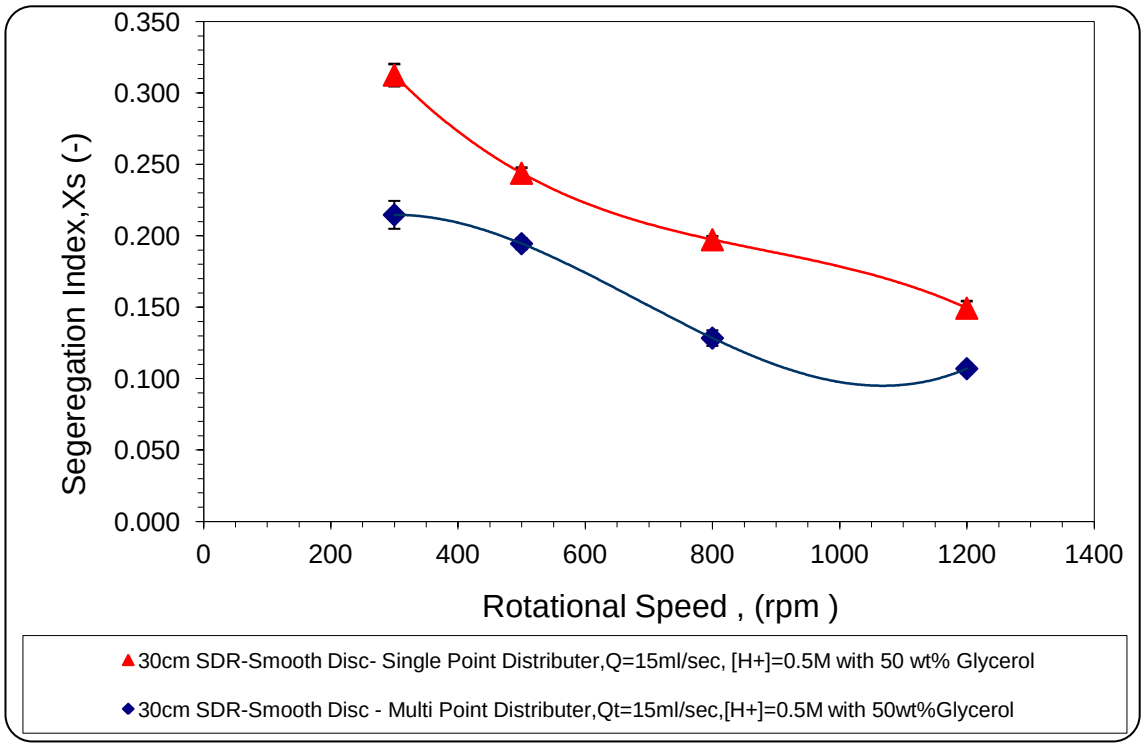

Figure 5.75: Effect of Disc Rotational Disc on segregation Index, (Xs) at Qt= 15 ml/sec, single-point distributor VS. Multi-point distributor – 50 wt% glycerol system with [H+] =0.5 M- (Smooth Disc)

Figure 5.76 below shows the influence of total flowrate on the segregation index using the water system flows on grooved disc. The acid ion concentration was 0.5 M. It is evident from the result that at the total flowrate of 15 ml/s with 70 mm Multi-Point Distributor, the Xs values were higher those with the Single-Point Distributor at the same flowrate which was not expected. This proved that the grooved disc failed to improve the micromixing despite the use of 70 mm Multi-Point Distributor. This could be attributed to the individual location of the injection points of each of the two reactant streams. Firstly, the $H_2BO_3^-$ solution is fed at a radial position of 20 mm from the centre of the disc, beyond which it produces an even film before it enters the first groove located at a radial position of 25 mm. On the other hand, the H_2SO_4feed stream is injected at a radial position of 25 mm from the disc centre through the multi-point distributor. The two phases then stay in the first groove until sufficient thickness causes the film to climb out of the groove. Consequence, more tri-iodide produced in the first grove before the reactants entering to the next grove. This is as result of bad design of 70 mm Multi-Point Distributor.

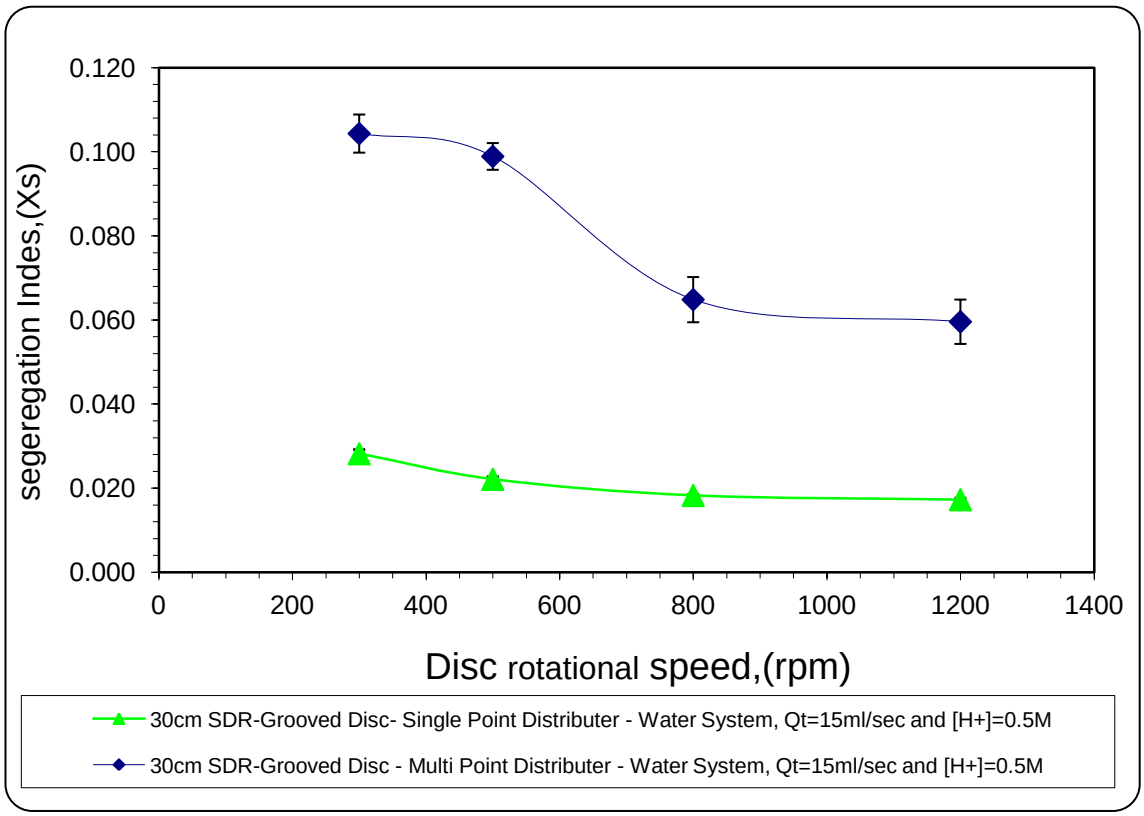

Figure 5.76: Effect of Disc Rotational Disc on segregation Index, (Xs) at Qt= 15 ml/sec, single-point distributor VS. Multi-point distributor – water system with [H+] =0.5 M- (Grooved Disc)

Similar trends with regards to the 30 cm performance using 70 mm Multi-Point Distribution and grooved disc as described above in Figure 5.76 were obtained when water system was replaced by 50 wt% glycerol as highlighted in Figure 5.77 for the disc speed range of 300-800 rpm. At the disc speed of 1200 rpm, the reactor started to show better performance. It seems to be that at this higher disc speed, the contact with the reactant has been improved even though rather poor distribution of sulphuric acid on the disc was still occurring.

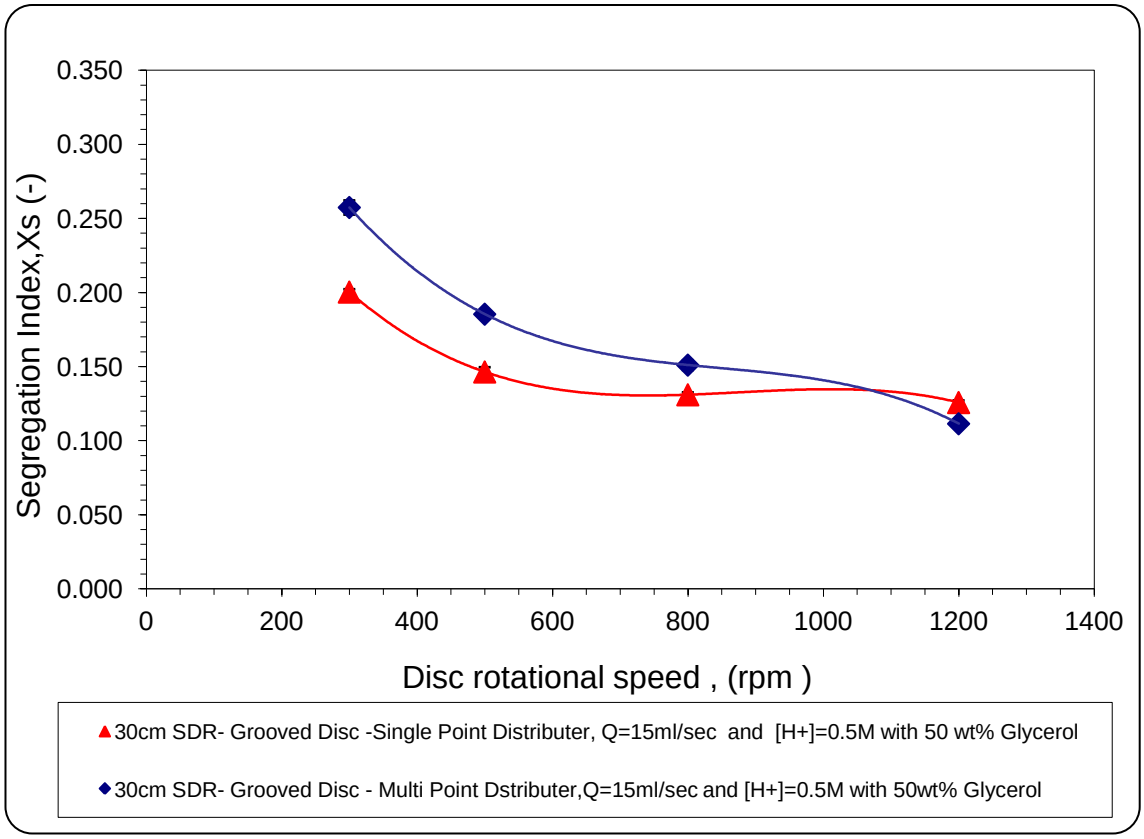

Figure 5.77: Effect of Disc Rotational Disc on segregation Index, (Xs) at Qt= 15 ml/sec, Single-Point Distributor VS. Multi-Point Distributor – 50 wt% glycerol system with [H+] =0.5 M- (Grooved Disc)

From the micromixing results attained using the Multi-Point Distributor, it can be concluded that to achieve the highest degree of micromixing using Multi-Point Distributor, some considerations need to be taken into account such as: the optimum flowrate, the dimensions of the distributor system i.e. the diameter, number and the position of holes of the distributor (how close to the centre of the disc and how close to the first groove of the disc - in the case of grooved disc). For the present design of the multipoint distributor with 4 holes of 0.2 mm diameter each, it is clear that the

distributor did not perform as well as expected in the range of flowrates tested (3 ml/s to 15 ml/s). It may well be that to obtain a more even jet flow of acid especially under conditions of very low flowrates, it may be necessary to have 4 holes of a much smaller diameter such as 0.05 mm so that increased liquid hold-up may prevail to give a uniform and continuous jet of acid at the injection point for improved acid distribution and micromixing.

5.3.5 Regression Analysis on Segregation index, (Xs), for 30cm SDR

Regression analyses were performed for all the 30 cm SDR smooth disc data (i.e. aqueous solution, 50 wt% Glycerol) using the regression tool in the Minitab 15 software. Two Empirical models between Segregation index, (Xs) and the three variables (angular velocity of the disc,ω, total flowrate, Q, and dynamic liquid Viscosity, μ) investigated at $[H^+]$ = 0.5 and 1.0 M.

For the regression analyses it was assumed that the segregation index, (Xs), could be represented by equation (5.13) which can written in a more appropriate form similar to equation (5.14).Table (5.13) represent the calculated values of the parameters and R^2 for X_S models

Table 5.13: Segregation index Regression analysis results for 30 cm SDR smooth disc

[H+],M	A	B	C	D	R^2(Adj)
0.50	+0.454	-0.327	-0.285	+0.543	79.5%
1.0	+0.778	-0.454	-0.160	+0.491	96.3%

Therefore following model equations which describe the segregation index in a 30 cm SDR smooth disc could be written as:

$$\text{For } [H+] = 0.5M: \quad X_S = 0.454\ (\omega)^{-0.327}(Q_t)^{-0.285}(\mu)^{0.543} \tag{5.19}$$

$$\text{For } [H+] = 0.5M: \quad X_S = 0.7780\ (\omega)^{-0.454}(Q_t)^{-0.160}(\mu)^{0.491} \tag{5.20}$$

From the 30 cm SDR smooth disc model equations that have been produced, it can be seen clearly that increases in angular velocity of the disc and liquid total flowrate cause significant decreases in X_s . While increases in dynamic liquid viscosity cause an increasein X_s. Furthermore, increases in acid concentration cause increases in X_s. This corresponds well with what was observed in the experimental data.

As indicated in Table (5.9) R^2 values for the three correlations were between 79.5 and 96.3 suggest a good fit of the regression line to the data. P-values were obtained corresponding to the significance of each parameter with the regression. With assuming a significance level of 0.05 (i.e. 95 % confidence interval) the p-values was 0 to three decimal places indication each parameter to be of significance within the regression.

In order to check the validity of the model equations, X_s values were calculated using the regression models (equation 5.19 and 5.20) and compared to experimental values by plotting the experimental values against Predicted data.

If the experimental values and Predicted data were in good agreement, the best linear fit would be y = x. It will be more realistic to expect that y = M x, where constant is close to 1.
Figures (5.78 and 5.79) demonstrate a good degree of correlation between the predicted and experimental results.

For the regressions, the model equations are applicable within the following rage of operation parameters:

$$52.3 \text{ sec}^{-1} \leq \omega \leq 83.7 \text{ sec}^{-1}$$

$$3 \text{ ml/sec} \leq Q_t \leq 9 \text{ ml/sec}$$

$$1.005 \text{ mPa.s} \leq \mu \leq 6.0 \text{ mPa.s}$$

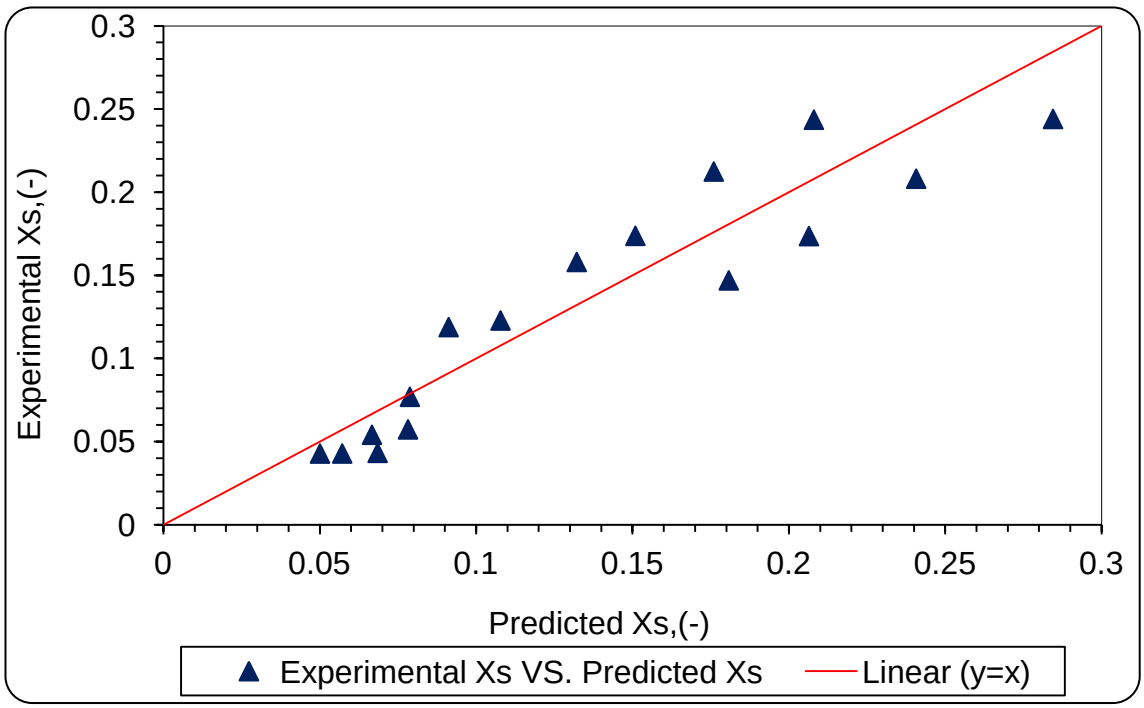

Figure 5.78: 30 cm SDR with smooth disc- Experimental segregation index data against segregation index as predicted by Empirical model for [H+] = 0.5 M

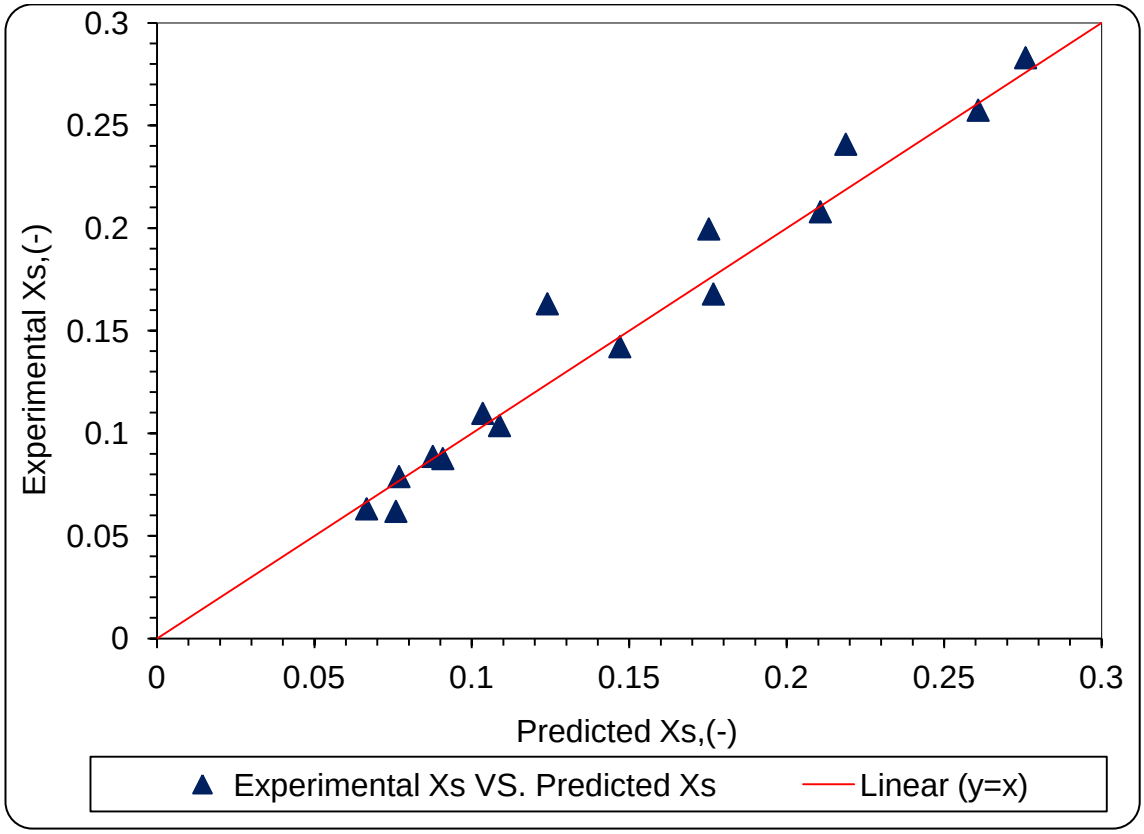

Figure 5.79: 30 cm SDR with smooth disc- Experimental segregation index data against segregation index as predicted by Empirical model for [H+] = 1.0 M

5.4 Micromixing Experimental Results: Narrow channel Reactors (NCRs)

As stated earlier, one of the objectives aimed in this research is to compare the efficiency of micromixing in SDR in terms of segregation index, (Xs), with that in continuous tubular flow reactors in the form of narrow channels. In this context, the degree of mixing was assessed in six different designs of narrow channel reactors (NCRs) in order to evaluate the influence of the length and of the junction type (Y and T-shape on the quality of mixing. For this purpose, six different narrow channel reactors made of borosilicate glass were utilised. Table (5.14) demonstrate the junction type the dimensions of the NCRs were utilised in this work.

Table 5.14: The NCRs dimensions

junction type,(-)	Channel Length,(mm)	Channel diameter,(mm)
T	5	1
T	10	1
T	15	1
Y	5	1
Y	10	1
Y	15	1

The effects of variables such as total feed flow rate (Qt), acid ion concentration,([H+]), feed viscosity,(μ), channel length and junction type were studied on the micromixing process in the NCRs, with the range of operating conditions as shown in section 5.4.1 below The characterisation of micromixing in the NCR'S adopted much the same procedure as for the SBR and SDRs, three replicates were carried out for each experiment, the mean value of absorbance D_λ (mean), the average segregation index Xs (-), the standard deviation (σ) and standard error (S) and relative error were estimated. The relative maximum relative error of experiments was only (3.0 %) and the results were satisfactorily reproducible.

5.4.1 NCR Experimental design

Minitab 15 was utilized in order to generate an appropriate randomized general full factorial experimental design for both water and 50wt% Glycerol systems (see Table AK1 in appendix K). The variables incorporated into the experimental design were:

- Total flowrate : 0.25, 0.5,1.0 and 2 ml/s ;
- Acid ion concentration: 0.1, 0.25, 0.5 and 1.0 M;
- Viscosity: water system (μ=1.005 mP.s at 20°C), 50 wt% glycerol system (μ = 6.0 mPa.s at 20 °C) ;
- Channel length: 5 cm, 10 cm and 15 cm ;
- Junction Type: Y- Junction (90°) and T- Junction (180°).

The individual flowrates of the iodide-iodate-borate ions stream, (Q_I), and the acid ions stream, (Q_H), corresponding to each total flowrate indicated above are given in Tables 5.15 to 5.18 for acid ion concentrations of 0.1, 0.2, 0.5 and 1.0 M corresponding to the volumetric flowrate ratio,(R), of 7, 17.5, 35 and 70 respectively.

Table 5.15: The individual flowrates of (QI) and (QH) corresponding to each total flowrate for acid concentrations 0.1 M and volumetric flowrate ratio of 7, (R= QI / QH)

Qt,(ml/s)	Q_I,(ml/s)	Q_H,(ml/s)
0.25	0.219	0.031
0.5	0.437	0.063
1.0	0.875	0.125
2.0	1.750	0.250

Table 5.16: The individual flowrates of (QI) and (QH) corresponding to each total flowrate for acid concentrations 0.25 M and volumetric flowrate ratio of 17.5, (R= QI / QH)

Qt,(ml/s)	Q_I,(ml/s)	Q_H,(ml/s)
0.25	0.236	0.014
0.5	0.473	0.027
1.0	0.946	0.054
2.0	1.892	0.108

Table 5.17: The individual flowrates of (QI) and (QH) corresponding to each total flowrate for acid concentrations 0.5 M and volumetric flowrate ratio of 35, (R= QI / QH)

Qt,(ml/s)	Q_I,(ml/s)	Q_H,(ml/s)
0.25	0.243	0.007
0.5	0.486	0.0138
1.0	0.973	0.027
2.0	1.945	0.055

Table 5.18: The individual flowrates of (QI) and (QH) corresponding to each total flowrate for acid concentrations 1.0 M and volumetric flowrate ratio of 70, (R= QI / QH)

Qt,(ml/s)	Q_I,(ml/s)	Q_H,(ml/s)
0.25	0.246	0.004
0.5	0.493	0.007
1.0	0.986	0.014
2.0	1.972	0.028

5.4.2 Effect of total flow rate on segregation index, (Xs)

The typical effect of total flowrate on the segregation index (X_S) of the mixed fluid in the channel is illustrated in Figures 5.80 and 5.81 which depict the trends obtained using water medium and 50 wt% glycerol system respectively in the 5 cm long NCR with the Y-junction. Table 5.19 below shows the total flow rates and the Reynolds numbers are implemented with for water system and 50 wt% glycerol system, are implemented and the flow in the outlet channel is laminar in most cases.

Table 5.19: The total flowrates and the Reynolds numbers employed in the in NCRs

Total flowrates in NCRs (ml/sec)	Reynolds number, Re (-) for water system	Reynolds number, Re (-) for 50 wt% glycerol system
0.25	318	60
0.5	637	120
1.0	1273	239
2	2547	478

The acid ion concentration was 0.1 M, 0.25 M, 0.5 M and 1.0 M. It can be seen from Figures 5.80 and 5.81 that segregation index, X_S, decreased and therefore micromixing intensity was enhanced as the total flowrate increased. Similar trends for the effect of flowrate are observed for all junction channel lengths, junction type studied (as shown in Figures AK1 to AK5 Appendix K)

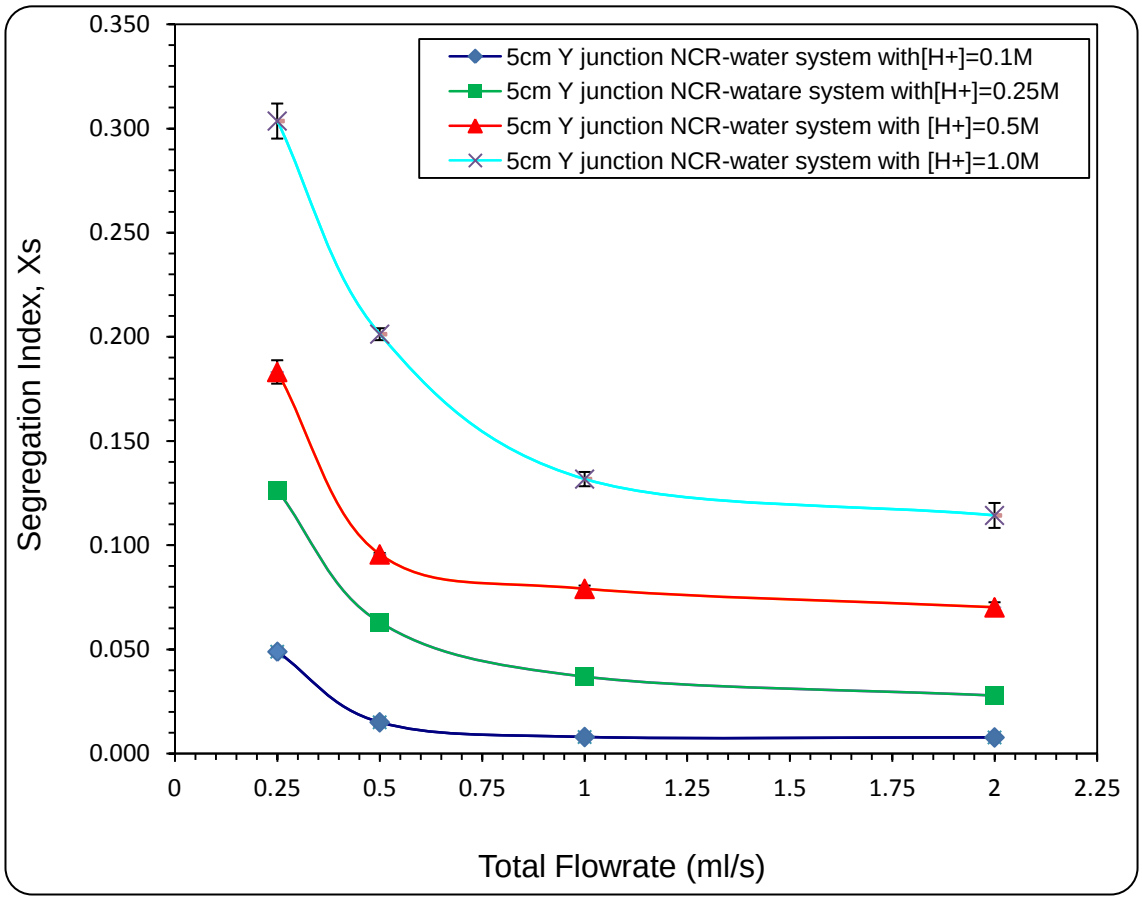

Figure 5.80: Effect of total flowrate on segregation index, Xs (-) for 5 cm Y junction NCR- Water system with different acid ion concentrations

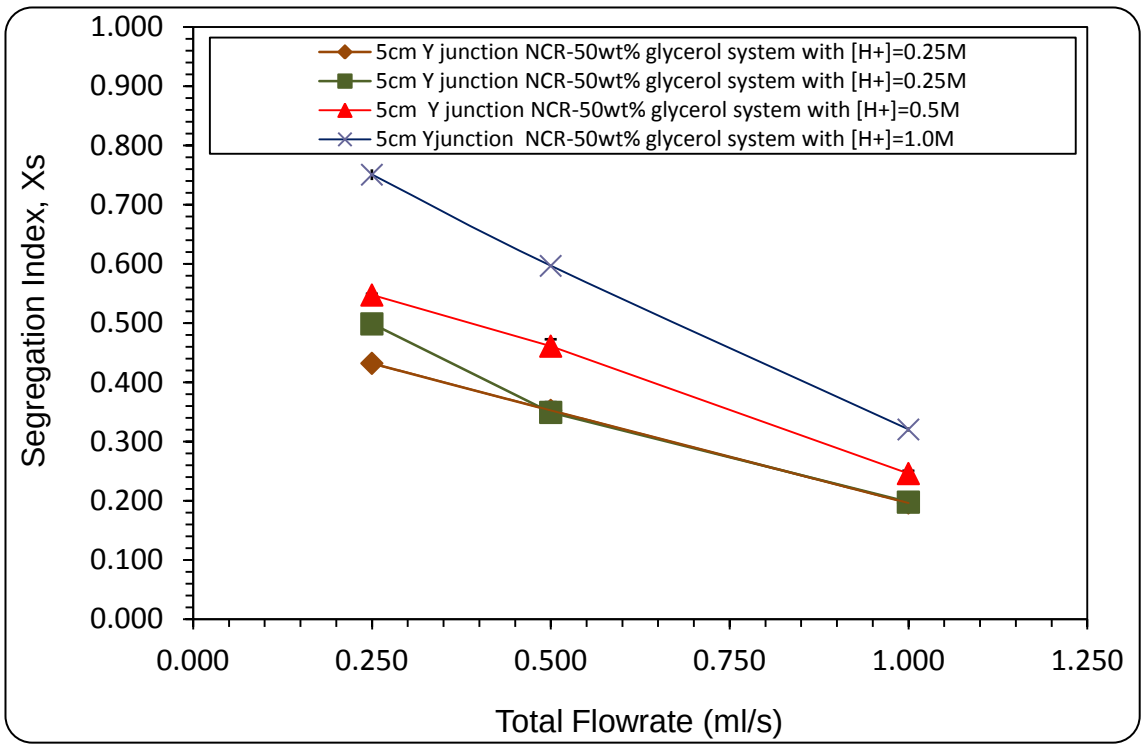

Figure 5.81: Effect of total flowrate on segregation index, Xs (-) for 5 cm Y junction NCR- 50 wt% glycerol system with different acid ion concentrations

With the increase in total flowrate, the mean velocity of the reactants in the channel increases. Consequently, three effects will occur in the reactor which, when combined, will have a significant impact on the mixing intensity. Firstly, more aggressive impinging will occur between the iodide-iodate-borate ions solution stream and the sulphuric acid stream at the junction area (the meeting point of two streams). Secondly, with increasing flow velocity, the mean shear rate between the fluid layers and the channel wall along the length of the channel will increase as shown in Figure 5.82. Subsequently, the rate of mass transfer for the system is increased via reorientation and stretching of fluid interfaces (Adeosun and Lawal, 2005). This leading to a reduction in segregation indexes (i.e. enhancing the intensity of micro-mixing efficiency) and this can be observed in Figure 5.83 For the three Y-junction NCRs with channel length of 5, 10, 15cm using both water and 50wt% glycerol system and $[H^+]$ =0.25 M. The wall shear rate for the NCRs was simply calculated from the equation below (Leveson et al., 2004):

$$\gamma = \frac{8V}{d} \qquad (5.21)$$

Where γ is the shear rate (s^{-1}), V is the bulk velocity (m/s), and d is the channel diameter (m). Thirdly, with increasing flow velocity, the laminar flow starts to form symmetrical vortices. Therefore, the diffusive mixing is assisted by these vortices and intensity of micro-mixing is enhanced (Mansur et al., 2008; Engler et al., 2004).

These three effects arising from increased flowrates contribute to the enhancement of micromixing in narrow channel.

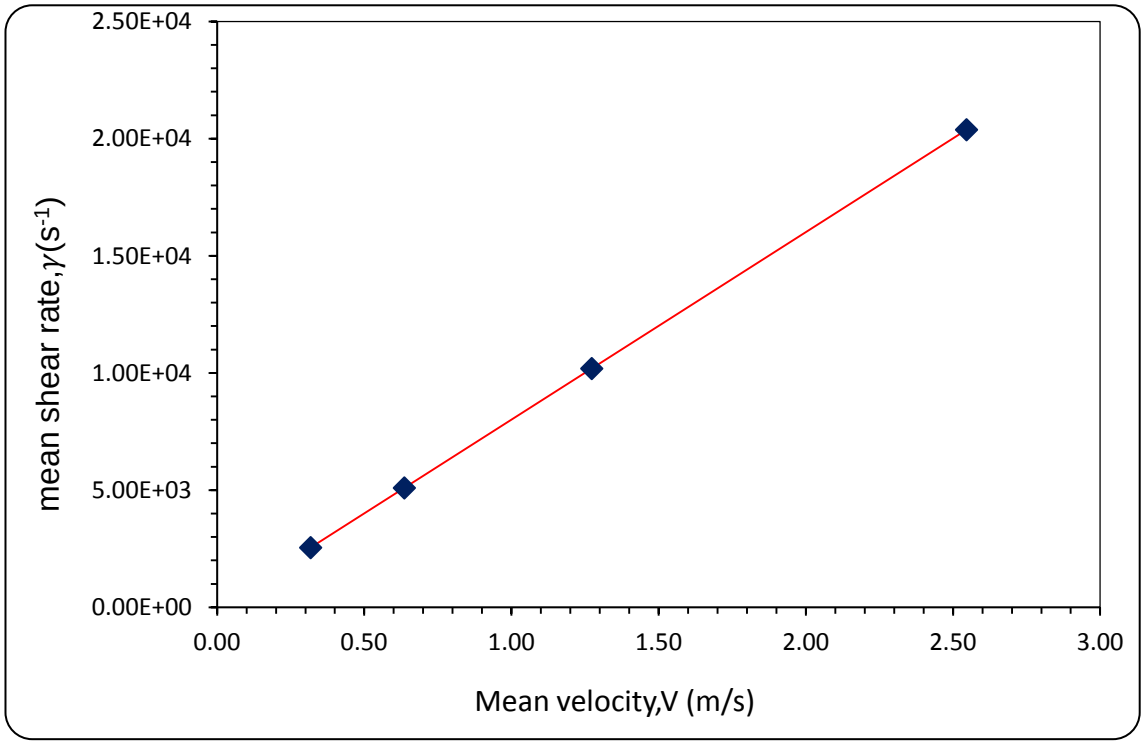

Figure 5.82: Effect of the mean velocity on the mean shear rate in the NCRs at different total flowrates

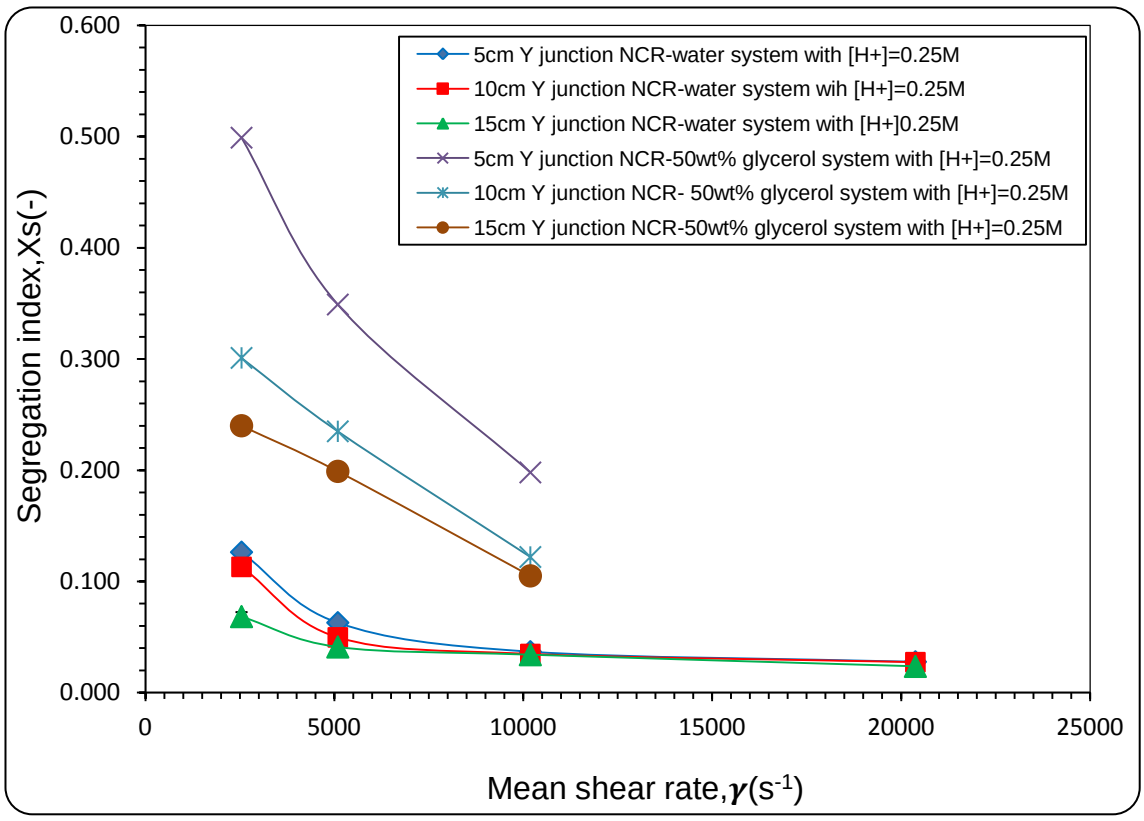

Figure 5.83: Effect of total mean shear rate on segregation index, Xs (-) for 5cm, 10cm and 15 cm Y Junction NCR-Water and 50 wt% glycerol systems with [H+]=0.25 M

The decrease in the segregation index with increasing flowrate has also been observed by (Ehrfeld et al., 1999) within a mixer array, whilst the inverse trend was observed by (Schneider et al., 2004). In the latter work, the flowrates considered only covered a range to 40 µl/min (6.6 x10^{-4} ml/s), in comparison to 120 ml/min (2 ml/s) used in our experiments. The segregation index decreases significantly between a total flowrate of 0.25 ml/s and 1.0 ml/s, whereas between 1.0 ml/s and 2.0 ml/s only a slight decrease in the segregation index is observed. This would seem to suggest that at given acid ion concentration, the intensity of mixing reach the maximum degree and there is no much benefit from increasing the total flowrate beyond 1ml/s.

In order to have a complete characterization of the mixing intensity in the NCRs, the variation of the segregation index as a function of parameters that depend on total flow rate and channel length was examined. In particular, the mean velocity of the mixed streams, the mean residence time and the Peclet number, Pe (-) in NCRs were considered.

The mean velocity is given by the ratio of total flowrate Qt (m^3/s) and the cross section area of NCR channel A (m^2) as shown below.

$$U = \frac{Q_t}{A} \tag{5.22}$$

For the circular channel, the Reynolds number is calculated from equation (5.23) as reproduced below (Holland and Bragg, 1995).

$$R_e = \frac{\rho U d_i}{\mu} \tag{5.23}$$

The residence time in the channel is given by the ratio of channel length (m) and the fluid velocity (m/s) equation (5.24).

$$t_{res} = \frac{L}{U} \tag{5.24}$$

Figure 5.84 shows how the segregation index varies with changing fluid mean velocity in 15 cm Y-NCR using water system and [H+]=0.1 M,0.25 M,0.5 M and 1.0 M. As mentioned earlier, when total flowrate rate increased the reactants mean velocity in the channel will increased. Thus, the segregation index in narrow channel decreased considerably because of the mean shear rate between the fluid layers and the channel wall increased also vigorous impinging between two streams at the junction area will occur which therefore results in the increase of the micromixing intensity.

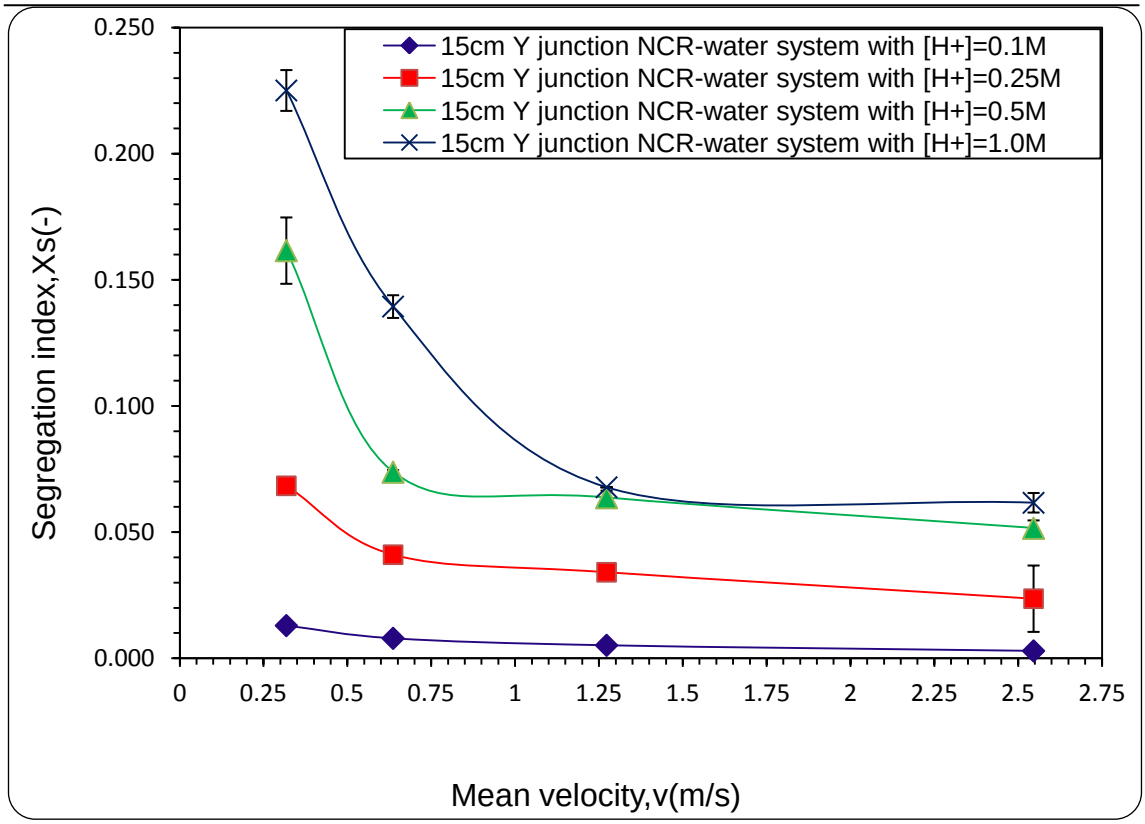

Figure 5.84: Effect of reactants mean velocity on segregation index, Xs (-) for 15 cm Y

With considering the acid concentration of $[H^+]$ =0.1 M and the lowest mean fluid velocity of 0.318 m/sec, the segregation index equalled 0.013. On the other hand, with the same acid ion concentration and the highest fluid velocity of 2.546 m/s, the segregation index equalled 0.003.The reduction in segregation index of 90% was attained. With replacing $[H^+]$ =0.1 M by $[H^+]$ =1.0 M, the segregation index equalled 0.225 at the lowest mean fluid velocity and 0.062 at the highest fluid velocity. The reduction in segregation index of 72.4 % was reached. Similar trends are observed when the acid concentration of 0.25 M and 0.5 M are used.

One important parameter needs to be considered when the micromixing taking place in the NCRs is the residence time of the fluid in the channel. The liquid residence time in the channel needs to be greater than the required micromixing time for the micromixing process to take place in the channel. The liquid residence time in the channels was calculated from equation (5.24), while the micromixing time (micromixing due to diffusion and shear force) in the NCRs was estimated by equation (5.25) proposed by Falk and Commenge (2010) as shown below :

$$t_{DS} = \frac{d}{8U\eta}\ln(1.52Pe\,\eta) \tag{5.25}$$

It is well known that the flow field and the concentration field do not match in the NCRs. In addition, the mechanical energy is used to achieve the flow in the NCRs, but in zones of pure component A with no interface with other component B, this mechanical energy does not contribute to mixing(Falk and Commenge, 2010). Due to only a part of the consumed mechanical energy is used for mixing, the energetic efficiency,(η), was considered as only 3.0% in this work as approximation(Falk and Commenge, 2010).

Table 5.20 shows the predicted values of the residence and the micromixing times for the NCR'S experiments (water and 50 wt% Glycerol systems). It is clear that the residence times are higher than the mixing times.

Table 5.20: Residence time and mixing time in NCR's for water and 50 wt% glycerol Systems

Total Flowrate (ml/s)	Residence time ,(s)			Mixing time for water system,(s)	Mixing time for 50 wt% glycerol system,(s)
	5 cm Channel Length	10 cm Channel Length	15 cm Channel Length		
0.25	0.157	0.314	0.471	0.125	0.138
0.50	0.079	0.157	0.236	0.067	0.073
1.00	0.039	0.079	0.118	0.035	0.039
2.00	0.020	0.039	0.059	0.0190	0.020

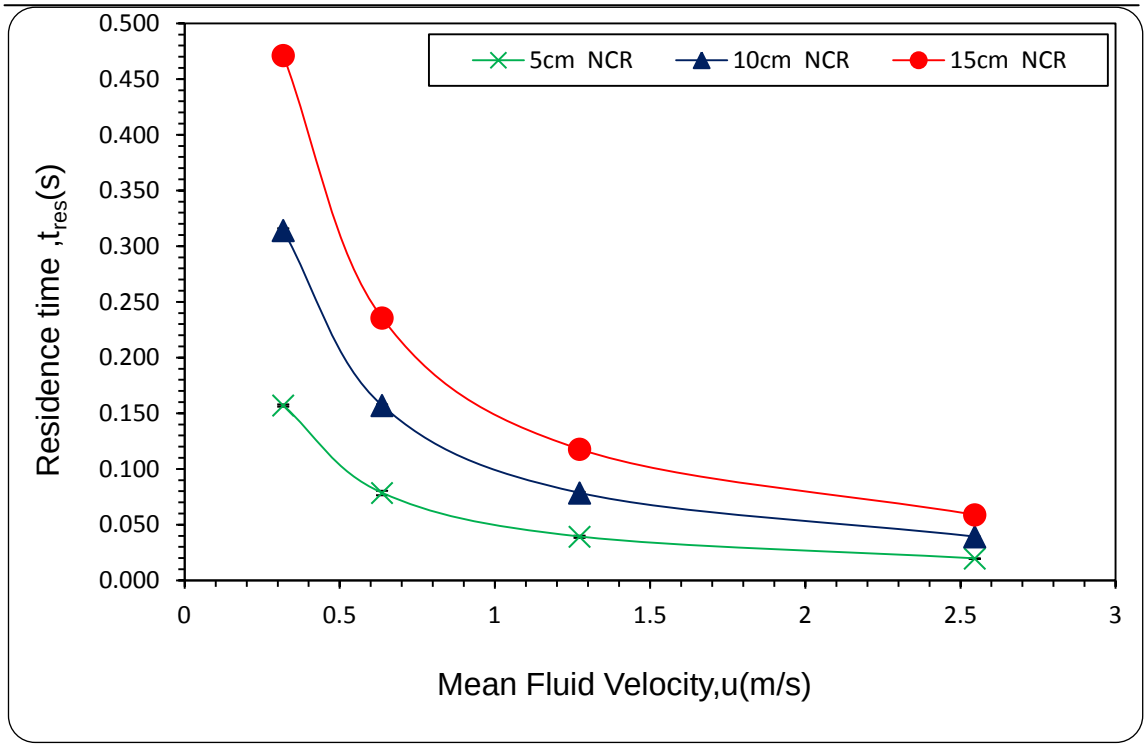

Figure 5.85: Effect of reactants mean velocity on residence time, tres (s) for Y and T NCRs junctions

Figure 5.85 illustrates the effect of the mean fluid velocity in the NCRs, an increase in residence time in a given channel results in decreases in residence time. In our experiments, the residence time was varied by changing the channel length and total flow rate in each channel. Therefore, when considering one length of NCR, the residence time varied only by changes in fluid velocity. For this case therefore the variation of segregation index with residence time can be related directly to the effect of velocity on the mixing intensity.

Figure 5.86 shows the effect of residence time of the fluid in the 5cm, 10cm and 15cm channel lengths with the total flowrates of 0.25 ml/s, 0.5 ml/s, 1 ml/s and 2 ml/s. This plot indicates that an increase in residence time in a given channel results in an increase in the segregation index, (Xs), where the residence time was 0.471 s in the longest channel (15 cm) for the lowest flowrate (0.25 ml/sec). This trend is opposite to that of Figure 5.83, depicting the effect of shear rate on Xs. As mentioned earlier, increased residence time in a fixed length channel occurs when the total flowrate in the channel is lowered. This causes the reduction in the mean velocity of the reactants and consequently the shear rate to be decreased. Higher residence time in a given channel is

therefore synonymous to lower shear rate, which accounts for the trend seen in Figure 5.86.

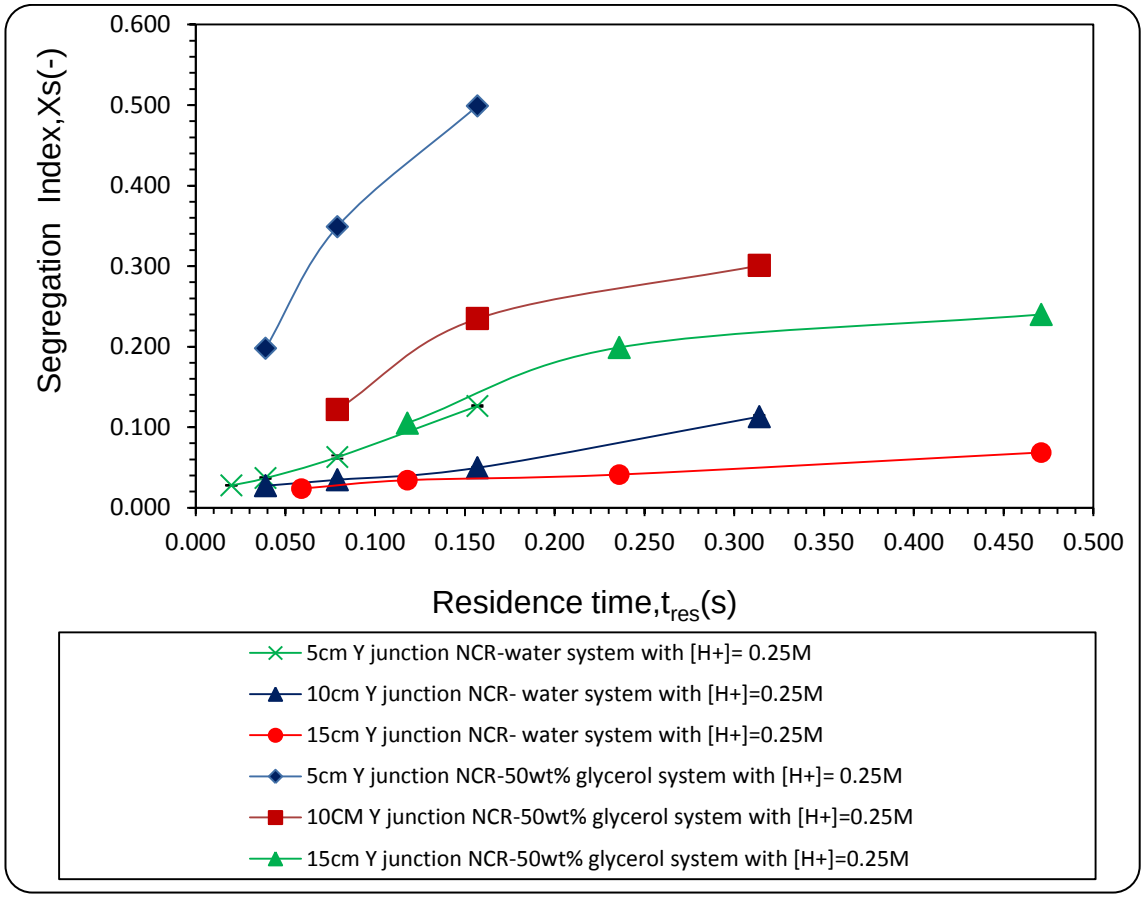

Figure 5.86: Effect of reactants residence time, tres.(s) on segregation index, Xs in individual Y-junction channels with water and 50 wt% glycerol systems at [H+]=0.25 M

When analysing the effect of flowrate on the performance of the NCRs, it is important to consider the mechanisms of mass transfer that are possible in the main channel section, namely convective mass transfer in the axial direction and diffusive mass transfer in the radial direction. Axial diffusion is considered to be negligible since longitudinal movement in the channel is controlled by convection (McCarthy et al., 2007). In order to assess the relative importance of each mechanism on the micromixing process in the NCR, the effect of Peclet number,(Pe), on Xs has been analysed and shown in Figure 5.87.

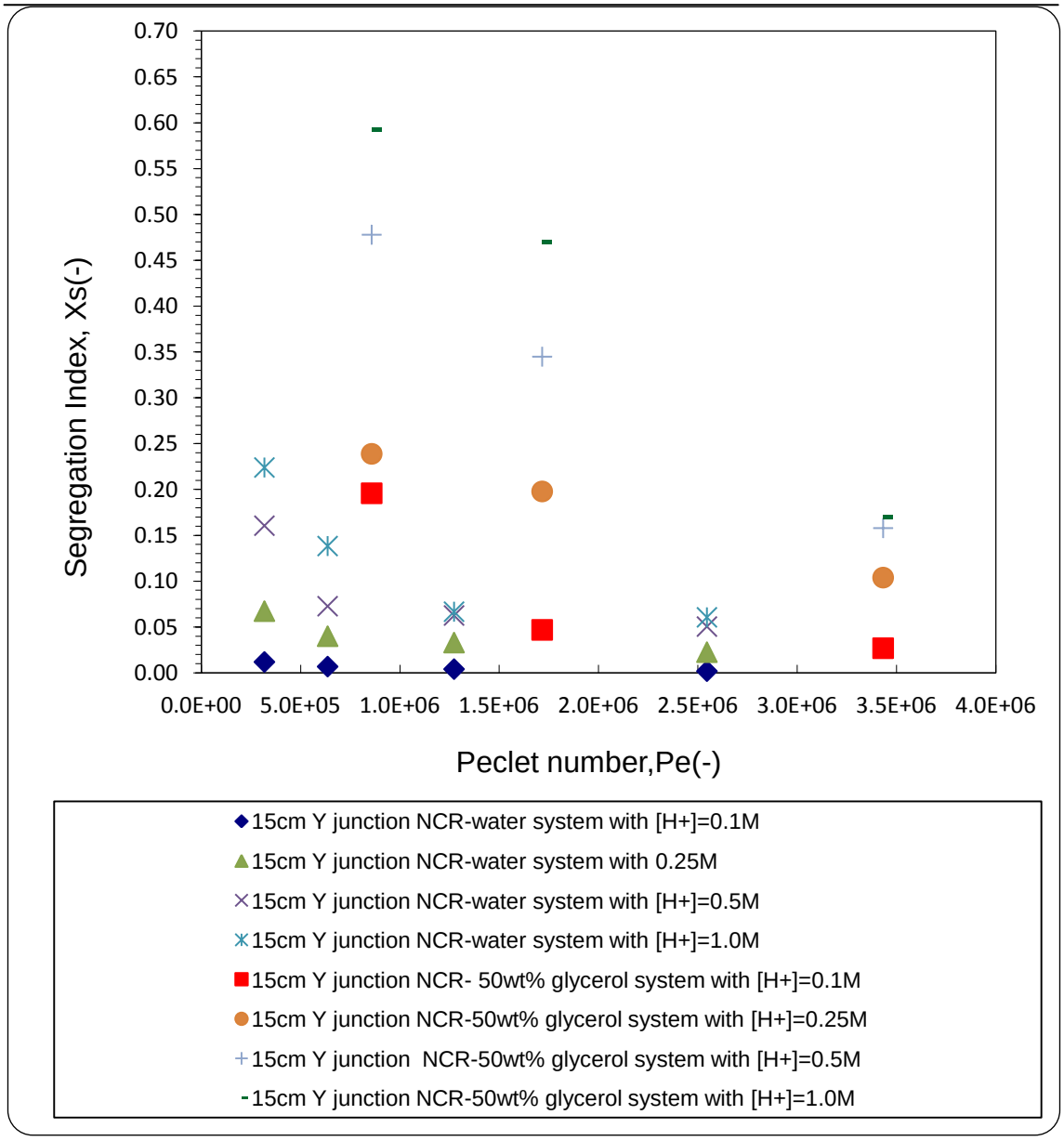

Figure 5.87: Effect of Peclet number, Pe (-) on segregation index, Xs (-) for 15cm Y Junction NCR-Water system with different acid ion concentrations

The plot shows the segregation index values as a function of the Peclet number, (Pe), in 15 cm Y junction NCR. It is noTable that the segregation index decreases with increasing Peclet number indicating that mixing efficiency is not mainly controlled by diffusion processes. In fact, if only diffusive mass transfer in the radial direction was responsible for the mixing of the two solutions, then the mixing efficiency would depend only on the diffusion path length, which is a function of channel diameter (McCarthy et al., 2007; Ehrfeld et al., 1999). If this was the case, then increasing the fluid velocity by increasing the total flowrate in the channel should not lead to a decrease in segregation index, as observed in this study.

Barresi *et al.,* 1999 and McCarthy *et al.,* 2007 have determined the relative contributions of the convective and diffusive mass transfer to the total mass transfer to characterise mixing for a barium sulphate precipitation in a Couette reactor and narrow channel reactor respectively by use of the Peclet number (Pe). The Peclet number (Pe) can be defined as the ratio of mass transfer occurring by convection in a system to that occurring by diffusion (Tilton, 1997) . The Peclet number (Pe) could be given as (Tilton et al., 1998):

$$Pe = ReSc = \frac{Ud_i}{D} \tag{5.26}$$

The convective mass transfer has a dominant influence on the overall mass transfer process if Pe >> 1. If Pe << 1 then diffusion dominates the mixing process. An analysis based on Pe has been adopted in this study following the previous work by McCarthy et al. (2007) and Baresi et al. (1999). The range of Pe applicable in the present work is between 3.186×10^5 < Pe < 2.546×10^6 for the water system and 8.585 $x10^5$ < Pe < 6.868 $x10^6$ for the 50 wt% glycerol system, values indicating the dominance of convection over diffusion under the flow regime attained in the NCRs studied. The calculations have been based on diffusion coefficient of 10^{-9} m^2/sec for the water system (Guichardon et al., 1997) and 3.708×10^{-10} m^2/sec for the 50 wt% system. The calculation of the diffusion coefficient for the 50 wt% glycerol system was based on the Diffusivity correlation (Reid et al., 1977) as shown in appendix M.

5.4.3 Effect of viscosity on segregation Index, (Xs)

In order to investigate the influence of viscosity on the micromixing intensity in terms of segregation index, glycerol was used to increase the viscosity of the aqueous reaction solution. A liquid mixture consisting of 50 wt% glycerol and 50 wt% water was used, which had a viscosity of 6 mPa.s at 20 ^oC (Dow Chemical Company), which is 6 times higher than the viscosity of the water medium. The pH of iodide – iodate - borate solution was maintained close to 11.0 for all viscous media experiments to prevent the

initial formation of iodine in the solution before any addition of the sulphuric acid is added (Guichardon et al., 1997). This was achieved by reducing the concentration of $H_2BO^-_3$ to 50% of its corresponding concentration in the in the aqueous reaction solution (water system), i.e. 0.0909 M. Selected experimental results for the viscosity effect on the segregation index in the NCRs are presented in this section whilst a complete set of results can be found in Figures AK6 to AK8 in Appendix K.

Figure 5.88 shows the effect of viscosity on segregation index (Xs) in 5cm Y junction NCR at different total flowrates with four acid concentrations. From Figure 5.88, it is clear that the segregation index is increased by the increasing the viscosity of the feed at given total flowrate and acid ion concentration. A similar effect was observed by (Yang et al., 2009b). For example, at 0.25 ml/sec and $[H^+]$ =0.1 M, the segregation index, (Xs) increased from 0.049 for the aqueous reaction solution to 0.432 for more viscous solution of 50 wt% glycerol-50 wt% water solution. , representing an increase of 89% in Xs. Similar trends were obtained at acid concentration of 0.25 M, 0.5 M and 1.0 M at all flowrates and all three channel lengths studied.

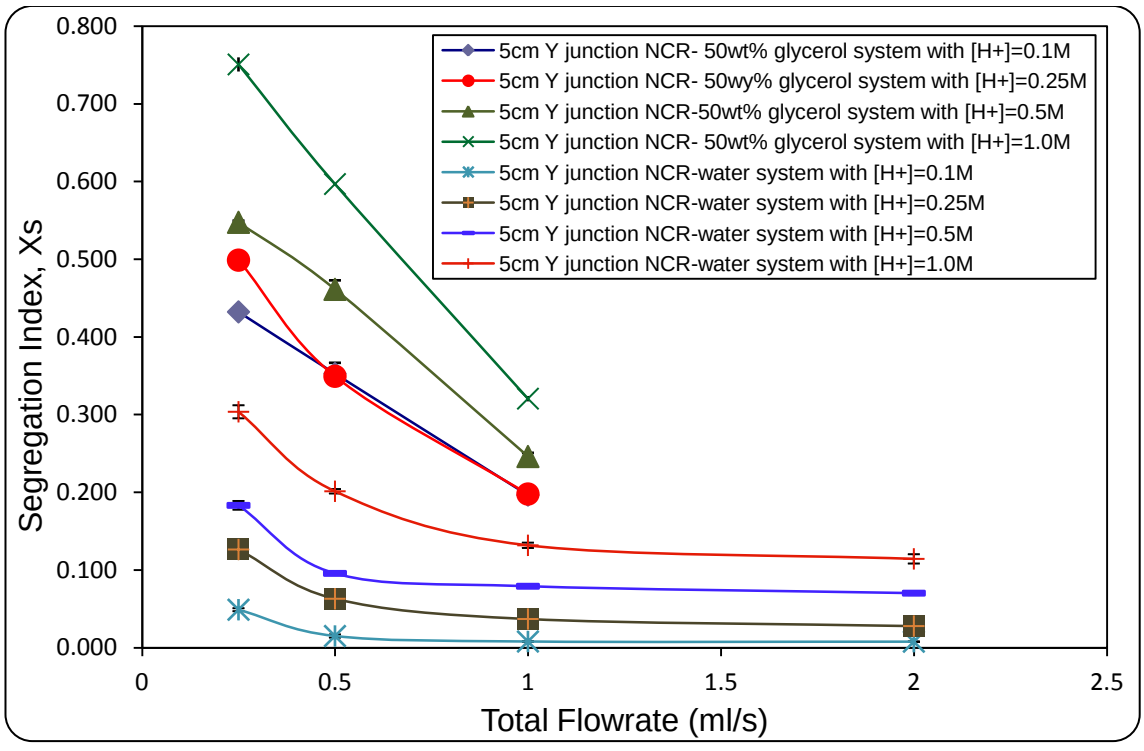

Figure 5.88: Effect of feed viscosity on segregation Index, (Xs) in 5 cm Y-Junction with different total flowrates and acid ion concentrations

Similar trends as described above were obtained for 10 cm and 15 cm length Y junction at all flowrates and acid concentrations as highlighted in Figure 5.89 and Figure 5.90 in this section and also for the three lengths of T junction as shown in Figures (AK6 to AK8 to in the Appendix K .

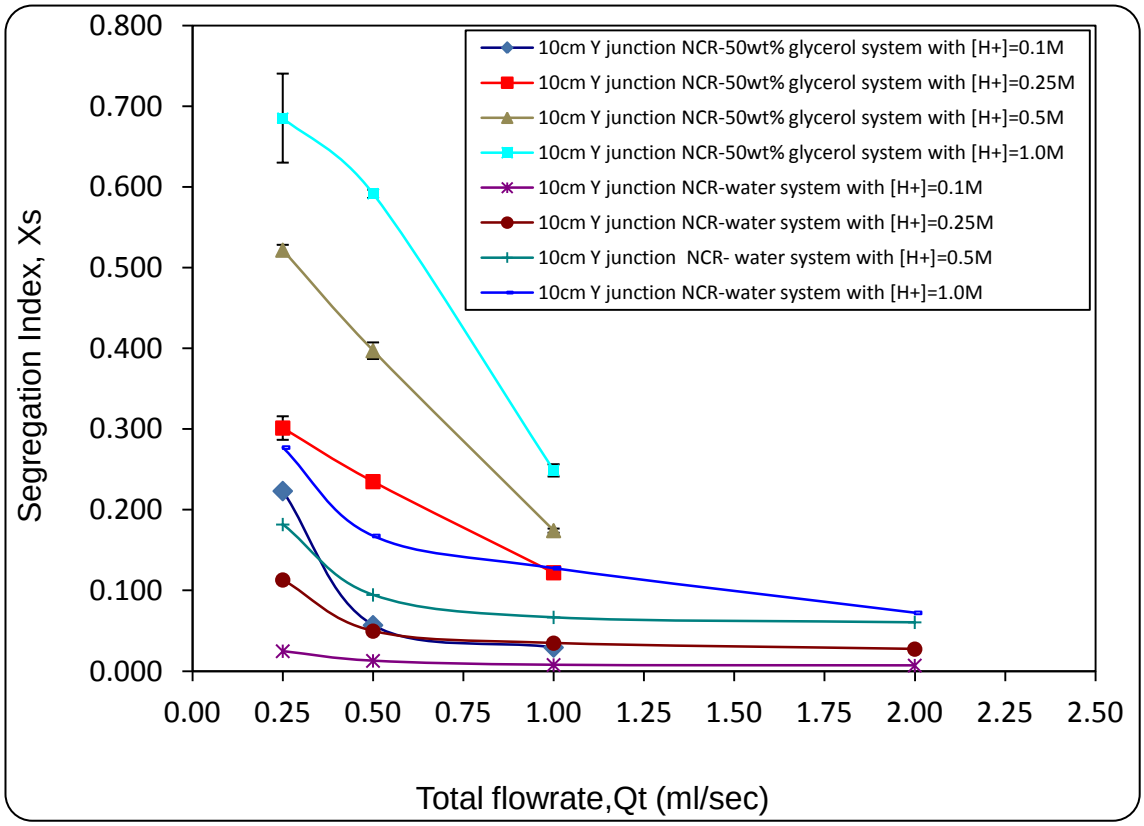

Figure 5.89: Effect of feed viscosity on segregation Index, (Xs) in 10 cm Y-Junction with different total flowrates and acid ion concentrations

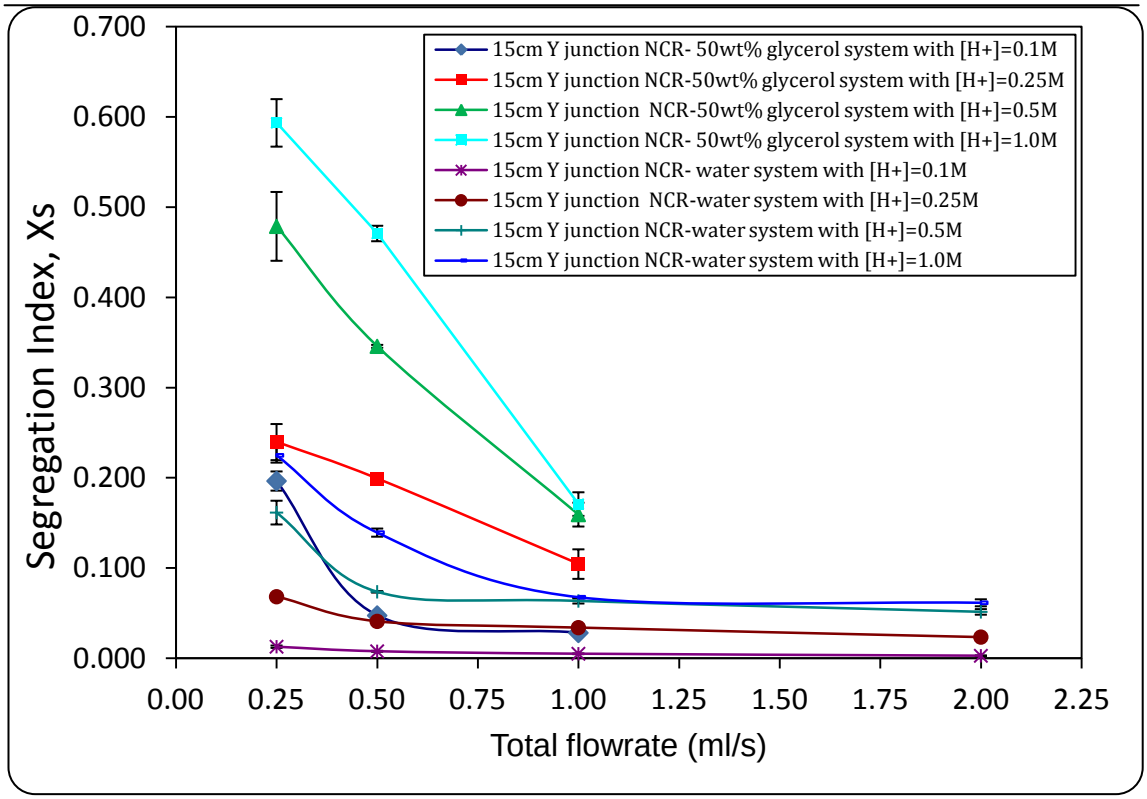

Figure 5.90: Effect of feed viscosity on segregation Index, (Xs) in 15 cm Y-Junction with different total flowrates and acid ion concentrations

The effect of viscosity on the segregation index, (Xs), can be related to a decrease in convective mass transfer based on Reynolds Number, (Re), as shown in Figure 5.91. Consequently, the rate of reaction in *neutralization reaction* will be reduced. Therefore, the *Dushman reaction* will tend to occur to a larger extent in the presence of an excess of localised acid ion concentration and iodine/tri-iodide will be produced, giving higher Xs. In general and as explained previously in SBR and SDRs experimental results (sections 5.1.4, 5.2.6 and 5.3.2.2), the viscous media will slow down the micromixing rate and alter the intrinsic kinetics of the reaction (Yang et al., 2009b; Yu-Shao CHEN, 2004; Guichardon et al., 1997) . It is to be noted that even at the higher viscosities, the NCRs still has positive influence on micromixing. For example when the $[H^+]$ =0.1 M was used, a 55% reduction of Xs was obtained at 6 mPa.s as the total flowrate increased from 0.25 to 1 ml/s. When $[H^+]$ =1.0 M, a 57% reduction of Xs was obtained over the same flowrate range.

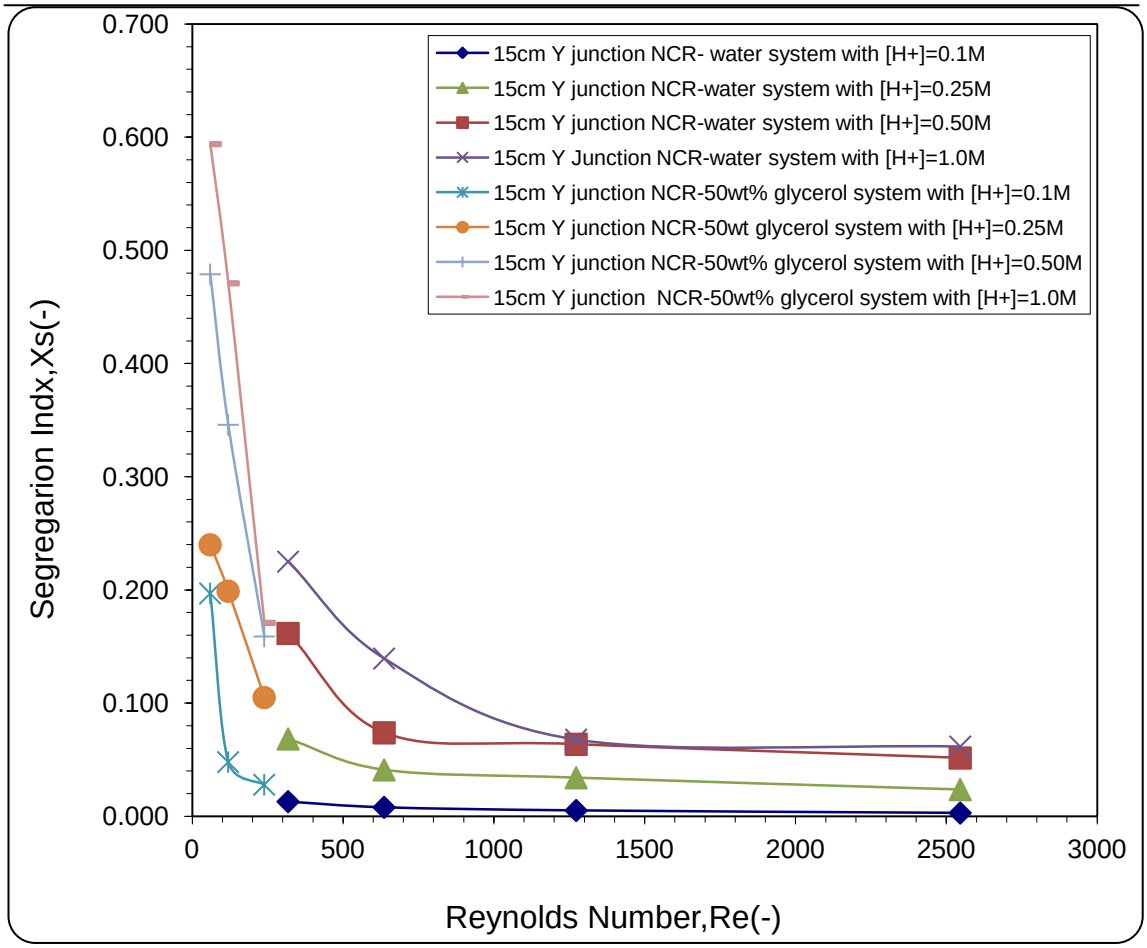

Figure 5.91: Effect of Reynolds Number, Re(-) on segregation Index, (Xs) in 15 cm Y Junction using water and 50 wt% glycerol system with different total flowrates and acid ion concentrations

5.4.3.1 Effect of acid concentration on segregation Index, (Xs)

The effect of acid concentration on segregation index in T and Y Junctions 10cm length NCR at different total flow rate is illustrated in Figures 5.92 and 5.93 below. The acid ion concentrations were 0.1, 0.25 and 0.5 M. In order to test the effect the acid concentration on the segregation index, (Xs), the total volumetric flow rate ratio was kept at R=7 with all the implemented acid concentrations.

One important issue need to be mentioned, it has been tried to investigate the effect of acid concentration on segregation Index, (Xs) with 1.0 M.The samples from these runs had pH values less that 7 and the absorbance values were higher than 2.0. For these reason, the results of this set of experiments has been rejected.

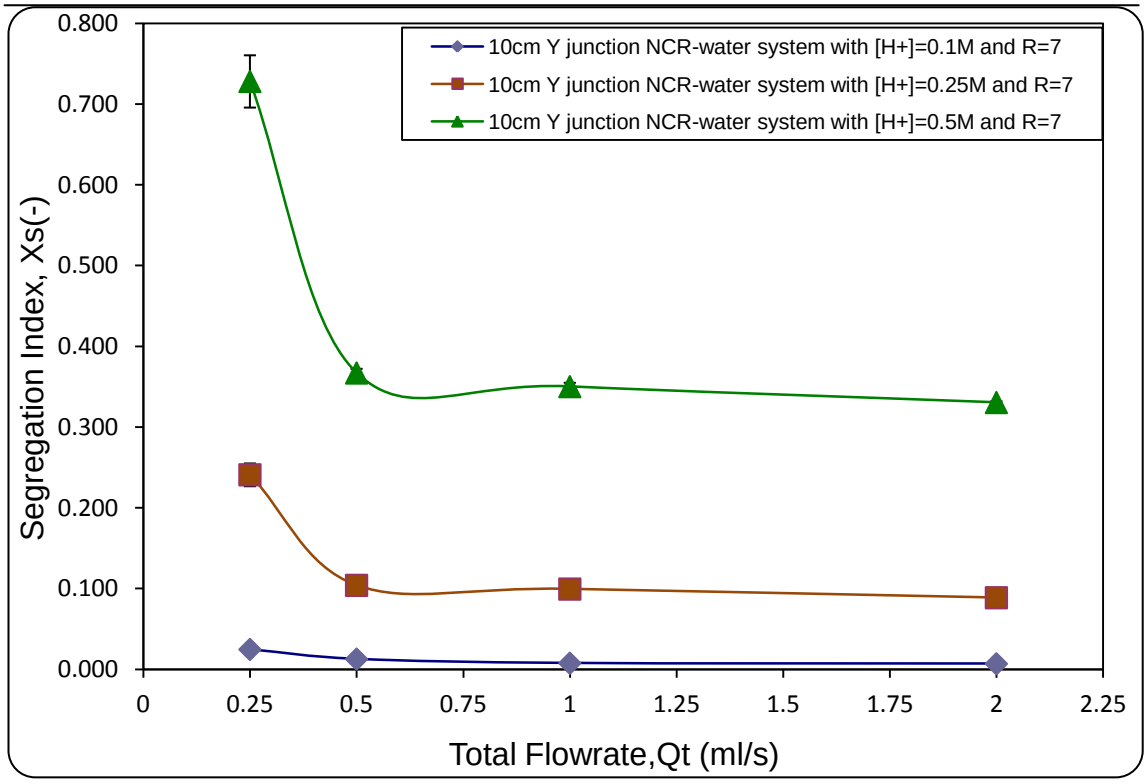

Figure 5.92: Effect of acid concentration on the segregation index in 10 cm Y- junction with different total flowrates -water system , The total volumetric flow rate ratio, (R=7), [H+] = 0.1,0.25, and 0.5 M

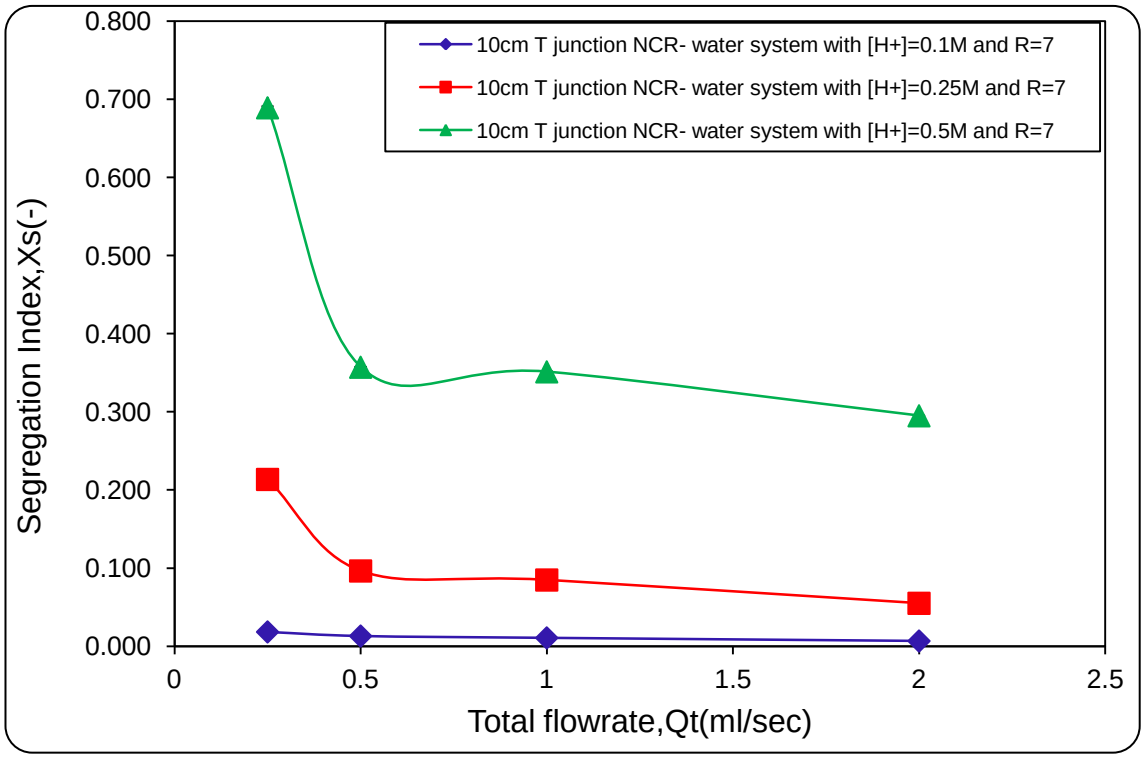

Figure 5.93: Effect of acid concentration on the segregation index in 10cm T- junction with different total flowrates -water system , The total volumetric flow rate ratio, (R=7), [H+] = 0.1,0.25, and 0.5 M

From the experimental results for the two NCR with different junction configurations, it can be observed that the segregation index is sensitive to the acid concentration. At the total flowrate in the range 0.25 ml/s to 2 ml/s, an increase of segregation index was observed as the acid concentration was increased. For instance, from Figure 5.92 using the Y-junction, at the total flowrate of 0.25 ml/s, the segregation index increased from 0.025 to 0.728 as acid concentration was raised from 0.1 M to 0.5 M, representing an increment in segregation index of 97%. Similar effects were observed at all flowrates tested. Also similar trends with regards to the increase of segregation index with increasing acid ion concentration as highlighted in Figure 5.92 were obtained when 10cm T junction NCR was tested, as seen in Figure 5.93 These findings support the results that have been achieved in 10cm and 30 cm SDR's experiments (sections 5.2.4 and 5.3.2.3). In addition, these findings were in agreement with other micromixing efficiency studies carried in rotating packed bed reactors (Yang et al., 2009a; Chu et al., 2007; Yang et al., 2006; Hai-Jian Yang, 2005) .The reason behind the increase in segregation index with the increase in acid concentration can be explained in the same manner as stated previously in small and large SDRs results section (sections 5.2.4 and 5.3.2.3) In brief, it is because of the rate of Dushman reaction, i.e. reaction (5.2) is more sensitive to acid concentration than that of reaction (5.1) as its reaction order with respect to acid is higher, reaction (5.2) increases at a faster rate than reaction (5.1) when the acid concentration is increased. Consequently more iodine and therefore more tri-iodide is formed. This causes segregation index (X_S) to be increased.

5.4.4 Effect of channel length and junction type on segregation Index, (Xs)

The degree of mixing was assessed in three different lengths and two different junctions (Y and T junctions) in order to evaluate the influence of the length and of the geometry of the channel on the quality of mixing. The channel lengths used were 5 cm, 10 cm and 15 cm and experimental runs were completed with the varying lengths using the acid concentrations and total flowrates as mentioned in the previous section 5.4.1. Figures 5.94 and 5.95 demonstrate the effect of increasing the channel length for both Y and T-junction narrow channel reactors with using water system and acid concentration of 1.0 M.

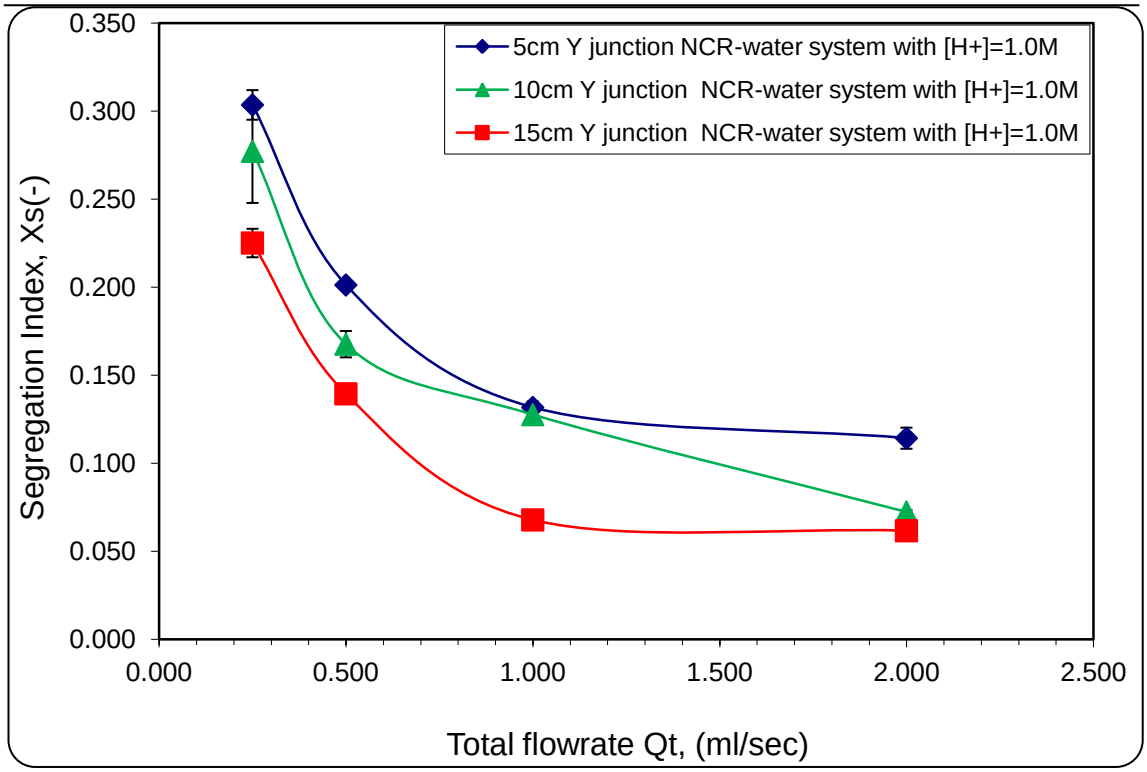

Figure 5.94: Effect of channel length on segregation Index, (Xs) for 5,10 and 15 cm Y junction-water system with [H+] =1.0 M

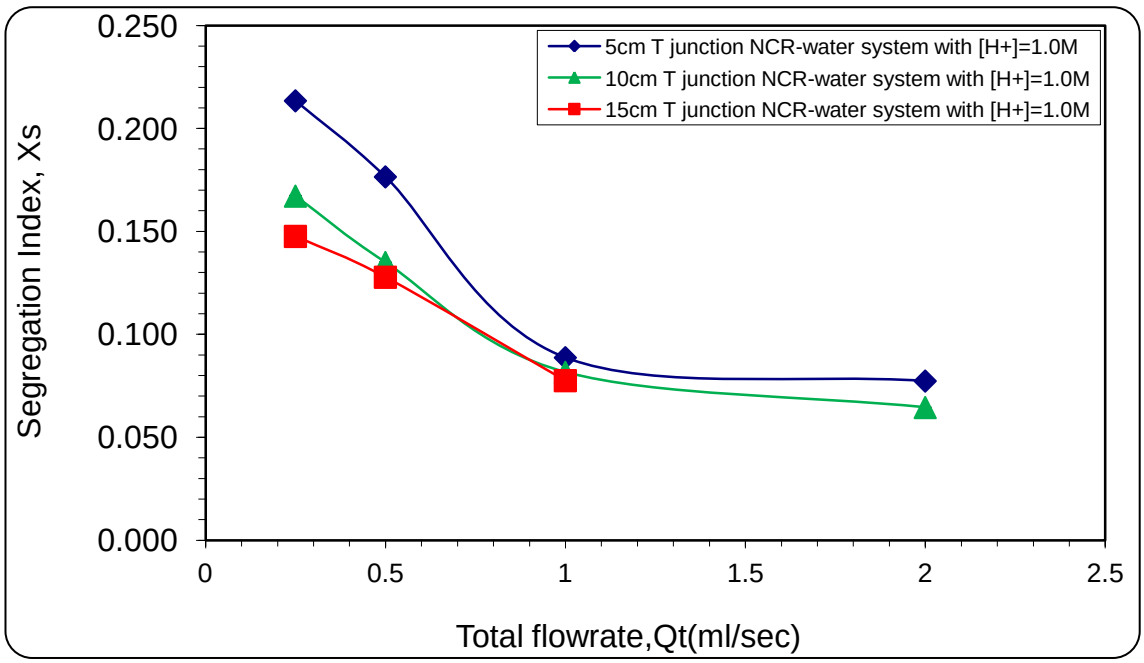

Figure 5.95: Effect of channel length on segregation Index, (Xs) for 5,10 and 15 cm T junction-water system with [H+] =1.0 M

One important point need to be mentioned, it has been tried to investigate the effect of Effect of channel length on segregation Index, (Xs) for the 15 cm T junction with the

total flowrate of 2 ml/s. unfortunately, the back pressure has been experienced with the pumping system. For these reason, the total flowrate of 2 ml/s has been ignored.

The Figures clearly demonstrate that at given total flowrate, increasing the length of the reactor leads to a decrease in the segregation index. This behaviour is expected since the reactants residence time in the NCRs is also longer. This trend was also observed by Schneider et al. (2004) when the intensity of mixing in three different channel deigns with the internal diameter of 0.25 mm and lengths of 2.85 mm, 11.30 mm and 18.75 mm was assessed by the iodide-iodate reaction system in order to evaluate the influence of the length and shape of the channel. This phenomenon therefore suggests that the mixing does not only occur at the meeting of the two streams, but continues along the length of the reactor which is expected due to the increased residence time.

Similar trends with regards to the decrease in segregation index with increase in the channel length as highlighted in Figures 5.94 and 5.95 were obtained in Figures (AK9 and AK10) in appendix K when the water system replaced by 50 wt% glycerol system.

The effect of the junction angle between the two feeds was considered and its effect on the segregation index. For this work two junction types were considered for comparison, Y and T, with the angle between the feed streams 90° and 180° respectively. The graph below, Figure 5.96, shows a comparison of segregation index values for both the Y and T junctions with channel length 5cm over the acid concentration range studied.

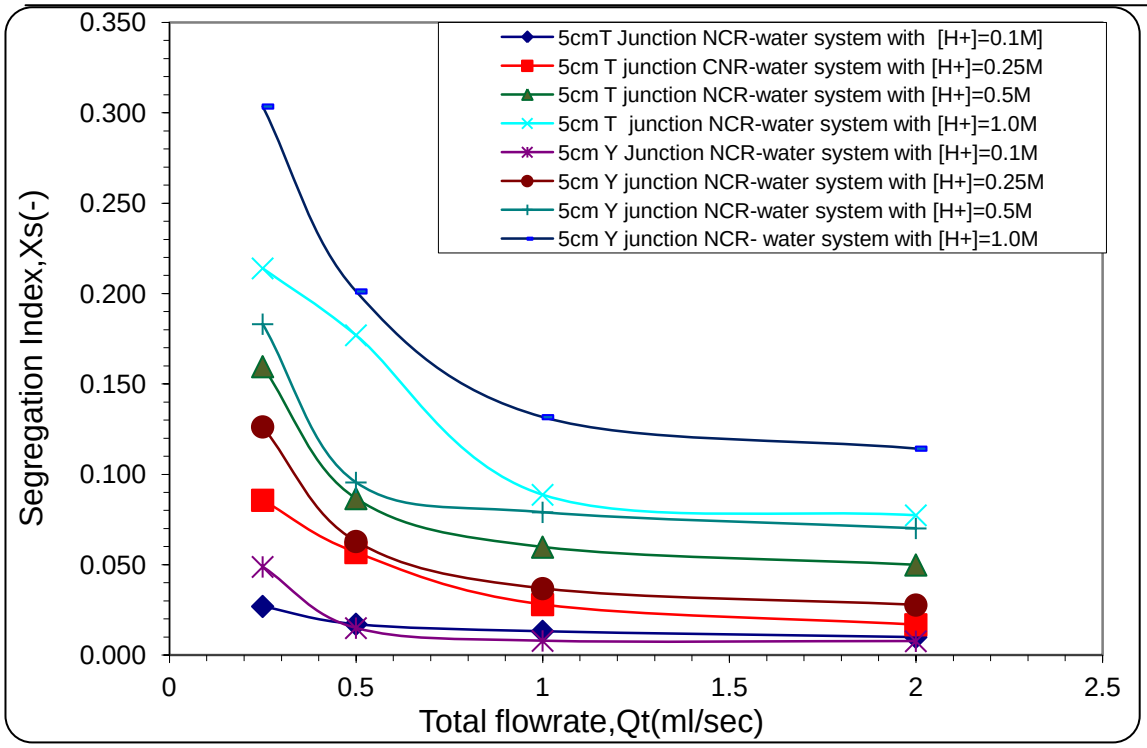

Figure 5.96: Effect of junction type on segregation Index, (Xs) for 5cm length -water system

It is observed that the use of the Y-junction results in higher values of the segregation index throughout the acid ion concentration range. This means that superior micromixing is achieved with the T-junction. Additionally, the same trend is observed for the reactors with 10 cm and 15 cm channel lengths as shown in Figures AK11 and AK12 in appendix K.

The explanation for the difference in micromixing performance with different junction types is necessarily related to the way the individual streams make contact with each other at the junction. For the T-junction narrow channel reactors, the two streams meet in a direct collision, whereas for the Y-junction the meeting of the streams is more graduated where not all layers of the feed streams make contact on initial impact, i.e. the border face surface area is larger for the T-junction than the Y-junction. This mechanism is demonstrated in Figure 97.

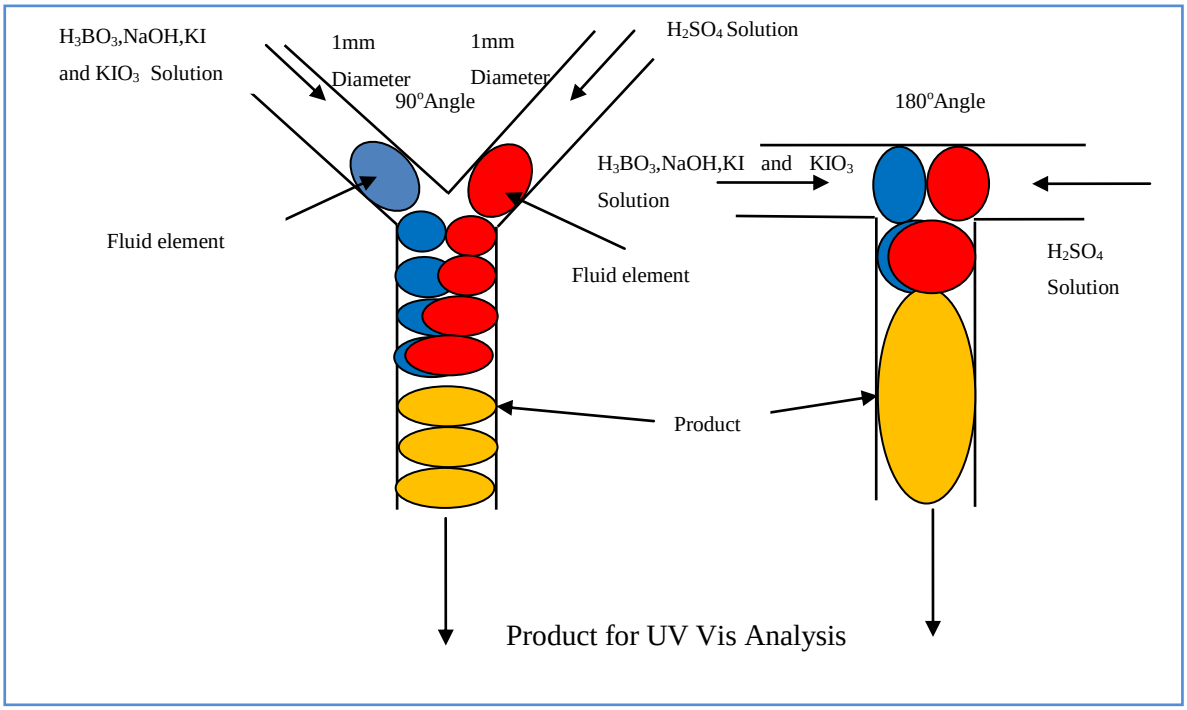

Figure 5.97: The contact mechanism of Fluid elements in the Y and T junctions

Theoretical simulations completed by Gigras and Pushpavanam (2008) have compared the mixing in three junctions in terms of percentage mixing quality. The junctions considered are Y, T and U. Differences in the simulations and this project included a Y-junction angle of 60°, a T-junction angle of 90°, a square channel with a width of 300 μm, and Reynolds numbers between 30 and 210. However, the simulation predicted that the T-junction would achieve increased mixing quality over the Y-junction across the range, i.e. an increase in the junction angle leads to an increase in the mixing intensity, as has been found experimentally in the present study. It was found that the U junction outperforms both the T and the Y-junction reactors. This superior mixing was explained in terms of the faster induction of secondary vortices at the U-junction

In addition, Aoki and Mae (2006) carried out an intensive experimental work considering the effects of channel geometry on mixing performance of micromixing using collision of fluid segments. They applied T- and Y- shape microchannnel mixers made of glass to the study on effects of the collision zone diameter on mixing performance. Two fluid streams collide at the angle of 90° in Y junction and 180° in T junction. In the whole of the channels of both mixers, the channel width and depth are 0.5 mm, and the channel length after collision of two fluid streams is 5 cm. Villermaux/Dushman reaction adopted to evaluate mixing performances of T- and Y-

junction microchannnel. The total flow rate has been increased to reduce the absorbance at 352 nm less than 0.05. The results shows that the mixer Y- junction microchannnel needs much higher total flowrate to reach this criterion than T- junction microchannnel. The researchers discuss this difference using shear rate applied to fluid segments at the collision zone. Though the Reynolds numbers of the two mixers are the same at the same total flow rate, the shear rate at the collision zone in the width direction of T-junction was $\sqrt{2}$ times larger than that of Y junction. The difference in mixing performance between the two microchannels was large in the high *Re* range, where a high shear rate is applied to fluid segments. The results also confirm that shear rate affects mixing performance in the high *Re* range. These findings support the results that have been achieved in this work with regards to the effect of junction type on mixing performance.

5.4.5 Effect of Power input (power dissipation) on segregation index, (Xs)

The Power input (power dissipation) in the NCRs was estimated according to the equation below (Falk and Commenge, 2010):

$$\varepsilon = \frac{32\nu(U^2)}{d_i^2} \tag{5.27}$$

Figure 5.98 show the effect of power rate dissipation on the segregation index in 10cm T junction NCR using both water and 50 wt% glycerol system. The acid ion concentrations were 0.1 and 1.0M. The total flowrates were 0.25 ml/s, 0.5ml/s, 1ml/s and 2ml/s. The power dissipation was in the range of 3.2 - 1105.4 W/kg. These values depend on the total flow rate, water system or 50wt% glycerol system as shown in Figure 5.99.

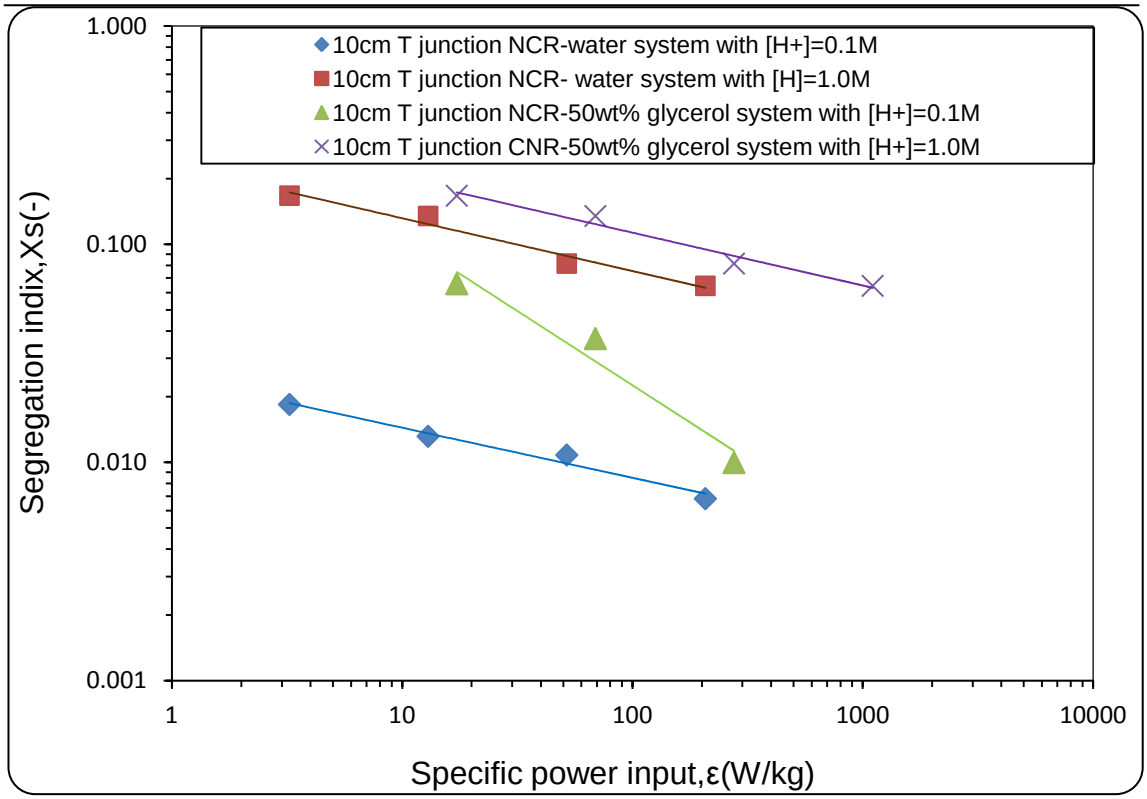

Figure 5.98: Effect of Power dissipation on Segregation Index, (-) - T junction -water system and 50 wt% Glycerol, [H+] =0.1 and 1.0 M

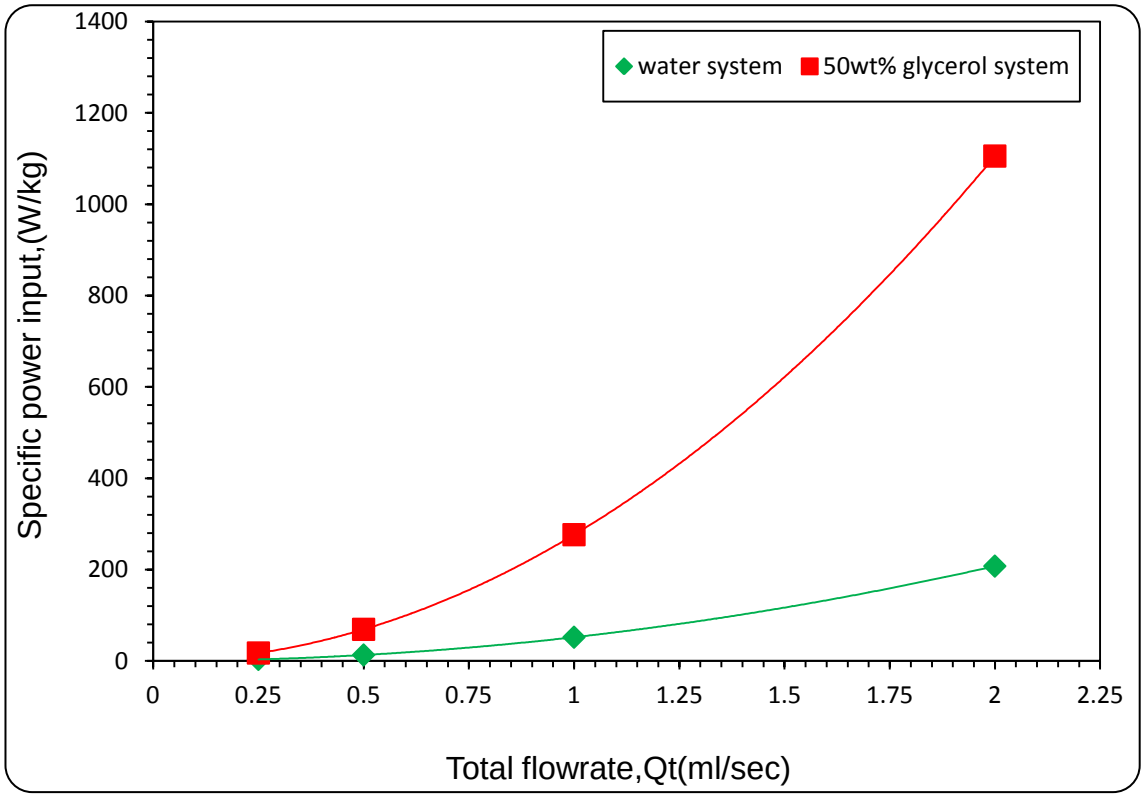

Figure 5.99: Effect of Total flowrate on Specific power input (Power dissipation) in NCR's for water system and 50 wt% Glycerol

From Figure 5.98, it is evident that the segregation index in 10cm NCR decreases consistently with increase in power dissipation. Considering water system with an acid ion concentration of 0.1 M, the specific power input increased from 3.2 W/kg at the total flowrate of 0.25 ml/s to its highest value of 208 W/kg at the total flowrate of 2 ml/s. This represents an increase of 98% in the power dissipation which results in a corresponding reduction of segregation index from 0.018 at total flowrate of 0.25 ml/s to its lowest value of 0.007 at total flowrate of 2 ml/s thereby representing a 61% drop in Xs. Similar trends were observed at all acid ion concentrations studied as well as when 50 wt% glycerol system was used.

From Figure 5.98 and Figure 5.99, certain facts were confirmed. At constant fluid kinematic viscosity (ν), the higher values of specific power input (ε) could be attained in the NCR channel by increasing the reactants total flowrate (Qt). This could be attributed to the fact that increasing the total flowrate results in increase in the mean velocity, (u_m) of the fluid in the NCR channel. Accordingly, the mean shear rate ($\dot{\gamma}$) in the channel increased and the kinetic energy given to the liquid increased as well. For that reason, the intensity of micromixing in terms of segregation index was improved.

5.4.6 Effect of mixing time on segregation index, (Xs)

Figure 5.100 below shows a logarithmic plot of the estimation of theoretical micromixing time from equation (5.25) for both the water system and 50 wt% glycerol system as function of specific power input for four different total flow rates namely, 0.25, 0.5,1 and 2 ml/s as shown in Figures 2.101 and 5.102 for 15 cm Y junction NCR and for 5 cm T junction NCR respectively. The energetic efficiency, (η), was considered as only 3.0%. As stated in section (5.4.2), the micromixing time in NCR's is controlled by molecular diffusion and shear rate which was calculated on the basis of the hydrodynamic properties of the fluid, channel size and the specific power input in the channel. The selectivity, quality or distribution of the final product could be controlled by degree of mixing if $t_m >> t_r$ and in this case the mixing process is the controlled step .

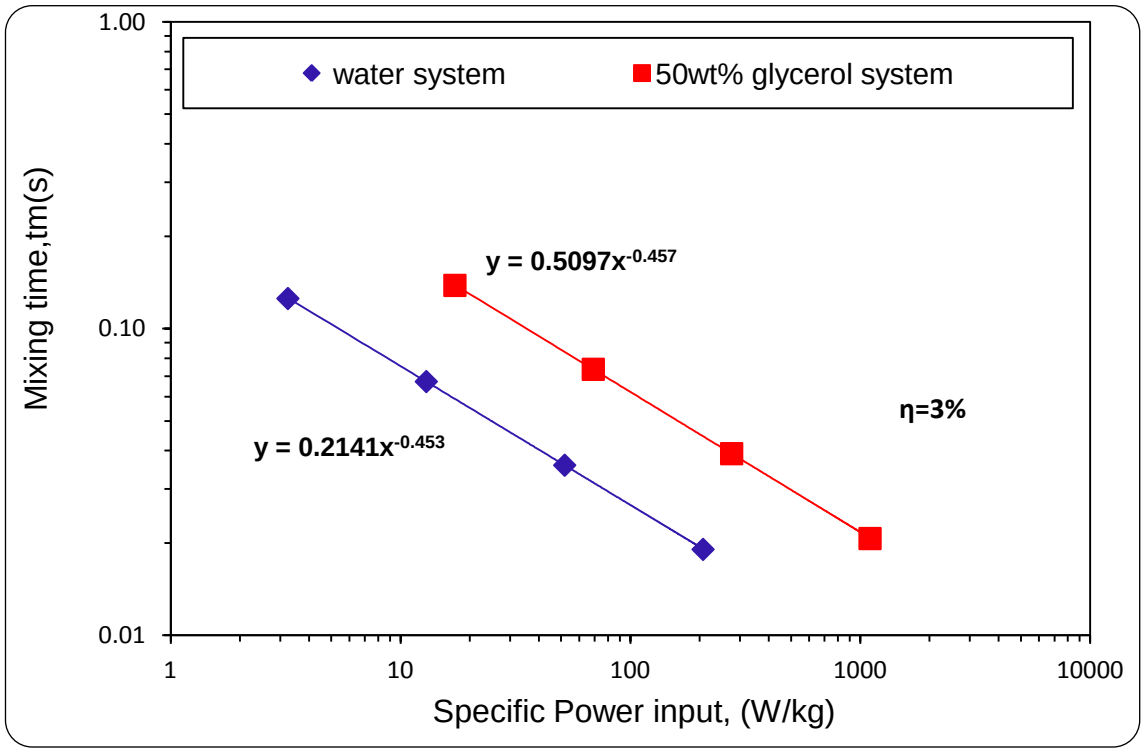

Figure 5.100: Theoretical mixing time versus Specific Power input in NCR's of 1 mm diameter for water and 50 wt% glycerol systems

It can be noticed that the mixing time is inversely proportional to the specific power input. As the specific power input increases, the micro-mixing time required for the molecules to contact and diffuse to one another decreases. Accordingly, the micromixing intensity will be improved. This also supports the explanation for the increases in the mixing efficiency in NCR's with increased total flowrates, which resulted in power input increase.

Figures 5.101 and 5.102 display the relationship between the micromixing time and the segregation index, (Xs), for 15 cm Y junction NCR and 5 cm T-junction NCR respectively under various operating conditions. From both Figures, it is clear that the shorter the micromixing time, the lower the value of segregation index achieved. Using the 15 cm Y-junction (Figure 5.101), for example the lowest Xs and therefore best mixing performance is achieved with the water system and [H+] =0.1 M at the lowest micromixing time of 0.019 s attained at the highest flowrate of 2 ml/s and therefore

highest power input. The effect of acid ion concentration on Xs at a fixed micromixing time is also clearly apparent from these plots.

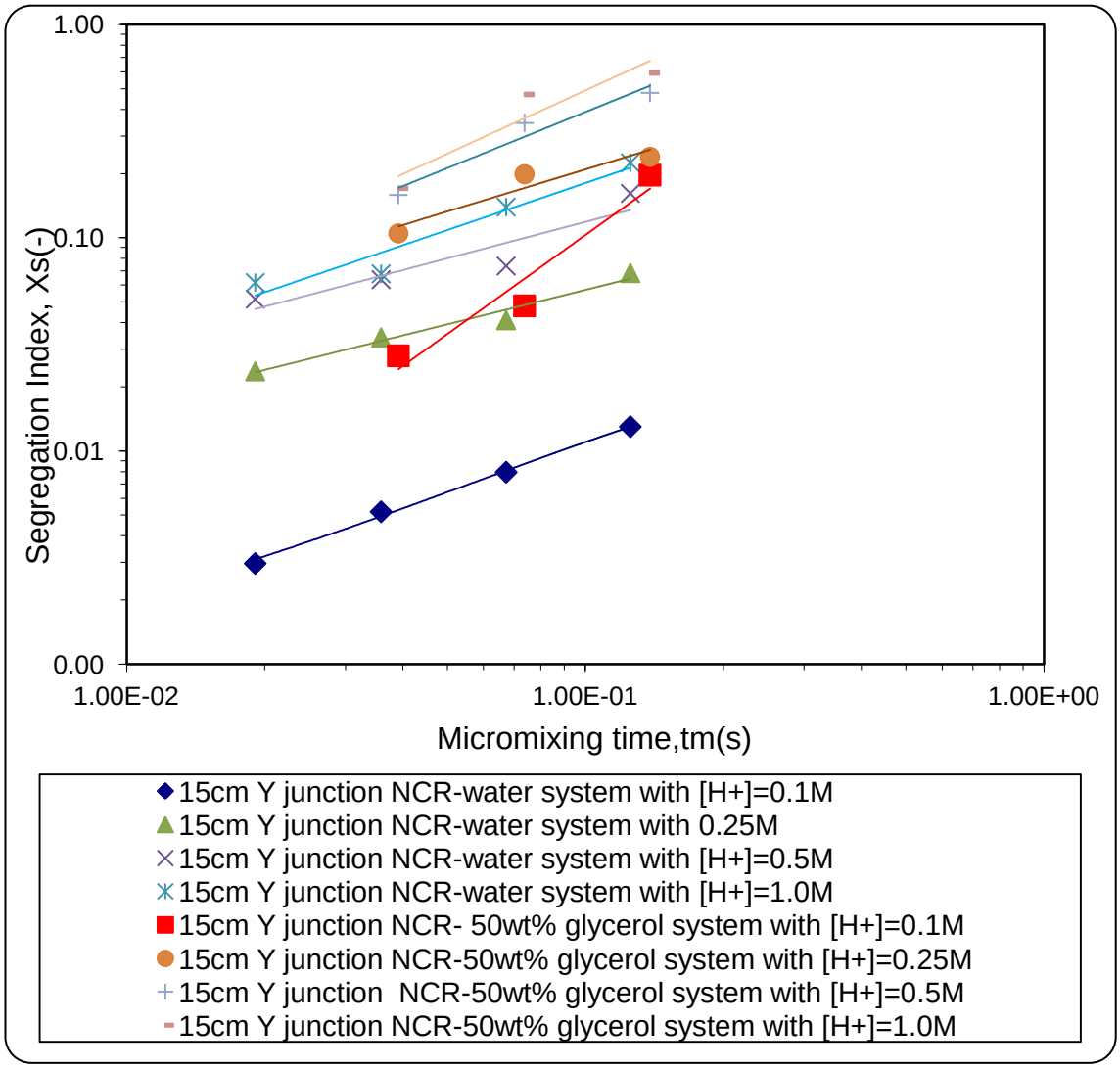

Figure 5.101: Relationship between Theoretical mixing time and segregation index for 15 cm Y junction NCR- water and 50 wt% glycerol systems

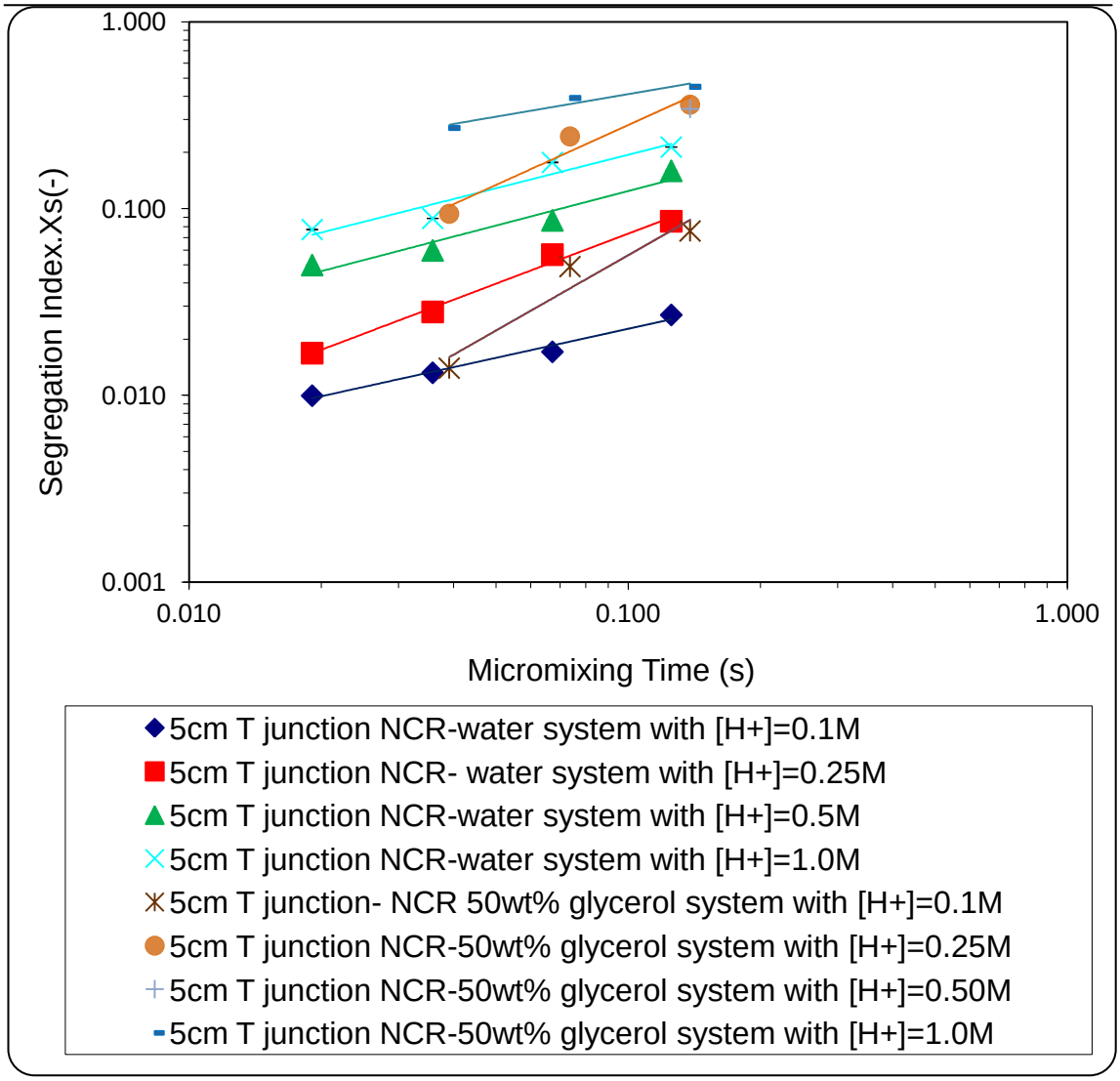

Figure 5.102: Relationship between Theoretical mixing time and segregation index for 5 cm T junction NCR- water and 50 wt% glycerol systems

Similar trends with regards to the relationship between the micromixing time and segregation index as highlighted in Figure 5.101 were obtained in Figure 5.102 when 5cm T junction NCR was tested with both water system and 50wt% glycerol.

From the findings above, it can be concluded that at given kinematic viscosity (ν) and NCR channel size, the higher values of specific power input (ε) could be attained in the NCR channel by increasing the reactants total flowrate (Qt). This in turn leads to shorter micro-mixing time between reacting molecules. These findings were in agreement with the findings made from the previous two intensified reactors (10 cm and 30 cm SDR experiments) as part of this present research and also in agreement with the findings in NCRs (Falk and Commenge, 2010; Yang et al., 2009b).

5.5 Reactor performance comparison by micromixing efficiency

One of the main objectives in this research project is to compare the SDR micromixing efficiency with the performance of other types of reactor i.e. semi-batch reactor (SBR) and narrow channel reactor (NCR). The reactors are in different operating modes i.e. semibatch in SBR and continuous flow in SDRs and NCRs. This makes the direct comparison between segregation index or micromixedness ratio as function of impeller rotational speed and disc rotational speed for SBR and SDR respectively or total flow rate in the three different reactors not possible. Instead, the mixing time, the segregation index or micromixedness ratio as function of the power dissipation in each of the reactors at given operating parameters was adopted for comparison between the three different reactors.

One of the important parameters which needs to be considered when drawing a comparison between the performance of the various reactor types studied is the ratio of the molar quantities of acid and the borate ions contacting each other. This parameter has to be maintained constant in the continuous reactors NCRs and SDRs as well as in the SBR for a valid comparison (Guichardon and Falk, 2000), as discussed in detail in Chapter 4. Sample calculation of the sulphuric acid volumes which needs to be injected in the SBR and also the ratios (R) of the solution of iodide-iodide-borate ions and the acid volumetric flow rates in the continuous reactors i.e. SDR and NCR is shown in appendix B.

5.5.1 Water system

The 10cm and 30 cm SDRs are identical except they are different in the size. The Reynolds number in both SDRs were kept constant by varying the total flow rate of the reactant streams (as shown in Table 5.21) for the purpose of a direct comparison of micromixing efficiency between two SDRs on the basis of disc rotational speed.

Table 5.21: Reynolds numbers values for both SDR are at given total flowrates implemented in the 10cm and 30 cm SDR's experiments

Total flowrates in 10cmSDR, ml/s	Total flowrates in 30cm SDR, ml/s	Reynolds number, Re(-)
1	3	14.29
3	9	42.29
5	15	71.48

Figure 5.103 below shows the effect of disc rotational speed on the segergation index for 10 cm and 30 cm SDRs. All the experiments were carried out with water system and at the same reactants concentration. The two SDR reactors operated at different total flow rates and with constant Reynolds number in both SDRs for the purpose of a direct comparison of micromixing efficiency between the two SDRs on the basis of disc rotational speed as mentioned above .

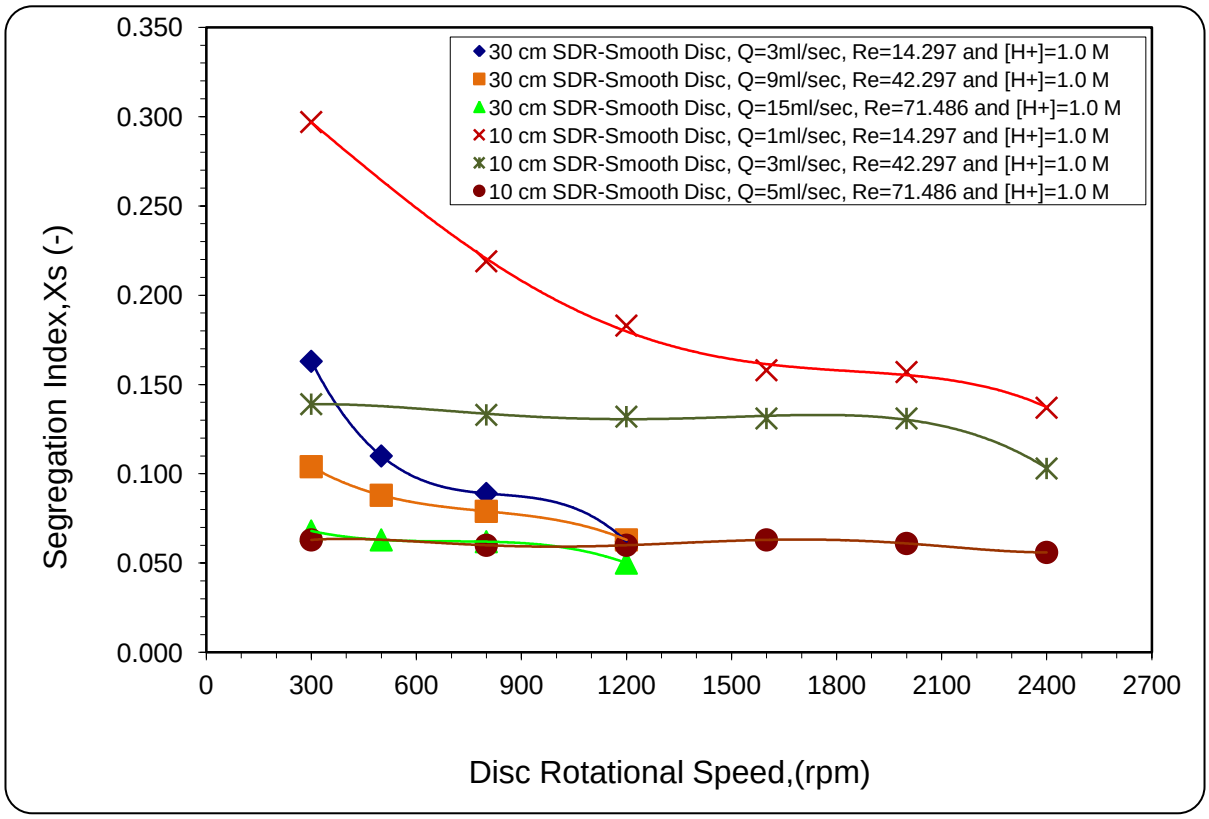

Figure 5.103: Effect of disc rotational speed,(rpm) on the segregation index ,(Xs), at various liquid total flowrates for 10 cm SDR and 30 cm SDR-Smooth Discs – water system with [H+]=1.0 M

Figure 5.103 shows the micromixing performance of the 10 cm SDR and 30 cm SDR in terms of segergation index using water system with acid ion concentration of 1.0 M corresponding to the flow rate ratios R=70 (where $R=Q_I/Q_H$). The total flow rates for

the 10 cm SDR were 1,3 and 5ml/s. On the other hand, the total flowrate were 5,9 and 15ml/s for the 30 cm SDR. From figure 5.103 , it could be concluded that at a given disc rotational speed, the highest micromixing performance (i.e. the lowest segergation index) has been achieved by the 30 cm SDR. This was at all the implemented total flowrates. From Figure 5.103, under optimised conditions in the 10 cm SDR corresponding to a rotational speed of 2400 rpm, 1.0 M acid ion concentration and total flowrate of 5.0 ml/s, the segergation index,(X_s), was estimated to be about 0.056. Using 30 cm SDR with disc rotational speed of 1200 rpm and total flowrate of 15 ml/s, the corresponding value for X_s, was estimated to be about 0.050. At the mentioned operating conditions, it is clear that the 30 cm SDR performs better than the 10cm SDR. The results from the 30 cm SDR were even higher than those from the 10 cm SDR at their respective maximum disc rotational speeds. In fact, the maximum disc rotational speed of the 10cm SDR was twice higher than the maxmum disc rotational speed in 30cm SDR. This is attributed to a larger disc surface area available within the 30cm SDR compared with the surface area of 10cm SDR (the surface area avilable at the 30 cm SDR is almost nine times higher than the surface area avilable at the 10 cm SDR). Consequently, more surface disc is available for contacting with the reactants and as result of that, the 30 cm SDR has the highest shear forces created between liquid film and the disc surface and more thinner liquid film are formed. The higher shear rates and the thinner films will cause the lower segregation index, (Xs). In addition, the larger the disc available, the longer the residence time for the reactants on the disc surface and thus higher the chance of micromixing process to occur.

Figure 5.104 below shows a logarithmic plot of the estimation of theoretical micromixing time received from the four different reactors as function of power dissipation. All the experiments were carried out with water system and at the same reactants concentration i.e $[H_2BO^-_3]$ = 0.0909 M; [NaOH] = 0.0909 M; [KI] =0.01167 M; $[KIO_3]$ =0.00233 M; $[I_2]_{potential} = 7\times10^{-3}$ M; $[H^+]$ =1.0 M .The reactors operated with water system and different total flow rates. The correlations between micromixing time t_m and power dissipation ε developed on the basis of the plots shown in Figure 5.104 are given in Table 5.22.

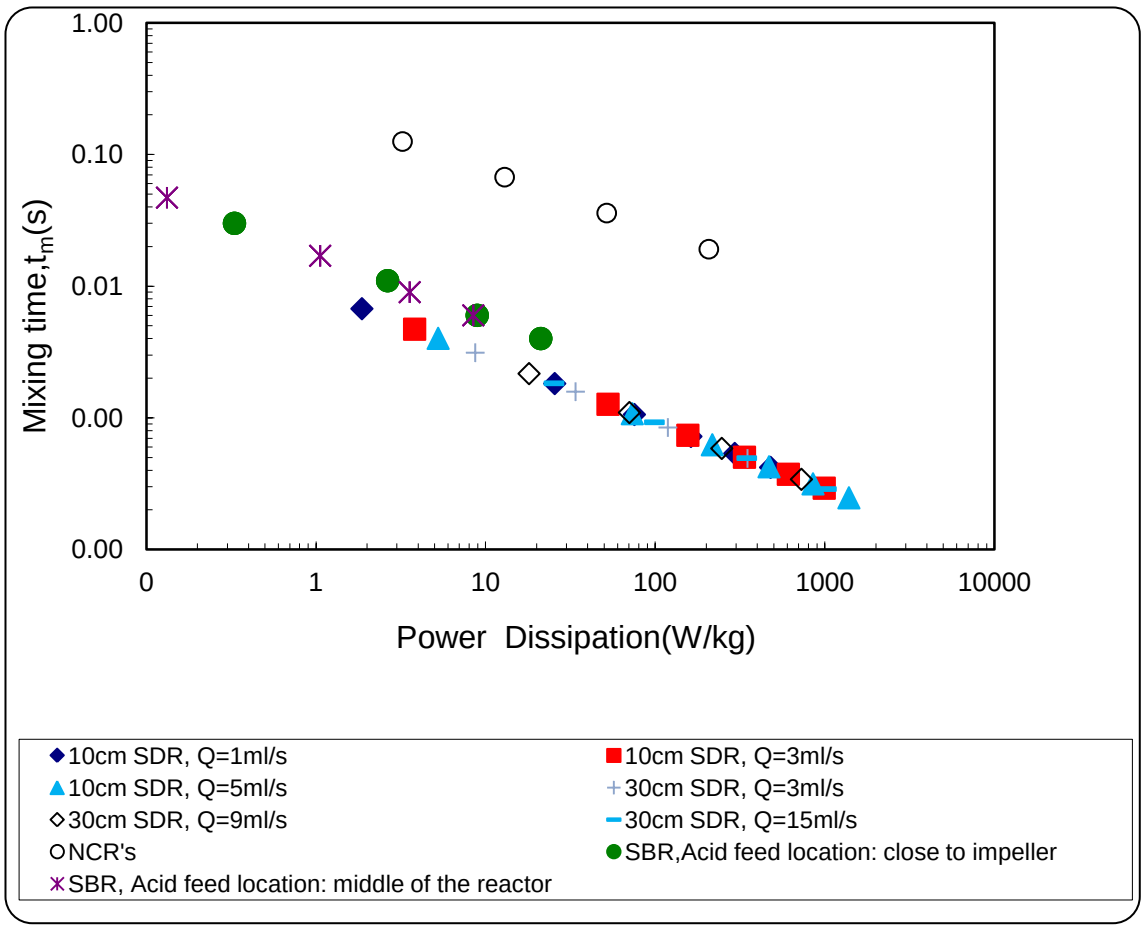

Figure 5.104: Evolution of the mixing time, (tm), versus the power dissipation for SBR, Semi-batch reactor reactor ; 10 and 30 cm SDR- smooth discs, spinning disc reactor, NCRs; narrow channel reactors – water system

Table 5.22: Correlations for theoretical mixing time with respect to the power dissipation for SDRs-smooth discs, SBR and NCR-water system

Reactor type	Correlation	R^2
10 and 30 cmSDR	$t_m = 0.0092\ \varepsilon^{-0.5}$	1.0
SBR : acid feed location close to impeller	$t_m = 0.0176\ \varepsilon^{-0.486}$	0.99
SBR : acid feed location: middle of the reactor	$t_m = 0.0173\ \varepsilon^{-0.497}$	0.99
NCR's	$t_m = 0.2141\ \varepsilon^{-0.453}$	1.0

From Figure 5.104 and Table 5.22, it is clear that the theoretical mixing times behave as a power-law function of the power dissipation with an order of -0.5,-0.486 and -0.453 for SDRs, SBR and NCRs respectively. The order value for the NCRs is similar to the value that Falk and Commenge (2010) achieved which was -0.5 for different designs of NCRs.

From both Figure 5.104 and Table 5.22, it is evident that the highest values of power dissipation corresponding to the lowest values of mixing time have been achieved by the SDRs. Achieving high power dissipation and lower mixing times are dependent on the total flowrate and disc rotational speed. The worst case of micromixing efficiency was achieved by using NCRs whilst intermediate performance was achieved in the SBR. It is noted that, for the same value of the power dissipation, the theoretical micromixing time remains largely lower in the SDRs than the semi-batch reactor (SBR) and narrow channel reactor (NCRs). This confirms that the micromixing efficiency in SDRs at a given power dissipation is better than in SBR and NCRs.

Other criteria of comparative analysis of the micromixedness ratio, (α) is also carried out on the basis of the power dissipation. Figure 5.105 show the effect of power dissipation on the micromixedness ratio (α), for SBR, semi-batch reactor; 10 and 30cm SDR, spinning disc reactor, NCR'S; narrow channel reactors - water system with $[H^+]$=1.0M.

From Figures 5.104 and 5.105, under optimised conditions in the 10 cm SDR corresponding to a rotational speed of 2400 rpm, 1.0 M acid ion concentration and total flowrate of 5.0 ml/s, the micromixing time (t_m), power dissipation (ε) in the film on the disc and micromixedness ratio (α) were estimated to be about 0.25 ms, and 1392 W/kg and 16.9 respectively. Using 30 cm SDR with disc rotational speed of 1200 rpm and total flowrate of 15 ml/s, the corresponding values for t_m, ε, and α were estimated to be about 0.3 ms, and 1025 W/kg and 19.0 respectively. At the mentioned operating conditions, it is clear that the 30 cm SDR performs better than the 10 cm SDR as a result of a larger disc surface area available within the 30cm SDR comparing with the surface area of 10 cm SDR. Consequently, more surface disc is available for contacting with the reactants. The larger the disc available, the longer the residence time for the reactants on the disc surface and thus higher the chance of micromixing process to occur. Alternatively, using a semi-batch Reactor (SBR) with an impeller rotational speed of 1200 rpm and acid concentration of 1.0 M injected close to the impeller, the micromixing time(t_m) was 4.0 ms, the power dissipation (ε) equalled only 21 W/kg and micromixedness ratio (α) was 7. On the other hand, using 15 cm Y junction narrow channel reactor (NCR) with total flow rate of 2 ml/s and acid concentration of 1.0 M,

the micromixing time(t_m) was 19.1 ms, the power dissipation (ε) equalled 207.506 W/kg and micromixedness ratio (α) was 15.21.

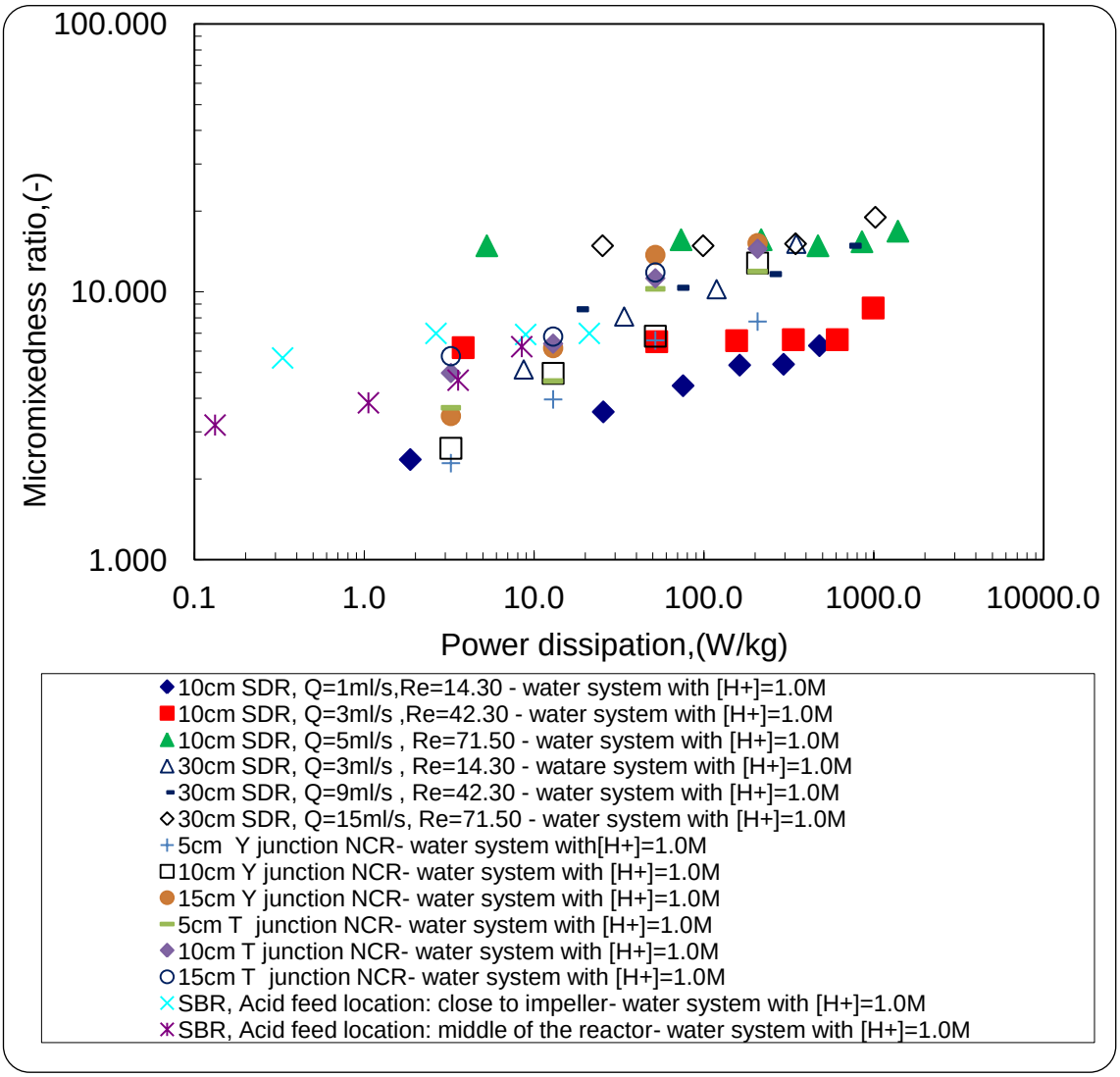

Figure 5.105: Effect of power dissipation on the micromixedness ratio ,(α), for SBR, semibach reactor; 10 and 30 cm SDRs-smooth discs, spinning disc reactor, NCRs; narrow channel reactors – water system with [H+]=1.0 M

Table 5.23 shows the performance of the 10 cm SDR, 30 cm SDR, SBR and NCRS in order from the highest to lowest using water system with acid ion concentration of 1.0 M and its micromixedness ratio correlations as function of power dissipation correlations. From Table 5.23 there some conclusions can be drawn, firstly, at a given power dissipation, the highest performance has been achieved by the SDRs particularly at higher total flowrates. Secondary, the SBR was the second performed reactor in terms of the intensity of the mixing when the acid ejection was close to impeller. The worst micromixing performance was achieved by the NCRs particularly for Y junction type with the 5cm length. In general, the NCRs did not show good performance when

compared with the other two types of reactors as their power range was small compared with the power dissipation range for the other two reactors.

Table 5.23: the performance of the reactors in order from the highest to lowest at the acid ion concentration of 1.0 M and its micromixedness ratio correlations as function of power dissipation correlations

Order NO.	Reactor type	Operating condition	Correlation	R^2
1	10 cm SDR-smooth disc	Q=5 ml/s, N=300 rpm-2400 rpm	$\alpha = 14.56\ \varepsilon^{0.0124}$	0.300
2	30 cm SDR-smooth disc	Q=15 ml/s ,N=300 rpm-1200 rpm	$\alpha = 11.745\ \varepsilon^{0.0585}$	0.607
3	SBR	acid feed location: close to impeller, N=300-1200 rpm	$\alpha = 6.2086\ \varepsilon^{0.0508}$	0.771
4	30 cm SDR-smooth disc	Q=9 ml/s, N=300-1200 rpm	$\alpha = 5.653\ \varepsilon^{0.1412}$	0.972
5	10 cm SDR	Q=3 ml/s, N=300-2400 rpm	$\alpha = 5.6492\ \varepsilon^{0.0387}$	0.419
6	NCR	T junction- 15 cm length, Qt=0.25-2 ml/s	$\alpha = 3.9803\ \varepsilon^{0.2595}$	0.933
7	SBR	acid feed location: middle of the reactor, N=300-1200 rpm	$\alpha = 4.1187\ \varepsilon^{0.1527}$	0.914
8	NCR	T junction- 10 cm length, Qt=0.25-2 ml/s	$\alpha = 3.507\ \varepsilon^{0.2717}$	0.974
9	30 cm SDR-smooth disc	Q=3 ml/s, ,N=300 rpm-1200 rpm	$\alpha = 2.8401\ \varepsilon^{0.2813}$	0.990
10	NCR	Y junction- 15 cm length, Qt=0.25-2 ml/s	$\alpha = 2.3743\ \varepsilon^{0.3793}$	0.932
11	NCR	T junction- 5 cm length, Qt=0.25-2 ml/s	$\alpha = 2.463\ \varepsilon^{0.3107}$	0.926
12	10 cm SDR-smooth disc	Q=1 ml/s, N=300 rpm-2400 rpm	$\alpha = 2.0958\ \varepsilon^{0.1743}$	0.990
13	NCR	Y junction- 10 cm length, Qt=0.25-2 ml/s	$\alpha = 1.7528\ \varepsilon^{0.3677}$	0.985
14	NCR	Y junction- 5 cm length, Qt=0.25-2 ml/s	$\alpha = 1.7528\ \varepsilon^{0.3677}$	0.954

It is worth comparing the micromixing efficiency of spinning disc reactors with the other intensified reactors. (Rousseaux et al., 1999), (Chu et al., 2007) and (Nouri et al., 2008) have characterised the micromixing efficiency in a novel sliding-surface mixing device (S-S-M), a rotor–stator reactor (R-S-R) and torus reactor(T-R) respectively, by use of iodide-iodate reaction test. The reactants concentrations including the acid ions concentration were similar to the concentration of the reactants used in this work. The local energy dissipation rate was correlated in the S-S-M, , the R-S-R and the T-R as shown in equations 5.28, 5.29 and 5.30 respectively:

$$\alpha = 3.3\varepsilon^{0.2} \quad (5.28)$$

$$\alpha = 0.0794\varepsilon^{0.498} \quad (5.29)$$

$$\alpha = 5.1\varepsilon^{0.236} \quad (5.30)$$

Comparing with the correlations for the 10 cm SDR and 30 cm SDR with the total flowrate of 5 ml/sec and 15 ml/s respectively (as shown in Table 5.23), it can be noted that for the same value of power dissipation, (ε), the micromixedness ratio in the spinning disc reactors remains largely higher than in the sliding-surface mixing device, the rotor–stator reactor and torus reactor. Table 5.24 shows the values of the micromixedness ratio at the power dissipation, (ε), of 1 W/kg using equations in Table 5.23 and equations 5.28 to 5.30. The results from Table 5.24 clearly show that the 10 and 30 cm SDR give significantly better micromixing performance which highlights its potential as an alternative device for processes where a high degree of mixing is critically important.

Table 5.24: The performance of the reactors in order from the highest to lowest at the acid ion concentration of 1.0 M and its micromixedness ratio correlations as function of power dissipation correlations

Reactor type and reactor speed	Total flowrate, Qt	micromixedness ratio,α (-)
10 cm spinning disc reactor,(SDR) with Rotating disc speed ranged of 300-2400 rpm	1 ml/s	2.096
	3 ml/s	5.649
	5 ml/s	14.560
30 cm spinning disc reactor,(SDR) with Rotating disc speed ranged of 300-1200 rpm	3 ml/s	2.840
	9 ml/s	5.653
	15 ml/s	11.745
Sliding-surface mixing device, (S-S-M) with Rotating disk speed up to 50 rps	Recirculation flow rate up to 500 ml/min	3.3
Rotor–stator reactor,(R-S-R) with reactor speed ranged of 300-2400 rpm	Total flowrate of 340 l/h	0.079
torus reactor(T-R) with Stirring speed ranged of 100 -1300 rpm	N/A	5.1

5.5.2 50% water/50% glycerol system

The reactor comparison also has been performed using 50wt% glycerol system corresponding to viscosity of $6.0x10^{-3}$ Pa.s. From Figure 5.106 and Table 5.25, the theoretical mixing time for each reactor type is influenced by the power dissipation into the fluid, according to a power-law correlation similar to the one observed previously for the water system.

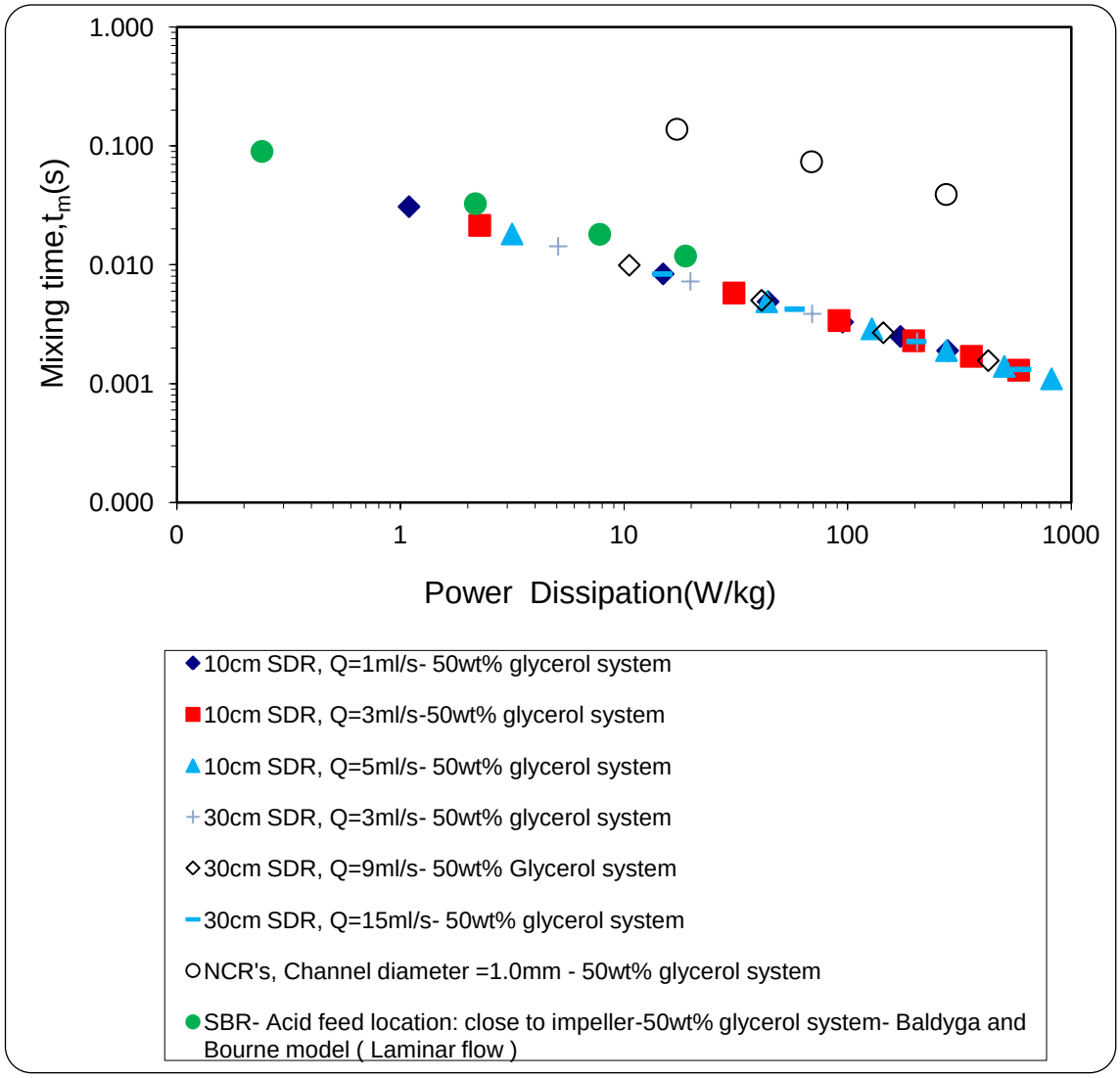

Figure 5.106: Evolution of the mixing time, (tm), versus the power dissipation for SBR, semibach reactor; 10 and 30 cm SDRs-smooth discs, spinning disc reactor, NCR's; narrow channel reactors – 50wt% glycerol system

Table 5.25: Shows the correlations for theoretical mixing time with respect to the power dissipation for SDRs-smooth discs, SBR and NCR in order of from the lowest to the highest mixing time for 50wt% glycerol system

Reactor type	Correlation	R^2
10 cm and 30 cm SDRs	$t_m = 0.033\ \varepsilon^{-0.5}$	0.99
SBR : acid feed location close to impeller	$t_m = 0.0467\ \varepsilon^{-0.464}$	0.99
NCR's	$t_m = 0.5097\ \varepsilon^{-0.456}$	1

From both Figure 5.106 and Table 5.25 and similar to the water system experiments results, it is clear that the highest values of power dissipation corresponding to the lowest values of mixing time have been achieved by both SDRs. It is again evident from these data that the lowest micromixing efficiency was achieved by NCRs, as observed with the water system.

At a given value of power dissipation, the theoretical micromixing time still remains largely lower in the SDRs than the other two types of reactors. Figure 5.107 show the effect of power dissipation on the micromixedness ratio, (α), for SBR, Semibatch reactor; 10 and 30 cm SDR, spinning disc reactor, NCR'S; narrow channel reactors – 50wt% glycerol system with $[H^+]$=1.0M. From Figures 5.105 and 5.106 with considering the optimised conditions in the 10cm SDR corresponding to a rotational speed of 2400 rpm, 1.0M acid ion concentration and total flowrate of 5.0 ml/s, the micromixing time(t_m), Power dissipation (ε) of the film on the disc and micromixedness ratio (α) were estimated to be about 1.1ms, and 818 W/kg and 5.2 respectively. Using 30 cm SDR with disc rotational speed of 1200 rpm and total flowrate of 15 ml/s, the corresponding values for t_m, ε and α were estimated to be about 1.3 ms, and 599 W/kg and 3.8 respectively. similar observations with regarding to the t_m, ε and α of the SDRs using water system as highlighted in Figures 5.104 and 5.105 were obtained in Figures 5.106 and 5.107. Even with using 50wt%.

Instead, using a semi-batch reactor (SBR) with an impeller rotational speed of 1200rpm and acid concentration of 1.0 M injected close to the impeller, the micromixing time(t_m) was 12.0 ms, the power dissipation (ε) equalled only 19 W/kg and micromixedness ratio (α) was 6.752. On the other hand, using 15 cm Y junction narrow channel reactor (NCR) with total flow rate of 1ml/s and acid concentration of 1.0 M, the micromixing

time(t_m) was 39.1 ms, the power dissipation (ε) equalled 276.3 W/kg and micromixedness ratio (α) was 4.85.

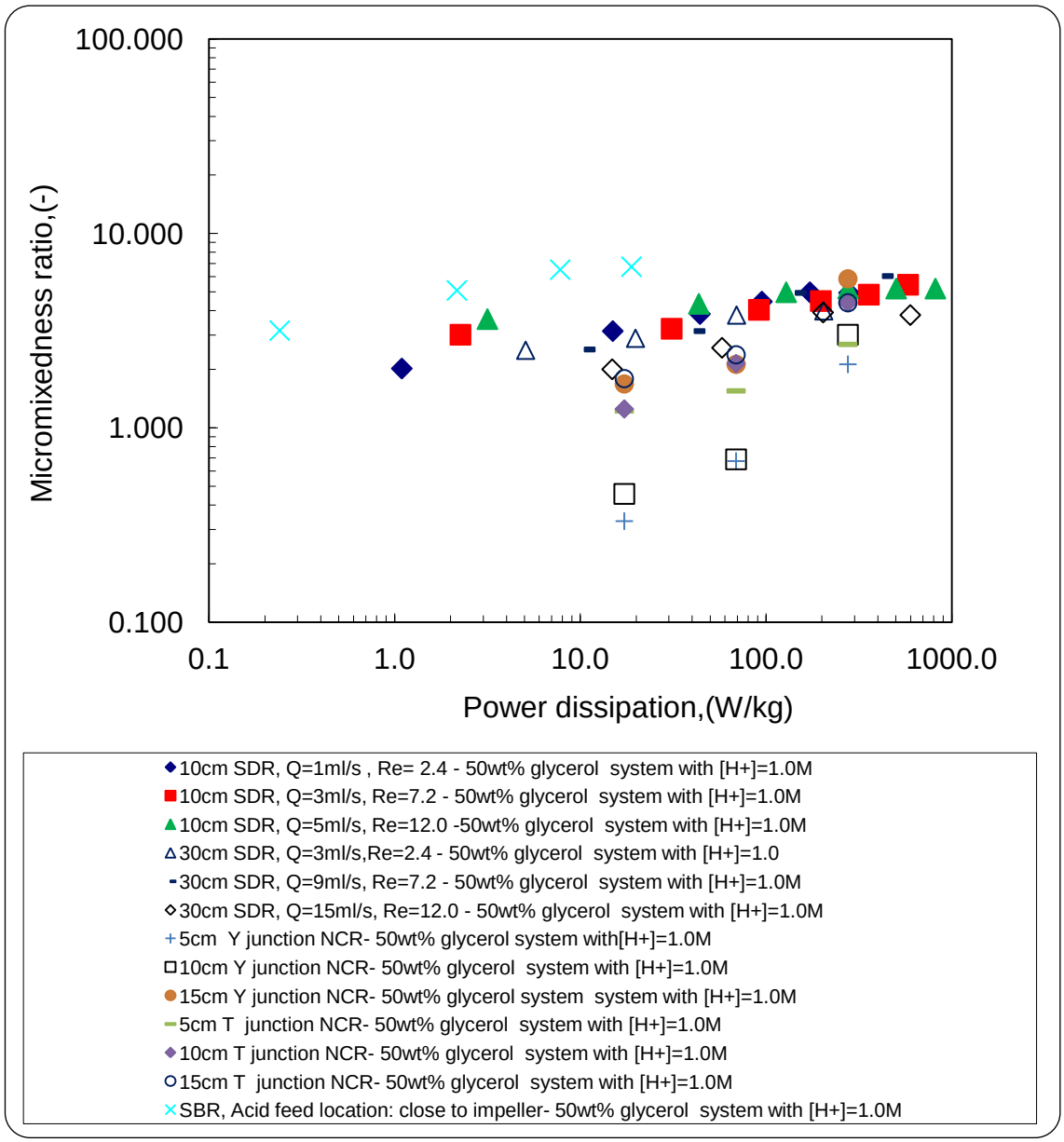

Figure 5.107: Effect of power dissipation on the micromixedness ratio ,(α), for SBR, semibach reactor; 10 and 30 cm SDRs-smooth discs, spinning disc reactor, NCR'S; narrow channel reactors – 50wt% glycerol system with [H+]=1.0 M

Table 5.26 shows the performance of the 10 SDR, 30cm SDR, SBR and NCR'S in order from the highest to lowest using 50 wt% glycerol system with acid ion concentration of 1.0 M and its micromixedness ratio correlations as function of power dissipation. From the correlations shown in Table 5.26, it is clear that the 10 and 30 cm SDRs show less mixing performance that the SBR with injecting the acid close to the impeller. The

NCR's shows the lowest mixing performance comparing with the SDR's and SBR. Although the SDRs shows better mixing performance in terms of mixing time as shown in Table 5.25, the SDRs fails to show high mixing intensity in terms of micromixedness ratio when the 50 wt% glycerol was used. Viscous materials are usually harder to mix in the reactors and consequentially require longer resentence time in the reactors to reach a high degree of mixing. Obviously the reactants have shorter resentence time in SDRs comparing with the ones in the SBR. The resentence time of the reactants in SBR is in the range of 22.2 min - 5.6 min, on the other hand the resentence time of the reactants in SDR is in the range of (0.1-2.0 s) it depends on the disc size, disc rotational speed and the total flowrate. It is clearly the reactants resentence time in SBR is much longer in the SDR and this will help the reactants to be longer in the mixing environment. Consequently, higher intensity of mixing may be achieved. Viscous materials would benefit from multi-pass SDRs (stacked Disc or series set ups) this would increase the reactants resentence time on the SDRs. Consequently, higher intensity of mixing may be achieved.

In this work when the 50 wt% glycerol was used, the Acid ions were injected to SBR by injection point close to impeller i.e. only 2.0 mm away from the edge of the impeller tip and this is an ideal situation. Usually in the industry the injection points are typically near the top of the vessel as it is favoured because of its convenience. In this work, if the micromixing intensity comparison between SDRs and SBR using injection point located in middle of reactor or higher which is not available, possibly the SDRs will show better micromixing performance than the SBR.

As will be recommended in this work, it would be important to estimate the micromixing in the SDRs by determination of the micromixing time and theoretical segregation index by using a simple mixing model, i.e., the incorporation model (Fournier et al., 1996b) which describes the coupling between mixing and chemical reaction in order to obtain the best agreement between theoretical predictions and experimental data over a wide range of operating conditions which was adopted in this research.

Table 5.26: The performance of the reactors in order from the highest to lowest using acid ion concentration of 1.0 M and 50 wt% glycerol system

Order NO.	Reactor type	Operating condition	Correlation
1	SBR	acid feed location: close to impeller	$\alpha = 4.0476\ \varepsilon^{0.1904}$
2	10 cm SDR-smooth discs	Q=5 ml/s	$\alpha = 3.387\ \varepsilon^{0.0705}$
3	10 cm SDR-smooth disc	Q=3 ml/s	$\alpha = 2.5549\ \varepsilon^{0.1075}$
4	10 cm SDR-smooth disc	Q=1 ml/s	$\alpha = 2.0036\ \varepsilon^{0.1703}$
5	30 cm SDR-smooth disc	Q=3 ml/s	$\alpha = 1.9996\ \varepsilon^{0.1363}$
6	30 cm SDR-smooth disc	Q=9 ml/s	$\alpha = 1.3631\ \varepsilon^{0.2476}$
7	30 cm SDR smooth disc	Q=15 ml/s	$\alpha = 1.22\ \varepsilon^{0.1924}$
8	NCR	T junction- 15 cm length	$\alpha = 0.6736\ \varepsilon^{0.3242}$
9	NCR	T junction- 10 cm length	$\alpha = 0.5158\ \varepsilon^{0.2845}$
10	NCR	Y junction- 15 cm length	$\alpha = 0.4111\ \varepsilon^{0.4491}$
11	NCR	T junction- 5 cm length	$\alpha = 0.3283\ \varepsilon^{0.4585}$
12	NCR	Y junction- 10 cm length	$\alpha = 0.0552\ \varepsilon^{0.68}$
13	NCR	Y junction- 5 cm length	$\alpha = 0.0457\ \varepsilon^{0.67}$

Currently there is no data available in the literature with regards to the intensified reactors using high viscosity systems. So at the moment the comparison of the micromixing efficiency of spinning disc reactors with the other intensified reactors is not possible.

6. Experimental Results and Discussion: Residence time Distribution (RTD) Studies

The main objectives of this part of research project is to predict experimentally the conditions under which the flow of the thin film on the 30 cm rotating disc approaches either a plug flow or a backmixed profile. These objectives could be achieved by implementing the Residence Time Distribution (RTD) concept. The variance and mean residence time were used to calculate the dispersion number of the fluid in the spinning disc reactor under different operating conditions. As mentioned in Chapter 2, the significance of the dispersion number is that it characterizes the degree of back mixing during flow. If the dispersion number approaches zero, backmixing is considered to be negligible and the behaviour of the reactor approaches that of a plug-flow reactor, (PFR). If the dispersion number approaches infinity, there is a large degree of dispersion, and the behaviour of the reactor approaches mixed flow as in a stirred tank reactor (STR).

Determination of the mean residence time (t_{mean}) and variance (square of the standard deviation, σ^2) by the method of moments are implemented for analysing the RTD curves that are obtained from the step injection technique, following the method presented in the existing chemical engineering literature (Fogler, 2006; Levenspiel, 1999). The effects of disc rotational speed, the total flow rate, fluid viscosity, and the use of smooth and grooved discs on the RTD curves have been examined.

The values of the residence time distribution E (t) and the mean residence time, (t_{mean}), as defined by the integrals in equations (2.50) and (2.56), were evaluated numerically using techniques such as the Simpson's rule in the case of even number of samples and the trapezoidol rule in the case of an odd numbers of samples (Interactive Mathematics, 2009; Fogler, 1992) . It should be emphasised that the time interval (Δt) between each sample collected should be the same for the above rules to apply. In the present work, the time interval (Δt) is ten seconds.

The experimental programme produced a large number of concentration curves, the cumulative distribution curves F(t), the residence time distribution curves E (t). This

Chapter will focus on the residence time distribution curves E (t) for 30cm smooth and grooved disc using water and 50wt% water -50 wt% glycerol system.

6.1 Experimental design

Randomized general full factorial experimental designs DOE for both water and 50wt% Glycerol systems were performed using Minitab 15 (Table AL1, appendix L) For the residence time distribution experiments in 30 cm SDR, the variables incorporated into the experimental design were:

- Disc rotational speed, N: 300 rpm, 500 rpm, 800 rpm and 1200 rpm (A disc speed of 1200 rpm was the maximum speed at which the reactor could be safely operated)
- Total flowrate, Qt: 3, 6, 9 and 15 ml/s;
- Working fluid: water and 50 wt% Glycerol systems;
- Disc surface: stainless steel smooth disc and grooved disc.

The total number of experiments carried out in this part of the research were sixty four experiments i.e. sixteen experiments for each system (water and 50wt % Glycerol system) using two different types of discs (Stainless steel smooth disc and Grooved disc).

6.2 Methylene blue spectra and molar extinction coefficient, (ε_λ), measurements

The molar extinction coefficient, (ε_λ), was determined by measuring the absorbance of different samples of methylene blue of known concentration. A calibration curve of absorbance vs. concentration enabled the value of the molar extinction coefficient to be calculated.

According to the spectra of methylene blue for all the measured samples, the peak of interest was observed at wavelength (λ_{max}) in the range 662.7-664.8 nm for both water and 50 wt% glycerol liquid media. These findings were in agreement with spectral data of methylene blue obtained from the literature (Genina et al., 2008;

Khalid, 2001; Gorman and Shnider, 1988). Figures 6.1 and 6.2 show the spectra of methylene blue in water and 50wt% glycerol/water system respectively.

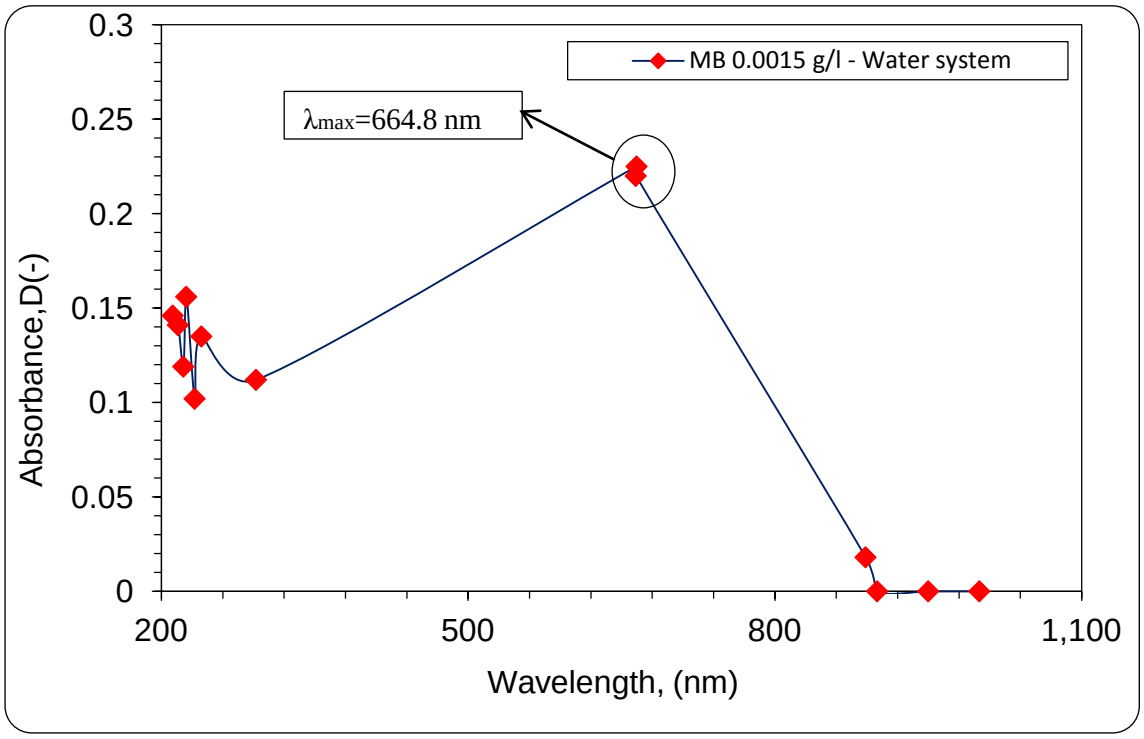

Figure 6.1: Absorbance spectra of methylene blue in water system using a single-beam spectrophotometer (UNICAM UV- PU8750)

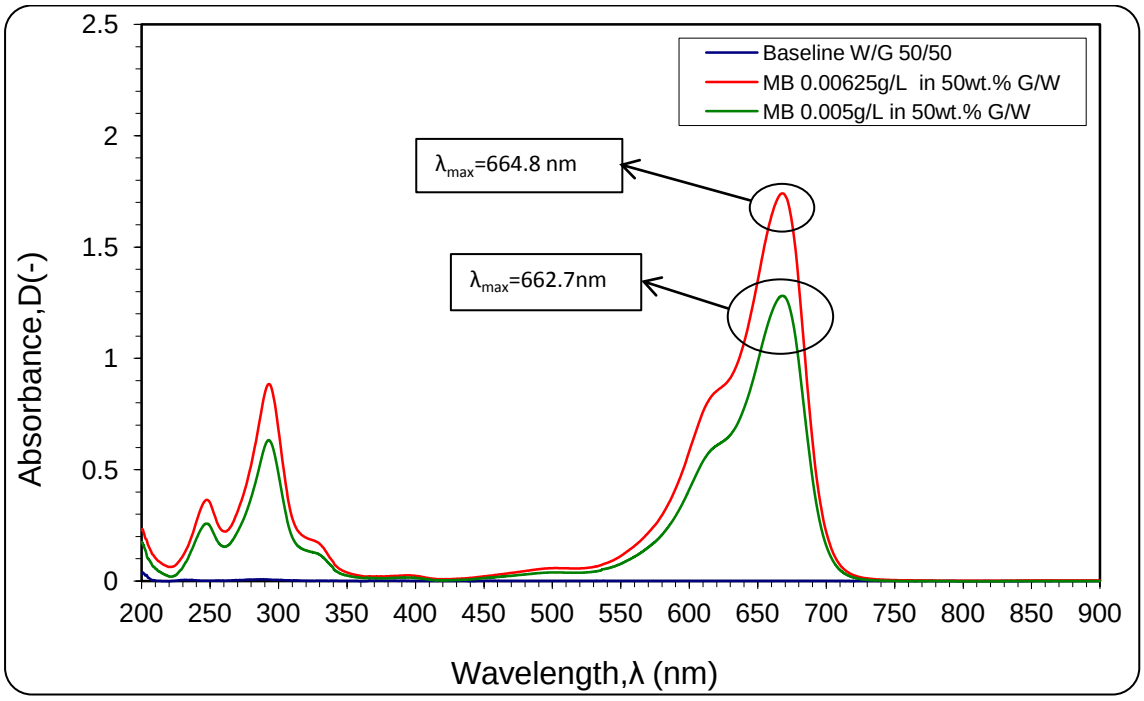

Figure 6.2: Absorbance spectra at different concentration of methylene blue in 50wt% glycerol/water system using a single-beam spectrophotometer (shimadsu UV- mini 1240)

Figure 6.3 shows the calibration plots for water and water/glycerol (50 wt% of component) obtained with a single-beam spectrophotometer of type (PU8750-UNICAM). The straight lines obtained confirm the validity of the Beer- Lambert law at the methylene blue concentrations used. The slope of the linear calibration profile is used in the calculation of the molar extinction coefficient, (ε_λ) as follows:

$$\varepsilon_{\lambda\,(\text{m.b water system})} = \frac{\text{slope}}{\text{cell length}} = \frac{63379\ (\text{l/mol})}{1\text{cm}} = 63379\ \frac{\text{l}}{\text{mol.cm}}$$

$$\varepsilon_{\lambda\,(\text{m.b 50wt\% glycerol system})} = \frac{\text{slope}}{\text{cell length}} = \frac{73609\ (\text{l/mol})}{1\text{cm}} = 73609\ \frac{\text{l}}{\text{mol.cm}}$$

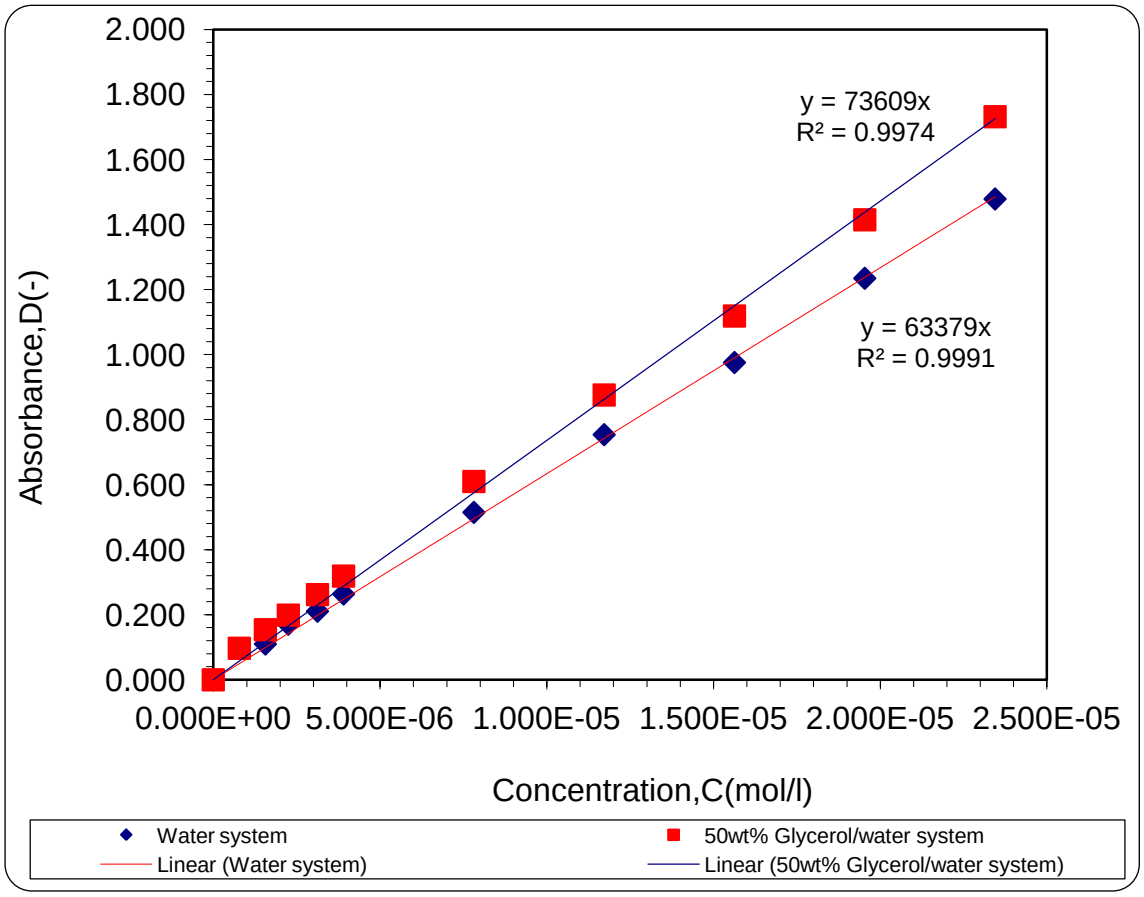

Figure 6.3: Calibration plot for the determination of molal absorption coefficient for methylene blue - water and 50wt% glycerol systems

6.3 Kinetics measurements of methylene blue / 50wt% glycerol-water mixture

As mentioned in Chapter 2, one of characteristics that the selection of tracer should be based on is that the tracer should not be reactive species with the working fluid, here in our case the methylene blue should not react with water or glycerol. To ensure this criterion is satisfied in our system, a kinetic test has been implemented on the 0.005 g/l of methylene blue in 50 wt% glycerol-water system, in terms of absorbance changes with time. The test has been run for 900 s at wavelengths of 664.8 nm with 0.1 ml of 0.05 g/l methylene blue added to 2 ml of 50 wt% glycerol-water system. Figure 6.4 show the absorbance values for the methylene blue in 50 wt% glycerol-water system within 15 min at wavelength of 664.8 nm. The plot was generated using a single-beam spectrophotometer (shimadsu UV- mini 1240). From Figure 6.4 it is clear that there is no change in the absorbance values and therefore concentration with time. Therefore, there is no reaction occurring between the tracer and the components in the liquid medium, confirming that methylene blue is a suiTable tracer for the liquid media used in this study.

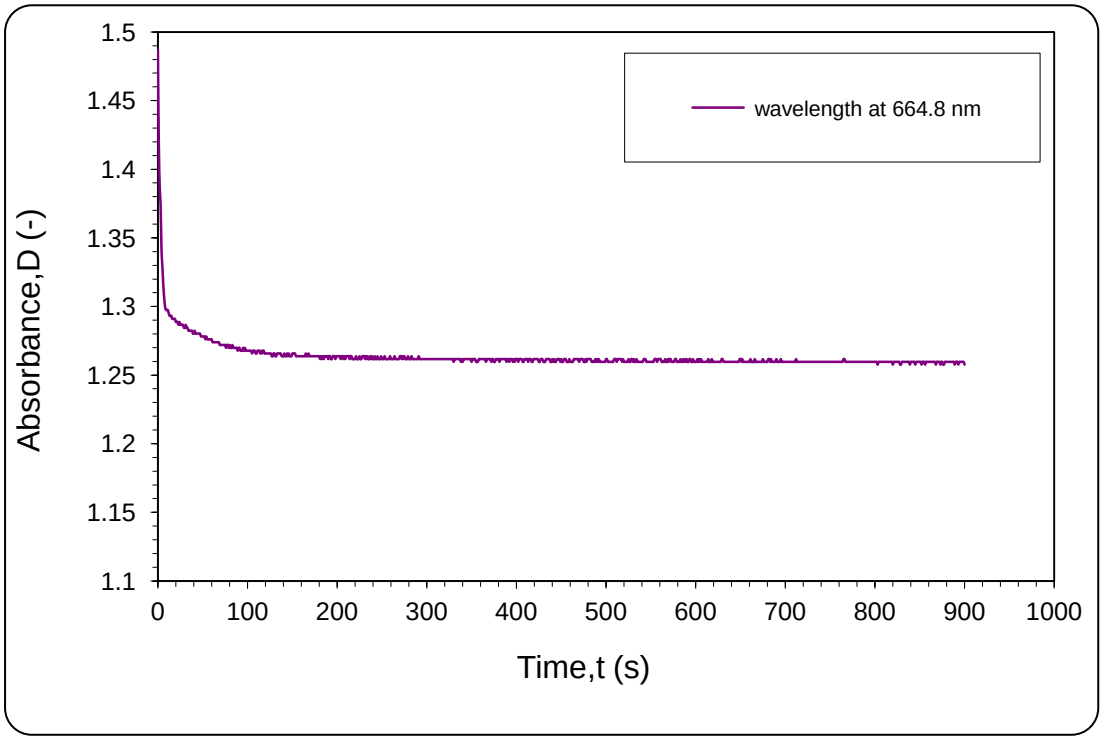

Figure 6.4: UV-Vis spectrophotometer Kinetics test at the wavelengths of 664.8nm for 0.005 g/l of methylene blue in 50 wt% glycerol-water system

6.4 Construction of Concentration C(t), Cumulative function F(t), and residence time distribution function E(t) curves

In order to construct the residence time distribution function E(t) curves using a step input technique for the SDR at different operating conditions, three steps are typically followed:

I. The outlet concentration is measured in terms of absorbance for the methylene blue/water or water-glycerol mixture flowing off the edge of the SDR surface. The measurements were taken from time, t = 0, until a constant reading is obtained i.e. steady state. In this work twelve samples were collected from the bottom of the shoe collector every ten seconds and absorbance were measured. The absorbance values allowed us to determine the concentration of methylene blue sample at a given time. The samples concentration were measured by using UV/VIS spectrophotometer based upon the Beer-Lambert absorption law as follows:

$$D_\lambda = C\, \varepsilon_\lambda\, l \tag{6.1}$$

$$C = \frac{D_\lambda}{\varepsilon l} \tag{6.2}$$

Where:

D_λ = absorbance, (-)

C = concentration, (mol/l)

l = cell length, (0.1cm)

ε_λ = the molar extinction coefficient, (= 63379 l/mol cm)

II. The second step involves calculating the cumulative function F (t); this is done by dividing the sample concentration at a given time (C_{out}) by the known inlet sample concentration (C_0), the latter being equivalent to the final steady-state concentration at the end of the step-input test. This yields the cumulative function (equation 2.50).

III. The third step is differentiate the F(t) to obtain the RTD function E(t) (equation 2.51).

Example calculations for C (t), F (t) and E (t):

A sample of computed results for the cumulative function *F (t)* and the residence time distribution function *E (t)* are displayed in Table (6.1) for the 30 cm smooth disc with water system, Qt=3 ml/s and N=300 rpm. The concentration C(t) for each sample collected is first determined from the corresponding absorbance value using equation (6.2):

$$C = \frac{D_\lambda}{\varepsilon l} \qquad (6.3)$$

Using the absorbance of 0.112 for sample 1 as an example, the concentration is calculated as:

$$C = \frac{0.112}{63379 * 0.1} = 1.767 * 10^{-5}\ mol/l$$

Similarly the final steady state concentration (C_0) is computed as 3.661x10^{-5} mol/l, based on an absorbance value of 0.232.The cumulative function F (t) value for sample 1 can then be calculated from equation (2.50):

$$F(t) = \left[\frac{C_{out}}{C_0}\right]_{Step} = \frac{1.767 * 10^{-5}}{3.661 * 10^{-5}} = 0.483$$

Finally, the RTD can be calculated from equation (2.51):

$$E(t) = \frac{d}{dt}\left[\frac{C(t)}{C_0}\right]_{step} = \frac{dF}{dt} = \frac{F(t)_2 - F(t)_1}{t_2 - t_1} = \frac{0.483 - 0}{10 - 0} = 4.83 * 10^{-2}\ s^{-1}$$

Table 6.1: Calculating the cumulative function F (t), the residence time distribution function E (t) for the 30 cm using smooth disc with water system, Qt=3 ml/s and N=300 rpm

Sample no.	Time t(sec)	absorbance D(-)	Concentration C(mol /l)	$F(t) = [Ct/C_0]$	$E(t)=d/dt\ [Ct/C_0]_{step}$
0	0	0.000	0.000E+00	0.000	0.0000E+00
1	10	0.112	1.767E-05	0.483	4.8270E-02
2	20	0.200	3.156E-05	0.862	3.7926E-02
3	30	0.215	3.392E-05	0.927	6.4647E-03
4	40	0.225	3.550E-05	0.970	4.3098E-03
5	50	0.231	3.645E-05	0.996	2.5859E-03
6	60	0.232	3.661E-05	1.000	4.3098E-04
7	70	0.232	3.661E-05	1.000	0.0000E+00
8	80	0.232	3.661E-05	1.000	0.0000E+00
9	90	0.232	3.661E-05	1.000	0.0000E+00
10	100	0.232	3.661E-05	1.000	0.0000E+00
11	110	0.232	3.661E-05	1.000	0.0000E+00
12	120	0.232	3.661E-05	1.000	0.0000E+00

By plotting the concentration values (C) as function of time, using the data in Table (6.1), the curve shown in Figure (6.5) is obtained. Figure (6.6) and Figure (6.7) are the Cumulative distribution curve F(t) and the RTD function E(t) respectively.

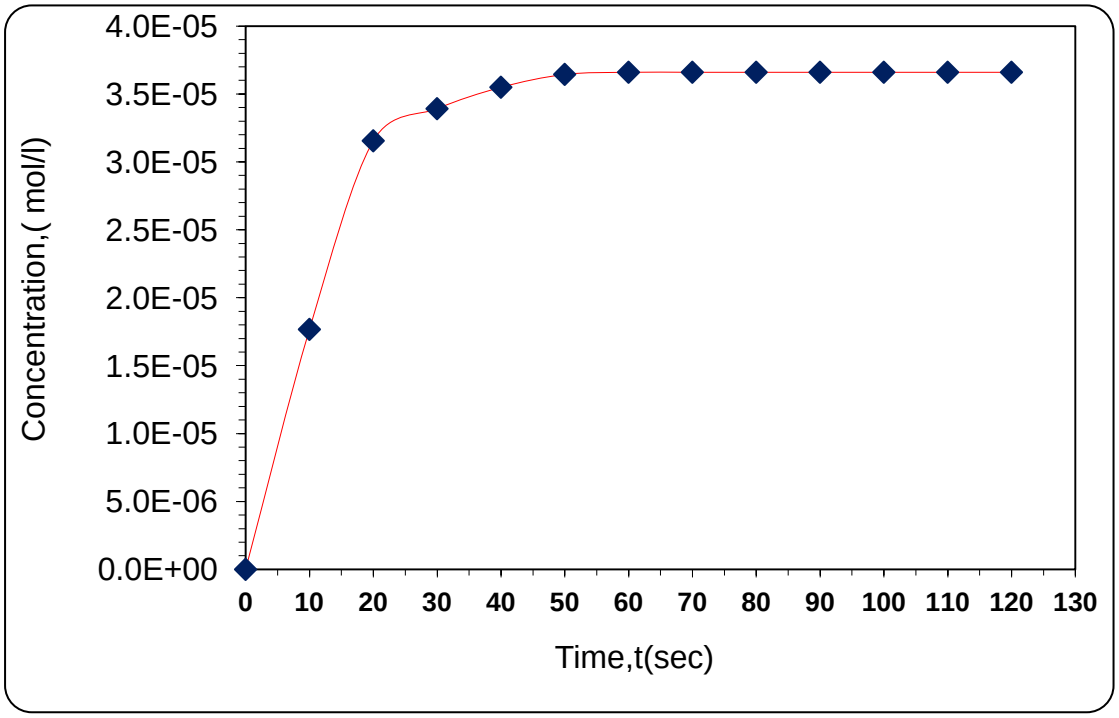

Figure 6.5: The concentration curve for 30cm SDR using smooth disc with water system, Qt=3 ml/s, N=300 rpm

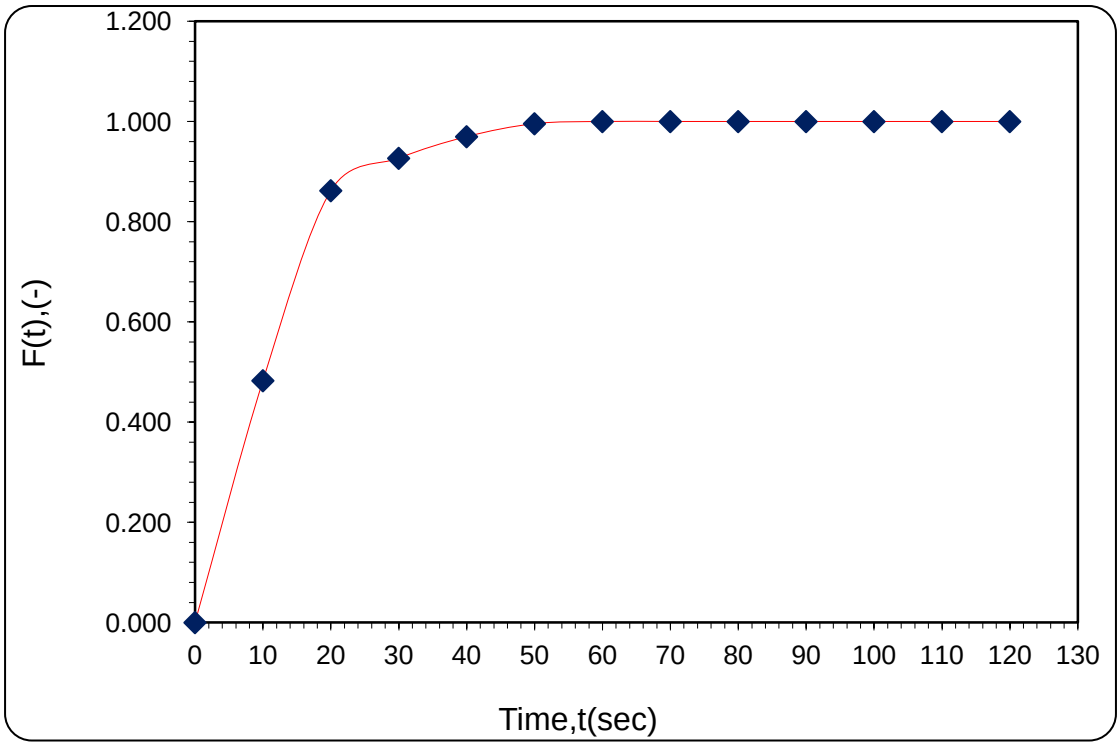

Figure 6.6: The cumulative distribution curve, F (t) for 30 cm SDR using smooth disc with water system, Qt=3 ml/s, N=300 rpm

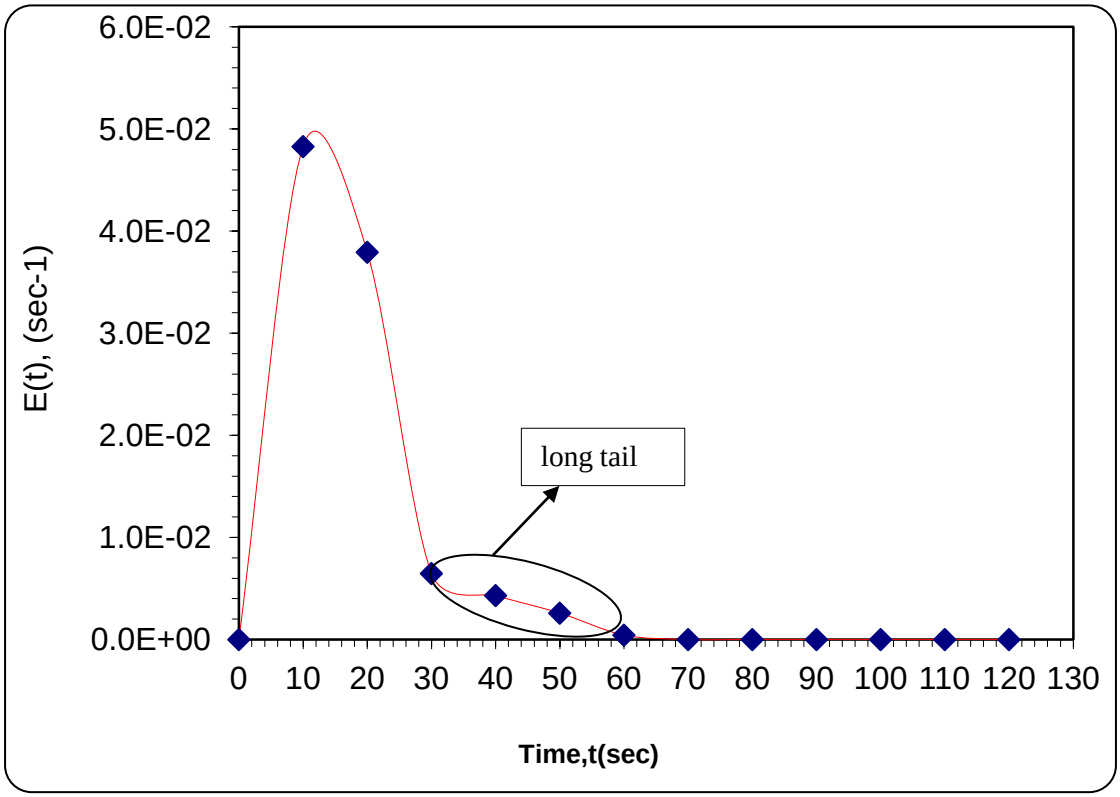

Figure 6.7: Calculating the residence time distribution function, E(t) for 30 cm SDR using smooth disc with water system, Qt=3 ml/s, N=300 rpm

One important point needs to be mentioned about Figure 6.6; it is well known that for systems approaching plug flow behaviour, an S-shaped curve is usually expected. If we had more data points at time intervals between 0 and 10 s and even 10 and 20 s, it may have seen this S-shape. In the present work, due to the limitation of the system measurement, the maximum time interval (Δt) between each sample collected was ten seconds.

Other important issue was noticed in Figure 6.7, a long tail appeared within the E (t) curve at the Qt=3 and N=300 rpm. Usually the long tail indicative of stagnant backwaters existing on the disc (Levenspiel, 1999). This abnormal behaviour negatively affects the intensity of mixing on the SDR disc surface. This kind of behaviour disappeared at the higher disc rotational speed and high flowrates i.e. N=1200 rpm and Qt=15 ml/s (Figure 6.13). From Figure 6.7, the tail is that portion of curve between 30-60 s.

6.5 Mean residence Time and Variance calculations

Other important values needed to be calculated are the first and the second moments of the RTD, namely is the experimental mean residence time (Exp. t_{mean}) and the Variance, or square of the standard deviation. The variance characterizes the width of the distribution of the RTD function and its spread around the average. The RTD of ideal plug flow reactors has a variance of zero. Real reactors, on the other hand, always show a deviation from ideal plug flow behaviour due to the axial dispersion, resulting in value of variance (σ^2) > 0.0. However, the smaller the value variance (σ^2), the narrower is the RTD and the lower is the axial dispersion.

The purpose for calculating theses two moments is to analyse and compare the RTDs produced by the 30cm SDR at different operating condition i.e. total flowrates, disc rotational speeds, disc configuration and feed viscosity. The mean residence time can be calculated as follows:

$$t_m = \int_0^\infty tE(t)dt \qquad (6.4)$$

The second moment of the RTD can be evaluated as follows:

$$\sigma^2 = \int_0^\infty (t - t_m)^2 E(t)dt \qquad (6.5)$$

To calculate the mean residence time (t_m) and the variance (σ^2), Table (6.3) was constructed from the data given and interpreted in Table (6.2). Using the data in Table (6.1), the tE(t), ($t-t_m$) and $(t-t_m)^2$ E(t) can be calculated as shown in Table (6.2)

Table 6.2: Calculating the experimental mean residence time (Exp. tm), the variance (σ2) for the 30cm using smooth disc with water system, Qt=3ml/s and N=300rpm

Run no.	t,(sec)	C,(mo l /l)	$E(t)=d/dt[Ct/C_0]_{step}$	t*E(t)	(t-tm)	$(t-tm)^2$	$(t-tm)^2$*E(t)
0	0	0.000E+00	0.0000E+00	0.000	-17.038	290.293	0.000
1	10	1.767E-05	4.8270E-02	0.483	-7.038	49.533	2.391
2	20	3.156E-05	3.7926E-02	0.759	2.962	8.773	0.333
3	30	3.392E-05	6.4647E-03	0.194	12.962	168.013	1.086
4	40	3.550E-05	4.3098E-03	0.172	22.962	527.253	2.272
5	50	3.645E-05	2.5859E-03	0.129	32.962	1086.493	2.810
6	60	3.661E-05	4.3098E-04	0.026	42.962	1845.733	0.795
7	70	3.661E-05	0.0000E+00	0.000	52.962	2804.973	0.000
8	80	3.661E-05	0.0000E+00	0.000	62.962	3964.213	0.000
9	90	3.661E-05	0.0000E+00	0.000	72.962	5323.453	0.000
10	100	3.661E-05	0.0000E+00	0.000	82.962	6882.693	0.000
11	110	3.661E-05	0.0000E+00	0.000	92.962	8641.933	0.000
12	120	3.661E-05	0.0000E+00	0.000	102.962	10601.173	0.000

Example for calculating t_m and σ^2, :

With adopting the data in Table (6.2), the mean residence time can be determined by using the Simpson's rule with even number of samples to evaluate the integral using the data in columns two and five as follows:

$$t_m = \int_0^\infty tE(t)dt = \frac{\Delta t}{3}(f_0 + 4f_1 + 2f_2 + 4f_3 + 2f_4 + 4f_5 + f_6)$$

$$= \frac{10}{3}[(1) * (0.00) + (4) * (0.483) + (2) * (0.759) + (4) * (0.194) +$$

$$2*0.172 + 4*0.129 + 1*0.026$$

$$= \underline{17.04 \text{ s}}$$

Where $f_0, f_1, \ldots . and f_6,$ are the values of t*E(t) for each sample number, the area under the curve of a plot of *tE(t)* as function of time (*t)* will also yield t_m as shown in Figure (6.8). The area under the curve should be approximately equal to the value obtained by Simpson's rule above.

It is to be noted that the value of the reactants mean residence time obtained by the RTD concept using step input injection method in this study is not, strictly speaking, the actual disc residence time. Rather, since the samples were collected not from the edge of the disc but from the bottom of the reactor through the sampling shoe, the value of 17.04 s represents the overall reactants residence time which is the time of the reactants residence time on the disc plus the time taken by the reactants to flow from the entrance of sampling shoe to the sampling collecting point at the bottom of the reactor.

Recalling equation 2.8 for the mean residence time of the reactants on the 30 cm SDR disc at the operating conditions of Qt=3 ml/s , N=300 rpm and water system, the value of exact mean residence was predicted to be only 1.2 s. Although it would have been better to collect samples right after the fluid comes off the discthis option was unfortunately not possible in this present work due to difficult mechanical modification issues. Nevertheless, in spite of the residence time measurements not being representative of the disc residence time, it is expected that residence time *distributions*

estimated in this study should not be significantly affected by the sample collection technique if steady flow of the stream to the outlet tube can be maintained.

By finding the mean residence time, the variance can be determined using the Simpson's rule with even number of samples to evaluate the integral using the data columns (two and seven) as following:

$$\sigma^2 = \int_0^\infty (t - t_m)^2 E(t) dt = \frac{\Delta t}{3}(f_0 + 4f_1 + 2f_2 + 4f_3 + 2f_4 + 4f_5 + f_6)$$

$$= \frac{10}{3}[(1) * (0.00) + (4) * (2.391) + (2) * (0.333) + (4) * (1.086) + (2) * (2.272) + (4) * (2.810) + (1) * (0.795)] = 103.8\ s^{-2}$$

As mentioned earlier in Chapter 2, the variance represents the spread of the distribution, the greater the value of this factor, the greater the distribution spread existing. The variance calculated above is an estimation of the area under the curve of a plot of $(t-t_m)^2E(t)$ as a function of time (t) as shown in Figure (6.9).

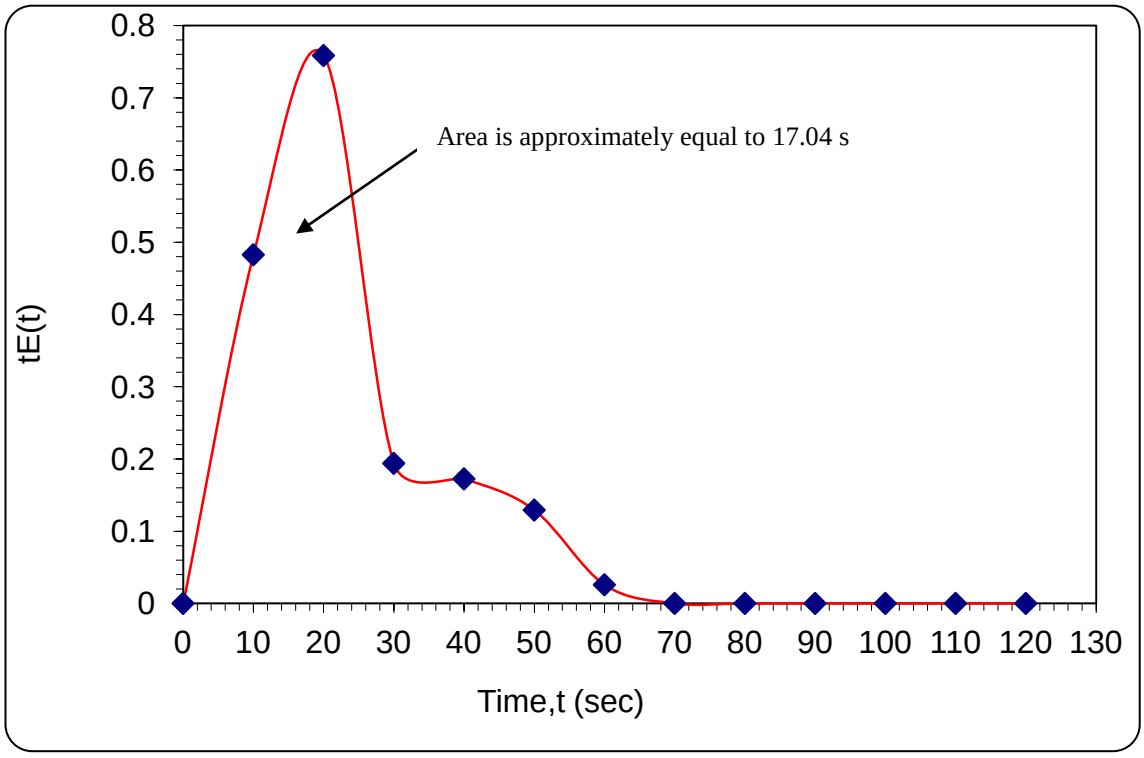

Figure 6.8: Graphical method for calculating the mean residence time for 30 cm SDR using smooth disc with water system, Qt=3 ml/s, N=300 rpm

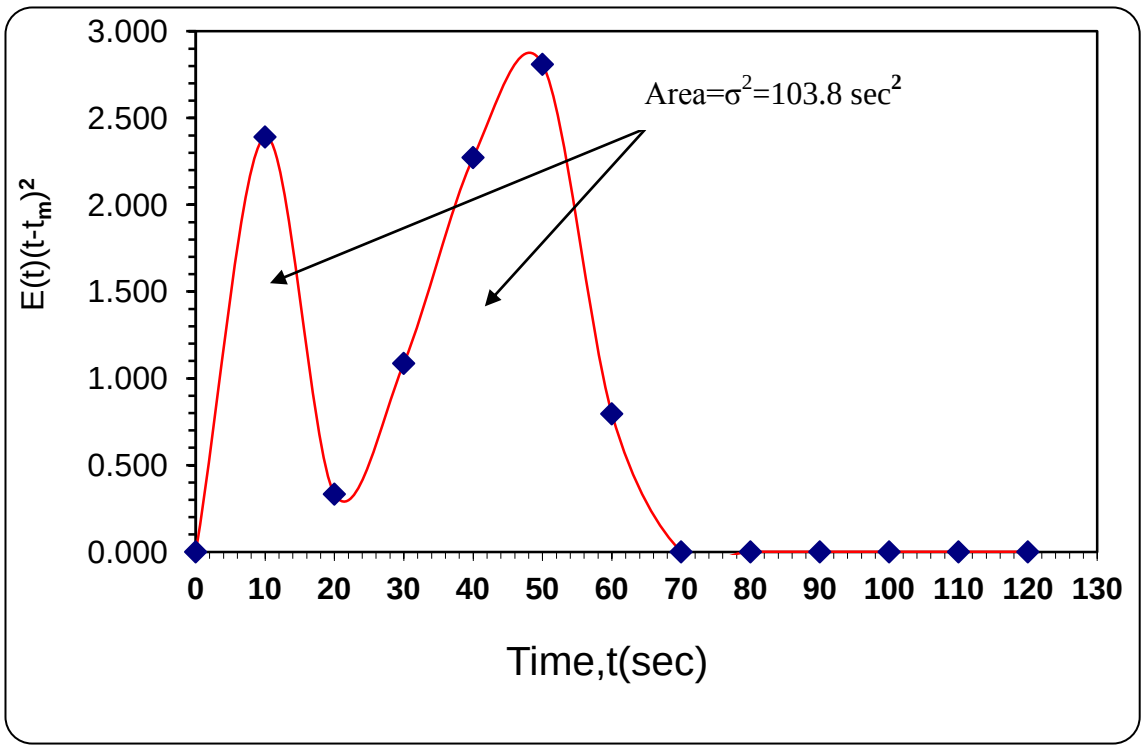

Figure 6.9: Graphical method for calculating the variance for 30 cm SDR using smooth disc with water system, Qt=3 ml/s, N=300 rpm

The above plots for F(t) and E(t) as well as calculations for mean residence time and variance were generated for each set of data collected for a given set of operating conditions in the SDR to assess the effect of a range of SDR parameters on the RTD. These will be analysed and discussed below.

6.6 30cm smooth stainless steel disc RTD results

6.6.1 Influence of disc rotational speed on RTD

The influence of the smooth 30cm disc rotational speed on RTD characteristics is shown in Figure 6.10 and Figure 6.11. The disc rotational speed was 300, 500, 800 and 1200 rpm. Four different total flow rates have been implemented in this set of experiments (3, 6,9 and 15 ml/s). The total flowrate ratio was, $R=Q_{m.b} / Q_w= 0.028$. The flowrate of and the initial concentration of methylene blue were 5ml/s and 0.5 g/l respectively.

Figure 6.10 shows the influence of disc rotational speed at total flowrates of 3ml/s on the RTD. There is an indication that, at the higher disc rotational speeds, the RTD curves become narrower. As underlined by Todd and Irving (Todd and Irving, 1969), the width of the RTD spread, (or equivalently the RTD variance) can be considered as a measure of the axial mixing which makes the reactor deviate from the ideal plug-flow model. The RTD dimensionless variance (σ_θ^2) or the normalized variance of residence time distribution value (the ratio of the variance to the square of the mean residence time) is zero for the ideal plug-flow reactor where as real reactors tend to give values of dimensionless variance(σ_θ^2) > zero. The smaller the value of σ_θ^2, the narrower the RTD and the lower the axial dispersion. Therefore, the analysis of the variance of RTDs is essential for investigating the flow and mixing in reactors.

From the data plotted in Figure 6.10, the area under the E (t) vs. t curve was evaluated. It was found that the fraction of material leaving the reactor, which spent 10 s in the reactor, was 24% and 26% at the disc rotational speed of 300 and 500 rpm respectively. This was numerically estimated by using the Trapezoidal rule (two-point). On the other hand, at both disc rotational speeds of 800 and 1200 rpm, the fraction of material leaving the reactor, which spent 10 s in the reactor, was 38%.

According to the experimental mean residence time values or the centroid of the distribution, which has been calculated at mentioned disc rotational speeds as shown in Table 6.3, it can be seen that when the disc rotational speed increases from the 300 to 1200 rpm, the experimental mean residence time, (MRT_{Exp}. i.e. the reactants residence time on the disc plus the time taken by the fluid to flow to the sampling collecting), decreased from 17.04 to 13.92 s with the percent of reduction of 18.35%.. In addition, as shown in Table 6.3, at the total flowrate of 3ml/s, the corresponding experimental variance is 103.8, 71.2, 64.9 and 63.1 for the disc rotational speed of 300, 500, 800 and 1200 rpm, respectively. The reduction of variance reached up to 39.27% when the disc speed increased from 300 to 1200 rpm. It is clear that at the higher disc speed, a lower variance is obtained. Therefore, the flow behaviour in the spinning disc reactor approaches plug-flow regime at higher disc rotational speeds, whereby RTD curves at these speeds become closer to the distorted bell shaped (Fogler, 2006). Consequently, more uniformity in the fluid properties can be expected e.g. composition across the surface of the disc, which makes the SDR closer to the near plug-flow reactor and this

will have positive influence on the yield and selectivity of reactions. These finding are in agreement with the results has been achieved for micromixing experiments (Chapter 5).

Another very important observation from Figure 6.10, the RTD curves almost coincide together and are not differentiable at the disc rotational speed of 800 and 1200 rpm. This could be attributed to the fact that, the mixing intensity has attained its maximum level at 800 rpm and increasing the disc rotational speed will not add any benefit to the mixing process.

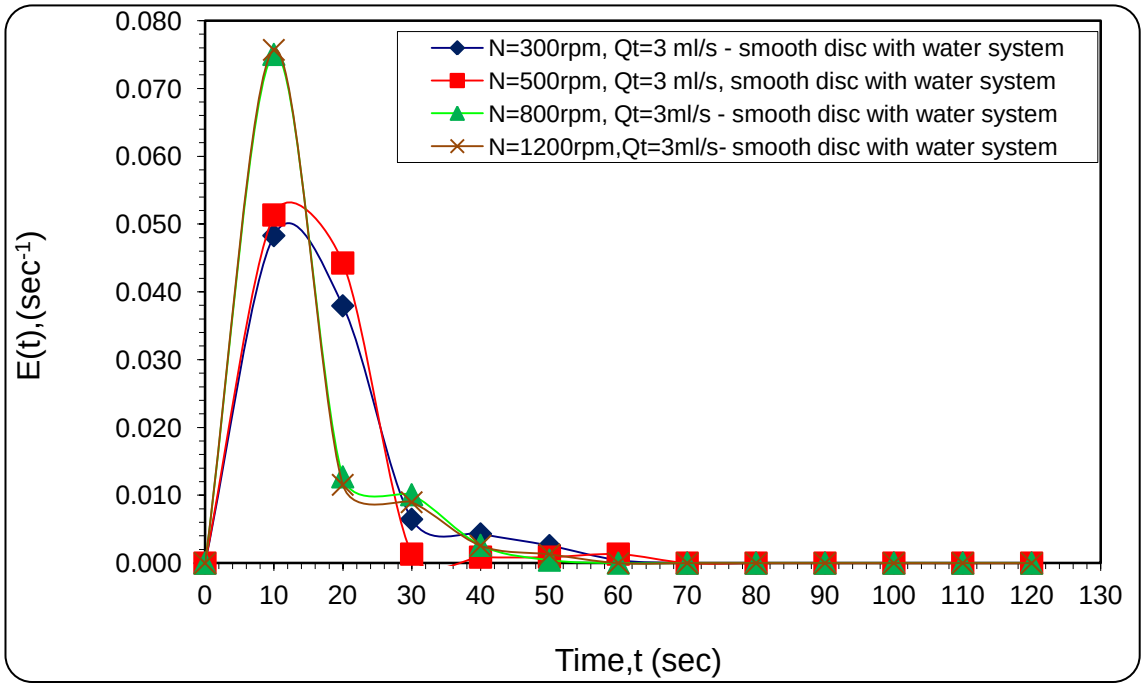

Figure 6.10: Effect of disc rotational speed on RTD at total flowrate of (Qt=3 ml/s)-smooth disc with water system

Table 6.3: Experimental mean residence time and the variance for the 30cm SDR using water system with smooth disc, Qt=3 ml/s

N, rpm	overall mean residence time, tm (s)	Variance,σ^2(sec^2)
300	17.04	103.840
500	14.37	71.247
800	14.24	64.929
1200	13.92	62.061

Figure 6.11 shows the influence of disc rotational speed at total flowrates of 6 ml/s on the RTD. Similar trends have been achieved at this total flowrate when compared with the RTD curves shown in Figure (6.10) for the lower flowrate Qt=3 ml/s i.e. the higher disc rotational speed, the narrower the RTD curves.

From the data plotted in Figure 6.11, the area under the E (t) vs. t curve was evaluated. It was found that the fraction of material leaving the reactor, which spent 10 s in the reactor, was 27% and 47 % at the disc rotational speed of 300 and 500 rpm respectively. In contrast, at the higher disc rotational speeds i.e. 800 and 1200 rpm, the fraction of material leaving the reactor, which spent 10 s in the reactor, was 48% and 49% respectively. As mentioned earlier, this was numerically estimated by using the Trapezoidal rule (two-point).

Based on the above findings, it can be concluded that at the highest disc rotational speed (1200 rpm), more percentage of materials is leaving the reactor within 10 s. This means that the flow is approaching plug flow behaviour at the higher speed when compared to the lower disc rotational speed (300 rpm).

The mean residence time and the variance values at the total flowrate of 6ml/s and the disc rotational speed in the range 300 to 1200 rpm are also shown in Table 6.4. It can be seen that when the disc rotational speed increases from the 300 to 1200 rpm, the mean resident time which is the measure of the average time spent by the molecules in the reactor,($MRT_{Exp.}$), decreased from 13.991 to 10.190 s with the percent of reduction of 27.16%. Moreover, at the Qt=6 ml/s, the reduction of variance reached up to 91.81% when the disc speed increased from 300 to 1200 rpm. The smaller the value of variance (σ^2), the narrower the RTD and the lower the axial dispersion occurring in the SDR.

The findings in Figure 6.11 were similar to the ones in Figure 6.10, in that the RTD curves become narrower and the values of mean residence time and the variance decreased as the disc rotational speed increased at a given total flowrate.

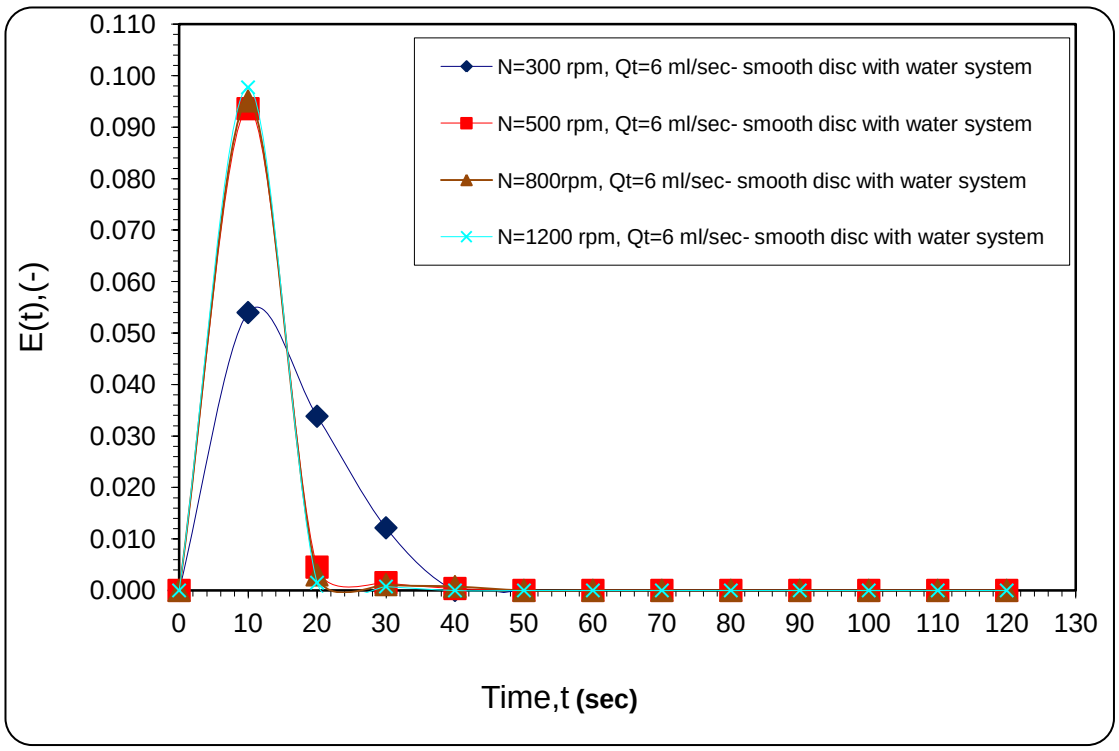

Figure 6.11: Effect of disc rotational speed on RTD at total flowrate of (Qt=6 ml/s)-smooth disc with water system

Table 6.4: Experimental mean residence time and the variance for the 30 cm SDR, using water system with smooth disc, Qt= 6ml/s

N, rpm	Mean resident time, tm (s)	Variance,σ^2(sec^2)
300	13.991	36.407
500	13.740	5.642
800	13.640	5.127
1200	10.190	2.9802

The effect of the disc rotational on the RTD and its variance were also examined with the total flowrate of 9 and 15 ml/s. Similar trends and observations with regards to the decreasing in mean residence time and the variance with increasing the disc rotational speed as highlighted in Figures 6.10 and 6.11 were obtained in Figures (AL1 and AL2) and Tables AL2 and AL3 in appendix L.

6.6.2 Influence of total feed flowrate on RTD

The effect of the total feed flowrate on the RTD curves is shown in Figures 6.12, 6.13 and Tables 6.5, 6.6 for the disc rotational speed of 800 and 1200 rpm respectively. Figures AL3 and AL4 and Tables AL4 and AL5 in appendix L are shown the effect of total feed flowrate on the RTD curves at disc rotational speed of 300 and 500 rpm.

Figure 6.12 indicates that, at the lower total feed flowrate i.e. Qt=3 ml/s, the RTD curve becomes much broader compared with the other higher flowrates, Qt= 6, 9 and 15 ml/s. This leads to an increase in mean residence time and the variance as shown in Tables 6.5. From these findings it is clear that the intensity of macromixing on the 30 cm SDR depends on the total feed flowrate. In addition, the higher the total feed flowrate, the more uniformity of mass flow rate and fluid composition is obtained across the surface of the disc, which results in the SDR behaving more like a plug flow reactor with improved the intensity of macromixing.

Figure 6.13 show the influence of total flow feed flowrate at the disc rotational speed of 1200rpm.The findings in Figure 6.13 were similar to the ones in Figure 6.12, in that the RTD curves become more narrower and the values of mean residence time and the variance decreased as the total flowrate increased from 3 ml/s to 6 ml/s. The curve at 6 ml/s is narrower than 3 ml/s but not so if compared 6 ml/s with 9 ml/s or 15 ml/s. In addition, the mean residence time and the variance values decreased as total feed flowrate increased from 3 ml/s to 6ml/s at disc rotational speed of 1200 rpm. At the total flowrate of 9 ml/s and 15 ml/s and disc rotational speed of 1200 rpm, the mean residence time and the variance values are almost unchanged as shown in Table 6.6.

One interesting observation from both Figures 6.12 and 6.13 is that at the Qt=6 ml/s, the RTD curve coincide with the other two RTD curves at the Qt=9 and 15ml/s. This means that beyond the total feed flowrate of 6 ml/s, the mixing intensity has reached the maximum level and increasing the total feed flowrate will not add much benefit to the intensity of macromixing.

Similar trends with regards to the effect of total feed flowrate on the RTD and its moments in Figures 6.12 and 6.13 and Tables 6.5 and 6.6 were obtained in Figures (AL3 and AL4) and Tables AL4 and AL5 in the appendix L at the total flowrate of 3 and 6 ml/s.

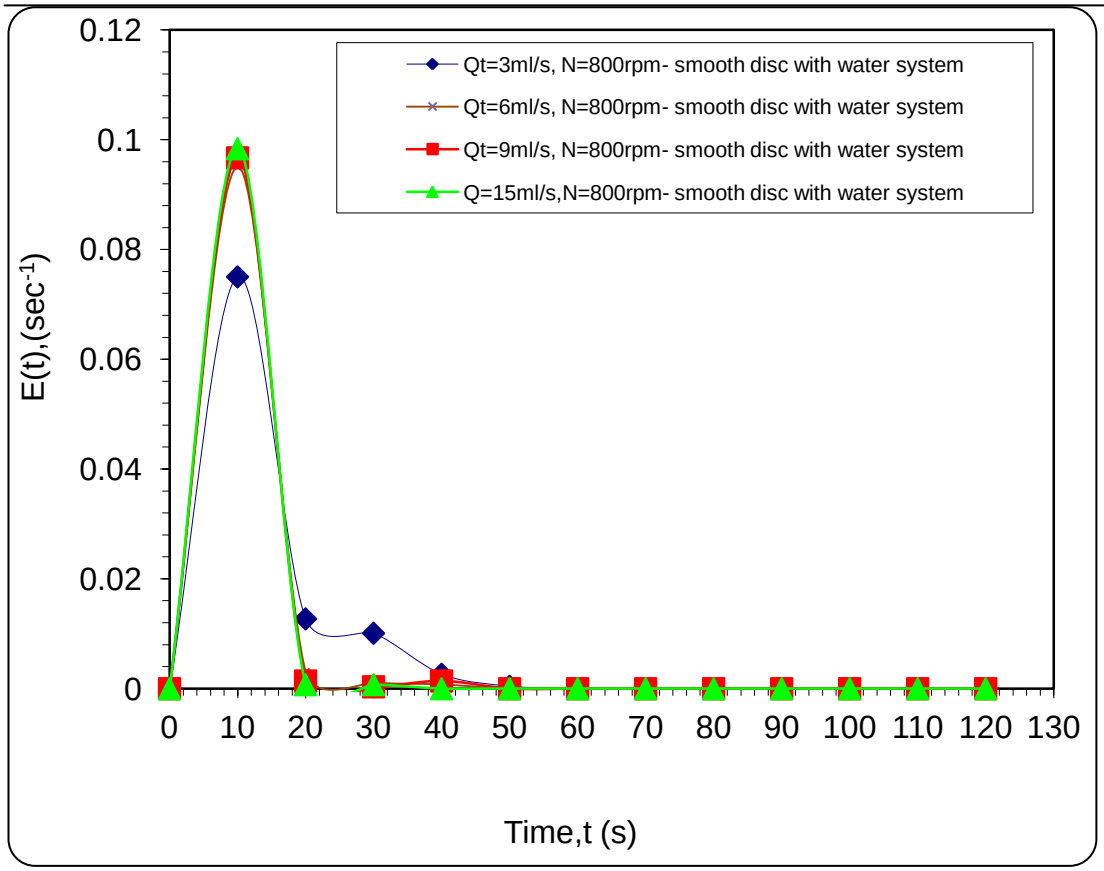

Figure 6.12: Effect of liquid total flowrate on the RTD in 30 cm SDR at disc rotational speed of 800 rpm –smooth disc with water system

Table 6.5: Experimental mean residence time and the variance for the 30cm SDR at different total flowrates and N=800 rpm using water system with smooth disc

Total flowrate, Qt (ml/s)	Mean resident time, tm (s)	Variance,σ^2(sec^2)
3	14.24	64.929
6	13.64	5.127
9	10.25	2.620
15	10.18	2.618

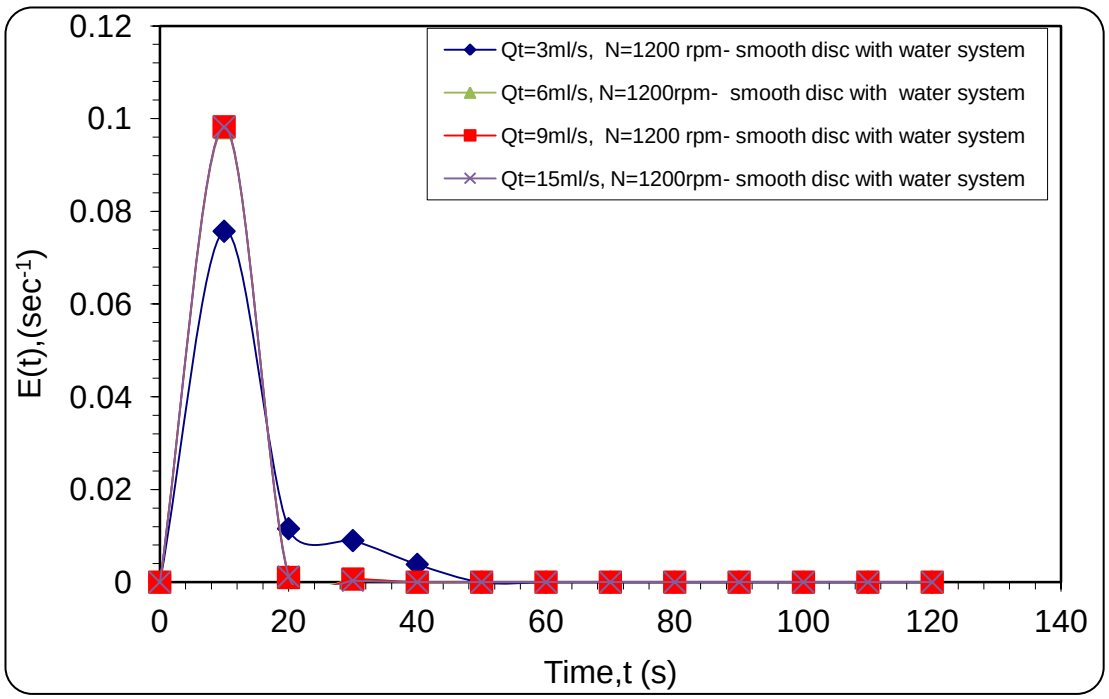

Figure 6.13: Effect of liquid total flowrate on the RTD in 30cm SDR at disc rotational speed of 1200 rpm –smooth disc with water system

Table 6.6: Experimental mean residence time and the variance for the 30cm SDR at different total flowrates and N=1200 rpm using water system with smooth disc

Total flowrate, Qt (ml/s)	Mean resident time, tm (s)	Variance,σ^2(sec^2)
3	13.92	63.061
6	10.190	2.9802
9	10.130	2.620
15	10.130	2.618

P Chao et al. (2009) studied the residence time distribution in a reciprocating single-screw pin-barrel extruder. An intensive a numerical method and experimental work investigating the effects of the influence of the feed rate and screw speed of single-screw pin barrel extruder on the RTD. Low- density polyethylene (LDPE) was used in the experiments as tracer material and it was pre-compounded with 16.7% red day companied with 83.3 wt% matrix material and chopped into the similar size of the LDPE. Digital image processing (DIP) method was used to measure the RTD. The experimental results of RTD show that for a given feed rate, the RTD shifts to the shorter times with the increasing the screw speed and also showed the larger throughput resulted in sharper RTD and smaller time delay with the increased feed rate for a given

screw speed. Other important fact confirmed in this particular study is that when the screw speed increased, the mean residence time and the variance of distribution decreases and vice versa. These findings support the results that have been achieved in our work with regards to the effect of feed flow and disc rotational speed on the RTD produced by 30 cm SDR.

6.6.3 Influence of feed viscosity on RTD

In order to investigate the effect of the feed viscosity on the mean residence time and the variance, glycerol was used to increase the viscosity of the working fluid (deionised water). A liquid mixture consisting of 50 wt% glycerol and 50 wt% deionised water was used, which had a viscosity of 6 mPa.s at 20 ^{O}C. The effect of feed viscosity on the RTD and its first and second moments in 30 cm SDR at four different total flowrates are shown in Figures 6.14 and 6.15 and Tables 6.7 and 6.8 below.

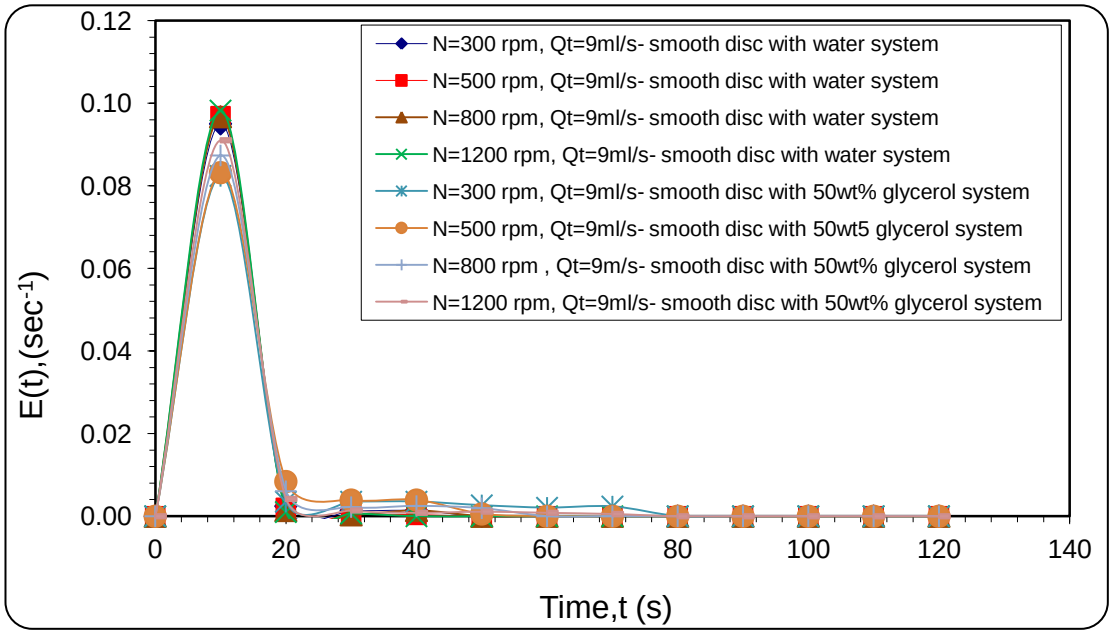

Figure 6.14: Effect of viscosity on the RTD in 30 cm SDR at total flowrate 9 ml/s and different disc rotational speeds –smooth disc with 50 wt% glycerol system

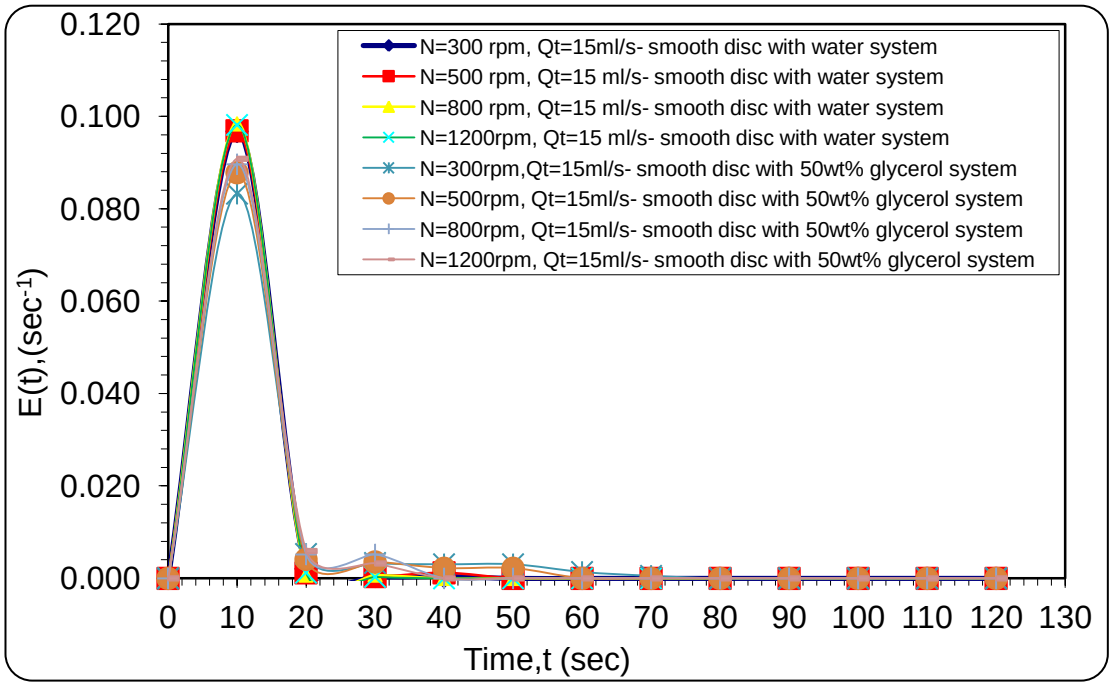

Figure 6.15: Effect of viscosity on the RTD in 30 cm SDR at total flowrate 15 ml/s and different disc rotational speeds –smooth disc with 50 wt% glycerol system

Table 6.7: Experimental mean residence time and the variance for the 30cmSDR using water system and 50 wt% glycerol system with smooth disc, Qt=9 ml/s

N, rpm	Water system		Water/glycerol system	
	Mean resident time , tm (s)	Variance,σ^2(sec^2)	Mean resident time, tm (s)	Variance,σ^2(sec^2)
300	13.47	5.000	14.780	7.272
500	10.27	2.837	12.890	5.015
800	10.25	2.620	12.080	4.917
1200	10.130	2.507	11.96	3.802

Table 6.8: Experimental mean residence time and the variance for the 30cmSDR using water system and 50wt% glycerol system with smooth disc, Qt=15 ml/s

N, rpm	Water system		Water/glycerol system	
	Mean resident time , tm (s)	Variance,σ^2(sec^2)	Mean resident time, tm (s)	Variance,σ^2(sec^2)
300	13.390	4.978	14.180	6.316
500	10.260	2.815	12.100	4.203
800	10.180	2.618	11.550	3.017
1200	10.130	2.500	10.760	2.573

It is clear from Figures 6.14, 6.15 and Tables 6.7, 6.8 which show the data for Qt=9 and 15 ml/s and disc rotational speed ranging between 300-1200 rpm, that the shape of the determined RTD becomes significantly influenced by the viscosity at a given flowrate. More specifically, it is noticeable that the RTD curves become broader with an increase of the feed viscosity from 1 to 6 mPa.s at any given disc rotational speed, this leading to increasing in mean residence time and the variance values as well.

From fig 6.14, when a water system (1 mPa.s) was used for the operating conditions of total flowrate of 9ml/s and the disc rotational speed of 300rpm, the material leaving the reactor (which spent 10s in the reactor) was 48%. In contrast, at similar operating condition, by replacing the water system with 50wt% glycerol system, the material leaving the reactor, which spent 10 s in the reactor, was only 41%. On the other hand, when the disc rotational speed increased to 1200rpm, the material leaving the reactor, which spent 10 s in the reactor, was 49% for both water system and 50 wt% glycerol system. It can be seen that viscosity had little or no effect on the RTD at the highest disc rotational speed (1200 rpm).

Again from Figure 6.14, It is evident that at Qt=9 ml/s and the disc rotational speed ranged 800-1200 rpm, the viscosity dependence nearly disappeared. This may be proves that the performance of the 30 cm can be enhanced by increasing the total flowrates which makes the larger area of disc were covered by liquid. Subsequently, greater uniformity of mass flow rate and fluid composition is taking place across the surface of

the disc. This results in the RTD curves resembling distorted bell shaped curves and the behaviour of SDR becoming more like a plug-flow reactor, with improved macromixing.

The findings in Figure 6.14 and Table 6.7 were similar to the ones in Figure 6.15 and Table 6.8 where the Qt=15 ml/s, in that the RTD curves become narrower and the values of mean residence time and the variance increased as the feed viscosity increased at a given disc rotational speed and total flow rate. A similar effect was observed by (Gao et al., 2011; Köhler et al., 2010) in their respective studies.

Similar trends with regards to the effect of feed viscosity on the RTD and its moments in Figures 6.14 and 6.15 and Tables 6.7 and 6.8 were obtained in Figures AL5 and AL6 and Tables AL6 and AL7 in the appendix L at given disc rotational speed and the total flowrate of 3 and 6 ml/s.

In general, the effect of viscosity on the RTD may be explained in terms of increased viscous shear forces acting against centrifugal forces on the surfaces of the disc, causing the flow to be retarded. Consequently, the percentage of material leaving the reactor at a given time and operating conditions is lower than that of water system within the same conditions. This makes the behaviour of the SDR to deviate from the plug flow behaviour especially at lower disc rotational speeds and lower flow rates.

6.7 30cm Grooved stainless steel disc RTD results and its Comparison with Smooth Disc Results

Referring to the micromixing results discussed in Chapter 5, the 30 cm SDR Grooved stainless steel disc showed strong indications of superior degree of mixing compared to the the smooth disc. To extend this comparative analysis between the smooth and the grooved discs further, an RTD study was performed to assess the macromixing intensity on the grooved stainless steel disc and to verify whether backmixing could be occurring due to the presence of grooves. If the backmixing was shown to occur to a significant extent, this would result in some of the products from the mixing process being transferred to the inner sections of the disc to combine with the fresh reagents being fed to the reactor. This could result in decreased efficiency of the overall mixing process which may not be reflected in the results of the micromixing experiments.

To verify all the issues mentioned above, sixteen experiments for each system (water and 50 wt% Glycerol system) were carried out using the grooved disc. The effects of disc rotational speed, total flowrate and feed viscosity on RTD were studied and compared with those from the smooth disc.

6.7.1 Effect of disc rotational speed on the RTD (Smooth Disc vs. Grooved Disc)

Figures 6.16 and 6.17 show the influence of the disc rotational speed on the RTD characteristics for both the grooved and smooth disc surfaces for the purpose of comparison. Four different total flow rates have been implemented in this set of experiments (3, 6, 9 and 15 ml/s). The disc rotational speed was 300, 500, 800 and 1200 rpm. The total flowrate ratio was, $R=Q_{m.b} / Q_w= 0.028$. The total flowrate and the initial concentration of methylene blue were 5ml/min and 0.5 g/l respectively.

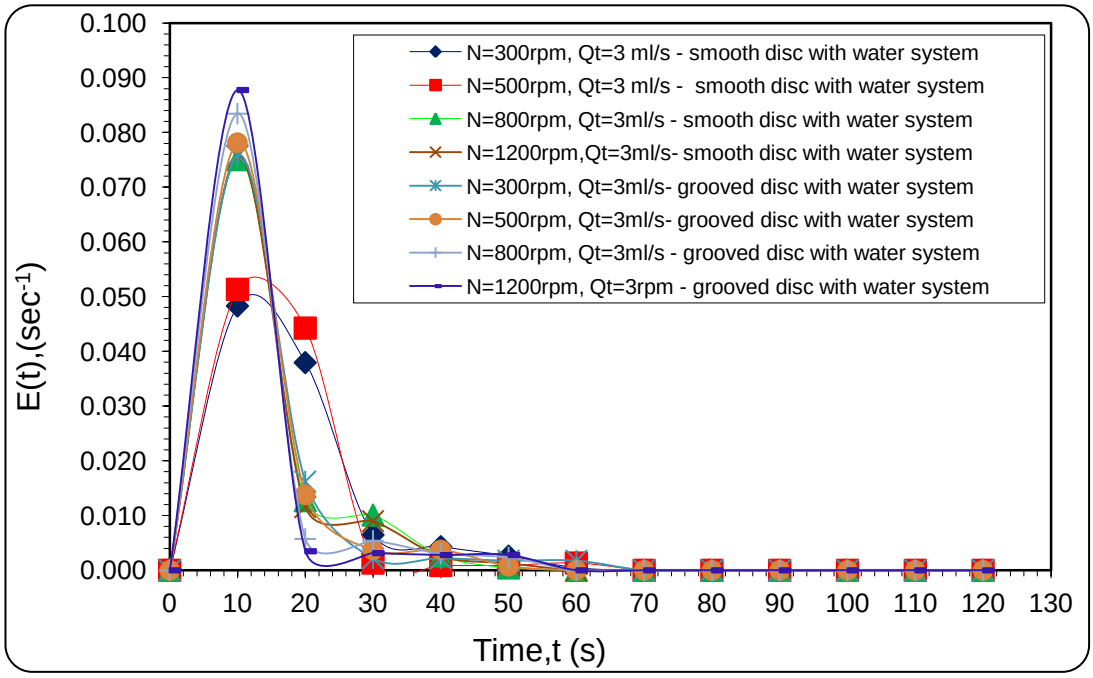

Figure 6.16: Effect of Disc Rotational speed on RTD at total flowrate of 3 ml/sec – water system (Smooth disc Vs. Grooved Disc)

Table 6.9: Experimental mean resident time and the variance for the 30 cmSDR using water system with grooved and smooth discs, Qt=3 ml/s and water system

N, rpm	Water system with using Grooved disc		Water system with Smooth disc	
	Mean residence time , tm (s)	Variance,σ^2(sec^2)	Mean residence time, tm (s)	Variance,σ^2(sec^2)
300	15.252	5.571	17.04	103.840
500	13.360	5.133	14.37	71.247
800	12.920	3.071	14.24	64.929
1200	15.252	5.571	13.92	63.061

From Figure 6.16, it is apparent at Qt=3 ml/s and the disc rotational speed of 300 rpm, the materials leaving the reactor, which spent 10 s in the reactor, were 24% and 38% for the smooth disc and grooved disc respectively with increment of 14% when the smooth disc was replaced by the grooved disc. From Figure 6.16 and at the mentioned speed and total feed flowrate, it is evident that the RTD curve produced by using grooved disc becomes narrower compared with curve produced by smooth disc. This leads to lower mean residence time and variance values on the grooved disc at identical operating conditions of disc speed and feed flowrate (Table 6.9). Accordingly, RTD curves for the grooved disc become closer to the distorted bell shaped curve described by Fogler (2006) for near plug-flow behaviour.

On the other hand, at the maximum disc rotational speed of 1200 rpm, the materials leaving the reactor, which spent 10s in the reactor, were 49% and 88% for the smooth disc and grooved disc respectively with an increment of 39% when the smooth disc was replaced by the grooved disc. Hence, with the grooved disc, the behaviour of the SDR becomes more like plug flow reactor with improvement in the intensity of the macromixing when compare with the smooth disc operating at the same conditions.

It is obvious from Figure 6.16 that the RTD curves become narrower for both smooth disc and grooved disc with increasing of the disc rotational speed from 300 rpm to 1200 rpm but the grooved disc shows better performance comparing with the smooth disc performance in terms of Mean residence time and Variance,σ^2 as shown in Table 9.6.

Similar trends with regards to the effect of rotational disc speed as described above were obtained at the total feed flow rate of 6 ml/sec and entire disc rotational speed range as highlighted in Figure 6.17 and Table 6.10.

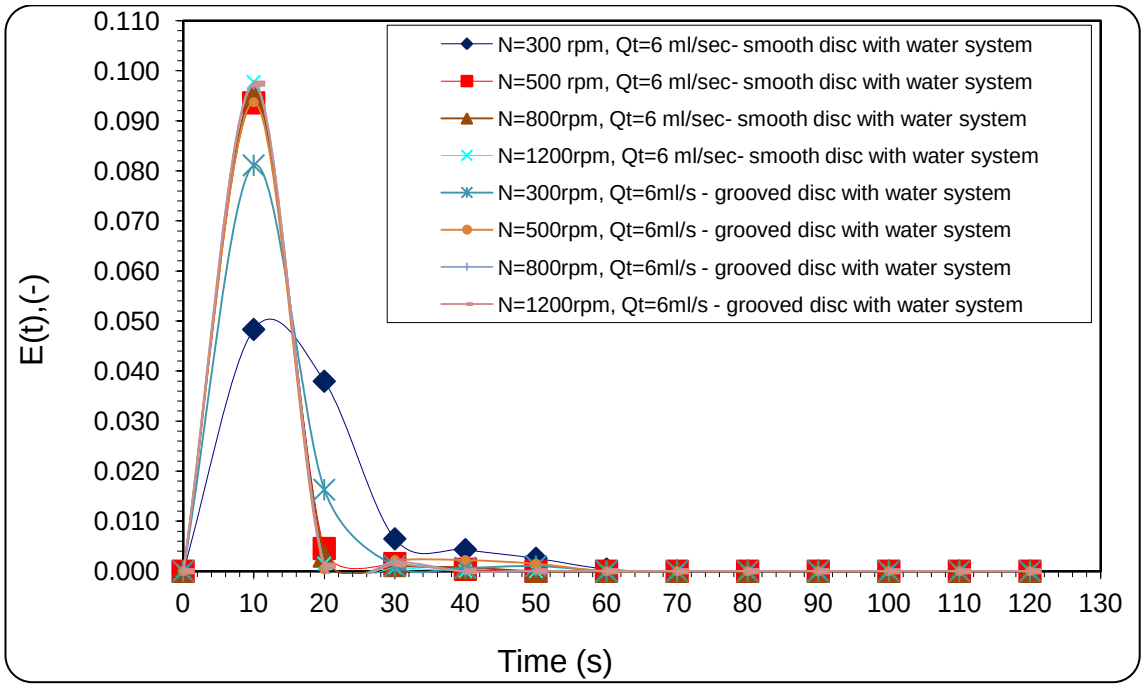

Figure 6.17: Effect of Disc Rotational speed on RTD at total flowrate of 6ml/sec – water system (Smooth disc Vs. Grooved Disc)

Table 6.10: Experimental mean resident time and the variance for the 30 cmSDR using water system with grooved and smooth discs, Qt=6 ml/s and water system

N, rpm	Water system with using Grooved disc		Water system with Smooth disc	
	Mean residence time , tm (s)	Variance,σ^2(sec^2)	Mean residence time, tm (s)	Variance,σ^2(sec^2)
300	12.20	3.271	13.991	36.407
500	11.70	2.513	13.740	5.642
800	10.20	1.740	13.640	5.127
1200	10.18	1.530	10.190	2.980

Figure 6.18 and 6.19 and Tables 11 and 12 show the effect of total feed flowrate of 9 and 15 ml/s and entire range of disc rotational speed ranged of 300-1200 rpm on RTD and the associated variance of the curves. From these two Figures, it can be concluded that the RTD curves for both smooth and grooved disc start to be almost coincide and the SDR exhibits similar behaviour for both smooth and grooved discs.

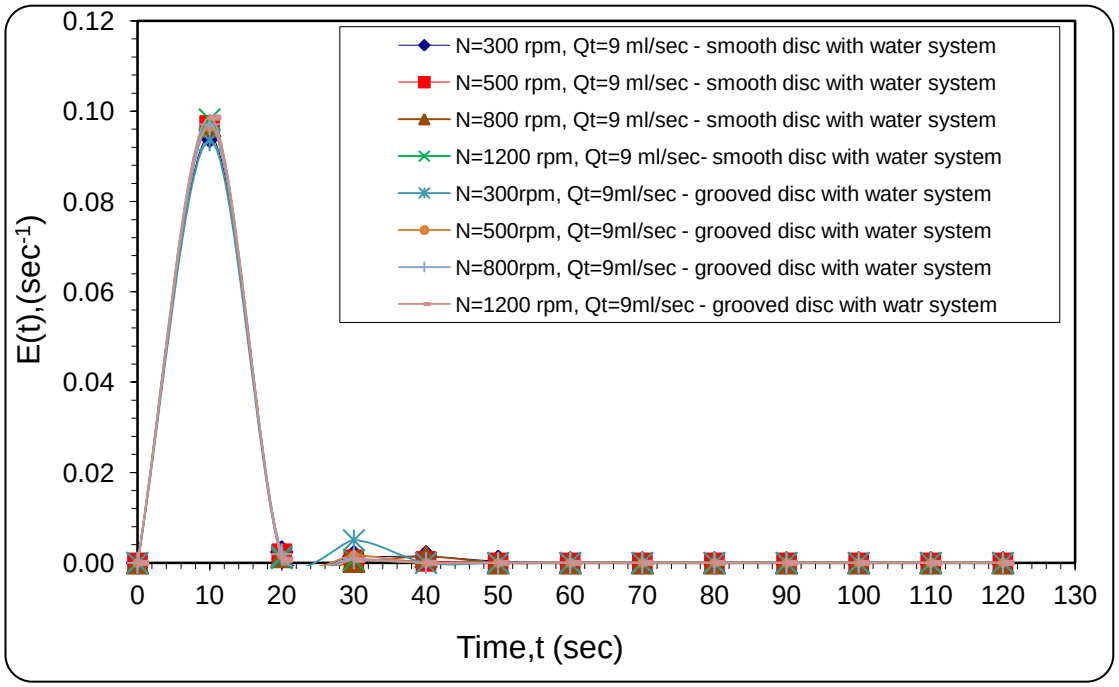

Figure 6.18: Effect of Disc Rotational speed on RTD at total flowrate of 9 ml/sec – water system (Smooth disc Vs. Grooved Disc)

Table 6.11: Experimental mean resident time and the variance for the 30 cmSDR using water system with grooved and smooth discs, Qt=9 ml/s and water system

N, rpm	Water system with using Grooved disc		Water system with Smooth disc	
	Mean residence time , tm (s)	Variance,σ^2(sec^2)	Mean residence time, tm (s)	Variance,σ^2(sec^2)
300	10.72	1.936	13.47	5.000
500	10.26	1.437	10.27	2.837
800	10.24	1.227	10.25	2.620
1200	10.10	1.033	10.13	2.507

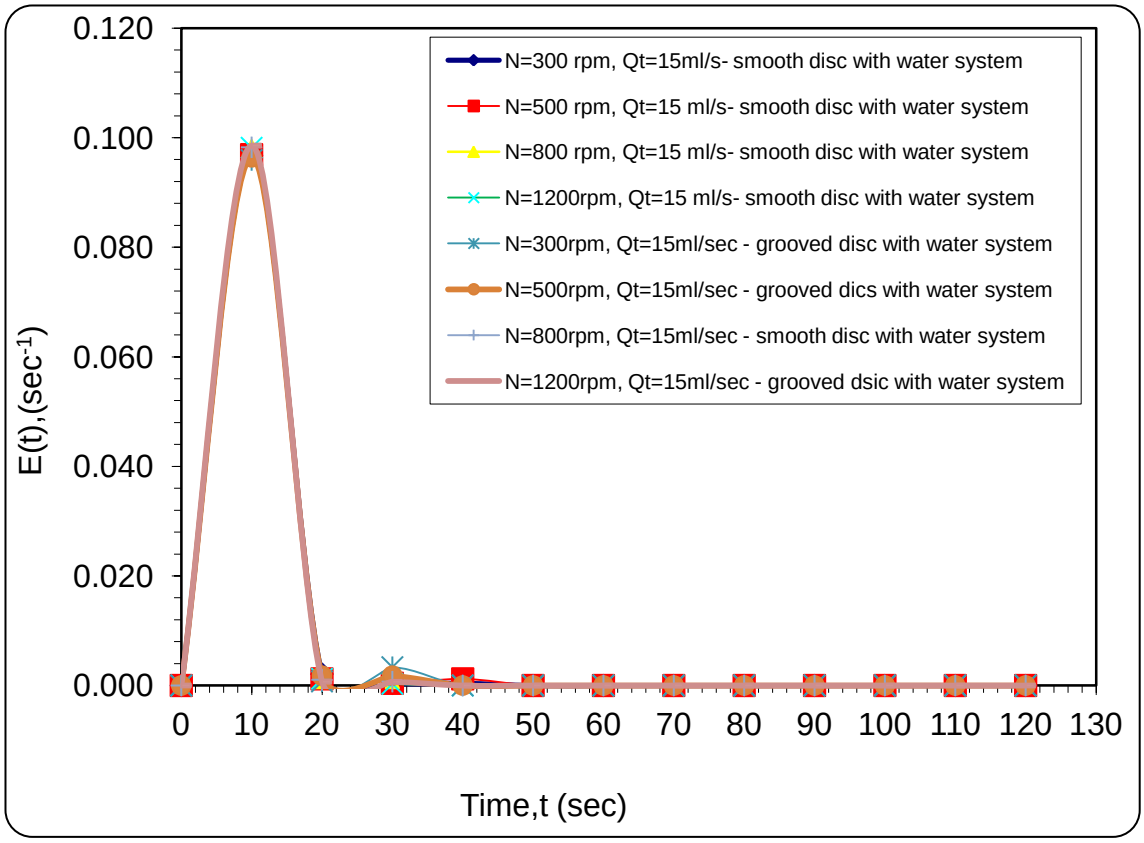

Figure 6.19: Effect of Disc Rotational speed on RTD at total flowrate of 15 ml/sec – water system (Smooth disc Vs. Grooved Disc)

Table 6.12: Experimental mean resident time and the variance for the 30cmSDR using water system with grooved and smooth discs, Qt=15 ml/s and water system

N, rpm	Water system with using Grooved disc		Water system with Smooth disc	
	Mean resident time , tm (s)	Variance,σ^2(sec^2)	Mean resident time, tm (s)	Variance,σ^2(sec^2)
300	10.69	1.739	13.390	4.978
500	10.27	1.373	10.260	2.815
800	10.14	1.201	10.180	2.618
1200	10.10	1.007	10.130	2.500

According to the mean residence times and the variance values which have been calculated for both smooth disc and grooved disc at the total feed flowrate of 3, 6, 9 and 15ml/s and disc rotational speeds ranged of 300-1200 rpm as shown in Tables 6.9 -6.12, It is clear that at the total flow rates of 9 ml/s and 15 ml/s and the entire range of disc rotational speed, a lower variance is obtained for both the smooth and grooved discs. As a result, more uniformity in the fluid properties such as composition across the surface of the disc is expected at higher rotational speeds for both disc surface configurations,

whereby near plug-flow profile is achieved. As mentioned earlier this will have intense positive influence on the yield and selectivity of certain types of reactions.

Referring to the mean residence time and variance values that has been calculated for both smooth disc and grooved discs, in general it is noticeable that at low to moderate total flowrates (i.e 3 to 15 ml/s in this study) and at a given disc rotational speed, the shortest mean residence time and the lowest variance values are achieved by grooved disc with comparing with the corresponding values obtained on the smooth disc. This could be attributed to the fact that, at low to moderate flowrates on a grooved disc only some of the grooves will perform as they are supposed to i.e. fill up then overflow radially. At larger radial positions, a continuous film may not form due to the larger surface area of the disc. Instead, the liquid may flow in the form of rivulets which may be characterised by separate jets flowing along radial paths to the periphery of the disc, thus reducing the mean residence time. On the smooth disc, this can still happen but usually happens at a greater radius. Hence, greater surface area is evenly covered per unit volume on the smooth disc. Smooth discs form uniform thin films more readily at a given flow conditions where as grooves discs tend to change from thin film to circumferential reservoirs with each radial groove, with more potential to form rivulets from the grooves. Higher flowrates will allow better use of available surface area of grooved discs as more grooves are able to be filled before rivulets form, this could increase the velocity of any rivulet could form and also result in better mixing. Flowrate which are so small as to not have enough volume to create a uniform film over the total surface area of a disc will eventually break up and form rivulets. Grooved discs tend to do this at smaller radii.

6.7.2 Effect of total flow rate on the RTD (Smooth Disc VS. Grooved Disc)

The influence of the total feed flowrate on the RTD characteristics is shown in Figures 6.20 and 6.21 for the 30 cm grooved and smooth disc for the purpose of comparison. Four different total feed flow rates have been used in this set of experiments (3, 6, 9 and 15 ml/s). The disc rotational speed range was 300-1200 rpm.

Figure 6.20 and Table 6.13 show the influence of the total feed flow rate at the disc rotational speed of 300rpm on the RTD curves for both smooth and grooved disc.

It indicates that, at Qt=3 ml/s and 6ml/s, the materials leaving the reactor, which spent 10 s in the reactor, were 24% and 27% for the smooth disc and grooved disc respectively with increment of 3% when the smooth disc was replaced by the grooved disc.

From the Figure 6.20 and at disc rotational speed of 300 rpm and given total feed flowrate, it is evident that the RTD curve produced by using grooved disc becomes narrower compared with curve produced by smooth disc. This leads to lower mean residence time and variance values on the grooved disc than the ones attained by the smooth disc at identical operating conditions of disc speed and feed flowrate (Table 6.13). On the other hand, at the other two total feed flowrate Qt=9 and 15 ml/s, the materials leaving the reactor, which spent 10 s in the reactor, were 48% and 49% for the smooth disc and grooved disc respectively with increment of 1% when the smooth disc was replaced by the grooved disc, so no significant improvement at these two higher total flowrates.

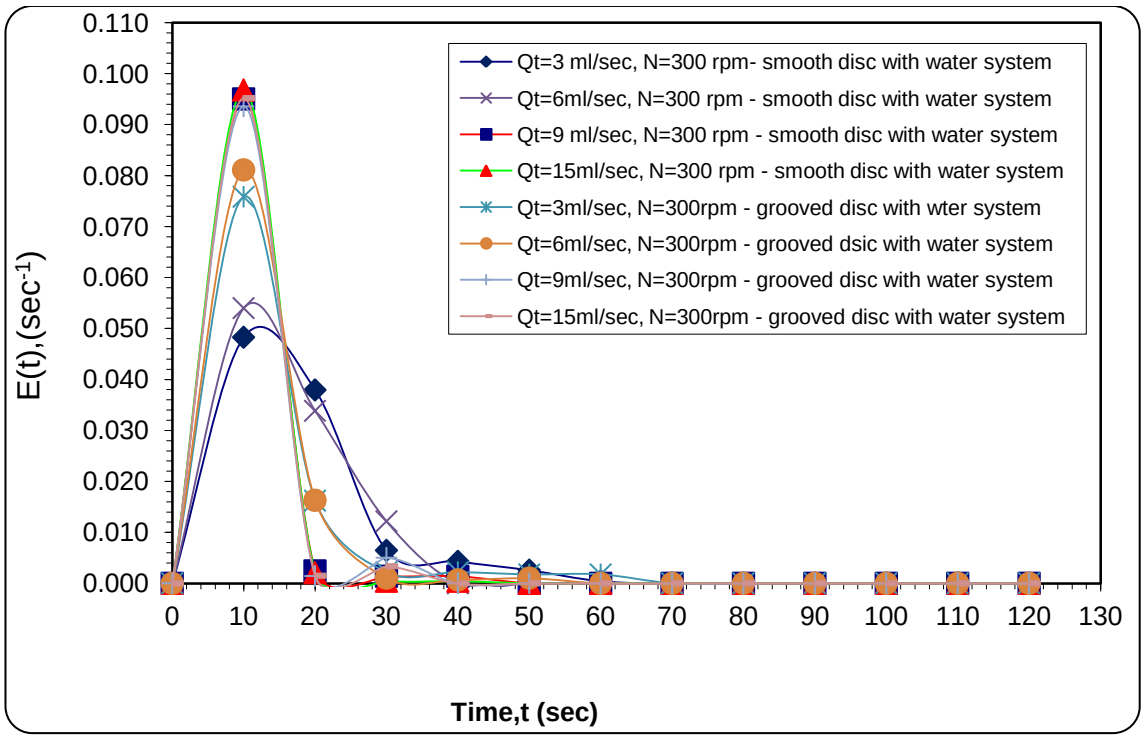

Figure 6.20: Effect of total flowrate on RTD at disc rotational speed 300 rpm – water system (Smooth disc Vs. Grooved Disc)

Table 6.13: Experimental mean resident time and the variance for the 30 cmSDR at different total flowrates, (Qt), using water system with grooved and smooth discs, N=300 rpm

Qt,ml/s	Water system with using Grooved disc		Water system with Smooth disc	
	Mean residence time , tm (s)	Variance,σ^2(sec^2)	Mean residence time, tm (s)	Variance,σ^2(sec^2)
3	15.252	5.571	17.04	103.840
6	13.360	5.133	13.991	36.407
9	12.920	3.071	13.47	5.000
15	12.230	2.030	13.390	4.978

Figure 6.21 and Table 6.14 show the influence of the total feed flow rate at the disc rotational speed of 500 rpm on the RTD curves for both smooth and grooved disc. At the Qt=3 ml/s, the RTD curve generated from flow on the grooved disc become narrower compared with the curve produced by smooth disc. Interestingly, at Qt=6, 9 and 15 ml/s, the RTD curves for both smooth and grooved disc are remarkably similar. This means the flow characteristic of the smooth disc approaches that of the grooved disc at these higher flowrates. Similar trends with regards to the effect of total feed flowrate as described above were obtained at the disc rotational speeds 800 and 1200 rpm as highlighted in Figures AL7, AL8 and Tables AL8, AL9) in the appendix L.

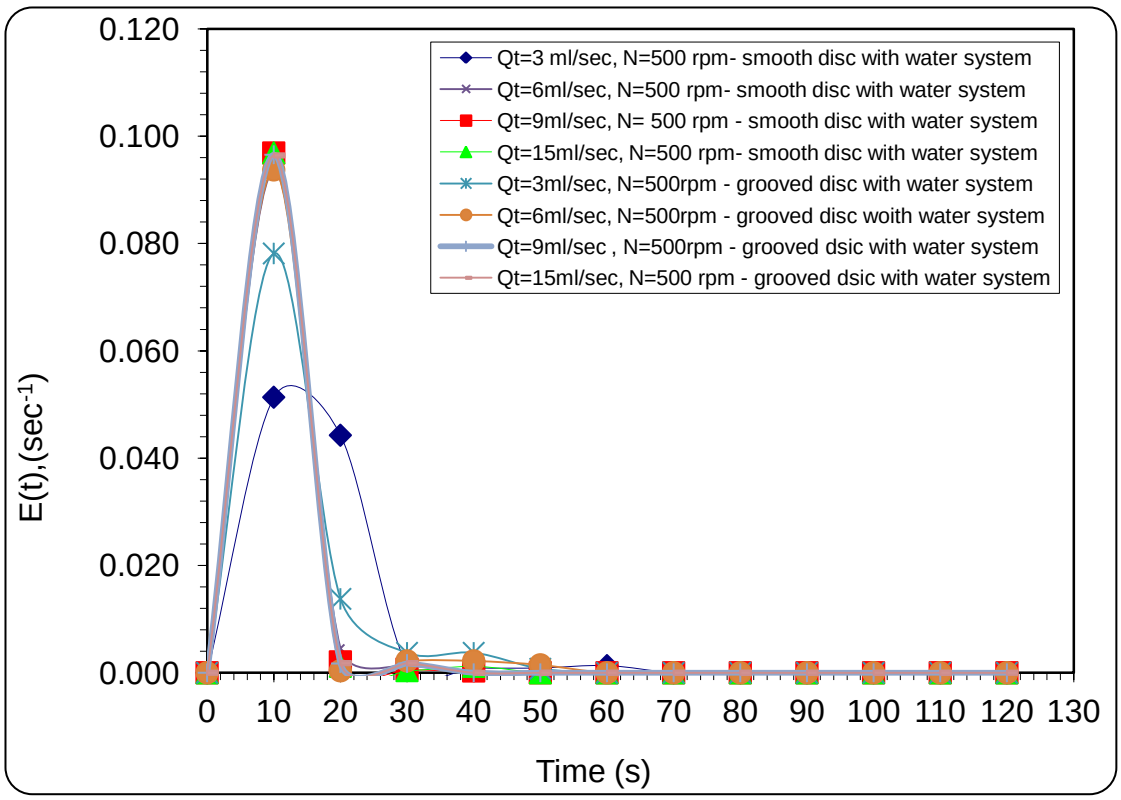

Figure 6.21: Effect of total flowrate on RTD at disc rotational speed 500 rpm – water system (Smooth disc Vs. Grooved Disc)

Table 6.14: Experimental mean resident time and the variance for the 30 cm SDR at different total flowrates, (Qt), using water system with grooved and smooth discs, N=500 rpm

Qt,ml/s	Water system with using Grooved disc		Water system with Smooth disc	
	Mean residence time , tm (s)	Variance,σ^2(sec^2)	Mean residence time, tm (s)	Variance,σ^2(sec^2)
3	13.360	5.133	14.370	71.247
6	11.70	2.513	13.740	5.642
9	10.27	1.437	10.270	2.837
15	10.27	1.373	10.260	2.815

6.7.3 Effect of feed viscosity on the RTD (Smooth Disc VS. Grooved Disc)

In order to investigate the RTD characteristics of the grooved disc in the presence of viscous media, a 50 wt% water / 50wt% glycerol system was employed to compare with the water medium. Similar conditions of the flow rate, disc rotational speed as described in previous sections in this Chapter were employed. Figures 6.22 and 6.23 show a comparison of the relevant RTD characteristics under selected operating conditions. Tables 6.15 and 6.16 lists the calculated values of the experimental mean residence time (MRTexp.) and the variance for the smooth disc and grooved disc with for water

system and 50 wt% glycerol system at a given disc rotational speed and total feed flowrate of 3 ml/s and 6 ml/s.

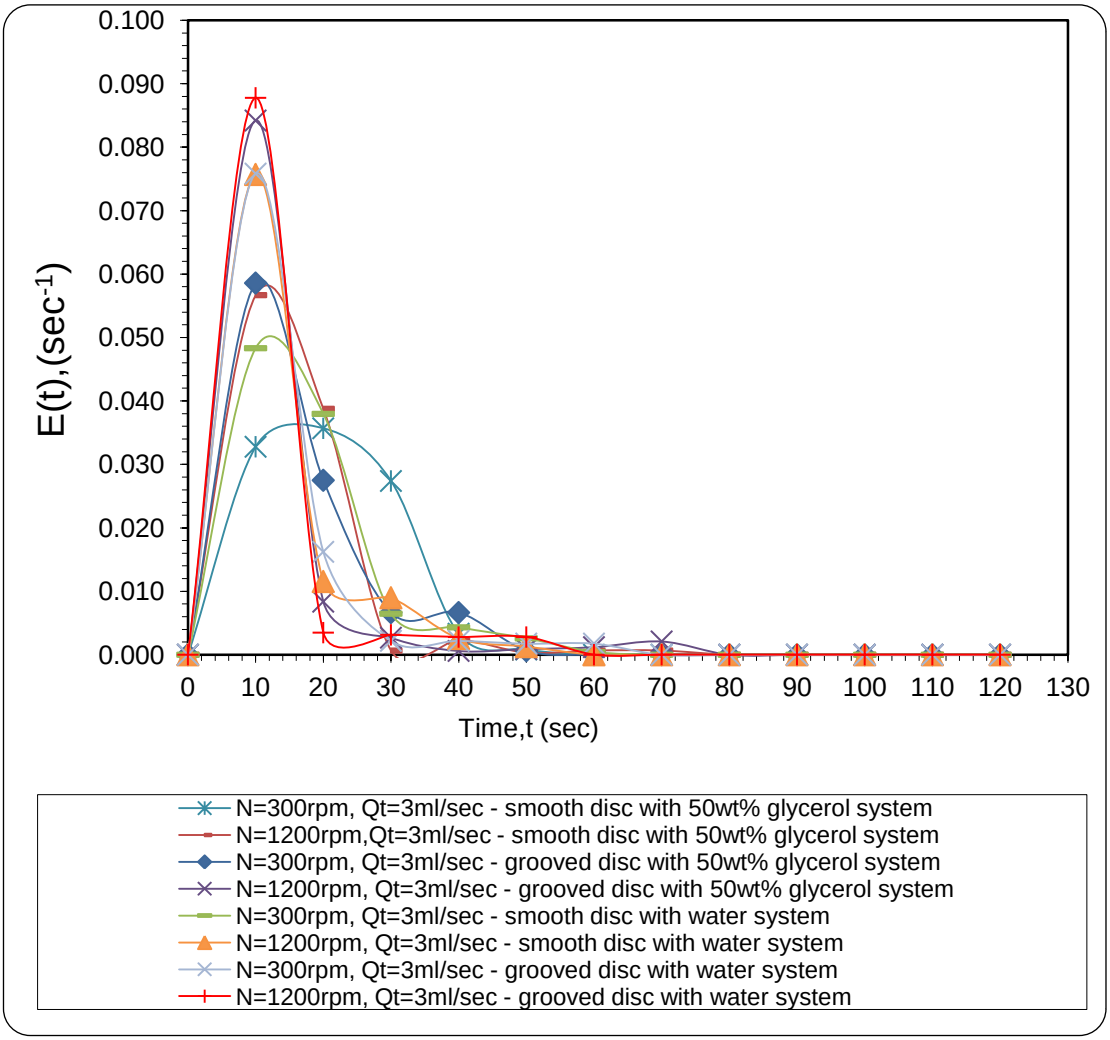

Figure 6.22: Effect of disc rotational speed on RTD at total flowrate of (Qt=3 ml/s) and disc rotational speeds of 300 and 1200 rpm -smooth disc vs. grooved disc with water and 50 wt% glycerol system

Table 6.15: Experimental mean resident time and the variance for the 30 cm SDR at disc rotational speeds of 300 and 1200 rpm using water system and 50 wt% glycerol system with grooved and smooth discs, Qt=3 ml/s

Disc type	Disc speed, N(rpm)	Water system		Glycerol system	
		Mean residence time , tm (s)	Variance,σ^2(sec^2)	Mean residence time, tm (s)	Variance,σ^2(sec^2)
Smooth	300	17.04	103.840	20.166	153.375
Smooth	1200	13.92	63.061	14.610	73.291
Grooved	300	15.252	5.571	16.167	85.615
Grooved	1200	12.230	2.030	13.030	9.724

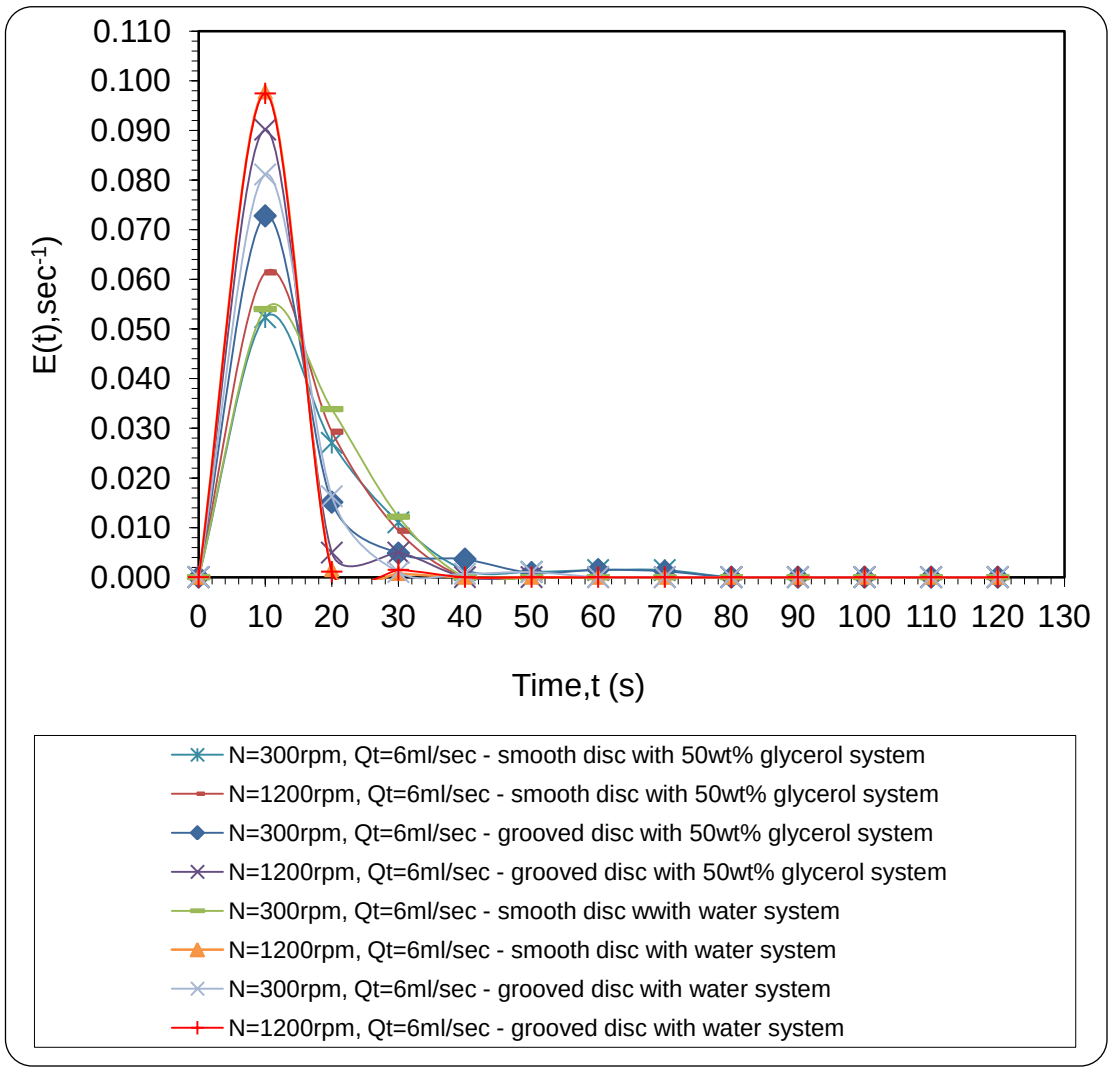

Figure 6.23: Effect of disc rotational speed on RTD at total flowrate of (Qt=6 ml/s) - smooth disc vs. grooved disc with water and 50 wt% glycerol system

Table 6.16: Experimental mean resident time and the variance for the 30 cm SDR at disc rotational speeds of 300 and 1200 rpm using water system and 50 wt% glycerol system with grooved and smooth discs, Qt=6 ml/s

Disc type	Disc speed, N(rpm)	Water system		Glycerol system	
		Mean residence time , tm (s)	Variance,σ^2(sec^2)	Mean residence time, tm (s)	Variance,σ^2(sec^2)
Smooth	300	13.991	36.407	16.408	93.566
Smooth	1200	10.190	2.9802	13.400	30.027
Grooved	300	12.20	3.271	14.97	17.814
Grooved	1200	10.18	1.530	10.74	3.847

It is clear from Figures 6.22 and 6.23 that the shape of the determined RTD curves becomes significantly influenced by the viscosity for both smooth and grooved disc. It is apparent that when the 50 wt% glycerol was used, the RTD curves become narrower for the grooved disc in comparison to the to the RTD characteristics with a smooth disc. It is clear from Figures 6.22, 6.23 and Tables 6.15, 6.16 which show the data for Qt=3 and 6 ml/s and disc rotational speeds of 300 and 1200 rpm, that the shape of the determined RTD become significantly influenced by the viscosity at a given flowrate for both smooth and grooved discs. More specifically, for both smooth and grooved discs, it is noticeable that the RTD curves become broader with an increase of the feed viscosity from 1 to 6 mPa.s at the higher disc rotational speed, this leading to increasing in mean residence time and the variance values as well.

From Figure 6.22 using smooth disc with water system (1 mPa.s) and operating conditions of total flowrate of 3ml/s, the disc rotational speed of 300 rpm, the material leaving the reactor, which spent 10 s in the reactor, was 24%. In contrast, at similar operating condition, by replacing the water system with 50wt% glycerol system, the material leaving the reactor, which spent 10 s in the reactor, was only 16%. On the other hand, when the disc rotational speed increased to 1200 rpm, the material leaving the reactor, which spent 10 s in the reactor, was 38% for water system and 28% for 50 wt% glycerol system.

On the other hand, when the smooth disc was replaced by grooved disc, the material leaving the reactor, which spent 10 s in the reactor, was 38%. When the water system was used with operating conditions of Qt=3 ml/s and N=300 rpm. In contrast, at similar operating condition, by replacing the water system with 50 wt% glycerol system, the

material leaving the reactor, which spent 10 s in the reactor, was only 29%. On the other hand, when the disc rotational speed increased to 1200rpm, the material leaving the reactor, which spent 10 s in the reactor, was 88% for water system and 42% for 50 wt% glycerol system.

The findings in Figure 6.22 and Table 6.15 were similar to the ones in Figure 6.23 and Table 6.16 where the Qt=6 ml/s, in that the RTD curves become more broader and the values of mean residence time and the variance increased as the feed viscosity increased at a given disc rotational speed and total flow rate for both smooth and grooved discs. In addition, it is noticeable that at total flowrates of 3 ml/s and 6 ml/s at a given disc rotational speed, the shortest mean residence time and the lowest variance values are achieved by grooved disc with comparing with the corresponding values obtained on the smooth disc for both water system and 50 wt% glycerol system (see the interpretation in section 6.7.1). Similar trends with regards to the effect of feed viscosity on the RTD and its moments in Figures 6.22 and 6.23 and Tables 6.15 and 6.16 were obtained in Figures (AL9) and (AL10) and Tables (AL10) and (AL11) in the appendix (L) at the disc rotational speed speeds of 500 and 800rpm and the total flowrate of 3 and 6 ml/s.

Similar observations with regards to the RTD characteristics of the grooved disc compared with smooth disc as highlighted in Figures 6.22 and 6.23 at the total feed flowrate Qt=3 and 6 ml/s and the disc rotational speeds of 300 and 1200 rpm were obtained in Figures AL11, AL12 and Tables AL12, AL13 in appendix (L) when the total feed flowrate are Qt=9 and 15 ml/s and disc rotational speed ranged of 300 -1200 rpm.

From Figures AL11 and AL12, It is evidence that at Qt=9 ml/s and 15 ml/s with the disc rotational speed ranged 800-1200 rpm, the viscosity dependence nearly disappears. As mentioned earlier, this may be evidence that the performance of the 30 cm can be enhanced by increasing the total flowrates which makes the larger area of disc were covered by liquid. Subsequently, greater uniformity of mass flow rate and fluid composition is taking place across the surface of the disc. This resulting to the RTD curves to resemble distorted bell shaped curves and the behaviour of SDR becoming more like a plug-flow reactor and macromixing is improved.

In general, the effect of viscosity on the RTD may be explained in terms of increased viscous shear forces acting against centrifugal forces on the surfaces of the disc, causing the flow to be retarded. Moreover, the mean residence time and variance values were decreased when the smooth disc replaced with the grooved disc as shown in Table 6.15 and 6.16. These findings prove that the intensity of mixing was reduced by increasing the feed viscosity. On the other hand, the intensity of mixing was enhanced when the smooth disc replaced by grooved disc and there is no evidence of backmixing as was expected.

6.8 The Dispersion number and Peclet number for the 30cm smooth and grooved disc

It has been shown in the previous sections of this Chapter that the RTD curves for the SDR for water and glycerol systems using both smooth and grooved discs give a more or less distorted bell shaped curves whose spread depends on the flow conditions. In general, the flow profile in the SDR approaches plug flow conditions reactor under the implemented operating conditions.

In order to estimate the extent of deviation from ideal plug flow conditions, the variance has been estimated, presented and discussed in earlier sections. A more established way of characterising the extent of deviation from ideal plug flow involves determination of the degree of dispersion in the thin film flow on the rotating disc. This can be achieved by calculating the dipersion number and the Peclet number (Rivera et al., 2010; Fogler, 2006; Apruzzese et al., 2003; Philipossian and Mitchell, 2003).

As mentioned earlier in section 2.5.6.2, the dispersion number is a measure of the ratio of the rate of transport by radial diffusion in the case of fluid flows on the SDR disc to the rate of transport by convection and cloud estimated by equation 2.56. The dispersion number is uniquely used to describe non-ideal reactors, where the axial dispersion is superimposed on the plug flow of a fluid and the radial dispersion is not considered. If the dispersion number approaches zero, the dispersion is considered to be negligible and the behaviour of the reactor is approaches that of a plug flow reactor . If the dispersion number approaches infinity, there is a large degree of dispersion, and the behaviour of

the reactor approaches mixed flow as in a continuance stirred tank reactor (CSTR). In addition, the degree of dispersion in the radial direction in the case of SDR can be also presented in terms of Peclet number (Pe) which is the inverse of the dispersion number, i.e., Pe = UL/ D. As stated in section 2.95.2.2, Higgins,(2000) and Levenspiel,(1972) categorize the degree of dispersion depending on the Peclet number (Pe) values as below:

- Pe = <10 → large amount of dispersion;
- Pe = 10 -100 → Intermediate amount of dispersion;
- Pe = >100 → small amount of dispersion.

Assumptions:

- The flow on the disc assumed to be flow in pipe, with the length of the pipe replaced by the radius of the disc and the diameter of the pipe replaced by the thickness of the film flowing on the disc.

- At the centre of the disc where the water stream and the methylene blue just start to contact each other and there is no diffusion, no dispersion, no mixing process occur and at this section, the SDR can be considered as closed system. On the other hand, when the fluid is ejected from the edge of the disc into the shoe collector with significant velocity, the mixing process may still continue and at this section, the SDR is considered to be an open system. With considering to this situation, the SDR is close- open system. For simplicity and as an approximation, the SDR was considered as an open-open system. As shown in Chapter 2, Figure 2.31 illustrates the various boundary conditions used with the dispersion model for open and close vessels.

For small extents of dispersion, (D/UL< 0.01), the normalized variance of residence time distribution for the SDR can be estimated by equation 2.57 (Levenspiel, 1999). For large Deviation from plug flow, (D/UL > 0.01), the normalized variance of residence time distribution can be estimated by equation 2.59 (Levenspiel, 1999).

Example for calculating σ_θ^2 and (D/UL):

With adopting the run performed with 30cm grooved disc at N=1200rpm with the total feed flowrate of 15ml/s, water system in Table 6.12 showed the mean resident time and the variance are 10.10s and 1.007s^2 respectively.

First we need to calculate the dimensionless variance (σ_θ^2) as follows:

$$\sigma_\theta^2 = \frac{\sigma^2}{t_m^2} = \frac{1.007}{(10.10)^2} = 0.009$$

As first approximation, a small extents of dispersion, D/UL < 0.01 was assumed,

$$\sigma_\theta^2 = 2\left(\frac{D}{UL}\right)$$

$$0.009 = 2\left(\frac{D}{UL}\right)$$

$$\left(\frac{D}{UL}\right) = \frac{0.009}{2} = 0.0045 \approx 0.005 \ < 0.01$$

The original guess was correct: The (D/UL) value is well below 0.01, where this first approximation should be used.

The Peclet number is obtained as:

Pe = UL/ D = 1/0.005= 200 (small amount of dispersion)

The dispersion number and Peclet number has been calculated for smooth and grooved disc using water and 50wt% glycerol system with the total flowrates of 3,6,9 and 15ml/s and disc rotational speeds ranged 300-1200rpm that has been implemented in RTD experiments. As example, Table 6.17 and 6.18 show the values of the dispersion

number and Peclet number using water system at total flowrate 15ml/sec for both smooth and grooved disc at disc rotational speeds range of 300 -1200rpm.

Table 6.17: The Dispersion number (D/UL) and Peclet number, Pe (-) for the 30cmSDR using smooth disc with water system, Qt=15ml/s

Disc rotational speed,N (rpm)	Dispersion number,D/UL,(-)	Peclet number, Pe= UL/ D (-)
300	0.013	76.923
500	0.013	76.923
800	0.012	83.333
1200	0.012	83.333

Table 6.18: The Dispersion number (D/UL) and Peclet number, Pe (-) for the 30 cm SDR using grooved disc with water system, Qt=15 ml/s

Disc rotational speed N,(rpm)	Dispersion number D/UL, (-)	Peclet number Pe,(-)
300	0.007	142.857
500	0.006	166.666
800	0.005	200.000
1200	0.005	200.000

Tables (AL14) to (AL27) in appendix (L) display the dispersion number and Peclet number for the remaining operating conditions. The lowest value of the dispersion number and the highest value of Peclet number were 0.005 and 200 respectively that has been achieved on grooved disc using water system and Qt=15 ml/s and N=1200 rpm. The highest value of the dispersion number and the lowest value of Peclet number were 0.126 and 7.936 respectively that has been achieved on smooth disc using 50 wt% glycerol system and Qt=3 ml/s and N=300 rpm.

The Dispersion number and Peclet number for the 30cmSDR using smooth and grooved discs with water system and 50 wt% glycerol system, Qt= 3,6 and 9 and 15 ml/s where displayed in Tables AL14 to AL27 in appendix L. The degree of dispersion in the SDR can be summarised in Table 6.19 below.

Table 6.19: The degree of dispersion for the smooth and grooved disc at different

Disc type and fluid system type	Disc rotational speed,(prm)	Total flowrate,(Qt)	The degree of dispersion,(-)
Smooth disc/ water system	300/500/800/1200	Qt=3 ml/s	Larger amount of dispersion
		Qt=6,9 and 15 ml/s	Intermediate amount of dispersion
Smooth disc/50wt% glycerol system	300/500/800/1200	Qt=3 ml/s	Larger amount of dispersion
	300 and 500	Qt=6 ml/s	Larger amount of dispersion
	800 and 1200	Qt=6 ml/s	Intermediate amount of dispersion
	300/500/800/1200	Qt=9 and 15 ml/s	Intermediate amount of dispersion
Grooved disc/ water system	300	Qt=3 and 6 ml/s	Intermediate amount of dispersion
	500/800/1200	Qt=3 and 6ml/s	small amount of dispersion
	300/500/800/1200	Qt=9 and 15ml/s	small amount of dispersion
Grooved disc/ 50wt% glycerol system	300 and 500	Qt=3 ml/s	Larger amount of dispersion
	800 and 1200	Qt=3 ml/s	Intermediate amount of dispersion
	300/500/800/1200	Qt=6 and 9 ml/s	Intermediate amount of dispersion
	300	Qt=15 ml/s	Intermediate amount of dispersion
	500/800/1200	Qt=15 ml/s	small amount of dispersion

From Table 6.19 it can be concluded that at a given operating conditions, the grooved disc shows less degree of dispersion comparing with the smooth disc under the same operating conditions. Thus, greater uniformity of mass flow rate and fluid composition is taking place across the surface of the disc. This leads to the RTD curves to resemble distorted bell shaped curves and the behaviour of the spinning disc reactor becoming more like a plug-flow reactor than a smooth disc. These features enable the grooved disc to give a superior degree of mixing compared to the smooth disc, with little evidence of backmixing on the groove disc, contrary to what was expected.

It is essential to compare the degree of dispersion in the SDR with the other intensified devices. Higgins (2000) have used the RTD analysis to characterise the mixing regime within a model and a prototype hydrodynamic vortex separator, (HDVS). The hydrodynamic vortex separator was operated with and without a base flow component and with and without the sludge hopper for a range of inlet flow rates. The RTD was obtained using a pulse tracer injection method. One of the analysis techniques which was employed in RTD analysis is the axial dispersion model (ADM). In this study, at the flow rate of 15-480 ml/min (250-8000 ml/s), the prototype HDVS- NO Baseflow has a Peclet number, (Pe), ranges from less that 1-4.42 depending on the flow rate. On the other hand, at the flow rate of 4-90 ml/min (66.6-1500 ml/s), the model HDVS-NO Baseflow has the Peclet number, (Pe), ranges between 1-3.48 depending on the flow rate. The results show that the HDVS has a complex imperfect plug-flow mixing regime (non-ideal flow behaviour) and high dispersion. In our study, the highest Peclet numbers for the 30 cm SDR using water system with grooved disc was found to be 200 at the Qt=15 ml/s and N=1200 rpm. This is an evidence of the 30 cm SDR giving significantly better macromixing performance than the other devices.

7. CONCLUSION AND RECOMMENDATIONS

The aim of this Chapter is to present the conclusions of the findings that have been made in the light of this research. In addition, a section of this Chapter has been dedicated to recommendations for future work to be carried out in the field of micromixing using spinning disc reactor (SDR).

7.1 CONCLUSION

7.1.1 Micromixing in 10cm and 30cm Spinning Disc Reactor (SDR)

I. The influence of disc rotational speed, feed flowrate, disc size and disc surface configuration, feed viscosity, feed distributor system have all been shown to be important parameters in assessing the micromixing characteristics in SDRs.

II. The individual contributions of the film thickness and residence time parameters as well as the film surface instabilities to the performance of the SDRs have all been extensively discussed in relation to the micromixing strength on the disc surface. These hydrodynamic factors were shown to be functions of total flow rate, disc rotational speed, feed viscosity, radial position and disc size.

III. The best micromixing conditions in the SDRs were generally achieved at high disc rotational speeds, high feed flowrates and on the large rotating discs. These parameters provided the conditions for the thinnest, highly sheared films, with a large number of surface ripples to be formed thereby enhancing molecular diffusion. It was observed that, at an acid concentration of 1M, the lowest segregation index of 0.05 was achieved for a feed of 0.001Ns/m^2 viscosity at the highest flowrate of 5ml/s (corresponding to Re_{film}=72) and highest rotational speed of 2400rpm on the 10cm diameter disc. On the other hand, a significantly improved micromixing was obtained on the larger disc of 30cm diameter, especially at the lower total flowrate of 3ml/sec and 9ml/s (lower Re_{film} of 15 and 42) , in comparison to the smaller disc of 10cm diameter.

IV. The SDRs micromixing intensity in high viscosity feeds was lower than in water-like fluids. This could be explained in terms of shear forces acting against centrifugal forces on the disc surface, causing the flow to be retarded. Furthermore, the viscous media will slow down the micromixing rate and alter the intrinsic kinetics of the reaction. Higher disc rotation speeds and high flowrates can nevertheless improve the micromixing significantly.

V. Based on the Baldyga and Pohorecki (1995a) model, the micromixing time for 10cm and 30cm SDRs was estimated for the given operating conditions and the relationship between the t_m and the power dissipation was reported. At the optimum conditions using water system, the micromixing time and the power dissipation values for the 10cm were 0.2 ms and 1390 W/kg respectively. In contrast, the micromixing time and power dissipation values for the 30 cm were 0.3 ms and 1025 W/kg respectively. These findings proved that the SDRs have excellent micromixing efficiency.

VI. Using a grooved disc with low flowrates can reduce the SDRs micromixing efficiency due to rivulet flow resulting from insufficient wetting of the larger surface area. Therefore, the grooved surfaces were better suited to high throughputs flowrates.

VII. A multi-point distributor was introduced to the 30 cm SDR in order to eliminate the bad distribution of sulphuric acid with the iodide-iodate-borate ions solution that occurred when the single-point distributor was used with the highest total flowrate of 15 ml/sec and the acid concentration was [H+]=0.5 M. The results show that at Qt=15 ml/s with the multi-point distributor, the micromixing was slightly better than that of the single-point distributor at the same flowrate for all disc speeds. For example, at a disc speed of 300 rpm, the Xs was 0.128 and 0.146 for multi-point distributor and single-point distributor respectively whilst when the disc rotational speed was 1200 rpm, the Xs achieved was 0.053 and 0.079 for multi-point distributor and single-point distributor respectively.

VIII. It was concluded that to achieve the highest degree of micromixing using multi-point distributor, some considerations were needed to be taken into account (as discussed in detail in the recommendation section of this Chapter). In general, the feeding mechanism can have a dramatic influence on the micromixing in the SDRs. Multipoint distributors are more effective than single point distributors at high feed flowrates, giving enhanced liquid distribution as one stream feeds into another.

7.1.2 Reactor Performance Comparison

1. In order to compare the SDR micromixing efficiency with the performance of other types of reactor i.e. semi-batch reactor (SBR) and narrow channel reactors (NCRs), correlations between micromixing time t_m and power dissipation ε using water system and 50 wt% glycerol system corresponding to viscosity of $1.01x10^{-3}$and $6.0x10^{-3}$ Pa.s respectively have been developed for these four different reactors under different operating conditions. From these correlations, it has been shown that with the water system the theoretical mixing times behave as a power-law function of the power dissipation with an order of -0.5,-0.486 and -0.453 for SDRs, SBR and NCRs respectively. When the 50wt% glycerol system was used, the theoretical mixing time for each reactor type is also influenced by the power dissipation into the fluid, according to a power-law correlation similar to the ones observed previously for the water system with an order of -0.50,-0.464 and -0.456 for SDRs, SBR and NCRs respectively. Similar behaviour for the SDRs was achieved even when the feed viscosity was increased to $6.0x10^{-3}$ Pa.s. From the correlations, it was concluded that the highest values of power dissipation corresponding to the lowest values of mixing time were attained by the SDRs when both water system and 50 wt% glycerol system were used. The worst case of micromixing efficiency was achieved by using NCRs whilst intermediate performance was achieved in the SBR. It was confirmed that, for the same value of the power dissipation, the theoretical micromixing time remains largely lower in the SDR's than the SBR and NCRs. From these experimental observations, it can be concluded that even when the SDRs operated with the higher feed viscosities (the severe conditions) the

intensity of the micromixing in SDRs at a given power dissipation would still be better than in SBR and NCRs.

2. Correlations between micromixing efficiency in terms of micromixedness ratio, (α), and power dissipation ε have also been developed for these four different reactors with feed viscosity of $1.0x10^{-3}$ Pa.s ,i.e. water system and at a given operating conditions. These correlations clearly show that the 10cm and 30cm SDR give significantly better micromixing performance compared with the NCRs and SBR particularly at higher total flowrates. The micromixedness ratio, (α), of well above 15 for the 10 cm and 30 cm SDRs, which is more than double that achieved in the STR or NCRs under similar power dissipation. In addition, the micromixing efficiency of the SDRs was also compared with the micromixing efficiency of the other intensified reactors such as the sliding-surface,(S-SM), mixing device, the rotor–stator reactor,(R-S-R), and torus reactor,(T-R). At the same value of power dissipation, (ε), the micromixedness ratio,(α), in the spinning disc reactors remains largely higher than in the sliding-surface mixing device (S-SM), the rotor–stator reactor (R-S-R), and torus reactor (T-R) which proved that the 10cm and 30cm SDR give significantly better micromixing performance than the above mentioned intensified reactors. Correlations between the micromixedness ratio, (α), and power dissipation ε were also developed for the four different reactors used in this study with feed viscosity of $6.0x10^{-3}$ Pa.s. It was clear from these correlations that the 10 cm and 30 cm SDRs show lower mixing performance than the SBR when the acid was injected close to the impeller in the latter. Although the correlations between the theoretical micromixing time t_m and the power dissipation ε show better SDRs performance, the micromixedness ratio correlations shows the opposite. This effects need to be investigated by using the incorporation model as will be recommended later in the section below. The NCRs shows the lowest mixing performance compared with the SDRs and SBR.

3. The comparison of micromixing performance in various reactors using water systems show that, under conditions of high feed flowrates, the 10 cm and 30 cm SDR give significantly better micromixing performance than the SBR and NCRs

under similar power dissipation. This highlights the potential of the SDR as an alternative device for processes where a high degree of mixing is critically important.

7.1.3 Residence Time Distribution for 30cm Spinning Disc Reactor

1. The influence of disc rotational speeds, total flow rates, the feed viscosity and the disc configuration (smooth vs grooved) on RTD and its moments have been investigated and the findings are summarised below:

   I. The RTD results collected from both the smooth and grooved discs show that at the higher disc rotational speeds and higher total flowrates, the RTD curves become narrower and the overall mean residence time ($t_{overall\ mean}$) is also lower The lowest value for the ($t_{overall\ mean}$), of 10.1 s was achieved for a feed of 0.001 Ns/m^2 viscosity at the highest flowrate of 15ml/s and highest rotational speed of 1200 rpm on the smooth disc with corresponding variance, σ^2, of 2.16. With the grooved disc under the above mentioned operating conditions the $t_{overall\ mean}$ was unchanged at 10.10 s with corresponding σ^2 of 1.03, indicating a narrower RTD profile.

   II. The increase of the feed viscosity also affected the RTD and its moments. The RTD curves become broader with an increase of the feed viscosity from 1 to 6 mPa.s at identical disc rotational speed and feed flowrate, leading to increased $t_{overall\ mean}$ and σ^2 values. The lowest value for the $t_{overall\ mean}$, of 10.76 s was achieved for a feed of 6mPa.s viscosity at the highest flowrate of 15 ml/s and highest rotational speed of 1200 rpm on the smooth disc with corresponding σ^2 of 2.57. When the smooth disc was replaced by the grooved disc, the $t_{overall\ mean}$ was almost unchanged at 10.22 s with corresponding σ^2 of 2.01.

III. With reference to the data shown above for both the smooth and grooved discs, it was clear that the grooved disc showed better performance than the smooth disc in terms of $t_{overall\ mean}$ and σ^2. These findings proved that the intensity of mixing was enhanced when the smooth disc replaced by grooved disc and there was no evidence of backmixing as was expected.

2. The dispersion number and Peclet number for the 30cm smooth and grooved disc were estimated at a given operating conditions to characterise the extent of deviation from ideal plug flow i.e. determination of the degree of dispersion in the thin film flow on the rotating disc. The results show that the grooved disc shows less degree of dispersion compared with the smooth disc under the same operating conditions. The lowest value for the dispersion number was 0.012 achieved for a feed of 1 mPa.s viscosity at the highest flowrate of 15 ml/s and highest rotational speed of 1200 rpm on the smooth disc with corresponding Peclet number of 83.3. When the smooth disc replaced by the grooved disc, the dispersion number was 0.005 with corresponding Peclet number of 200. These characteristics allow the grooved disc to give a superior degree of mixing compared to the smooth disc, with little evidence of backmixing on the groove disc, contrary to what was expected.

7.2 RECOMMENDATIONS FOR FUTURE WORK

This study has confirmed that SDRs give significantly better micromixing performance which highlights its potential as an alternative device for processes where a high degree of mixing is critically important. However, a number of issues still remained to be explored before a complete and thorough understanding of the principles behind the spinning disc technology as an alternative device for processes where a high degree of mixing is critically needed.

It is hoped that the following recommendations would give a valuable suggestions in the future exploration of Spinning Disc Reactors for micromixing characteristics.

I. The use of Computational Fluid Dynamics (CFD) to model the behaviour of liquid flow and intensity of micromixing on the SDR is a very challenging area of investigation but should be investigated. It is recommended that the behaviour of the thin film flows on SDR discs operating under different operating conditions be modelled for different types of discs, feeding system and feed locations in order to make it more attractive. In addition, the use of more advanced CFD code such as Fluent software which would enable the prediction of the flow and concentration field on the SDR disc and the local power dissipation at a given radius can be used to validate the micromixing results obtained from this study.

II. It is recommended that a comprehensive film flow visualization study on rotating disc be performed in order to investigate the thin film behaviour on disc surface under the effect of the operating parameters that has been implemented in this study i.e. disc rotation rates, total feed flowrates, disc surface configurations (stainless steel smooth and grooved) and liquid viscosity. This can be used to relate the behaviour of the thin film flows on the disc surface with the SDR micromixing results collected from this investigation which will give a clearer picture and better explanation for the micromixing and RTD results achieved by the SDR. It is important to mention that one of the objectives of this research was to carry out flow film visualization study on 30cm rotating disc; a phantom V7 camera supplied by EPSRC (Engineering Instrument Pool) was used for this purpose. Unfortunately, the captured photos were not clear and efficient enough to serve the purpose of the interpretation. Hence it is recommended that selection of the proper camera for the visualization purpose needs to be carried out in future works on SDR.

III. It would be valuable to assess the micromixing in the SDR by determination of the micromixing time and theoretical segregation index by using a simple mixing model, i.e., the incorporation model which describes the coupling between mixing and chemical reaction in order to obtain the best agreement between theoretical predictions and experimental data over a wide range of operating conditions which was adopted in this research.

IV. Investigation into the distribution of Xs at different radial positions on the disc surface, i.e., the effect of radial positions on Xs by collecting the samples at the various radius of the SDR disc surface. This was not possible to carry it out in this study. The sampling probe (scooper) was designed and constructed for this purpose. As was mentioned in the Chapter 4, due to the thinner film of the disc, it was not possible to collect the samples by this scooper. So it is recommended to run the micromixing and experiments at higher flowrates that has been adopted in this investigation (higher then 15ml/s) by using larger pump capacity than was used in this research. This can help to increase the film thickness and build a pool within the probe tube which could then be drawn up the samples via a syringe for later analysis. Subsequently, the target can be achieved.

V. Regarding the RTD Experiments, it is recommended to collect samples at the edge of the disc, i.e. the samples will be collected right after it comes off the disc, rather than collected from the end of the tubing attached to the sampling system, which was extending the residence time. In addition, in this work an offline sample analysis method was used, it will be more accurate to take online measurements by using a different tracer/analytical system, e.g. using a solution of potassium chloride (KCl) or Sodium hydroxide (NaOH) as tracer and the tracer concentration can be measured by its electrical conductivity .

VI. This study involved the use of a normal grooved rotating disc whose hydrodynamic measurements are yet to be determined. Hence there is need to for carrying out tests to measure the film thickness and the velocity at various radial positions and the residence times for different geometry and types of grooves like the normal and re-entry. There is also the need to develop the empirical correlations and models that are similar to the centrifugal model for smooth discs in order to establish the dependencies of film thickness, velocity distribution and residence time on the different operating variables such as disc speed and liquid flowrate and viscosity.

VII. *Suggestions related to SDR design:*

The present investigation proves that the disc surface area of the SDR was one of the factors affecting the intensity of the micromixing. For the purpose of increasing the surface area of the surface disc of the SDR, it is suggested to use a multi SDRs in series where the product from one SDR is fed onto next one and so on, or stacking of the discs in one SDR (one disc above the other) and then feeding the product onto lower discs from the above and so on.

VIII. *Suggestions related to SDR surface design:*

- It is recommended that investigation of the micromixing performance of the SDR using the roughened disc surface that could be produced mechanically be perfomed. These kinds of surfaces could be in the shape of reverse spirals of varying depth or metal sprayed rough surface. The experimental results collected from these kinds of surfaces can be compared with the results achieved in this investigation.

- Combinations of grooves with the incorporation of the above modifications, on the whole groove surfaces or just only on the flat areas should be carried out.

IX. *Suggestions related to Multi-Point Distributor design:*

In the present design of the multipoint distributor with 4 holes of 0.2 mm diameter each, it was clear that the distributor did not perform as well as expected in the range of flowrates tested (3 ml/s to 15 ml/s). It may well be that to obtain a more even jet flow of acid especially under conditions of very low flowrates, it is recommended to have 4 holes of a much smaller diameter such as 0.05 mm so that increased liquid hold-up may prevail to give a uniform and continuous jet of acid at the injection point for improved acid distribution and micromixing. To further improve the intensity of micromixing, it may be more advantageous to change the location of the distributor itself in terms of the radial position of the outlet holes from the centre and their vertical distance from the disc surface. This may be especially relevant when grooved discs are used so that the jet is introduced before the first groove position.

X. Suggestions related to the initial concentration of the reactants:

The reactant concentrations implemented in this work ware adopted from the work of Guichardon and Falk (2000a). There is a lot of work can be done to expand the knowledge of the effect of the reactant concentrations and the value of the flow rate ratios,(R), on the SDRs micromixing performance. It is suggested to implement a different set of reactants concentration as well as use the value of the flow rate ratio R=1, (where $R=Q_I/Q_H$) and to find out how the values of Xs is effected.

References

Dow Chemical Company,Data sheets for Physical Properties of Glycerine 99.7% USP/EP, . Available at: http://www.dow.com/glycerine/products/optim.htm (Accessed: 02/04/2009).

Adeosun, J. T. and Lawal, A. (2005) 'Mass transfer enhancement in microchannel reactors by reorientation of fluid interfaces and stretching', *Sensors and Actuators B: Chemical*, 110, (1), pp. 101-111.

Akay, G., Mackley, M. R. and Ramshaw, C. (1997) *IChemE Research Event Proceedings* Nottingham, Chameleon Press, London, UK, April 8 – 9,

Andreev, A. F. (1964) ' Stability of the laminar flow of the thin liquid layers', *J. Exp. Theo. Phys.*, 18 (2), pp. 519-521.

Anxionnaz, Z., Cabassud, M., Gourdon, C. and Tochon, P. (2008) 'Heat exchanger/reactors (HEX reactors): Concepts, technologies: State-of-the-art', *Chemical Engineering and Processing: Process Intensification*, 47, (12), pp. 2029-2050.

Aoki, N. and Mae, K. (2006) 'Effects of channel geometry on mixing performance of micromixers using collision of fluid segments', *Chemical Engineering Journal*, 118, (3), pp. 189-197.

Aoune, A. and Ramshaw, C. (1999) 'Process intensification: Heat and mass transfer characteristics of liquid films on rotating discs', *International Journal of Heat and Mass Transfer*, 42, (14), pp. 2543-2556.

Apruzzese, F., Pato, J., Balke, S. T. and Diosady, L. L. (2003) 'In-line measurement of residence time distribution in a co-rotating twin-screw extruder', *Food Research International*, 36, (5), pp. 461-467.

Aris, R. (1958) 'On the Dispersion of Linear Kinematic Waves', *Proceedings of the Royal Society of London. Series A. Mathematical and Physical Sciences*, 245, (1241), pp. 268-277.

Assirelli, M., Bujalski, W., Eaglesham, A. and Nienow, A. W. (2002) 'Study Of Micromixing in a Stirred Tank Using a Rushton Turbine: Comparison of Feed Positions and Other Mixing Devices', *Chemical Engineering Research and Design*, 80, (8), pp. 855-863.

Assirelli, M., Bujalski, W., Eaglesham, A. and Nienow, A. W. (2008) 'Macro- and micromixing studies in an unbaffled vessel agitated by a Rushton turbine', *Chemical Engineering Science*, 63, (1), pp. 35-46.

Aubry, C. (1972) *Représentation des états de micromélange résultant de la mise en contact de deux courants d'un fluide homogène.* Ph.D thesis. Université de Nancy I.

Awtrey, A. D. and Connick, R. E. (1951) 'The absorption spectra of I2, I3 -, I-, IO3 -, S4O6 = and S2O3 =. Heat of the reaction I3 - = I2 + I', *Journal of the American Chemical Society,* 73, (4), pp. 1842-1843.

Baldyga, J. and Bourne, J. R. (1984a) 'A Fluid Mechanical Approach to Turbulent Mixing and Chemical Reaction - Part II Micromixing in the Light of Turbulence Theory', *Chem. Eng. Commun.,* 28, pp. 243-258.

Baldyga, J. and Bourne, J. R. (1984b) 'FLUID MECHANICAL APPROACH TO TURBULENT MIXING AND CHEMICAL REACTION. PART III. COMPUTATIONAL AND EXPERIMENTAL RESULTS FOR THE NEW MICROMIXING MODEL', *Chemical Engineering Communications,* 28, (4-6), pp. 259-281.

Baldyga, J. and Bourne, J. R. (1989a) 'Simplification of micromixing calculations. I. Derivation and application of new model', *The Chemical Engineering Journal,* 42, (2), pp. 83-92.

Baldyga, J. and Bourne, J. R. (1989b) 'Simplification of micromixing calculations. II. New applications', *The Chemical Engineering Journal,* 42, (2), pp. 93-101.

Baldyga, J. and Bourne, J. R. (1992) 'Interactions between mixing on various scales in stirred tank reactors', *Chemical Engineering Science,* 47, (8), pp. 1839-1848.

Baldyga, J. and Bourne, J. R. (1999) *Turbulent mixing and Chemical Reactions.* John Wiley & sons.

Baldyga, J., Bourne, J. R. and Walker, B. (1998) 'Non-isothermal micromixing in turbulent liquids: theory and experiment', *Canadian Journal of Chemical Engineering,* 76, (3), pp. 641-649.

Baldyga, J. and Pohorecki, R. (1995a) 'Turbulent micromixing in chemical reactors -- a review', *The Chemical Engineering Journal and the Biochemical Engineering Journal,* 58, (2), pp. 183-195.

Baldyga, J. and Pohorecki, R. (1995b) 'Turbulent micromixing in chemical reactors - a review', *The Chemical Engineering Journal and the Biochemical Engineering Journal,* 58, (2), pp. 183-195.

Ball, C. (1975) *The hydrodynamics and heat transfer characteristics of liquid films on a rotating disc* PhD thesis. Newcastle University.

Barthole, J. P., David, R. and Villermaux, J. (1982) 'A new chemical method for the study of local micromixing conditions in industrial stirred tanks', *ACS Simp. Ser.,* 196, pp. 545-553.

Bhattacharya, S. and Kresta, S. M. (2002) 'CFD simulations of three-dimensional wall jets in a stirred tank', *Canadian Journal of Chemical Engineering,* 80, (4), pp. 695-709.

Binnie, A. (1957) 'Experiments on the onset of water formation on a film of water flowing down a vertical plane', *J. Fluid Mech.*, 2, pp. 551-553.

Boodhoo, K. V. K. (1999) *Process Intensification: Spinning Disc Reactor for Styrene Polymerisation.* PhD Thesis thesis. University of Newcastle Upon Tyne.

Boodhoo, K. V. K., Dunk, W. A. E. and Jachuck, R. J. (2002) 'Influence of centrifugal field on free-radical polymerization kinetics', *Journal of Applied Polymer Science*, 85, (11), pp. 2283-2286.

Boodhoo, K. V. K., Dunk, W. A. E. and Jachuck, R. J. J. (2003) 'Continuous Photopolymerization in a Novel Thin Film
Spinning Disc Reactor: Photoinitiated Polymerization', in *ACS Symposium Series.* Vol. 847 ACS pp. 437- 450

Boodhoo, K. V. K., Dunk, W. A. E., Jassim, M. S. and Jachuck, R. J. (2004) 'Thin film solvent-free photopolymerization of n-butyl acrylate. I. Static film studies', *Journal of Applied Polymer Science*, 91, (4), pp. 2079-2095.

Boodhoo, K. V. K., Dunk, W. A. E., Vicevic, M., Jachuck, R. J., Sage, V., Macquarrie, D. J. and Clark, J. H. (2006) 'Classical cationic polymerization of styrene in a spinning disc reactor using silica-supported BF3 catalyst', *Journal of Applied Polymer Science*, 101, (1), pp. 8-19.

Boodhoo, K. V. K. and Jachuck, R. J. (2000a) 'Process intensification: spinning disk reactor for styrene polymerisation', *Applied Thermal Engineering*, 20, (12), pp. 1127-1146.

Boodhoo, K. V. K. and Jachuck, R. J. (2000b) 'Process intensification: spinning disc reactor for condensation polymerisation', *Green Chemistry*, 2, (5), pp. 235-244.

Bosworth, R. C. L. (1948) 'Distribution of reaction times for laminar flow in cylindrical reactors', *Philosophical Magazine Series*, 7, (39), pp. 847-862.

Bourne, J. R. (1993) 'What Does the Modelling of Reactive Flows Ask of CFD ?', *Oil & Gas Science and Technology*, 48, (06), pp. 615 - 630.

Bourne, J. R. (2003) 'Mixing and the selectivity of chemical reactions', *Organic Process Research and Development*, 7, (4), pp. 471-508.

Bourne, J. R., Crivelli, E. and Rys, P. (1977) 'Chemical Selectivities Disguised by Mass Diffusion.V.Mixing-Disguised Azo Coupling Reactions', *Helvetica Chimica Acta*, 60,, pp. 2944- 2957.

Bourne, J. R. and Hilber, C. P. (1990b) 'The productivity of micromixingcontrolled reactions: effect of feed distribution in stirred tanks', *Trans IChemE*, 68, pp. 51-56.

Bourne, J. R. and Kozicki, F. (1977) 'Mixing effects during the bromination of 1,3,5-trimethoxybenzene', *Chemical Engineering Science*, 32, (12), pp. 1538-1539.

Bourne, J. R., Kozicki, F. and Rys, P. (1981) 'Mixing and fast chemical reaction--I: Test reactions to determine segregation', *Chemical Engineering Science,* 36, (10), pp. 1643-1648.

Bourne, J. R., Kut, O. M. and Lenzner, J. (1992) 'An improved reaction system to investigate micromixing in high-intensity mixers', *Industrial and Engineering Chemistry Research,* 31, (3), pp. 949-958.

Bourne, J. R., Kut, O. M., Lenzner, J. and Maire, H. (1990) 'Kinetics of the Diazo Coupling between 1-Naftol and Diazotized Sulfanilic Acid. Industrial & Engineering Chemistry Research', *Industrial & Engineering Chemistry Research,* 29, pp. 1761-1765.

Bourne, J. R. and Maire, H. (1991) 'Influence of the kinetic model on simulating the micromixing of 1-naphthol and diazotized sulphanilic acid', *Ind. Eng. Chem. Res.,* 30, pp. 1389-1390.

Bourne, J. R. and Rohani, S. (1983) 'Micro-mixing and the Selective Iodination of I-Tyrosine', *Chemical Engineering Research & Design,* 61, pp. 297-302.

Bourne, J. R., Rys, P. and Suter, K. (1977b) 'Mixing effects in the bromination of resorcin', *Chemical Engineering Science,* 32, (7), pp. 711-716.

Bourne, J. R. and Thoma, S. A. (1991) 'Some factors determining the critical feed time of a semi-batch reactor', *Chemical Engineering Research and Design,* 69, (4), pp. 321-323.

Bourne, J. R. and Yu, S. (1994) 'Investigation of micromixing in stirred tank reactors using parallel reactions', *Industrial & Engineering Chemistry Research,* 33, (1), pp. 41-55.

Brauner, N. and Maron, D. M. (1982) 'Characteristics of inclined thin films, waviness and the associated mass transfer', *International Journal of Heat and Mass Transfer,* 25, (1), pp. 99-110.

Bums, J. R. (1996) *Liquid distribution in a rotating packed bed.* thesis. Newcastle

Burns, J. R., Jamil, J. N. and Ramshaw, C. (2000) 'Process intensification: operating characteristics of rotating packed beds -- determination of liquid hold-up for a high-voidage structured packing', *Chemical Engineering Science,* 55, (13), pp. 2401-2415.

Burns, J. R. and Ramshaw, C. (1996) 'Process intensification: Visual study of liquid maldistribution in rotating packed beds', *Chemical Engineering Science,* 51, (8), pp. 1347-1352.

Cafiero, L. M., Baffi, G., Chianese, A. and Jachuck, R. J. J. (2002) 'Process Intensification: Precipitation of Barium Sulfate Using a Spinning Disk Reactor', *Industrial & Engineering Chemistry Research,* 41, (21), pp. 5240-5246.

Charwat, A. F. and Kelly, R. E. (1972) 'The flow and stability of thin liquid films on a rotating disk', *J. Fluid Mech.,* 53, (2), pp. 227-255.

Cheremisinoff, N. P. (2000) 'Handbook of Chemical Processing Equipment', in Elsevier.

Chia-Chang, L. and Hwai-Shen, L. (2000) 'Adsorption in a centrifugal field: Basic dye adsorption by activated carbon', *Industrial and Engineering Chemistry Research*, 39, (1), pp. 161-167.

Chu, G.-W., Song, Y.-H., Yang, H.-J., Chen, J.-M., Chen, H. and Chen, J.-F. (2007) 'Micromixing efficiency of a novel rotor-stator reactor', *Chemical Engineering Journal*, 128, (2-3), pp. 191-196.

Costes, J. and Couderc, J. P. (1988) 'Study by laser Doppler anemometry of the turbulent flow induced by a Rushton turbine in a stirred tank: Influence of the size of the units-I. Mean flow and turbulence', *Chemical Engineering Science*, 43, (10), pp. 2751-2764.

Cozewith, C. and Squire, K. R. (2000) 'Effect of reactor residence time distribution on polymer functionalization reactions', *Chemical Engineering Science*, 55, (11), pp. 2019-2029.

Custer, J. J. (1949) 'Spectrophotometric determination of microquantities of iodine', *Analytical Chemistry*, 21, (8), pp. 1003-1005.

Danckwerts, P. V. (1953) 'Continuous flow systems : Distribution of residence times', *Chemical Engineering Science*, 2, (1), pp. 1-13.

Danckwerts, P. V., Jenkins, J. W. and Place, G. (1954) 'The distribution of residence-times in an industrial fluidised reactor', *Chemical Engineering Science*, 3, (1), pp. 26-35.

David, R., Barthole, J. P. and Villermaux, J. (1985) 'Interpretation of micromixing experiments involving consecutive competitive reactions in a stirred tank by a simple interaction model', *Proc.5th European Conference on Mixing*. Wurzburg, West Germany, pp. 433-441.

Deckwer, W. D. and Schumpe, A. (1993) 'Improved tools for bubble column reactor design and scale-up', *Chemical Engineering Science*, 48, (5), pp. 889-911.

Detrez, C., David, R. and Villermaux, J. (1988) 'New developments of the precipitation method for the study of local micromixing efficiency in mixing devices', *6th European conference on Mixing*. Pavia Italy, 1988. pp. 153 -159.

Dow Chemical Company *Data sheets for Physical Properties of Glycerine 99.7% USP/EP*. Available at: http://www.dow.com/glycerine/products/optim.htm (Accessed: 02/04/2009).

Edward, P., Victor, A. and Suzanne, K. (2004) *handbook of industrial mixing - Wiley-Interscien.*

Ehrfeld, W., Golbig, K., Hessel, V., LÃ¶we, H. and Richter, T. (1999) 'Characterization of mixing in micromixers by a test reaction: Single mixing units and mixer arrays', *Industrial and Engineering Chemistry Research,* 38, (3), pp. 1075-1082.

Ekpo, O. (1972) *The Effect of Wall Fow on theLiquid Residence Time Distribution in Randomly Packed Columns* PhD thesis. Victoria University of Machester.

Emslie, A. G., Bonner, F. T. and Peck, L. G. (1958) 'Flow of a Viscous Liquid on a Rotating Disk', *J. Appl. Phys.* , 29, pp. 858.

Engler, M., Kockmann, N., Kiefer, T. and Woias, P. (2004) 'Numerical and experimental investigations on liquid mixing in static micromixers', *Chemical Engineering Journal,* 101, (1-3), pp. 315-322.

Falk, L. and Commenge, J. M. (2010) 'Performance comparison of micromixers', *Chemical Engineering Science,* 65, (1), pp. 405-411.

Falk, L., Fournier, M. C. and Villermaux, J. (1994) 'Scale-up of micomixing effects in stirred tank reactors by a parallel competing reaction system', *icheme Symposium Series,* 136, pp. 251-258.

Ferrouillat, S., Tochon, P. and Peerhossaini, H. (2006) 'Micromixing enhancement by turbulence: Application to multifunctional heat exchangers', *Chemical Engineering and Processing,* 45, (8), pp. 633-640.

Fogler, H. S. (1992) *Elements of chemical reaction engineering.*Second edition ed: Prentice Hall International Editions.

Fogler, H. S. (2006) *Elements of chemical reaction engineering.*fourth edition ed: Pearson education Inc.

Fournier, M. C., Falk, L. and Villermaux, J. (1996a) 'A new parallel competing reaction system for assessing micromixing efficiency--Experimental approach', *Chemical Engineering Science,* 51, (22), pp. 5053-5064.

Fournier, M. C., Falk, L. and Villermaux, J. (1996b) 'A new parallel competing reaction system for assessing micromixing efficiency--Determination of micromixing time by a simple mixing model', *Chemical Engineering Science,* 51, (23), pp. 5187-5192.

Friedman, S. J. and Miller, C. O. (1941) 'Liquid Films in the Viscous Flow Region', *Industrial & Engineering Chemistry,* 33, (7), pp. 885-891.

Fulford, G. D. (1964) 'The flow of liquids in thin films', *Advances in Chemical Engineering :Academic Press, New York,* 5, pp. 151-236.

Fulford, G. D., Thomas B. Drew, J. W. H. J. T. V. and Giles, R. C. (1964) 'The Flow of Liquids in Thin Films', in *Advances in Chemical Engineering.* Vol. Volume 5 Academic Press, pp. 151-236.

Gao, Y., Vanarase, A., Muzzio, F. and Ierapetritou, M. (2011) 'Characterizing continuous powder mixing using residence time distribution', *Chemical Engineering Science,* 66, (3), pp. 417-425.

Geisler, R., Krebs, R. and Forschner, P. (1994) 'Local turbulent shear stress in stirred vessels and its significance for different mixing tasks', *IChemE Symposium Series,* 21, (9), pp. 243-250.

Genina, E. A., Bashkatov, A. N. and Tuchin, V. V. (2008) 'Effect of ethanol on the transport of methylene blue through stratum corneum', *Medical Laser Application,* 23, (1), pp. 31-38.

Gigras, A. and Pushpavanam, S. (2008) 'Early induction of secondary vortices for micromixing enhancement', *Microfluidics and Nanofluidics,* 5, (1), pp. 89-99.

Gilliland, E. R. and Mason, E. A. (1952) 'Gas mixing in beds of fluidised solids', *Industrial and Engineering Chemistry,* 44, pp. 218-234.

Gorman, E. S. and Shnider, M. R. (1988) 'Effect of methylene blue on the absorbance of solutions of haemoglobin', *British Journal of Anaesthesia,* 60, (4), pp. 439-444.

Goto, H., Goto, S. and Matsubara, M. (1975) 'A generalized two-environment model for micromixing in a continuous flow reactor-II. Identification of the model', *Chem. Engng Sci.* , 30, pp. 71–77.

Green, D. W. and Perry, R. H. (2008) 'Perry's Chemical Engineers' Handbook (8th Edition)', in McGraw-Hill,pp 2-112.

Guichardon, P. and Falk, L. (2000) 'Characterisation of micromixing efficiency by the iodide-iodate reaction system. Part I: experimental procedure', *Chemical Engineering Science,* 55, (19), pp. 4233-4243.

Guichardon, P. and Falk, L. (2000a) 'Characterisation of micromixing efficiency by the iodideâ€“iodate reaction system. Part I: experimental procedure', *Chemical Engineering Science,* 55, (19), pp. 4233-4243.

Guichardon, P., Falk, L., Fournier, M. C. and Villermaux, J. (1995) 'Study of micromixing in a liquid-solid suspension in a stirred reactor', *AIChE Symp. Series,* 91, pp. 123-130.

Guichardon, P., Falk, L. and Villermaux, J. (1997) 'Extension of a chemical method for the study of micromixing process in viscous media', *Chemical Engineering Science,* 52, (24), pp. 4649-4658.

Guichardon, P., Falk, L. and Villermaux, J. (2000b) 'Characterisation of micromixing efficiency by the iodide-iodate reaction system. Part II: kinetic study', *Chemical Engineering Science,* 55, (19), pp. 4245-4253.

Hai-Jian Yang, G.-W. C., Jian-Wen Zhang, Zhi-Gang Shen, and Jian-Feng Chen. (2005) 'Micromixing Efficiency in a Rotating Packed Bed: Experiments and Simulation', *Ind. Eng. Chem. Res.*, 44 (20), pp. pp 7730–7737.

Hall, C. and Hughes, T. L. (1993) *Proceedings of the 1993 SPE International Symposium on Oilfield Chemistry.*

Harnby, N., Edwards, M. F. and Nienow, A. W. (1992) *Mixing in the process industries.* New York: Butterworth-Heinemann.

Hartley, D. E. and Murgatroyd, W. (1964) 'Criteria for the break-up of thin liquid layers flowing isothermally over solid surfaces', *International Journal of Heat and Mass Transfer,* 7, (9), pp. 1003-1015.

Harvey, A. P., Mackley, M. R. and Seliger, T. (2003) 'Process intensification of biodiesel production using a continuous oscillatory flow reactor', *Journal of Chemical Technology and Biotechnology,* 78, (2-3), pp. 338-341.

Harvey, A. P., Mackley, M. R. and Stonestreet, P. (2001) 'Operation and optimization of an oscillatory flow continuous reactor', *Industrial and Engineering Chemistry Research,* 40, (23), pp. 5371-5377.

Hassan-Beck, H. M. (1997) *Process intensification: Mass transfer and pressure drop for counter-current rotating packed beds.* PhD thesis. Newcastle.

Hessel, V. and Lowe, H. (2003a) 'Microchemical engineering: Components, plant concepts user acceptance - Part I', *Chemical Engineering and Technology,* 26, (1), pp. 13-24.

Hessel, V. and Lowe, H. (2003b) 'Microchemical engineering: Components, plant concepts, user acceptance - Part II', *Chemical Engineering and Technology,* 26, (4), pp. 391-408.

Hessel, V., Löwe, H. and Schönfeld, F. (2005) 'Micromixers - a review on passive and active mixing principles', *Chemical Engineering Science,* 60, (8-9), pp. 2479-2501.

Higgins, P. R. (2000) *The Characterisation of the Hydrodynamic Vortex Separator using Residence Time Distribution Analysis.* thesis. Liverpool John Moores University.

Holland, F. and Bragg, R. (1995) *Fluid Flow for Chemical and Process Engineers* Second ed: Butterworth-Heinemann.

Horstwood, J. (2009) *Characterisation of micromixing effects in a narrow channel reactor.* M.Sc. thesis. Newcastle.

Interactive Mathematics (2009) *Integration*. Available at: http://www.intmath.com/integration/integration-intro.php (Accessed: 11th November).

Jachuck, R. J. and Ramshaw, C. (1994a) 'Process Intensification: Heat transfer characteristics of tailored rotating surfaces', *Heat Recovery Systems and CHP* 14, (5), pp. 475-491.

Jachuck, R. J. J. and Ramshaw, C. (1994b) 'Process intensification: Heat transfer characteristics of tailored rotating surfaces', *Heat Recovery Systems and CHP*, 14, (5), pp. 475-491.

Johnson, B. K. and Prud'homme, R. K. (2003) 'Chemical processing and micromixing in confined impinging jets', *AIChE Journal*, 49, (9), pp. 2264-2282.

Keairns, D. L. and Manning, F. S. (1969) 'Model simulation of adiabatic continuous flow stirred tank reactors ', *AIChE J.* , 15, (5), pp. 660–665.

Keeler, R. N., Petersen, E. E. and Prausnitz, J. M. (1965) ' Mixing and chemical reaction in turbulent flow reactors ', *A.I.Ch.E. J.* , 11 (2), pp. 221–227.

Khalid, Z. (2001) *Studies of the photochemical hinetics of methylene blue with reductants.* thesis. University of Karachi.

Khan, J. R. (1986) *Heat Transfer on A rotating surface with and without phase change.* PhD thesis. Newcastel University.

Kirkbride, C. G. (1934) 'Heat Transfer by Condensing Vapor on Vertical Tubes', *Industrial & Engineering Chemistry*, 26, (4), pp. 425-428.

Klein, J. P., David, R. and Villermaux, J. (1980) ' Interpretation of experimental liquid phase micromixing phenomena in a continuous stirred reactor with short residence times', *Ind. Eng. Chem. Fundam.* , 19, pp. 373–379.

Kockmann, N., Kiefer, T., Engler, M. and Woias, P. (2006) 'Convective mixing and chemical reactions in microchannels with high flow rates', *Sensors and Actuators B: Chemical*, 117, (2), pp. 495-508.

Köhler, J. M., Schleiff, B., Schneider, S., Boskovic, D., Henkel, T. and Groß, G. A. (2010) 'Characterization of viscosity dependent residence time distribution in the static micromixer Statmix6', *Chemical Engineering Journal*, 160, (3), pp. 845-851.

Kusch, H. A., Ottino, J. M. and Shannon, D. M. (1989) 'Analysis of impingement mixing-reaction data: Use of a lamellar model to generate fluid mixing information', *Industrial and Engineering Chemistry Research*, 28, (3), pp. 302-315.

Larosa, P. and Manning, F. S. (1964) ' Intensity of segregation as a measure of incomplete mixing', *Can. J. Chem. Eng.* , 42, pp. 65–68.

Laufhuette, H. D. and Mersmann, A. (1987) 'LOCAL ENERGY DISSIPATION IN AGITATED TURBULENT FLUIDS AND ITS SIGNIFICANCE FOR THE DESIGN OF STIRRING EQUIPMENT', *Chemical Engineering and Technology*, 10, (1), pp. 56-63.

Lee, E. T., Rehkopf, P. G., Warnicki, J. W., Friberg, T., Finegold, D. N. and Cape, E. G. (1997) 'A new method for assessment of changes in retinal blood flow', *Medical Engineering and Physics*, 19, (2), pp. 125-130.

Levenspiel, O. (1972) *Chemical reaction engineering* second edition ed New York:

Levenspiel, O. (1999) *Chemical reaction engineering* third edition ed New York: John Wiley & Sons.

Levenspiel, O. and Bischoff, K. (1959) 'Backmixing in the Design of Chemical Reactors', *Industrial & Engineering Chemistry,* 51, (12), pp. 1431-1434.

Leveson, P., Dunk, W. A. E. and Jachuck, R. J. (2004) 'Investigation of shear effects on styrene free radical polymerization using a narrow channel reactor', *Journal of Applied Polymer Science,* 94, (4), pp. 1365-1369.

Lin, C. C., Liu, W. T. and Tan, C. S. (2003) 'Removal of carbon dioxide by absorption in a rotating packed bed', *Industrial and Engineering Chemistry Research,* 42, (11), pp. 2381-2386.

Lin, W. W. and Lee, D. J. (1997) 'Micromixing effects in aerated stirred tank', *Chemical Engineering Science,* 52, pp. 3837-3842.

Lintz, H. G., Riekert, L. and Weber, W. (1975) 'Untersuchung des Mischvorgangs in einem kontinuierlich betriebenen Rührkessel mit Hilfe einer chemischen Reaktion', *Chemie Ing. Techn.* , 47 (3), pp. 103.

Liu, H. S., Lin, C. C., Wu, S. C. and Hsu, H. W. (1996) 'Characteristics of a rotating packed bed', *Industrial and Engineering Chemistry Research,* 35, (10), pp. 3590-3596.

Makataka, S. and Kobayashi, J. (1976) 'Micromixing model and experimental study in a continuous stirred-tank reactor', *Int. Chem. Eng.* , 16 (1), pp. 148–154.

Mansur, E. A., Ye, M., Wang, Y. and Dai, Y. (2008) 'A State-of-the-Art Review of Mixing in Microfluidic Mixers', *Chinese Journal of Chemical Engineering,* 16, (4), pp. 503-516.

Mao, K. W. and Toor, H. L. (1971) 'Second-order chemical reactions with turbulent mixing', *Ind. Eng. Chem. Fundam.* , 10 (2), pp. 192–197.

McCarthy, E. D., Dunk, W. A. E. and Boodhoo, K. V. K. (2007) 'Application of an intensified narrow channel reactor to the aqueous phase precipitation of barium sulphate', *Journal of Colloid and Interface Science,* 305, (1), pp. 72-87.

Meeuwse, M. (2011) *Rotor-Stator Spinning Disc Reactor.* PhD thesis. Eindhoven University of Technology.

Meeuwse, M., Lempers, S., van der Schaaf, J. and Schouten, J. C. (2010b) 'Liquid - Solid Mass Transfer and Reaction in a Rotor - Stator Spinning Disc Reactor', *Industrial & Engineering Chemistry Research,* 49, (21), pp. 10751-10757.

Meeuwse, M., van der Schaaf, J., Kuster, B. F. M. and Schouten, J. C. (2010a) 'Gas - liquid mass transfer in a rotor - stator spinning disc reactor', *Chemical Engineering Science,* 65, (1), pp. 466-471.

Méthot, J. C. and Roy, P. H. (1973) 'Experimental evaluation of a model-based degree of segregation in a CSTR', *Chem. Engng Sci,* 28, pp. 1961–1966.

Meyer, T., Fleury, P. A., Renken, A., Darbellay, J. and Larpin, P. (1992) 'Bariumsulfate precipitation as a model reaction for segregation studies at pilot scale', *Chem. Eng. Process.,* 31, pp. 307-310.

Miyairi, Y., Kamiwano, M. and Yamamoto, K. (1971) ' Turbulent mixing in a tubular flow reactor', *Int. Chem. Eng.* , 11 (2), pp. 344–352.

Miyawaki, O., Tsujikawa, H. and Uragughi, Y. (1975) 'Chemical reactions under incomplete mixing. ', *J. Chem. Eng. Japan* 8 (1), pp. 63–68.

Monnier, H., Wilhelm, A. M. and Delmas, H. (1999a) 'The influence of ultrasound on micromixing in a semi-batch reactor', *Chemical Engineering Science,* 54, (13-14), pp. 2953-2961.

Monnier, H., Wilhelm, A. M. and Delmas, H. (1999b) 'Influence of ultrasound on mixing on the molecular scale for water and viscous liquids', *Ultrasonics Sonochemistry,* 6, (1-2), pp. 67-74.

Monnier, H., Wilhelm, A. M. and Delmas, H. (2000) 'Effects of ultrasound on micromixing in flow cell', *Chemical Engineering Science,* 55, (19), pp. 4009-4020.

Moore, S. R. (1986) *Mass Transfer into Thin Liquid Films With and Without Chemical Reactions.* Ph.D.
thesis. University of Newcastle-upon-Tyne, UK.

Nabholz, F. and Rys, P. (1977) 'Chemical Selectivities Disguised by Mass Diffusion. IV. Mixing-Disguised Nitrations of Aromatic Compounds with Nitronium Salts', *Helvetica Chimica Acta,* 60
(
), pp. 2937-2943.
.

Nauman, E. B. and Buf ham, B. A. (1983) *Mixing in continuous flow systems.* New York: Wiley & Sons.

Nauman, E. B. and Buffham, B. A. (2003) *Mixing in Continuous Flow Systems.* J Wiley & Sons

Nguyen, N. T. and Wu, Z. (2005) 'Micromixers - A review', *Journal of Micromechanics and Microengineering,* 15, (2), pp. R1-R16.

Ni, X. (1994) 'Residence time distribution measurements in a pulsed baffled tube bundle', *Journal of Chemical Technology and Biotechnology,* 59, (3), pp. 213-221.

Nienow, A. W. (1997) 'On impeller circulation and mixing effectiveness in the turbulent flow regime', *Chemical Engineering Science*, 52, (15), pp. 2557-2565.

Nouri, L. h., Legrand, J., Benmalek, N., Imerzoukene, F., Yeddou, A.-R. and Halet, F. (2008) 'Characterisation and comparison of the micromixing efficiency in torus and batch stirred reactors', *Chemical Engineering Journal*, 142, (1), pp. 78-86.

Nusselt, W. and Ver.Deut. Ingr. Z. (1916) 60, pp. 549.

Okamoto, Y., Nishikawa, M. and Hashimoto, K. (1981) 'ENERGY DISSIPATION RATE DISTRIBUTION IN MIXING VESSELS AND ITS EFFECTS ON LIQUID-LIQUID DISPERSION AND SOLID-LIQUID MASS TRANSFER', *International chemical engineering*, 21, (1), pp. 88-94.

Oliveros, G. and Smith, J. M. (1982) 'Dynamic studies of dispersion and channelling in fixed Beds', *AIChE Journal*, 28, pp. 751-759.

Palmer, D. A., Ramette, R. W. and Mesmer, R. E. (1984) 'Triiodide ion formation equilibrium and activity coefficients in aqueous solution', *Journal of Solution Chemistry*, 13, (9), pp. 673-683.

Paul, E. L., Atiemo-Obeng, V. and Kresta, S. M. (2004) *Handbook of Industrial Mixing: Science and Practice.* Wiley-Interscien.

Paul, E. L., Mahadevan, H., Foster, J., Kennedy, M. and Midler, M. (1992) 'The effect of mixing on scaleup of a parallel reaction system', *Chem. Engng Sci.* , 47, , pp. 2837–2840.

Paul, E. L. and Treybal, R. E. (1971) 'Mixing and product distribution for a liquid-phase, second- order, competitive- consecutive reaction', *AIChE Journal*, 17, (3), pp. 718-724.

Phelan, K. G. and Stedman, G. (1981) ' Nitrogen tracer evidence for a cyclic azide species', *J. Chem. Soc. Commun.* , 6, pp. 299–300.

Philipossian, A. and Mitchell, E. (2003) 'Dispersion number studies in CMP of interlayer dielectric films', *Journal of the Electrochemical Society*, 150, (12), pp. G854-G860.

Rahman, M. M. and Faghri, A. (1993) 'Gas absorption and solid dissolution in a thin liquid film on a rotating disk', *International Journal of Heat and Mass Transfer*, 36, (1), pp. 189-199.

Ramshaw, C. (1999) 'Process intensification and green chemistry', *Green Chemistry*, 1, (1), pp. G15-G17.

Ramshaw, C. (2003) *Process Intensification Master degree level course* Newcastle university pp:

Ramshaw, C. and Mallinson, R. H. (1981) *Mass Transfer Process*.

Reay, D., Ramshaw, C. and Harvey, A. (2008) *Process Intensification: Engineering for efficiency sustainability and flexibility.* Elsevier.

Reid, R. C., Pausnitz, J. M. and Sherwood, T. K. (1977) *The properties of Gases and Liquids.*3rd ed: McGraw-Hill New York, U.S.A.

Rhodes, F. H. and Barbour, C. B. (1923) 'The Viscosities of Mixtures of Sulfuric Acid and Water', *Industrial & Engineering Chemistry,* 15, (8), pp. 850-852.

Rivera, F. F., Cruz-Diaz, M. R., Rivero, E. P. and Gonzalez, I. (2010) 'Analysis and interpretation of residence time distribution experimental curves in FM01-LC reactor using axial dispersion and plug dispersion exchange models with closed-closed boundary conditions', *Electrochimica Acta,* 56, (1), pp. 361-371.

Robinson, B. A. and Tester, J. W. (1984) 'DISPERSED FLUID FLOW IN FRACTURED RESERVOIRS: AN ANALYSIS OF TRACER-DETERMINED RESIDENCE TIME DISTRIBUTIONS', *Journal of Geophysical Research,* 89, (B12), pp. 10374-10384.

Rousseaux, J. M., Falk, L., Muhr, H. and Plasari, E. (1999) 'Micromixing efficiency of a novel sliding-surface mixing device', *AIChE Journal,* 45, (10), pp. 2203-2213.

Sanchez Perez, J. A., Rodriguez Porcel, E. M., Casas Lopez, J. L., Fernandez Sevilla, J. M. and Chisti, Y. (2006) 'Shear rate in stirred tank and bubble column bioreactors', *Chemical Engineering Journal,* 124, (1-3), pp. 1-5.

SCHNEIDER, M. A. (2004) *DEVELOPMENT OF A NOVEL MICROREACTOR-BASED CALORIMETER FOR THE STUDY OF FAST EXOTHERMAL REACTIONS IN LIQUID PHASE.* thesis. ÉCOLE POLYTECHNIQUE FÉDÉRALE DE LAUSANNE.

Schneider, M. A., Maeder, T., Ryser, P. and Stoessel, F. (2004) 'A microreactor-based system for the study of fast exothermic reactions in liquid phase: characterization of the system', *Chemical Engineering Journal,* 101, (1-3), pp. 241-250.

Sparks, T. (1996) *Fluid Mixing in Rotor/Stator Mixers.* PhD thesis. Cranfield University

Stankiewicz, A. and Moulijn, j. A. (2004) *RE-Engineering the Chemical Processing Plant.* Marcel Dekker,I nc.

Stankiewicz, A. I. and Moulijn, J. A. (2000a) 'Process intensification: Transforming chemical engineering', *Chemical Engineering Progress,* 96, (1), pp. 22-33.

Stankiewicz, A. I. and Moulijn, J. A. (2000b) 'Process Intensification :Transforming Chemical Engineering', *Chemical Engineering Progress,* 88, pp. 22-34.

Tatterson, G. B. (1994) *Scaleup and Design of Industrial Mixing Processes.* McGraw-Hill,Inc.

Tilton, J. N. (1997) '*Fluid and particle Dynamics in Perry's Chemical Engineers' Handbook (7th Edition)', in*: McGraw-Hill.

Tilton, J. N., Perry, R. H. and Green, D. W., Editors (1998) ' Perry's Chemical Engineering Handbook ', in McGraw–Hill, New York pp. 6-48.

Todd, D. B. and Irving, H. F. (1969) 'AXIAL MIXING IN SELF-WIPING REACTOR', *Chemical Engineering Progress*, 65, (9), pp. 84-89.

Torrest, R. S. and Ranz, W. E. (1969) ' Improved conductivity system for measurement of turbulent concentration fluctuations', *Ind. Eng. Chem. Fundam.*, 8 (4), pp. 810–816.

Treleaven, C. R. and Tobgy, A. H. (1973) 'Residence times, micromixing and conversion in an unpremixed feed reactor—II Chemical reaction measurements', *Chem. Engng Sci.* , 28, pp. 413–425.

Truong, K. T. and Methot, J. C. (1976) 'Segregation effects on consecutive competing reaction in a CSTR', *The Canadian Journal of Chemical Engineering*, 54, (5), pp. 572-577.

Venkataraman R.S. (1966) *Mass Transfer to an Expanding Interface.* PhD thesis. University of Leeds,Great Britain.

Vicevic, M. (2004) *Catalytic rearrangement of alpha pinene oxide using spinning disc reactor technology.* PhD thesis. Newtastle university.

Villermaux, J. (1986) 'Micromixing phenomena in stirred reactors', in *Encyclopedia of Fluid Mechanics.* Houston, TX.: Gulf Pub., pp. Chapter 27, pp. 707-771.

Villermaux, J., Falk, L. and Fournier, M. C. (1993) 'Potential use of a new parallel reaction system to characterize micromixing in stirred reactors', *AIChE Symp. Series,*, 90, pp. 50 -54.

Villermaux, J., Falk, L., Fournier, M. C. and Detrez, C. (1992) 'Use of parallel competing reactions to characterise micromixing efficiency', *AIChE Symp. Series*, 286, pp. 6-10.

Wenger, K. S., Dunlop, E. H. and MacGilp, I. D. (1992) 'Investigation of the chemistry of a diazo micromixing test reaction', *AIChE Journal*, 38, pp. 1105-1114.

Wolf, D. and White, D. H. (1976) 'EXPERIMENTAL STUDY OF THE RESIDENCE TIME DISTRIBUTION IN PLASTICATING SCREW EXTRUDERS', *AIChE Journal*, 22, (1), pp. 122-131.

Wood, R. M. and Watts, B. E. (1973) 'The flow, heat and mass transfer characteristics of liquid films on rotating discs', *Trans Instn Chem Engrs*, pp. 315-322.

Woods, W. (1995) *The hydrodynamics of thin liquid films flowing over a rotating disc.* PhD thesis. University of Newcastle upon Tyne, Newcastle Upon Tyne - UK.

Worrell, G. R. and Eagleton, L. C. (1964) 'An experimental study of mixing and segregation in a stirred tank reactor', *Can. J. Chem. Eng.* , 42, pp. 254–258.

Wu, H. and Patterson, G. K. (1989) 'Laser-Doppler measurements of turbulent-flow parameters in a stirred mixer', *Chemical Engineering Science,* 44, (10), pp. 2207-2221.

Yang, H. J., Chu, G. W., Xiang, Y. and Chen, J. F. (2006) 'Characterization of micromixing efficiency in rotating packed beds by chemical methods', *Chemical Engineering Journal,* 121, (2-3), pp. 147-152.

Yang, K., Chu, G.-W., Shao, L., Luo, Y. and Chen, J.-F. (2009a) 'Micromixing efficiency of rotating packed bed with premixed liquid distributor', *Chemical Engineering Journal,* 153, (1-3), pp. 222-226.

Yang, K., Chu, G., Shao, L., Xiang, Y., Zhang, L. and Chen, J. (2009b) 'Micromixing Efficiency of Viscous Media in Micro-channel Reactor', *Chinese Journal of Chemical Engineering,* 17, (4), pp. 546-551.

Yoshida, J. I., Nagaki, A., Iwasaki, T. and Suga, S. (2005) 'Enhancement of chemical selectivity by microreactors', *Chemical Engineering and Technology,* 28, (3), pp. 259-266.

Yu-Shao CHEN, H.-S. L., Chia-Chang LIN and Wen-Tzong LIU. (2004) 'Micromixing in a Rotating Packed Bed', *Journal of Chemical Engineering of Japan,* 37, (9), pp. 1122-1128.

Zoulalian, A. (1973.) *Etude par voie chimique du micro-mélange dans un réacteur agité continu en phase liquide.* Ph.D thesis. Université de Nancy I, Nancy.

Zoulalian, A. and Villermaux, J. (1974) 'INFLUENCE OF CHEMICAL PARAMETERS ON MICROMIXING IN A CONTINUOUS STIRRED TANK REACTOR (CSTR)', *Adv Chem Ser,* (13), pp. 348-361.

Zoulalian, A. and Villermaux, J. (1970) ' An experimental investigation of the state of mixing of the fluid in a chemical reactor', *Chem. Eng. J.* , 1, pp. 76–78.

Zwietering, T. N. (1959) 'The degree of mixing in continuous flow systems', *Chemical Engineering Science,* 11, (1), pp. 1-15.

Appendix A: Calibration carves for SBR pumping system

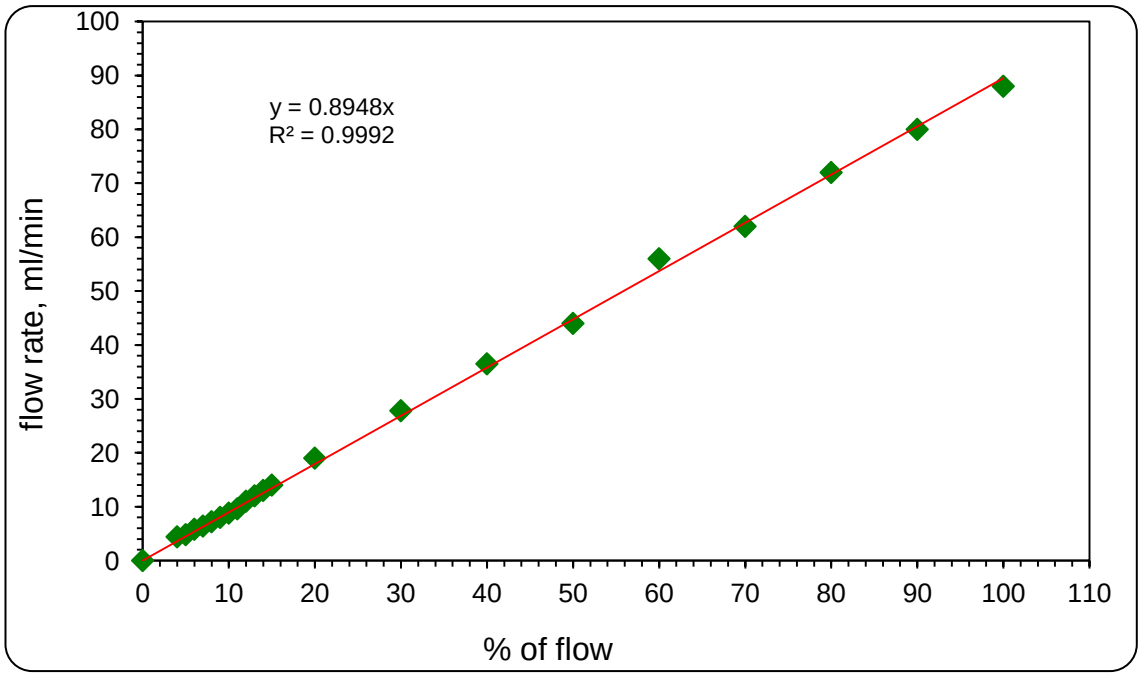

Figure AA-1: Calibration curve for syringe pump, model 353 sage instruments (one syringe of 60 ml)

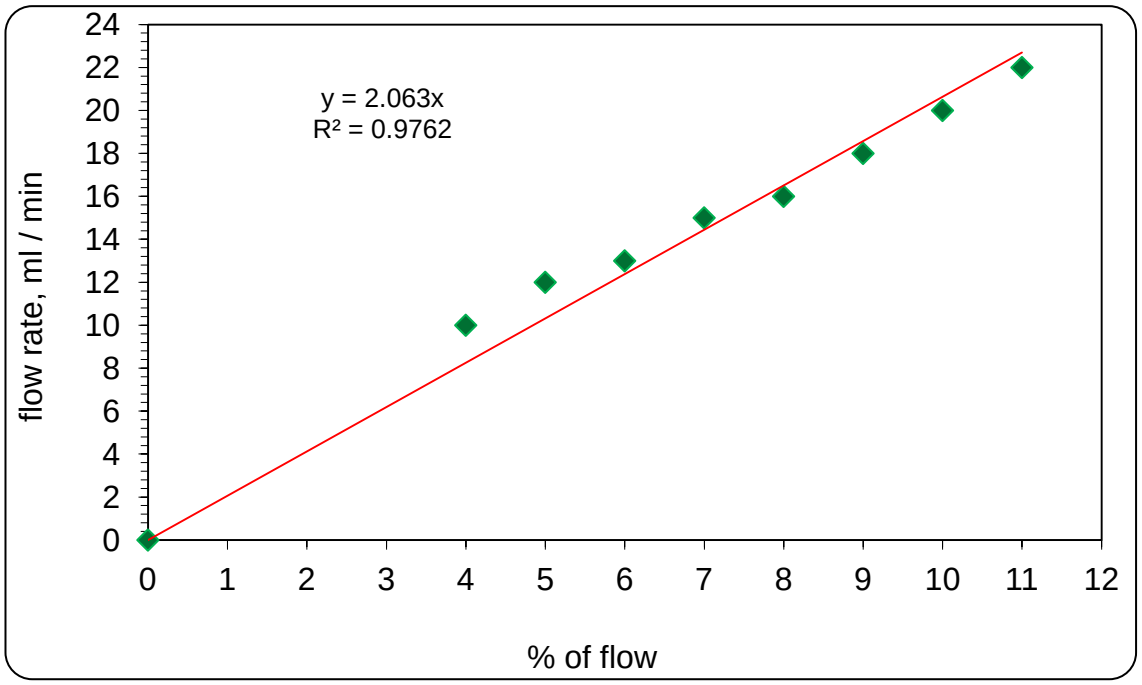

Figure AA-2: Calibration curve for syringe pump, model 353 sage instruments (Two syringes of 60 ml each)

Appendix B: Calculations the feed ratios, Q_H and Q_I for SDRs and NCRs and the sulphuric acid volumes which were injected into the SBR

Calculation of the Feed Ratios, (R), and Q_H & Q_I

The feed ratio, R, was calculated for each of the acid concentrations. The ratio ensures that the sulphuric acid is the limiting reagent. Once this had been found, the flowrate of both the feed streams could be found for the all the flowrates.

The following outlines the procedure for calculating the ratio and the flowrates, for 0.1M acid concentration and a total flowrate of 0.5ml/s.

$$R = \frac{Q_I}{Q_H} \qquad AB.1$$

Where :

R = the feed ratio
Q_I = the iodide, iodate, borate solution volumetric flowrate
Q_H = the acid volumetric flowrate

The concentrations known: $[H^+]_0$ = 0.1M and $[H_2BO_3]_0 = 0.0909$ M.

From section 4.2.1.2.4 it is known that:

$$\left(\frac{n_{H_2BO_3^-}}{n_{H,o^+}}\right)_{Batch} = \left(\frac{q_{H_2BO_3^-}\ [H_2BO_3^-]_0}{q_{H,_O^+}\ [H^+]_0}\right)_{Continuous} = 6.363 \qquad AB.2$$

$$\left(\frac{q_{H_2BO_3^-}[H_2BO_3]_0}{q_{H_0^+}[H^+]_0}\right)_{SDRs\&NCRs} = 6.363$$

$$\left(\frac{q_{H_2BO_3^-}[H_2BO_3]_0}{q_{H_0^+}[H^+]_0}\right)_{SDRs\&NCRs} = 6.363 = R\left(\frac{[H_2BO_3]_0}{[H^+]_0}\right)$$

Therefore R can be found from: $6.363 = R\left(\frac{0.0909}{0.1}\right) \Longrightarrow R = 7$

Once R has been calculated, it is used to find the required flowrates. For a total feed of 0.5ml/s:

$$Q_t = Q_I + Q_H \qquad AB.3$$

$$R = \frac{Q_I}{Q_H}$$

$$RQ_H = Q_I$$

$$Qt = RQ_H + Q_H$$

$$Qt = (R+1)Q_H$$

$$Q_H = \frac{Q_t}{R+1}$$

$$Q_H = \frac{3}{7+1} = \frac{0.0625\ ml}{s} = \frac{3.75\ ml}{min}$$

$$Q_I = Q_t - Q_H = 0.5 - 0.0625 = \frac{0.4375\ ml}{s} = 26.25\ ml/min$$

Calculation of the injected sulphuric acid volumes into the SBR:

As mentioned in Chapter 4. One of the restrictions that needed to be taken into account when carrying out a comparison between the performance of the various types of reactors studied is the ratio of the molar quantities of acid and the borate ions contacting each other. This parameter has to be maintained at a constant ratio in the NCRs and SDRs, as well as in the SBR for a valid comparison.

To utilise the above conditions for continuous reactor systems and to make a possible comparison between the micromixing performance of various reactor types (SBR vs. SDRs and NCRs), the ratio of the molar quantities of acid and the borate ions that are in contact with each other has to be considered. This ratio has to be maintained constant in the continuous reactors as well as in SBR for a valid comparison. Recalling equation AB.2:

$$\left(\frac{n_{H_2BO_3^-}}{n_{H,o^+}}\right)_{Batch} = 6.363 \qquad (4.6)$$

$$n_{H_2BO_3^-} = [CH_2BO_{3,0}^-] * V_{CH_2BO_{3,0}^-} = 0.09 * 1.37l = 0.1233\ moles$$

$$\left(\frac{0.1233}{n_{H,o^+}}\right)_{Batch} = 6.363 \implies n_{H,o^+} = \frac{0.1233}{6.363} = 0.020\ moles\ of\ H_{,0}^+$$

IF $[H_{,0}^+] = 1.0M$:

$$n_{H,o^+} = [H_{,0}^+] * V_{H_{,0}^+}$$

$$V_{H_{,0}^+} = \frac{0.020}{1.0} = 0.02\ l = 20\ ml\ of\ H_{,0}^+\ need\ to\ be\ injected\ into\ SBR$$

IF $[H_{,0}^+] = 0.5M$:

$$V_{H_{,0}^+} = \frac{0.020}{0.5} = 0.04\ l = 40\ ml\ of\ H_{,0}^+\ need\ to\ be\ injected\ into\ SBR$$

IF $[H_{,0}^+] = 0.25M$:

$$V_{H_{,0}^+} = \frac{0.020}{0.25} = 0.08\ l = 80\ ml\ of\ H_{,0}^+\ need\ to\ be\ injected\ into\ SBR$$

Appendix C: Calibration carves for 10cm SDR pumping system

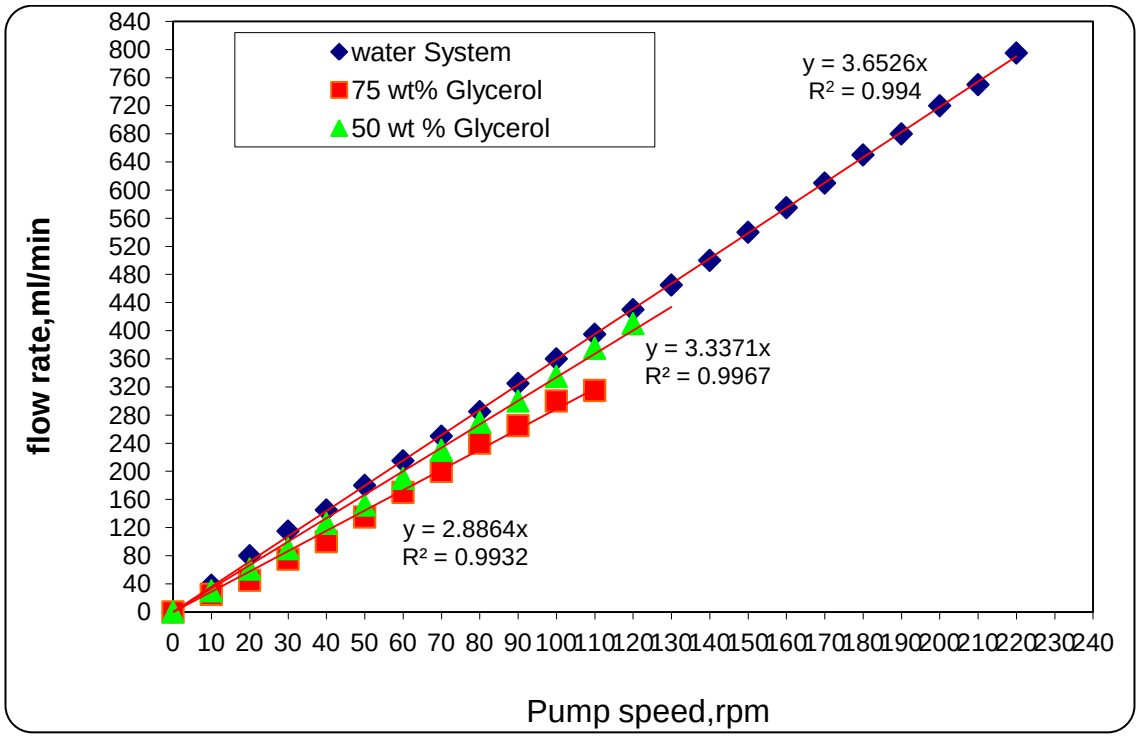

Figure AC-1: Calibration curve for Watson Marlow pump505S with 4.8 mm diameter tubing feed pipe.

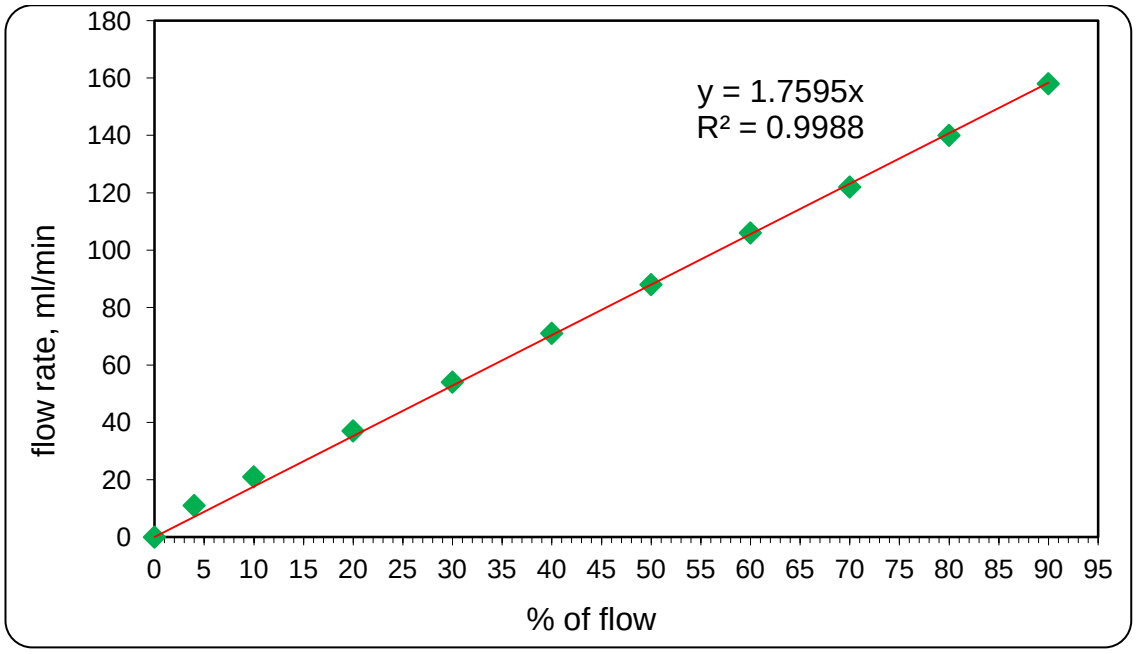

Figure AC-2: Calibration curve for syringe pump, model 353 sage instruments (two syringes of 60ml) with 4.8 mm of tubing pipe, 1.65mm diameter of feed system and 1.0 of pumping range

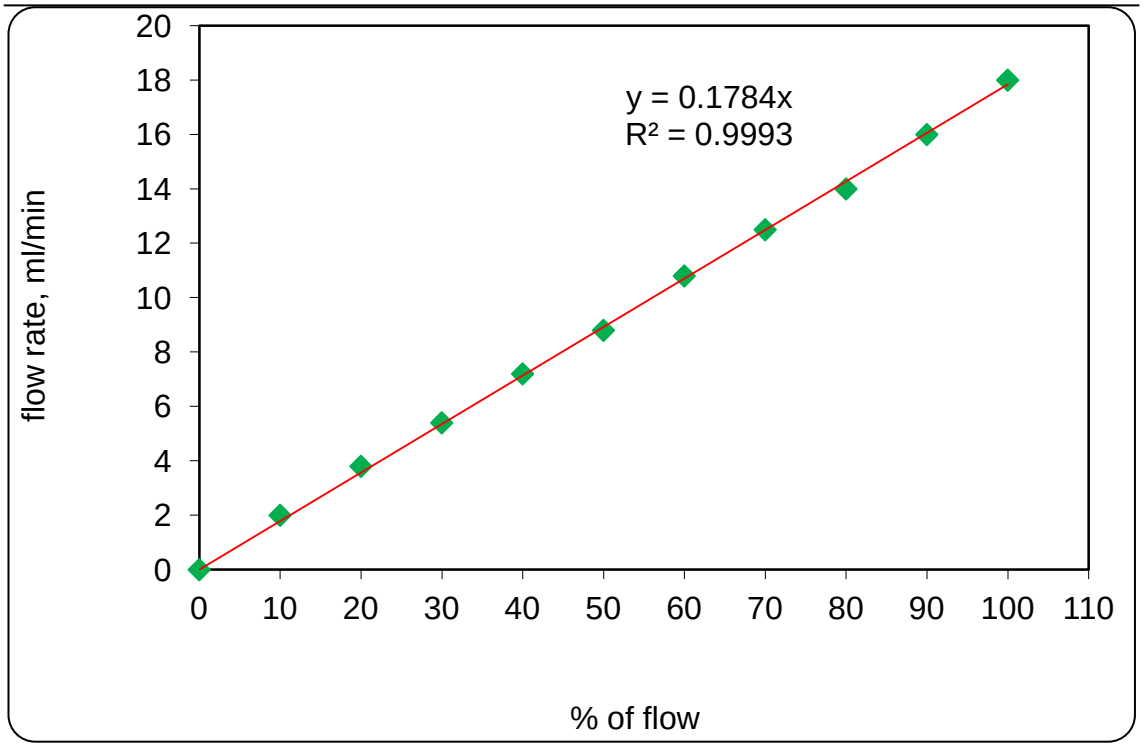

Figure AC-3: Calibration curve for syringe pump, model 353 sage instruments (two syringes of 60 ml) with 4.8 mm of tubing pipe, 1.65mm diameter of feed system and 0.1 of pumping range

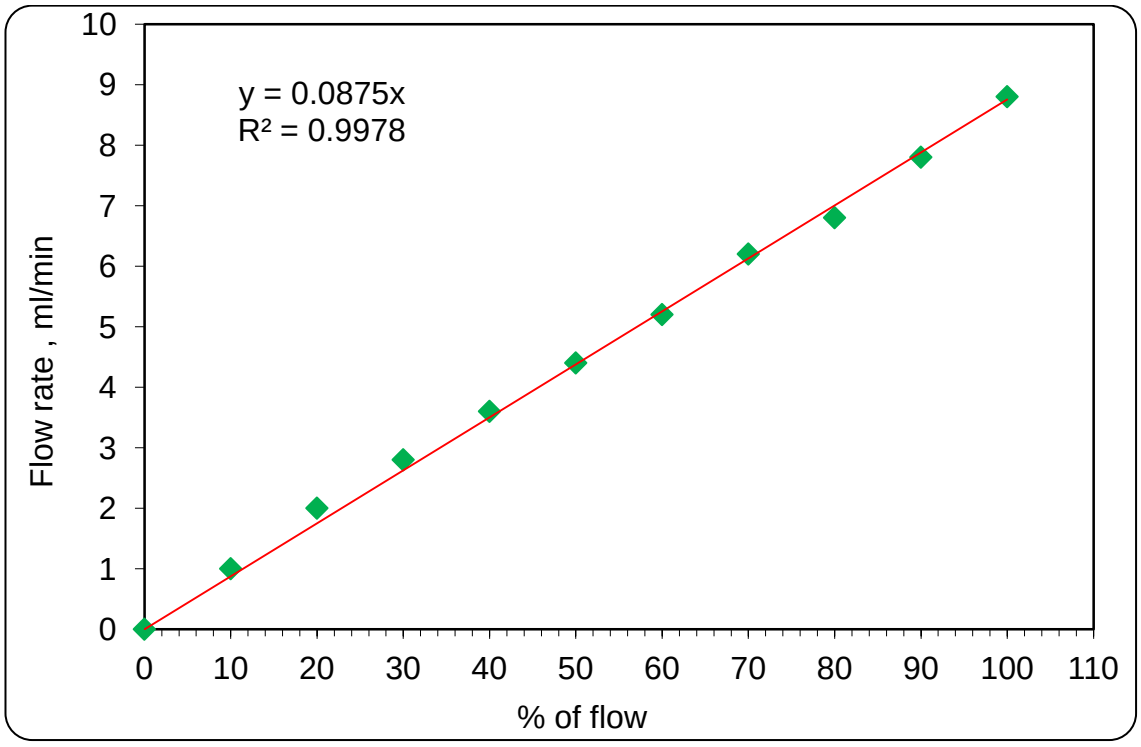

Figure AC-4: Calibration curve for syringe pump, model 353 sage instruments (one syringe of 60 ml) with 4.8 mm of tubing pipe, 1.65 mm diameter of feed system and 0.1 of pumping range

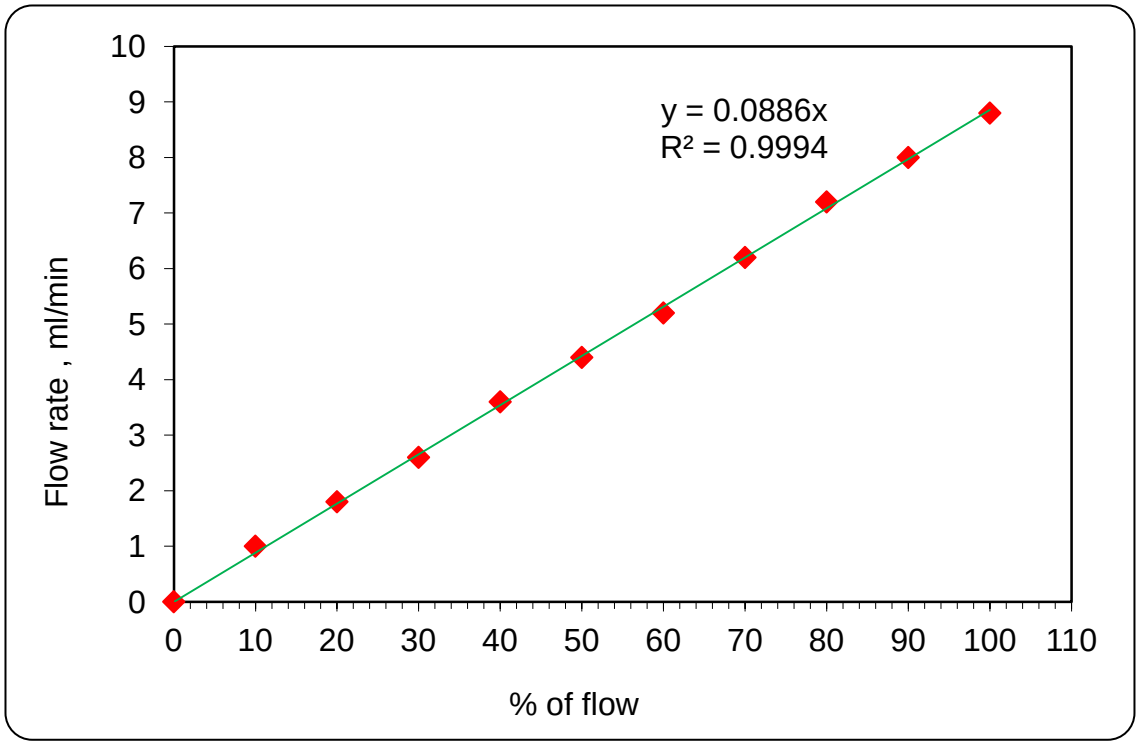

Figure AC-5: Calibration curve for syringe pump, model 353 sage instruments (one syringe of 60 ml) with 4.8 mm of tubing pipe, 0.65 mm diameter of feed system and 0.1 of pumping range

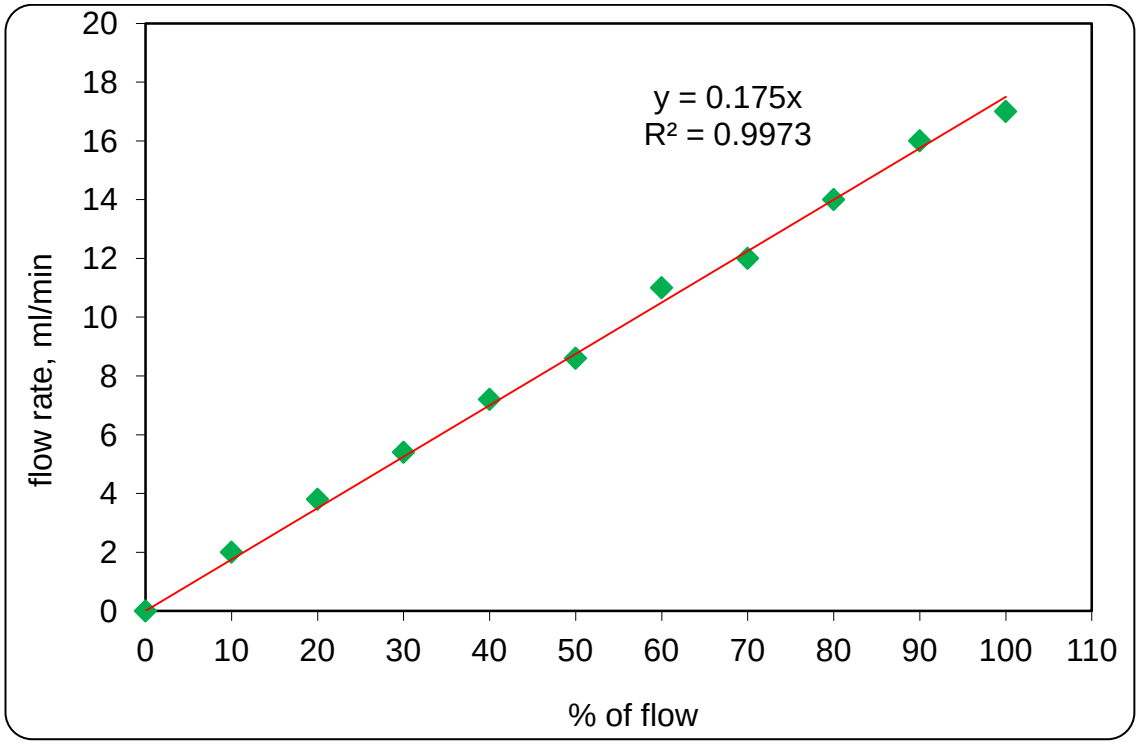

Figure AC -6: Calibration curve for syringe pump, model 353 sage instruments (two syringes of 60 ml) with 4.8 mm of tubing pipe, 0.65 mm diameter of feed system and 0.1 of pumping range

Appendix D: Calibration carves for 30 cm SDR disc speed

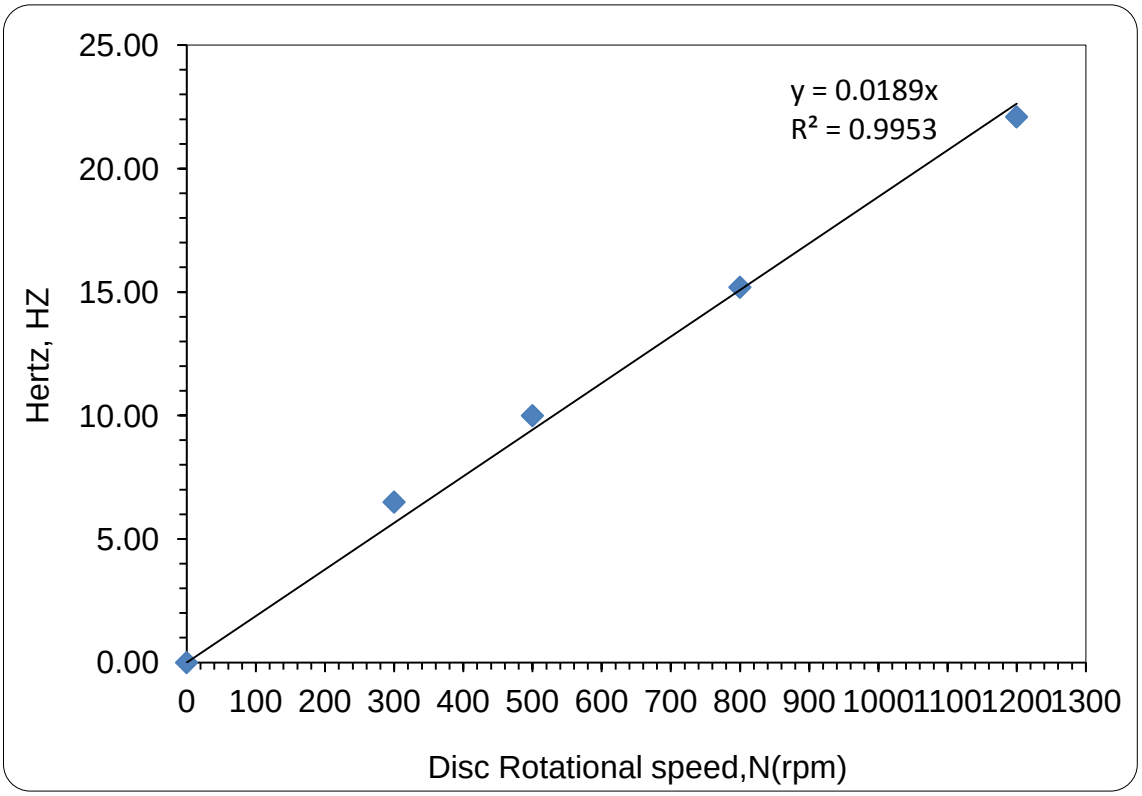

Figure AD-1: Calibration carve for 30 cm SDR disc speed

Appendix E: Calibration Carves for the Pumping system of 30 cm SDR Rig

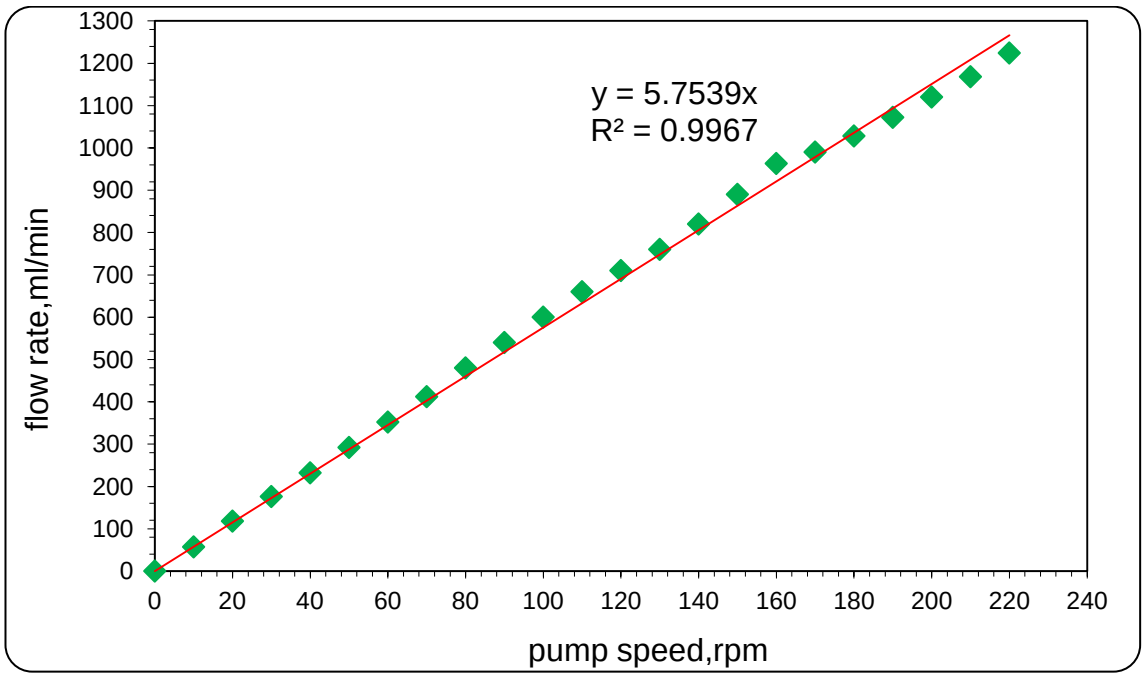

Figure AE-1: Calibration curve for Watson Marlow pump505S with 6.4 mm diameter tubing feed pipe and 3 mm diameter of H_3BO_3 solution-water system stream (water system) – 30 cm SDR

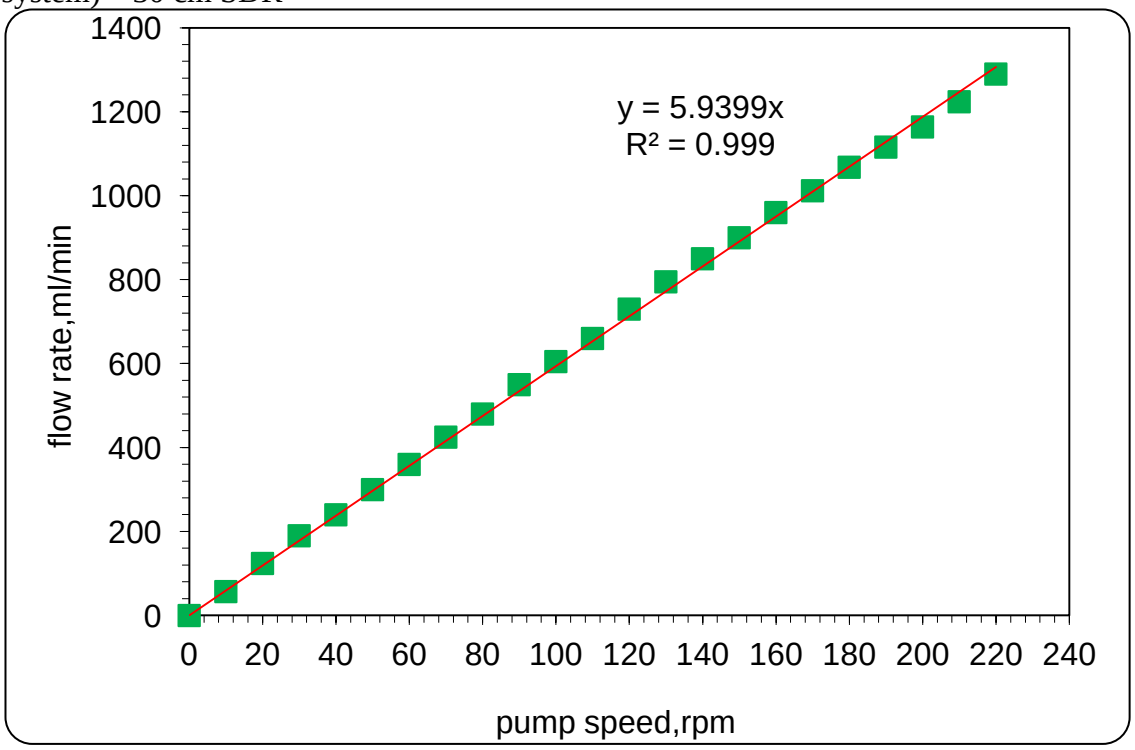

Figure AE-2: Calibration curve for Watson Marlow pump505S with 6.4 mm diameter tubing feed pipe and 3 mm diameter of H_3BO_3 solution system stream (50 wt% glycerol system) – 30 cm SDR

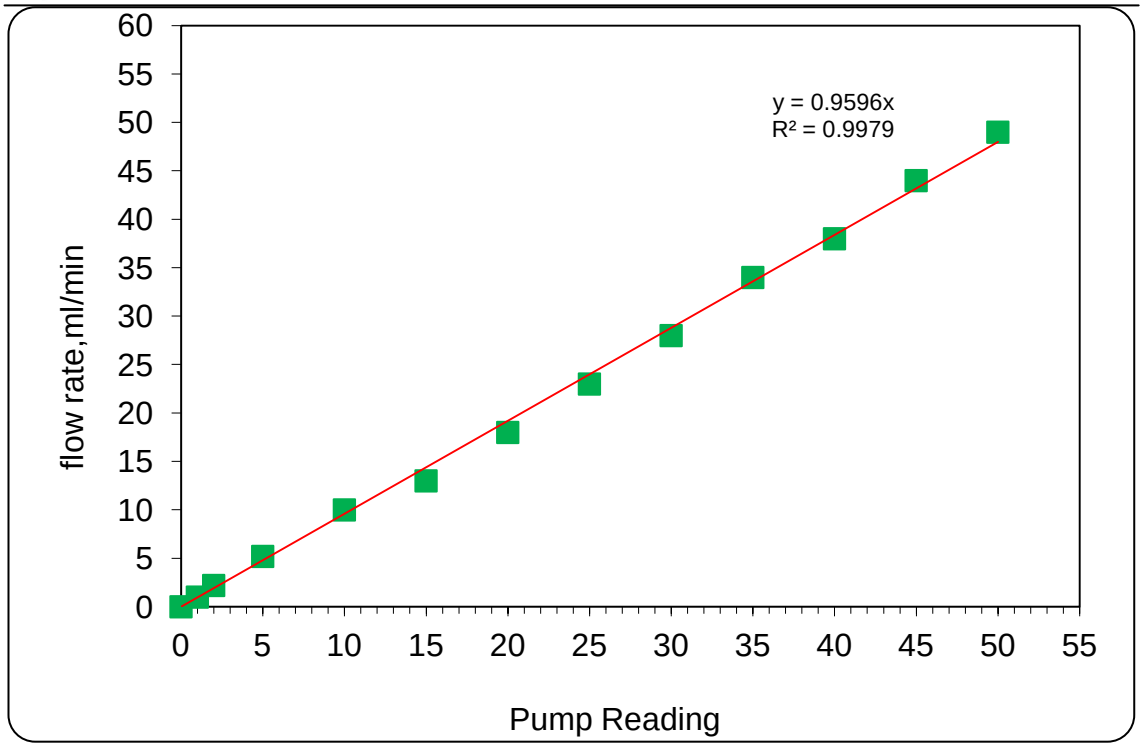

Figure AE-3: Calibration curve for syringe pump, model (NE-1000, New Era Syringe) for pumping H_2SO_4 , (One syringes of 60 ml with 6.4 mm of tubing pipe and 1.7 mm diameter of feed system). 30 cm SDR Rig

Appendix F: Calibration Carves for the Pumping system of NCRs Rig

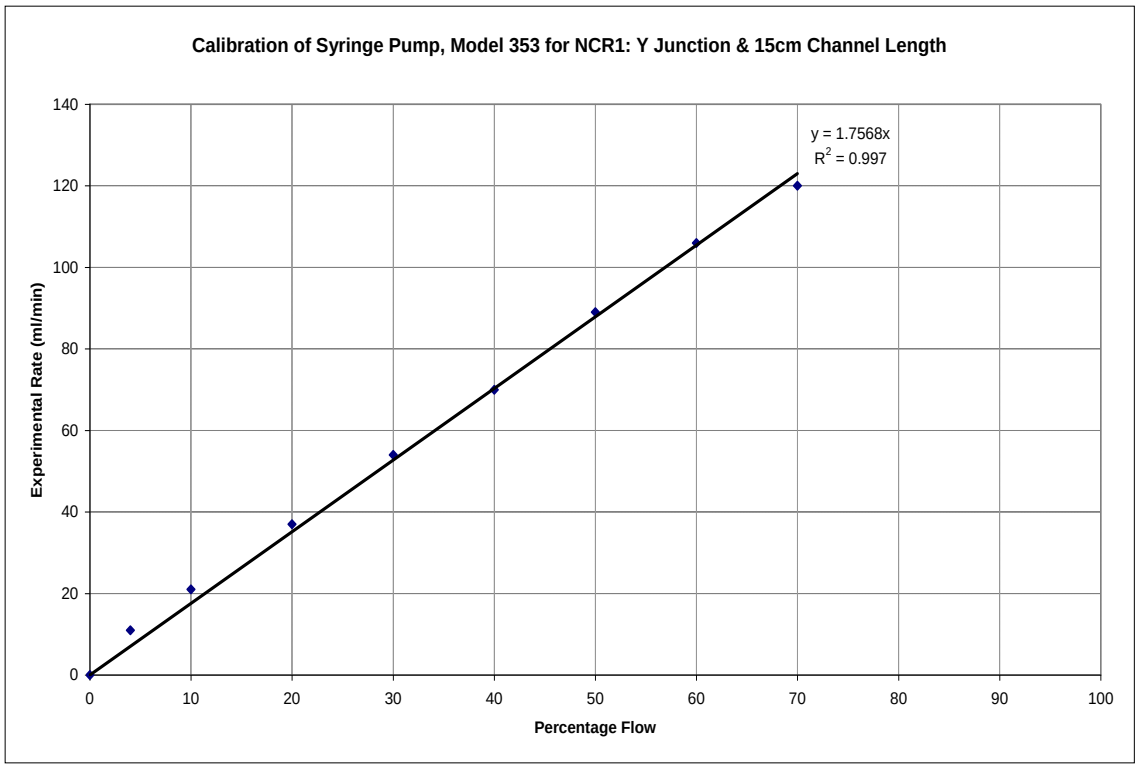

Figure AF-1: Calibration of Syringe Pump, Model 353: Iodide, Iodate, Borate Solution for 15 cm Y junction NCR- Water System

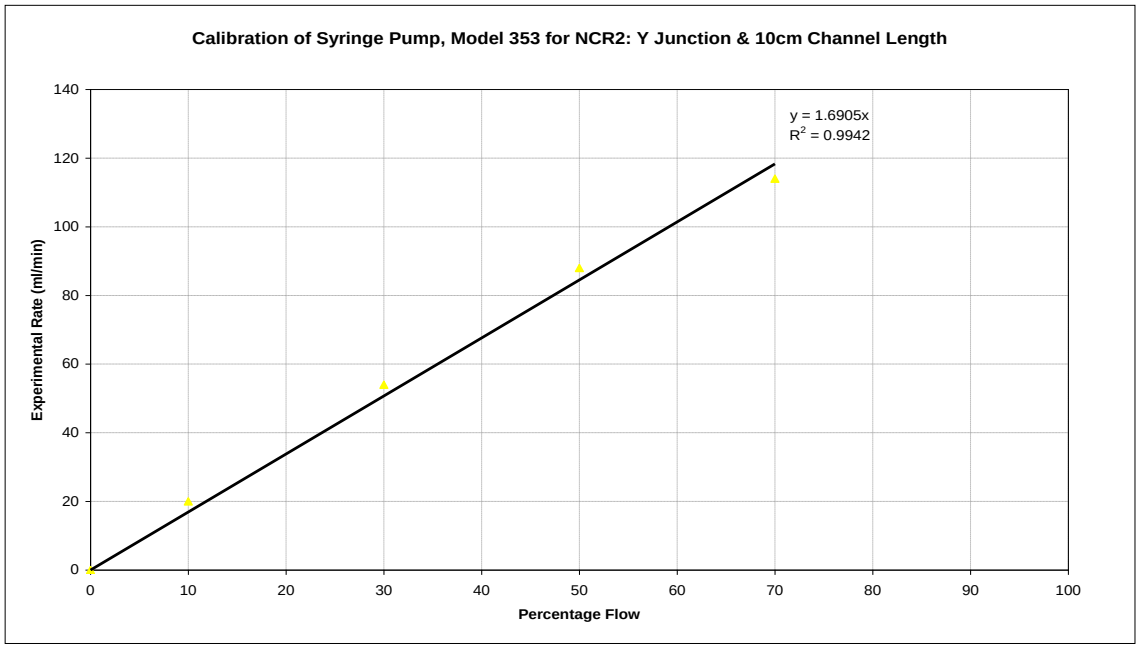

Figure AF-2: Calibration of Syringe Pump, Model 353: Iodide, Iodate, Borate Solution for 10 cm Y junction NCR- Water System

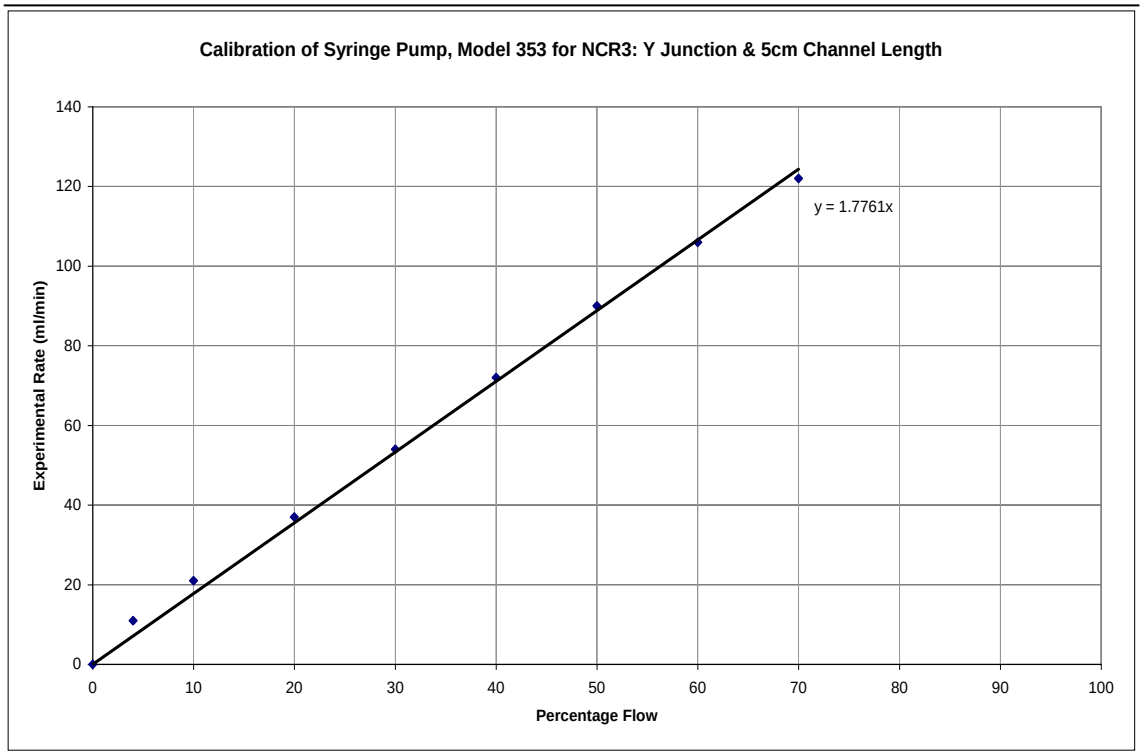

Figure AF-3: Calibration of Syringe Pump, Model 353: Iodide, Iodate, Borate Solution for 5 cm Y junction NCR- Water System

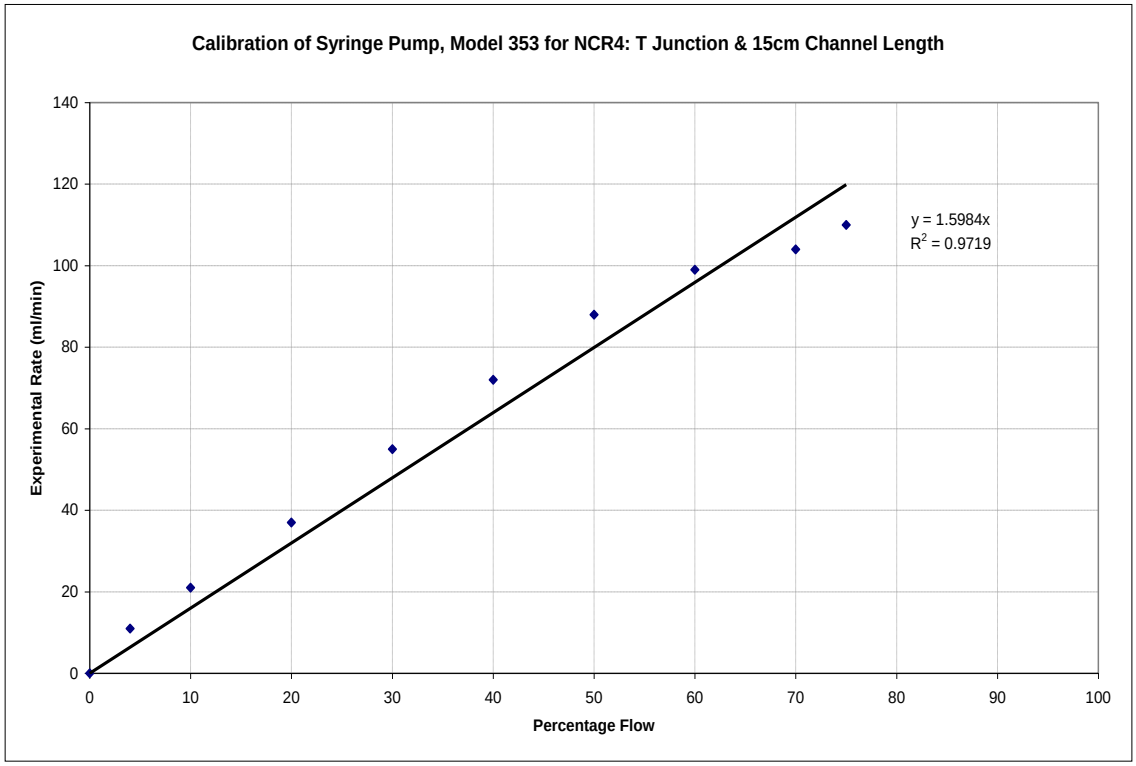

Figure AF-4: Calibration of Syringe Pump, Model 353: Iodide, Iodate, Borate Solution for 15 cm T junction NCR- Water System

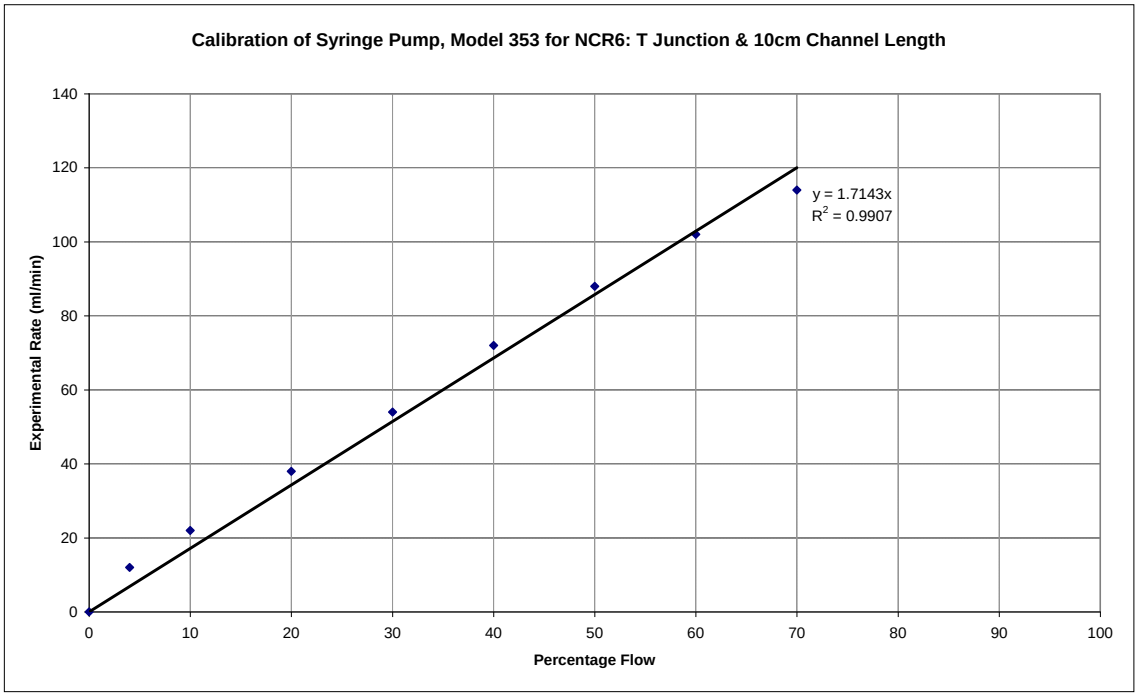

Figure AF-5: Calibration of Syringe Pump, Model 353: Iodide, Iodate, Borate Solution for 10 cm T junction NCR- Water System

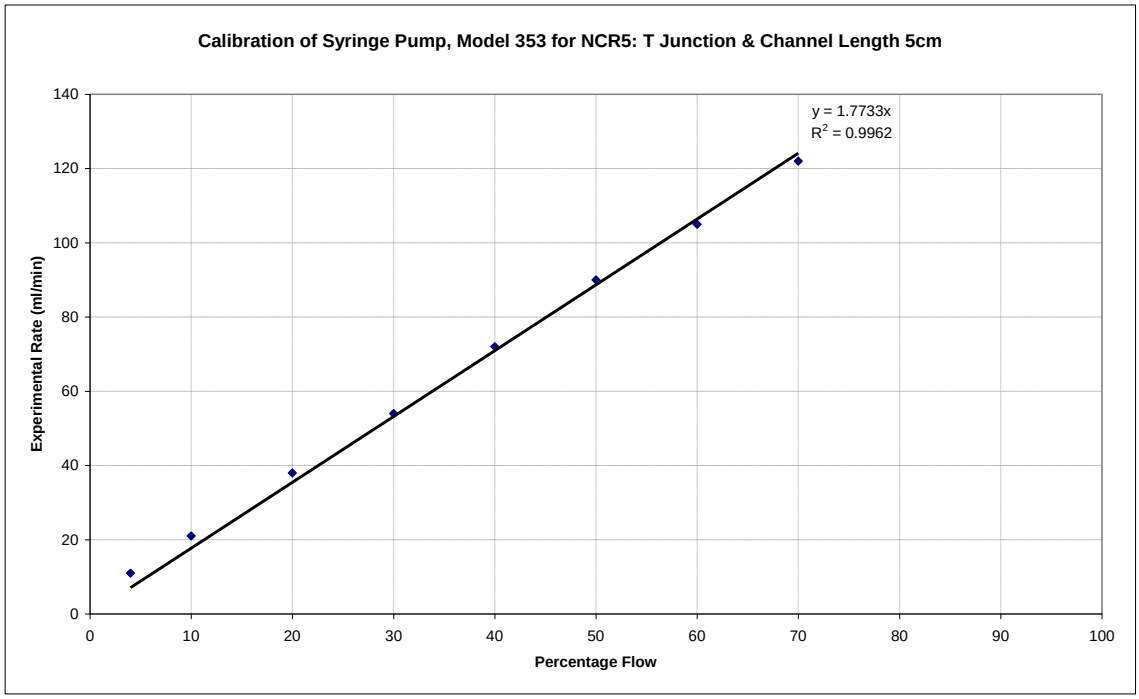

Figure AF-6: Calibration of Syringe Pump, Model 353: Iodide, Iodate, Borate Solution for 5 cm T junction NCR- Water System

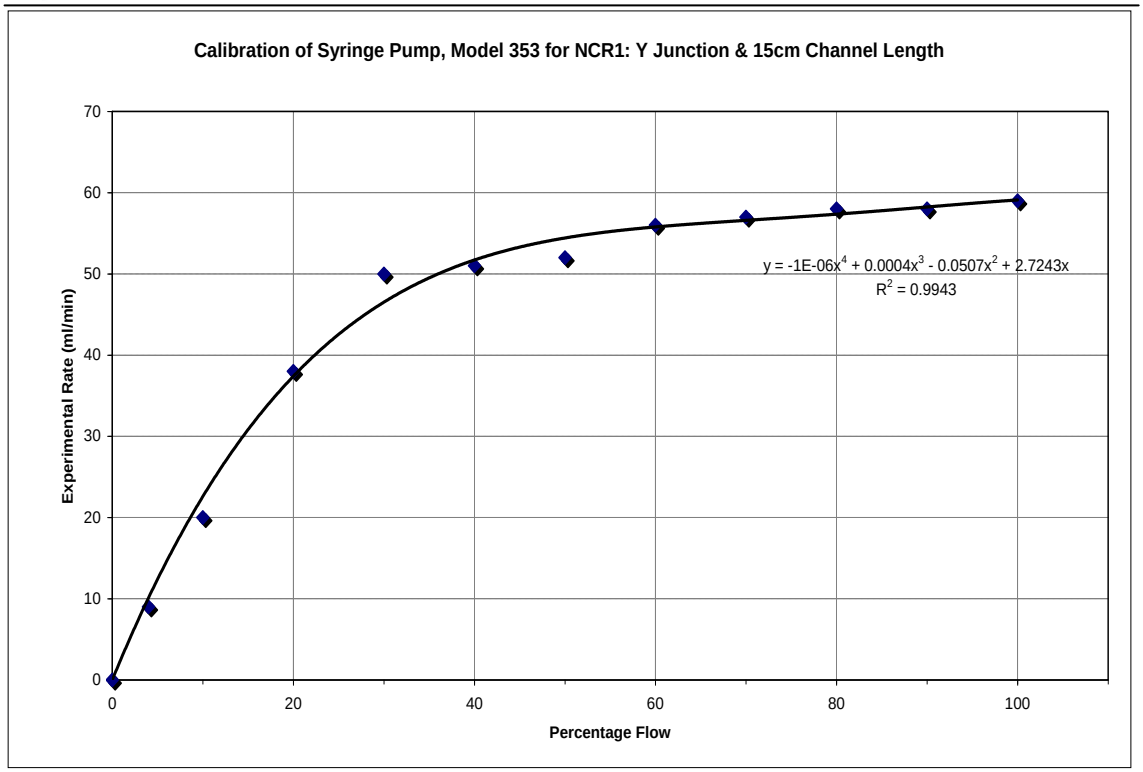

Figure AF-7: Calibration of Syringe Pump, Model 353: Iodide, Iodate, Borate Solution for 15 cm Y junction NCR- 50 wt% Viscous System

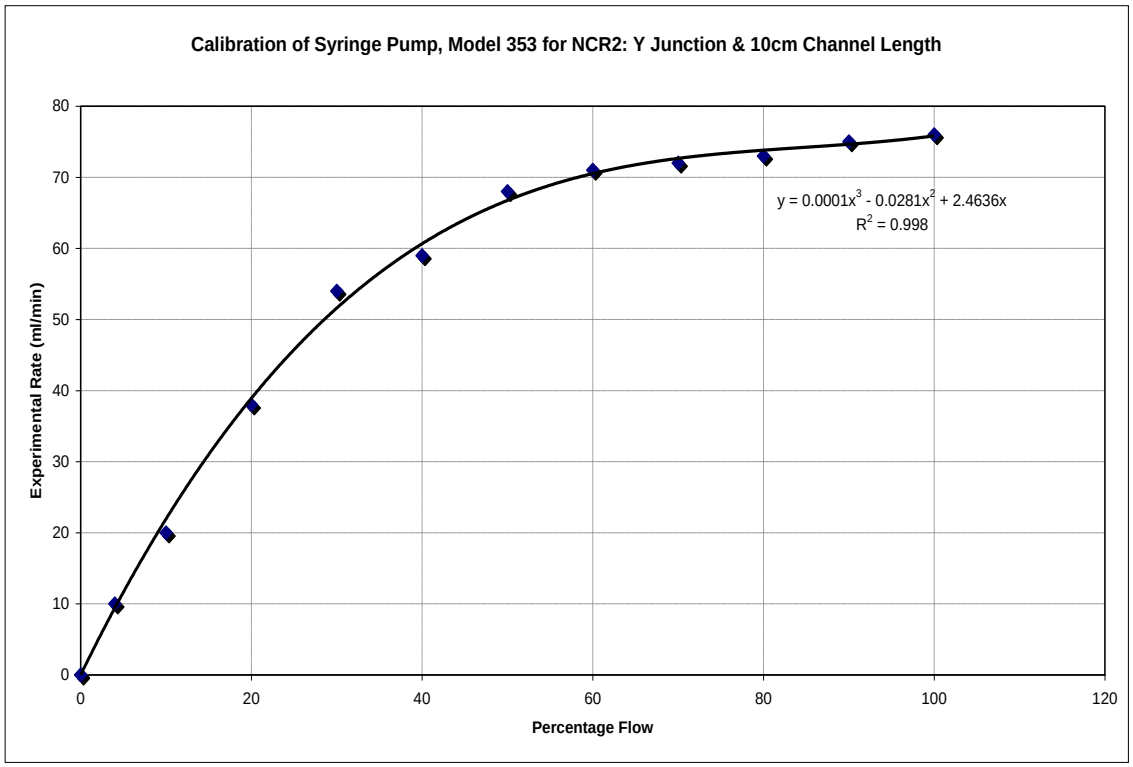

Figure AF-8: Calibration of Syringe Pump, Model 353: Iodide, Iodate, Borate Solution for 10 cm Y junction NCR- 50 wt% Viscous System

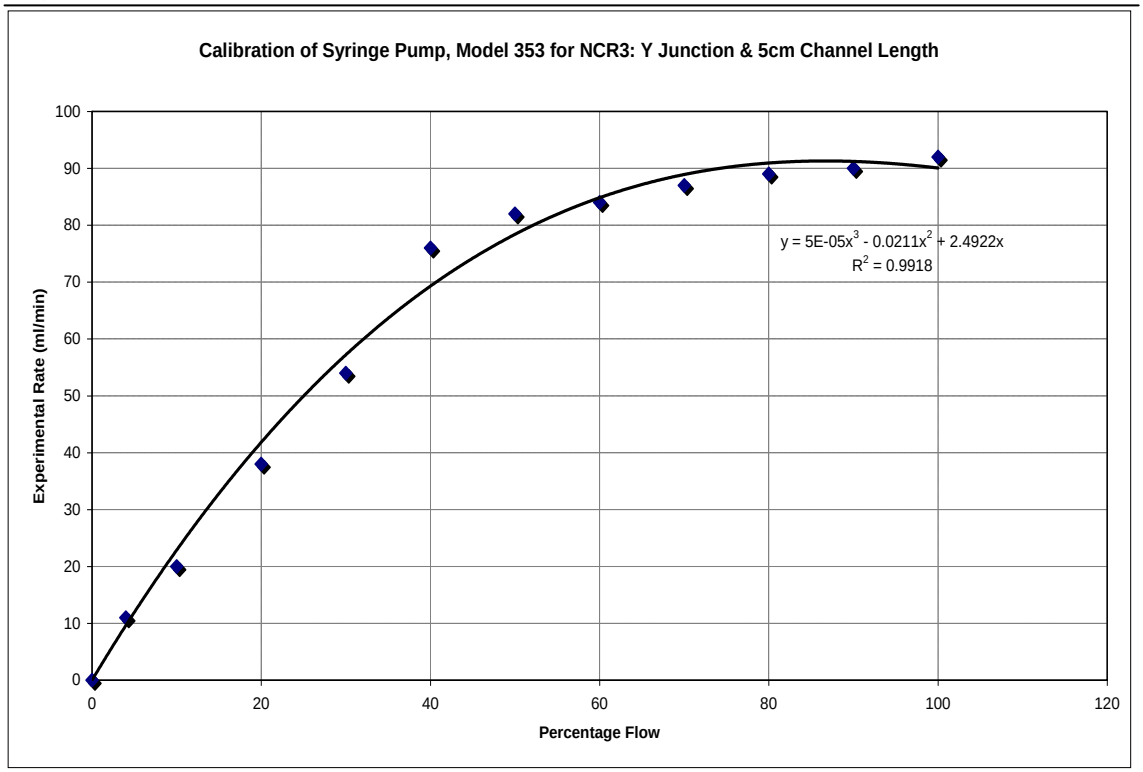

Figure AF-9: Calibration of Syringe Pump, Model 353: Iodide, Iodate, Borate Solution for 5 cm Y junction NCR- 50 wt% Viscous System

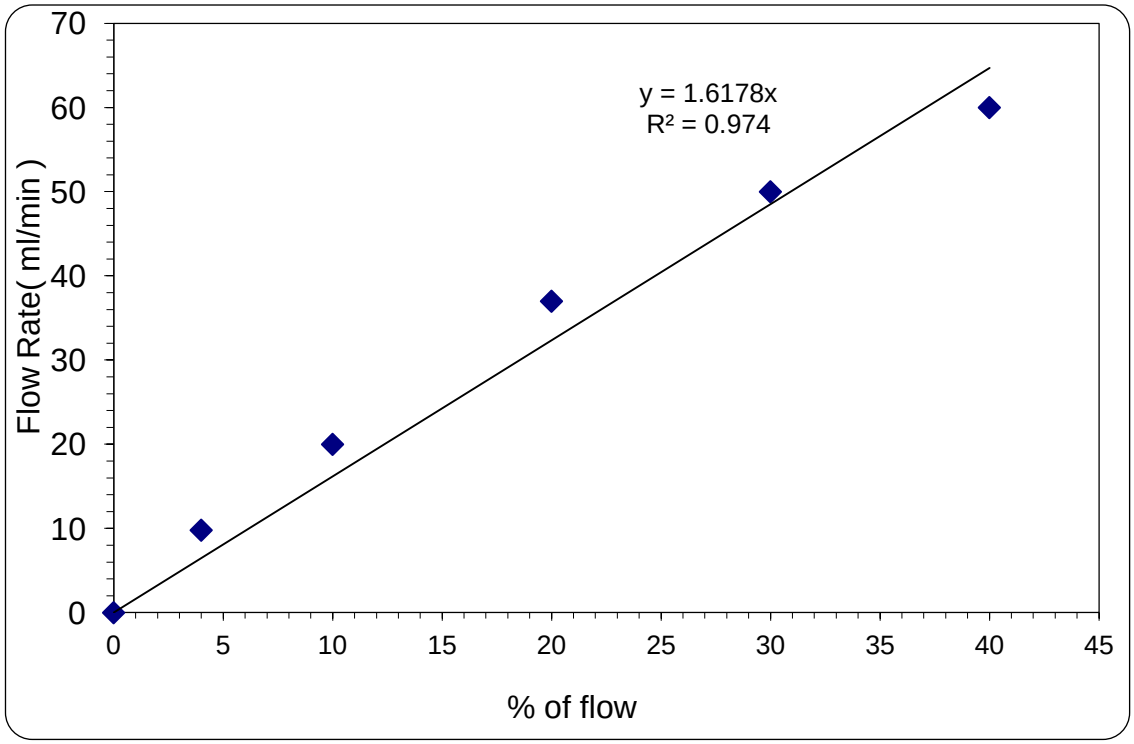

Figure AF-10: Calibration of Syringe Pump, Model 353: Iodide, Iodate, Borate Solution for 15 cm Y junction NCR- 50 wt% Viscous System

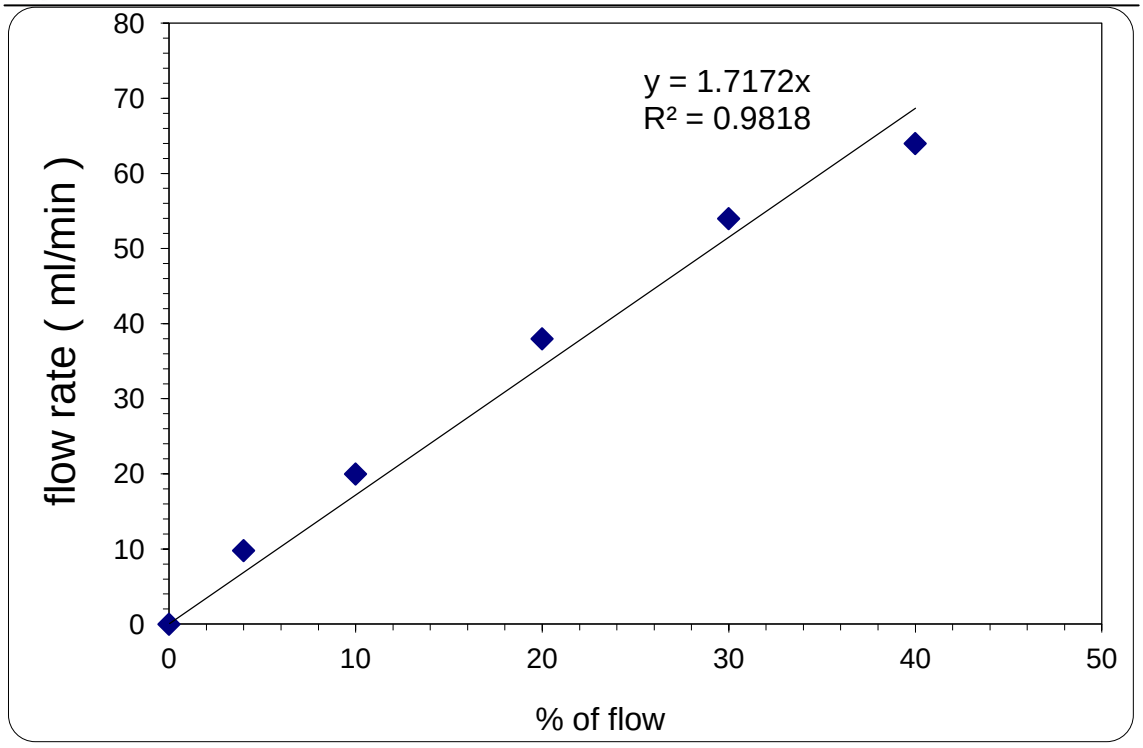

Figure AF-11: Calibration of Syringe Pump, Model 353: Iodide, Iodate, Borate Solution for 10 cm Y junction NCR- 50 wt% Viscous System

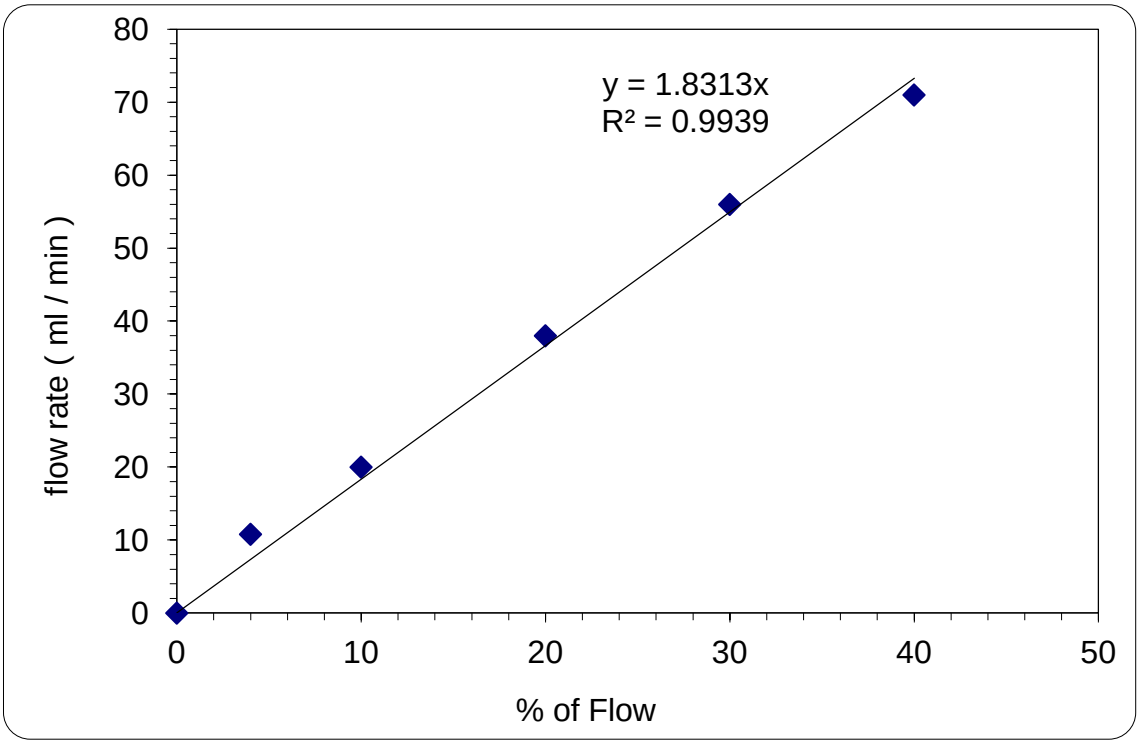

Figure AF-12: Calibration of Syringe Pump, Model 353: Iodide, Iodate, Borate Solution for 5 cm Y junction NCR- 50 wt% Viscous System

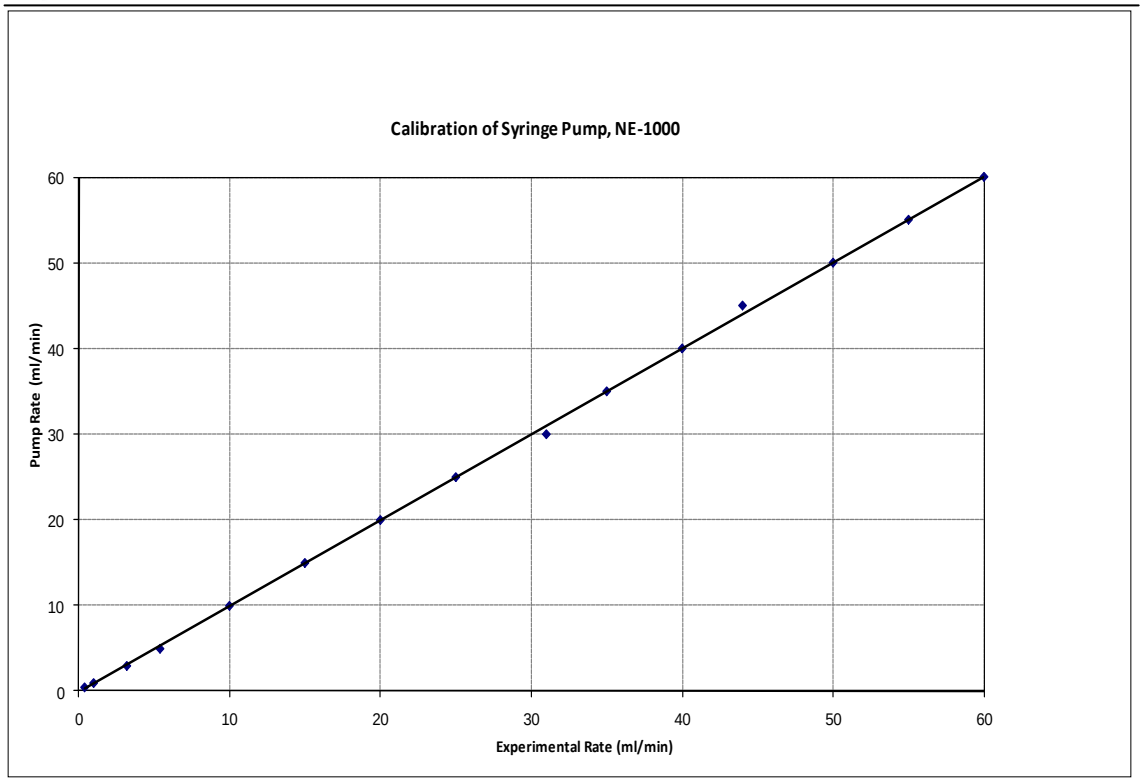

Figure AF-13: Calibration of Syringe Pump, Model NE-1000 for pumping sulphuric acid

Appendix G: Semi-Batch Reactor (SBR) Experiments

Table AG1: Factorial Experimental Design – SBR Experiments

Run Order	Acid Concentration, M	Agitation Speed, rpm	Acid Feed Injection location
1	1.00	1200	middle point
2	1.00	1200	close
3	1.00	600	middle point
4	0.50	1200	close
5	0.50	600	middle point
6	1.00	900	close
7	0.25	600	middle point
8	0.50	900	close
9	0.50	900	middle point
10	0.50	1200	middle point
11	0.25	900	close
12	1.00	900	middle point
13	0.50	300	middle point
14	1.00	300	middle point
15	0.25	1200	close
16	0.25	300	close
17	0.50	300	close
18	0.25	600	close
19	1.00	600	close
20	0.50	600	close
21	0.25	300	middle point
22	0.25	1200	middle point
23	1.00	300	close
24	0.25	900	middle point

Table AG2: Influence of the acid feed rate on segregation index, (Xs) at N=300 rpm; Acid n Injection point located at the Middle of the reactor; $[H^+]$ =1.0 M – Water system

Run Order	Flow rate (ml/min)	Average Xs (-)	Relative error (%)
1	3.6	0.217	2.093
2	5.4	0.221	1.290
3	7.2	0.230	0.580
4	8.9	0.232	1.231
5	10.7	0.221	0.877
6	12.5	0.224	0.756
7	17.9	0.228	1.596
8	35.8	0.227	0.881
9	53.7	0.245	2.080
10	71.6	0.274	0.777
11	89.5	0.302	0.626

Table AG3: Influence of the acid feed rate on segregation index, (Xs) at N=300 rpm; Acid n Injection point located at the Middle of the reactor; [H+] =1.0 M – 75 wt% Glycerol system

Run Order	Flow rate, (ml/min)	Average Xs, (-)	Relative error, (%)
1	3.6	0.360	2.081
2	5.4	0.360	1.929
3	7.2	0.361	1.755
4	8.9	0.362	2.068
5	10.7	0.360	2.005
6	12.5	0.362	1.737
7	17.9	0.361	1.542
8	22.4	0.362	0.198
9	26.8	0.368	1.169
10	35.8	0.371	2.079
11	44.7	0.373	1.980
12	53.7	0.380	1.738
13	67.1	0.383	1.843
14	71.6	0.387	1.823
15	89.5	0.391	1.648

Appendix H: Error analysis

Every experimental determination carries a certain amount of uncertainty. Uncertainty can be defined as the possible value the error may have. When determining the results, the investigator must provide an estimate of their uncertainty in order to draw significant conclusions from the data.

The Errors in individual results are a combination of:

- Systematic - random scatter around the true value;
- Instrument errors;
- Personal errors - depending on personal reaction.

Statistical analysis was used in this research as tool to predict the Error analysis using the standard deviation (σ), standard error (S) and relative error formulas. In the micromixing part, each experiment was repeated three times.

If a number n of measurements of the same variables are taken the arithmetic mean or Average can be calculated from the expression:

$$x_m = \frac{1}{n}\sum_{i=1}^{n} X_i \qquad AH.1$$

The deviation for d_i for each reading is defined by:

$$d_i = x_i - x_m \qquad AH.2$$

And the Standard deviation (σ) can be estimated by the equation:

$$\text{Standard deviation } (\sigma) = \sqrt{\frac{\left(x_{1-x_m}\right)^2 + \left(x_{2-x_m}\right)^2 + \cdots \ldots \ldots + \left(x_{n-x_m}\right)^2}{n-1}} \qquad AH.3$$

Where $x_1 \rightarrow x_n$ are n results and x_m is their mean

From the Standard deviation, (σ), the standard error can be estimated by dividing the standard deviation by the square root of the number of measurements.

$$\text{Standard error (S)} = \frac{\text{Standard deviation, } (\sigma)}{\sqrt{n}} \qquad \text{AH. 4}$$

And the % of relative error is defined by:

$$\%\text{ of relative error} = \frac{\text{Standard error (S)}}{\text{Average measured value}} \text{ x } 100 \qquad \text{AH. 5}$$

Appendix I: 10 cm SDR Experiments

Table AI1: Factorial Experimental Design - 10 cm SDR for each acid concentration

Run Order	Total flow rate, (ml/sec)	Disc rotational speed, (rpm)
1	1	300
2	5	1200
3	3	1200
4	1	600
5	1	1200
6	5	600
7	3	900
8	5	600
9	3	600
10	1	900
11	3	1200
12	5	900
13	5	1200
14	1	900
15	5	1200
16	3	900
17	3	900
18	1	300

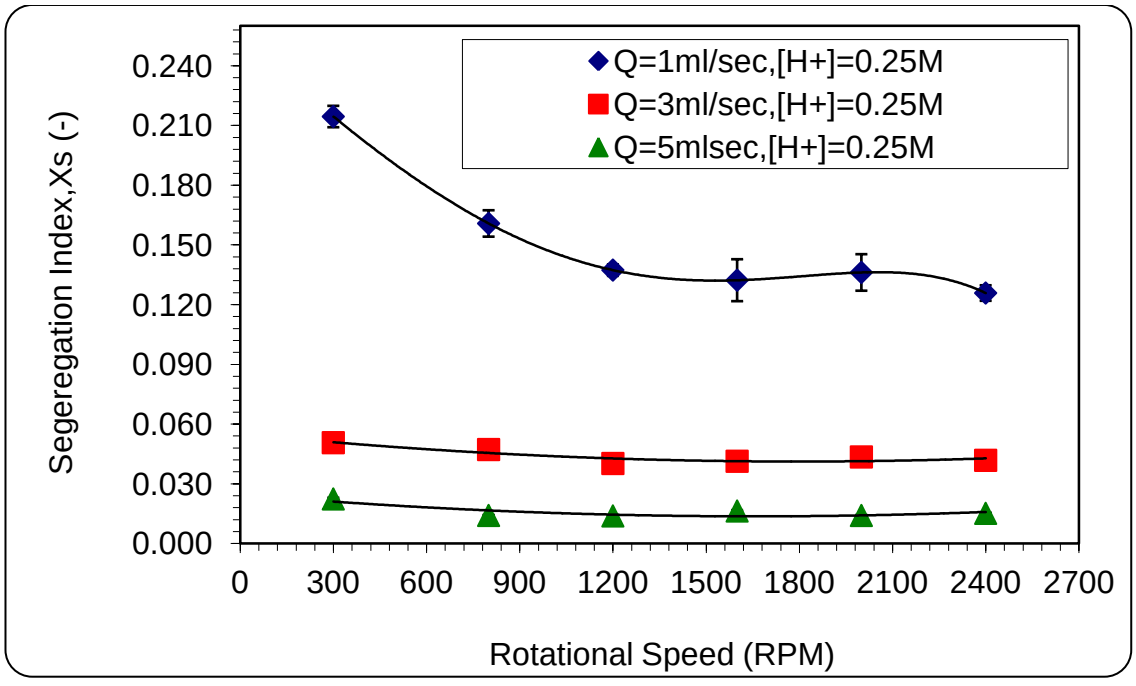

Figure AI1: Effect of rotational speed and total flowrate on the segregation index at [H+] =0.25 M

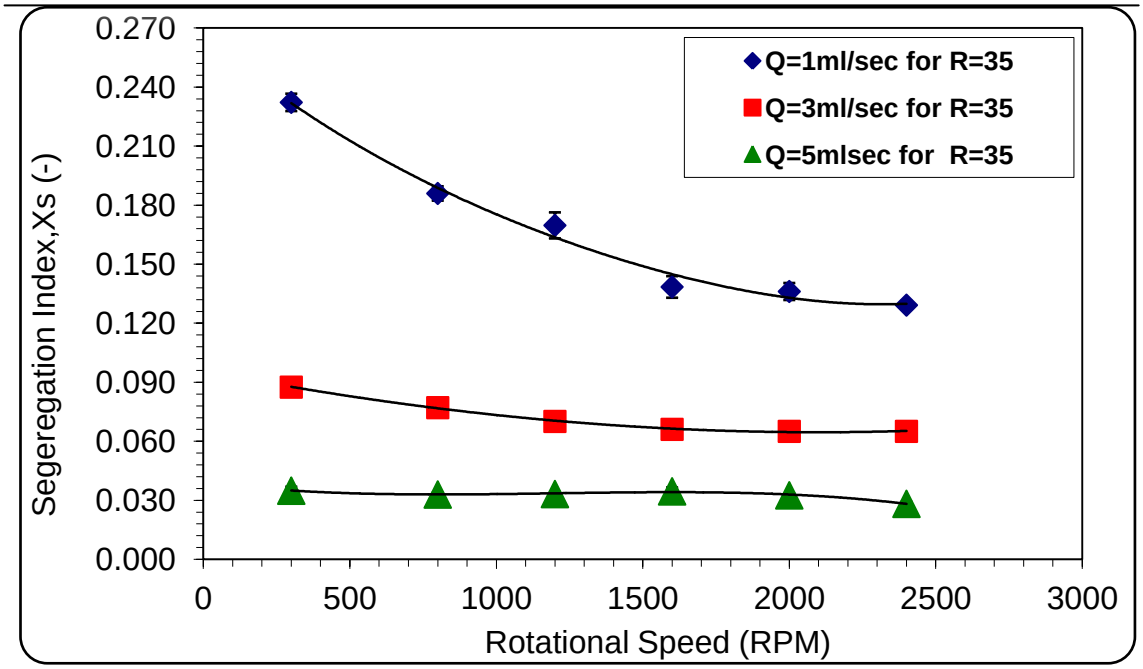

Figure AI2: Effect of rotational speed and total flowrate on the segregation index at [H+] =0.50 M

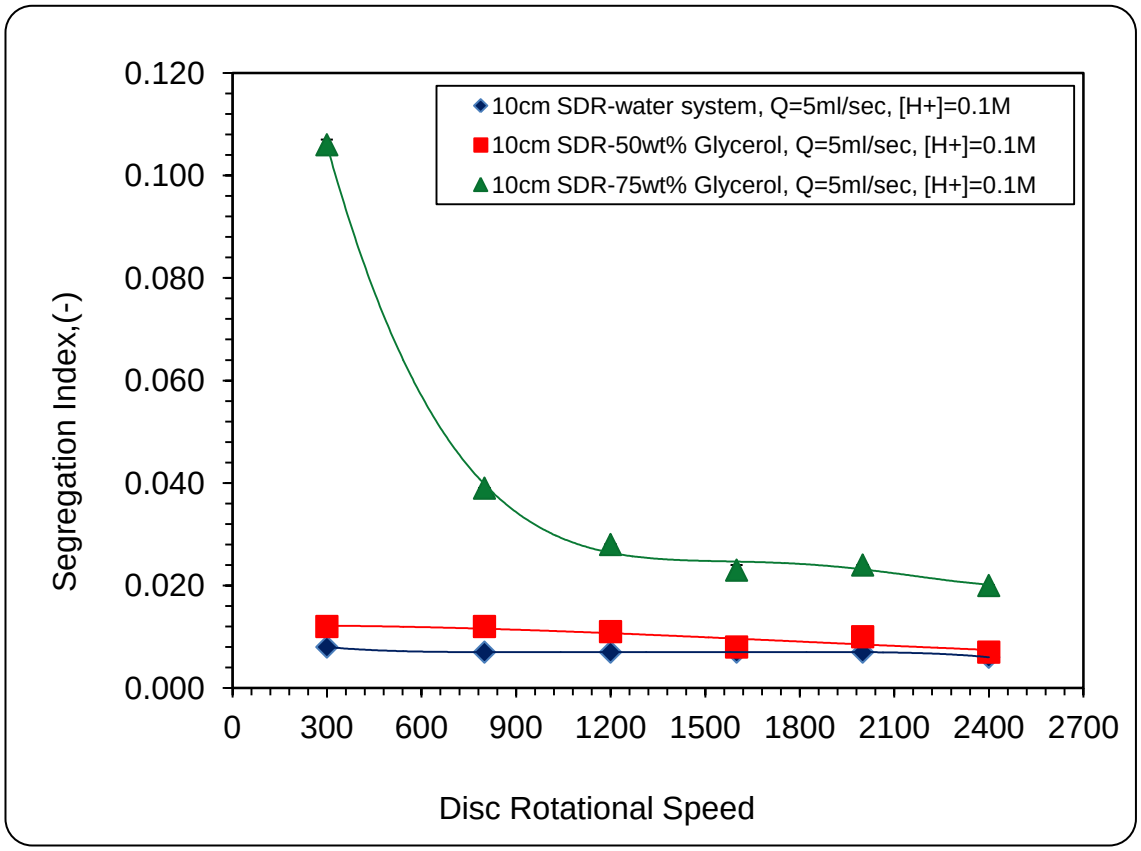

Figure AI3: Effect of feed viscosity on segregation Index (Xs) in SDR at Q=5 ml/sec, Total Flow rates and [H+] =0.1 M

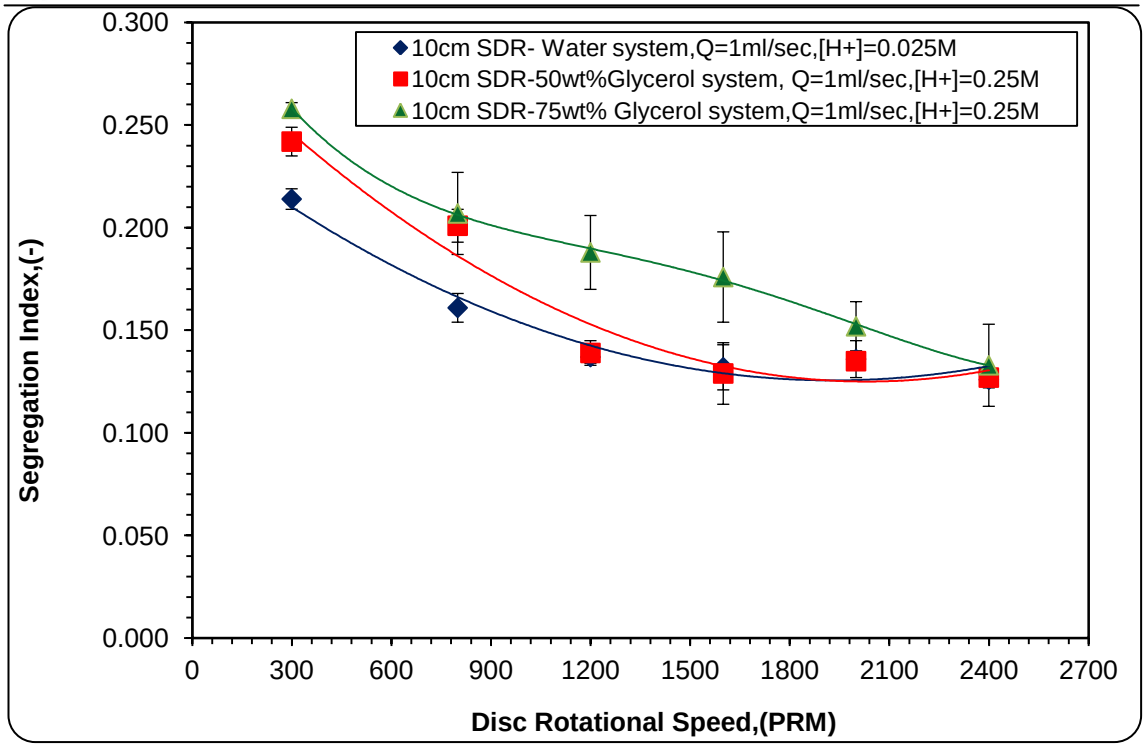

Figure AI4: Effect of feed viscosity on segregation Index (Xs) in SDR at Q=1 ml/sec, Total flowrate and [H+] =0.25 M

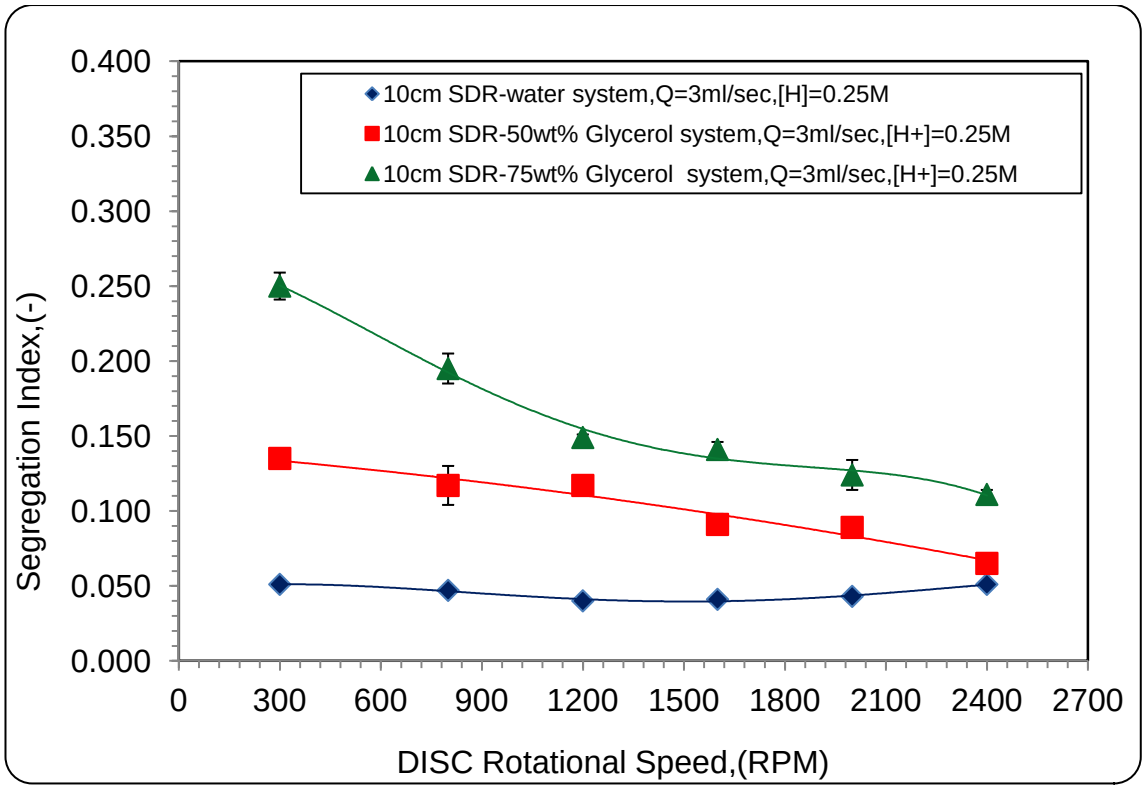

Figure AI5: Effect of feed viscosity on segregation Index (Xs) in SDR at Q=3 ml/sec, Total flowrate and [H+] =0.25 M

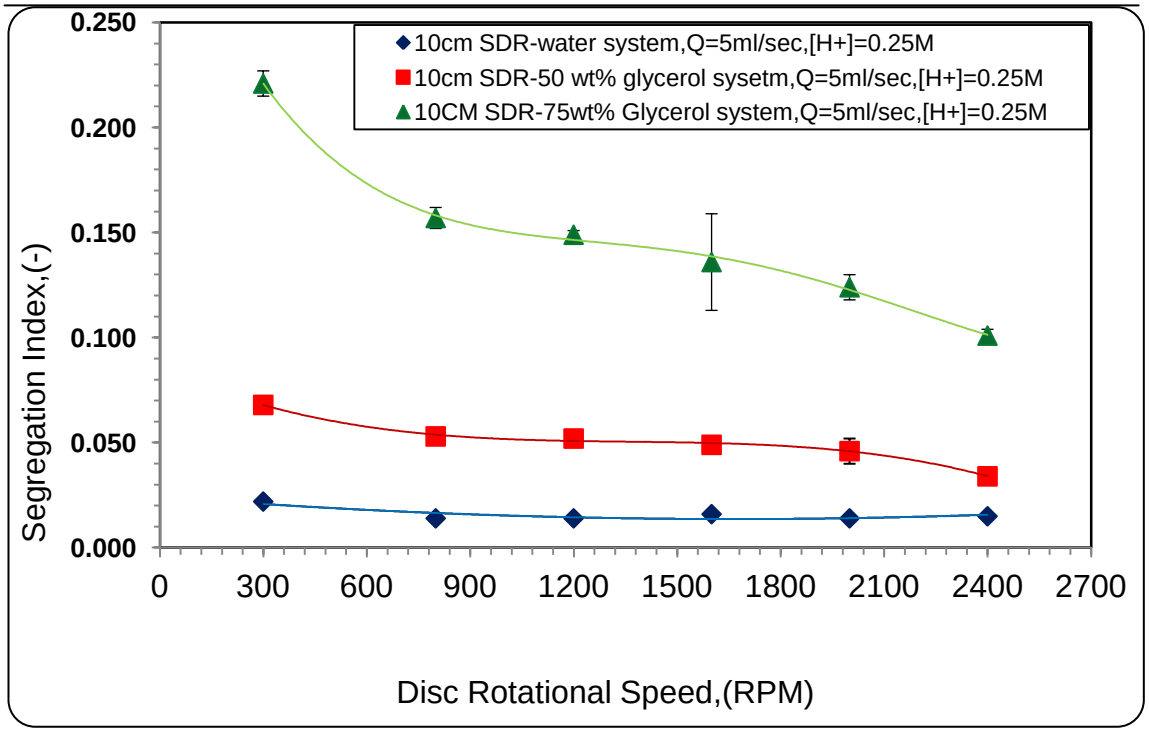

Figure AI6: Effect of feed viscosity on segregation Index (Xs) in SDR at Q=5 ml/sec, Total flowrate and [H+] =0.25 M

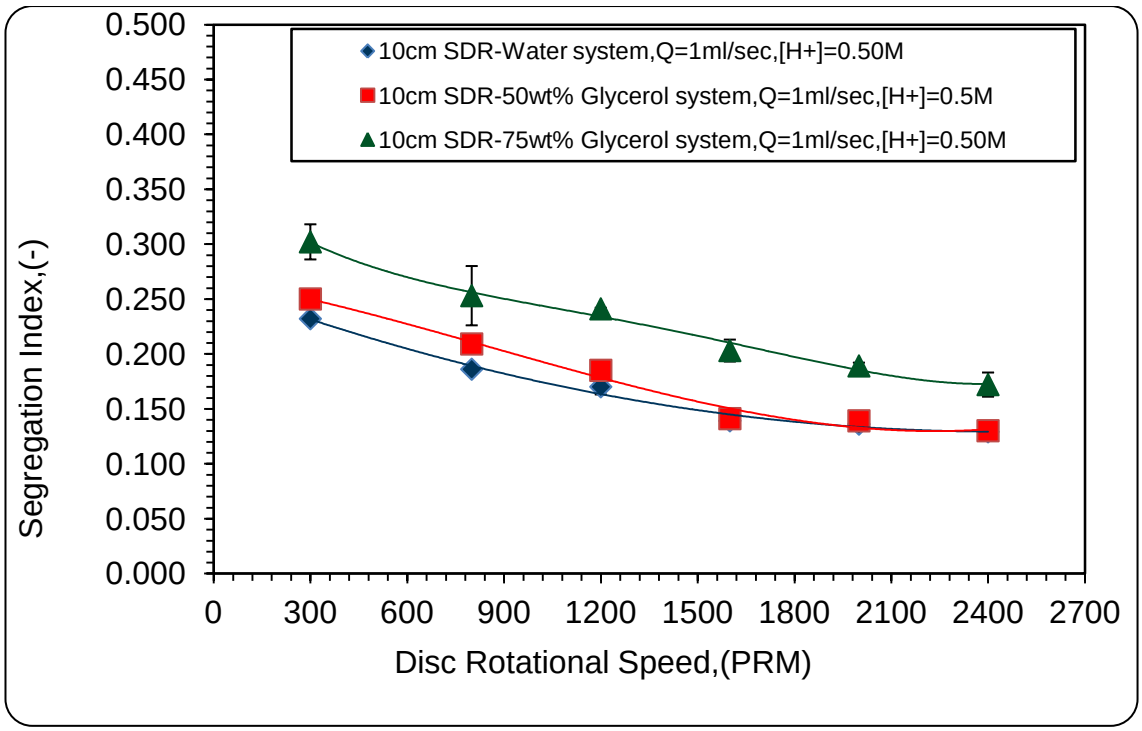

Figure AI7: Effect of feed viscosity on segregation Index (Xs) in SDR at Q=1 ml/sec, Total flowrate and [H+] =0.50 M

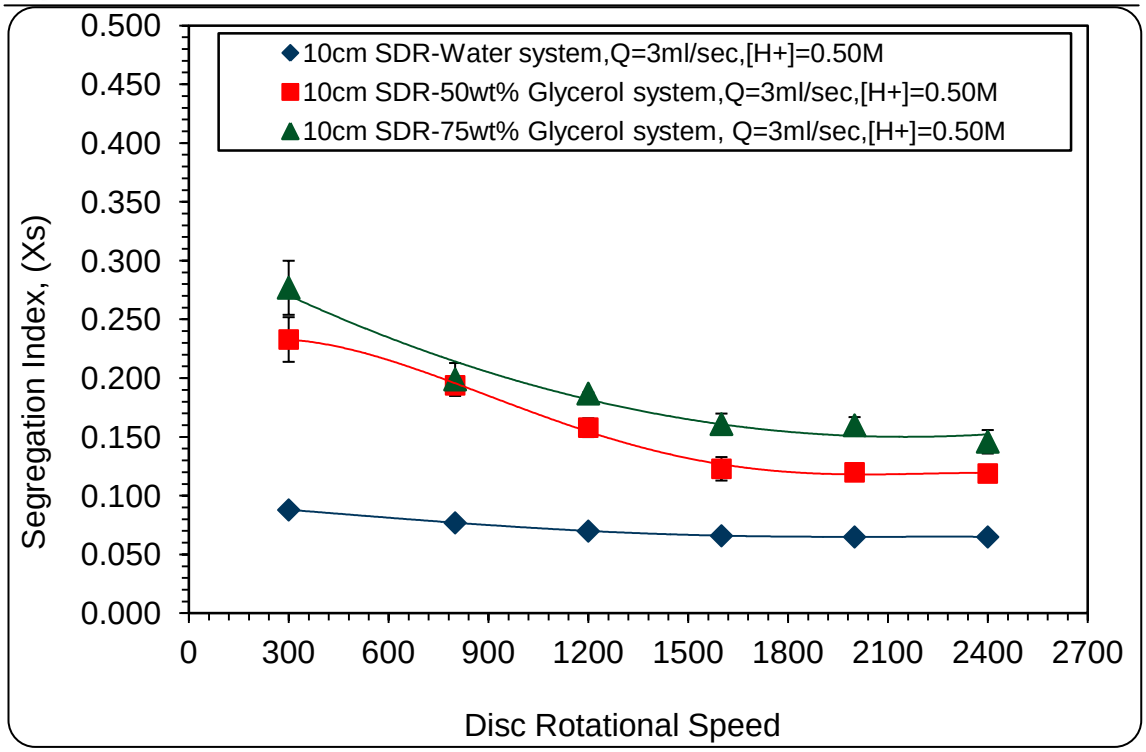

Figure AI8: Effect of feed viscosity on segregation Index (Xs) in SDR at Q=3 ml/sec, Total flowrate and [H+] =0.50 M

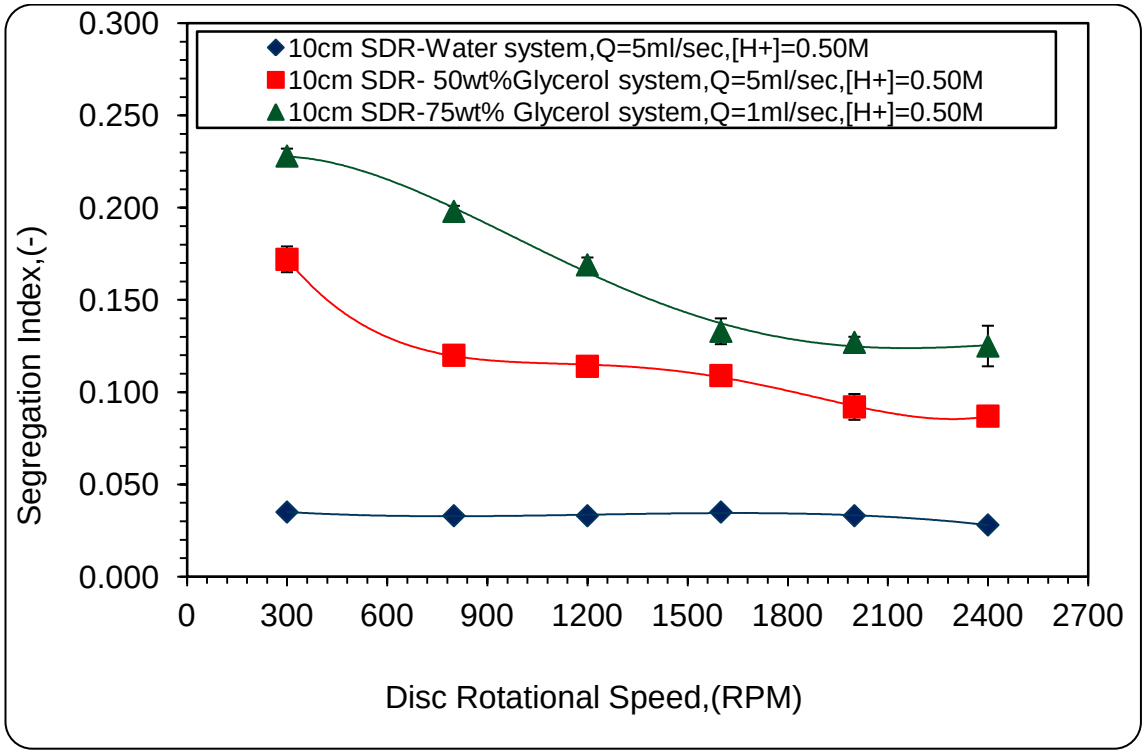

Figure AI9: Effect of feed viscosity on segregation Index (Xs) in SDR at Q=5 ml/sec, Total flowrate and [H+] =0.50 M

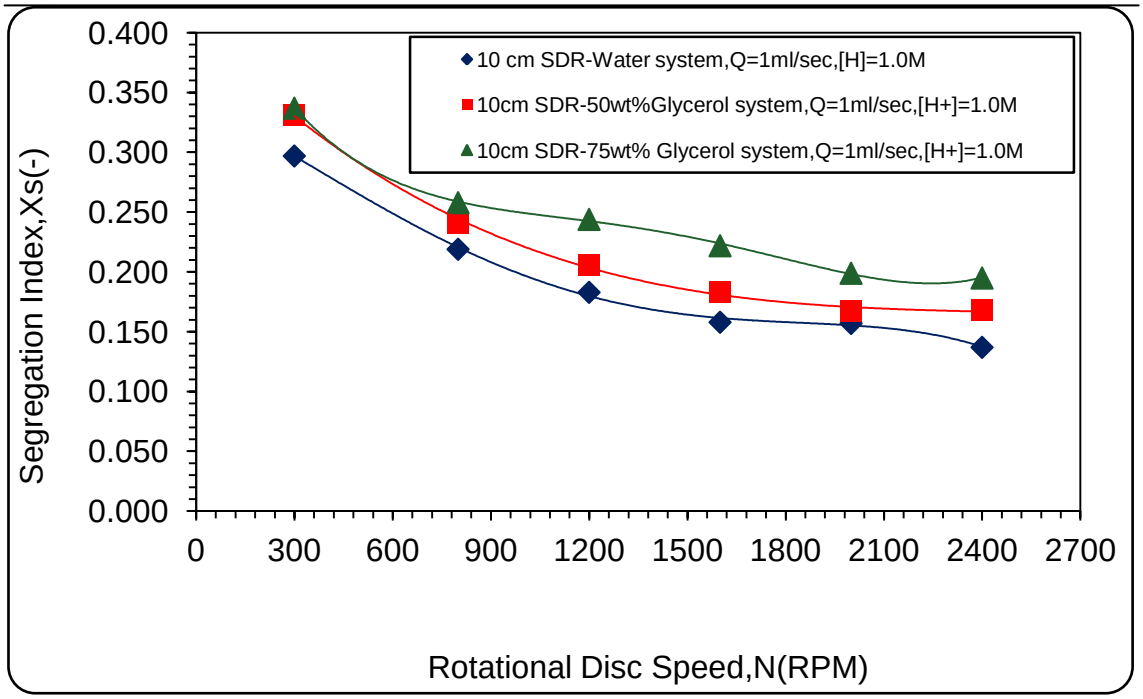

Figure AI10: Effect of feed viscosity on segregation Index (Xs) in SDR at Q=1 ml/sec, Total flowrate and [H+] =1.0 M

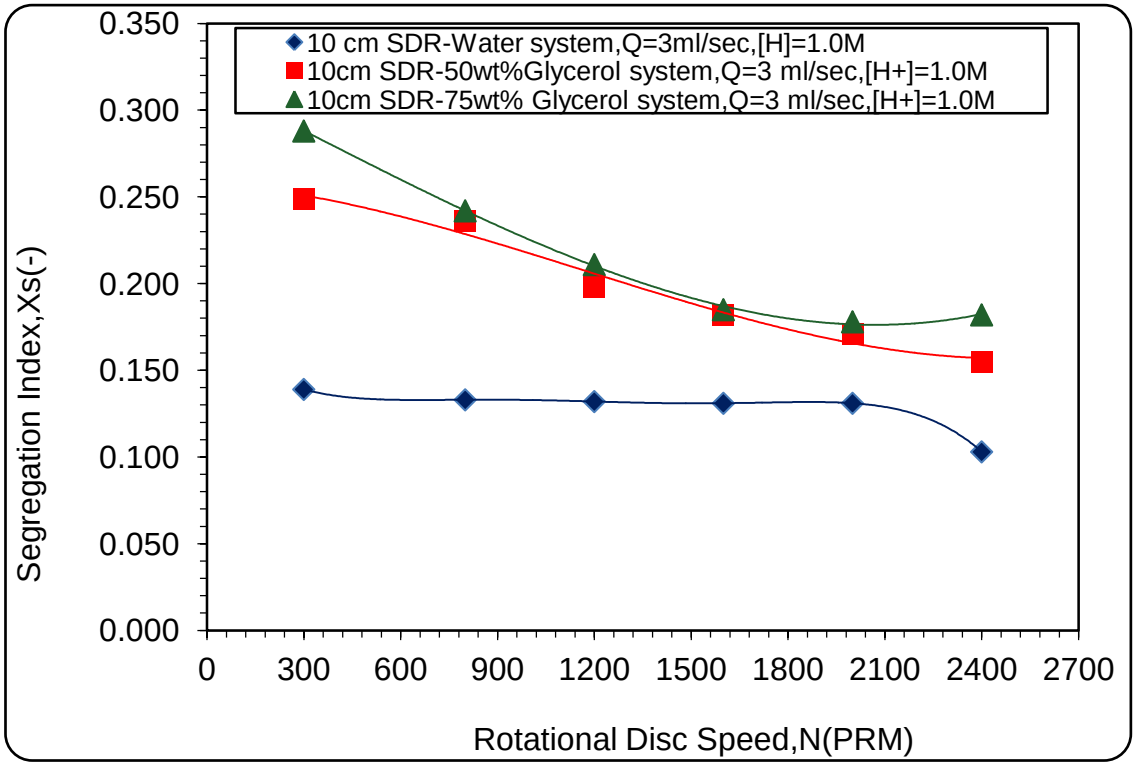

Figure AI11: Effect of feed viscosity on segregation Index (Xs) in SDR at Q=3 ml/s, Total flowrate and [H+] =1.0 M

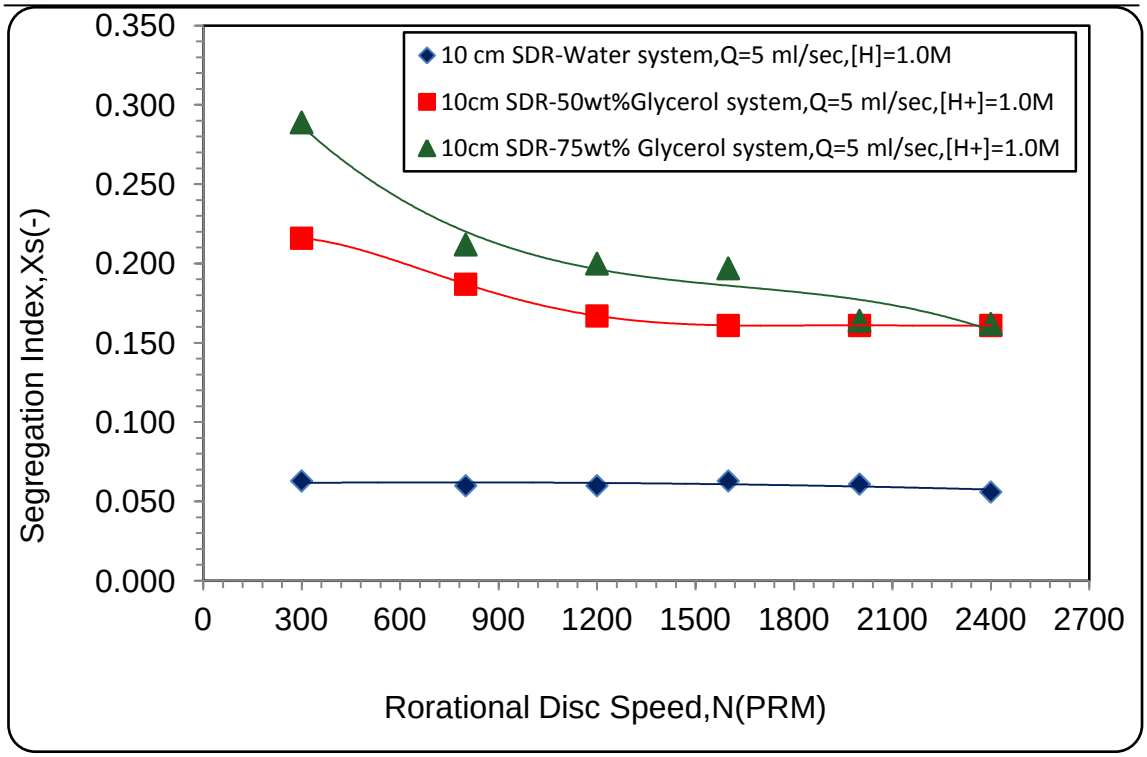

Figure AI12: Effect of feed viscosity on segregation Index (Xs) in SDR at Q=5 ml/s, Total flowrate and [H+] =1.0 M

Appendix J: 30 cm SDR Experiments

Table AJ1: Factorial Experimental Design – 30 cm SDR for each acid concentration

Run Order	Total flow rate, (ml/sec)	Disc rotational speed, (rpm)
1	9	500
2	15	800
3	3	300
4	15	500
5	3	1200
6	15	1200
7	15	300
8	3	500
9	3	800
10	9	1200
11	9	300
12	9	800

Table AJ2: Residence time and mixing time on 30 cmSDR for water System

Disc rotational speed,(rpm)	Liquid total flowrate Qt, (ml/sec)	Residence time $t_{res,}$ (sec)	Micromixing time $t_{mix,}$ (sec)
300	3	1.195	0.0031
500		0.849	0.0016
800		0.621	0.0008
1200		0.474	0.0005
300	9	0.574	0.0022
500		0.408	0.0011
800		0.298	0.0006
1200		0.227	0.0003
300	15	0.408	0.0018
500		0.291	0.0009
800		0.212	0.0005
1200		0.162	0.0003

Table AJ3: Residence time and mixing time on 10cmSDR for 50 wt% Glycerol System

Disc rotational speed,(rpm)	Liquid total flowrate Qt, (ml/sec)	Residence time $t_{res,}$ (sec)	Micromixing time $t_{mix,}$ (sec)
300	3	2.045	0.0143
500		1.45	0.0073
800		1.06	0.0039
1200		0.811	0.0023
300	9	0.983	0.0099
500		0.699	0.0050
800		0.511	0.0027
1200		0.390	0.0016
300	15	0.699	0.0084
500		0.497	0.0042
800		0.363	0.0023
1200		0.277	0.0013

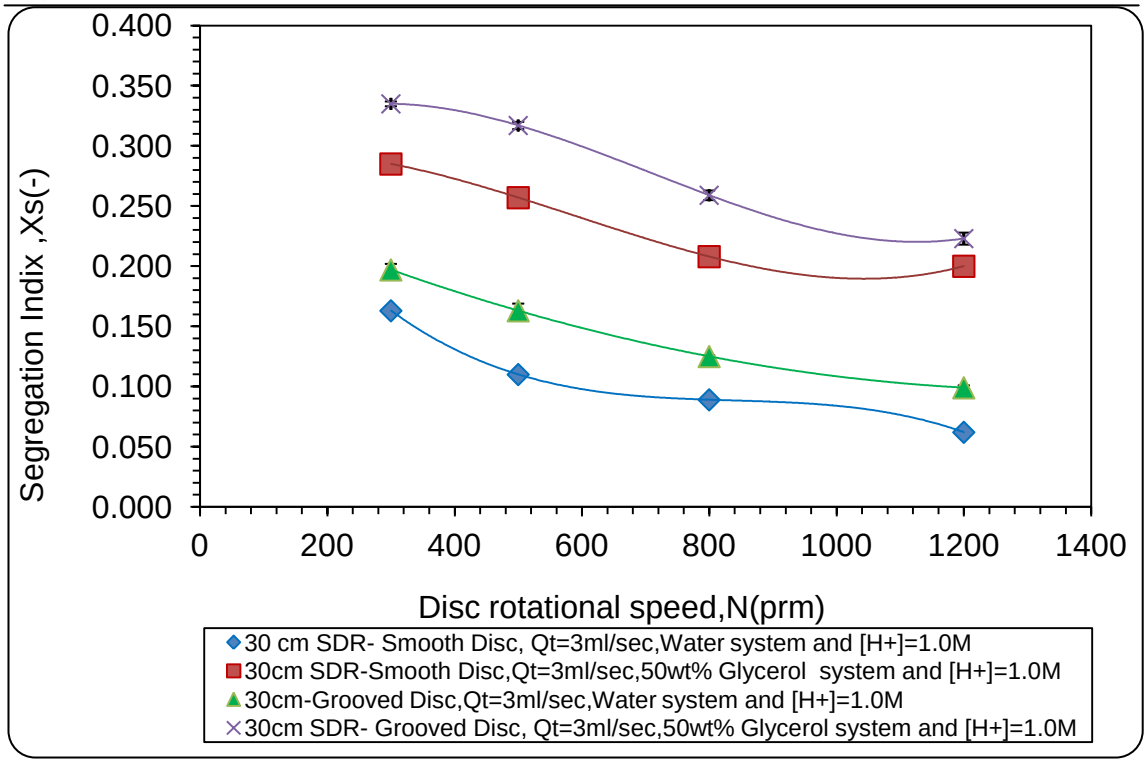

Figure AJ1: Effect of feed viscosity on segregation Index (Xs) in 30 cm SDR At Qt =3 ml/sec and [H+] =1.0 M (Smooth disc Vs. Grooved Disc)

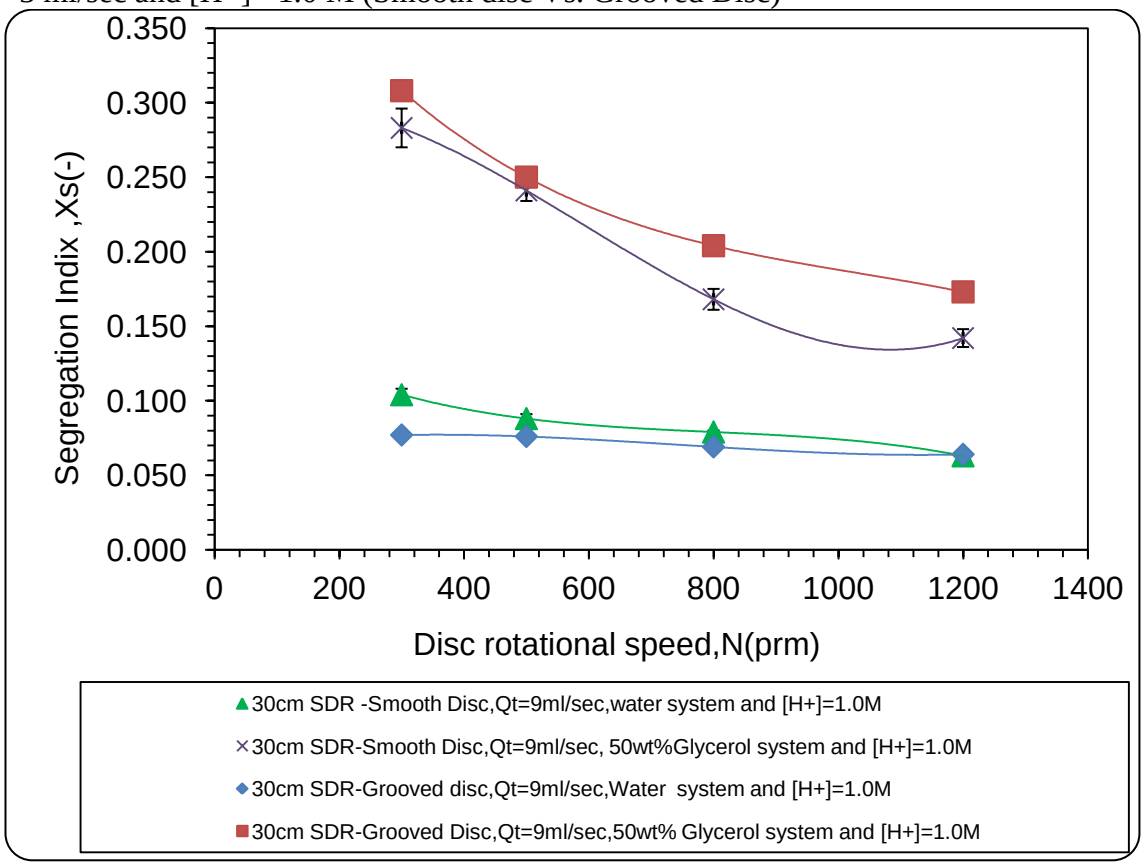

Figure AJ2: Effect of feed viscosity on segregation Index (Xs) in 30 cm SDR at Qt =9 ml/sec and [H+] =1.0 M (Smooth disc Vs. Grooved Disc)

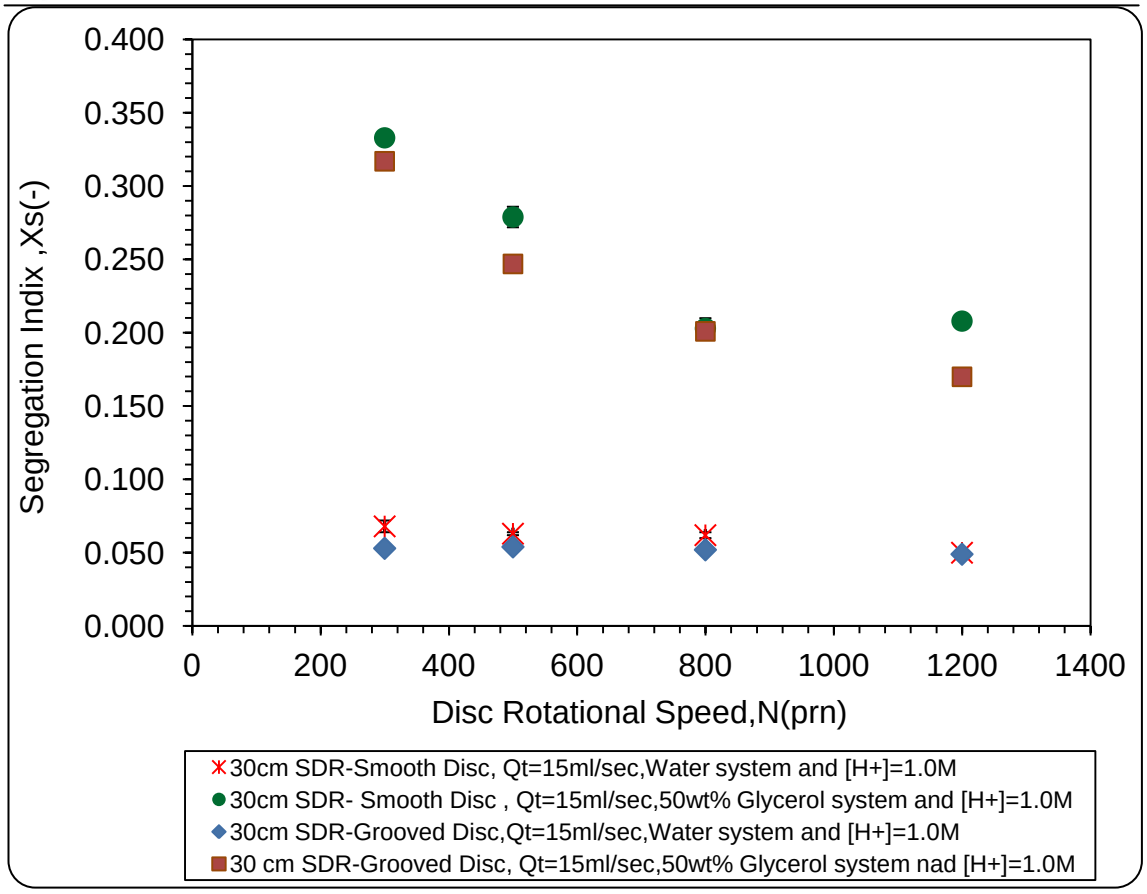

Figure AJ3: Effect of feed viscosity on segregation Index (Xs) in 30 cm SDR At Qt =15 ml/sec and [H+] =1.0 M (Smooth disc Vs. Grooved Disc)

Appendix K: NCR Experiments

Table AK1: Factorial Experimental Design – for each NCR

Run Order	Total flow rate, (ml/sec)	Acid concentration [H^+], M
1	0.50	0.25
2	1.00	1.00
3	0.50	0.50
4	0.25	0.10
5	0.50	0.10
6	0.25	0.50
7	0.50	1.00
8	1.00	0.10
9	2.00	0.10
10	2.00	0.25
11	1.00	0.25
12	0.25	1.00
13	2.00	1.00
14	1.00	0.50
15	2.00	0.50
16	0.25	0.25

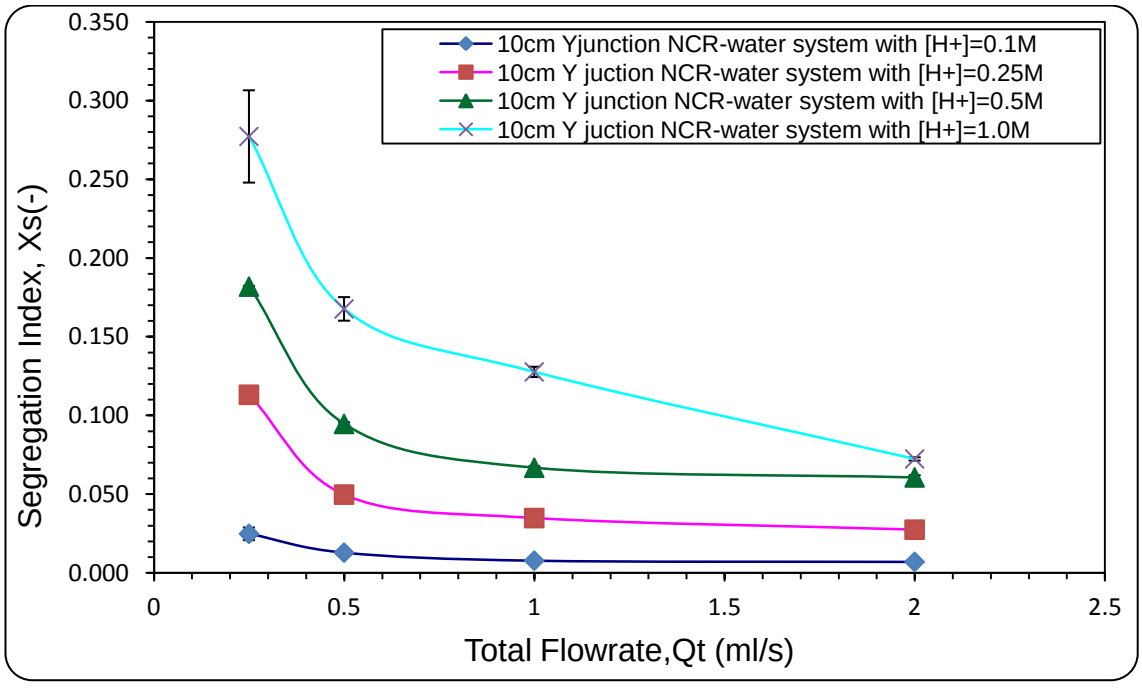

Figure AK1: Effect of total flowrate on segregation index, Xs (-) for 10 cm Y junction NCR-Water system with different acid ion concentrations

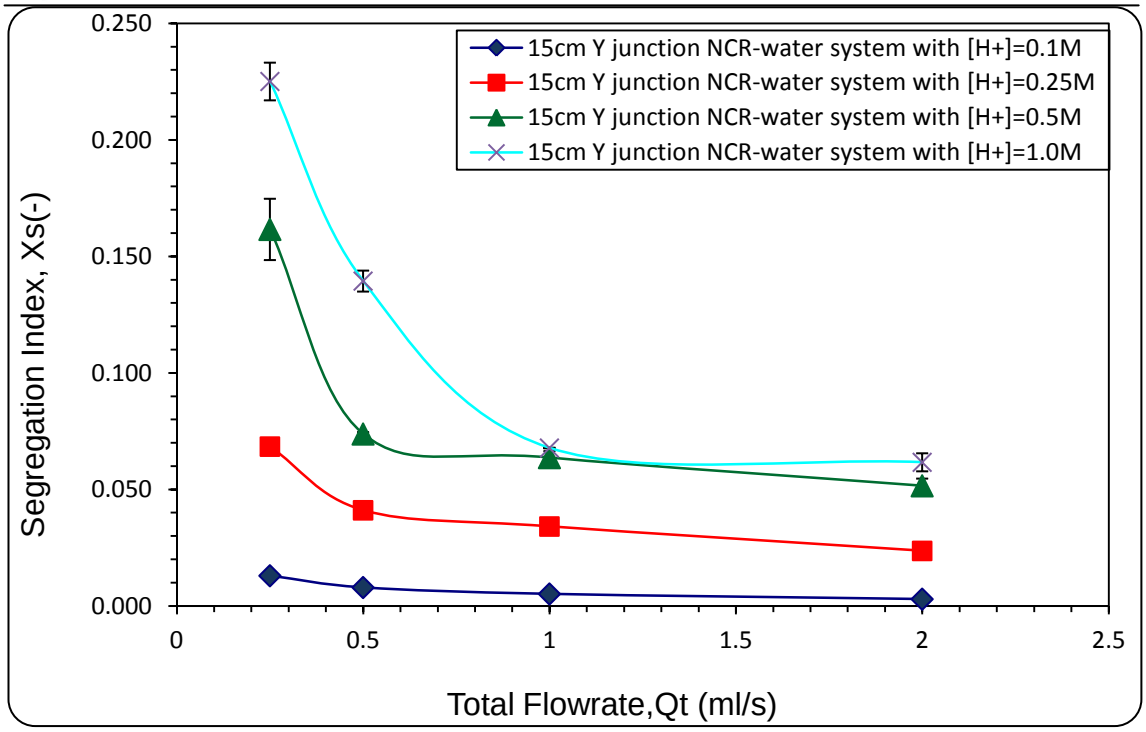

Figure AK2: Effect of total flowrate on segregation index, Xs (-) for 15 cm Y Junction NCR-Water system with different acid ion concentrations

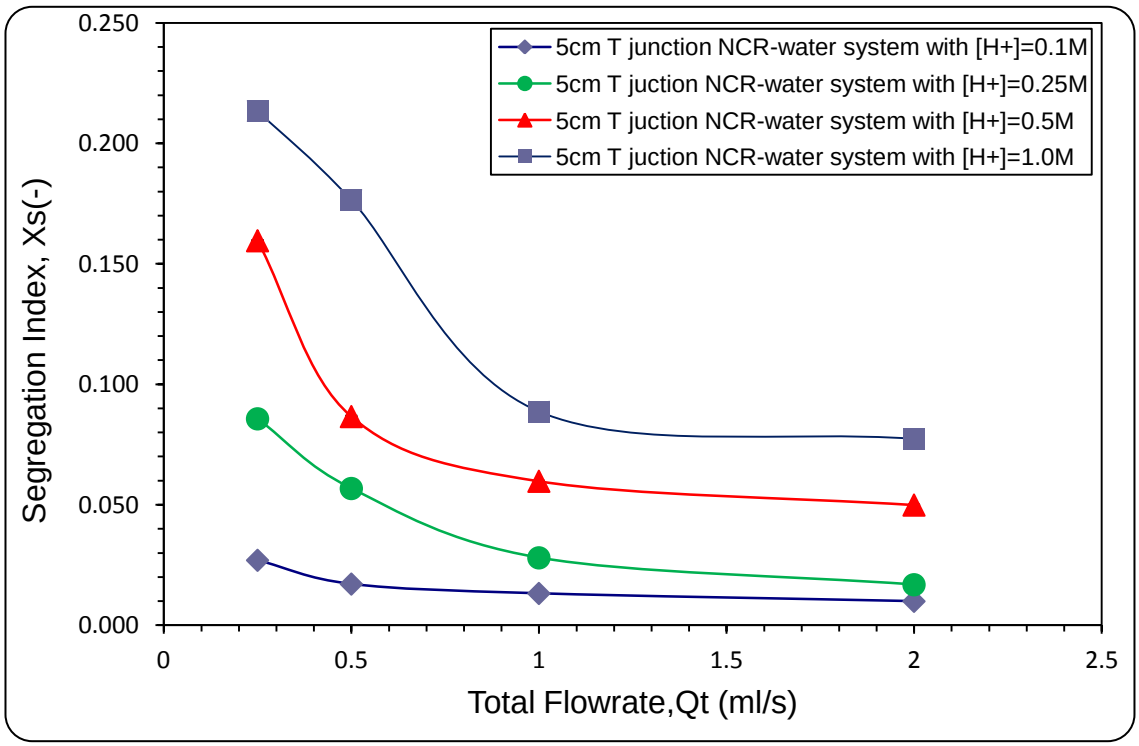

Figure AK3: Effect of total flowrate on segregation index, Xs (-) for 5 cm T Junction NCR-Water system with different acid ion concentrations

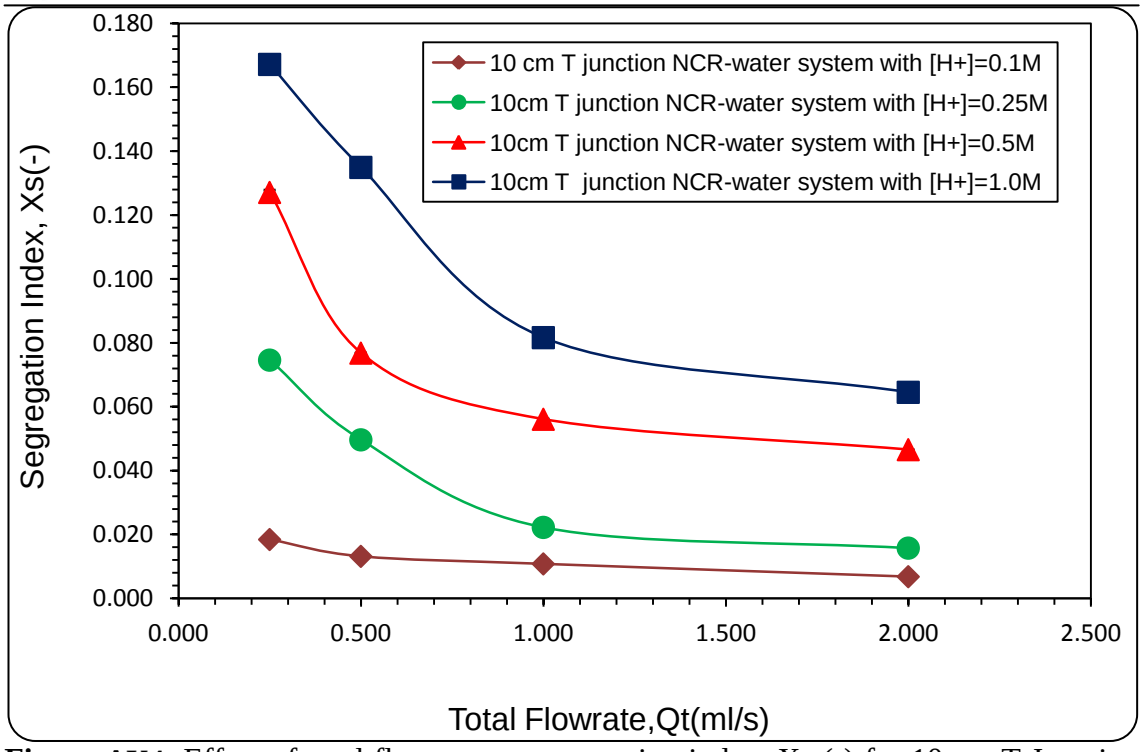

Figure AK4: Effect of total flowrate on segregation index, Xs (-) for 10 cm T Junction NCR-Water system with different acid ion concentrations

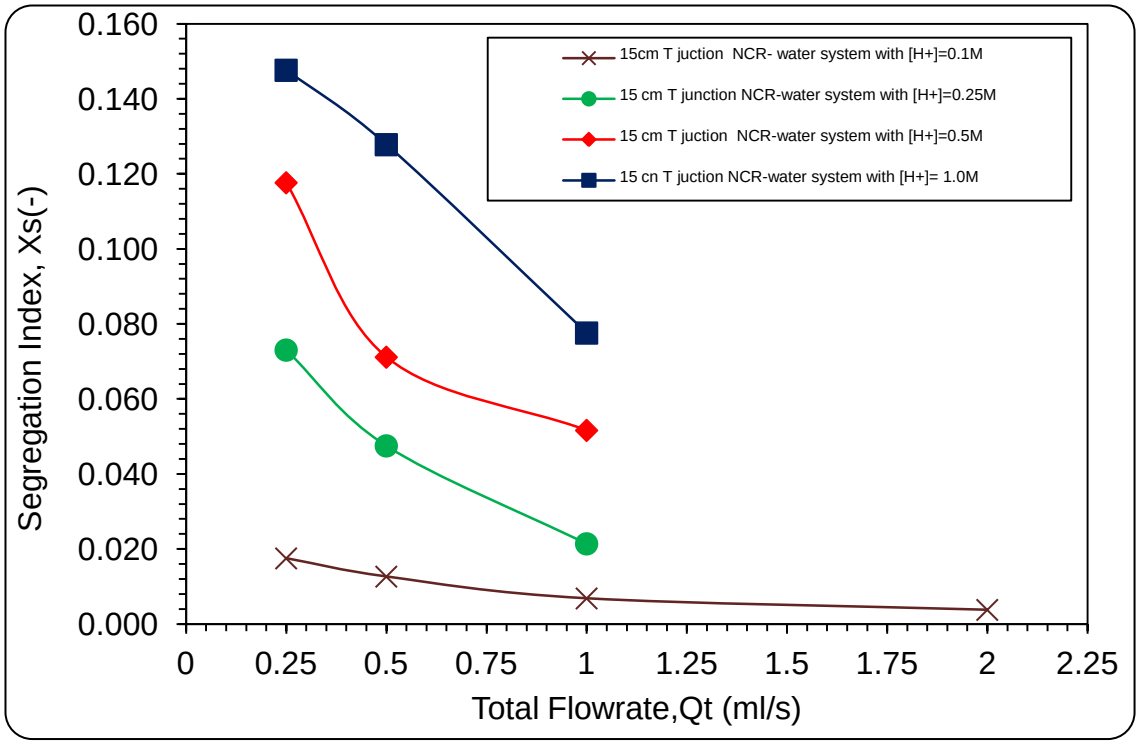

Figure AK5: Effect of total flowrate on segregation index, Xs (-) for 15 cm T Junction NCR-Water system with different acid ion concentrations

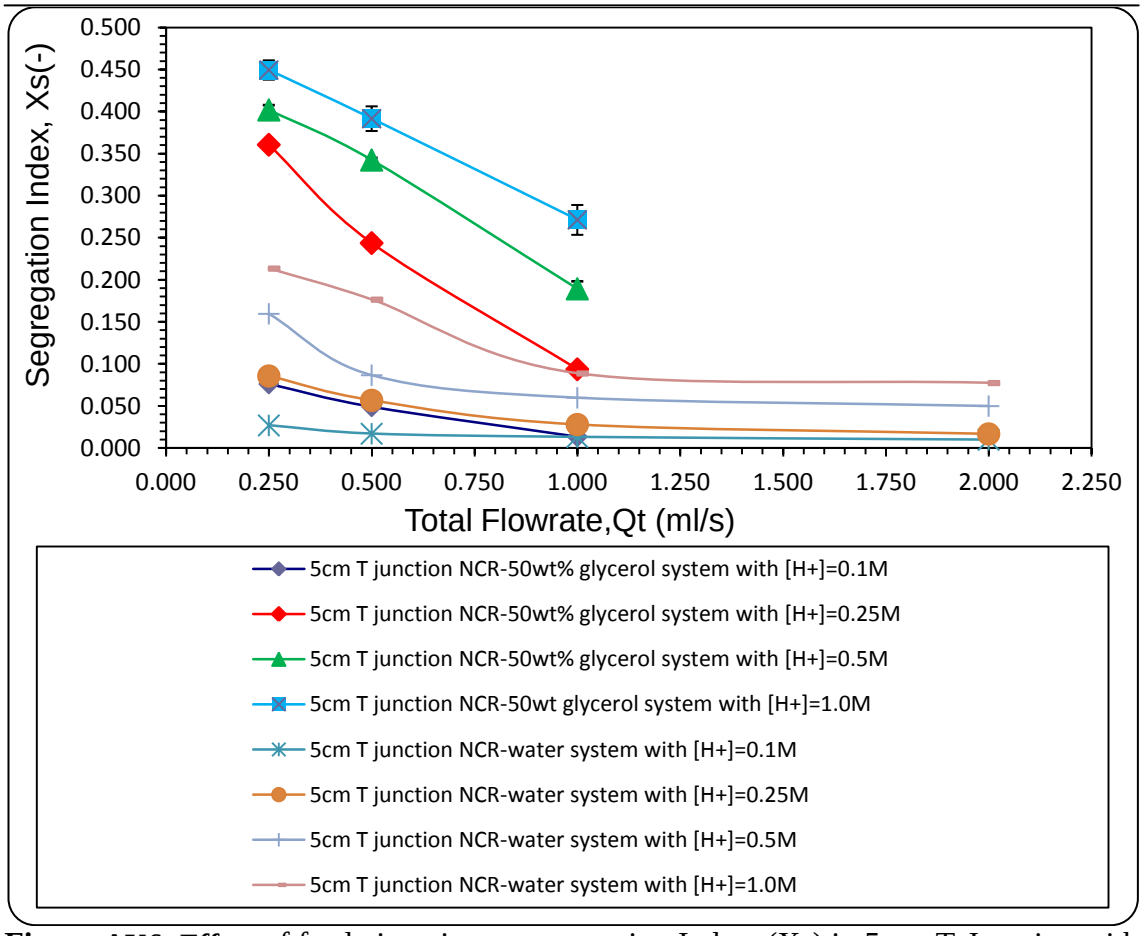

Figure AK6: Effect of feed viscosity on segregation Index, (Xs) in 5 cm T-Junction with different total flowrates and acid ion concentrations

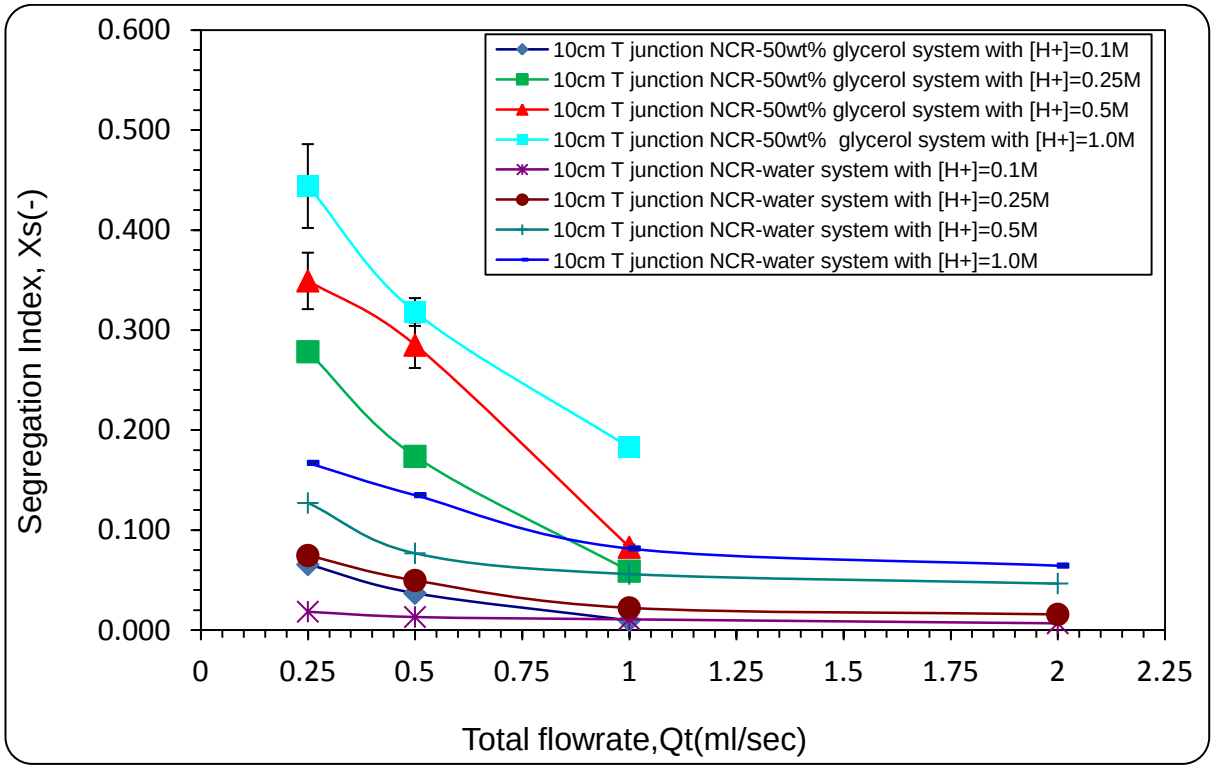

Figure AK7: Effect of feed viscosity on segregation Index, (Xs) in 10 cm T-Junction with different total flowrates and acid ion concentrations.

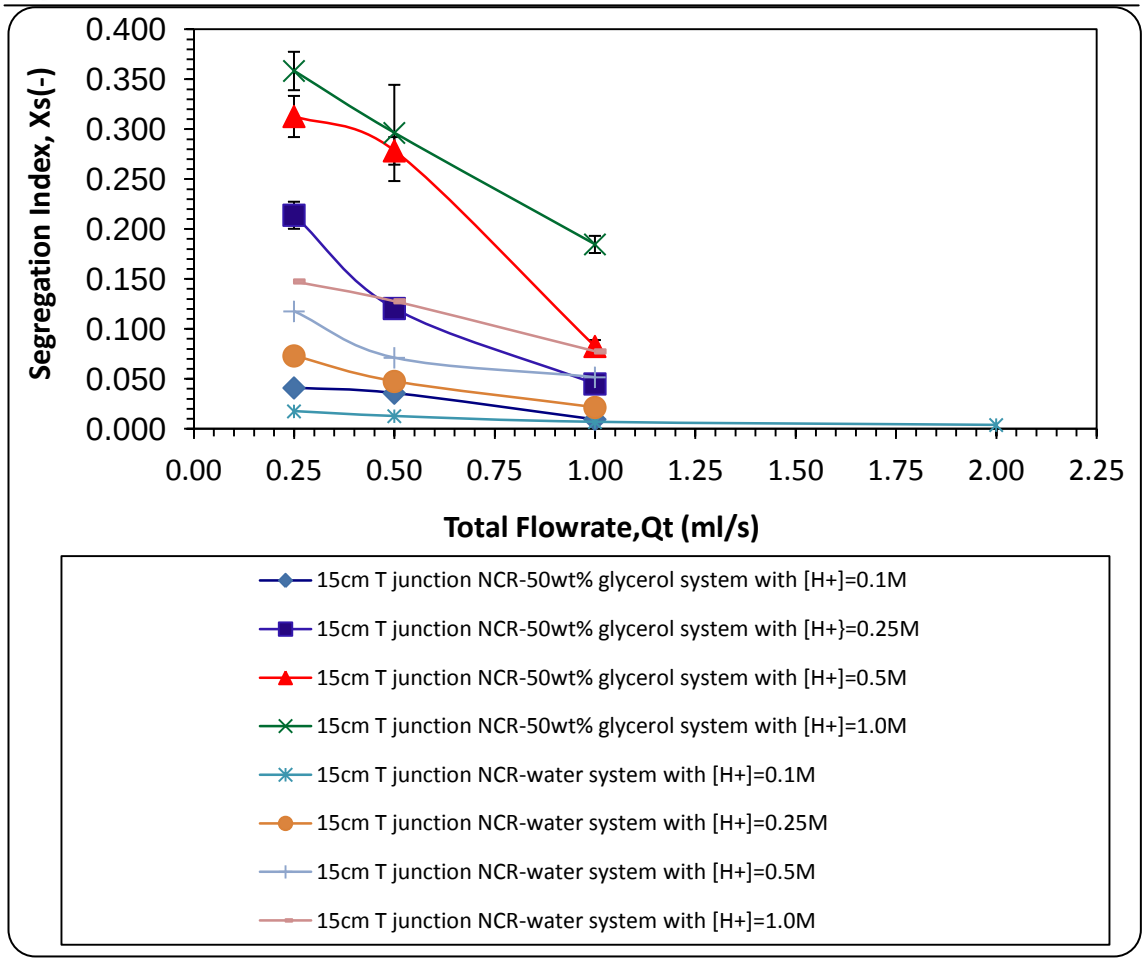

Figure AK8: Effect of feed viscosity on segregation Index, (Xs) in 15 cm T-Junction with different total flowrates and acid ion concentrations

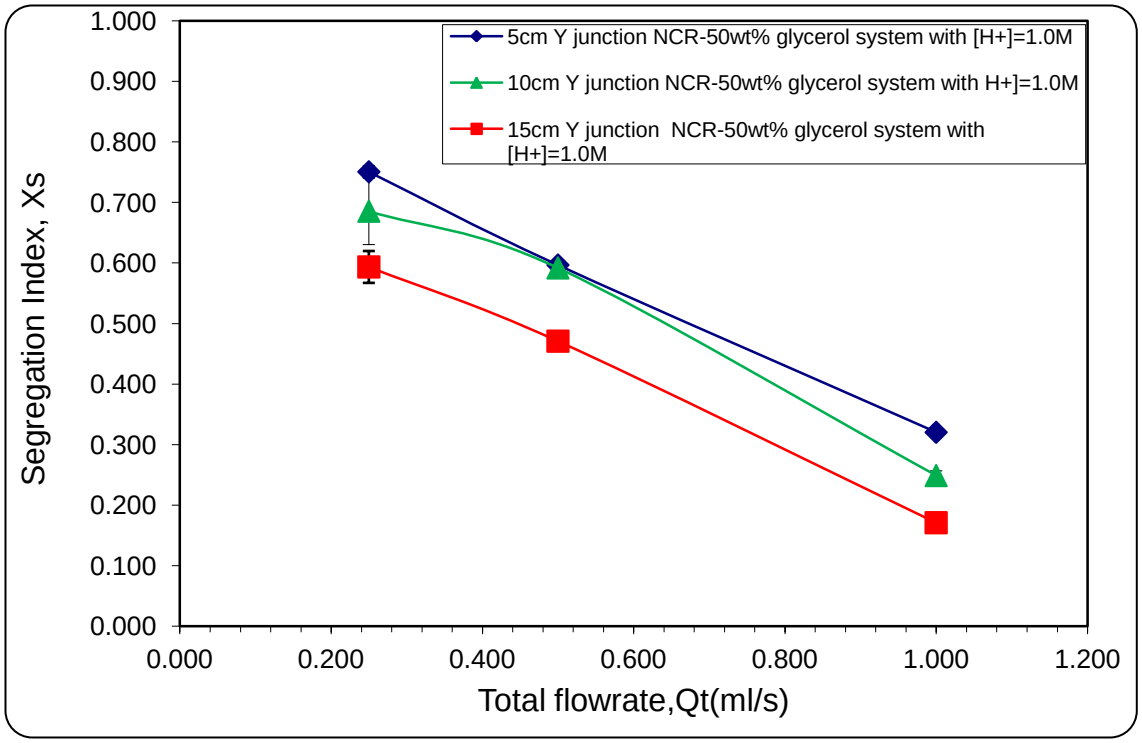

Figure AK9: Effect of channel length on segregation Index, (Xs) for 5,10 and 15 cm Y junction-50wt% system with $[H^+]$ =1.0 M

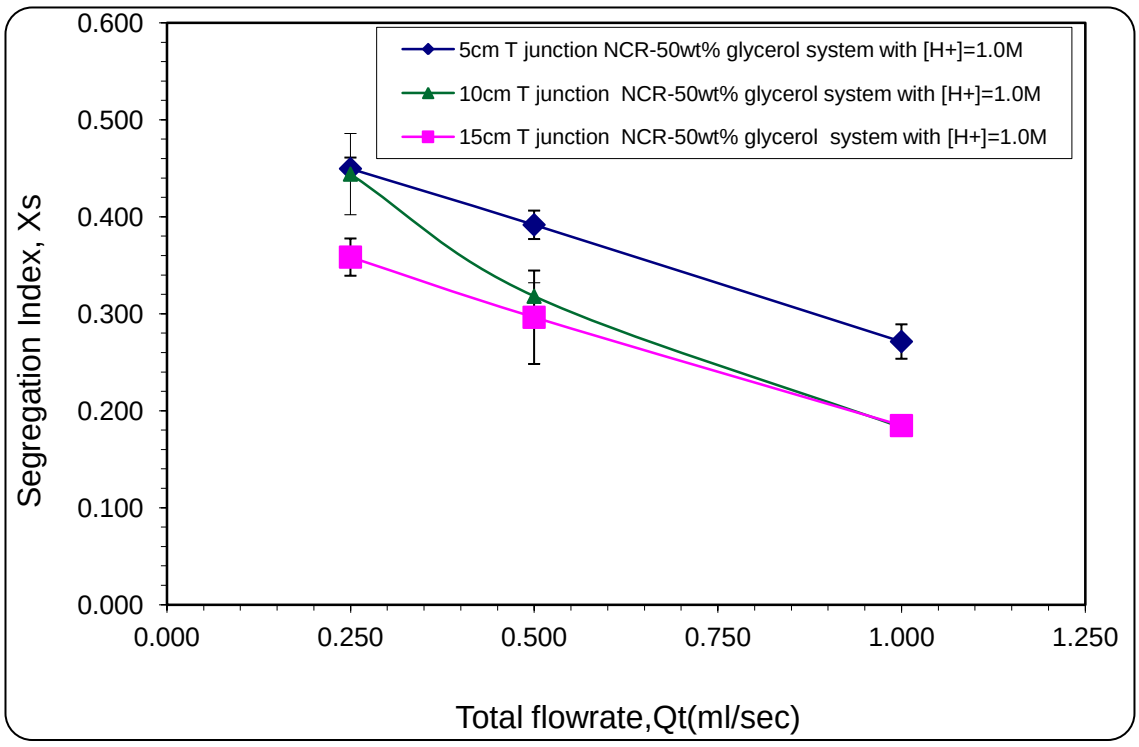

Figure AK10: Effect of channel length on segregation Index, (Xs) for 5,10 and 15 cm T junction- 50 wt% system with $[H^+]$ =1.0 M

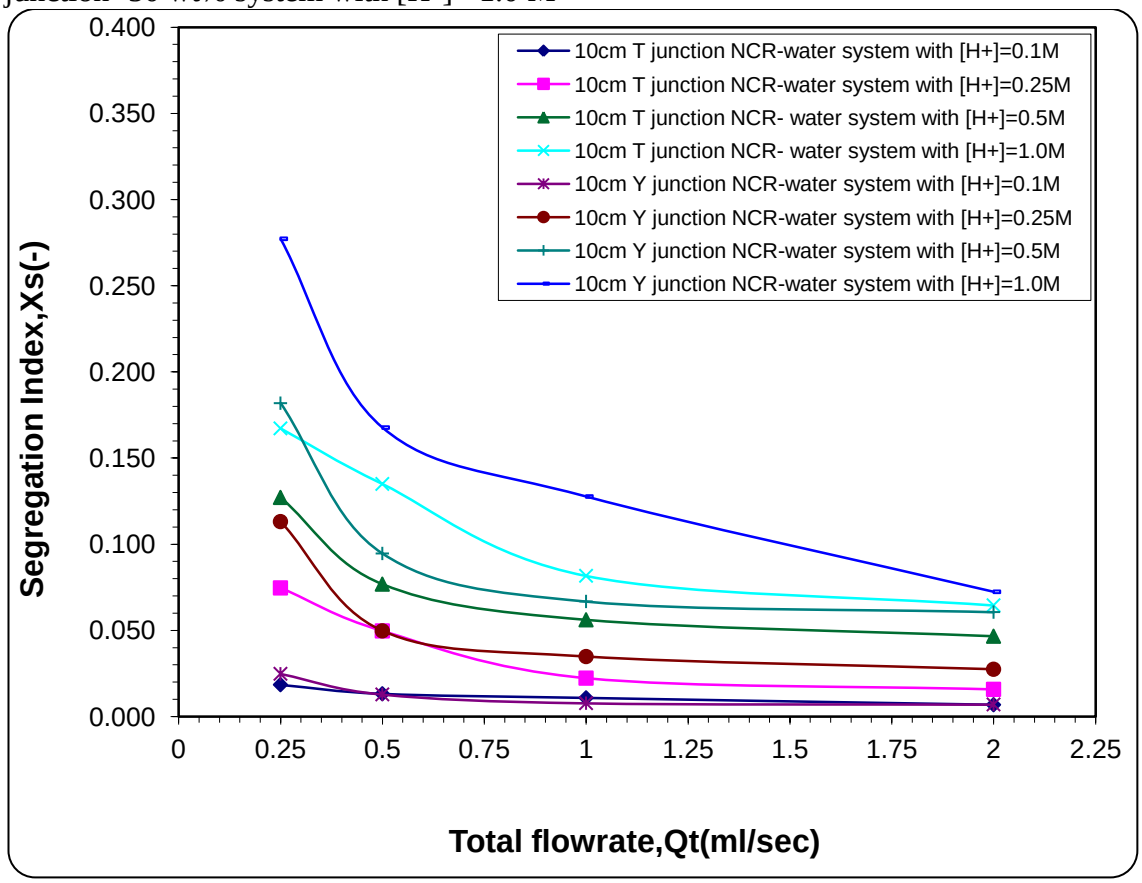

Figure AK11: Effect of junction type on segregation Index, (Xs) for 10 cm length - water system

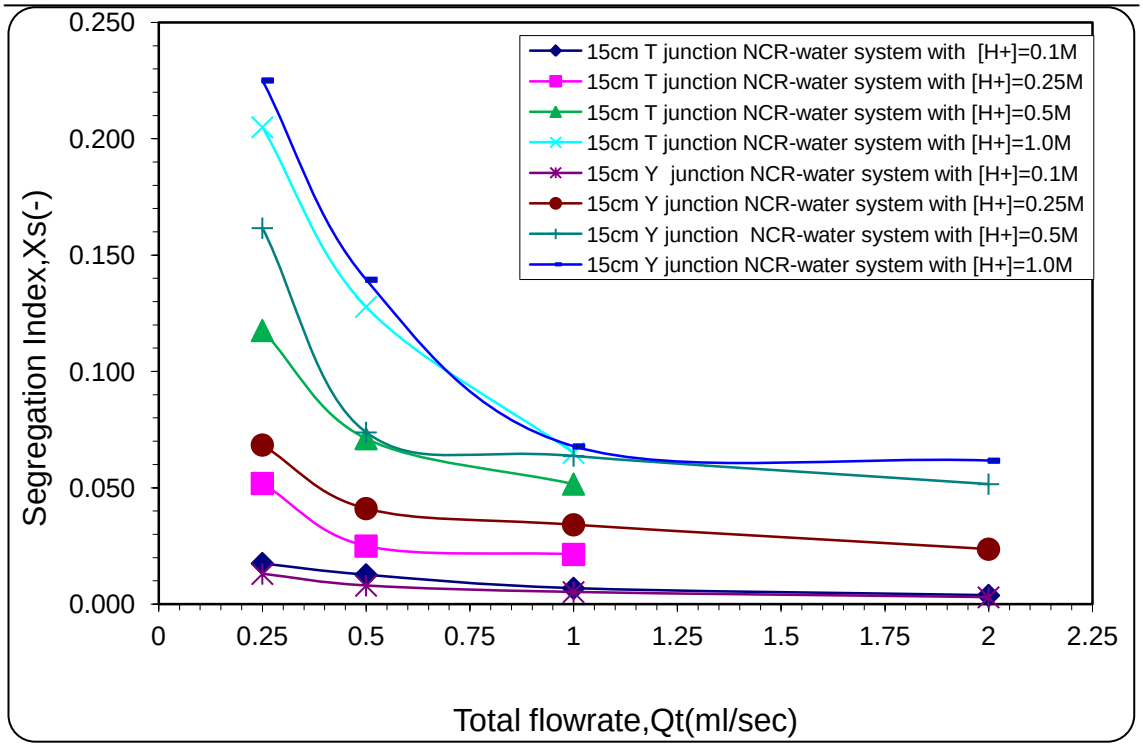

Figure AK12: Effect of junction type on segregation Index, (Xs) for 15 cm length - water system

Appendix L: Residence time distribution (RTD) Experiments

Table Al1: Factorial Experimental Design – RTD Experiments on 30 cm SDR disc. 32 runs for each type of disc surface

Run Order	Total flow rate, Qt(ml/sec)	Disc rotational speed ,(rpm)	Feed viscosity, (μ) mPa.s
1	6	800	1.005
2	9	300	1.005
3	6	1200	6.000
4	9	300	6.000
5	15	300	6.000
6	15	500	1.005
7	9	800	1.005
8	6	300	1.005
9	9	800	6.000
10	15	1200	6.000
11	9	500	6.000
12	6	500	6.000
13	3	300	6.000
14	15	300	1.005
15	15	1200	1.005
16	3	500	6.000
17	6	1200	1.005
18	6	300	6.000
19	9	500	1.005
20	15	800	6.000
21	9	1200	1.005
22	3	300	1.005
23	15	500	6.000
23	3	800	1.005
24	3	500	1.005
25	15	800	1.005
26	3	1200	1.005
27	6	800	6.000
29	3	800	6.000
30	6	500	1.005
31	3	1200	6.000
32	9	1200	6.000

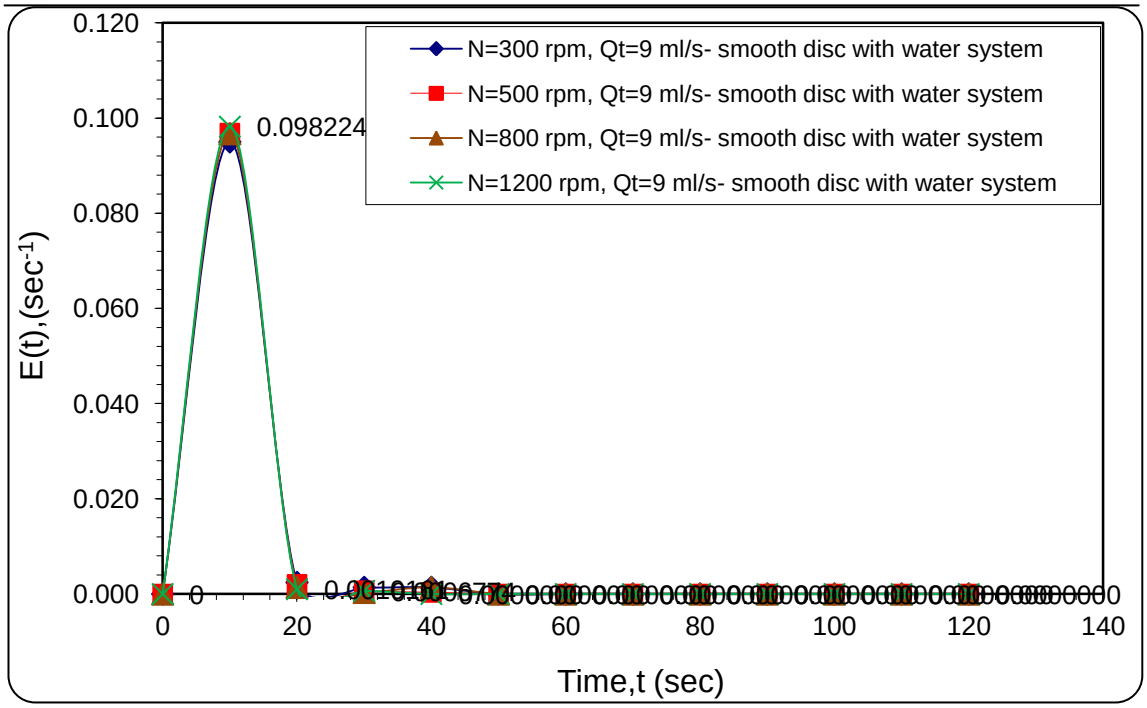

Figure AL1: Effect of disc rotational speed on RTD at total flowrate of (Qt=9 ml/s)-smooth disc with water system

Table AL2: the experimental mean resident time and the variance for the 30 cmSDR, Using smooth disc with water system, Qt=9 ml/s and disc rotational speeds of 300,500,800 and 1200 rpm.

N, rpm	Mean resident time, tm (s)	Variance,σ^2(sec^2)
300	13.55	5.000
500	13.50	2.837
800	13.22	2.620
1200	10.13	2.507

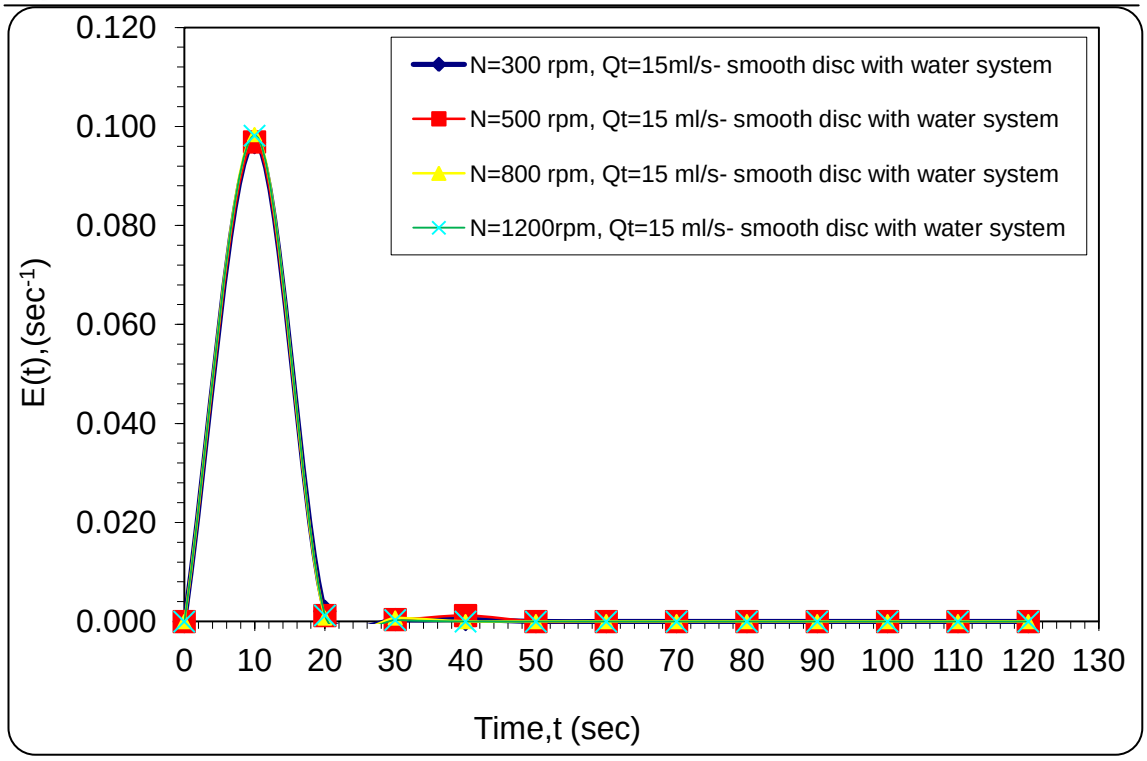

Figure AL2: Effect of disc rotational speed on RTD at total flowrate of (Qt=15 ml/s)-smooth disc with water system

Table AL3: the experimental mean resident time and the variance for the 30 cmSDR using smooth disc with water system ,Qt=15 ml/s and disc rotational speeds of 300,500,800 and 1200 rpm.

N, rpm	Mean resident time, tm (s)	Variance,σ^2(sec^2)
300	13.40	4.978
500	10.26	2.815
800	10.20	2.618
1200	10.13	2.155

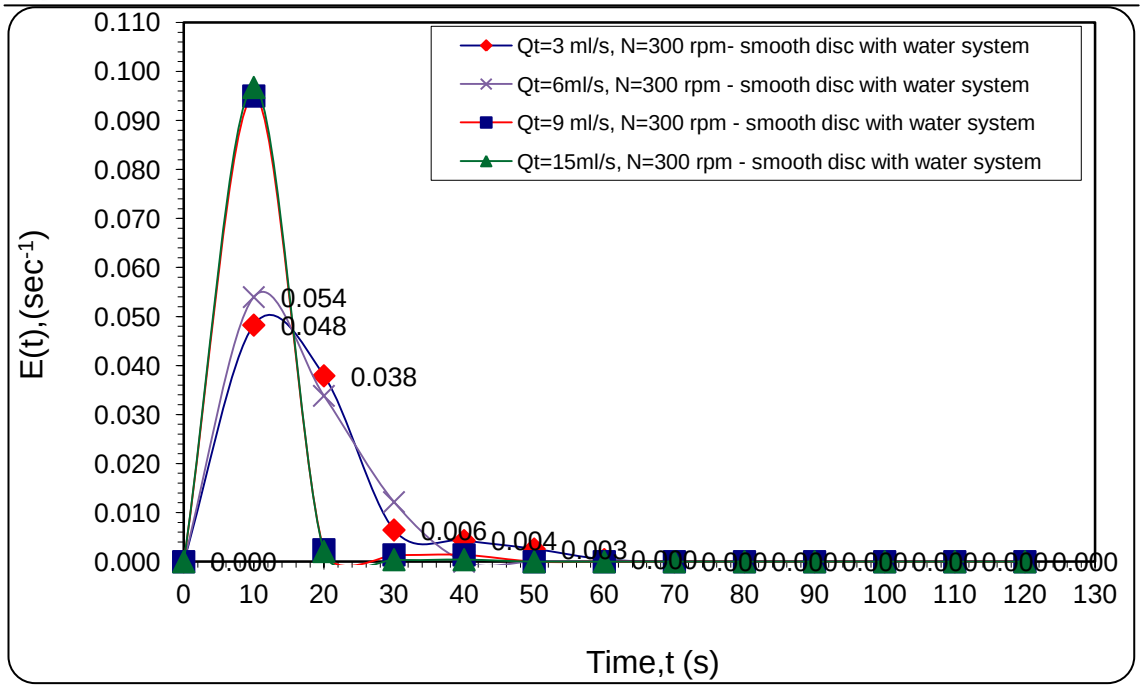

Figure AL3: Effect of liquid total flowrate on the RTD in 30 cm SDR at disc rotational speed of 300 rpm –smooth disc with water system

Table AL4: Experimental mean residence time and the variance for the 30 cm SDR at different total flowrates and N=300 rpm using water system with smooth disc

Total flowrate, Qt (ml/s)	Mean resident time, tm (s)	Variance,σ^2(sec^2)
3	17.040	103.840
6	13.991	36.407
9	13.470	5.000
15	13.390	4.978

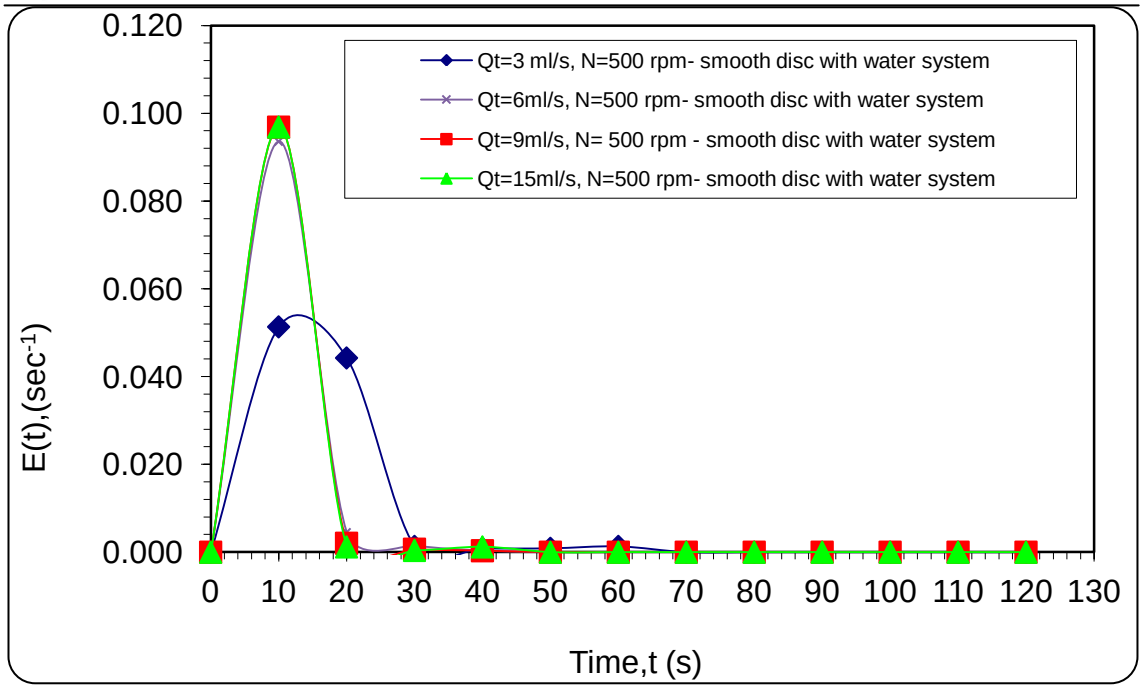

Figure AL4: Effect of liquid total flowrate on the RTD in 30cm SDR at disc rotational speed of 500 rpm –smooth disc with water system

Table AL5: Experimental mean residence time and the variance for the 30 cm SDR at different total flowrates and N=500 rpm using water system with smooth disc

Total flowrate, Qt (ml/s)	Mean resident time, tm (s)	Variance,σ^2(sec^2)
3	14.37	71.247
6	13.740	5.642
9	10.27	2.837
15	10.260	2.815

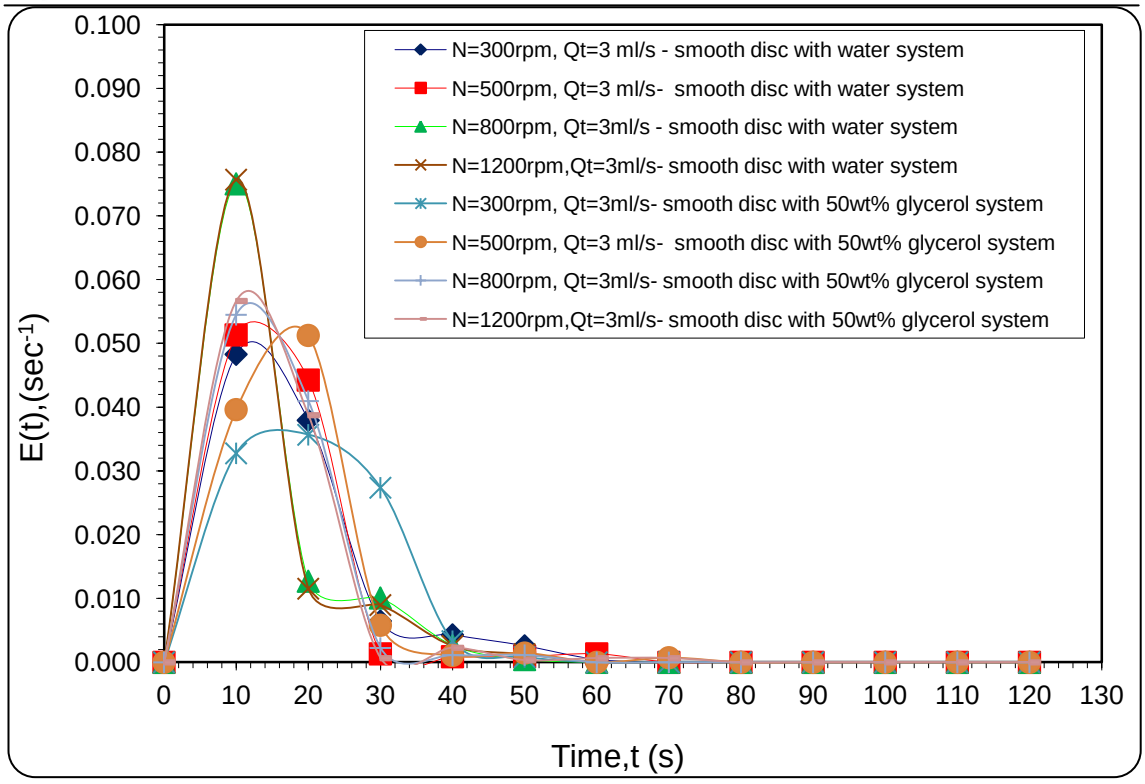

Figure AL5: Effect of viscosity on the RTD in 30 cm SDR at total flowrate 3ml/s and different disc rotational speeds –smooth disc with 50 wt% glycerol system

Table AL6: Experimental mean residence time and the variance for the 30 cm SDR using water system and 50 wt% glycerol system with smooth disc, Qt=3 ml/s

N, rpm	Water system		Water/glycerol system	
	Mean resident time , tm (s)	Variance,σ^2(sec^2)	Mean resident time, tm (s)	Variance,σ^2(sec^2)
300	17.04	103.840	20.166	153.375
500	14.37	71.247	16.250	95.615
800	14.24	64.929	15.060	80.810
1200	13.92	63.061	14.610	73.291

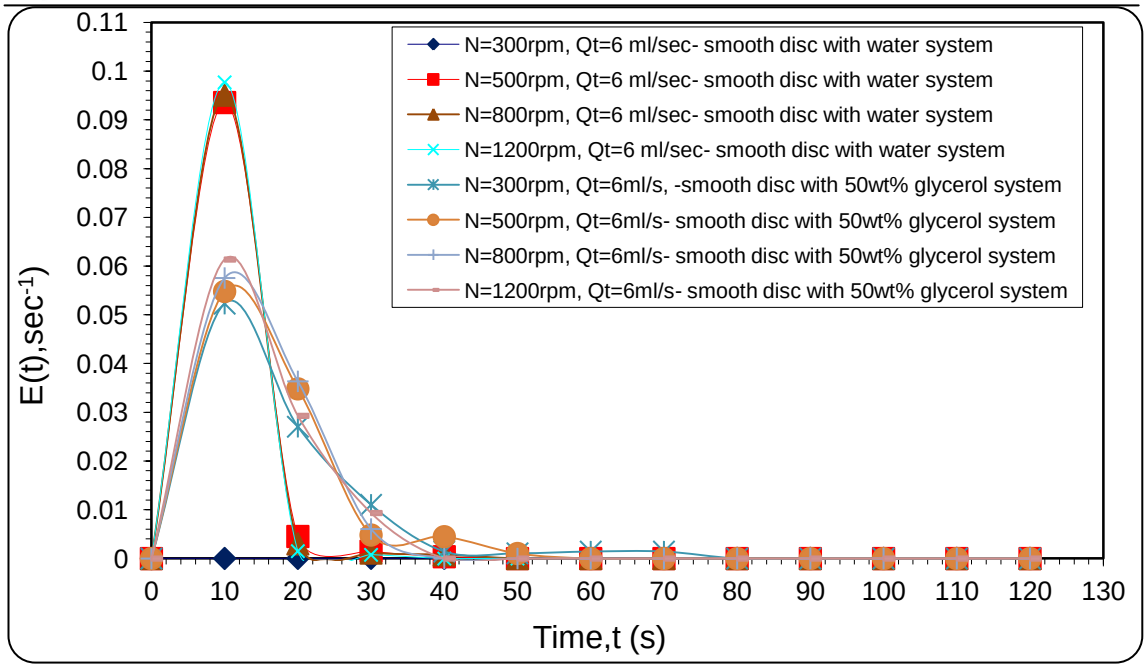

Figure AL6: Effect of viscosity on the RTD in 30 cm SDR at total flowrate 6ml/s and different disc rotational speeds –smooth disc with 50 wt% glycerol system

Table AL7: Experimental mean residence time and the variance for the 30 cmSDR using water system and 50 wt% glycerol system with smooth disc, Qt=6 ml/s

N, rpm	Water system		Water/glycerol system	
	Mean resident time , tm (s)	Variance,σ^2(sec^2)	Mean resident time, tm (s)	Variance,σ^2(sec^2)
300	13.991	36.407	16.408	93.566
500	13.740	5.642	15.950	76.573
800	13.640	5.127	13.940	30.106
1200	10.190	2.980	13.400	30.027

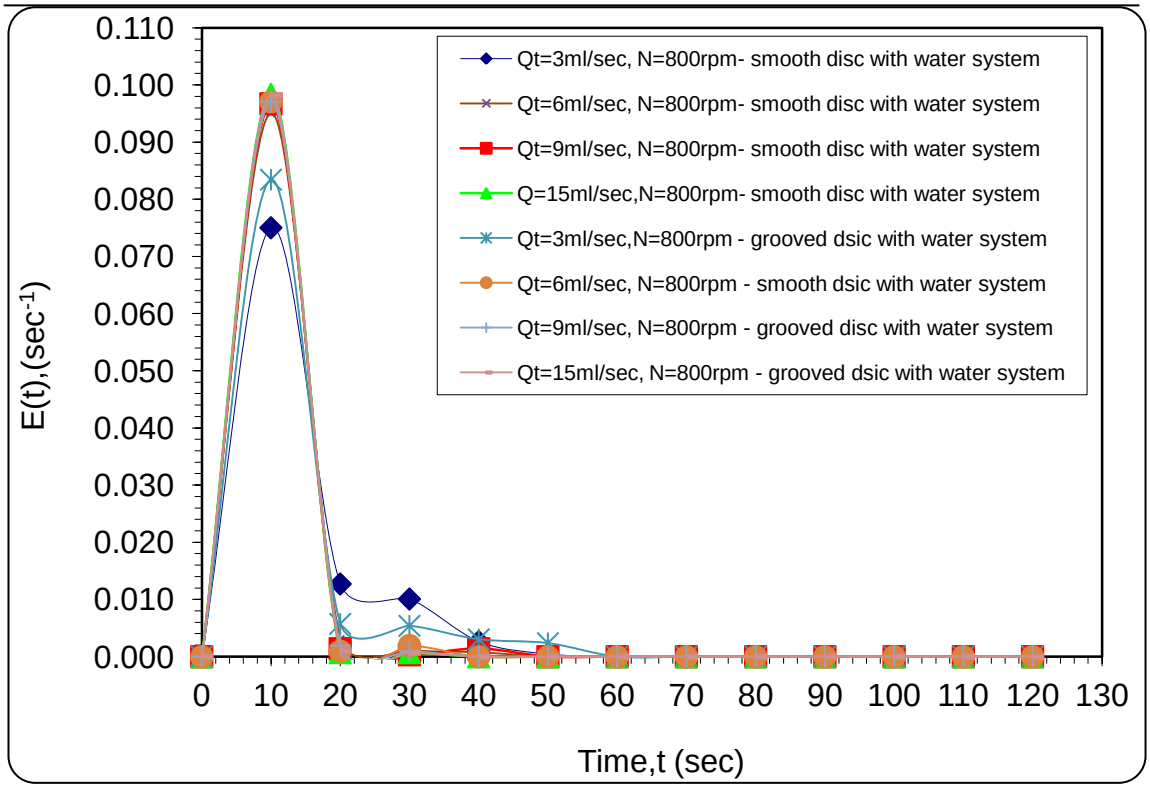

Figure AL7: Effect of total flowrate on RTD at disc rotational speed 800 rpm – water system (Smooth disc Vs. Grooved Disc)

Table AL8: Experimental mean resident time and the variance for the 30 cmSDR at different total flowrates, (Qt), using water system with grooved and smooth discs, N=800 rpm

Qt,ml/s	Water system with using Grooved disc		Water system with Smooth disc	
	Mean residence time , tm (s)	Variance,σ^2(sec^2)	Mean residence time, tm (s)	Variance,σ^2(sec^2)
3	12.920	3.071	14.24	64.929
6	10.20	1.740	13.640	5.127
9	10.24	1.227	10.25	2.620
15	10.14	1.201	10.180	2.618

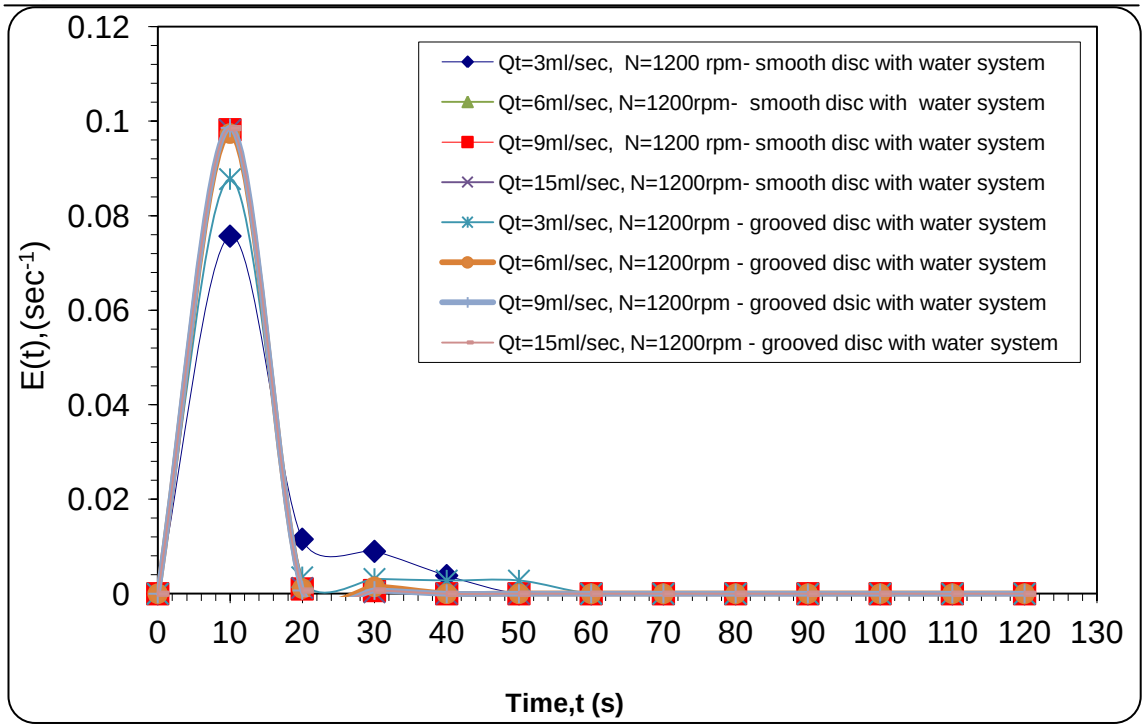

Figure AL8: Effect of total flowrate on RTD at disc rotational speed 1200 rpm – water system (Smooth disc Vs. Grooved Disc)

Table AL9: Experimental mean resident time and the variance for the 30 cm SDR at different total flowrates, (Qt), using water system with grooved and smooth discs, N=1200 rpm

Qt,ml/s	Water system with using Grooved disc		Water system with Smooth disc	
	Mean residence time , tm (s)	Variance,σ^2(sec^2)	Mean residence time, tm (s)	Variance,σ^2(sec^2)
3	12.230	2.030	13.920	63.061
6	10.180	1.530	10.190	2.980
9	10.100	1.033	10.130	2.507
15	10.100	1.027	10.130	2.500

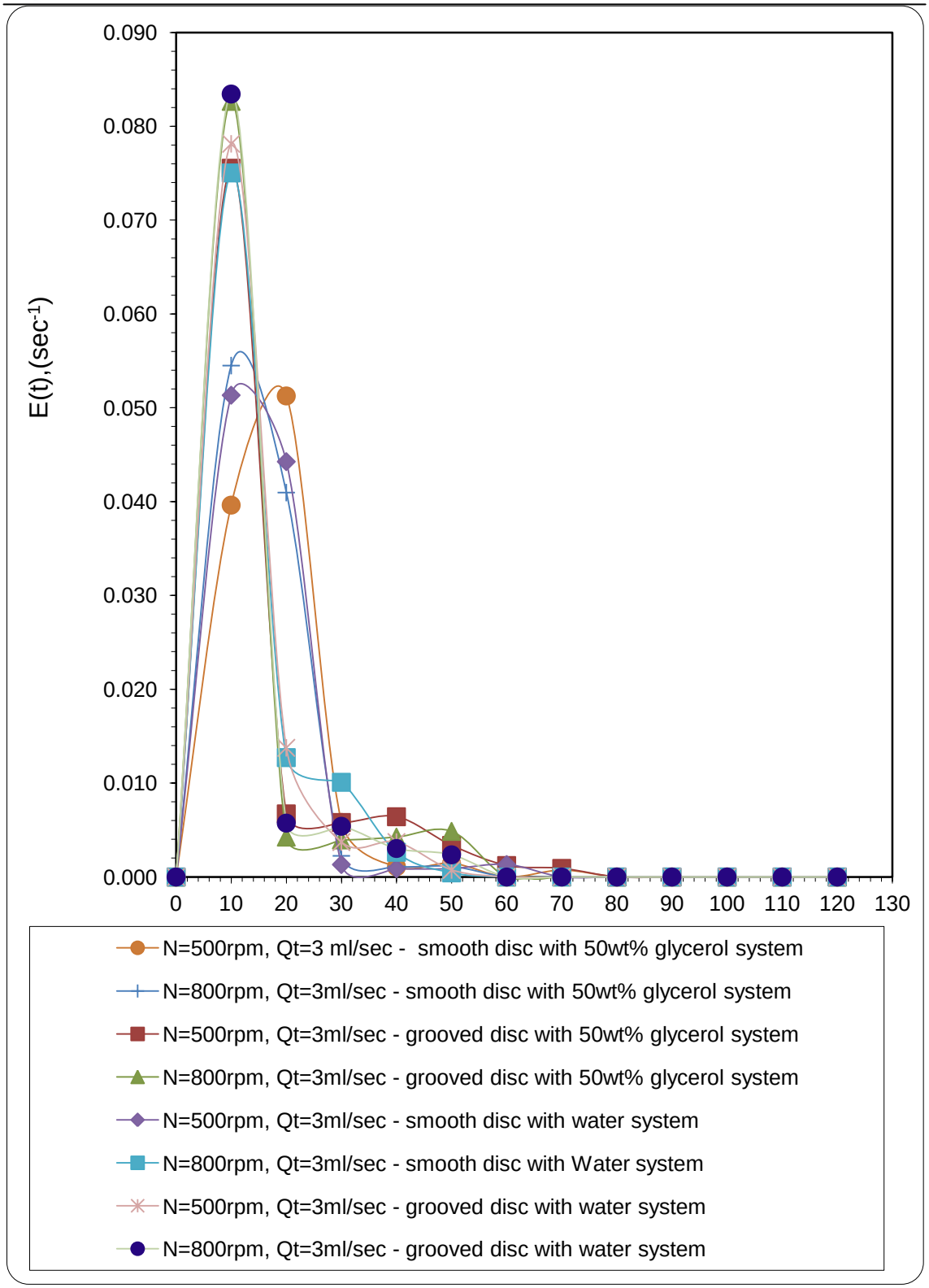

Figure AL9: Effect of disc rotational speed on RTD at total flowrate of (Qt=3 ml/s) and disc rotational speeds of 500 and 800 rpm -smooth disc vs. grooved disc with water and 50wt% glycerol system

Table AL10 : Experimental mean resident time and the variance for the 30 cmSDR at disc rotational speeds of 500 and 800 rpm using water system and 50 wt% glycerol system with grooved and smooth discs, Qt=3ml/s

Disc type	Disc speed, N(rpm)	Water system		Glycerol system	
		Mean residence time , tm (s)	Variance,σ^2(sec^2)	Mean residence time, tm (s)	Variance,σ^2(sec^2)
Smooth	500	14.370	71.247	16.250	95.615
Smooth	800	14.240	64.929	15.060	80.810
Grooved	500	13.360	3.071	15.950	73.284
Grooved	800	12.920	2.030	13.220	22.016

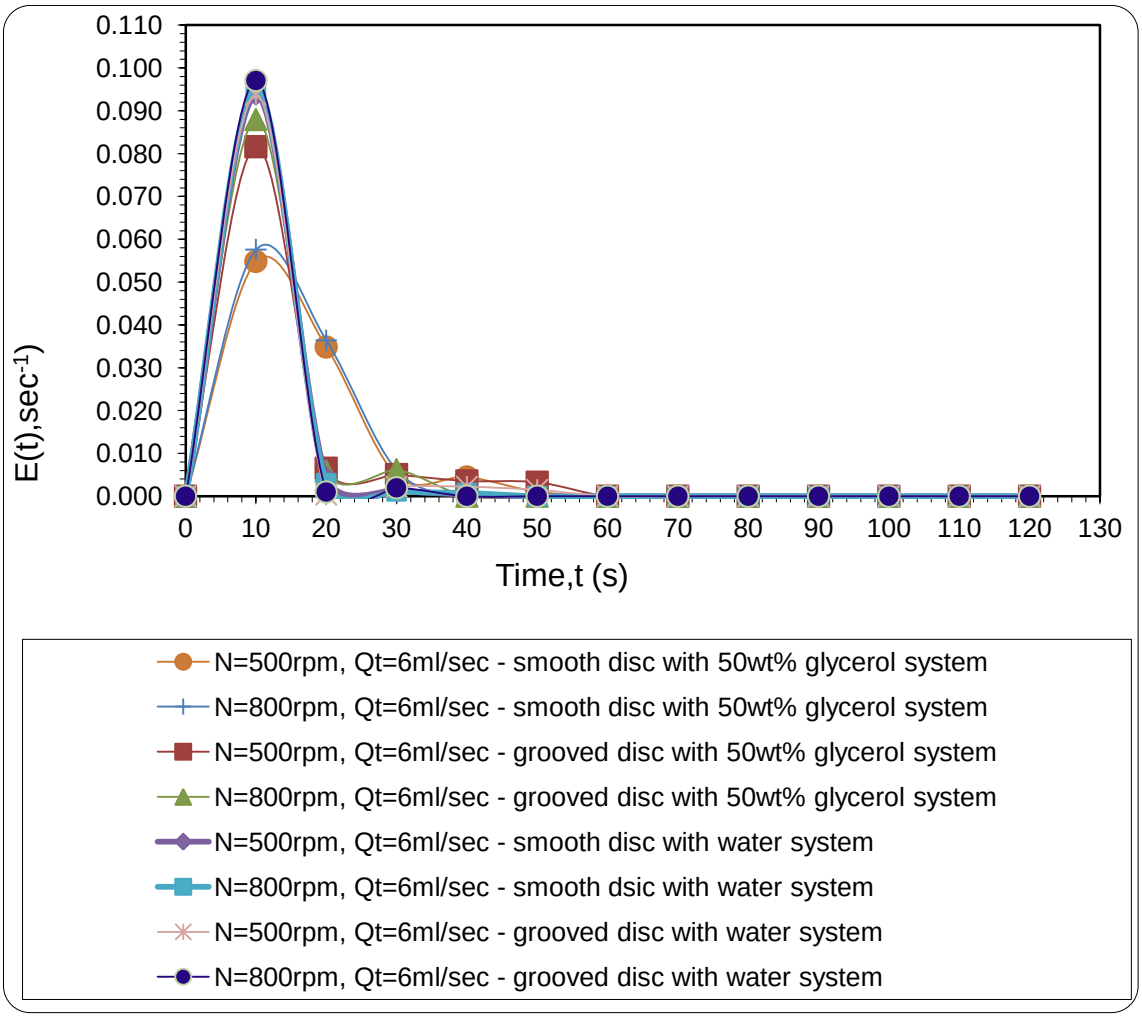

Figure AL10: Effect of disc rotational speed on RTD at total flowrate of (Qt=6 ml/s) and disc rotational speeds of 500 and 800 rpm -smooth disc vs. grooved disc with water and 50 wt% glycerol system

Table AL11: Experimental mean resident time and the variance for the 30 cm SDR at disc rotational speeds of 500 and 800 rpm using water system and 50 wt% glycerol system with grooved and smooth discs, Qt=6 ml/s

Disc type	Disc speed, N(rpm)	Water system		Glycerol system	
		Mean residence time , tm (s)	Variance,σ^2(sec^2)	Mean residence time, tm (s)	Variance,σ^2(sec^2)
Smooth	500	13.740	5.642	15.950	76.573
Smooth	800	13.640	5.127	13.940	30.106
Grooved	500	11.700	2.513	13.22	4.011
Grooved	800	10.200	1.740	10.90	3.847

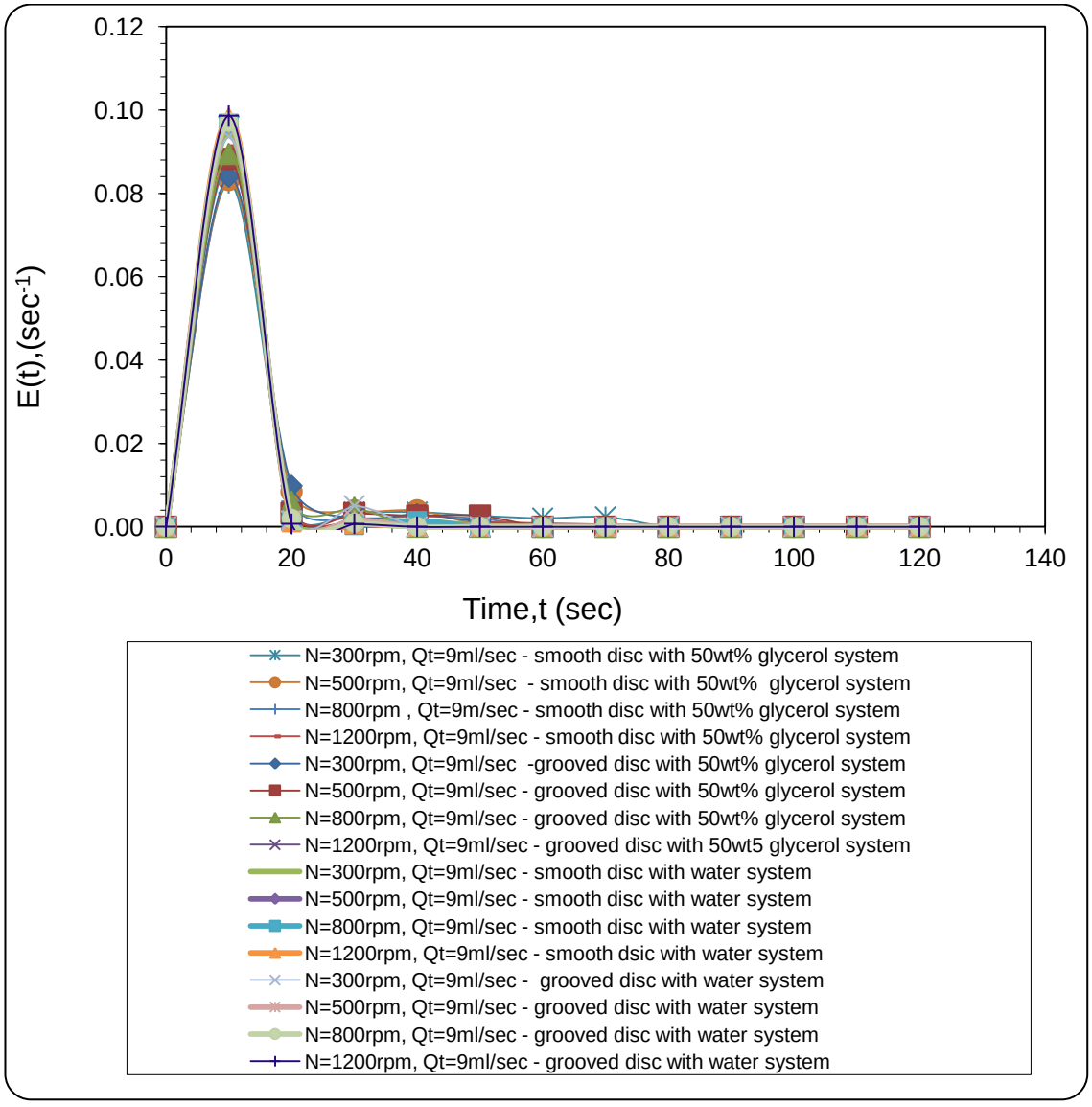

Figure AL11: Effect of disc rotational speed on RTD at total flowrate of (Qt=9 ml/s)-smooth disc vs. grooved disc with water and 50 wt% glycerol system

Table AL12: Experimental mean resident time and the variance for the 30 cm SDR at disc rotational speeds of 500 and 800 rpm using water system and 50 wt% glycerol system with grooved and smooth discs, Qt=9 ml/s

Disc type	Disc speed, N(rpm)	Water system		Glycerol system	
		Mean residence time , tm (s)	Variance,σ^2(sec^2)	Mean residence time, tm (s)	Variance,σ^2(sec^2)
Smooth	500	10.270	2.837	12.890	5.015
Smooth	800	10.250	2.620	12.080	4.917
Grooved	500	10.240	1.437	12.160	4.699
Grooved	800	10.240	1.227	10.82	3.648

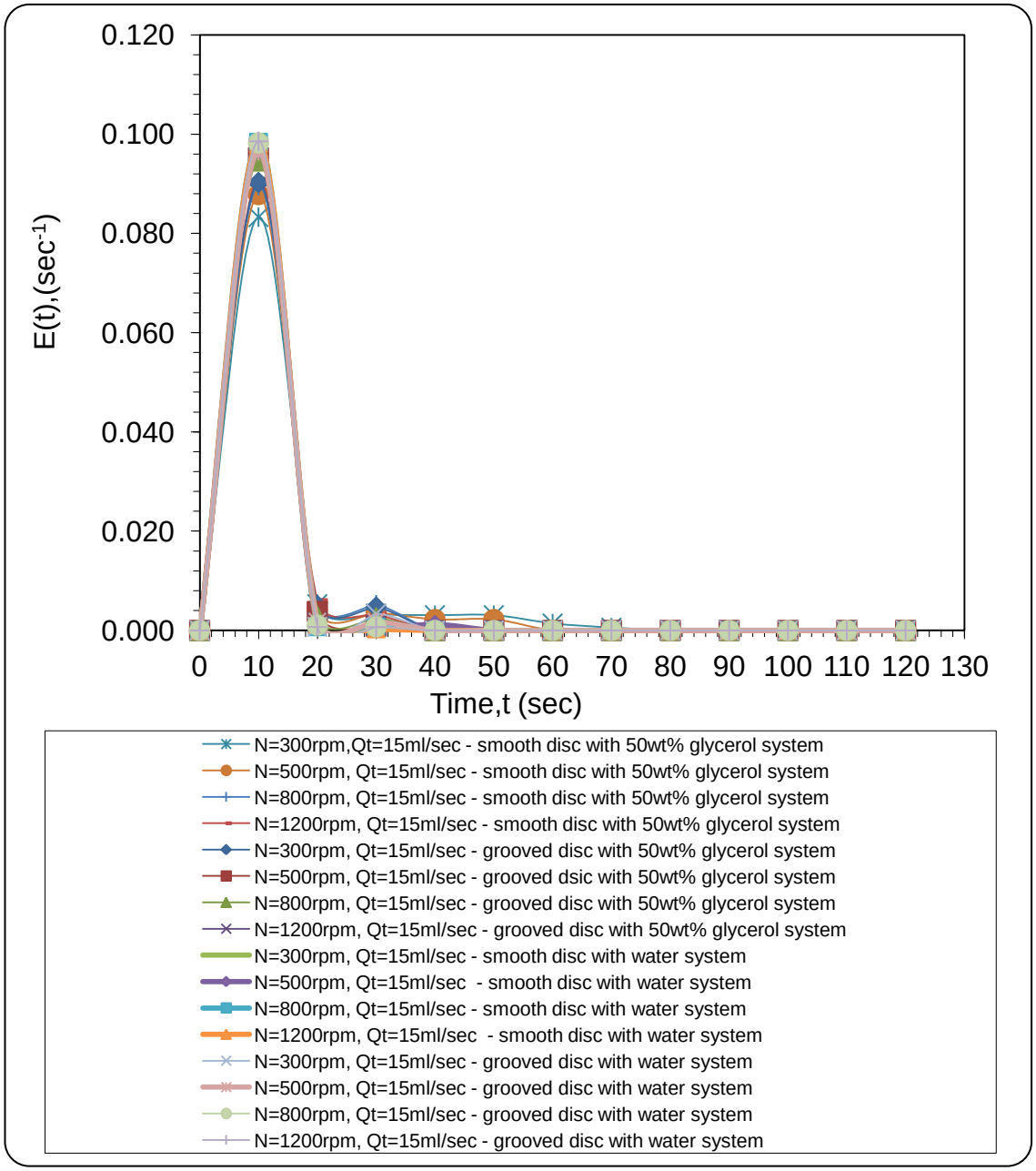

Figure AL12: Effect of disc rotational speed on RTD at total flowrate of (Qt=15 ml/s)-smooth disc vs. grooved disc with water and 50 wt% glycerol

Table AL13: Experimental mean resident time and the variance for the 30 cm SDR at disc rotational speeds of 500 and 800 rpm using water system and 50 wt% glycerol system with grooved and smooth discs, Qt=15 ml/s

Disc type	Disc speed, N(rpm)	Water system		Glycerol system	
		Mean residence time , tm (s)	Variance,σ^2(sec^2)	Mean residence time, tm (s)	Variance,σ^2(sec^2)
Smooth	500	10.260	2.815	12.10	4.203
Smooth	800	10.180	2.618	11.55	3.017
Grooved	500	10.26	1.373	10.420	3.217
Grooved	800	10.140	1.201	10.410	3.200

Table AL14:The Dispersion number (D/UL) and Peclet number, Pe(-) for the 30 cm SDR using water system with smooth disc, Qt=3 ml/s .

Disc rotational speed,N (rpm)	Dispersion number (D/UL)	Peclet number, Pe(-)
300	0.121	8.264
500	0.117	8.547
800	0.112	8.928
1200	0.112	8.928

Table AL15: The Dispersion number (D/UL) and Peclet number, Pe(-) for the 30 cm SDR ,using water system with smooth disc, Qt=6 ml/s .

Disc rotational speed,N (rpm)	Dispersion number (D/UL)	Peclet number, Pe(-)
300	0.072	13.888
500	0.014	71.428
800	0.013	76.923
1200	0.013	76.923

Table AL16: The Dispersion number (D/UL) and Peclet number, Pe(-) the 30 cm SDR, Using smooth disc with water system, Qt=9 ml/s.

Disc rotational speed,N (rpm)	Dispersion number (D/UL)	Peclet number, Pe(-)
300	0.013	76.923
500	0.013	76.923
800	0.012	83.333
1200	0.012	83.333

Table AL17: The Dispersion number (D/UL) and Peclet number, Pe (-) for the 30 cm SDR using 50 wt% glycerol system with smooth disc, Qt=3 ml/s.

Disc rotational speed, N (rpm)	Dispersion number, D/UL (-)	Peclet number, Pe(-)
300	0.126	7.936
500	0.122	8.196
800	0.120	8.333
1200	0.117	8.547

Table AL18:The Dispersion number (D/UL) and Peclet number, Pe (-)for the 30 cm SDR ,using 50 wt% glycerol system with smooth disc,Qt=6 ml/s .

Disc rotational speed, N (rpm)	Dispersion number, D/UL (-)	Peclet number, Pe(-)
300	0.118	8.474
500	0.106	9.433
800	0.098	10.204
1200	0.065	15.384

Table AL19:The Dispersion number (D/UL) and Peclet number, Pe (-)for the 30 cm SDR, using smooth disc with 50 wt% glycerol system, Qt=9 ml/s

Disc rotational speed N,(rpm)	Dispersion number D/UL, (-)	Peclet number Pe,(-)
300	0.015	66.66
500	0.014	71.428
800	0.013	76.923
1200	0.012	83.333

Table AL20: The Dispersion number (D/UL) and Peclet number, Pe (-) for the 30 cm SDR using smooth disc with 50 wt% glycerol system, Qt=15 ml/s

Disc rotational speed N,(rpm)	Dispersion number D/UL, (-)	Peclet number Pe,(-)
300	0.014	71.428
500	0.012	83.333
800	0.010	100
1200	0.010	100

Table AL21: The experimental mean resident time and the variance for the 30 cm SDR using water system with grooved disc, Qt=3 ml/s

Disc rotational speed N,(rpm)	Dispersion number D/UL, (-)	Peclet number Pe,(-)
300	0.012	83.333
500	0.010	100
800	0.009	111.111
1200	0.007	142.857

Table AL22: The experimental mean resident time and the variance for the 30 cm SDR ,using water system with grooved disc, Qt=6 ml/s

Disc rotational speed N,(rpm)	Dispersion number D/UL, (-)	Peclet number Pe,(-)
300	0.011	90.90
500	0.009	111.111
800	0.008	125
1200	0.007	142.857

Table AL23: The experimental mean resident time and the variance for the 30 cm SDR, Using grooved disc with water system, Qt= 9 ml/s

Disc rotational speed N,(rpm)	Dispersion numberD/UL, (-)	Peclet number,Pe(-)
300	0.008	125
500	0.007	142.857
800	0.005	200
1200	0.005	200

Table AL24: The experimental mean resident time and the variance for the 30 cm SDR Using grooved disc with 50wt% glycerol system, Qt=3 ml/s

Disc rotational speed N,(rpm)	Dispersion number D/UL, (-)	Peclet number Pe,(-)
300	0.113	8.849
500	0.102	9.803
800	0.052	19.230
1200	0.026	38.46

Table AL25: The experimental mean resident time and the variance for the 30 cm SDR, using grooved disc with 50wt% glycerol system, Qt= 6 ml/s.

Disc rotational speed N,(rpm)	Dispersion number D/UL, (-)	Peclet number Pe,(-)
300	0.034	29.412
500	0.016	62.500
800	0.015	66.666
1200	0.015	66.666

Table AL26: The experimental mean resident time and the variance for the 30 cm SDR, Using grooved disc with 50wt% glycerol system, Qt= 9 ml/s .

Disc rotational speed N,(rpm)	Dispersion number D/UL, (-)	Peclet number Pe,(-)
300	0.014	71.428
500	0.013	76.923
800	0.012	83.333
1200	0.011	90.909

Table AL27: The experimental mean resident time and the variance for the 30 cm SDR Using grooved disc with 50wt% glycerol system, Qt=15 ml/s.

Disc rotational speed N,(rpm)	Dispersion number D/UL, (-)	Peclet number Pe,(-)
300	0.013	76.923
500	0.009	111.111
800	0.009	111.111
1200	0.009	111.111

Appendix M: Calculations of the diffusion coefficient for the 50 wt% and 75 wt% glycerol systems

The Diffusion Coefficient for the glycerol-water system can be estimated from the empirical correlation below (Guichardon et al., 1997):

$$D_{mix} = X_w \left(\frac{\mu_w}{\mu_{mix}}\right)^{0.8} D_W + X_G \left(\frac{\mu_G}{\mu_{mix}}\right)^{0.8} D_G \qquad AM.1$$

Where:

D_{mix}= Diffusion coefficient for the mixture (m^2/s)

D_W= Diffusion coefficient for water (=10^{-9} m^2/s)

D_G= Diffusion coefficient for concentrated glycerol (=$1.33*10^{-11}$ m^2/s)

X_w= Mole fraction of water in the mixture (-)

X_G= Mole fraction of glycerol in the mixture (-)

μ_w= water dynamic viscosity at 20^{O}C (=1.005 cp)

μ_G= glycerol dynamic viscosity at 20^{O}C (=1410 cp)

μ_{mix}= mixture dynamic viscosity at 20^{O}C (50wt% = 6.00 cp)

Calculation of mole factions of water and glycerol in the 50wt% glycerol system:

Data:

Total volume of solution =10l
Volume of water =5577 ml
Volume of concentrated glycerol=4422.7 ml
Wt. of water =?
M. wt. of water=18 g/mol
M. wt. of glycerol=92.09 gm/mol
$\rho_w = 1\ gm/cm^3\ at\ 20\ ^O$C
$\rho_G = 1.26\ gm/cm^3\ 20\ ^O$C

$\rho = \frac{M}{V}$

Wt. of water =5577 gm

Wt. of glycerol =5577.0247 gm

Total wt. of solution=5577+5577.025=11154.025 gm

Basis =11154.025gm

Component	Wt., gm	Weight fraction,(-)	Molecular wt., gm/mol	No. of moles,(gm mol)	Mole fraction
water	5577	0.50	18	309.833	0.836
glycerol	5577.025	0.50	92.09	60.560	0.163
Total	11154.025	1.00	-	370.393	1.00

Mole fraction for water = 309.833/370.393=0.836

Mole fraction for glycerol = 60.560/370.393=0.163

Appling equation AM1, the Diffusion Coefficient for 50 wt% glycerol system equals $3.708*10^{-6}$ cm^2/s =$3.708*10^{-10}$ m^2/s

Calculation of mole factions of water and glycerol in the 75 wt% glycerol system:

Data:

D_W= Diffusion coefficient for water =10^{-9} m^2/s

D_G= Diffusion coefficient for concentrated glycerol =$1.33*10^{-11}$ m^2/s

μ_w= water dynamic viscosity at 20 ^{O}C =1.005 cp

μ_G= glycerol dynamic viscosity at 20 ^{O}C =1410 cp

μ_{mix}= mixture dynamic viscosity for 75 wt% glycerol system at 20 ^{O}C = 35.5 cp

Total volume of solution =10l

Volume of water =2959 ml

Volume of concentrated glycerol=7039 ml

Wt. of water =?

M. wt. of water=18 g/mol

M. wt. of glycerol=92.09 gm/mol

$\rho_w = 1\ gm/cm^3\ at\ 20^{O}C$

$\rho_G = 1.26\ gm/cm^3\ 20\ ^{O}C$

$\rho = \frac{M}{V}$

Wt. of water =2959 gm

Wt. of glycerol =8869.14 gm

Total wt. of solution=8869.14+2959=11828.14 gm

Basis=11828.14

Component	Wt., gm	Weight fraction,(-)	Molecular wt., gm/mol	No. of moles,(gm mol)	Mole fraction
water	2959	0.25	18	164.38	0.6305
glycerol	8869.14	0.75	92.09	96.309	0.3694
Total	11828.14	1.00	-	260.989	1.00

Mole fraction for water = 164.38/260.689=0.6305

Mole fraction for glycerol = 96.309/260.689=0.3694

Appling equation AM1, the Diffusion Coefficient for 75wt% glycerol system equals $1.264*10^{-6}$ cm^2/s = $\underline{1.264*10^{-10}\ m^2/s}$